The protective mechanisms of Protein Disulphide Isomerase in Amyotrophic Lateral Sclerosis

---

Emma Renee Perri

(Bachelor of Biomedical Science – Honours)

Submitted in total fulfillment of the requirements of the degree of
Doctor of Philosophy

October 2017

_____

Department of Biomedical Sciences

Faculty of Medicine and Health Sciences

Macquarie University

Sydney, Australia

Preface Contents

Abstract

Amyotrophic Lateral Sclerosis (ALS) is a devastating neurodegenerative disorder characterised by the degeneration of motor neurons. Numerous genes are linked to ALS both genetically and pathologically. Approximately 10% of ALS cases are familial, and of these cases, approximately 20% are due to mutations in the gene encoding superoxide dismutase 1 (SOD1), and approximately 10% are due to mutations in TAR DNA binding protein 43 (TDP-43) and fused in sarcoma (FUS). A major hallmark observed in ALS is the accumulation of misfolded proteins, containing either SOD1, TDP-43 and FUS, which form aggregates in the cytoplasm of degenerating motor neurons. However, the pathogenic mechanisms of disease in ALS remain poorly understood. Recent evidence suggests that dysfunction to the Endoplasmic Reticulum (ER), resulting in ER stress, is increasingly implicated in ALS pathogenesis. Protein Disulphide Isomerase (PDI) is an ER chaperone which functions as an oxidoreductase, utilising its disulphide interchange activity to oxidise, reduce and isomerase disulphide bonds. Our laboratory has previously demonstrated that PDI overexpression is protective against mutant SOD1, TDP-43 and FUS in neuronal cell cultures. Hence, here we examined that PDI overexpression is also protective against ALS mechanisms of pathogenesis triggered by mutant forms of novel ALS protein, Cyclin F. Previous studies have also identified that PDI's disulphide interchange activity is fundamental for its protective activity. Therefore, here we further investigated the properties of PDI which are important in mediating this activity. Results obtained suggest that PDI's *a* domain is essential for PDI's protective function, as well as its oxidase activity (capability to form disulphide bonds). These properties were verified in cell culture models expressing mutant FUS. Ultimately, there is a need for more effective therapeutics in ALS, thus, peptides mimicking PDI's *a* domain and oxidase activity were developed and analysed here for their protective effect in ALS cell models.

Declaration

This is to certify that the work presented in this thesis titled, "The Protective Mechanisms of Protein Disulphide Isomerase in Amyotrophic Lateral Sclerosis", has not previously been submitted, in either whole or part, for the purposes of obtaining any other degree at any other university or institution other than Macquarie University. I declare that due acknowledgement has been made in the text to all other material used and unless otherwise stated, this work was carried out by the author.

Signed: Emma Renee Perri

Date: 21/10/2017

Preface

All work described in this thesis was performed by the author, except where hereby stated. The author acknowledges the following people for their assistance in performing or assisting in the following experiments reported in this thesis:

Chapter 4

The design of the PDI domain mutants and the Dsb-like eukaryotic proteins were proposed in collaboration with Dr. Begoña Heras, La Trobe University, Melbourne, Australia. The constructs encoding these proteins were designed with the kind assistance of Dr. Damian Spencer, La Trobe University, Melbourne, Australia.

Chapter 5

The design of the PDI redox active site mutants and the cis-proline loop mutants was proposed in collaboration with Dr. Begoña Heras, La Trobe University, Melbourne, Australia.

Acknowledgements

To all my family and friends, who have supported me every step of the way and have always willingly lent an ear for me to vent. Thank you for reminding me that my life does not solely revolve around my PhD. A special thank you to my sisters, Sarah and Claudia, my main sources of happiness and laughter. Thank you for your constant love and for always being there. Also, a heartfelt thank you to my late dog, Cody, who was constantly by my side and kept me company whilst I wrote up my thesis until his untimely passing. Thank you for your companionship, love, and for how happy you made me, despite the task at hand.

To my parents, Laura and Otto. Throughout my childhood you encouraged me to work hard and to take all opportunities as they come. Without your unconditional love, advice, patience when I have been a handful, and all the sacrifices you have made along the way, I would not be where I am today. You have been my biggest support and I truly appreciate everything you have both done for me. I hope I have made you proud.

And finally, to my fiancé, Andrew. Words cannot express how grateful I am for you. You have been my rock, my voice of reason, and my escape over the past three and a half years. Thank you for putting me before yourself on countless occasions, enthusiastically joining me on my move to Sydney to complete the PhD, showering me with endless love and support, and patiently waiting for this all to be over. You have made it all that little bit easier and I cannot thank you enough. I wholeheartedly appreciate all that you have done for me.
We did it!

Dedicated to the loving memory of my late grandfather, Ben Sciartilli.

Here's to a future where no one succumbs to neurodegenerative disease.

Table of Contents

Abbreviations

AD	Alzheimer's Disease
ALS	Amyotrophic Lateral Sclerosis
ALS2	Alsin
ANOVA	Analysis of variance
ANG	Angiogenin
ASK1	Apoptosis signal-regulating kinase 1
ATF4	Activating transcription factor 4
ATF6	Activating transcription factor 6
ATXN2	Ataxin-2
A4V	Alanine mutated to valine at codon 4
BBB	Blood Brain Barrier
BCA	Bicinchoninic acid
BIM	BCL2 interacting mediator of cell death
BiP	Immunoglobulin binding protein
BMAA	β-N-methylamino-L-alanine
BMC	1,2 bis(mercaptoacetamido)cyclohexane
BSA	Bovine serum albumin
C9orf72	Chromosome 9 open reading frame 72
CCNF	Cyclin F
cDNA	Complementary Deoxyribonucleic Acid
CGHC	Cysteine-Glycine-Histidine-Cysteine
CGPC	Cysteine-Glycine-Proline-Cysteine
CHCHD10	Coiled-coil-helix-coiled-coil-helix domain-containing protein 10
CHMP2B	Charged multivesicular body protein 2B
CHOP	Enhancer binding protein (C/EBP) homologous protein
CNS	Central Nervous System
CPYC	Cysteine-Proline-Tyrosine-Cysteine
CSF	Cerebrospinal Fluid
DAO	D-amino acid oxidase
DAPI	4',6 diamidino-2-phenylindole

DCTN1	Dynactin 1
DMEM	Dulbecco's Modified Eagle's Medium
DMSO	Dimethyl Sulphoxide
DNA	Deoxyribonucleic Acid
ECL	Electrochemiluminescence
E. coli	Escherichia coli
EGFP	Enhanced green fluorescent protein
eIF2α	Eukaryotic translation initiation factor 2 subunit α
ELP3	Elongator acetyltransferase complex subunit 3
ERAD	ER-associated degradation pathway
ER	Endoplasmic Reticulum
ERBB4	Chorion protein gene ErB.4
ERGIC	ER-Golgi intermediate compartment
ERo1	ER oxidoreductin 1
ERp57	Endoplasmic reticulum protein 57
ERp72	Endoplasmic reticulum protein 72
fALS	Familial Amyotrophic Lateral Sclerosis
FCS	Fetal Calf Serum
FDA	Food and Drug Administration
FTD	Frontotemporal Dementia
FTLD	Frontotemporal Lobar Degeneration
FUS	Fused in sarcoma
GADD34	Growth arrest and DNA damage-inducible 34
GFP	Green fluorescent protein
GIP	Glycine-Isoleucine-Proline
GTP	Glycine-Threonine-Proline
GYP	Glycine-Tyrosine-Proline
HIV	Human immunodeficiency virus
hnRNP	Heterogenous nuclear ribonucleoprotein
IPSCs	Induced pluripotent stem cells
IRE1	Inositol-requiring kinase 1
JNK	c-Jun N-terminal kinase

KDEL	Lysine-Aspartic Acid-Glutamic Acid-Leucine
LB	Luria-Bertani
LMN	Lower motor neuron
MAM	Mitochondrial-associated ER membrane
MATR	Matrin 3
MND	Motor Neuron Disease
mRNA	Messenger Ribonucleic Acid
MW	Molecular weight
NEFH	Neurofilament heavy chain
NES	Nuclear export sequence
NLS	Nuclear localisation sequence
NO	Nitric Monoxide
OPTN	Optineurin
PAGE	Polyacrylamide gel electrophoresis
PARP1	Poly-adenosine diphosphate ribose polymerase
PBS	Phosphate buffered saline
PCR	Polymerase Chain Reaction
PD	Parkinson's Disease
PDI	Protein Disulphide Isomerase
PERK	PKR-like endoplasmic reticulum kinase
PFA	Paraformaldehyde
PFN1	Profilin 1
PON 1/2/3	Paraoxonase 1, 2 and 3
PRPH	Peripherin
Q331K	Glutamine mutated to lysine at codon 331
RIDD	Regulated IRE1 dependent decay
RNA	Ribonucleic Acid
ROS	Reactive oxygen species
R521G	Arginine mutated to glycine at codon 521
sALS	Sporadic Amyotrophic Lateral Sclerosis
SDS	Sodium dodecyl sulphate
SEM	Standard error of the mean

SETX	Sentaxin
SFP	Serine-Phenylalanine-Proline
SIGMAR1	Sigma nonopioid intracellular receptor 1
SIP	Serine-Isoleucine-Proline
siRNA	Small interfering ribonucleic acid
SOD1	Superoxide dismutase 1
SPG11	Spatacsin
STP	Serine-Threonine-Proline
TAE	Tris-Acetic Acid-EDTA
TAF15	TATA-binding protein associated factor 15
TBK1	TANK-binding kinase 1
TBS	Tris buffered saline
TBS-T	Tris buffered saline with tween-20
TDP-43	Transactive response DNA binding protein of 43 kDa
TUBA4A	Tubulin α1
UMN	Upper motor neuron
UAD	Ubiquitin association domain
UBL	Ubiquitin-like domain
UPR	Unfolded Protein Response
UPS	Ubiquitin Proteasome System
VAPB	Vesicle associated membrane protein-associated protein B
VCP	Valosin containing protein
WT	Wildtype
XBP-1	X-box binding protein-1

Units of magnitude and measure

C	Celsius
Da	Dalton/s
g	Acceleration due to gravity at Earth's surface
g	Gram/s
h	Hour/s
k	Kilo
L	Litre/s
m	Metre/s
M	Molar
min	Minute/s
N	Number of distinct units in a dataset
n	Nano
rpm	Revolution/s per minute
s	Second/s
V	Volt/s
μ	Micro

Publications

Review Papers

- <u>Perri ER</u>, Thomas CJ, Parakh S, Spencer DM, Atkin JD (2016) "The Unfolded Protein Response and the role of Protein Disulfide Isomerase in neurodegeneration". *Frontiers in Cell and Developmental Biology*, 3:80.

- <u>Perri ER</u>, Parakh S, Atkin JD (2017) "Protein Disulphide Isomerases: Emerging roles of PDI and ERp57 in the nervous system and as therapeutic targets for ALS". *Expert Opinion on Therapeutic Targets*, 21:1, 37-49.

- Shahheydari H, Ragagnin A, Walker AK, Toth RP, Vidal M, Jagaraj CJ, <u>Perri ER</u>, Konopka A, Sultana JM, Atkin JD (2017) "Protein quality control and the Amyotrophic Lateral Sclerosis/Frontotemporal Dementia continuum". *Frontiers in Molecular Neuroscience*, 10:119.

Experimental Papers in preparation

- Parakh S, Jagaraj CJ, Vidal M, Ragagnin AMG, Perri ER, Konopka A, Toth R, Galper J, Blair IP, Thomas CJ, Walker AK, Yang S, Spencer DM, Atkin JD (2017) "ERp57 is protective against mutant SOD1-induced cellular pathology in Amyotrophic Lateral Sclerosis". *Human Molecular Genetics.* Manuscript submitted for publication.

- Ragagnin AMG, Sundaramoorthy V, Soo KY, Parakh S, Perri ER, Rayner S, Chung R, Williams K, Blair IP, Atkin JD (2017) "Mutant cyclin F associates with stress granules and perturbs endoplasmic reticulum homeostasis, inducing apoptosis in Amyotrophic Lateral Sclerosis". Manuscript in preparation.

Chapter 1: General Introduction

1.1 Amyotrophic Lateral Sclerosis (ALS)

Amyotrophic Lateral Sclerosis (ALS), also known as Motor Neuron Disease (MND), is a fatal, adult-onset neurodegenerative disease, characterised by the premature degeneration of upper motor neurons (UMNs) of the motor cortex and lower motor neurons (LMNs) of the brainstem and spinal cord [1]. This degeneration manifests in symptoms of fatigue, muscle weakness and atrophy, followed by eventual muscle paralysis [2]. The aetiology of ALS is still under investigation, hence there is currently no cure for the disease and patients have a median lifespan of three years, with death usually occurring due to respiratory failure [3, 4]. Currently, there are only two Food and Drug Administration (FDA) approved pharmaceutical agents for ALS treatment, Riluzole, although this drug only extends the life span of patients by two to three months [5, 6], and the newly approved, Edaravone [7]. Thus, there is a dire need for identifying and developing novel therapeutics for the treatment of ALS.

Approximately 10% of ALS cases are inherited, termed familial ALS (fALS), with the remaining 90% of cases being sporadic (sALS) [8]. Of the familial cases, approximately 12-20% are caused by mutations in the gene encoding superoxide dismutase 1 (SOD1) and approximately 8% are caused by mutations in the genes encoding either TAR-DNA binding protein 43 (TDP-43) or fused in sarcoma (FUS) [9]. Furthermore, repeat expansions in the gene encoding Chromosome 9 open reading frame 72 (C9orf72) account for disease in over 40% of fALS cases [10]. However, as well as genetic influences, environmental risk factors for ALS have also been recently identified, such as smoking, exposure to cyanotoxins, and physical activity [11]. Nonetheless, clinical and pathological overlap exists between both fALS and sALS. Similar to other neurodegenerative diseases, such as Alzheimer's Disease (AD) and Parkinson's Disease (PD), protein misfolding and the presence of abnormal intracellular protein inclusions are major pathological hallmarks of ALS [12]. Unfortunately, however, the mechanisms of pathogenesis are yet to be fully elucidated, and further study is

warranted to understand the molecular mechanisms of ALS in order to design effective therapeutics for the disease. The induction of Endoplasmic Reticulum (ER) stress is increasingly implicated as a key pathological event relevant to ALS disease processes and the induction of ER chaperone Protein Disulphide Isomerase (PDI) has been demonstrated to play a protective role in ALS cell models. Therefore, this thesis focuses on determining the protective characteristics and mechanisms of PDI, with the objective of developing novel therapeutics for the treatment of ALS based on PDI's protective activity.

1.2 The epidemiology of ALS

ALS has a worldwide incidence of approximately 1.5-2 cases per 100,000 per year and a prevalence of approximately 5-6 per 100,000 per year, however these rates differ between populations [13]. For example, the median incidence of ALS in Europe is 2.1 per 100,000 whereas the median incidence in the United States is 1.75 per 100,000, and in Chinese populations it is only 0.45 per 100,000 [13]. Moreover, there is an overall reduced occurrence of ALS among Asian, African, American Indians and Alaskan populations, compared to Caucasian populations [14, 15]. ALS has a mean age onset of approximately 58-63 years for sporadic disease and 47-52 years for familial disease [16] and the incidence is higher in males than females, with an overall male-to-female ratio of 2.5:1, however this ratio declines with age to 1.4:1 after the age of 75 [17]. As the risk of developing ALS increases with age, therefore with an aging population, both the incidence and prevalence of the disease is expected to rise in the future [18].

1.3 The clinical features of ALS

The clinical features of ALS present with a loss of voluntary control of skeletal muscle, due to the degeneration of UMNs and LMNs [1]. Degeneration of the UMNs results in impaired voluntary movement, hyperreflexia and spasticity. If only the UMNs of a patient are affected, they are diagnosed with Primary Lateral Sclerosis (PLS) [19]. The median survival time of a patient with PLS is more than ten years [20]. Conversely, degeneration of the LMNs results in muscle denervation, causing subsequent muscle atrophy, weakness and fasciculation. Loss of LMNs only results in a disease termed 'Progressive Muscular Atrophy (PMA)' [21], in which the median survival time is approximately seven years [20]. Degeneration of UMNs in the brainstem causes dysphagia and impaired voluntary control of the bulbar muscles. This is

often referred to as progressive bulbar palsy, in which a patient develops slurred speech, and can be associated with emotional liability, such as inappropriate crying or laughing [22]. The median survival time of a patient with progressive bulbar palsy is two years [20]. In ALS, however, degeneration of the UMNs and LMNs is initiated simultaneously, primarily affecting specific regions of the body before spreading [23].

The initial clinical presentation of ALS can be classed by the body region primarily affected. Around 70% of cases result in limb-onset ALS, whereby symptoms originate in the upper and lower limbs, and this form is characterised by muscle weakness and fatigue [24]. Patients with limb-onset ALS experience fasciculations (fleeting twitches under the skin) and muscle atrophy, resulting in spasticity (stiff muscles). Due to this spasticity, gait and the ability to execute simple tasks are severely affected. Eventually, bulbar symptoms and respiratory issues ensue [25]. In contrast, around 25% of cases result in bulbar-onset ALS, characterised by facial weakness, dysarthria of speech, dysphagia (swallowing difficulties) and excessive drooling. Bulbar-onset is associated with a more rapid progression of disease, and spinal symptoms will eventually progress [24, 26, 27]. A small proportion of patients have a concurrent limb and bulbar onset [28]. Moreover, respiratory onset of ALS is rare (< 3% of ALS cases), and is usually linked to mutations in the SOD1 gene [29], however, advanced cases of ALS will eventually develop respiratory failure and this is the primary cause of death in patients [30]. The median survival time after prognosis for ALS is two and a half years [20]. Depression is also often associated with ALS, usually because cognitive function is still maintained. This has been shown to alter the quality of life of a patient, independent of their physical disability [31].

Although cognitive function is generally spared in ALS, between 5-40% of patients develop Frontotemporal Dementia (FTD) [32]. FTD represents a subgroup of neurological disorders that constitute Frontotemporal lobar degeneration (FTLD) and is characterised by behavioural

and cognitive dysfunction [32]. Moreover, approximately 15% of patients with FTD develop ALS and approximately 30% of FTD patients present signs of motor dysfunction [33]. In fact, genetic and neuropathological overlap exists between the two diseases [34]. This overlap was suggested by the discovery of common genetic causes for both diseases, including mutations in the genes encoding Chromosome 9 open reading frame 72 (C9orf72), TDP-43, FUS, TANK-binding kinase-1 (TBK-1), Ubiquilin 2 (UBQLN2), optineurin (OPTN) and Cyclin F (CCNF) [35].

1.4 The environmental factors of ALS

ALS is thought to be a multifactorial disease, where the interaction between genetics and environmental factors are considered to play a key role in triggering neurodegeneration. Many diverse environmental factors have been associated with ALS development, including but not limited to, smoking, toxins and cyanotoxins such as β-N-methylamino-L-alanine (BMAA), pesticides, physical activity, heavy metals, viral infections, Gulf war service and exposure to electricity [11]. Prevalence of ALS is also commonly observed in people with a history of brain trauma [36].

Smoking is considered to be a major environmental risk factor for ALS following assessment of many case studies [37, 38]. A longitudinal study also revealed that current tobacco smokers had almost twice the risk of developing ALS than non-smokers. Moreover, the number of years of smoking increased this risk, while the number of years since the cessation of smoking decreased this risk [39]. How smoking causes this risk is unknown, however exposure to the toxins present in the cigarette may be a possibility.

Exposure to cyanotoxins, such as BMAA, are also implicated in ALS disease processes. A large concentration of BMAA is present in cycad seeds ingested by Guam indigenous

populations [40]. Reports of a link between BMAA and ALS was initially based on elevated rates of ALS, and other neurodegenerative diseases such as PD and AD, in the island of Guam [41]. In fact, the incidence rate of ALS in Guam is three times higher than the overall world incidence [41]. Autopsies of nervous tissue of indigenous people from Guam affected with ALS demonstrate an increased BMAA concentration, compared to those who died from other reasons [42]. This finding was later confirmed when increased levels of BMAA were found in the brains of ALS patients in Florida, but not in the brains of healthy subjects [43]. More recent studies confirm that BMAA can be incorporated into nerve cell proteins, resulting in protein misfolding, aggregation and eventual cell death [44].

Physical activity has also been postulated as a risk factor for ALS. In particular, a wide range of studies have shown that professional soccer players have a surprisingly high prevalence of ALS [45-47]. This incidence of ALS in soccer players was not observed in basketball players or cyclists [48]. The reason for this high prevalence of ALS in soccer plays may be due to high physical demands which could result in the production of reactive oxygen species (ROS), leading to damaged nucleic acids [49]. Moreover, soccer players may suffer from repeated head injuries [50] caused by constantly hitting the ball with their heads. Exposure to pesticides on soccer fields may also be a risk factor for ALS, as pesticide exposure is believed to be implicated in ALS, however this has not been demonstrated conclusively.

A higher incidence of ALS is recorded among subjects from rural areas [51] and furthermore, ALS risk is associated with agricultural chemicals, solvents and heavy metals [52]. The interest in pesticides arose following an increased incidence of ALS among Gulf war veterans, who possess an almost two-fold greater risk of ALS than military personnel who were not deployed [53]. This increased incidence has been attributed to an environmental factor, possibly a pesticide, however the exact cause remains unknown [53].

Other environmental factors linked with ALS are occupational or residential exposure to electromagnetic fields and electric shocks [54, 55], as well as viral infections [56]. ALS has been identified in patients with human immunodeficiency virus (HIV) infection [56] and another study suggests that retroviral elements contribute to ALS pathophysiology [57]. Interestingly, in some cases of ALS, partial recovery of symptoms has been observed with antiretroviral treatment [56].

1.5 The genetics of ALS

Approximately 10% of all ALS cases are inherited (fALS), caused by mutations in specific genes associated with ALS. While the remaining 90% of cases are sporadic (sALS), gene mutations can still be implicated in sporadic disease and known genetic causes now account for 11% of sALS. In contrast, two-thirds of fALS now have a known genetic aetiology [8]. The first identified and hence most widely studied gene in ALS is SOD1, recognized in 1993 [58]. Since then, many genes have been linked with the disease, as illustrated in Table 1.1. For example, the hexanucleotide repeat expansion in C9orf72 is the most common mutation present in fALS [59, 60]. Furthermore, mutations in the genes encoding TDP-43 and FUS, are also commonly studied and are of great importance because, along with SOD1 and C9orf72, misfolded, wildtype forms of these four proteins are implicated in sALS pathology, demonstrating the overlap between fALS and sALS [61-64]. Mutations in these four genes account for more than 50% of fALS cases [8] and thus, are discussed in detail below. On overview of the other genes implicated in ALS is also presented below.

TABLE 1.1 An overview of the genes and loci associated with ALS.

Gene	Locus	Protein encoded	Inheritance	References
SOD1	21q22	Superoxide dismutase 1	AD, AR	[58]
C9orf72	9p21	Chromosome 9 open reading frame 72	AD	[60]
TARDBP	1p36	TAR DNA-binding protein 43	AD	[62]
FUS	16p11	Fused in sarcoma	AD, AR	[65]
UBQLN2	Xp11	Ubiquilin 2	XD	[66]
VCP	9p13	Valosin-containing protein	AD	[67]
SQSTM1	5q35	Sequestosome 1	AD	[68]
OPTN	10p13	Optineurin	AD, AR	[69]
PFN1	17p13	Profilin 1	AD	[70]
VAPB	20q13	Vesicle-associated-membrane-associated protein B	AD	[71]
MATR3	5q31.	Matrin 3	AD	[72]
TUBA4A	2q35	Tubulin α1	AD	[73]
DCTN1	2p13	Dynactin 1	AD	[74]
NEFH	22q12	Neurofilament heavy chain	AD	[75]
PRPH	12q12	Peripherin	AD	[76]
ALS2	2q33	Alsin	AR	[73, 77]
FIG4	6q21	FIG4 homolog	AD	[78]
CHMP2B	3p11	Charged multivesicular protein 2B	AD	[79]
SETX	9q34	Sentaxin	AD	[80]
ANG	14q11	Angiogenin	AD	[81]
SPG11	15q21	Spatacsin	AR	[82]
DAO	12q22-23	D-amino acid oxidase	AD	[83]
TBK-1	12q14	TANK-binding kinase 1	AD	[84]
HNRNPA1	12q13	Heterogenous nuclear ribonucleoprotein A1	AD	[85]
HNRNPA2B1	7p15	Heterogenous nuclear ribonucleoprotein A2B1	AD	[85]
SIGMAR1	9p13	Sigma nonopioid intracellular receptor 1	AD	[86]
ATXN2	12q24	Ataxin-2	AD	[87]
ELP3	8p21	Elongator acetyltransferase complex subunit 3	Undefined	[88]
CCNF	16p13	Cyclin F	AD	[89]
CHCHD10	22q11	Coiled-coil-helix-coiled-coil-helix domain-containing protein 10	AD	[90]
ERBB4	2q34	Chorion protein gene ErB.4	AD	[91]
PON1/2/3	7q21	Paraoxonase 1, 2 and 3	AD	[92]
ANXA11	10q22	Annexin A11	AD	[93]
NEK1	4q33	NIMA-related kinase 1	AD	[94]

AD: autosomal dominant, AR: autosomal recessive, XD: X-linked dominant

1.5.1 Superoxide dismutase 1 (SOD1)

The *SOD1* gene, encoding the antioxidant enzyme Cu/Zn superoxide dismutase (SOD1), was the first causative gene linked to ALS [58]. Since the discovery of its association with ALS in 1993, more than 180 mutations in SOD1 have been reported in the ALSoD Database (http://alsod.iop.kcl.ac.uk). Most mutations cause autosomal dominant ALS, although autosomal recessive inheritance occurs in rare instances, such as in the D90A (aspartic acid to alanine) and D96N (aspartic acid to asparagine) SOD1 mutations [95, 96]. Mutations in SOD1 account for approximately 12-20% of fALS cases and 1% of sALS [9].

SOD1 is a highly expressed, ubiquitous antioxidant and metalloenzyme that exists as a 32 kDa homodimer, comprising two 153 amino acid residue subunits [97]. Each subunit is stabilised by four cysteine residues, whereby two are linked by a disulphide bond, and contain one enzymatically active copper ion and one stabilising zinc ion which are essential for protein stability and SOD1's catalytic activity [97] (see Figure 1.1). SOD1 is predominantly located in the cytoplasm where it catalyses the degradation of harmful, free superoxide radicals (O_2^-) to dioxygen (O_2) and hydrogen peroxide (H_2O_2). Thus, SOD1 regulates and protects the cell from oxidative stress [98]. It is a highly conserved protein, accounting for 1-2% of the total soluble protein found in the nervous system [99]. Although primarily found freely in the cytoplasm, SOD1 is also localised in the mitochondria, lysosomes, peroxisomes and the nucleus [100]. Moreover, studies have shown that SOD1 can be found in the trans-Golgi network where it binds to neurosecretory vesicles, and thus, it can be secreted in the extracellular space, where it can promote microgliosis and motor neuronal damage [101]. In fact, both misfolded and wildtype SOD1 are detected in the cerebrospinal fluid (CSF) of ALS patients [102, 103].
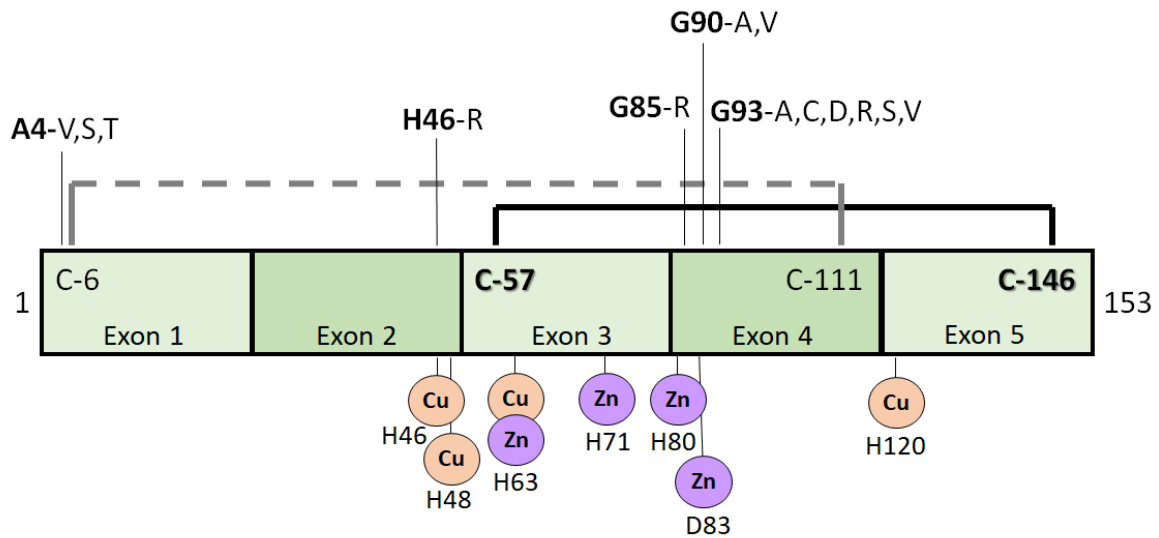
Figure 1.1: A schematic representation of the SOD1 gene.

One monomer of SOD1 contains four cysteine residues; Cys-6, Cys-57, Cys-111 and Cys-146. Cys-57 and Cys-146 form a stabilising intrasubunit disulphide bond (black solid line), however abnormal disulphide bonding is sometimes observed between Cys-6 and Cys-111 due to alterations in redox environment (grey perforated line). The copper (pink) and zinc (purple) binding histidine and aspartic acid residues are shown, as well as the location of several well studied ALS causative mutations within the protein.

Mutant SOD1 proteins have a destabilised structure compared to wildtype SOD1 and they are readily reduced into monomers by reduction of the disulphide bonds between Cys-57 and Cys-146 and demetallation at the dimer interface [104, 105]. Abnormal disulphide crosslinking of SOD1 also leads to the irreversible formation of oligomers [106]. Due to this monomerisation, mutant forms of the protein have an increased propensity to misfold and the accumulation of misfolded SOD1 in affected neurons leads to the formation of insoluble, intracellular ubiquitin positive aggregates or inclusions [104, 107]. In fact, around 2% of pathological inclusions in ALS contain accumulated SOD1 [108]. These SOD1 inclusions are visible by light microscopy in the motor neurons of SOD1 patients and animal models [109].

How mutant SOD1 is relevant to disease remains unknown. Initially, it was believed that mutant SOD1 was pathogenic due to a loss-of-function, however SOD1-/- (null) mice had a reduced lifespan but do not develop an ALS phenotype [110], arguing against this hypothesis. Several SOD1 mutations, including H46R (histidine to arginine), disrupt binding to copper which is required for SOD1's dismutase activity, however, other ALS-linked mutations, including the commonly studied G93A (glycine to alanine), retains full copper binding and dismutase activity [111, 112]. Moreover, the presence of the G93A mutation is associated with a rapid progression of disease, whereas the H46R mutation is associated with a slower progression of disease [113]. Interestingly, mutations in SOD1 have been linked with numerous cell defects, including oxidative stress, excitotoxicity, neuroinflammation, axonal transport dysfunction, ER stress and Golgi fragmentation (detailed further in Section 1.6) [114, 115]. Recent research has also identified misfolded forms of wildtype SOD1 in sALS patients and in fALS patients not associated with SOD1 [116-118]. It has also been established that wildtype SOD1 is capable of inducing pathological disease mechanisms similar to mutant SOD1 [116, 119], suggesting a role for misfolded, wildtype SOD1 in ALS pathogenesis. Interestingly, beneficial effects have been demonstrated for an active

immunisation strategy using a SOD1 exposed dimer interface antibody displayed on a branched peptide dendrimer to target monomer and misfolded SOD1 in mutant SOD1 transgenic mice. Immunisation with these antibodies delayed disease onset and extended disease duration, with survival times increasing by an average of 40 days in treated mice [120].

Many rodent models have now been developed which develop ALS-like symptoms at varying time-points. The transgenic SOD1 G93A mouse model is the most widely used ALS model [121]. Whilst it can recapitulate most characteristics of ALS pathology, it has also been heavily criticised as therapeutic strategies developed using this model have failed to translate into clinical trials.

1.5.2 TAR-DNA binding protein 43 (TDP-43)

TDP-43 is a ubiquitously expressed RNA and DNA binding protein, encoded by the *TARDBP* gene, with a molecular mass of 43 kDa [62]. TDP-43 contains two RNA recognition motifs, a nuclear localisation sequence (NLS), a nuclear export signal (NES), and a glycine-rich C-terminus, which is involved in ribonucleoprotein binding and splicing [122, 123] (see Figure 1.2). According to the ALSoD database, more than 50 mutations in TARDBP have been linked with ALS (http://alsod.iop.kcl.ac.uk). These pathogenic mutations are mostly located in the glycine-rich C-terminus [124]. Mutations in TARDBP account for approximately 4% of fALS and approximately 1% of sALS worldwide [8, 9], most of which are missense and autosomal dominant mutations [125].
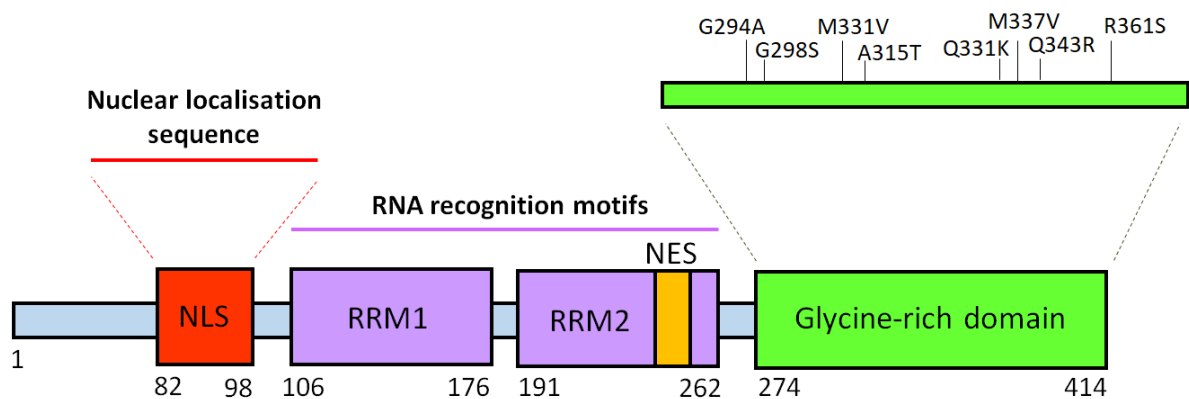
Figure 1.2: A schematic representation of the TARDBP gene encoding TDP-43.

TDP-43 contains a nuclear localisation sequence (NLS), two RNA recognition motifs (RRM1 and RRM2), a nuclear export sequence (NES) within one of the RNA recognition motifs, and a glycine-rich domain at the C-terminus. Most ALS causative mutations in TARDBP occur within the glycine-rich domain. Some of the most common and well-studied of these mutations are shown above.

TDP-43 is localised primarily in the nucleus where it is involved in RNA processing, such as transcription, pre-mRNA splicing, mRNA stabilisation and transport to dendrites, and miRNA biogenesis [108]. In ALS, TDP-43 is recruited to stress granules, ribonucleoprotein complexes where protein synthesis is temporarily halted, in conditions of oxidative stress [126]. It is thought that these stress granules are precursors for large TDP-43-positive inclusions that develop in ALS [127]. In fact, TDP-43 is the major constituent of cytoplasmic and intranuclear inclusions in spinal cord neurons and glia of fALS and sALS patients and cortical neurons of FTD patients [62, 128]. Moreover, ubiquitinated TDP-43 positive inclusions are present in 97% of total ALS cases, except in ALS cases with mutant SOD1, indicating a central role of TDP-43 in the pathogenesis of ALS [129]. Interestingly, a truncated, 25 kDa fragment of TDP-43, resulting from caspase cleavage, can also cause inclusion formation and cellular toxicity [130].

In ALS, mutated forms of TDP-43 are redistributed from the nucleus to the cytoplasm [62]. In the cytoplasm, TDP-43 is cleaved at the C-terminus and hyper-phosphorylated, and it then accumulates into inclusions [62, 131]. However, it remains unclear how TDP-43 mutations are associated with ALS, although the distribution of TDP-43 into the cytoplasm and its aggregation [132], loss of RNA processing [133], mislocalisation in mitochondria [134, 135], and axonal transport impairment [136] are key mechanisms linked to disease. Therefore, the discovery of TDP-43 in ALS pathogenesis highlights the importance of RNA processing and additional support for this hypothesis has arisen from the discovery of ALS mutations in FUS, another RNA-binding protein.

1.5.3 Fused in sarcoma (FUS)

Mutations in the gene encoding the 53 kDa protein, fused in sarcoma (FUS), were first identified in cases of autosomal dominant and recessive fALS by two groups in 2009 [65, 137]. Since then, multiple studies have reported FUS mutations in sALS and in patients with FTD [138-140]. FUS is an RNA and DNA-binding protein, sharing functional and structural homology with TDP-43. FUS consists of an N-terminal serine-tyrosine-glutamine-glycine (SYQG) rich domain, a glycine rich domain, a conserved RNA recognition motif, a RanBP2-type zinc finger motif and multiple C-terminal arginine glycine-glycine domains [141] (see Figure 1.3). Similar to TDP-43, FUS mutations are generally localised in the RNA-binding domain at the C-terminus of the protein. More specifically, mutations are usually found in the NLS and NES of the C-terminus [137]. Over 46 mutations in FUS are currently associated with ALS and these mutations account for approximately 4% of fALS and approximately 1% of sALS cases [8].
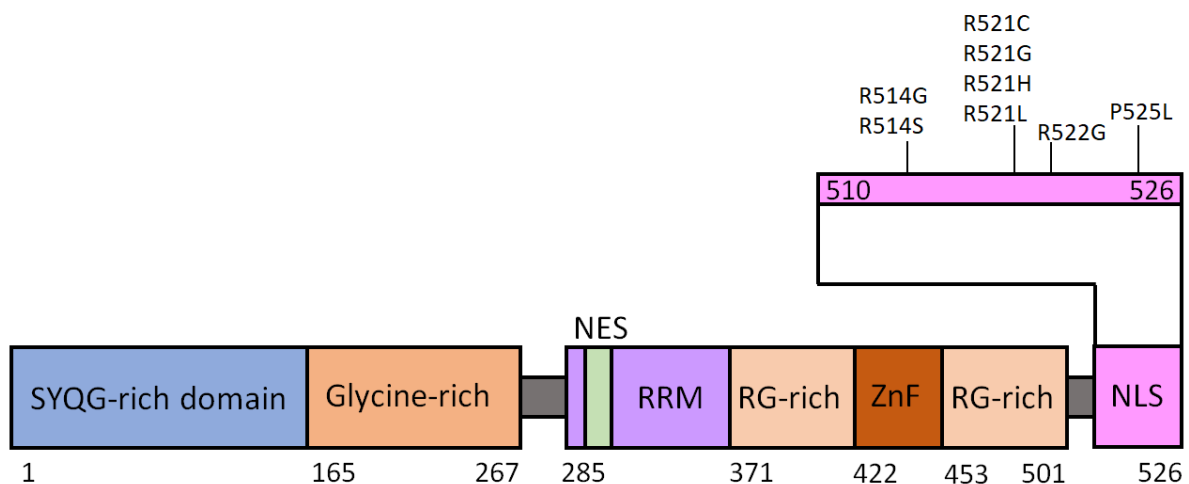
Figure 1.3: A schematic representation of the FUS gene.

FUS contains a serine-tyrosine-glutamine-glycine rich domain (SYQG-rich domain), a glycine-rich domain, an RNA recognition motif (RRM), a nuclear export sequence (NES) within the RNA recognition motif, two arginine-glycine rich domains (RG-rich), a zinc finger motif (ZnF), and a nuclear localisation sequence (NLS) at the C-terminus. Several ALS causative mutations occur in the nuclear localisation sequence of FUS and well-studied mutations are illustrated above.

FUS is normally localised in the nucleus, but it also plays a role in nuclear-cytoplasmic shuttling of mRNA in a transportin-mediated manner, hence it can also be found less commonly in the cytoplasm [142]. FUS also regulates RNA transcription and post-transcriptional processing, such as pre-mRNA splicing and mRNA trafficking [143], and it is also involved in mRNA transport and DNA repair [144]. It has been demonstrated that mutations in FUS prevent its nuclear import, causing mislocalisation to the cytosol, resulting in the generation of stress granules [145].

FUS mutations can be categorised into two groups: those localised in the prion-like domain and those found in the C-terminus, however both can lead to mislocalisation of FUS to the cytoplasm [65, 137]. In ALS, mutant FUS can alter the dynamics of stress granules, thus making them more resistant to autophagy [146, 147]. Moreover, distinct mutations of FUS can have different pathological effects. For example, expression of mutant FUS R521G (arginine to glycine) induces cytoplasmic inclusions formation in neuroblastoma cells, whereas expression of mutant FUS H517Q (histidine to glutamine) did not induce inclusions [137]. In fact, 2% of sALS patients display FUS immunoreactive inclusions [108]. FUS immunoreactive inclusions are also present in TDP-43 negative cases of FTD [148-150], indicating an overlap between ALS and FTD, as well as similarities between FUS and TDP-43.

1.5.4 Chromosome 9 open reading frame 72 (C9orf72)

A GGGGCC hexanucleotide repeat expansion present in the 5' non-coding region of C9orf72 represents the most common cause of fALS and FTD worldwide [60]. In fact, this pathogenic mutation accounts for approximately 40% of fALS cases [9] and also approximately 7% of sALS cases [8]. Normally, the number of hexanucleotide repeats is generally less than 30. Conversely, in ALS patients, this expansion can be up to several hundred or thousand copies of the repeat [10].

The normal cellular function of C9orf72 remains relatively unknown, however studies have shown that the localisation of C9orf72 is predominately cytoplasmic. Furthermore, it is structurally related to DENN domain protein's conserved GDP-GTP exchange factors that activate Rab-GTPases. This suggests that C9orf72 may regulate membrane traffic in conjunction with Rab-GTPase switches and plays a role in autophagy [151]. More recent studies have confirmed these observations and also established that C9orf72 interacts with SMCR8 and WDR41 to form a complex that regulates the autophagy-lysosome pathway [152, 153].

Moreover, the exact mechanisms by which C9orf72 causes ALS have not been fully elucidated. However, three hypotheses have been proposed; loss of the normal function of C9ORF72 protein caused by C9orf72 haploinsufficiency, and gain of function mechanisms, involving either toxicity of sense and anti-sense RNA transcripts, or expression of dipeptide repeat proteins from an unconventional mechanism of translation: repeat associated non-ATG (RAN) translation [154]. Decreased levels of C9orf72 protein have been detected in ALS patient motor neurons [155] and depletion of C9orf72 in primary cortical neurons has been reported to impair autophagy, leading to TDP-43 and p63 aggregates [156], however in vivo studies have yielded conflicting results as to whether haploinsufficiency is a valid pathogenic

mechanism [157]. Alternatively, abnormal repeat RNA transcripts accumulate within nuclear

foci in the brain and spinal cord of C9orf72 patients [60]. Moreover, expression of long

GGGGCC repeats form intracellular RNA foci that induce apoptosis in ALS cell lines and

zebrafish models, suggesting that RNA toxicity triggers ALS [158]. These transcripts

undergo unusual RAN translation resulting in dipeptide repeat proteins which aggregate in

ALS and FTD patients [159], as well as in affected neurons, resulting in the induction of ER

stress and neurotoxicity in vitro [159].

1.5.5 Other genes implicated in ALS

The other genes implicated in ALS cause uncommon or atypical forms of the disease and are

discussed below. It is important to note that genes implicated in ALS and FTD are also

implicated in patients with other neurological diseases.

1.5.5.1 Mutations in genes encoding proteins that function in proteostasis or autophagy

Ubiquilin 2 (UBQLN2)

Ubiquilin 2 is encoded by the gene *UBQLN2* and it is a member of the ubiquitin-like protein

family which is involved in the regulation of the ubiquitin proteasome system (UPS) and

autophagy [160]. Missense mutations in *UBQLN2* cause X-linked autosomal dominant ALS

and FTD, however these mutations are quite rare, accounting for less than 1% of fALS [8,

66]. All ubiquitin-like proteins possess a N-terminal ubiquitin-like domain (UBL), which

binds to subunits of the proteasome, and a C-terminal ubiquitin association domain (UAD),

which binds to poly-ubiquitin chains that are targeted for degradation [160]. A PXX region

located close to the UBA domain, not present in other ubiquilins, harbours most of the mutations associated with fALS [161].

Ubiquilin 2 mediates the delivery of ubiquitinated proteins to the proteasome for degradation by binding to these ubiquitinated proteins through its UBA domain and binding to the proteasome through its UBL domain [162]. Moreover, Ubiquilin 2 interacts with LC3 in the autophagosome, suggesting that it is able to deliver cargoes, such as misfolded proteins, to autophagosomes [163]. These findings suggest that normally Ubiquilin 2 plays a central role in protein quality control.

Ubiquilin 2 skein-like cytoplasmic inclusions are present in the brain and spinal cords of sALS patients [66], suggesting a broader role for Ubiquilin 2 in ALS in addition to the familial mutations in fALS. These inclusions also contain ubiquitin, optineurin, TDP-43 and FUS [66, 164], suggesting that the dysfunction of protein clearance is associated with ALS.

Valosin containing protein (VCP)

Valosin containing protein (VCP) is a ubiquitously expressed member of the ATPase associated with diverse cellular activities (AAA) protein superfamily [165]. It is a multifunctional ubiquitin sensitive chaperone that unfolds and disassembles protein complexes or directs misfolded proteins to be degraded via the UPS, suggesting an important role in ER associated degradation (ERAD) [166]. Mutations in VCP were first identified in patients with inclusion body myopathy with early onset Paget disease and FTD [167], and they now account for approximately 1-2% of fALS cases, but they are rare in sALS [8]. Most mutations are evident in VCP's N-domain which is responsible for assisting the transport of misfolded proteins from the ER to the cytoplasm with its ATPase activity [167, 168]. ALS-associated mutations in VCP have been shown to disrupt ERAD function [169] and decreased

levels of VCP has been demonstrated to induce ER stress, due to reduced ERAD substrates [170].

Sequestosome 1 (SQSTM1)

The *SQSTM1* gene encodes p62, a ubiquitin binding protein involved in protein degradation. It is also a major pathologic protein deposited in ubiquitin-positive inclusions in ALS, and other neurodegenerative diseases, such as AD and PD [171, 172]. In fact, p62 co-localises with TDP-43 and FUS ubiquitinated inclusions in the motor neurons in spinal cords of sALS patients, non-SOD1 fALS patients and in ALS patients with FTD [63]. Mutations in *SQSTM1* account for approximately 1% of fALS and approximately 4% of sALS [9].

Normally, p62 mediates the delivery of misfolded proteins to the autophagosome. Moreover, p62 and SOD1 co-localise in aggregates in mutant SOD1 transgenic mice, however, p62 does not associate with wildtype SOD1, suggesting that p62 plays an important role in inclusion formation [173]. It is speculated that mutations in *SQSTM1* result in a loss of function of p62, thus causing disturbances in protein homeostasis [174].

Optineurin (OPTN)

Optineurin was first associated with ALS when mutations in the *OPTN* gene were identified in six Japanese individuals [69]. In these patients, the presence of cytoplasmic inclusions containing optineurin, Lewy body-like inclusions containing optineurin and SOD1, and skein-like inclusions containing optineurin, ubiquitin and TDP-43, were observed [69]. It has since been recognised that mutations in optineurin are greater in Asian populations than in

European populations, however the worldwide incidence of optineurin mutations are approximately less than 1% in both fALS and sALS [175].

Optineurin is involved in vesicular trafficking, immune responses and transcriptional regulation in the cell [176]. It also plays a role in the trafficking of lysosomes during autophagy in association with myosin VI, whereby optineurin interacts with lysosomes and promotes autophagosome fusion to lysosomes [177]. However, mutations in optineurin result in the inhibition of this fusion of autophagosomes and lysosomes, resulting in autophagy dysfunction. Moreover, optineurin mutations cause a disruption of vesicular trafficking between the Golgi apparatus and plasma membrane due to a loss of interaction with myosin VI, which leads to ER stress and Golgi fragmentation [177]. These studies suggest that mutations in optineurin are involved in several mechanisms of ALS pathogenesis.

Charged multivesicular body protein 2B (CHMP2B)

CHMP2B regulates endosomal trafficking and plays a role in the sorting of integral membrane proteins in multivesicular bodies and the subsequent clearance by autophagy [178]. Mutations in *CHMP2B* have been linked to two ALS cases [79] and subsequent studies have identified several other ALS-specific mutations in the protein [179]. Mutant CHMP2B causes altered lysosomal localisation and impaired autophagy function in cell culture models [179]. However, the lack of studies demonstrating CHMP2B mutation detection in ALS indicates that these mutations are not a common cause of ALS [180].

<u>TANK-binding kinase 1 (TBK-1)</u>

TBK-1 is a serine-threonine kinase involved in the activation of proinflammatory cytokines [181] and in the maintenance of autophagy, whereby it phosphorylates autophagy receptors such as p62 [182] and optineurin [183]. More than 40 mutations in *TBK-1* have been identified since its discovery as an ALS-associated gene [184, 185], and it represents between 0.4%-4% of ALS patients [186].

The exact role that mutant TBK-1 plays in ALS pathogenesis is unknown, however mechanisms of protein quality control are hypothesised to be a prominent feature [35]. These mutations lead to a loss of function of the protein [84]. Due to disrupted binding to optineurin, mutant TBK-1 is unable to be recruited to damaged mitochondria [187, 188], and in contrast to wildtype TBK-1 which colocalises with mutant SOD1 aggregates, deletion of TBK-1 enhances the presence of these aggregates, and also inhibits autophagy [189]. This data suggests that TBK-1 plays a major role in the clearance of protein inclusions via autophagy.

1.5.5.2 Mutations in genes encoding cytoskeletal proteins

<u>Profilin 1 (PFN1)</u>

Profilin 1 is encoded by the *PFN1* gene and it is a member of the profilin family of small actin-binding proteins. Profilin 1 is primarily involved in actin regulation, by catalysing its polymerization, and thus promoting the assembly of globular actin [70]. Mutations in the Profilin 1 gene account for less than 1% of fALS and sALS cases [8], however their exact mechanism for triggering ALS is unknown. Two mechanisms have been hypothesised; the first is a proposed gain of function by the formation of aggregates, whereby profilin 1 mutations co-localise with TDP-43 to form ubiquitinated, insoluble aggregates [70]. The

second is by a loss of function due to alterations in actin dynamics which trigger disruptions to the cytoskeleton. It has been demonstrated that profilin 1 mutants inhibit axonal outgrowth by inhibiting actin polymerisation [70]. Regardless, mutations in profilin 1 demonstrate that cytoskeletal alterations can contribute to ALS pathogenesis.

Tubulin α1 (TUBA4A)

TUBA4A encodes Tubulin α1, a member of the alpha-tubulin family and a key component of microtubules [73]. Ten missense, one nonsense and one splice donor site mutations in TUBA4A have been identified in both classical fALS and sALS, as well as in ALS-FTD patients [190]. These mutations cause deleterious effects by destabilising the microtubule network and dynamics, and diminishing re-polymerisation capability [73]. Therefore, mutations in *TUBA4A* strengthen the hypothesis that alterations affecting cytoskeleton structure and function are linked to ALS pathogenesis.

Neurofilament heavy chain (NEFH)

Neurofilaments are cytoskeletal proteins involved in maintaining axonal integrity [191]. Small heterozygous deletions in the *NEFH* gene, encoding neurofilament heavy chain, have been reported in very few sALS and fALS cases (<1%) [75, 192]. ALS causing mutations in neurofilament heavy chain are located in a region containing a phosphorylation site essential for neurofilament cross-linking. Therefore, these mutations result in neurofilament aggregation and disorganisation, leading to toxicity [193]. Moreover, phosphorylated neurofilament proteins have been observed to accumulate into inclusions in motor neurons of fALS patients [194].

Peripherin (PRPH)

Peripherin is a neuronal intermediate filament, encoded by the gene *PRPH*, possessing sequence similarity with neurofilament proteins [76]. Three different frame-shift truncations and missense mutations have been detected in the *PRPH* gene, that cause ALS [76, 195, 196]. These mutants disrupt the normal neurofilament network and induce the formation of intracellular inclusions [76, 195]. Peripherin is a component of the inclusions present in the spinal cords of ALS patients and also in cell culture models overexpressing mutant peripherin [76, 195]. Aggregate-inducing isoforms of peripherin are also up-regulated in transgenic SOD1 mice models and ALS patients [197, 198].

1.5.5.3 Mutations in genes encoding proteins that function in intracellular transport

Vesicle-associated membrane protein-associated protein B (VAPB)

VAPB encodes an ER transmembrane protein involved in intracellular vesicle trafficking and the transport of lipids and microtubules [71, 199]. Mutations in *VAPB* can cause a rare, gradually progressing atypical form of ALS and late-onset SMA [71]. Moreover, decreased levels of VAPB have been observed in both mutant SOD1 transgenic mice [199] and in human fALS and sALS without VAPB mutations [200], suggesting a role for VAPB in more common forms of the disease.

Studies show that VAPB has a role in modulating ER stress, however the effect of mutant VAPB and how it causes disease remains to be determined [201, 202]. Mutant VAPB inclusions are ER derived, and they co-localise with ER proteins, including Protein Disulphide Isomerase (PDI), indicating that the ER plays a role in VAPB-associated ALS [201]. VAPB is also necessary for the maintenance of the Golgi and intracellular transport,

however mutant VAPB has been shown to cause Golgi fragmentation in primary neurons [203].

Dynactin 1 (DCTN1)

DCTN1 encodes the protein Dynactin 1, and mutations in this gene were identified in rare autosomal dominant ALS cases with an early-onset [204]. Dynactin is involved in microtubule- and dynein- based intracellular and axonal retrograde transport, however mutations in dynactin disrupt microtubule binding [204]. Transgenic mice expressing mutant dynactin develop a progressive motor neuron disease characterised by the accumulation of ubiquitinated inclusions, defects in vesicular trafficking, an abnormal ER morphology, an increase in vesicles, and autophagy activation [74, 205]. Therefore, the presence of mutations in dynactin imply that dysfunction to intracellular and axonal transport are involved in ALS. However, mutations in dynactin are now more commonly linked to Perry Syndrome [206].

Alsin (ALS2)

Mutations in the *ALS2* gene, encoding alsin, cause atypical autosomal recessive juvenile onset fALS or juvenile PLS [77]. Alsin is a guanine nucleotide exchange factor for the GTPase Rab5A which is involved in endosomal trafficking [207], axonal outgrowth [208], endocytosis [209], and AMPA receptor trafficking [210]. Deletion mutations in *ALS2* are thought to induce neurotoxicity by a loss of function mechanism [211] because knockdown of alsin in transgenic SOD1 mice models exuberated motor dysfunction and caused early disease onset and reduced survival [212]. Moreover, alsin-deficient neurons disrupt AMPA receptor trafficking and enhance glutamate induced cytotoxicity [210]. Interestingly, alsin mutations have never been reported in adult ALS [9].

FIG 4

Located in vacuolar membranes, FIG4 is a phosphoinositide which functions as a signalling molecule and plays a key role in vesicle trafficking, which is essential for the normal functioning of the endosome-lysosome system [213]. Mutations in FIG4 were first identified in pale tremor mice which exhibited neuronal degeneration, peripheral neuropathy and altered pigmentation [214]. Later, heterozygous missense, truncation and splice site loss of function mutations in FIG4 were identified in familial and sporadic forms of ALS and PLS [78]. Mutations in FIG4 demonstrate a decreased function of the endosome-lysosome system in both mammalian cell culture and in yeast [78, 214], suggesting that defects in membrane and vesicle trafficking are features of ALS.

Annexin A11 (ANXA11)

Annexin A11, encoded by *ANXA11*, is a phospholipid binding protein involved in vesicular transport and has been reported to play a role in apoptosis, exocytosis and cytokinesis [93]. Six rare mutations in Annexin A11 have recently been implicated in ALS patients, accounting for approximately 1% of fALS and 1.7& of sALS cases. Moreover, Annexin A11-positive aggregates have been observed in spinal motor neurons and hippocampal axons of a patient [215]. It is hypothesised that Annexin A11 mutations interfere with normal function [215].

Matrin 3 (MATR3)

Matrin 3 is an RNA/DNA binding protein that interacts with TDP-43 [72]. Two heterozygous, missense mutations in the gene encoding matrin 3, *MATR3*, have been identified in slow progressing fALS cases [72], and it is thought that these mutations result in a loss of protein function. It is hypothesised that matrin 3 plays a role in the repair of double strand breaks in DNA, and therefore, reports have demonstrated that a loss of matrin 3 induces DNA damage and also leads to the abnormal accumulation of cells at the S-phase of the cell cycle [216]. These results indicate a link between DNA damage and ALS pathogenesis.

NIMA-related kinase 1 (NEK1)

Loss of function mutations in NIMA-related kinase 1, encoded by *NEK1*, have recently been implicated in ALS [93]. Findings demonstrate that NEK1 constitutes a major ALS-associated gene with risk variants present in approximately 3% of European and European-American ALS cases [217]. Normally, NEK1 is associated with several cellular functions, including the DNA-damage response, cilia formation, microtubule stability, mitochondrial function, neuronal morphology, and axonal polarity [217]. Moreover, NEK1 plays a key role in preventing cell death induced by DNA damage [218]. Foci of damaged DNA in NEK1 null cells remain after the removal of a toxic insult, and these cells develop unstable chromosomes at a higher rate than identically cultured cells containing NEK1 [219].

In addition, *C21orf2* has recently been identified as a gene associated with ALS risk [220]. It is speculated that defects in C21orf2 may lead to dysfunction in primary cilium and mitochondria, or inefficient DNA repair [220]. Interestingly, studies have demonstrated that

the C21orf2 protein is required for efficient DNA damage repair and can interact with NEK1 [221]. DNA repair is less efficient in C21orf2-depleted cells and homologous recombination is impaired. However, this deficit can be rescued by the overexpression of NEK1 [221].

1.5.5.5 Mutations in genes encoding proteins that function in RNA metabolism

Sentaxin (SETX)

SETX encodes sentaxin, a large protein with a DNA/RNA helicase domain [80]. Sentaxin is localised in the nucleus and there is evidence to suggest it is protective against oxidative damage to DNA, and in RNA transcription [222, 223]. Missense and truncation mutations in *SETX* cause an atypical juvenile form of ALS, with an early-onset, under 25 years [80]. This rare disease is characterised by the absence of respiratory and bulbar symptoms and typically patients have a normal lifespan [80]. However, a novel mutation in *SETX* has been detected in one patient with typical sALS, indicating that sentaxin could possibly play a role in sporadic disease in rare instances [224]. Mutant sentaxin acts through a gain of function mechanism and it induces neurotoxicity by damaging DNA during replication thus creating genomic instability [225].

Angiogenin (ANG)

ANG encodes angiogenin which induces angiogenesis (the formation of new blood vessels) under hypoxic conditions and protects motor neurons from hypoxia [226]. It is also implicated in neurite outgrowth [227]. Angiogenin is a member of the ribonuclease A family of proteins, and mutations in this protein demonstrate decreased ribonuclease activity, suggesting that mutations are pathogenic by a loss of function mechanism [228]. Although

rare, more than 20 FALS mutations in the *ANG* gene have been observed in numerous populations [81, 229-232]. Patients with *ANG* mutations display an accumulation of TDP-43 and inclusion formation in motor neurons [233], and interestingly, SALS patients without mutations in ANG exhibit elevated serum angiogenin levels [234].

1.5.5.6 Mutations in genes encoding proteins linked to excitotoxicity

D-amino acid oxidase (DAO)

DAO is a peroxisomal enzyme that oxides D-serine, an activator of NMDA-type glutamate receptors which are responsible for the excitation of neurons. Mutations in the *DAO* gene cause a rare classical adult onset form of fALS [83]. Mutant DAO demonstrates decreased enzymatic activity despite its normal localisation in peroxisomes. This results in the induction of autophagy, the formation of ubiquitinated inclusions and cell death in transduced primary motor neurons [83, 235]. Interestingly, DAO controls the level of D-serine, which has been shown to accumulate in the spinal cords in sALS and in a mutant SOD1 mouse model of ALS [236], indicating that this abnormality may represent an important component of pathogenesis in both sALS and fALS. Moreover, the inactivation of DAO in mutant SOD1 mouse models results in spinal motor neuron degeneration and abnormal locomotor activity [237].

1.5.5.7 Mutations in genes encoding mitochondrial and ER proteins

Coiled-coil-helix-coiled-coil-helix domain-containing protein 10 (CHCHD10)

CHCHD10 encodes a protein located on the intermembrane space of mitochondria where it is involved in the maintenance of mitochondrial organisation [238]. The first report of a link between ALS and mutations in *CHCHD10* was found in a French family with ALS, FTD and

cerebellar ataxia, whereby all cases in this family demonstrated muscular abnormalities [238]. Although rare, *CHCHD10* mutations account for approximately 2.6% of FTD-ALS cases in France [239, 240]. Mutations in *CHCHD10* cause a loss of protein function [241] and studies have demonstrated that while normal CHCHD10 exerts a protective effect in mitochondrial and synaptic integrity, as well as in the retention of TDP-43 in the nucleus, mutant CHCHD10 exhibits a loss of function, resulting in mitochondrial and synaptic damage and the accumulation of cytoplasmic TDP-43 inclusions [242].

Paraoxonase 1, 2 and 3 (PON 1/2/3)

The paraoxonase proteins are involved in lipoprotein secretion, detoxification of neurotoxins and protection against oxidative and ER stress in the cell [243]. Whilst rare, eight different mutations in the *PON* genes, which result in a loss of function, have been identified in ALS patients [92], indicating a link between mutated forms of paraoxonase proteins and ALS pathogenesis. Paraoxonase 1 also exhibits a role in the detoxification of pesticides, herbicides and nerve gases, therefore it is hypothesised that these proteins can protect humans from environmental risk factors for ALS, whereas mutant paraoxonase proteins cannot [244].

Sigma nonopioid intracellular receptor 1 (SIGMAR1)

Mutations in Sigma 1 receptor (*SIGMAR1*) have been identified in fALS patients [86] Sigma 1 is a chaperone protein localised at the ER-mitochondrion interface that modulates calcium signalling [245]. Mutations in *SIGMAR1* cause abnormal ER morphologies, mitochondrial abnormalities and impaired endosomal trafficking and autophagic degradation [246], implying that these mutations cause a loss of protein function. Another study demonstrated that disruption in the function of Sigma 1 disturbed ER-mitochondria contacts and affected

intracellular calcium signalling, resulting in the induction of ER stress and mitochondrial defects [247]. Moreover, SIGMAR1$^{-/-}$ mice displayed locomotor deficits associated with muscle weakness, axonal degeneration and motor neuron loss [247].

1.5.5.8 Mutations in genes encoding proteins of unknown function

Ataxin 2 (ATXN2)

The *ATXN2* gene encodes the 150 kDa protein, ataxin 2, and mutations in this gene are linked to spinocerebellar ataxia type 2 [248]. Mutations in *ATXN2* are caused by an abnormal expansion of CAG repeats extending to 33, whereas the normal length is below 22 repeats [87]. The role of ataxin 2 is currently unknown, however studies have demonstrated that a greater frequency of ALS patients possess CAG repeats, compared to controls, indicating that more than 29 CAG repeats in *ATXN2* are a risk factor for ALS [87, 249]. In ALS, mutant ataxin 2 promotes TDP-43 aggregation in motor neurons, and genetic screening indicates a link between these two proteins [87].

Spatacsin (SPG11)

The exact function of Spatacsin, encoded by the *SPG11* gene, is unknown. However, twelve different homozygous or compound heterozygous mutations in the *SPG11* gene have been identified in ten distinct families with autosomal recessive hereditary spastic paraplegia [82]. Although this is the most common autosomal recessive juvenile form of ALS, fewer than 30 families have been reported in the literature over the past 20 years [250]. This rare disease has an early-onset (under 25 years of age) and is characterised by bulbar symptoms, muscle weakness and long disease duration with dysfunction in both upper and lower motor neurons

[82, 251]. In zebrafish models, spatacsin is necessary for axonal growth and muscular junction connectivity [252], suggesting a fundamental role for spatacsin in motor neuron functionality.

Other rarer genes linked to ALS include *hnRNPA1/A2B1, ELP3* and *ERBB4*. Mutations in the prion-like domains of hnRNP proteins usually cause multisystem proteinopathy but have been shown to cause ALS in rare instances [85]. Mutations in *ELP3* have demonstrated an association with motor neuron degeneration, however whether this causes ALS remains unknown [88]. Finally, mutations in *ERBB4* disrupt the neuregulin-ErbB4 pathway which can result in ALS type 19 [91].

Another gene recently implicated in ALS and FTD is *CCNF*, encoding the E3 ligase protein, Cyclin F [89]. The implication of mutations in this gene are discussed in detail in Chapter 3.

1.6 Current hypotheses for the mechanisms of ALS pathogenesis

The genetic studies presented above, as well as investigations into ALS cell culture and animal models, have provided an insight into several possible cellular mechanisms involved in the pathogenesis of ALS. Neurons are highly susceptible to oxidative stress and alterations in cellular proteostasis, due to their high metabolic requirements and larger size [253], however the mechanisms underlying the selective vulnerability of neurons to degeneration remain unknown. In particular, motor neurons are specifically affected in ALS, despite the ubiquitous expression of numerous ALS causative proteins, and disturbances to organelles that are present in almost all cell types, such as the ER, Golgi and mitochondria. Interestingly, ALS genetic studies demonstrate that mutations in dissimilar proteins, with diverse functions, still result in a similar ALS phenotype, suggesting that motor neuron degeneration may be due to multiple mechanisms triggered simultaneously.

Presently, the cause of ALS pathogenesis is not fully understood. However, evidence implicates the following mechanisms; protein misfolding and aggregation, impaired axonal transport and intracellular trafficking, excitotoxicity, mitochondrial dysfunction, abnormal RNA homeostasis and processing, non-cell autonomous toxicity, dysfunction in proteostasis and autophagy, ER-Golgi transport defects, prion-like mechanisms, DNA damage repair defects, oxidative stress, and ER stress (Figure 1.4). Notably, ER stress is emerging as a major mechanism involved in ALS pathogenesis [254-256]. These proposed mechanisms of ALS pathogenesis are described in this section below, with a subsequent focus on ER stress which forms the basis of this thesis.
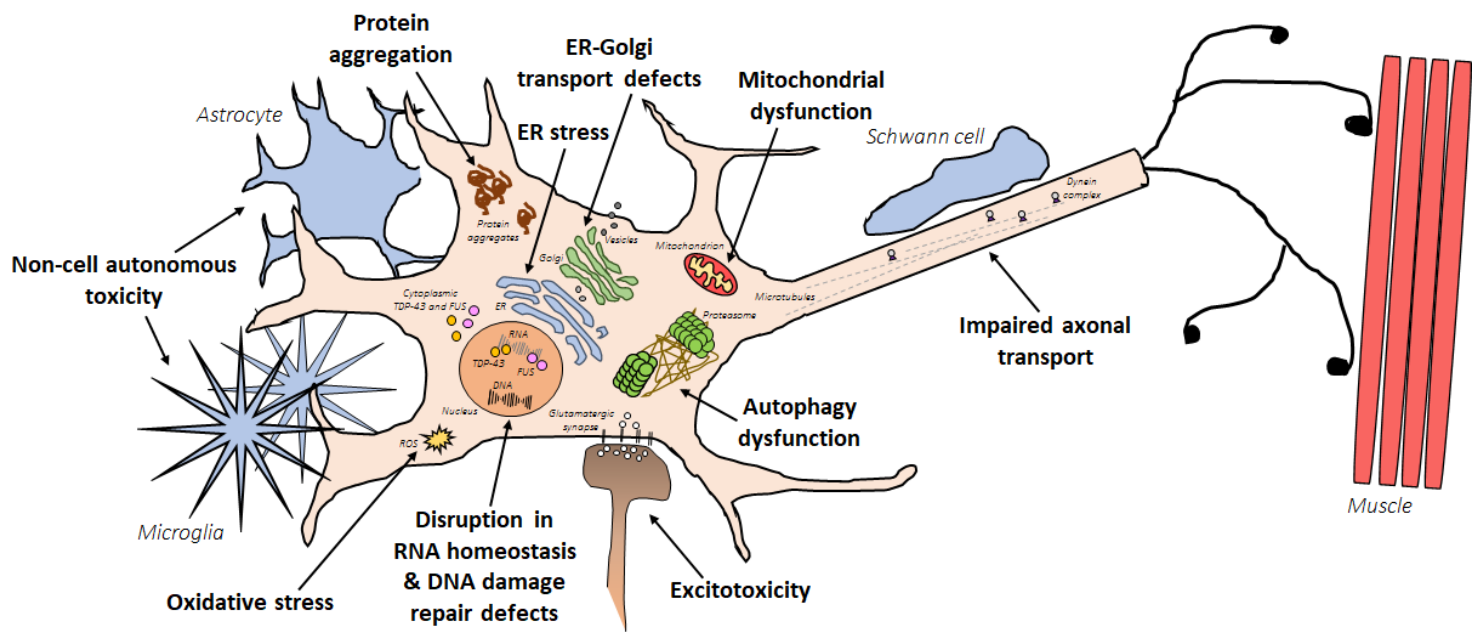
Figure 1.4: Cellular symptoms and phenotypes observed in ALS disease models.

Motor neurons are highly susceptible to degeneration in ALS. The proposed mechanisms of ALS pathogenesis are: Protein aggregation, ER-Golgi transport defects, ER stress, mitochondrial dysfunction, non-cell autonomous toxicity, oxidative stress, disruption in RNA homeostasis, DNA damage repair defects, excitotoxicity, autophagy dysfunction and impaired axonal transport. Refer to the text for detailed descriptions for each mechanism. Diagram not to scale.

1.6.1 Protein misfolding and aggregation

Despite having diverse clinical manifestations, protein misfolding and aggregation in affected areas of nervous tissue is a common feature and pathological hallmark among neurodegenerative diseases [257]. In conjunction with ALS, the most prevalent neurodegenerative diseases, AD, PD, Huntington's disease (HD), and transmissible prion encephalopathies, such as Creutzfeldt-Jakob disease (CJD), all present with protein aggregates, which can sequester into inclusions. These disorders differ in the proteins that misfold and the group of neurons which are affected [258]. It is unclear, however, whether protein aggregation is a direct cause of disease, a protective response mechanism, or whether it is a secondary product of other disease mechanisms.

Aggregation occurs when misfolded, unfolded, or partially folded, proteins expose hydrophobic regions that are normally hidden within a protein folded in its native conformation. The exposed hydrophobic regions promote hydrophobic interactions with other proteins, resulting in their accumulation, forming aggregates or inclusions [259]. Protein misfolding is triggered by either genetic mutations in familial cases of disease, or by cellular conditions which cause wildtype proteins to misfold in sporadic cases, although the latter mechanism is poorly understood [259]. Abnormal protein aggregation can result in the inhibition of important cellular functions, causing a dysregulation in cell proteostasis, which eventuates into neuronal death. The presence of prominent cytoplasmic inclusions in motor neurons is a classic pathological hallmark in ALS and these insoluble structures are observed at the onset of disease, where they progressively accumulate until disease end stage [260].

Inclusions observed in ALS have variable morphology, including ubiquitin-positive skein-like or Lewy body-like inclusions, or ubiquitin-negative Bunina bodies containing cystatin C and neurofilament proteins [261, 262]. The first study to demonstrate protein aggregation in

ALS described inclusions in the spinal cords of fALS patients carrying SOD1 mutations [58, 263]. Wildtype SOD1 aggregation has also been reported in post-mortem samples of spinal cords from sALS patients [61, 264]. Interestingly, the most inclusion-prone SOD1 mutants are linked with higher levels of cell death in cell culture, suggesting a correlation with SOD1 inclusion formation and toxicity [265]. Moreover, SOD1 mutations with a higher propensity to aggregate cause the most aggressive forms of disease with short duration in ALS patients [266, 267].

Examination of SOD1-negative ALS patients identified TDP-43 as a major constituent of ubiquitinated inclusions [62, 128]. In fact, wildtype TDP-43 inclusions are observed in motor cortices and spinal cords in 97% of ALS patients [125]. In addition to wildtype TDP-43, ALS causative mutations in TDP-43 result in the cytoplasmic accumulation of insoluble TDP-43 in patient neurons [268]. Similarly, post-mortem tissues of ALS patients carrying FUS mutations possess cytoplasmic inclusions within motor neurons and glial cells [65, 137]. In addition, FUS-positive inclusions have also been observed in sALS and non-SOD1 fALS cases [63]. In C9orf72 patients, the non-ATG translation of hexanucleotide repeat RNA results in inclusions containing abnormal dipeptide repeat (DPR) proteins [269]. The inclusions first isolated from C9orf72 patient neurons in the hippocampus and pyramidal, frontal and temporal cortices were all TDP-43 immuno-positive, however, inclusions from the cerebellum and neocortex were TDP-43 negative [270].

Interestingly, p62 is found in almost all pathological inclusions [271], indicating the induction of a cellular response to degrade these aggregates. Moreover, optineurin has also been detected in skein-like inclusions in the spinal cords of non-SOD1 fALS and sALS patients [272], however other studies dispute this [69, 273]. UBQLN2-positive inclusions are detected in the spinal cords of both sALS and fALS patients with mutations in SOD1, TDP-43, FUS and C9orf72 [66, 164]. Interestingly, ALS patients carrying UBQLN2 mutations

possess inclusions that are also immunopositive for other ALS associated proteins, such as FUS, OPTN and TDP-43 [164], suggesting that proteostasis dysregulation may play a role in inclusion formation.

1.6.2 Impaired axonal transport and intracellular trafficking

The intracellular trafficking of cargoes is a fundamental process for the maintenance of structure and function in all cell types [274]. Due to their remarkably long axons, motor neurons are particularly vulnerable to disturbances in intracellular trafficking, thus impaired axonal transport is typically implicated in ALS, observed early in disease [275-277]. Axonal transport mediates the movement of cargoes synthesised in the cell body; proteins, mRNA, lipids, and membrane-bound vesicles, to be distributed to sites along the axon [274]. Evidence for defects in axonal transport in ALS demonstrate damage to axonal transport machinery via an abnormal accumulation of phosphorylated neurofilaments, mitochondria and lysosomes in the axon [278-281], and axonal spheroids containing a variety of vesicles, lysosomes, mitochondria, neurofilaments and microtubules [282, 283].

In ALS patients and rodent models of ALS, retraction and denervation of neurons is observed in the early stages of disease, resulting in axonal dysfunction and connection failure [275, 276]. Microtubule-dependent kinesin and cytoplasmic dynein motor proteins mediate anterograde and retrograde transport, respectively [284]. The deceleration of both anterograde and retrograde axonal transport are early events observed in mutant SOD1 transgenic mice [114]. In these mice, mutant SOD1 binds preferentially to dynein, which may partially explain the slowing of axonal transport [114]. Furthermore, misfolded SOD1 associates with kinesin-associated protein 3 (KAP3) into aggregates which inhibits trafficking [285].

Proteomic studies demonstrate that the knockdown of TDP-43 reduces the levels of intracellular transport proteins, suggesting that a loss of TDP-43 function could induce transport defects [286]. Moreover, mutations in both TDP-43 and FUS may impair axonal transport by inducing stress granule formation and aggregation, or by reducing the availability of neurofilaments [287-289]. Furthermore, mutations in proteins linked to axonal transport, including DCTN1, VAPB and alsin, further support the notion that axonal transport defects contribute to ALS pathogenesis [71, 74, 208].

1.6.3 Excitotoxicity

There is strong evidence that altered excitatory neurotransmission plays a key role in ALS pathogenesis, mediated by an increased susceptibility to excitotoxicity. The over-stimulation of post-synaptic glutamate receptors NMDA and AMPA-type receptors, leads to the excessive influx of calcium cations, resulting in excitotoxicity [290]. This is facilitated by deleterious cellular responses to excitatory stimulation, such as ER stress, mitochondrial overload, and the activation of phospholipids and proteases, which cause organelle and DNA damage, eventually resulting in neuronal death [290, 291]. Currently, one of only two approved treatments for ALS is Riluzole, which blocks sodium currents by inhibiting the pre-synaptic release of glutamate, thus reducing excitability [292].

Evidence for altered glutamate levels in ALS is observed in electrophysiological studies demonstrating disturbances in UMNs and LMNs [293], and in transcranial magnetic stimulation demonstrating hyper-excitability in both sALS patients and fALS patients with SOD1 and C9orf72 mutations [294]. In patients with C9orf72 mutations, this hyper-excitability is observed before the onset of symptoms [295]. Moreover, the presence of fasciculations, or muscle twitching, in patients is a key clinical symptom that suggests hyper-

excitability occurs in ALS [296]. In addition to this, some groups have reported altered glutamate levels in post-mortem ALS tissue [297] and in the CSF from some ALS patients [298, 299], but the cause remains poorly understood. Interestingly, fasciculations are not observed in mutant SOD1 transgenic mice models, although this may be a limitation of the model. However, decreased levels of the excitatory amino acid transporter EAAT2, responsible for the rapid removal of glutamate from the synapse, is observed in both ALS patients and mutant SOD1 transgenic mouse models [300, 301]. Furthermore, the transgenic overexpression of EAAT2 in mutant SOD1 mice inhibits excitotoxicity, thus delaying the onset of disease, although it does not affect survival [301]. This suggests that excitotoxicity is involved in disease progression, however, it is not an upstream trigger of ALS.

1.6.4 Mitochondrial dysfunction

Changes in mitochondria morphology and function have been well-documented in ALS patients and mutant SOD1 mouse models [302]. Moreover, damage to mitochondria is an early phenomenon observed in ALS [303]. Analysis of motor neurons from mutant SOD1 transgenic mice reveal swelling of the mitochondria as early as two weeks of age, before symptom onset [304]. In fact, multiple studies have observed a detrimental effect of mutant SOD1 localisation and oligomerisation on mitochondria. Wildtype SOD1 can partially localise in mitochondria, and non-native mutant SOD1 proteins display an increased tendency to localise in this organelle [305, 306]. Furthermore, it has been shown that mutant SOD1 accumulates and thus, induces mitochondrial damage in cell culture [307, 308] and in ALS mouse models [309]. These studies demonstrate an association between SOD1 toxicity and mitochondrial dysfunction.

Similarly, wildtype TDP-43 also co-localises with mitochondria in motor neurons and this association is increased when TDP-43 is mutated [310], demonstrating a correlation of mutant TDP-43 with damage to mitochondria. TDP-43 also perturbs ER-mitochondria interactions resulting in disruption of cellular calcium homeostasis [311]. Moreover, a disturbance of calcium levels is also observed in mutant SOD1 cell and animal models, affecting the integrity of motor neurons [312-314]. Mutations in the *CHCHD10* gene, encoding a mitochondrial protein, have also recently been associated with ALS. These mutations cause fragmentation of the mitochondrial network and defects, such as the loss and disorganisation of cristae [238]. Furthermore, the activation of mitochondrial-dependent apoptotic pathways has been described in ALS cell culture, demonstrating that the release of cytochrome c and recruitment of pro-apoptotic Bax protein to mitochondria are involved in mutant SOD1-mediated cell death [315, 316].

Interestingly, however, recent research has demonstrated that low levels of mitochondrial stress regulates cytoplasmic proteostasis, enhances stress resistance and prolongs health span by inducing genes involved in the stress response [317]. Therefore, mitigating mitochondrial stress may also be detrimental to the cell by exacerbating toxicity, rather than protective.

1.6.5 Abnormal RNA homeostasis and processing

Mutations in genes that encode RNA-binding proteins, such as TDP-43 and FUS, have recently emerged as key determinants of ALS. Normally, RNA binding proteins directly bind to RNA and control RNA synthesis, maturation, localisation, translation and decay [318], however, mutations in these proteins have been reported to alter their native functions. Previous studies demonstrate that dysfunction of RNA binding proteins is an important

feature in ALS, including dysregulation of RNA processing, mislocalisation of these proteins to the cytoplasm, and their abnormal aggregation [319, 320].

The pathogenic mechanisms triggered by TDP-43 and FUS are thought to involve a combination of both loss of function and gain of toxic function processes [108, 321, 322]. For example, increased TDP-43 levels of either wildtype or mutant TDP-43 are highly deleterious, indicating a crucial role for an auto-regulatory pathway which maintains TDP-43 RNA levels [323, 324]. Conversely, the selective removal of TDP-43 from motor neurons produces progressive motor neuron degeneration with ALS-like pathology in mouse models [325]. TDP-43 and FUS are both constituents of stress granules which can induce pathogenicity by sequestering mRNA transcripts or other RNA binding proteins, and by providing a seed for the formation of pathological inclusions in ALS [288, 326]. The recruitment of these proteins into stress granules suggests a loss of function exists under these conditions.

Neurodegeneration induced by C9orf72 mutations are also associated with RNA toxicity by the production of toxic RNA containing the repeat sequence [327]. Additional neurodegenerative mechanisms may be triggered by complementary repeat-containing RNA produced by bidirectional transcription [328], or RAN translation [329], resulting in the production of potentially toxic RNA and protein species, respectively. The expression of RAN proteins reduces RNA-processing bodies, sequesters essential RNA-binding proteins, and induces the formation of cytoplasmic stress granules, thus triggering apoptosis. Hence these data imply that RNA homeostasis is perturbed by RAN translated C9orf72 peptides [330].

1.6.6 Non-cell autonomous toxicity

Although motor neurons are primarily implicated in ALS, non-neuronal cell types, such as astrocytes and microglia, also play a role in the modulation of disease [331]. This was first demonstrated in experiments utilising mutant SOD1. The expression of mutant SOD1 in either muscle or peripheral Schwann cells did not affect ALS disease onset or progression [332, 333], however, the expression of mutant SOD1 in microglia or astrocytes accelerates disease progression [331, 334]. Moreover, silencing mutant SOD1 expression in microglia and astrocytes delays disease progression and motor neuron loss [335, 336]. Interestingly, though, the ablation of 50% of reactive microglia from spinal cords of mutant SOD1 transgenic mice does not affect motor neuron degeneration [337].

Another study used embryonic stem cells derived from mice carrying either the normal or mutant transgenic alleles of the human SOD1 gene to generate motor neurons [338]. The results demonstrated that both the wildtype and mutant SOD1 motor neurons displayed neurodegenerative properties when co-cultured with mutant SOD1 glial cells, demonstrating that glial cells harbouring a human SOD1 mutation have a direct, non-cell autonomous effect on motor neuron survival [338]. Similarly, astrocytes cultured from both fALS and sALS patients induce toxicity in motor neurons, resulting in neuronal death [339]. Therefore, it is possible that non-neuronal cells in ALS modulate disease progression, however, further studies need to be undertaken to fully define this process.

1.6.7 Dysfunction in protein degradation

Autophagy is a major protein degradation pathway involved in the clearance of proteins, especially protein aggregates, in order to maintain cellular proteostasis. The presence of cytoplasmic aggregates in ALS suggests defects in the machinery that regulates protein

homeostasis, and abnormalities in autophagy have been observed in ALS [340]. The discovery of ALS-associated mutations in genes encoding for proteins involved in protein degradation pathways, such as UBQLN2, TBK-1, OPTN, VCP and p62, provides compelling evidence towards autophagy dysfunction as a mechanism of disease pathogenesis [66, 67, 84, 174, 175]. Interestingly, p62, encoded by *SQSTM1*, is found in almost all pathological inclusions [271] and UBQLN2-immunopositive inclusions have been detected in spinal cords of both fALS and sALS patients with mutations in SOD1, TDP-43, FUS or C9orf72 [66, 164]. This presence of proteasome-associated proteins within pathological inclusions implies a defect in the cellular response required to degrade these inclusions.

Other studies have demonstrated an induction of autophagy markers in spinal cords of ALS mouse models [341], sALS and fALS patients [342, 343]. Moreover, increased levels of LC3-II are observed in mutant SOD1 transgenic mice models at the symptomatic stage [344, 345], and increased levels of autophagosomes are observed in motor neurons of sALS patients [346]. Interestingly, the partial depletion of C9orf72 in neurons partly impairs autophagy, leading to the accumulation of TDP-43 and p62 aggregates [156], indicating that C9orf72 may regulate autophagy. Furthermore, C9orf72 interacts with UBQLN2 and LC3-positive vesicles, and co-migrates with lysosome-stained vesicles in neuronal cultures, providing further evidence for a possible role for C9orf72 in autophagy [153].

Rapamycin is an autophagy activator, and it has been shown to reduce mutant FUS-positive stress granules, neurite fragmentation and apoptosis in neuronal cell cultures expressing mutant FUS, under conditions of oxidative stress [347]. Furthermore, rapamycin administration to mutant optineurin expressing rat models inhibited the presence of optineurin-containing inclusions [348]. Trehalose is another autophagy enhancer, which demonstrated a reduction in the formation of SOD1 aggregates, enhanced motor neuron survival, and a prolonged lifespan when administered to mutant SOD1 transgenic mice [349].

Finally, an additional autophagy inducing agent, methotrimeprazine, improved TDP-43 clearance and localisation, and enhanced the survival of primary murine neurons, human stem cell-derived neurons and astrocytes expressing mutant TDP-43 [350]. These results demonstrate that pharmaceutical agents targeting autophagy may provide a beneficial effect in ALS, therefore, autophagy and proteasome dysfunction are important modulators of disease.

1.6.8 ER-Golgi transport and secretory pathway defects

The ER-Golgi secretory pathway mediates the transport of proteins and lipids between the ER and the Golgi apparatus [351]. Newly synthesised proteins in the ER are packed into vesicles and transported to the Golgi apparatus via the ER-Golgi intermediate compartment (ERGIC), before they are redistributed to their respective cellular destinations [352]. Impairment of ER-Golgi transport increases the accumulation of secretory proteins within the ER lumen, resulting in ER stress [353]. Moreover, impairment also leads to abnormal Golgi organisation and fragmentation [354].

ALS mutations in VAPB disrupt ER-Golgi vesicle transport [71], and mutations in optineurin disturb the interaction between optineurin and myosin VI, resulting in inhibition of secretory protein trafficking, ER stress and Golgi fragmentation [177]. Our laboratory has demonstrated that mutant SOD1 inhibits ER-Golgi transport, preceding the induction of ER stress, fragmentation of the Golgi, protein aggregation and apoptosis in ALS cell models [355]. Furthermore, our laboratory showed that extracellular wildtype SOD1 also induced ER-Golgi trafficking defects in human neuronal cell lines [119], indicating that wildtype SOD1 can also cause ER-Golgi impairment. Our group further demonstrated that mutant optineurin disrupts association with myosin VI, leading to abnormal diffuse cytoplasmic

distribution, inhibition of secretory protein trafficking, ER stress and Golgi fragmentation [177]. Furthermore, our group showed that C9orf72 mediates endosomal trafficking via its interaction with Rab proteins. The knockdown of C9orf72 inhibited transport of Shiga toxin from the plasma membrane to Golgi apparatus in neuronal cell lines, primary cortical neurons and spinal cord motor neurons [153]. In addition, greater colocalization was observed between C9orf72 and Rab proteins 7 and 11, which are involved in endosomal transport, in the motor neurons of ALS patients with the C9orf72 repeat expansion, compared to controls [153], thus suggesting that endosomal trafficking is dysregulated in ALS.

1.6.9 Prion-like mechanism of propagation of misfolded proteins

Recent data provides compelling evidence that pathogenic protein aggregates in ALS possess prion-like properties; they are capable of self-replicating by templating the misfolding of monomeric proteins, which then propagate between individual cells [356]. This concept was first proposed by Prusiner and colleagues after the discovery of protein-only infectious agents, termed 'prions', that cause transmissible spongiform encephalopathies [357]. In these diseases, aggregates form due to misfolding and this aggregation of the prion protein is spread to other cells via templated conformational change of normally-folded proteins [358]. The notion that this mechanism could be expanded to other neurodegenerative diseases, including ALS, was subsequently proposed. Evidence that this mechanism may operate in ALS was obtained by observing the brains of ALS patients at different time periods, revealing a stereotypical pattern of spread between the brain regions [23, 359]. Since then, numerous studies have demonstrated that both SOD1 and TDP-43 display prion-like behaviour [360-362].

Aggregates containing mutant SOD1 penetrate inside cells by micropinocytosis and exit the macropinocytic compartment to stimulate aggregation of mutant SOD1 [362]. Once initiated, it was demonstrated that mutant SOD1 aggregation is self-perpetuating, transferring efficiently from cell to cell, and it is dependent on the extracellular release of aggregates [362]. Another study utilising mutant SOD1 transgenic mice demonstrated an accelerated development of an ALS phenotype when a single sciatic nerve was injected with spinal homogenates from paralysed, previously inoculated mutant SOD1 mice. SOD1 inclusions formed outside of the injection site and spread along the spinal cords into motor and sensory neurons [360]. Moreover, SOD1 inclusions also become apparent in structures of the brain synaptically connected to the injection site [360]. These studies suggest that SOD1 aggregates propagate in a prion-like manner in neuronal cells and in ALS animal models.

TDP-43 contains a prion-like domain in the C-terminus glycine rich region, which is prone to aggregation [363]. When insoluble TDP-43 from ALS brains are introduced into cells expressing TDP-43, phosphorylated and ubiquitinated TDP-43 was aggregated in a self-templating manner [361]. Upon analysis, it was revealed that the C-terminal fragments of insoluble TDP-43 acted as seeds, inducing seed-dependent aggregation of TDP-43 in these cells [361], thus indicating that insoluble TDP-43 has prion-like properties. FUS also contains a prion-like domain which is required to induce aggregation [364], thus it is possible that FUS proteins may have prion-like tendencies, like TDP-43 and SOD1, although this has not yet been determined. Similarly, mutations in the prion-like domains of hnRNPA1 and hnRNPA2B1 cause ALS and multisystem proteinopathy [85]. However, further *in vivo* characterisation of the transmissibility of these proteins is required to determine if they play a role in ALS pathogenesis.

1.6.10 DNA damage and repair defects

In sporadic ALS patients, increased DNA damage is observed in the early stages of disease, accompanied by an increase in poly-adenosine diphosphate ribose polymerase (PARP1) and expression of enzymes involved in base-excision repair [365]. Once DNA is damaged, PARP1 binds to the DNA and signals the recruitment of DNA damage and repair proteins, including FUS [365]. It was hypothesised that DNA damage resulting from double-stranded breaks triggers the recruitment of wildtype FUS to DNA damage foci, where it interacts with chromatin remodelling factor, HDAC1 [366]. However, this interaction is impaired when FUS is mutated in ALS, thus limiting its protective activity in DNA repair [367]. Moreover, mutant FUS transgenic mice display enhanced DNA repair defects in cortical and spinal motor neurons [367], and human induced pluripotent stem cells (iPSC)-derived motor neurons expressing mutant FUS demonstrate enhanced DNA damage pathology [368]. In addition to FUS, motor neurons differentiated from iPSCs derived from C9orf72 patients, also display DNA damage [369]. Furthermore, a recent study from our group demonstrated that the DNA damage response was induced by the C9orf72 repeat expansion in ALS [370].

1.6.11 Oxidative stress

Oxidative stress is caused by an imbalance between the production of reactive oxygen species (ROS) and other oxidants, and the elimination of these species by the cellular antioxidant defence system [371]. Neurons are particularly vulnerable to oxidative stress, as they use ten times more oxygen than other tissues [372]. SOD1 is an antioxidant protein with a normal cellular function in preventing the production of ROS, implying a role for oxidative stress in the pathogenesis of ALS. Evidence of a role for oxidative stress in ALS is demonstrated in

post-mortem tissues of fALS and sALS patients, and mutant SOD1 transgenic mice, whereby widespread oxidative damage to proteins, lipids and DNA are observed [371].

The main source of ROS results from mitochondrial dysfunction, therefore oxidative stress may be linked to abnormalities in this organelle [373]. Moreover, mutant TDP-43 induces oxidative stress and mitochondrial dysfunction in neuronal cell cultures by the accumulation of nuclear factor E2 related factor 2 (Nrf2), a modulator of oxidative stress [374]. Oxidative stress is further aggravated by mutations in TDP-43 and FUS. Under conditions of oxidative stress, mutant TDP-43 is recruited into stress granules [126]. Similarly, mutant FUS is recruited to stress granules during oxidative stress more rapidly compared to wildtype FUS [145]. Finally, as ALS is a late-onset disease, it can be conceptualised that pathology arises during the normal aging process, such as through increases in oxidative stress and the production of free radicals which damage cells by decreasing antioxidant defences [375].

It is important to note, however, that ROS also plays a paradoxical role in regulating several signalling pathways through its direct interaction with critical signalling molecules, such as those in cell proliferation, metabolism, differentiation and survival, anti-oxidant and anti-inflammatory responses, DNA damage and iron homeostasis [376]. Therefore, while therapeutic strategies primarily focus on reducing ROS levels to prevent toxicity, it remains to be seen whether targeting the signalling molecules activated by ROS could produce viable therapies to prevent ROS-mediated disease.

1.7 The ER, ER stress and the Unfolded Protein Response (UPR)

ER stress is being increasingly recognised as a key cellular mechanism of pathogenesis in neurodegenerative diseases, such as ALS, and emerging evidence highlights the complexity of the Unfolded Protein Response (UPR) in these disorders, with protective and detrimental elements being described [254, 256, 377].

The ER is a vital redox-regulated cellular organelle, responsible for the folding, post-translational modification, transport and quality control of newly synthesised proteins [378]. Protein folding in the ER occurs in cisternae, and the capacity of protein folding is adjusted according to cellular requirements to maintain homeostasis [379]. The native folding of newly synthesised proteins is assisted by ER molecular chaperones, which are responsible for the correct folding of nascent proteins and the refolding of incorrectly folded proteins, thus preventing misfolded protein aggregation [380]. ER chaperone proteins include BiP, glucose regulated protein 94 (GRP94), calreticulin, calnexin, and the Protein Disulphide Isomerase (PDI) family [380]. Misfolded proteins that are not refolded in the ER are generally directed to the cytoplasm for endoplasmic reticulum-associated protein degradation (ERAD), where they are degraded by the proteasome or by autophagy [381], demonstrating an efficient protein quality control system to both refold and degrade incorrectly folded proteins. The ER is therefore a major component of cellular proteostasis.

The ER is closely associated with other organelles, such as the outer membrane of the nucleus [382], mitochondria [383], and particularly the Golgi apparatus, where newly synthesised and correctly folded proteins are transported in vesicles from the ER to the Golgi, from where they are secreted to their native cellular locations [384]. Moreover, the ER is also responsible for intracellular calcium storage, synthesis of lipids, and it also contributes to the biogenesis of autophagosomes and peroxisomes [385, 386]. There is evidence that the ER is

much more extensive in neurons than in other cells, extending throughout the entire dendritic arbour and axon [387]. Furthermore, due to the high demand for protein synthesis, the ER in neurons is particularly challenged and highly susceptible to a constant source of stress.

1.7.1 ER stress and the UPR

Disturbances in ER homeostasis, such as an ER calcium imbalance, redox dysregulation, ER-Golgi trafficking defects, or an excess accumulation of misfolded proteins in the ER lumen, can result in ER stress [256]. A proportion of proteins misfold under normal physiological conditions, however in some situations, the load of misfolded proteins becomes increased. The imbalance between the load of misfolded proteins and the rate of protein synthesis results in an accumulation of proteins in the lumen of the ER, triggering ER stress, which induces a cellular stress response known as the UPR. The UPR is an adaptive mechanism designed to control protein folding alterations in the ER, hence restoring proteostasis [388].

The UPR is mediated by three ER stress sensors; PKR-like endoplasmic reticulum kinase (PERK), inositol-requiring kinase 1 (IRE1), and activating transcription factor 6 (ATF). Under basal conditions, these ER stress sensors are bound to the ER chaperone, immunoglobulin binding protein (BiP), retaining them in an inactivated state. Upon induction of ER stress, BiP dissociates from ER stress sensors, to preferentially bind hydrophobic regions of the misfolded proteins, thus resulting in their activation [389].

Once PERK is dissociated from BiP, it undergoes dimerization and auto-phosphorylation, resulting in activation. In turn, PERK directly phosphorylates, and thus inhibits, the ubiquitous eukaryotic translation initiation factor 2α (eIF2α), which attenuates protein translation, ensuing a reduction in the entry of newly synthesised proteins into the ER lumen, therefore decreasing the load of ER protein folding [390]. The phosphorylation of eIF2α also

promotes the selective translation of mRNA encoding the transcription factor ATF4. ATF4 translocates to the nucleus where it specifically induces the expression of ER chaperones, thus increasing misfolded protein refolding in the ER [391]. ATF4 subsequently induces the expression of various genes involved in autophagy, the antioxidant response, redox control, and amino acid biosynthesis and transport [256, 392].

Similar to PERK, the IRE1 pathway is initiated by IRE1 dimerization and auto-phosphorylation. Upon activation, IRE1 degrades a subset of mRNAs which encode for ER-localised proteins by means of regulated IRE1 dependent decay (RIDD), thereby reducing protein synthesis in the ER [392]. IRE1 also catalyses the unconventional splicing of mRNA encoding transcription factor X-box binding protein 1 (XBP-1). This splicing removes a 26-base intron from XBP-1, resulting in a shift in the reading frame. Spliced XBP-1 is a stable transcription factor which translocates to the nucleus to induce the upregulation of ER chaperones to promote protein folding, and also proteins associated with ERAD, to enhance degradation of misfolded proteins, and proteins involved in phospholipid synthesis, in order to expand the volume of the ER to alleviate stress [393, 394].

The ATF6 pathway involves the translocation of ATF6 from its native localisation on the ER membrane to the Golgi apparatus, where it is cleaved by Golgi-localised site-1 and site-2 proteases. The resulting cytosolic ATF6 fragment translocates from the Golgi apparatus to the nucleus where it induces gene expression of ER chaperones, ERAD proteins and XBP-1 [395]. ATF6 can form heterodimers with XBP-1 to control the induction of specific patterns of gene expression [396].

Thus, the three ER stress sensors aim to alleviate ER stress by regulating the expression of a number of target genes encoding for proteins which modulate adaptation to stress. Previous studies have demonstrated that the ER stress sensors inhibit protein translation and synthesis,

promote protein refolding via the upregulation of ER chaperones, enhance degradation of misfolded proteins via ERAD, and they also control the redox environment of the ER and expand its volume by synthesising phospholipids. Therefore, the UPR promotes the survival of the cell when ER stress is first induced. However, under conditions of chronic or irreversible ER stress, such as those that arise during disease, there is a shift in the paradigm of the UPR from being pro-protective to pro-apoptotic.

1.7.2 Chronic activation of the UPR

During chronic or irreversible ER stress, the UPR induces apoptosis, which is mediated by overlapping mitochondria-dependent and independent apoptotic signalling mechanisms. The UPR activates apoptosis by signalling calcium release from the ER, the induction of microRNAs and mitogen-activated protein kinases, as well as activating all three ER stress sensors [397-399].

The sustained activation of PERK elicits a chain of transcriptional responses mediated by ATF4. ATF4 upregulates a key mediator of ER stress induced apoptosis, the transcription factor C/EBP-homologous protein (CHOP) and its target, growth arrest and DNA damage-inducible protein 34 (GADD34). CHOP can inhibit the expression of survival protein BCL-2 and it can simultaneously engage pro-apoptotic proteins, including Bcl-2-interacting mediator of cell death (BIM) and p53 upregulated modulator of apoptosis (PUMA) [400]. These events result in the activation of BAX- and BAK-dependent apoptosis at the mitochondria, and activation of the caspase cascade, which leads to subsequent apoptosis [401, 402]. Interestingly, a recent study has demonstrated that ATF4 and CHOP also trigger apoptosis by enhancing protein synthesis within stressed cells, resulting in the accumulation of additional misfolded proteins, ATP depletion, oxidative stress, and eventual cell death [403]. The

54

activation of GADD34 results in the de-phosphorylation of eIF2α, thus increasing protein synthesis [392, 403]. Furthermore, CHOP induces ERO1α, resulting in oxidative stress by transferring electrons from PDI to oxygen, to produce hydrogen peroxide [392]. ERO1α also promotes calcium release from the ER. Since calcium is required for ER chaperone function, the depletion of calcium in the ER further perturbs protein folding. Moreover, calcium released from the ER is loaded into mitochondria, resulting in oxidative stress and apoptosis [392].

IRE1 also mediates apoptosis through the recruitment of apoptosis signalling kinase (ASK1), which activates the c-Jun N-terminal kinase (JNK) pathway. The JNK pathway stimulates apoptotic pathways through pro-inflammatory responses [404], and by direct interaction with BAX and BAK [405]. Similarly, RIDD activity can induce apoptosis by degrading mRNA that encodes ER chaperones and by the downregulation of microRNAs that negatively regulate the expression of pro-apoptotic caspases [399].

Hence, the UPR comprises a complex mechanism of integrated signalling pathways that respond to ER stress by either cellular adaptation, thus promoting the survival of the cell, or by triggering cell apoptosis if ER stress is prolonged or severe (Figure 1.5).
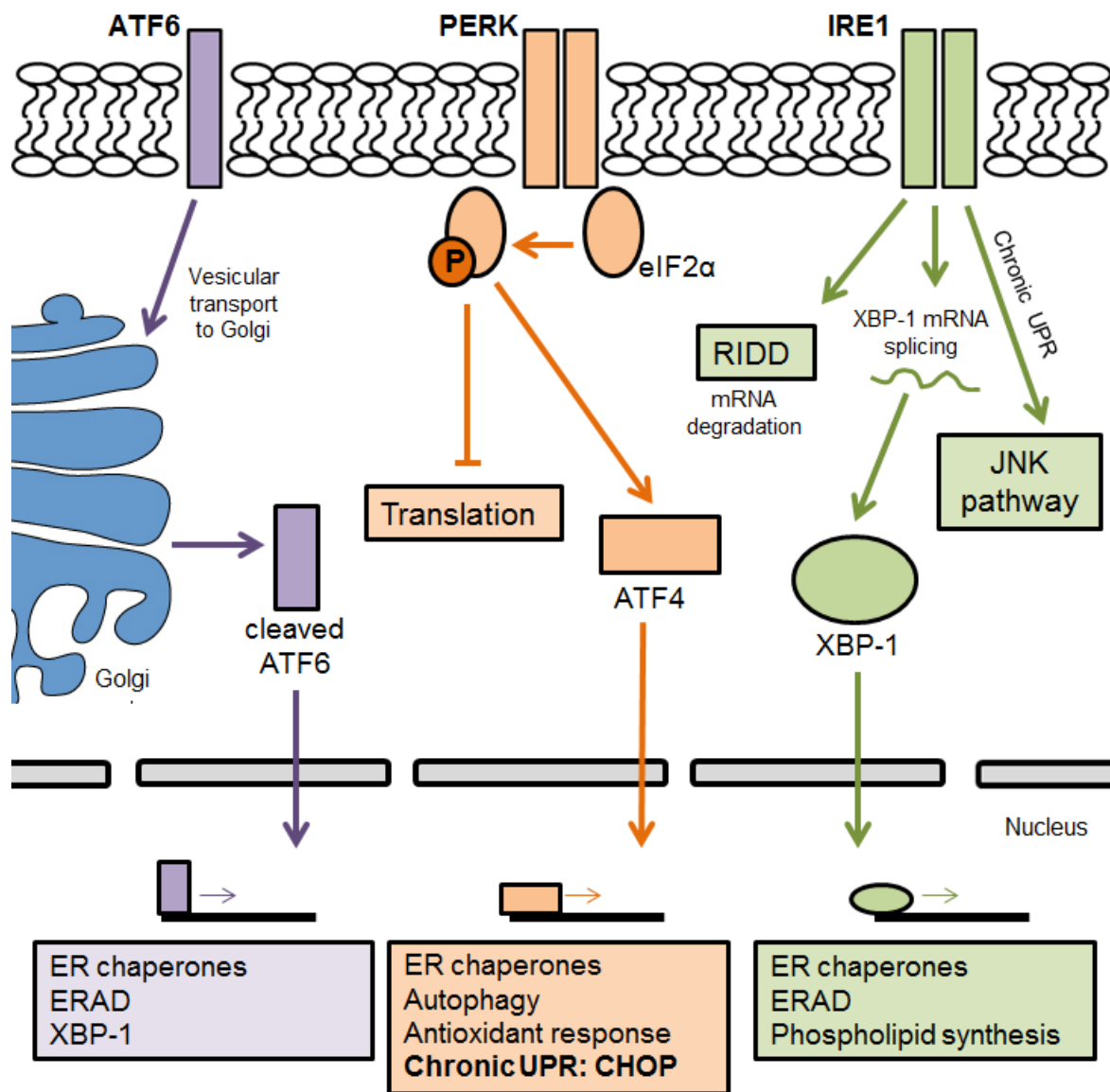
Figure 1.5: The UPR signalling pathways. In ALS, the accumulation of misfolded proteins in the ER induces the UPR by activating ER stress sensors, ATF6, IRE1 and PERK. ATF6 is transported to the Golgi, where it is cleaved, releasing the cytosolic ATF6 fragment which acts as a transcription factor. Cleaved ATF6 translocates to the nucleus where it induces genes required for the upregulation of ER chaperones and ERAD, and it also modulates XBP-1 mRNA levels. PERK phosphorylates eIF2α which inhibits protein translation. However, ATF4 is upregulated, and it translocates to the nucleus, inducing the expression of ER chaperones, genes related to autophagy and redox control. During chronic UPR, ATF4 induces CHOP, mediating ER stress associated apoptosis. IRE1 induces RIDD and the splicing of mRNA encoding XBP-1. Spliced XBP-1 upregulates ER chaperones, genes involved in ERAD and genes involved in phospholipid synthesis. During chronic UPR, IRE1 induces the JNK pathway, which results in apoptosis.

1.7.3 Evidence for induction of the UPR in neurodegenerative diseases

ER stress is induced in many conditions, including viral infection, diabetes, tumour development, and autoimmune disease [406]. Moreover, aging inhibits the early protective responses of ER stress [407]. There is increasing evidence that the UPR is induced in most neurodegenerative diseases, such as ALS, AD, PD, HD and CJD. The upregulation of UPR markers in disease-affected neurons has now been described in both cellular and animal models of disease, as well as in post-mortem patient tissues, for most of these disorders. It is generally thought that UPR induction in these diseases may initially be neuroprotective, however, sustained activation of the UPR may subsequently result in neurodegeneration. However, in some instances, induction of some phases of the UPR can be detrimental, so the relationship between the UPR and neurodegeneration is complex. The author wrote a review article on evidence for UPR induction in neurodegenerative diseases, thus the reader is directed to this review for more information [12]. However, a concise summary of UPR induction in neurodegenerative diseases, besides ALS, is presented below.

In patients with AD, UPR proteins PERK, BiP, IRE1 and eIF2α are upregulated in the temporal cortex and hippocampus [408, 409]. CHOP activation is detected in AD cell models [410] and is upregulated, along with JNK, in animal models of AD [411], indicating the activation of pro-apoptotic UPR in AD. In patients with PD, phosphorylated PERK and eIF2α are detected in the substantia nigra [412]. Moreover, PERK and IRE1, as well as downstream targets, eIF2α, ATF4 and CHOP are upregulated in PD cell culture models [413]. The induction of CHOP in the substantia nigra of PD mouse models has also been detected [414], indicating the activation of pro-apoptotic UPR in PD. BiP and CHOP are up-regulated in HD cell models [415], as well as in post-mortem brains from HD patients [416]. Similarly, the increased expression of XBP-1 is detected in the striatum of HD patients, however interestingly, CHOP and ATF4 are not elevated [417]. Further investigation into XBP-1 in

PD demonstrate that XBP-1 knockdown in HD mouse models reduces neuron loss and mutant Huntingtin protein levels, and improves motor performance [417]. The upregulation of ER chaperones, such as BiP, have been detected in the cortex of post-mortem CJD patients [418]. Moreover, in CJD cell models, toxicity is linked with an increase in intracellular calcium release from the ER and the upregulation of ER chaperones [418, 419], indicating a role for ER stress in prion diseases.

1.7.4 Evidence for ER stress and UPR induction in ALS

Emerging evidence highlights ER stress, and consequential UPR induction, as a key mechanism of ALS pathogenesis, observed in both fALS and sALS. Indeed, UPR activation is now well documented in cellular and animal models of ALS, as well as human patient tissues, and is discussed in this section.

Studies utilising mutant SOD1 transgenic mice reveal that ER stress sensors (IRE1, PERK, ATF6), ER chaperones (PDI, BiP, ERp57), and apoptotic effectors (CHOP, caspase-12) are upregulated in lumbar spinal cords during disease [377, 420], indicating that UPR activation is essential in mutant SOD1-associated ALS. Furthermore, UPR markers, including IRE1, PDI and CHOP, were observed to be induced prior to symptom onset in these mice, evident initially in the subtypes of motor neurons that degenerate first in ALS [254, 255], suggesting that ER stress is implicated in pathogenesis. When ER stress is induced using tunicamycin or thapsigargin in neuroblastoma cells expressing mutant SOD1, an increase in the formation of SOD1 inclusions was observed, and these inclusions co-localised with ER markers [421]. In Neuro-2A cells expressing mutant SOD1, increased phosphorylation of PERK and eIF2α, and cleavage of ATF6, were upregulated [422]. Furthermore, inhibiting ER stress in mutant SOD1 expressing cells by treatment with salubrinal prevents eIF2α de-phosphorylation,

inhibits mutant SOD1 inclusion formation and improves cellular viability [422], demonstrating that by suppressing this arm of the UPR, the induction of pro-apoptotic ER stress is inhibited. These results suggest that ER stress and mutant SOD1 aggregation in ALS are closely associated.

SOD1 mutations represent only 12% of fALS and 1% of sALS cases, and SOD1-ALS patients do not display the typical TDP-43 pathology characteristic of most forms of ALS. Hence, these cases may not accurately represent pathology in the more common forms of disease. However, similar findings of upregulation of UPR markers were obtained in post-mortem human spinal cords tissues of sALS patients [254, 423, 424], including PDI and phosphorylated eIF2α [423]. This was confirmed with a comprehensive analysis of the UPR, which demonstrated upregulation of all three ER stress sensors, ER chaperones, and ER stress-associated apoptotic effectors, caspase-4 and JNK, in lumbar spinal cord tissue from sALS patients [254]. Upregulation of CHOP and BiP, as well as alterations in ER structure in motor neurons of ALS patients, have also been described [424, 425].

More recently, ER stress has been detected in neuronal cells expressing ALS-associated mutants of FUS and TDP-43 [426, 427], and in animal models based on TDP-43 [427], implying that ER stress is implicated in TDP-43 and FUS-associated ALS. Similarly, the UPR is induced in cell culture by ALS-associated mutant VAPB [428] and hexanucleotide repeat expansions in C9orf72 [159]. Several mechanisms have been proposed for ER stress induction in ALS. In SOD1-associated ALS impairment of ERAD as a result of mutant SOD1 interacting with ER resident protein, Derlin-1, which is essential for ERAD function has been described. This triggers ER stress-mediated cell death via the ASK1 pathway [429]. Another mechanism implicated in triggering ER stress is the impairment of protein transport between the ER and Golgi apparatus by mutant SOD1 [119, 355], mutant TDP-43 and mutant FUS (Soo et al 2015 Acta). These studies imply that ER stress is triggered from the

cytoplasm, rather than the ER, although further studies are warranted to fully define the mechanisms involved. Interestingly, in studies using reprogrammed iPSCs ER stress was closely associated with the electrical excitability of motor neurons [430], and hyper-excitability of motor neurons may trigger ER stress [431].

Several studies have shown that modulation of the UPR genetically in animal models of ALS is protective. Deletion of BIM, XBP-1, ASK1, Puma or ATF4 either delays disease [432-434], or extends survival in transgenic mutant SOD1 mice [342, 429]. Similarly, pharmacological modulation of the UPR is protective in mutant SOD1 transgenic mice [255] and in *C.elegans* and zebrafish models expressing mutant TDP-43 [435]. Furthermore, the inhibition of eIF2α de-phosphorylation using salubrinal delays disease and extends survival of mutant SOD1 transgenic mice [390]. Interestingly, however, mutant SOD1 transgenic mice with hemizygous deletion of PERK had a considerably accelerated disease onset and shortened lifespan compared to mutant SOD1 transgenic mice with normal PERK expression [436], indicating that some aspects of the UPR are not protective, and may enhance disease. These findings suggest that PERK is a mediator of motor neuron survival in ALS, perhaps by decreasing protein misfolding [436], or by inducing autophagy [342]. Together, these results indicate that selectively targeting specific components of the UPR may be beneficial in ALS.

1.8 Protein Disulphide Isomerase (PDI)

PDI is a 55 kDa ER chaperone and oxidoreductase, primarily localised within the ER. It is normally upregulated during ER stress, as discussed above, where it aims to alleviate stress by engaging in protein folding [437]. PDI is the prototype of a large family of proteins which possess two distinct functions: 1) disulphide interchange activity, whereby PDI utilises its oxidoreductase capabilities to either oxidise, reduce or isomerise protein disulphide bonds, and 2) general chaperone activity (discussed in detail in Chapter 4). These two functions allow PDI to promote the correct folding of misfolded proteins into their native conformations, hence, PDI is a fundamental constituent of the ER proteostasis machinery [438].

As PDI can facilitate protein folding, it is not surprising that it is increasingly implicated in neurodegenerative diseases, such as ALS, where protein misfolding is a key component. PDI is often co-localised with misfolded proteins in disease-affected tissue, implying a possible role for PDI in preventing protein misfolding [426, 427, 439, 440]. In fact, there is evidence that PDI prevents protein aggregation and associated toxicity in ALS, suggesting that is has a protective function (discussed in detail in Chapter 3). Moreover, recent studies have identified unique functions of PDI family members, specific to the nervous system, including neuronal outgrowth and synaptic function [441]. Interestingly, novel variants in genes encoding two PDI family members, PDIA (PDI) and PDI3 (ERp57), were recently proposed as risk factors for developing ALS [441-444]. Hence, novel therapeutic strategies based on the functional activity of PDI may be beneficial in the treatment of protein misfolding disorders, such as ALS.

1.9 Summary and Aims

In order to develop novel therapeutics based on PDI's activity, the protective mechanisms of PDI need to be defined. To investigate and characterise these protective mechanisms, each chapter of this thesis addresses specific aims, as described below.

Chapter 3 – PDI is protective against ALS-associated mutant Cyclin F expressed in neuronal cells. The aims of the studies described in this chapter were to determine whether PDI is protective against cellular defects induced by mutant Cyclin F – a novel protein associated with ALS.

Chapter 4 – Characterising the protective properties of PDI.
The aims of the studies described in this chapter were primarily to determine which domains of PDI were involved in PDI's protective activity. Subsequently, the activities of prokaryotic thioredoxin-like proteins with differing redox properties to PDI were analysed to investigate differences in activity based on redox potential.

Chapter 5 – The role of redox activity for PDI's function.
The aims of the studies described in this chapter were to determine the role of PDI's redox potential on its protective activity, and to analyse which of PDI's oxidoreductase properties were imperative for its protective function.

Chapter 6 – The role of PDI and its redox activity in FUS-linked ALS.
The aims of the studies described in this chapter were to investigate how inhibiting PDI's oxidase activity affects its protective activity against ALS-associated mutant FUS.

Chapter 7 – Peptides based on PDI's active site are protective in neuronal cells expressing mutant SOD1. The aims of the studies described in this chapter were to determine if linear peptides, based on protective features of PDI defined in previous chapters, were protective against mutant SOD1 in neuronal cells.

Chapter 2: Materials and Methods

The general methods of the doctoral work are detailed in this chapter. Methods specific to a particular study are described later in the relevant experimental chapter.

2.1 Materials

Wildtype TDP-43 and mutant TDP-43 Q331K constructs encoding enhanced green fluorescent protein (EGFP)-tagged human TDP-43 at the N-terminus were a kind gift from Professor Benjamin Wolozin, Boston University, USA, and wildtype TDP-43 and mutant TDP-43 Q331K in pmCherry.N1 vector were as previously described [427]. Wildtype SOD1 and mutant SOD1 A4V constructs encoding EGFP-tagged human SOD1 at the C-terminus were previously described [265]. GFP FUS (wildtype and R521G) vectors were a gift from Dr. Justin Yerbury, University of Wollongong, Australia, and wildtype FUS and mutant FUS R521G constructs encoding hemagglutinin (HA)-tagged human FUS at the N-terminus were provided by Dr. Dorothee Dormann, Munich University, Germany. Wildtype Cyclin F and mutant Cyclin F S621G in pmCherry.N1 vector were supplied by Professor Roger Chung, Macquarie University, Australia. Wildtype PDI containing a v5 tag in pcDNA3.1(+) construct was provided by Professor Neil Bulleid, University of Glasgow, UK. Mutant PDI D292N and R300H were a kind gift from Professor Claudio Hetz, University of Chile, Chile. The PDI QUAD mutant was generated by a Masters student at La Trobe University, Australia, and the cytoplasmic PDIs (WT and QUAD) were created by a Post-doctoral researcher (Dr. Sonam Parakh), all using site-directed mutagenesis. The EGFP-SOD1 A4V cysteine mutants were also generated by a Masters student using site-directed mutagenesis. The XBP-1 venus reporter construct was as previously described [445], as well as the GFPu construct [446, 447]. The cyto-roGFP construct was a gift from Paul Schumacker (Addgene plasmid #49435). Expression constructs were re-suspended in nuclease free water and

transformed in TOP10 cells with glycerol stocks made for future experiments. All DNA

plasmids were verified by DNA sequencing before use.

2.2 Molecular Biology

2.2.1 Luria-Bertani (LB) medium

Luria-Bertani (LB) broth was used as a medium to maintain and support the growth of *E. coli*

throughout the project. 10 g bacto-tryptone (Oxoid), 5 g yeast extract (Oxoid) and 10 g NaCl

were mixed in 1 L dH$_2$O, with the pH adjusted to 7.0 with 1 mL 1 M NaOH, in order to make

LB broth. LB broth was autoclaved and stored at room temperature.

2.2.2 Antibiotic for bacterial culture

Ampicillin or kanamycin sulphate (Sigma) were dissolved in dH$_2$O at 100 mg/mL and filter

sterilised before storage at -20°C. The appropriate antibiotic was added to LB broth prior to

the broth's usage at a final concentration of 60 µg/mL for ampicillin and 100 µg/mL for

kanamycin.

2.2.3 LB agar plates

LB agar was prepared by adding 20 g of bacteriological agar (Oxoid) per 1 L LB broth prior

to autoclaving. LB agar was allowed to cool to approximately 55°C and appropriate antibiotic

was added before pouring ~ 15 mL into sterile Petri dishes in a laminar flow hood. Plates

were left to set before immediate use or storage at 4°C.

2.2.4 Transformation of competent cells

TOP10 competent cells (Invitrogen) were stored at -80°C. Upon use, cells were thawed on ice. The appropriate volume of DNA plasmid was added to 50 µL of competent cells in a tube, and gently mixed with a pipette tip. The cells were incubated on ice for 30 min, and then heat shocked at 42°C for 45 s, before immediately returned to ice for a further two minutes. 250 µL SOC medium (Invitrogen) was added to the cells and tubes were shaken at ~200 rpm in a 37°C shaking incubator for 1 h. Aliquots of 50 µL of the cell mixture were spread onto pre-prepared agar plates (section 2.2.3), which were incubated at 37°C overnight, inverted.

2.2.5 Small scale plasmid DNA production

DNA used for initial mammalian cell transfection optimisation and mutation screening was isolated from bacterial cultures using the QIAprep Spin Miniprep Kit (Qiagen). After overnight incubation of transformed LB agar plates, a single bacterial colony was collected with a pipette tip and inoculated in a Falcon tube containing 5 mL LB broth with antibiotic. The tube was incubated overnight at 200 rpm in a 37°C shaking incubator. 4 mL of bacterial culture was centrifuged using a FA-45-24-11 rotor, 1 mL at a time, at 13,000 rpm for 3 min the following day. The remaining 1 mL was used to make a glycerol stock (section 2.2.8). Supernatants were removed after each centrifugation and the resulting pellet was processed according to the manufacturer's protocol. 50 µL of DNA was eluted as a result of the protocol which was stored at -20°C. DNA was quantified by spectrophotometry (section 2.2.7).

2.2.6 Midi-scale plasmid DNA production

DNA used for all mammalian cell transfections was isolated using the QIAGEN Plasmid Plus Midi Kit (Qiagen). After overnight incubation of transformed LB agar plates, a single bacterial colony was collected with a pipette tip and inoculated in a Falcon tube containing 25 mL LB broth with antibiotic. The tube was incubated overnight at 200 rpm in a 37°C shaking incubator. The following day, bacterial cultures were centrifuged at 6,000 g for 15 min at 4°C. The supernatant was removed of and the resulting pellet was processed according to the manufacturer's protocol. 200 µL of DNA was eluted as a result of the protocol and this was stored at -20°C. DNA was quantified by spectrophotometry (section 2.2.7) and agarose gel electrophoresis (section 2.2.8) before use in transfection experiments.

2.2.7 DNA quantification by spectrophotometry

The concentration of DNA was analysed by using a Nanodrop ND-1000 spectrophotometer. A conversion of 1.0 A_{260} = 50 ng/µL was used to determine the original DNA concentration, and the A_{260}/A_{280} ratio was used to examine DNA purity, where a ratio of ~ 1.8 was generally accepted as "pure" for DNA.

2.2.8 DNA analysis by agarose gel electrophoresis

50x TAE buffer (40 mM Tris-acetate, 1 mM EDTA, pH 8.0) was diluted with dH_2O to a 1x working solution. 3 % (w/v) agarose was added to the buffer and heated until agarose had dissolved, followed by the addition of 0.1 % (v/v) Gel Red Nucleic Acid Stain (Biotium). Buffer was poured into a gel rig and allowed to set. Next, the gel rig was placed into the gel electrophoresis apparatus and 1x TAE buffer poured over the apparatus, ensuring the gel was

covered. 1 kb PLUS DNA ladder (Invitrogen) and plasmid samples were loaded to the wells

with 6x Gel Loading Dye (New England Biolabs). The voltage applied varied from 70 to 100

V for 30 – 90 min, depending on DNA size. Bands were visualised under UV light and

analysed using the desktop program Genesys (Syngene, Frederick, MD, USA).

2.2.9 Glycerol stocks

Glycerol stocks of overnight bacterial cultures were prepared by mixing 750 µL of bacterial

culture with 250 µL of 80 % glycerol. Stocks were mixed by vortexing and subsequently

stored at -80°C in order to preserve bacteria for a long period of time.

2.3 Mammalian Cell Culture

2.3.1 Fetal Calf Serum (FCS) heat inactivation

Fetal Calf Serum (FCS; Gibco) was stored at -20°C. Upon use, FCS was thawed to room

temperature, before being added to a 56°C water bath for 30 min with frequent mixing. The

heat-inactivated FCS was aliquoted in 50 mL tubes and stored at -20°C.

2.3.2 Cell maintenance

Mouse neuroblastoma Neuro2a cells were maintained in T75 flasks containing high glucose

Dulbecco's Modified Eagle Medium (DMEM; Gibco) with 10 % (v/v) heat-inactivated FCS

and 1 % (v/v) Pen-Strep. The cells were incubated at 37°C under 5 % CO_2 and upon 75-80 %

confluence, they were passaged. This involved briefly washing the cells with sterile

phosphate buffer saline (PBS; 3.2 mM Na_2HPO_4, 0.5 mM KH_2PO_4, 1.3 mM KCl, 135 mM NaCl, pH 7.4), followed by 37°C incubation with 1 mL Trypsin-EDTA (Gibco) for ~ 1 min to detach the cells from the flask. The cells were then collected with 5 mL DMEM with 10 % (v/v) FCS and centrifuged at 800 rpm for 5 min. The cell pellet was resuspended in 1 mL DMEM with 10 % (v/v) FCS and cell concentration was determined using a haemocytometer (Crown Scientific). Briefly, 10 µL of cell suspension was added to 90 µL DMEM and 100 µL Trypan Blue (Invitrogen), resulting in a 1:20 dilution. The number of viable cells in each of the four 1 mm^2 areas of the haemocytometer were counted and the mean number of cells was multiplied by 20 (dilution factor) and 10^4 to confer cell number per mL. Cells were plated onto 24-well plates comprising 13 mm coverslips (Menzel) in each well if performing immunocytochemistry or 6-well plates if preparing cell lysates, and the remaining cells were subcultured into a new T75 flask containing 10 mL DMEM with 10 % (v/v) FCS and 1 % (v/v) Pen-Strep. The number of cells plated were dependent on how long the cells were to be incubated for, the degree of growth, and the type of well-plate used, typically a range between 4 x 10^4 – 1 x 10^5 per well. The cell amount per well was kept constant within experiments.

2.3.3 Transfection

Neuro2A cells were transfected using Lipofectamine 2000 with PLUS reagent (Invitrogen) according to the manufacturer's protocol. Cells plated in 24-well plates were transfected with 500-1000 ng plasmid DNA. In cells which required two plasmid DNAs to be transfected, a concentration of 500 ng of each DNA plasmid was used. The DNA amount per well was kept constant within experiments to ensure reproducibility. Cells were incubated in a 37°C

incubator under 5 % CO_2. Cell media was replaced 5 h post-transfection and cells were

further incubated for between 18 h – 72 h, depending on experiment.

2.3.4 Long-term storage of cell lines

Confluent cells at a low passage number were treated with Trypsin-EDTA and collected in 5

mL antibiotic-free DMEM with 10 % (v/v) FCS. The cell suspension was centrifuged at 800

rpm for 5 min at room temperature and the resulting pellet was resuspended in 1 mL 95 %

FCS and 5 % DMSO. Cells in this medium were dispensed into cyrovials (1-2 million cells

per 1 mL aliquot) and frozen at -80°C. Cyrovials were transferred to liquid nitrogen for long

term storage.

2.3.5 Cell lysate preparation

Tris NaCl (TN) buffer (50 mM Tris-HCl pH 7.5, 150 mM NaCl) was prepared with 0.1 %

(w/v) sodium dodecyl sulfate (SDS) and 1% protease inhibitor cocktail (Sigma) (1 tablet/10

mL), and kept on ice. Cell lysates were collected in 250-500 µL TN buffer, depending on

confluence, and incubated on ice for 15 min. After incubation, remaining cells were detached

with a cell scraper and collected into labelled centrifuge tubes to be frozen at -20°C for 24 h.

2.3.6 Protein concentration determination

Samples were incubated on ice for 10 min before centrifugation with a FA-45-24-11 rotor at

15,000 rpm for 15 min to clear the supernatant. The pellet was removed. The concentration of

protein within the cell lysates was determined using the BCA Protein Assay (Thermo

Scientific) by comparing concentrations with a bovine serum albumin (BSA) standard curve

of known concentrations ranging from 0 to 2.0 mg/mL, according to the manufacturer's protocol. All cell lysate samples were analysed in duplicates on a 96-well plate, and the absorbance at 560 nm was determined using a PHERAstar FS microplate reader (BMG Labtech, Ortenberg, Baden-Wűrttemberg, Germany).

2.4 Immunocytochemistry

2.4.1 Cell fixation

At the appropriate time point for analysis, transfected Neuro2A cells in 24-well plates were taken out of 37°C and 5 % CO_2 incubation. DMEM was aspirated and cells were washed once with 1 x PBS. Cells were then fixed with 4 % (w/v) paraformaldehyde (PFA) and incubated in the dark at room temperature for 20 min. Cells were again washed with PBS and stored in PBS at 4°C if not used immediately.

2.4.2 Immunofluorescence assay

After fixation, cells were permeabilised with 0.1 % (v/v) Triton-100 in PBS for 10 min and blocked with 3 % (w/v) BSA in PBS for 1 h, both at room temperature with gentle rocking. After washing twice with PBS, the appropriate primary antibody (Table 2.1) was diluted and added to the cells, followed by an overnight incubation at 4°C. Primary antibodies were diluted in 1 x PBS.

TABLE 2.1: Primary antibodies used for immunocytochemistry.

Antibody	Dilution factor	Species raised in	Manufacturer
Anti-V5 tag	1:200	Mouse	Invitrogen (#R960-25)
Anti-HA tag	1:200	Rabbit	Sigma (#H6908)
Anti-CHOP	1:50	Mouse	Santa Cruz (#sc-7351)
Anti-XBP-1	1:20	Rabbit	Santa Cruz (#sc-8015)
Anti-Bax	1:200	Mouse	BD Biosciences (#556467)
Anti-Cleaved Caspase-3	1:400	Rabbit	Cell Signalling (#9661)
Anti-Calreticulin	1:200	Rabbit	Abcam (#ab2907)

The following day, cells were washed three times with PBS over 10 min, and then incubated with the appropriate secondary antibody at 1:250 dilution in PBS for 1 h in the dark at room temperature. Secondary antibodies used were goat anti-rabbit IgG Alexa Fluor 594 conjugate or goat anti-rabbit IgG Alexa Fluor 488 conjugate for primary antibodies hosted in rabbit, and goat anti-mouse IgG Alexa Fluor 594 conjugate or rabbit anti-mouse IgG Alexa Fluor 488 conjugate for primary antibodies hosted in mouse (all from Molecular Probes). Cells were washed three times with PBS over 10 min after secondary antibody incubation. Nuclei were stained using Hoechst 33342 (Thermo Scientific) diluted to a concentration of 0.5 µg/mL in dH$_2$O for 15 min in the dark. Again, cells were washed three times with PBS. Coverslips were carefully removed from wells and mounted onto slides, cell side down, using Dako fluorescent mounting media, and allowed to air dry in the dark overnight.

2.4.3 Nuclear morphology apoptosis analysis

Neuro2A cells were grown on coverslips in 24-well plates, and then transfected with suitable plasmids, as indicated in section 2.3.3. Cells were washed with PBS and fixed with 4 % (w/v) PFA for 20 min in the dark at room temperature. Cells were subsequently washed and then treated with Hoechst 33342 at a concentration of 0.5 µg/mL for 15 min in the dark at room temperature. After a final two washes with PBS, cells were mounted onto slides, cell side down, with Dako fluorescent mounting medium. Images for counting and analysis were acquired using a Zeiss AxioImager epifluorescence microscope, and accompanying Zen software. At least 100 cells co-expressing both transfected plasmids per treatment were counted and analysed, and three independent experiments were performed. Apoptotic nuclei were defined as condensed (under 5 µM in diameter), fragmented, or having an abnormal morphology (not circular) and were counted as a percentage of non-apoptotic cells. Cells which expressed just one transfected plasmid and cells which were undergoing cell division were omitted from the study.

2.4.5 Fluorescence microscopy

Once slides were dried, they were observed under 40x magnification on a Zeiss AxioImager epifluorescence microscope. DAPI (nuclei, blue fluorescence), FITC (green fluorescence) and TRITC (red fluorescence) filters were used for viewing the different channels, and images were taken using the microscope's Zen software for cell counting and analysis. Photomultiplier sensitivities were set to minimise 'bleed through' effects from one channel to another. At least 100 cells co-expressing both transfected plasmids were counted and analysed per treatment. Confocal imaging was performed using a Zeiss LSM 880 confocal laser scanning microscope for the attainment of high-resolution images.

2.5 SDS-PAGE and Immunoblotting

2.5.1 Materials

<u>10x running buffer</u>

30 g Tris, 148 g glycine and 10 g SDS were dissolved in 1 L dH$_2$O. For a 1x working

solution, the stock was diluted by 1 in 10 in dH$_2$O. 1x running buffer was used when running

the gel through electrophoresis.

<u>1x transfer buffer</u>

3.03 g Tris and 14.4 g glycine were dissolved in 200 mL methanol and made up to 1 L with

dH$_2$O. The working solution contained 25 mM Tris, 192 mM glycine and 20 % (v/v)

methanol. 1x transfer buffer was used when transferring the gel to a nitrocellulose membrane.

<u>10x Tris-buffered saline (TBS)</u>

12.1 g Tris and 88 g NaCl were dissolved in 1 L dH$_2$O and stored at 4°C. The stock was

diluted by 1 in 10 in dH$_2$O and the pH adjusted to 8.0 with HCl to achieve a 1x working

solution. The working solution contained 10 mM Tris-HCl and 150 mM NaCl.

<u>10x Tris-buffered saline with tween-20 (TBS-T)</u>

In each 1 L of 10x TBS, 5 mL of Tween-20 (polyoxyethylene sorbitol monolaureate, Sigma)

was added. The stock was diluted by 1 in 10 in dH$_2$O and the pH adjusted to 8.0 with HCl to

achieve a 1x working solution. The working solution contained 10 mM Tris-HCl, 150 mM

NaCl and 0.05 % (v/v) Tween-20.

2.5.2 SDS-PAGE

40 µg of protein sample (sections 2.3.5 and 2.3.6) were added to 10 µL of 4 x Laemmli

Sample Buffer (Biorad) and NuPage Sample Reducing Agent (10x) (Invitrogen). Samples

were vortexed and briefly centrifuged before denaturation at 95°C for 5 min. Samples and the

Precision Plus Protein™ Dual Color Standards molecular weight marker (Bio-Rad) were run

through a 4-15 % precast polyacrylamide gel and transferred to a nitrocellulose membrane.

2.5.3 Immunoblotting

Nitrocellulose membranes were blocked with 5 % (w/v) skim milk in TBS-T for 30 min, and

then incubated with primary antibodies (Table 2.2) at 4°C overnight or at room temperature

for 1 h. Primary antibodies were diluted in 5 % (w/v) skim milk in TBS-T.

TABLE 2.2: Primary antibodies used for immunoblotting.

Antibody	Dilution factor	Species raised in	Manufacturer
Anti- V5 tag	1:2000	Mouse	Invitrogen (#R960-25)
Anti- GFP	1:2000	Rabbit	Abcam (#ab290)
Anti- β-actin	1:2000	Mouse	Sigma (#A2228)
Anti- mCherry	1:2000	Rabbit	Abcam (#ab183628)

After primary antibody incubation, membranes were washed once with TBS-T for 4 min,

followed by a further two washes with TBS for 4 min each. Membranes were then incubated

with secondary antibodies (Chemicon) for 1 h at room temperature: HRP-conjugated goat

anti-rabbit, or goat anti-mouse (1:2000 dilution in TBS-T). After another three washes,

signals were detected Clarity™ Western ECL Substrate (Bio-Rad), according to the

manufacturer's protocol. Membranes were analysed and images obtained using the Bio-Rad

ChemiDoc MP system and Image Lab™ software. Blots were stripped using Restore™

PLUS Western Blot Stripping Buffer (Thermo Scientific) according to the manufacturer's

protocol and re-probed as above.

2.6 Statistical Analysis

Each experiment was performed a minimum of three times at differing cell passage number,

with at least one blind experiment. Differing cell passage numbers were used to demonstrate

that the results obtained were still consistent, despite variations to cell passage number. The

data are represented as mean ± standard error of the mean (SEM) and comparisons were

performed using one-way analysis of variance (ANOVA) followed by Tukey *post hoc* test

(GraphPad Prism, San Diego, CA, USA). P-values of 0.05 were considered significant, where

$* \ p < 0.05$, $** \ p < 0.01$, and $*** \ p < 0.001$.

Chapter 3: PDI is Protective Against ALS-Associated Mutant Cyclin F Expressed in Neuronal Cells

3.1 Introduction

PDI is a multifunctional protein, acting as both an ER chaperone and an oxidoreductase. Upregulated by the induction of ER stress, PDI is a fundamental molecular defence against protein misfolding, both in the ER and in the cytoplasm [438]. In studies investigating the role of ER stress in ALS, PDI upregulation was detected in both mutant SOD1 transgenic mouse models and human ALS patient spinal cord tissues [254, 440]. Moreover, PDI was found to be co-localised with misfolded proteins in disease-affected tissue, suggesting a role for PDI in ALS [426, 427]. Investigations into the role of PDI in ALS has established a possible protective role for PDI against ER stress and various other ALS hallmarks induced by ALS-associated proteins SOD1, TDP-43 and FUS [448] (Parakh et al., 2017 in preparation), as discussed in the following sections.

Cyclin F is an E3 ligase protein, responsible for mediating the ubiquitination and proteasomal degradation of target proteins. Therefore, Cyclin F is an essential constituent of the UPS [449]. Recently, novel mutations in the gene encoding Cyclin F have been associated with ALS and FTD [89], and further studies from our group have demonstrated that ALS/FTD associated-mutant forms of the protein inhibit ER-Golgi transport and ERAD, which induces ER stress and apoptosis, similar to other proteins linked to ALS (Ragagnin et al., 2017 in preparation).

Given that we have obtained evidence that PDI is protective against similar mechanisms of ALS pathogenesis induced previously, it was hypothesised that PDI would also exert a protective effect against mutant Cyclin F induced-cellular defects. Thus, this chapter focuses specifically on the role of PDI against ALS/FTD associated- mutant Cyclin F in neuronal cells.

3.1.1 The involvement of PDI in ALS

PDI was first identified as a key player in ALS when it was found to be upregulated in the spinal cords of mutant SOD1 transgenic mouse models of ALS at pre-symptomatic, symptomatic and end stages of disease [254]. In addition, PDI levels were upregulated in the spinal cords of sALS patients, compared to non-ALS controls [254, 423]. PDI was subsequently observed in swollen neurites [440] and upregulated in the CSF of both sALS and fALS patients [254], consistent with reports that PDI is localised in other cellular locations besides the ER, and secreted by several cell types [450]. Proteomic screening also detected an upregulation of PDI in the blood of ALS patients during disease, suggesting that PDI may have potential as a biomarker for diagnosis [451].

PDI co-localises with mutant SOD1 inclusions in both mutant SOD1 transgenic mouse models and in neuronal cells expressing mutant SOD1, indicating that it may be protective against mutant SOD1 misfolding. This was subsequently confirmed in ALS cell models expressing mutant SOD1 in which co-expression with PDI prevented the formation of SOD1 inclusions and insoluble ubiquitinated proteins [448]. Conversely, the knockdown of PDI in these cells increased the proportion of SOD1 inclusions [448], demonstrating that PDI is protective against the formation of SOD1 inclusions. Furthermore, overexpression of PDI also reduces the levels of UPR markers BiP, phosphorylated PERK, and pro-apoptotic CHOP, as well as reduces the proportion of apoptotic cells compared to control populations [448], implying that PDI is also protective against ER stress and toxicity induced by mutant SOD1.

In addition to mutant SOD1, PDI also co-localises with inclusions formed by other ALS-linked mutant proteins; TDP-43 [427, 440], FUS [426], and VAPB [201]. Moreover, PDI has been detected in motor neuronal inclusions in sALS patients where it associates with TDP-43

and SOD1 [440], suggesting that PDI is associated with general protein misfolding in ALS. The neuroprotective role for PDI was also further supported in vivo, by studies involving the deletion of Reticulon-4A. Knockdown of Reticluon-4A, responsible for PDI distribution to intracellular subdomains, accelerates the degeneration of motor neurons in SOD1 mouse models [452].

Recently, unique roles for PDI and its family member, ERp57, have been identified in the nervous system. Overexpression of PDI and ERp57 enhances neurite outgrowth in motor neuronal cells, primary neurons and human motor neurons produced from differentiation of embryonic stem cells. Moreover, ERp57 is protective at the synapse [441]. Conditional ERp57 knockout mice display abnormal synapses, reduced muscle innervation, aberrant skeletal muscle fibres and dysfunctional neuromuscular connectivity, resulting in a significant decline in motor performance, a reduction in body mass, and premature death [441]. Hence, these data suggest that PDI family members have novel roles in motor control and neuromuscular connectivity.

PDI's profile in ALS has recently become more prominent by the identification of PDI variants as a genetic risk factor [442]. In this study, single nucleotide polymorphisms (SNPs) in the gene encoding PDI were associated with fALS and sALS [442]. In addition, a second study demonstrated a significant association of SNPs in the PDI gene with sALS in the Chinese Han population, implying that genetic variations in the PDI gene may be a contributing risk factor for developing sporadic forms of ALS in these populations [443]. Interestingly, a further study identified 16 variants in both PDI and ERp57, with 1-2% present in all fALS and 1% present in all sALS cases analysed [444]. This frequency is similar to that of other ALS-linked gene variants [4]. Structural analysis of proteins encoded by PDI variants, D292N and R300H, predicted a change in the catalytic functioning of these proteins [444]. These variants are discussed in detail in Chapter 6.

Recent unpublished data in our laboratory has demonstrated that PDI is protective against ER stress and ER-Golgi transport defects induced by mutant TDP-43 and mutant FUS (Parakh et al., 2017 in preparation), similar to its protective effect against mutant SOD1. Moreover, PDI is able to inhibit mutant TDP-43 and mutant FUS mislocalisation to the cytoplasm (Parakh et al., 2017 in preparation), demonstrating that PDI is protective against various ALS-associated proteins and against similar ALS mechanisms of pathogenesis.

3.1.2 Cyclin F (CCNF)

First reported in 1994, Cyclin F, encoded by the gene *CCNF*, is an orphan member of the cyclin protein family [453]. It is involved in regulating several cell cycle processes, including centrosome duplication [454], genome stability maintenance [455], and DNA replication and repair [456]. Usually, cyclins are important regulators of the cell cycle by activating cyclin-dependent kinases (CDKs), however, Cyclin F does not perform this function [449]. In contrast to other cyclins, which exploit the catalytic subunits of CDKs to phosphorylate protein substrates and promote cell cycle events, Cyclin F regulates the cell cycle independent of CDK activity. Instead, it ubiquitinates or directly interacts with substrates using its F-box motif [449, 456, 457]. This process has important roles in the ubiquitination and degradation of proteins involved in the cell cycle, but it also marks other proteins for degradation [458].

Cyclin F is the founding member of the F-box family of proteins, characterised by the presence of an F-box motif [453]. By binding directly to S-phase kinase-associated protein 1 (Skp1), F-box proteins, including cyclin F, act as the substrate recognition subunits of the Skp1-Cul1-F-box (SCF) E3 ubiquitin-protein ligase complex, which recognise and mediate the ubiquitination and proteasomal degradation of target proteins via an enzyme cascade

[449, 453] (see Figure 3.1). Therefore, this E3 ubiquitin-protein ligase complex (SCF$^{\text{Cyclin F}}$) is a fundamental component of the UPS. Moreover, E3 ubiquitin ligases, including F-box proteins, are involved in maintaining ER homeostasis by directing target proteins for degradation via ERAD [459, 460].
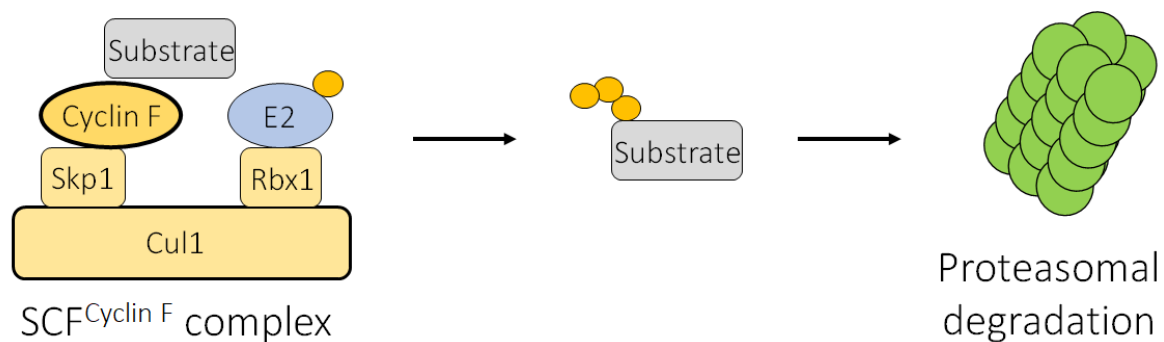
Figure 3.1: The SCF$^{\text{Cyclin f}}$ complex in the UPS pathway.

Cyclin F, Skp1 and Cul1 form a Skp1-Cul1-F-box (SCF) E3 ubiquitin-protein ligase complex. Target substrates bind to Cyclin F's F-box motif. Ubiquitinated E2 enzymes bind to RING box protein 1 (Rbx1), which is bound to Cul1, which then interacts with the SCF$^{\text{Cyclin F}}$ complex to transfer ubiquitin to a target substrate. The ubiquitinated substrate is then directed to the proteasome for degradation.

Cyclin F has a molecular weight of 87 kDa, and along with an F-box domain, it contains a cyclin box, two functional D-box motifs, two NLS motifs, and a PEST sequence rich in proline (P), glutamic acid (E), serine (S) and threonine (T) residues (see Figure 3.2). The two NLS motifs ensure cyclin F localises predominantly in the nucleus [461]. The F-box domain binds to Skp1 within the SCF complex [462], whereas the two D-box motifs, composed of an RXXL sequence, are required for anaphase promoting complex/cyclosome (APC/C)-mediated degradation of Cyclin F [463]. The cyclin box domain shares structural similarities with other cyclin proteins, and it is responsible for binding substrates through hydrophobic residues [454-456]. The PEST sequence, located at cyclin F's C-terminus, is typically present in proteins which are rapidly degraded. Indeed, expression of Cyclin F lacking a PEST sequence leads to the accumulation of Cyclin F in cells [464].
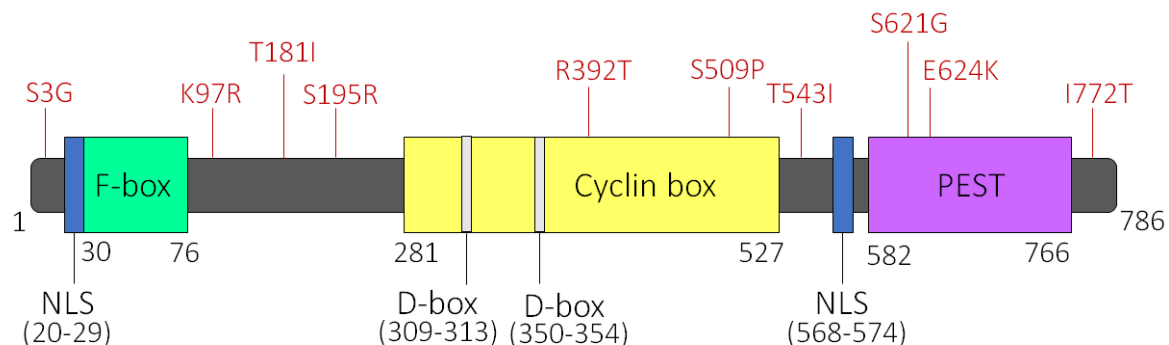
Figure 3.2: The domain organisation of the Cyclin F protein.

Cyclin F is a 786-amino acid protein which contains two NLS motifs (blue), an F-box motif (green), a cyclin box (yellow) containing two D-box motifs (light grey) and a PEST region (purple). The red text above the sequence indicates the location of each of the ALS/FTD-linked mutations identified to date within the CCNF gene.

3.1.3 Cyclin F mutations are implicated in ALS and FTD

The role of Cyclin F is neurons has not been well investigated, however recently, genome-wide linkage analysis in a large ALS/FTD pedigree and whole-exome sequencing was utilised to identify a CCNF missense mutation on chromosome 16p13.3. Upon investigation of international cohorts, additional novel *CCNF* variants in both fALS and sALS, as well as FTD, were discovered, indicating that mutant forms of Cyclin F are associated with ALS and FTD [89].

To date, ten missense mutations in *CCNF* have been identified in fALS, sALS and FTD patients. Interestingly, these mutations are scattered throughout the distinct domains of the protein and their functional consequences are yet to be determined. However, no mutations in the F-box domain of Cyclin F have been identified as of yet. Nonetheless, no relationship has yet been identified between the location of mutations in cyclin F and clinical phenotype [89]. Familial ALS and FTD mutations in *CCNF* were present in overall cohorts from diverse geographic populations at frequencies ranging from 0.6% to 3.3%, which is comparable to the frequency of mutations observed in *TARDBP*, which encodes TDP-43, and FUS, that have been reported in fALS cohorts [89].

Cyclin F is a fundamental component of the UPS [449]. Usually, aberrant misfolded proteins are targeted for degradation by the UPS, however there is increasing evidence that this system is dysfunctional in ALS patients [108]. Interestingly, expression of mutant Cyclin F in neuronal cells resulted in UPS dysfunction, as well as abnormal ubiquitination and accumulation of ubiquitinated proteins, including TDP-43 [89]. Furthermore, overexpression of mutant Cyclin F in zebrafish resulted in an aberrant motor neuron phenotype, reminiscent of ALS [465]. These studies suggest that mutant forms of Cyclin F may contribute to overall proteostasis dysfunction in ALS.

3.1.4 Cyclin F induces ER stress, mislocalisation, promotes cell death and activates UPS

Recent unpublished studies performed in our laboratory have demonstrated that mutant Cyclin F S621G induces pathogenic mechanisms previously observed in ALS (Ragagnin et al., 2017 in preparation). Similar to mutant forms of TDP-43 and FUS, mutant Cyclin F S621G mislocalises to the cytoplasm, whereas wildtype Cyclin F is localised in the nucleus, as expected. This suggests that the presence of ALS/FTD-associated mutations in Cyclin F induce its redistribution to the cytoplasm. Mutant Cyclin F S621G also perturbs ER-Golgi protein transport and induces fragmentation of the Golgi apparatus into tubular and vesicular structures. Moreover, mutant Cyclin F S621G induced ER stress, upregulating levels of IRE1, spliced XBP-1 and pro-apoptotic CHOP, in neuronal cells (Ragagnin et al., 2017 in preparation). CHOP levels were also slightly, but significantly, upregulated in cells expressing wildtype Cyclin F, similar to previous findings that wildtype SOD1 induces low levels of ER stress [119]. Furthermore, expression of mutant Cyclin F S621G was also found to impair ERAD in neuronal cells, and interestingly, wildtype Cyclin F also inhibited ERAD, but again to a lesser extent that mutant Cyclin F. In addition, mutant Cyclin F S621G became associated with stress granules in neuronal cells, and triggered apoptotic cell death, indicating that cellular mechanisms stimulated by mutant Cyclin F are associated with neuronal loss (Ragagnin et al., 2017 in preparation). These studies therefore reveal that ALS-associated mutant Cyclin F perturbs ER homeostasis and triggers apoptosis in human neuronal cell lines, similar to other ALS-associated proteins, revealing novel insights into the pathogenic mechanisms induced by Cyclin F in ALS/FTD. These studies also provide further evidence of a relationship between ER and Golgi defects and cellular pathology in ALS.

3.1.5 Aims of this chapter

Despite their diverse functions, ALS mutant proteins SOD1, TDP-43 and FUS share several pathogenic mechanisms implicated in ALS, including the accumulation of abnormally folded proteins, the induction of ER stress and inhibition of ER-Golgi transport. Previous studies from our group have demonstrated that PDI is protective against these events in cells expressing mutant forms of SOD1, TDP-43 and FUS. Mutant forms of novel ALS/FTD-associated protein, Cyclin F, also induce similar cellular mechanisms. The following experiments described in this chapter involved examining whether the overexpression of PDI is protective against these mechanisms induced by mutant Cyclin F S621G in neuronal cell lines.

3.2 Materials/Methods

3.2.1 Constructs

A pcDNA3.1 vector containing full-length PDI and a V5 tag at the C-terminus was provided by Dr. Neil Bulleid, University of Glasgow, UK. The V5 tag is a short peptide sequence of 14 amino acids which is used to detect expression of tagged proteins [466]. Wildtype Cyclin F and mutant Cyclin F S621G constructs in pmCherry.N1 vector were supplied by Associate Professor Ian Blair, Macquarie University, Australia. mCherry is commonly used as a tag to aid the visualisation of proteins in neuronal cells by its bright red fluorescence. It has been previously shown not to alter the native function or localisation of proteins [467]. The GFPu construct, used to indicate activation of the UPS, was as previously described [447]. Similarly, the XBP-1 venus reporter construct was used to signal XBP-1 activation and hence, induction of ER stress [445]. The DNA plasmids used in this chapter were verified by DNA sequencing before use.

3.3 Results

3.3.1 Wildtype PDI is localised in the ER of Neuro-2A cells.

First, the localisation of overexpressed V5-tagged PDI protein was analysed in Neuro-2A cells using confocal microscopy. Cells were transfected with the PDI construct for 24 h and then immunocytochemistry was performed using a V5 antibody to visualise PDI, and a calreticulin antibody to probe for calreticulin, an ER-resident protein. As expected, PDI co-localised with calreticulin in all transfected cells, indicating that PDI is localised within the ER (Figure 3.3). This is consistent with previous reports [468]. Single colour controls were also performed to ensure there was no evidence of bleed through from one channel to another (Supplementary figure 1).
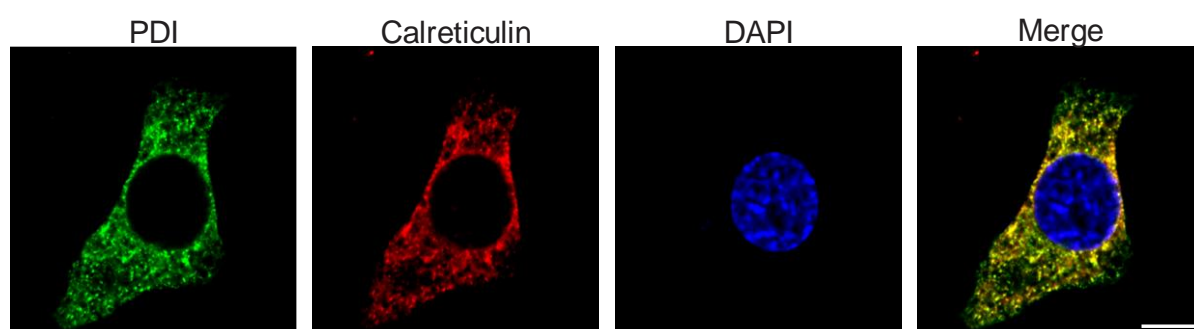
Figure 3.3: Wildtype PDI is localised in the ER of Neuro-2A cells.

Neuro-2A cells were transfected with pcDNA3.1 vector encoding PDI and a V5 tag (left column). After 24 h transfection, cells were fixed and immunocytochemistry was performed using antibodies for the V5 tag and calreticulin (second column from the left), and the nucleus was stained using Hoechst (third column). The yellow in the merge panel (last column) illustrates co-localisation of PDI and calreticulin, illustrating that PDI is localised primarily in the ER, as expected. Scale bar represents 30 µM.

3.3.2 Wildtype PDI V5 is co-expressed in almost all Neuro-2A cells co-transfected with Cyclin F mCherry.

Next, the co-transfection efficiency of PDI and Cyclin F was examined in Neuro-2A cells. Cells were transfected with PDI-V5 and Cyclin F mCherry constructs for 72 h, before fixing and performing immunocytochemistry using an anti-V5 antibody and staining the nuclei with Hoechst. Co-transfection was verified by fluorescence microscopy examining mCherry expression (red) for Cyclin F and performing immunocytochemistry with an Alexa Fluor 488-tagged secondary antibody to detect the V5 tag of PDI (Figure 3.4 A). The overall transfection efficiency of Cyclin F constructs was calculated to be approximately 35 % in Neuro-2A cells when observed 72 h post-transfection. For each of the three replicate experiments, fluorescent microscopy was utilised to visualise at least 100 cells expressing Cyclin F. These cells were further analysed for co-expression with PDI. Quantification revealed that approximately 95 % of Cyclin F transfected cells also co-expressed PDI (Figure 3.4 B). Thus, it was assumed in all further experiments that detection of Cyclin F expression reflected co-expression of both Cyclin F and PDI. Hence, in all future experiments including co-transfection of Cyclin F and PDI, immunocytochemistry using a V5 antibody was not performed.
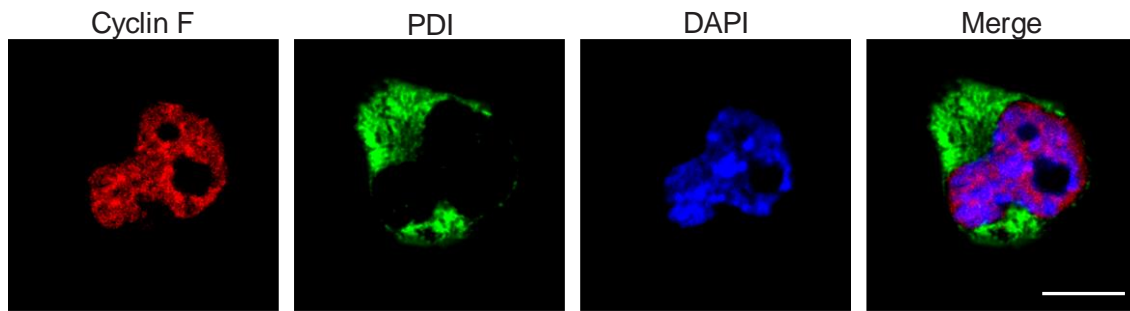
Figure 3.4: Wildtype PDI V5 is co-expressed in almost all Neuro-2A cells co-transfected with Cyclin F mCherry. A) Neuro-2A cells were transfected for 72 h with Cyclin F tagged with mCherry (left column) and PDI tagged with V5 (second column from the left). Cells were fixed and immunocytochemistry was performed using an anti-V5 antibody and the nucleus was stained with Hoechst (third column). The merge column demonstrates co-expression of PDI and Cyclin F in the cell shown. Scale bar = 30 µM.

3.3.3 Western blotting of PDI and Cyclin F in Neuro-2A cells.

Prior to performing cellular assays using overexpressed Cyclin F and PDI, Western blotting analysis was performed to ensure that transfection of each construct resulted in similar levels of expression and to confirm that the expressed proteins were of the expected size (Figure 3.5 A and B). Cell lysates were prepared from the following cell populations; mCherry vector alone, wildtype Cyclin F co-expressed with either empty pcDNA3.1 vector or PDI, and mutant Cyclin F S621G co-expressed with either empty pcDNA3.1 vector or PDI. Immunoblotting using an anti-mCherry antibody revealed that wildtype and mutant Cyclin F mCherry proteins were expressed at the expected size of 130 kDa, and mCherry alone was expressed at 30 kDa, as expected. PDI was detected in transfected cell lysates using an anti-V5 tag antibody (62 kDa). β-actin was used as a loading control, detected using anti-β-actin antibody (40 kDa). These studies revealed that the levels of expression of PDI and Cyclin F were similar across cell lysate populations and that overexpression of PDI did not alter the expression of Cyclin F. The expression levels of mCherry was significantly higher than the expression of Cyclin F proteins, however, this was to be expected.

A
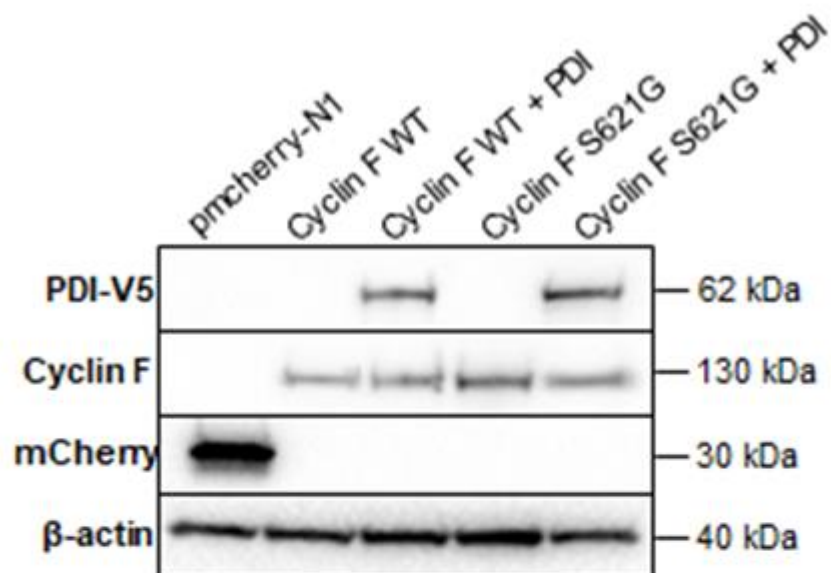
B
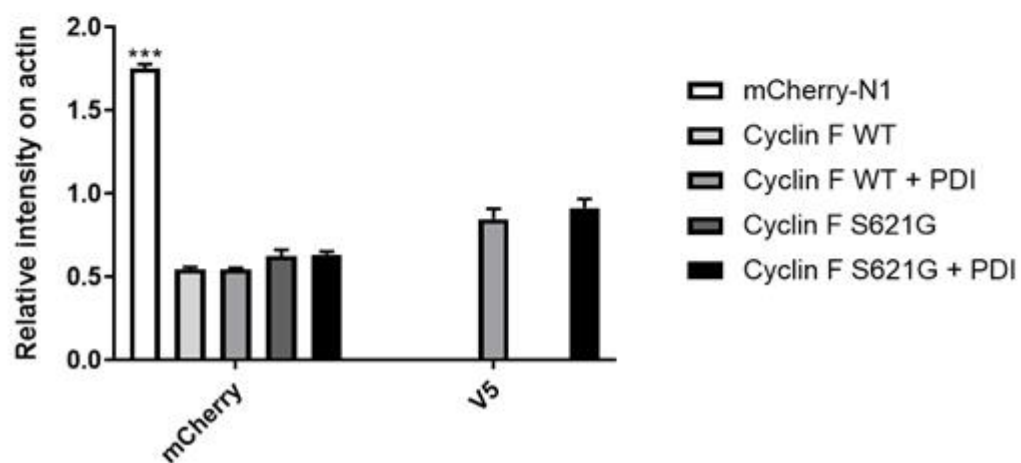
Figure 3.5: Expression of PDI-V5 and Cyclin F-mCherry proteins in Neuro-2A cells.

A) Western blotting analysis of cell lysates was performed and to ensure that proteins were expressed at the expected size and that expression levels were similar between groups. Cell lysates examined were from cells expressing mCherry alone, wildtype Cyclin F with either empty pcDNA3.1 vector or PDI, and mutant Cyclin F S621G with either empty pcDNA3.1 vector or PDI. PDI was detected at 62 kDa, as expected (PDI = 61 kDa, V5 tag = 1 kDa), whereas wildtype and mutant Cyclin F were detected at 130 kDa (Cyclin F = 100 kDa, mCherry = 30 kDa) and mCherry vector at 30 kDa. β-actin was used as a loading control and was detected at 40 kDa, as expected. **B)** The relative intensity of proteins was quantified against β-actin. The levels of expression of Cyclin F and PDI were confirmed to be similar between groups. The expression levels of mCherry were significantly ($p < 0.001$) higher than the expression levels of Cyclin F-mCherry proteins, as expected. N = 3, Mean ± SEM, *** p < 0.001.

3.3.4 Overexpression of PDI inhibits mutant Cyclin F localisation to the cytoplasm.

Our laboratory has previously shown that mutant Cyclin F mislocalises from its native location in the nucleus to the cytoplasm (Ragagnin et al., 2017 in preparation). This finding is consistent with prior studies demonstrating that cytoplasmic mislocalisation of TDP-43, FUS and C9orf72 is present in ALS, revealing that nucleo-cytoplasmic shuttling is dysregulated [469-471]. The mislocalisation of TDP-43 and FUS in ALS patient motor neurons is a common observation [62, 65, 128, 137], and it has been demonstrated in our laboratory that the over expression of PDI in neuronal cells expressing mutant TDP-43 and FUS can prevent mislocalisation of mutant TDP-43 and FUS (Parakh et al., 2017 in preparation). Therefore, it was next investigated whether PDI overexpression could also protect against mutant Cyclin F mislocalisation to the cytoplasm in Neuro-2A cells.

The cellular location of Cyclin F was analysed 72 h post-transfection to ensure maximal levels of protein expression, based on previous observations in our laboratory. Immunocytochemistry was carried out using an anti-V5 antibody to detect PDI expression, and DAPI staining using Hoechst was performed to clearly visualise the nuclei. Cells were examined for localisation using fluorescence microscopy, and at least 100 cells co-transfected with Cyclin F and PDI were examined. Cyclin F was considered nuclear when it completely co-localised with the DAPI-stained nucleus. In contrast, Cyclin F was categorised as cytoplasmic when fluorescence was detected in both the nucleus and the cytoplasm or only within the cytoplasm of Cyclin F expressing cells (Figure 3.6 A). Low magnification images are also shown (Supplementary figure 2).

A significantly higher proportion of cells expressing mutant Cyclin F S621G ($p < 0.05$) displayed cytoplasmic rather than nuclear Cyclin F ($54.3\% \pm 3.4$), compared to cells expressing wildtype Cyclin F. However, overexpression of PDI in cells expressing mutant

Cyclin F S621G resulted in significantly ($p < 0.001$) fewer cells with cytoplasmic Cyclin F localisation (30.7% ± 2.9), compared to cells expressing mutant Cyclin F S621G alone (Figure 3.6 B). Wildtype Cyclin F was localised in the cytoplasm in 41.0% ± 2.5 of cells expressing Cyclin F. Moreover, co-expression of PDI with wildtype Cyclin F reduced the proportion of cells with Cyclin F cytoplasmic mislocalisation to 31.0% ± 2.0 of cells, although this decrease was not statistically significant. Therefore, these data suggest that overexpression of PDI is protective against the cytoplasmic mislocalisation of ALS-associated mutant Cyclin F S621G. The cells displaying mislocalised Cyclin F were also stratified into fixed expression levels to ensure that the co-expression of PDI did not decrease the expression of Cyclin F, thus resulting in less mislocalisation. These results demonstrated that the expression levels of Cyclin F were similar between groups, suggesting that alterations in expression were not a co-variate in determining PDI's protective effect against mislocalisation (Supplementary figure 3).

A

| | mCherry | PDI | DAPI | Merge |

Cyclin F WT

Cyclin F WT + PDI

Cyclin F S621G
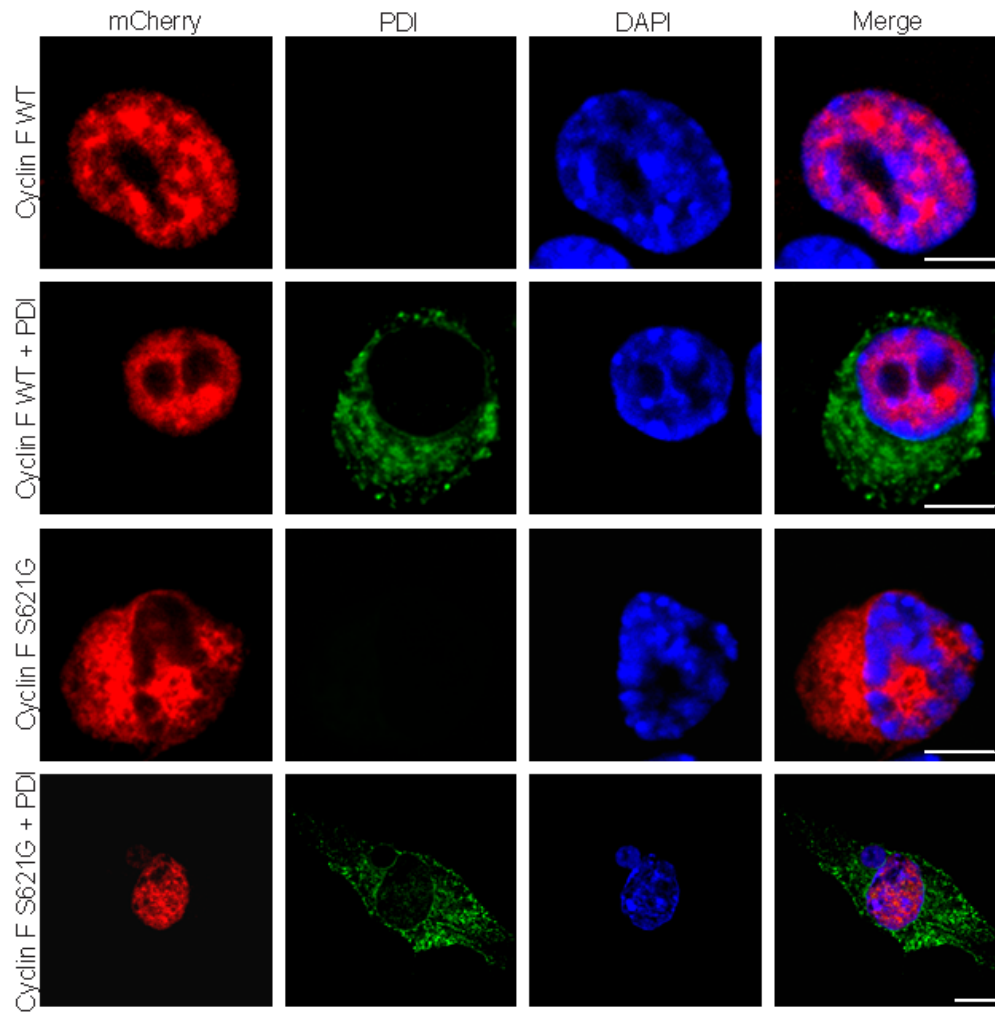
Cyclin F S621G + PDI

B
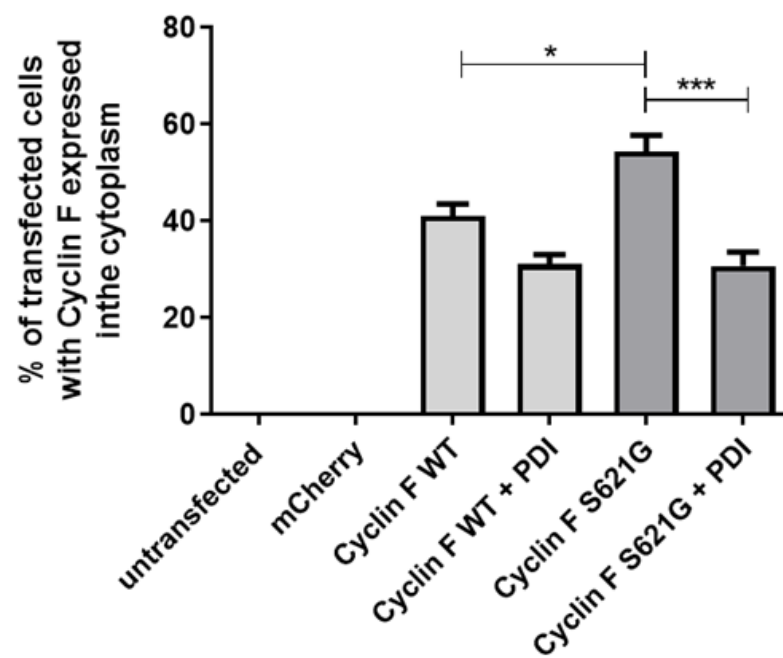
Figure 3.6: Overexpression of PDI inhibits ALS mutant Cyclin F localisation to the cytoplasm. A) Immunofluorescence images of Neuro-2A cells expressing either wildtype or mutant Cyclin F S621G (first column), with or without co-expression of PDI (second column). DAPI stained nuclei are illustrated in column three, and a merged image of the cell is shown in column four. Cells expressing wildtype Cyclin F displayed mainly nuclear localisation of Cyclin F (first and second panel; Cyclin F WT, Cyclin F WT + PDI), whereas more cells expressing mutant Cyclin F S621G (third panel) displayed cytoplasmic localisation, as indicated with the white arrowhead. However, when PDI was co-expressed with mutant Cyclin F S621G, significantly fewer cells displayed cytoplasmic Cyclin F (fourth panel; Cyclin F S621G + PDI). Scale bar = 30 µM. **B)** Quantification of Neuro-2A cells with cytoplasmic localisation of Cyclin F in A). There was a significant increase ($p < 0.05$) in the proportion of cells with cytoplasmic localisation of mutant Cyclin F S621G, compared to wildtype Cyclin F. A significant decrease in the proportion of cells with cytoplasmic localisation of Cyclin F was observed when mutant Cyclin F S621G, but not wildtype Cyclin F, was co-expressed with PDI ($p < 0.001$). N=3, Mean ± SEM, * $p < 0.05$, *** $p < 0.001$.

3.3.5 Overexpression of PDI is protective against ER stress induced by mutant Cyclin F.

Our laboratory previously demonstrated that ALS-associated Cyclin F induces ER stress in neuronal cell lines (Ragagnin et al., 2017 in preparation). As PDI has been shown to be protective against mutant SOD1-induced ER stress in neuronal cells [448], it was next investigated whether PDI was also protective against ER stress induced by mutant Cyclin F S621G in cell culture. Two markers of ER stress were used; XBP-1 and CHOP. The activation of XBP-1 was used as a marker of UPR induction in its early, pro-survival stages, and is indicative of the activation of the IRE-1 pathway of the UPR [393, 472]. A reporter construct for XBP-1 was used to detect XBP-1 activation. The XBP-1 Venus reporter contains the GFP variant, Venus, downstream of a partial sequence of XBP-1. Under normal non-stressed conditions, it is expected that the mRNA generated from this fusion construct will not be spliced, and translation will be terminated at the stop codon between the XBP-1 and Venus genes. Conversely, during ER stress, this mRNA is spliced, leading to a frame shift which results in termination of translation at the stop codon after venus. Thus, a fusion protein of XBP-1 and Venus will be produced in cells undergoing ER stress. The fluorescence from Venus will therefore be observed in the nucleus if XBP-1 is activated, where nuclear immunoreactivity to XBP-1 is indicative of its activation, and thus, ER stress [445] (Figure 3.7 A).

Neuro-2A cells were co-transfected with constructs encoding XBP-1 Venus reporter, either wildtype Cyclin F-mCherry or mutant Cyclin F S621G-mCherry, and with either pcDNA3.1 empty vector (as a control) or PDI-V5 pcDNA3.1. Cells were also transfected with constructs encoding mCherry or XBP-1 Venus reporter constructs alone as controls to ensure that mCherry or XBP-1 reporter alone does not induce ER stress. After 72 h transfection, the cells were fixed and stained with Hoechst to visualise the nuclei.

In untransfected cells and cells transfected with mCherry alone, very little XBP-1 activation (less than 5% of cells) was detected. Mutant Cyclin F S621G cells co-expressing empty vector displayed significantly more ($p < 0.001$) XBP-1 activation ($41.3\% \pm 2.7$) compared to cells co-expressing wildtype Cyclin F with empty vector ($20.7\% \pm 3.3$). Moreover, co-expression of mutant Cyclin F S621G with PDI significantly reduced ($p < 0.001$) the proportion of cells with XBP-1 activation to $22.7\% \pm 1.8$, similar to levels seen in cells expressing wildtype Cyclin F (Figure 3.7 B). Interestingly, XBP-1 activation was detected in an increased percentage of cells expressing wildtype Cyclin F ($20.7\% \pm 3.3$) compared to mCherry alone ($p < 0.001$). This result is similar to previous findings obtained from our laboratory where wildtype forms of Cyclin F and SOD1 induced low levels of ER stress (Ragagnin et al., 2017 in preparation) [119]. However, PDI did not inhibit XBP-1 activation in cells expressing wildtype Cyclin F ($19.3\% \pm 1.2$). Hence, these results indicate that overexpression of PDI is protective against XBP-1 nuclear immunoreactivity, and hence ER stress, induced by ALS-associated mutant Cyclin F S621G.

A

	mCherry	XBP-1	DAPI	Merge
mCherry				
Cyclin F WT				
Cyclin F WT + PDI				
Cyclin F S621G				
Cyclin F S621G + PDI				

B

% of transfected cells with XBP1 activation

untransfected, mCherry, Cyclin F WT, Cyclin F WT + PDI, Cyclin F S621G, Cyclin F S621G + PDI

103
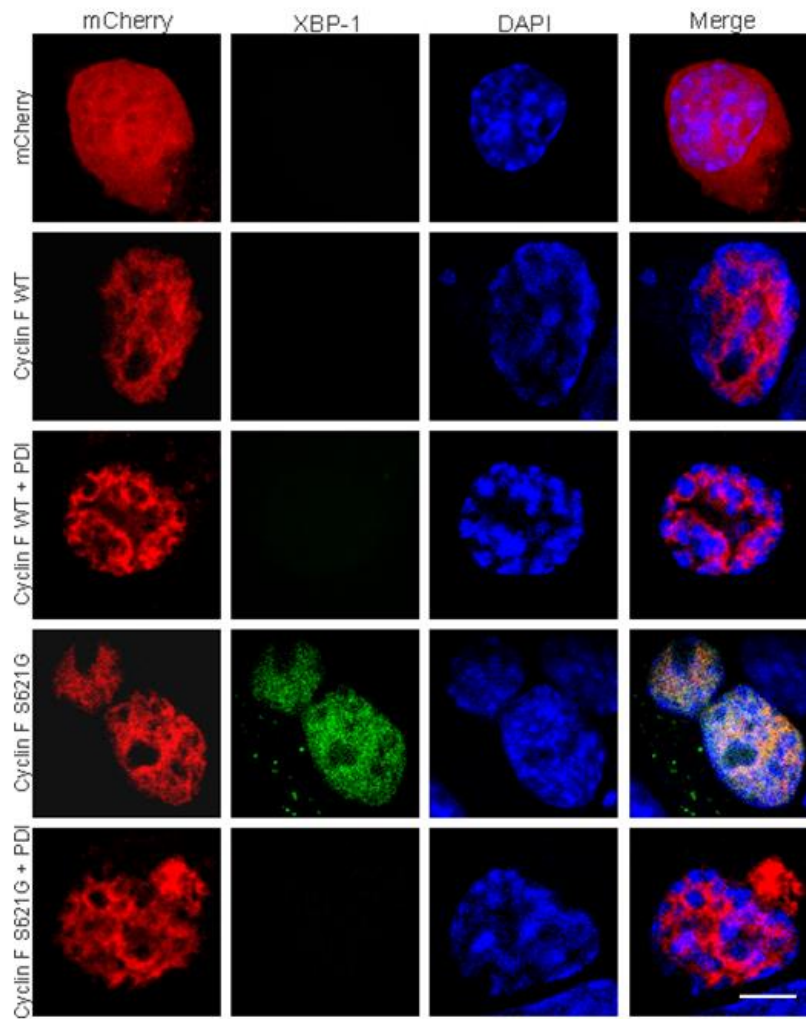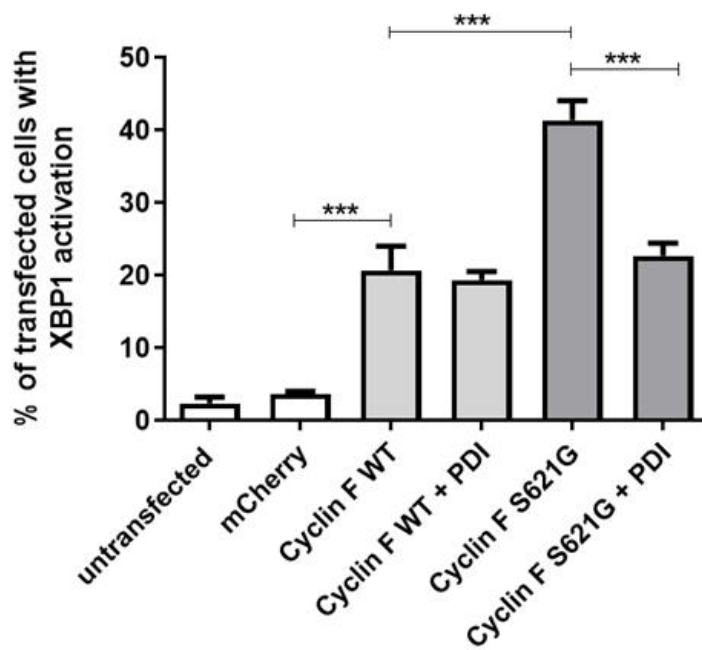
Figure 3.7: Overexpression of PDI is protective against XBP-1 activation induced by mutant Cyclin F. A) Immunofluorescence images of Neuro-2A cells expressing mCherry alone and either wildtype or mutant Cyclin F S621G (first column), with or without co-expression of PDI-V5 (second column). The third column illustrates DAPI-stained nuclei and the fourth column depicts a merged image. Cells expressing mCherry alone, or wildtype Cyclin F (first, second and third panels; mCherry, Cyclin F WT, Cyclin F WT + PDI) displayed low levels of nuclear XBP-1 immunoreactivity, and hence, XBP-1 activation. In contrast, more cells expressing mutant Cyclin F S621G displayed XBP-1 activation (fourth panel; Cyclin F S621G), as indicated by GFP expression in the nucleus in the second column. However, when PDI was co-expressed with Cyclin F S621G, significantly fewer cells displayed XBP-1 activation (fifth panel; Cyclin F S621G + PDI). Scale bar = 30 µM. **B)** Quantification of the cells in A) with XBP-1 nuclear immunoreactivity. The proportion of cells with XBP-1 activation was significantly higher in cells expressing Cyclin F S621G, compared to wildtype Cyclin F ($p < 0.001$). When PDI was co-expressed with Cyclin F S621G, significantly fewer cells ($p < 0.001$) displayed XBP-1 activation, implying that PDI is protective against ER stress induced by mutant Cyclin F, but not by wildtype Cyclin F. N=3, Mean ± SEM, *** $p < 0.001$.

To confirm these results, a second marker of ER stress was examined in cells co-expressing Cyclin F and PDI. CHOP is a pro-apoptotic protein induced via the PERK arm of the UPR and it is usually activated at a later phase than XBP-1 [397]. Activation of CHOP plays a fundamental role in facilitating the transition from the pro-survival to pro-apoptotic phases of the UPR. Therefore, nuclear immunoreactivity to CHOP, signifying CHOP activation, indicates that ER stress-induced apoptotic signalling has been induced within cells.

Cells were fixed 72 h after transfection and immunocytochemistry was performed using an anti-CHOP antibody, where nuclear immunoreactivity to CHOP indicated activation of pro-apoptotic UPR, similar to previous studies [448] (Figure 3.8 A). Nuclei were stained with Hoechst to clearly visualise the nucleus of each cell.

Quantification revealed that untransfected cells and cells expressing mCherry alone displayed almost no nuclear immunoreactivity to CHOP ($3.0\% \pm 0.6$ and $2.3\% \pm 0.3$ of cells respectively), as expected. There was a significant increase ($p < 0.001$) in the proportion of cells expressing mutant Cyclin F S621G with nuclear immunoreactivity to CHOP ($35.7\% \pm 3.0$), compared to wildtype Cyclin F expressing cells, consistent with previous observations. In contrast, co-expression of PDI with Cyclin F S621G resulted in a significant decrease ($p < 0.01$) in the proportion of cells with CHOP activation ($23.7\% \pm 1.2$), compared to cells co-expressing Cyclin F S621G with empty vector. Moreover, there was a slight, but significant ($p < 0.05$), increase in the proportion of cells displaying CHOP activation in cells expressing wildtype Cyclin F ($14.7\% \pm 1.5$), as for XBP-1. Similarly, co-expression of PDI with wildtype Cyclin F did not alter the proportion of cells with CHOP activation ($12.3\% \pm 1.2$) (Figure 3.8 B). Hence, these findings imply that PDI is protective against ER stress-induced apoptotic signalling stimulated by mutant Cyclin F in Neuro-2A cells.

A
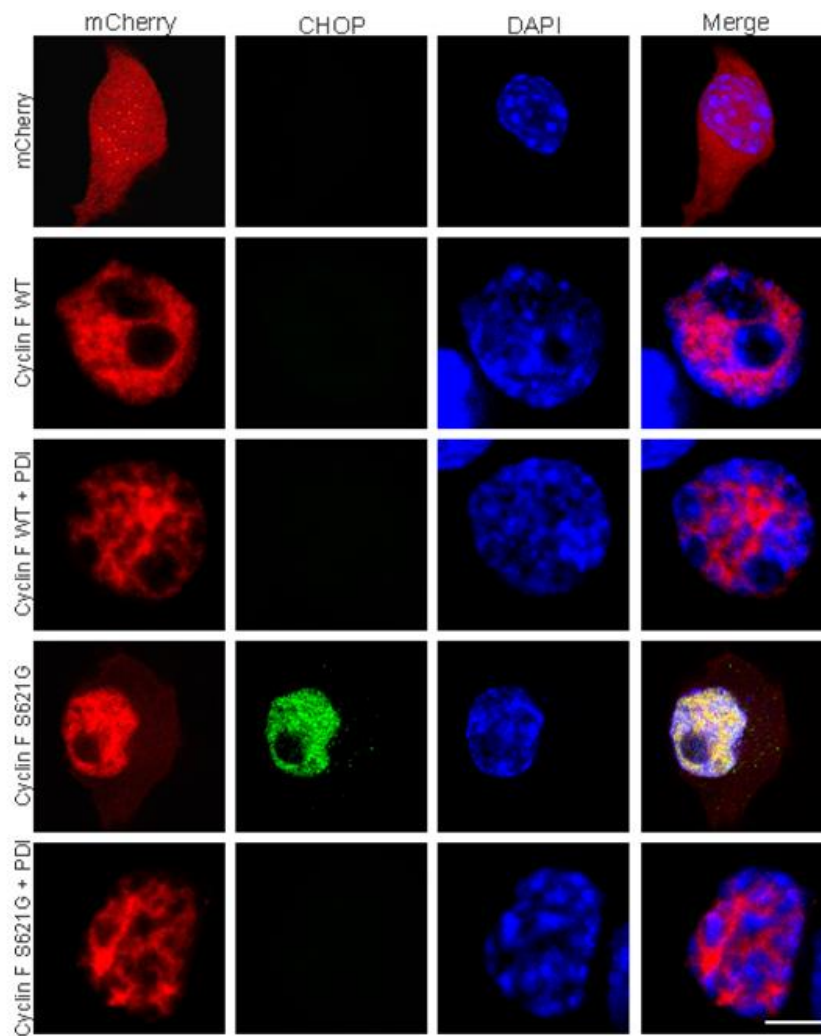
B
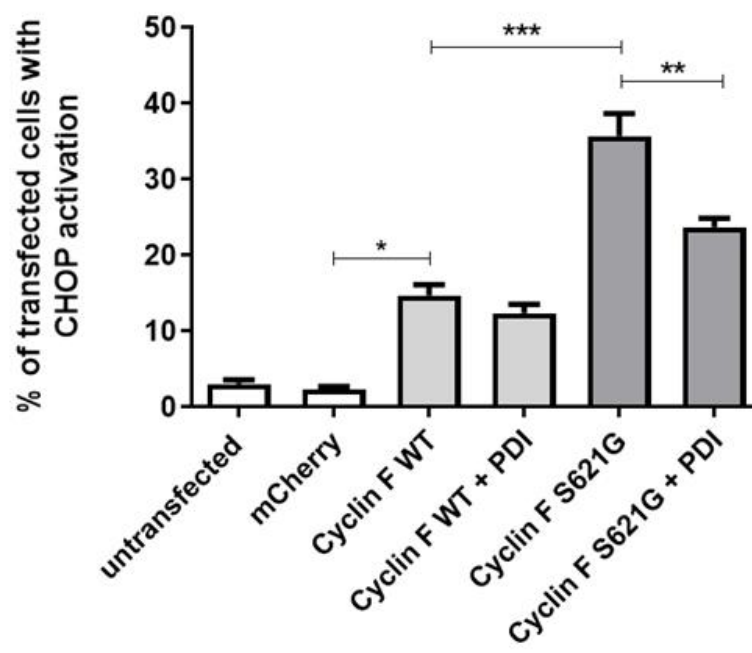
Figure 3.8: Overexpression of PDI is protective against CHOP activation induced by mutant Cyclin F. A) Neuro-2A cells were transfected with mCherry alone (first panel), wildtype Cyclin F co-expressed with either empty vector (second panel; Cyclin F WT) or PDI-V5 (third panel; Cyclin F WT + PDI), or mutant Cyclin F S621G co-expressed with either empty vector (fourth panel; Cyclin F S621G) or PDI-V5 (fifth panel; Cyclin F S621G + PDI). Cells expressing mCherry or wildtype Cyclin F displayed little nuclear immunoreactivity to CHOP. In contrast, in cells expressing Cyclin F S621G, GFP expression in the nucleus was more commonly visualised (fourth panel, second column). However, when PDI was co-expressed with Cyclin F S621G, the proportion of cells with nuclear immunoreactivity to CHOP was reduced (fifth panel). Scale bar = 30 µM. **B)** Quantification of cells in A) displaying CHOP activation. Very few untransfected cells and cells expressing mCherry alone displayed nuclear CHOP immunoreactivity. There was a significant increase ($p < 0.05$) in the proportion of cells with CHOP activation in the population expressing wildtype Cyclin F, compared to cells expressing mCherry. Moreover, significantly more ($p < 0.001$) cells expressing Cyclin F S621G displayed nuclear immunoreactivity to CHOP, compared to cells expressing wildtype Cyclin F. However, significantly fewer ($p < 0.01$) Cyclin F S621G cells displayed CHOP activation when PDI was co-expressed, compared to cells transfected with the empty vector. N=3, Mean ± SEM, * $p < 0.05$, ** $p < 0.01$, *** $p < 0.001$.

3.3.6 Overexpression of PDI inhibits dysfunction of the UPS induced by mutant Cyclin F.

Our group previously demonstrated that ALS-associated mutant Cyclin F impairs ubiquitin-mediated proteasomal degradation in neuronal cells [89]. Therefore, it was next examined whether PDI could prevent UPS dysfunction induced by ALS-associated mutant Cyclin F.

To investigate this possibility, a UPS reporter construct, GFPu, was utilised. This construct consists of a 16 amino acid degron (CL1, a specific substrate for the UPS), fused to the carboxyl terminus of GFP [473]. Through the degron sequence, GFP is degraded by the UPS. Therefore, the accumulation of GFPu (visualised by its fluorescence) is indicative of UPS impairment [473]. Wildtype and mutant Cyclin F constructs tagged with mCherry were co-transfected with GFPu, and either empty vector pcDNA3.1 or V5-tagged PDI. After 72 h transfection, cells were fixed and the nuclei were stained with Hoechst. Cells were analysed using confocal microscopy and the percentage of Cyclin F expressing cells with clearly visible GFPu expression (indicated by bright green fluorescence) was quantified (Figure 3.9 A).

Very few cells expressing mCherry, pcDNA3.1 vector or GFPu alone displayed GFPu expression (less than 10%), as expected, demonstrating that the proteasome is functioning as normal in these cells. In contrast, a marked increase in the proportion of cells expressing wildtype Cyclin F with GFPu fluorescence (40.3% ± 1.8) was observed, indicating that degradation of GFPu was impaired in these cells. Hence, this implies that wildtype Cyclin F induces UPS dysfunction. However, upon co-expression of wildtype Cyclin F with PDI, there was a significant decrease ($p < 0.05$) in the proportion of cells with GFPu activation (29.3% ± 2.2). Moreover, the proportion of cells with GFPu fluorescence in populations expressing mutant Cyclin F S621G was significantly higher (52.0% ± 2.6, $p < 0.05$) than in those expressing wildtype Cyclin F. However, when Cyclin F S621G was co-expressed with PDI,

the proportion of cells with GFPu fluorescence was significantly reduced (31.7% $\pm$ 4.5, p <

0.001) (Figure 3.9 B). These findings demonstrate that PDI is protective against impairment

of the UPS triggered by both wildtype and ALS-associated mutant Cyclin F. To confirm the

results obtained, the absolute expression levels of GFPu were also analysed in this

experiment, and this data can be viewed in the Appendix (Supplementary figure 4).

A

	mCherry	GFPu	DAPI	Merge
mCherry				
Cyclin F WT				
Cyclin F WT + PDI				
Cyclin F S621G				
Cyclin F S621G + PDI				
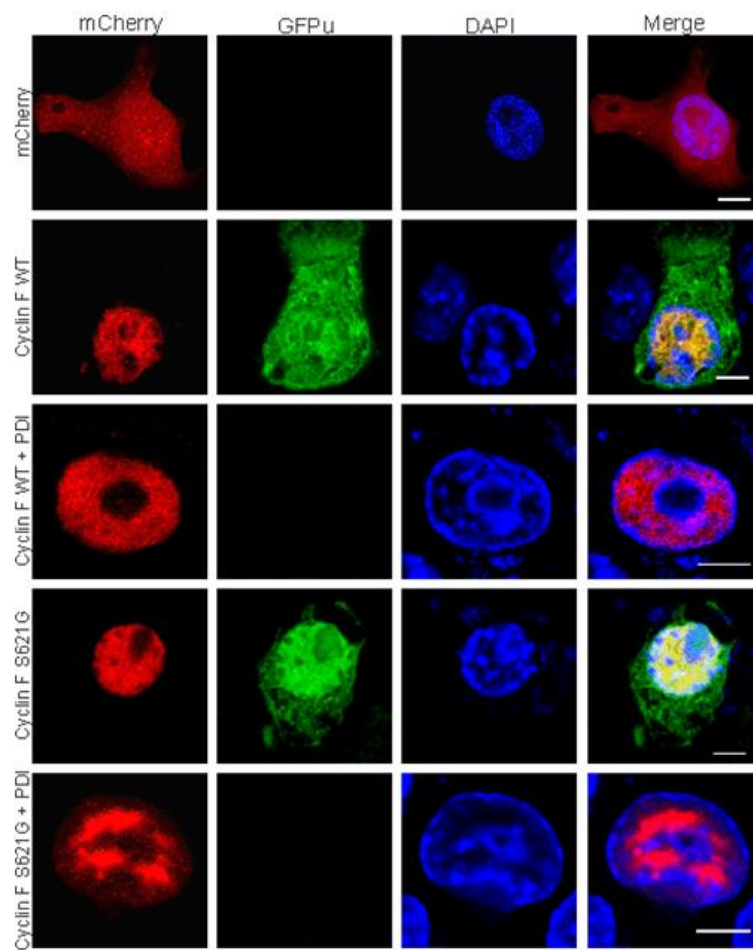
B
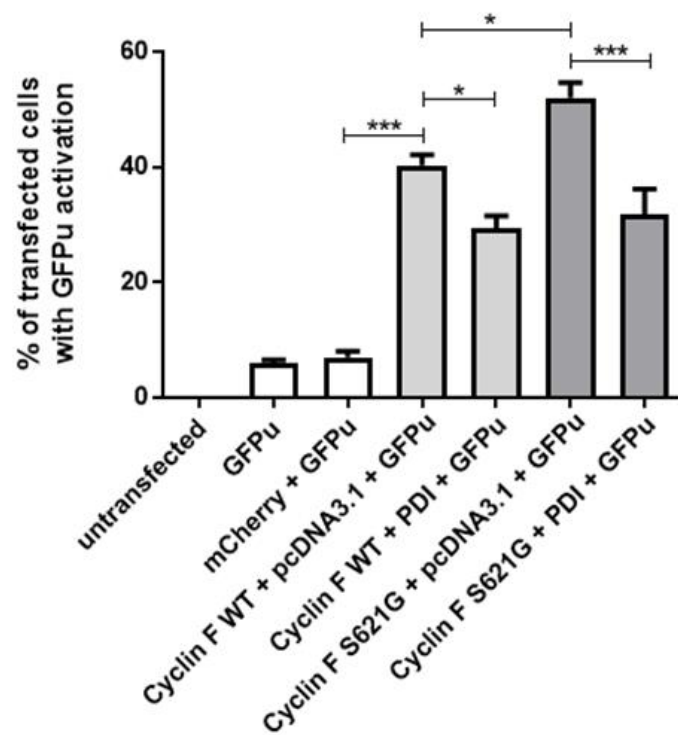
Figure 3.9: Overexpression of PDI inhibits UPS dysfunction induced by mutant and wildtype Cyclin F. A) Neuro-2A cells expressing mCherry only (first panel; mCherry) display minimal levels of GFPu activation, indicating that the proteasome is functioning normally in these cells. In contrast, more cells expressing wildtype Cyclin F (second panel; Cyclin F WT) display GFP expression, indicating GFPu activation (as shown in the second panel, column two), implying dysfunction in the UPS. However, co-expression of PDI with wildtype Cyclin F resulted in fewer cells with GFP expression (third panel; Cyclin F WT + PDI). Similarly, whilst mutant Cyclin F S621G expressing cells displayed more GFPu activation (fourth panel; Cyclin F S621G) compared to wildtype Cyclin F, this was reduced when PDI was co-expressed with mutant Cyclin F (fifth panel; Cyclin F S621G + PDI). Scale bar = 30 µM. **B)** Quantification of the cells in A); the proportion of Cyclin F expressing cells with GFPu expression, indicating UPS dysfunction. Very few untransfected cells and mCherry expressing cells displayed activation of GFPu. Significantly more cells ($p < 0.001$) expressing wildtype Cyclin F demonstrated UPS dysfunction as detected by GFPu activation, however this proportion was significantly decreased ($p < 0.05$) when PDI was co-expressed. There was a significant increase ($p < 0.05$) in the proportion of cells with GFPu activation in populations expressing mutant Cyclin F S621G, compared to wildtype Cyclin F. Moreover, this proportion was significantly reduced ($p < 0.001$) when PDI was co-expressed with mutant Cyclin F S621G. N=3, Mean ± SEM, * $p < 0.05$, *** $p < 0.001$.

3.3.7 PDI overexpression inhibits mutant Cyclin F induced nuclei condensation, indicative of apoptosis.

The activation of CHOP in cells expressing mutant Cyclin F S621G, compared to cells expressing wildtype Cyclin F, implies that the presence of the ALS mutation triggers apoptotic cell death. Our laboratory has previously demonstrated by flow cytometry and examination of nuclear morphology that mutant Cyclin F induces apoptosis in neuronal cell lines (Ragagnin et al., 2017 in preparation), and that PDI inhibits apoptosis induced by mutant SOD1 in Neuro-2A cell lines [448]. Hence, next it was examined whether overexpression of PDI was protective against apoptosis induced by mutant Cyclin F.

Neuro-2A cells were transfected with wildtype Cyclin F or Cyclin F S621G mCherry with either pcDNA3.1 empty vector or PDI-V5. After fixing and staining with Hoechst, cells were examined for the presence of condensed nuclei, indicative of apoptosis. Nuclear morphology was examined in at least 100 cells expressing Cyclin F, with or without PDI, per experiment. Cells were considered apoptotic if the nucleus was condensed (under ~5 µM in diameter) or fragmented (multiple condensed Hoechst-positive structures in one cell), following previous methods [316, 448] (Figure 3.10 A). Cells undergoing cell division were excluded from the study, as these cells can sometimes appear condensed.

Condensed nuclei, indicative of apoptosis, were rarely present in untransfected cells or cells expressing mCherry alone ($1.0\% \pm 0.6$ and $2.0\% \pm 0.6$ of cells, respectively). Approximately 10% of cells co-expressing wildtype Cyclin F with either empty vector pcDNA3.1 or PDI displayed condensed nuclei. Apoptotic nuclei were more common in cells expressing mutant Cyclin F S621G ($24.0\% \pm 3.5$), compared to those expressing wildtype Cyclin F ($p < 0.001$), consistent with previous observations. However, significantly fewer ($p < 0.001$) apoptotic nuclei were detected in cells co-expressing PDI with mutant Cyclin F S621G ($10.0\% \pm 1.5$),

indicating that PDI overexpression is protective against mutant Cyclin F -induced apoptosis

(Figure 3.10 B).

A
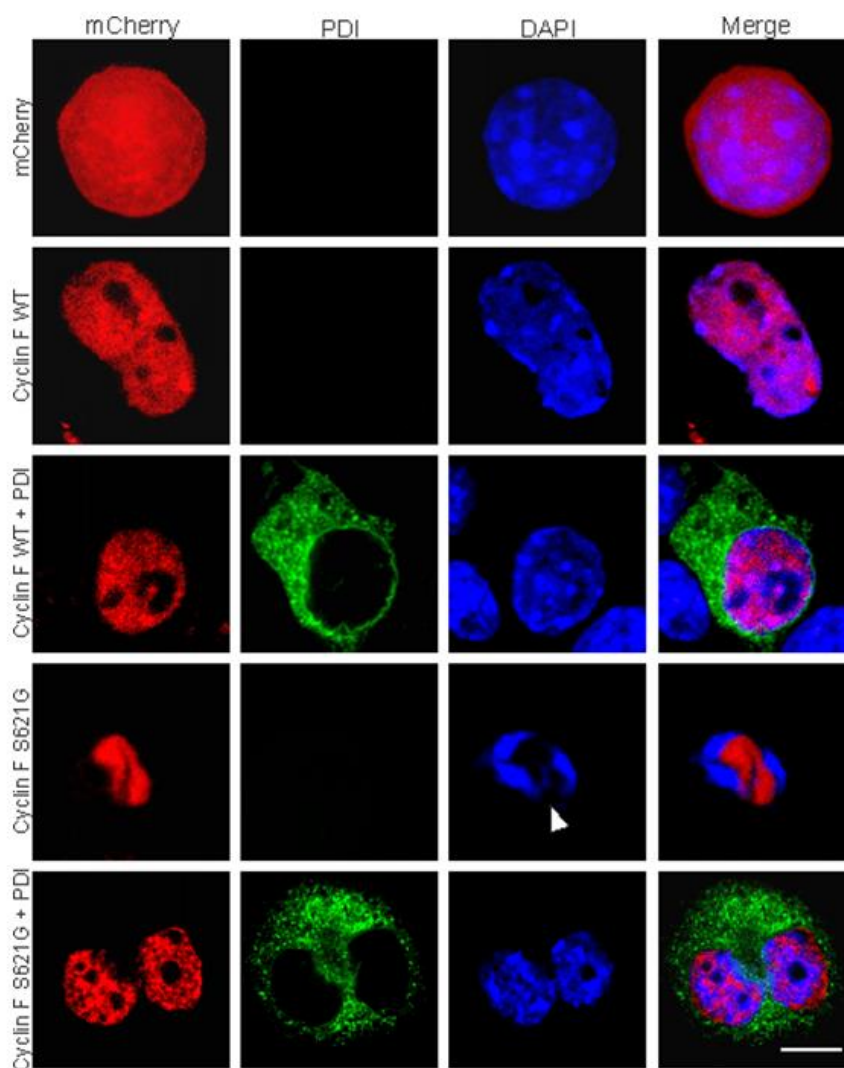
B
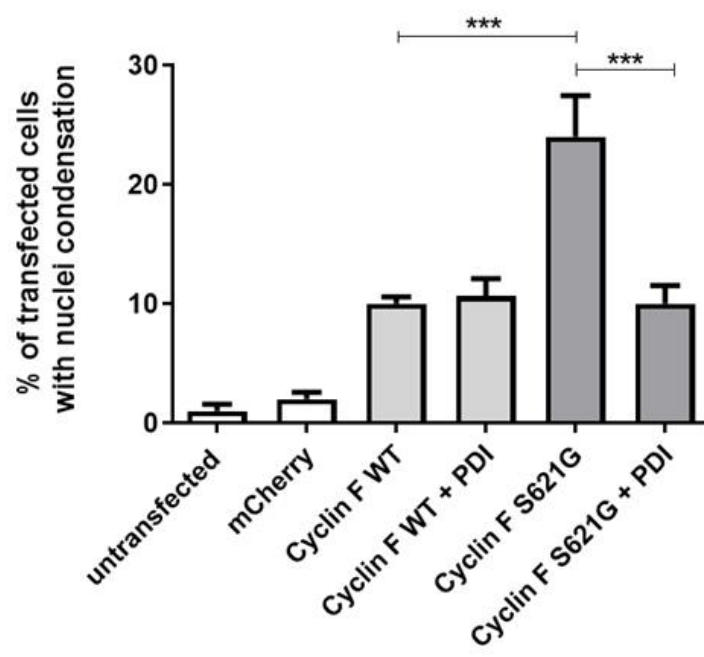
Figure 3.10: PDI overexpression inhibits mutant Cyclin F induced nuclei condensation, indicative of apoptosis. A) Neuro-2A cells expressing mCherry (first panel; mCherry) or wildtype Cyclin F (second and third panel; Cyclin F WT, Cyclin F WT + PDI) display few apoptotic nuclei, indicated by cells with regular nuclear morphology and size. In contrast, more cells expressing mutant Cyclin F S621G (fourth panel, Cyclin F S621G) display condensed nuclei (fourth panel, column three). However, the proportion of cells with apoptotic nuclei is reduced in mutant Cyclin F S621G cells co-expressing PDI (fifth panel, Cyclin F S621G + PDI). Scale bar = 30 µM. **B)** Quantification of Cyclin F expressing cells exhibiting apoptotic nuclei in A). There was a significant increase in the proportion of cells with condensed nuclei in mutant Cyclin F S621G populations, compared to those expressing wildtype Cyclin F or mCherry ($p < 0.001$). When PDI was co-expressed with Cyclin F S621G, however, there was a significant decrease in the proportion of cells with apoptotic nuclei ($p < 0.001$) to similar levels observed in wildtype Cyclin F expressing cells. N=3, Mean ± SEM, *** $p < 0.001$.

3.3.8 PDI overexpression reduces the activation of Caspase-3 induced by mutant Cyclin F.

To confirm these findings, another marker of apoptosis was examined. Caspase-3 is activated during the caspase cascade of apoptotic signalling, following activation of Bax and the release of cytochrome c from mitochondria [474]. Therefore, activation of caspase-3 indicates that a cell is undergoing apoptosis.

Neuro-2A cells were co-transfected with mCherry alone, and wildtype Cyclin F or mutant Cyclin F S621G, with either empty vector pcDNA3.1 or PDI-V5. After 72 h transfection, cells were fixed and immunocytochemistry was performed using an anti-cleaved Caspase-3 antibody. This antibody is specific for the cleaved, or activated form, of Caspase-3. Hence, nuclear immunoreactivity to Caspase-3 indicated its activation (Figure 3.11 A).

Less than 10% of untransfected cells or cells expressing mCherry displayed Caspase-3 activation. Consistent with previous findings, there was a significant increase in the proportion of cells with nuclear immunoreactivity to Caspase-3 in cells expressing mutant Cyclin F S621G (56.0% ± 3.1), compared to cells expressing wildtype Cyclin F ($p < 0.01$). However, when PDI was co-expressed with mutant Cyclin F S621G, significantly fewer cells displayed Caspase-3 activation (38.7% ± 4.4 of cells, $p < 0.05$), further confirming that overexpression of PDI is protective against apoptosis induced by ALS-associated mutant Cyclin F (Figure 3.11 B). Compared to cells expressing mCherry alone, a significantly greater ($p < 0.05$) proportion of cells expressing wildtype Cyclin F were found to be undergoing apoptosis, indicated by activation of Caspase-3 (31.3% ± 6.0), and this proportion did not significantly alter when PDI was co-expressed (37.0% ± 1.7). This result suggests that PDI is only protective against the mutant form of Cyclin F in reducing the activation of Caspase-3.

A
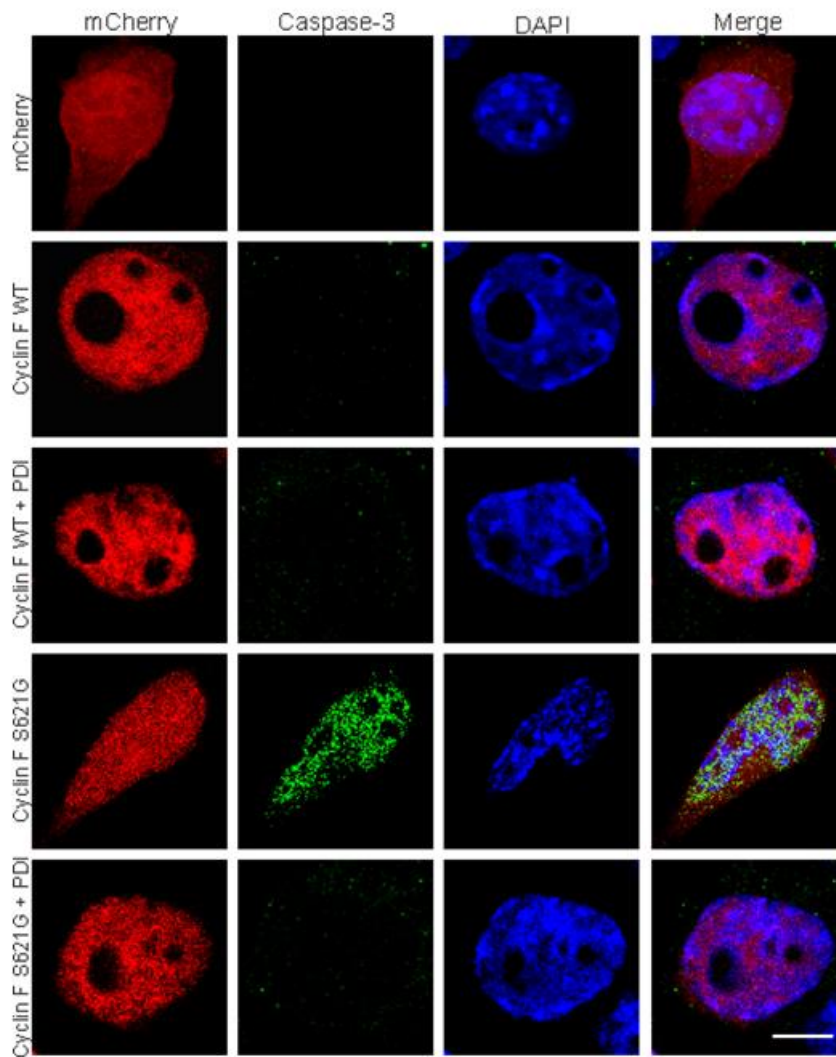
B
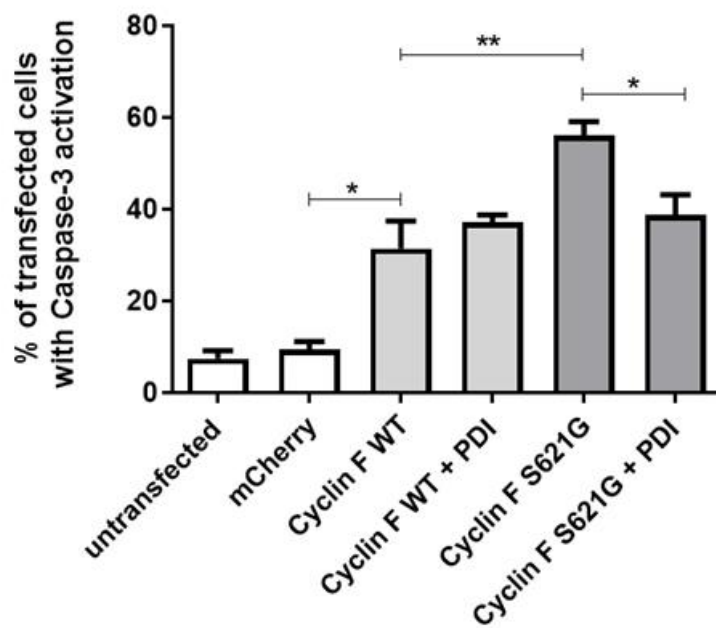
Figure 3.11: PDI overexpression inhibits activation of Caspase-3 induced by mutant Cyclin F. A) Neuro-2A cells expressing wildtype or mutant Cyclin F, and either empty vector pcDNA3.1 or PDI-V5. Few cells expressing mCherry or wildtype Cyclin F display Caspase-3 activation (first three panels; mCherry, Cyclin F WT, Cyclin F WT + PDI), whereas a greater proportion of cells expressing mutant Cyclin F S621G (fourth panel; Cyclin F S621G) exhibit Caspase-3 activation, indicated by nuclear immunoreactivity to Caspase-3 (fourth panel, column two). When PDI was co-expressed with mutant Cyclin F S621G, fewer cells displayed Caspase-3 activation (fifth panel; Cyclin F S621G + PDI). Scale bar = 30 μM. **B)** Quantification of the proportion of Cyclin F expressing cells with Caspase-3 activation in A). There was no significant difference in the proportion of cells displaying Caspase-3 activation between populations expressing wildtype Cyclin F and either empty vector pcDNA3.1 or PDI. In contrast, there was a significant increase in the proportion of mutant Cyclin F S621G expressing cells with Caspase-3 activation, compared to wildtype Cyclin F expressing cells ($p < 0.01$). The proportion of cells with Caspase-3 activation was significantly reduced when PDI was co-expressed with mutant Cyclin F S621G ($p < 0.05$). N=3, Mean ± SEM, * $p < 0.05$, ** $p < 0.01$.

3.4 Discussion

Cyclin F has recently been genetically and pathologically linked to ALS and FTD. Mutations in the gene encoding Cyclin F, *CCNF*, were identified in both patients with familial or sporadic ALS/FTD [89]. Cyclin F is a component of the SCF E3 ubiquitin-protein ligase complex, an integral part of the UPS, and it utilises its F-box domain to promote the ubiquitination of target substrates. Thus, Cyclin F is fundamental for the ubiquitination and degradation of proteins, particularly those involved in the cell cycle [453, 458].

Cyclin F exhibits a unique function compared to other ALS-associated proteins. There have been few studies examining pathogenic mechanisms linked to Cyclin F mutations, however unpublished work from our laboratory has revealed that the several mechanisms of pathogenesis implicated are similar to those of other proteins linked to ALS. Mutant forms of TDP-43 and FUS mislocalise from their normal location in the nucleus to the cytoplasm [62, 65]. Moreover, ER stress and dysfunction of ER-Golgi transport have emerged as important mechanisms linked to ALS pathogenesis that are be induced by mutant forms of SOD1, TDP-43 and FUS [355, 426, 427, 448]. Our group has recently demonstrated that a Cyclin F ALS-associated mutant, S621G, also perturbs ER homeostasis and induces cellular mechanisms similar to that of other proteins implicated in ALS. Mutant Cyclin F S621G mislocalises from the nucleus to the cytoplasm, similar to mutant TDP-43 and FUS, where it induces ER stress, inhibits ER-Golgi transport, impairs the UPS, and triggers apoptosis in cell culture (Ragagnin et al., 2017 in preparation).

Recently, in unpublished work, it has been demonstrated that PDI is protective against ER stress induced by mutants TDP-43 and FUS, mutant TDP-43 and FUS mislocalisation to the cytoplasm, ER-Golgi transport defects induced by mutant SOD1, TDP-43 or FUS, and UPS impairment induced by mutant SOD1 and TDP-43 (Parakh et al., 2017 in preparation). In

light of these findings, it was speculated in this study whether PDI would be protective against similar mechanisms induced by ALS-associated mutant Cyclin F S621G. In this chapter, it was demonstrated in cell culture models that PDI is, in fact, protective against each of these cellular mechanisms of pathogenesis induced by mutant Cyclin F S621G.

In Neuro-2A cells co-expressing PDI with mutant Cyclin F S621G, over-expression of PDI was found to be protective against mutant Cyclin F localisation to the cytoplasm, ER stress, UPS impairment, and apoptosis. Previous studies have demonstrated that although PDI is upregulated in ALS patients, it undergoes post-translational modification and is S-nitrosylated, therefore losing its normal protective function [448]. It is possible then, that over-expressing PDI may compensate for the loss of endogenous PDI activity, and thus, is able to overcome these cellular defects induced by mutant Cyclin F. Although in this study it has been demonstrated that PDI is protective against ALS-associated mutant Cyclin F, the mechanism of its protective activity remains unknown. Possible mechanisms of protection by PDI in ALS are explored further in subsequent chapters.

Cyclin F is usually localised in the centrosomes and the nucleus, however increased levels of mutant Cyclin F S621G are detected in the cytoplasm in ALS. Overexpression of PDI was found to inhibit mutant Cyclin F S621G localisation in the cytoplasm, albeit it being a normally ER resident protein. In this study, the predominant ER localisation of overexpressed V5-tagged PDI was confirmed. Interestingly, however, PDI has been shown to be redistributed away from the ER as punctate vesicular structures by reticulon proteins, and in this location PDI was observed to have higher enzymatic activity [475]. Moreover, the knockdown of Reticulon 4A and 4B accelerates axonal degeneration and early death of transgenic SOD1 G93A mice, suggesting that the redistribution of PDI away from the ER modulates disease progression [452]. In fact, PDI has been detected in the cytoplasm, nucleus and extracellular space, although the mechanisms by which PDI leaves the ER in these

instances are poorly understood [450]. These studies suggest that PDI plays a protective role outside of the ER and that the location of PDI is relevant to disease in ALS. Therefore, it may be possible that PDI interacts with mutant Cyclin F in the cytoplasm where it exhibits its protective function.

ER stress and the induction of the UPR is now regarded as a central mechanism of pathogenesis in ALS. Two markers of the UPR, XBP-1 and CHOP, were used to investigate the activity of PDI on mutant Cyclin F induced ER stress. XBP-1 is a marker of early phase UPR, and CHOP activation is an indicator of late phase UPR, whereby the UPR switches from protective to pro-apoptotic. Hence, the data obtained in this study demonstrate a protective role for PDI during both early and late phase UPR in Neuro-2A cells against ER stress induced by mutant Cyclin F S621G. Our laboratory has previously demonstrated that mutant Cyclin F triggers ER stress from either the ER or cytoplasm (Ragagnin et al., 2017 in preparation). Previous studies from our group and others have proposed that mutant SOD1 induces ER stress from the cytoplasm [355, 429] and that mutant TDP-43 triggers ER stress from the cytoplasmic face of the ER [476]. Hence it remains unclear whether mutant Cyclin F induces ER stress from either the ER or cytoplasm, or both. ER chaperones, in particular PDI, are upregulated during induction of the UPR [256]. As an oxidoreductase, PDI may function during UPR induction by refolding misfolded proteins into their correct and native conformation [477]. However, in this study, misfolded or aggregated Cyclin F was not detected in cells, nor were visible inclusions formed. It may also be that oligomers were present, however, these were not detected in this study in cells with or without PDI.

Alternatively, PDI could promote protein degradation in order to reduce protein load by facilitating ER-associated degradation (ERAD) [478]. Interestingly, our laboratory also recently demonstrated that mutant Cyclin F S621G impedes ERAD (Ragagnin et al., 2017 in preparation), so it is possible that PDI reverses this effect. Mutant Cyclin F has also been

found to abnormally increase the ubiquitination of TDP-43 and its transport to the proteasome, and thus may be accountable for wider changes in protein homeostasis [89]. Therefore, it may be possible that mutant Cyclin F accelerates the presence of abnormal misfolded proteins, such as TDP-43, and the accumulation of protein aggregates, and that PDI plays a protective role in preventing these defects, as has been previously reported for SOD1.

Several future studies follow on from this work. Our laboratory has also demonstrated that impairment of ER-Golgi transport by mutant Cyclin F S621G precedes and may induce ER stress (Ragagnin et al., 2017). Therefore, further study is warranted to determine whether overexpression of PDI is protective against ER-Golgi transport defects induced by mutant Cyclin F. However, the protective effect of PDI against ER stress in these cells suggests that this is possible. Recently, a study by Lee and colleagues (2017) demonstrated that mutant Cyclin F S621G disrupted Lys48-specific ubiquitylation, leading to the accumulation of substrates and defects in the autophagy pathway, specifically resulting in the impairment of autophagosomal-lysosome fusion [479]. These results indicate that mutant Cyclin F can indirectly impair the autophagy degradation pathway which is implicated in ALS pathogenesis. Therefore, it would also be interesting to assess whether PDI is protective against autophagy induced by mutant Cyclin F and other ALS-associated proteins. In other future studies, it would also be interesting to study the effect of PDI on other ALS-associated proteins, particularly those which induce ER-Golgi defects and ER stress, such as VAPB. PDI interacts with VAPB inclusions in a *Drosophila melanogaster* model of ALS [201], and mutations in VAPB have been shown to induce ER stress [428], implying that PDI has a broader role than previously recognised.

Several caveats of this study should be mentioned, and additional future experiments could be performed to address these points. It will be important in future studies to further investigate

the protective role of PDI against mutant Cyclin F using *in vivo* models, given the limitations of utilising cell culture only, as in this study. Mutant Cyclin F transgenic zebrafish are available in our group which display impaired motor performance and shorter, branched axons [465]. These zebrafish could therefore be injected with human PDI RNA and examined *in vivo* for improvement in motor neuron axonopathy and motor performance, which are clearly not possible to examine using cell culture models. Conditional knockout or transgenic PDI animal models could also be utilised to further investigate the role of PDI in ALS, by crossing these rodents with established mouse models, although as of yet, there are no mouse models available based on cyclin F. It would also be beneficial to repeat the experiments performed in this chapter in primary neuronal cell cultures or IPSC-derived motor neurons, to validate the results observed, as neurons would more closely mimic the physiological state of motor neurons in ALS patients. Furthermore, this study only investigated the effects of one mutant of Cyclin F, thus, it may be worthwhile to confirm the protective activity of PDI against other ALS/FTD-associated mutants of Cyclin F. Indeed, studies in our laboratory performed since the completion of this work, have demonstrated that two other ALS/FTD-associated Cyclin F mutants also induce similar cellular events to S621G, so PDI could next be over-expressed with both of these mutants in neuronal cells.

In summary, this study demonstrated that PDI is protective against mutant Cyclin F induced cellular mechanisms relevant to ALS pathogenesis in Neuro-2A cells. PDI was able to inhibit mutant Cyclin F localisation to the cytoplasm, as well as inhibit induction of ER stress and UPS impairment, and reduce the proportion of mutant Cyclin F cells undergoing apoptosis. A schematic diagram outlining these events in shown in Figure 3.12.
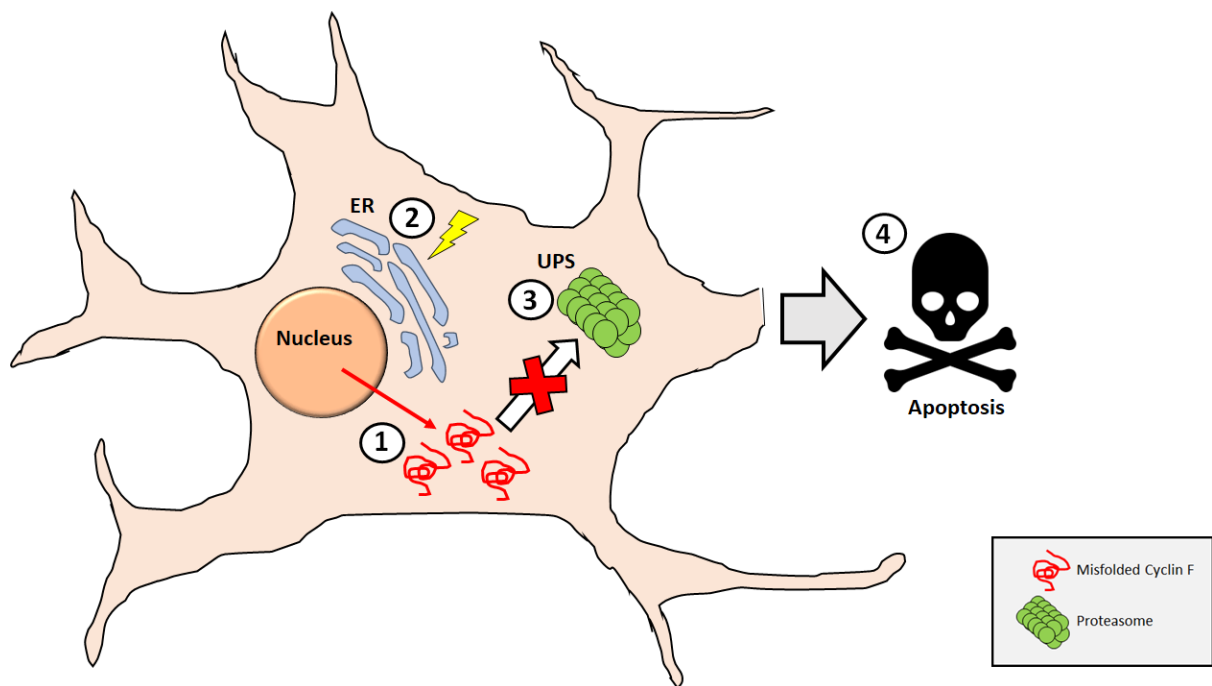
Figure 3.12: A schematic diagram illustrating the impairment of ER homeostasis, resulting in apoptosis, in neuronal cells expressing mutant Cyclin F S621G.

The Cyclin F mutation S621G triggers Cyclin F mislocalisation from the nucleus to the cytoplasm (1). Misfolded Cyclin F in the cytoplasm induces ER stress (2) and inhibition of the UPS (3), therefore resulting in apoptosis of the cell (4). PDI is protective against all four of these mechanisms of ALS pathogenesis induced by mutant Cyclin F S621G.

Hence, this study is consistent with previous studies demonstrating that PDI is broadly protective against ALS-associated proteins. Moreover, this study provides further evidence to suggest that PDI may be a potential therapeutic target in ALS, or that drugs based on PDI's protective activity may lead to novel, effective treatments. Therefore, it is imperative that the underlying mechanisms whereby PDI is protective in ALS are investigated and fully defined so that they can be applied to the design of possible therapeutic agents. In depth studies investigating these mechanisms and defining the protective characteristics of PDI are presented in the following chapters.

Chapter 4: Characterising the Protective Properties of PDI Against Misfolded Proteins in ALS

4.1 Introduction

The ER is equipped with numerous ER chaperones which assist protein quality control mechanisms, such as mediating protein folding and directing misfolded proteins to ERAD. Moreover, the ER lumen provides an optimal environment for the oxidative folding of proteins [480]. PDI is a fundamental protein localised in the ER because it can facilitate both oxidative folding, via cysteine-based redox reactions to form disulphide bonds, as well as performing general chaperone functions [481]. Previous studies in our laboratory have demonstrated that PDI's disulphide interchange activity is essential to its protective function against misfolded proteins SOD1, TDP-43 and FUS in ALS, more so than its chaperone capabilities, which was only protective against mutant FUS (Parakh et al., 2017 in preparation).

Therefore, the next series of experiments, as described in this chapter, involve investigating which of PDI's domains mediate this protective function, in the anticipation of designing small therapeutic agents based on the activity of PDI in the future. Moreover, in this chapter, the effect of PDI's chaperone activity and cytoplasmic localisation on mutant SOD1-induced cell apoptosis was examined, as well as the role of mutant SOD1's cysteine residues on the induction of ER stress. Finally, this chapter concludes with a brief study on PDI-like proteins DsbA and DsbC, which possess differing redox properties to PDI.

4.1.1 The structure and expression of PDI

Encoded by the *P4HB* gene, PDI (also known as PDI1) is a 508 amino acid, 55 kDa molecular chaperone, primarily localised within the ER lumen [481]. It is the prototype of a large thioredoxin-like family of proteins, responsible for oxidative folding, which vary in length, domain arrangement and substrate specificity [437]. PDI is a highly abundant ER protein constituting 0.8% of total cellular protein [482].

The structure of PDI consists of four domains; two catalytic domains (*a* and *a'*) and two non-catalytic domains (*b* and *b'*). The catalytic domains are separated by the non-catalytic domains and an x-linker region. PDI also contains a highly acidic C-terminus, comprising an ER-retention signal sequence (KDEL), and a signal sequence at the N-terminus. The KDEL sequence and signal sequence are responsible for retaining PDI in the ER (Figure 4.1) [483, 484]. The catalytic domains share 33.3% similarity and they contain PDI's two thioredoxin-like active site motifs, each possessing two cysteine residues (CGHC), which facilitate disulphide bond formation, reduction and isomerisation, by interacting with the thiol group of a substrate protein [483, 485]. The two active site motifs co-operate in disulphide bond formation, however, each motif comprises independent enzymatic activity in the full-length protein [486]. Moreover, the catalytic domains can only catalyse basic disulphide exchange, but all domains are required to isomerise a protein substrate that has undergone conformational change [487, 488]. The non-catalytic domains share 28% identity and are principally involved in the binding of protein substrates [489]. Indeed, studies have identified that the *b'* domain of PDI is the major substrate-binding site because of its hydrophobic pocket, although the other domains also contribute to the binding of substrate proteins [487]. In its 3D conformation, PDI is arranged in a "U" shape, in which the *a* and *a'* domain active site motifs face each other across the long sides of the "U". The *b* and *b'* domains form the

hydrophobic base for the U-shaped molecule, thought to be involved in substrate interaction [489].

Overall, the CGHC active sites modulate the redox potential of PDI, and thus regulate its catalytic activity. The redox potential of PDI is -160 mV, higher than other PDI family members, and it has a low pKa value of 6.7, which renders PDI a proficient oxidising agent in the ER [490-492].
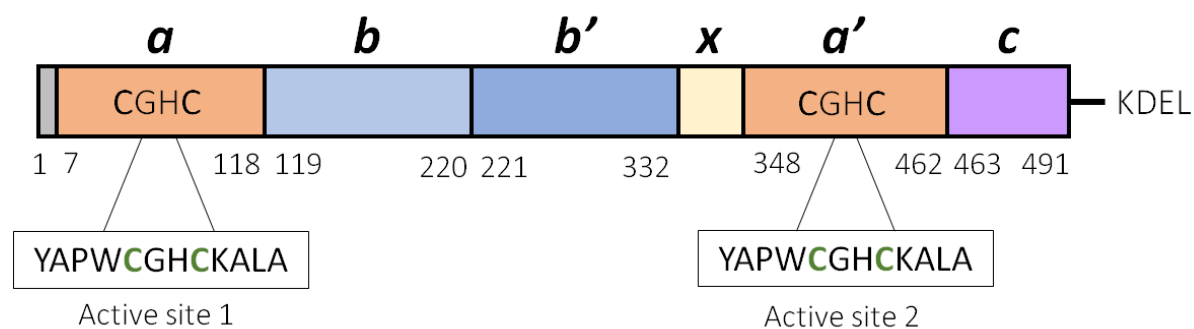
Figure 4.1: Schematic diagram illustrating the structure of PDI. PDI comprises four domains, *a, b, b'* and *a'*. The two catalytic *a* and *a'* domains (shaded in orange) possess the thioredoxin-like CGHC active site motif, responsible for oxidative protein folding. The catalytic domains are separated by the substrate-binding *b* and *b'* domains (shaded in blue) and the x-linker region (shaded in yellow). The highly acidic C-terminus (termed 'c' and shaded in purple) comprises an ER-retention signal, KDEL. The N-terminus consists of a signal sequence (shaded in grey).

4.1.2 The functions of PDI

PDI has two major functions; firstly, it is an oxidoreductase that mediates oxidative protein folding, as it is responsible for the oxidation (formation), reduction (break down) and isomerisation (rearrangement) of native disulphide bonds in proteins, via disulphide interchange activity. Secondly, PDI also possesses general chaperone capabilities [437]. These functions are described in detail below. Other secondary functions of PDI include the retro-translocation of misfolded cholera toxin from the ER to the cytoplasm by interaction with Derlin-1 [493], and the cellular export of some proteins, such as thyroglobulin [494].

4.1.2.1 PDI's chaperone function

Being a major chaperone in the ER, PDI binds to misfolded proteins to prevent their aggregation and subsequently translocates them to the cytoplasm for degradation [380]. For this purpose, PDI has the ability to distinguish between partially folded, unfolded and correctly folded substrates [495]. Moreover, PDI is able to bind misfolded proteins with high affinity and broad specificity via hydrophobic interactions with these misfolded proteins and its conformational flexibility [495, 496]. Together, these properties make PDI a highly efficient chaperone in the ER.

PDI is upregulated during ER stress where the accumulation of misfolded proteins activates the UPR. The UPR induces chaperones, such as PDI, to increase protein folding capacity and to facilitate the degradation of misfolded proteins via ERAD, demonstrating a role in protein quality control [256, 478, 497]. The *b'* domain of PDI comprises the principal substrate-binding site which binds substrate proteins, however, whilst the *b'* domain is sufficient alone to bind small substrates, the binding of larger substrates requires additional contributions from the other domains [487]. Other specific functions involving PDI's chaperone activity

have been described, such as the maintenance of the active conformation of the β subunit of collagen prolyl 4-hydroxylases [498], and stabilisation of the peptide loading complex of the major histocompatibility complex (MHC) class 1, which mediates MHC class 1 folding [499].

4.1.2.2 PDI's disulphide interchange activity

As PDI is an oxidoreductase, it is able to act as either an oxidase (to form disulphide bonds), a reductase (to break down disulphide bonds) or an isomerase (to rearrange disulphide bonds) (Figure 4.2). The catalytic *a* and *a'* domains are responsible for this disulphide interchange activity due to the presence of two cysteine residues in the thioredoxin-like CGHC motif [500, 501]. Interestingly, the *a* and *a'* domains act independently of one another, as it has been demonstrated that abolishment of one active site decreases catalytic activity by 50%, and abolishment of both active sites results in the complete removal of catalytic activity [502].

In an oxidation reaction, PDI utilises oxidative protein folding to form disulphide bonds in nascent, unfolded proteins. During this process, the substrate protein's dithiol groups (SH) are oxidised to form a disulphide (S-S). To facilitate this event, the substrate protein's reduced cysteine thiols bind to PDI's active site CGHC motif to form a PDI-substrate complex. A second reduced thiol from the substrate protein reacts with this complex and forms a disulphide with the first cysteine thiol, producing a disulphide with one another, resulting in a correctly folded protein [500]. This causes PDI to become subsequently reduced due to its donation of a disulphide bond to the substrate protein. However, it is soon re-oxidised due to the oxidising environment of the ER, via interaction with endoplasmic reticulum oxidoreductin 1 (Ero1) [503, 504].

However, oxidative protein folding is not unflawed, and at times incorrectly folded proteins can result. Hence, non-native disulphide bonds need to be corrected by either reduction or isomerisation to recover the native conformation of these proteins [505]. In a reduction reaction, whereby PDI breaks down disulphide bonds, a disulphide bond within a substrate protein is reduced to the dithiol state, via the formation of a disulphide bond with PDI's active site. For this process, PDI needs to be in a reduced state, therefore, reductants such as glutathione (GSH) and NADPH donate electrons to reduce the disulphide in PDI to a dithiol state [483]. Finally, the isomerisation, or rearrangement, of disulphide bonds is essential for the formation of abnormal disulphides by misfolded proteins, in order to return them to their native conformation. To facilitate isomerisation of disulphides, one of PDI's active sites must be in a reduced dithiol state [503]. Next, the N-terminal cysteine residue in the active site binds to the substrate protein's disulphide group, which results in an intra-molecular rearrangement within the substrate protein itself [505]. Conversely, isomerisation can be regarded as repeated cycles of reduction and oxidation [500]. These processes are illustrated in Figure 4.2.

Ultimately, impairment of PDI's disulphide interchange activity results in the accumulation of misfolded proteins, which are prone to aggregation. Furthermore, aggregation of mutant SOD1 is at least partially dependent upon disulphide bonds, because disulphide-reduced monomers and high molecular weight oligomers are present in both cell and animal models of ALS [506-508]. Hence it is possible that PDI prevents mutant SOD1 aggregation by correcting abnormal disulphide bonding.

Disulphide oxidation
(the formation of disulphide bonds)

Nascent protein

Oxidised protein

S-H   S-H

S — S

PDI

Oxidised PDI

S — S

S-H

PDI

S-H   S-H

PDI

Reduced PDI
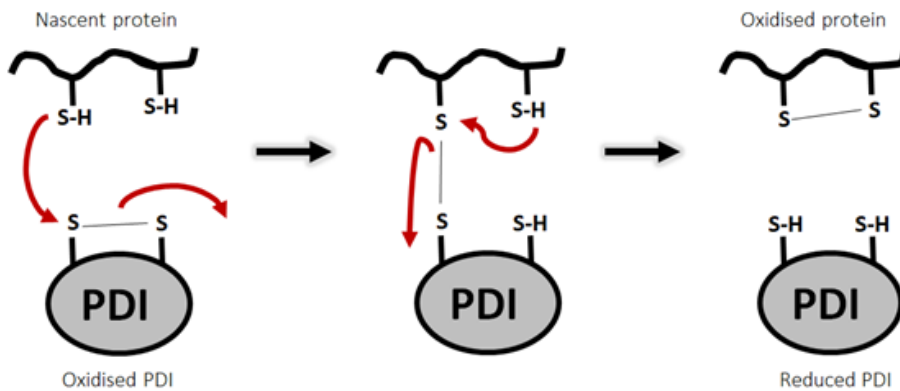
Disulphide isomerisation
(the rearrangement of disulphide bonds)

Misfolded protein

Correctly folded protein

S-H

S — S

S-H   S-H

PDI

Reduced PDI

S-H

S   S-H

S   S-H

PDI

S

S   S-H

S-H   S-H

PDI
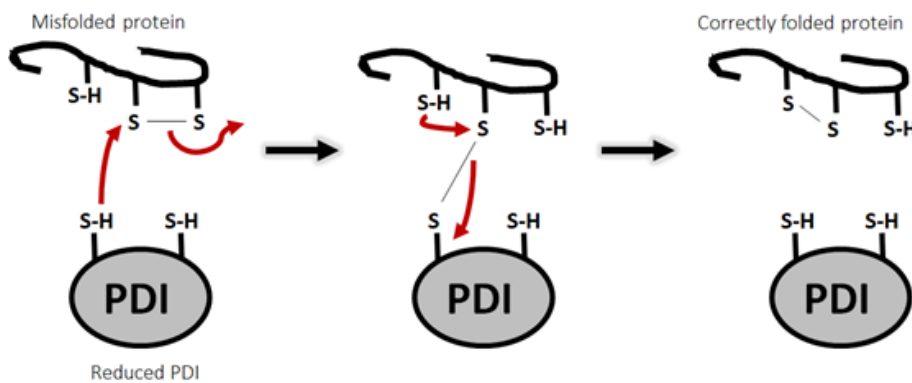
Figure 4.2: The disulphide interchange activity of PDI. Being an oxidoreductase, PDI can catalyse the oxidation (formation), reduction (break down) and isomerisation (rearrangement) of disulphide bonds in nascent and misfolded proteins via the cysteine residues of its thioredoxin-like active site motif (CGHC). This ensures the correct and native conformation of substrate proteins.

4.1.3 PDI and SOD1: Non-native disulphide bonding in mutant SOD1 aggregation

Misfolded SOD1-containing aggregates in motor neurons are a common feature of mutant SOD1-mediated ALS [263]. Previous studies have demonstrated that PDI is present within abnormal inclusions found in SOD1 G93A rodents, motor neuronal cells and ALS patients [254], implying that PDI may function as a cellular defence against SOD1 misfolding and aggregation. Consistent with this notion, it has been demonstrated in our laboratory that over-expression of PDI in motor neuron-like cell lines significantly reduced the percentage of cells expressing SOD1 inclusions in a dose dependent manner [448]. Moreover, knockdown of PDI in these cell lines using siRNA increased the proportion of cells bearing mutant SOD1 inclusions [448], indicating an important role for PDI in protecting the cell from mutant SOD1 protein aggregation.

The SOD1 protein consists of four cysteine residues at amino acid positions Cys-6, Cys-57, Cys-111 and Cys-146. The Cys-57 and Cys-146 residues form an intra-subunit disulphide bond, which is necessary for the stabilisation and correct folding of SOD1 [509]. The loop containing Cys-57 is involved in the formation of the non-covalently bonded dimer interface, thus dissociation of this disulphide bond results in destabilisation of the physiological SOD1 homodimer [98]. Interestingly, several studies have demonstrated that cellular stressors in ALS transgenic mouse models induce abnormal disulphide bonding between Cys-6 and Cys-111 residues, which normally do not form disulphide bonds, leading to the presence of high molecular weight oligomers containing non-native disulphide-bonded aggregates. These aggregates have been observed in the spinal cords of mutant SOD1 transgenic mice and also in ALS cellular models [506, 510, 511]. Furthermore, it has been shown that mutagenesis of Cys-6 and Cys-111 to serine inhibits mutant SOD1 aggregation, inclusion formation and cell toxicity [510, 512], although this has been disputed by other studies [513]. Moreover, the reduction of non-native disulphide bonds in mutant SOD1 can inhibit aggregation in neuronal

cell cultures [512], suggesting that the reduction or isomerisation of aberrant non-native SOD1 disulphide bonds via PDI may be protective against mutant SOD1-induced pathogenic mechanisms. Additionally, by preventing the formation of non-native disulphide bonds in mutant SOD1, PDI could be protective in ALS.

If PDI interacts directly with SOD1, this interaction implies a redistribution of either PDI to the cytoplasm, or SOD1 to the ER. Interestingly, PDI has been observed in non-ER locations, including the cytoplasm [450]. In fact, acute ER stress can cause leakage of PDI from the ER to the cytoplasm, suggesting that this could be how PDI interacts with SOD1 [514].

4.1.4 The cellular locations of PDI

Although primarily localised in the ER, PDI has been identified in other sub-cellular compartments, although the exact mechanisms by which PDI leaves the ER in these situations is poorly understood. PDI has been detected in the cytosol, endosomes and plasma membrane, where it acts as a reductase, due to the reducing environment of these cellular locations [515]. PDI is also localised in the nucleus, extracellular space and on the cell surface, where it facilitates several different functions [450, 516].

PDI is involved in the metabolism of insulin in the cytoplasmic fraction of human liver cells [517]. PDI is also expressed in the cytoplasm of leukocytes [518] and in the cytoplasm of glial astrocytes where it regulates actin polymerisation [519]. Cell surface PDI is involved in cell signalling through its interaction with membrane receptors, however it remains unclear how PDI is transported to this location [520, 521]. At the cell surface, PDI is also involved in the adhesion of leukocytes, where the reducing activity of PDI assists in the interaction with thyroid stimulating hormone receptor of thyrocytes [494, 522]. Moreover, cell surface PDI facilitates thrombus formation on the surface of platelets [523], and it can have detrimental

effects in this location, such as mediating the entry of pathogens during infectious disease [524, 525].

Furthermore, PDI has been detected in the nuclear matrix of human lymphocytes and monocytes [526]. Nuclear PDI has been linked to several transcription factors as it activates the binding of immunoglobulin enhancer binding factors (E2A) and NF-κB via redox regulated mechanisms [527, 528]. Together, these studies support the hypothesis that PDI in a non-ER location interacts with SOD1, and they demonstrate that PDI is secreted from a variety of cell types. For example, PDI is secreted from hepatocytes, pancreatic exocrine cells and endothelial cells, although the biological relevance of the presence of PDI in these secretions is unclear [521, 529, 530].

In 2009, a study identified that reticulons, a family of ER membrane proteins, are essential modulators of PDI subcellular localisation, and they mediate its redistribution to the cytoplasm. Interestingly, deletion of Reticulon-4A accelerates motor neuron degeneration in mutant SOD1 transgenic mouse models, implying that the cellular location of PDI is relevant to disease in ALS [452]. Consistent with this study, redistribution of PDI increases its enzymatic activity and reduces the intracellular levels of PDI which are aberrantly modified by S-nitrosylation [475].

4.1.5 The S-nitrosylation of PDI

Although PDI is normally protective against protein misfolding, under conditions of cellular stress, such as in ALS, PDI can become aberrantly modified by post-translational modification. Whilst the ER is capable of enduring mild insults of stress, a build-up of ROS and reactive nitrogen species can result in oxidative and nitrosative stress [531]. Typically, oxidative and nitrosative stress increases in cells throughout the ageing process due to a

decline in antioxidant defences, however neurons are particularly vulnerable to these conditions. This also renders them susceptible to late-onset neurodegenerative disorders, such as ALS. Moreover, proteostasis in the ER also declines with age, resulting in higher levels of stress [532].

The excessive generation of nitric oxide (NO) has been implicated in ALS and in other neurodegenerative diseases, including AD and PD. In these disorders, and during conditions of elevated nitrosative stress, the active sites of PDI undergo a post-translational modification called S-nitrosylation [500]. S-nitrosylation involves the covalent addition of an NO group to one or both cysteine thiols of the active site. This modification inhibits the normal disulphide interchange activity of PDI and it results in the accumulation of misfolded proteins [500]. Previous studies have demonstrated that the levels of S-nitrosylated PDI in the lumbar spinal cords of ALS patients are five-fold greater compared to controls [448], suggesting that although PDI is normally protective, it is functionally inactive in ALS. S-nitrosylated PDI is also evident in the brains of AD and PD patients [533]. In addition to inhibiting the function of PDI, S-nitrosylation is linked to the redistribution of PDI away from the ER by reticulon proteins [475]. This is associated with increased mutant SOD1 aggregation, induction of ER stress and resultant neuronal cell death [534].

4.1.6 The PDI family of proteins

The PDI family of proteins comprises more than 21 members that share several similar features, including a signal sequence and a thioredoxin-like domain. These domains may present as a catalytically active *a* or *a'* domain comprising a CXXC active site motif, or as a catalytically inactive *b* or *b'* domain [535, 536]. The most common active site motif is CGHC, present in PDI, ERp57 and ERp72. Moreover, sequence alignment reveals that these

three proteins are the most similar [537, 538]. Although it is speculated that all PDI family members possess disulphide interchange activity, only specific members have actually demonstrated this activity *in vivo* [539]. In addition, only a number of family members have specifically displayed chaperone-like capabilities, such as facilitating misfolded protein degradation via ERAD [540]. The other members of the PDI family are related through evolution, rather than function [536]. Ultimately, PDI family members primarily vary in their substrate specificity and enzymatic activity [485], due to their contrasting redox potentials, which is determined by the two residues between the active site cysteines [540].

4.1.6.1 ERp57

ERp57, which is also known as PDIA3, is the second most abundant soluble protein after PDI localised in the ER. It can also localise in other non-ER compartments such as the cytosol, mitochondria, cell surface and nucleus [541]. Sequence alignment reveals that ERp57 is the most similar PDI family member to PDI [537]. It shares the same active site motif (CGHC) and the same domain architecture (*a-b-b'-a'-c)* as PDI, as well as being an oxidoreductase similar to PDI. However, ERp57 mediates disulphide bond formation primarily in glycosylated proteins, by interacting with the ER-resident lectins calnexin (CNX) and calreticulin (CRT), as part of the CNX/CRT cycle [542]. This cycle selectively recruits newly synthesised glycoproteins, thus promoting their folding by exposing them to oxidoreductases, such as ERp57 [543]. Moreover, ERp57 has a lower redox potential than PDI, rendering it more reducing in nature [544]. Like PDI, ERp57 is upregulated in spinal cords of mutant SOD1 transgenic mouse models, in human patient spinal cords, in the CSF and blood of ALS patients [254, 451]. Recent reports have also demonstrated that ERp57 has novel roles in the nervous system, in enhancing neurite outgrowth, facilitating axonal regeneration, regulating the expression of synapse proteins, inhibiting neuromuscular junction defects, and ensuring normal muscle innervation and function [441].

4.1.7 Dsbs – prokaryotic PDI-like proteins

Bacteria express a spectrum of disulphide-bonded virulence factors, such as secreted toxins, adhesins, pili, and secretion systems [545]. Many of these proteins must be oxidatively folded to be functionally active [546]. As PDI comprises the machinery that catalyses oxidative protein folding in eukaryotes, the Dsb (disulphide bond) system is the equivalent bacterial machinery that facilitates oxidative protein folding in prokaryotes. The Dsb system consists of several enzymes that form two distinct pathways in the periplasm; the oxidative pathway which introduces disulphide bonds into substrate proteins, and the isomerisation pathway which rearranges incorrectly folded, non-native disulphide bonds, thereby correcting misfolded substrates to their native conformation [547].

4.1.7.1 The Dsb oxidation pathway

Two Dsb proteins, DsbA and DsbB, comprise the oxidative pathway in *E. coli.* DsbA is an oxidase and it is therefore responsible for the introduction of disulphide bonds into nascent proteins that are translocated to the periplasm [548, 549]. The structure of DsbA consists of a thioredoxin-like domain, a common structural fold observed in thiol-disulphide oxidoreductases, and an inserted helical domain [550, 551]. Consistent with thioredoxin-like proteins, DsbA contains a CXXC active site motif of CPHC, and a cis-proline residue that is closely associated with the active site motif , which plays a key role in the function of the protein [552]. DsbA has a redox potential of -120 mV, rendering it one of the most oxidising proteins yet identified [492]. DsbA displays broad specificity and it reacts quickly with unfolded nascent proteins via cysteines in its CPHC motif [553]. In the process of oxidising substrate proteins, the two cysteines in the CPHC motif become subsequently reduced. Afterward, DsbB catalyses the re-oxidation of these cysteines, thereby restoring DsbA to its

active oxidised form, in order to interact with another unfolded substrate protein [554, 555]. Interestingly, DsbB has a strict substrate specificity for DsbA and it does not participate in disulphide exchange reactions with reduced unfolded proteins [547].

4.1.7.2 The Dsb isomerisation pathway

Similar to protein folding in eukaryotic cells, the Dsb oxidation pathway is not unflawed, and it can give rise to non-native disulphide substrates. To avoid this, the Dsb isomerisation pathway, comprising DsbC and DsbD, corrects non-native disulphides [547]. DsbC is an isomerase, with a redox potential of approximately -140 mV [492], which rearranges non-native disulphides in misfolded bacterial proteins introduced by either DsbA [556] or under conditions of copper oxidative stress [557]. No functional role has been described for DsbG, another isomerase protein in *E. coli*, with a redox potential of approximately -130 mV [492]. Both DsbC and DsbG contain a thioredoxin-like domain with a CXXC motif in the active site (CGYC in DsbC and CPYC in DsbG), which is adjacent to the cis-proline residue. In contrast to DsbA, DsbC and DsbG are linked to an amino-terminal dimerization domain, resulting in a V-shaped homodimer [558, 559]. This dimerization provides a hydrophobic pocket where misfolded substrate proteins can bind, however this prevents interaction with DsbB [554]. DsbC and DsbG are maintained in their active reduced form by interaction with DsbD [560]. Interestingly, DsbC possesses a chaperone function, similar to PDI [561].

4.1.8 Aims of this chapter

PDI is a unique protein, possessing two fundamental properties; an oxidoreductase facilitating disulphide interchange activity, as the prototype of the major groups of enzymes mediating protein disulphide bond formation, and an ER chaperone. In Chapter 3 it was demonstrated that PDI is protective against mutant forms of a novel ALS-associated protein, Cyclin F, in neuronal cells, suggesting that PDI's protective activity is broader than its protective effect against the more well-studied ALS mutant proteins; SOD1, TDP-43 and FUS. Therefore, therapeutics based on PDI's activity may be beneficial in the treatment of ALS. Previous studies undertaken in our laboratory have verified that PDI's disulphide interchange activity is required for PDI's protective function, rather than its chaperone capabilities (Parakh et al., 2017 in preparation), implying that therapeutics based on the disulphide interchange activity would be most effective against pathogenic mechanisms of ALS. However, full-length PDI, being a 55kDa protein, is too large to be delivered in the brain as an effective therapeutic agent by itself.

Thus, the aim of this chapter was to investigate which of PDI's domains were essential for PDI's protective activity. To perform these studies, PDI domain mutants were created, to assess the individual protective activity of each domains. Furthermore, eukaryotic forms of Dsb proteins, DsbA and DsbC, were also synthesised to investigate the role of redox potential on protective activity. The effect of mutant SOD1's cysteine residues on ER stress activation was also examined to determine if PDI's interaction with SOD1 is protective against mutant SOD1 protein misfolding, and thus, ER stress. Finally, the effect of PDI's chaperone function and the cytoplasmic localisation of PDI were examined for their protective effect against mutant SOD1-induced apoptosis.

4.2 Materials/Methods

4.2.1 Constructs used in this chapter

A pcDNA3.1 vector, containing full-length PDI and a V5 tag, was provided by Dr. Neil Bulleid, University of Glasgow, UK. Wildtype and mutant A4V constructs encoding EGFP-tagged human SOD1 at the C-terminus were as previously described [265]. Wildtype and mutant Q331K constructs encoding EGFP-tagged human TDP-43 at the N-terminus was a gift from Professor Benjamin Wolozin, Boston University, USA, and GFP FUS (wildtype and mutant R521G) vectors were provided by Dr. Justin Yerbury, University of Wollongong, Australia. The EGFP-SOD1 A4V cysteine mutants and the PDI QUAD mutant constructs were generated by Masters students in the laboratory (Ray Ma, Navya Bilia). The constructs encoding cytoplasmic PDI (wildtype and QUAD) were synthesised by a post-doctoral researcher in the laboratory (Sonam Parakh), using site-directed mutagenesis. All DNA plasmids used in this chapter were verified by DNA sequencing before use.

4.2.2 Analysing Bax activation vs. Bax recruitment to the mitochondria

To determine the proportion of transfected cells in which Bax is activated or recruited to mitochondria, immunocytochemistry using anti-Bax antibodies was performed (section 2.4.2). To examine Bax recruitment, cells were permeabilised with 0.1 % (v/v) Triton-100 in PBS for 10 min to permeabilise the cell membrane. To analyse for Bax activation, cells were permeabilised with CHAPS buffer for 10 min to lyse the nuclear membrane.

4.2.3 Generating PDI domain constructs

To determine the protective effects of the individual domains of PDI, three constructs were designed and synthesised by Genscript (Piscataway, New Jersey, USA). The constructs were based on the two individual '*a'* domains and the '*b'* domains of PDI, as shown in Table 4.1.

TABLE 4.1. PDI domain variants

Variant name	Modification
PDIa	Remove *b*, *b'*, *a'* and *c* domains
PDIbb'	Remove *a*, *a'* and *c* domains
PDIa'	Remove *a*, *b*, *b'* and *c* domains

Constructs were designed so that the unwanted domains were removed from full-length PDI, whilst retaining the signal sequence at the N-terminus and KDEL ER-retention signal at the C-terminus. A V5 tag was added to the C-terminus of each construct. Once constructs were received, transformation into *E. coli* was performed (section 2.2.4), followed by a midi-scale plasmid DNA production (section 2.26). The resulting plasmids were sequenced to ensure the desired mutations had been incorporated and that specific domains had been removed.

4.2.4 Generating Dsb constructs for transfection into Neuro-2A cells

To express DsbA and DsbC in mammalian cells, new constructs were designed and synthesised by Genscript. DNA sequences encoding Dsbs were inserted into a pcDNA3.1 backbone, with PDI's signal sequence at the N-terminus of the Dsb sequence, and PDI's KDEL ER-retention signal at the C-terminus of the sequence. A V5 tag was added to the C-terminus of both constructs. Once constructs were received, transformation into *E. coli* and a midi-scale plasmid DNA preparation was performed, followed by sequencing of the plasmids to confirm that the desired constructs contained the expected sequence.

4.3 Results

4.3.1 PDI-V5 is co-expressed in almost all cells transfected with either EGFP-SOD1, EGFP-TDP-43 or GFP FUS

The experiments described in this chapter examine the effect of PDI when co-expressed in neuronal cells with ALS-associated proteins, SOD1, TDP-43 and FUS. Hence, the percentage of cells co-expressing PDI with each of these three proteins was primarily quantified. Previous studies in our laboratory demonstrated that almost all cells co-expressing SOD1 also expressed PDI, so it was expected that these experiments would yield the same results.

Neuro-2A cells were transfected with constructs encoding PDI-V5 and either EGFP-SOD1, EGFP-TDP-43, or GFP FUS for 72 h, before fixing and performing immunocytochemistry. An anti-V5 primary antibody was used with an Alexa Fluor 568-tagged secondary antibody to detect the V5 tag and thus, analyse PDI expression. Expression of SOD1, TDP-43 or FUS was verified by examining the green fluorescence from GFP by fluorescent microscopy (Figure 4.3). Fluorescent microscopy was used to examine at least 100 cells expressing either SOD1, TDP-43 or FUS and they were further analysed for co-expression with PDI. The overall transfection efficiency of the constructs encoding SOD1, TDP-43 or FUS was found to be approximately 75-80% in Neuro-2A cells when observed 72 h post transfection. Quantification demonstrated that approximately 99% of mutant SOD1 expressing cells, 97% of mutant TDP-43 expressing cells, and 98% of mutant FUS expressing cells also co-expressed PDI. Therefore, it was assumed in all further experiments in which PDI-V5 was not examined by immunocytochemistry using a V5 antibody, that expression of either SOD1, TDP-43 or FUS in a cell also reflected co-expression with PDI.
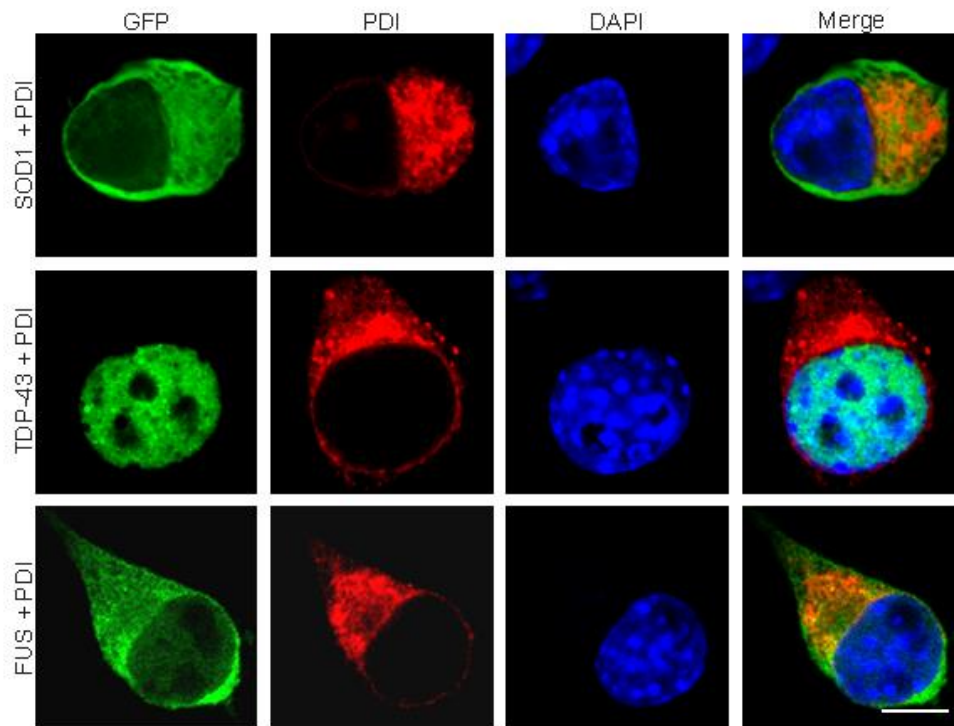
Figure 4.3: Wildtype PDI-V5 is co-expressed in almost all Neuro-2A cells co-transfected with either EGFP-SOD1, TDP-43 or FUS. A) Neuro-2A cells were transfected with either EGFP-SOD1, TDP-43 or FUS (left column, GFP) and PDI-V5 (second column, PDI). Cells were stained with Hoechst to visualise nuclei (third column, DAPI). The merge column illustrates co-expression of PDI with either SOD1, TDP-43 or FUS in a cell. Scale bar = 20 μM.

The effect of the individual domains of PDI on its protective activity.

The first half of this chapter primarily focuses on the individual domains of PDI and their role in mediating PDI's protective activity against selective ALS-associated cellular mechanisms of pathogenesis. The two catalytic domains, *a* and *a'*, were analysed, as well as the non-catalytic domains, *bb'*. Previous studies have demonstrated that PDI's catalytic domains, containing the CGHC active site, are responsible for PDI's disulphide interchange activity. On the other hand, the *bb'* domains of PDI were selected as they contain the hydrophobic cleft responsible in substrate binding, thus play a fundamental role in facilitating PDI's chaperone function [483]. These constructs were synthesised so that the unwanted domains were eliminated from the cDNA sequence, leaving only the domain to be examined. Constructs were inserted into the pcDNA3.1 vector and a V5 tag was attached to the C-terminal of the sequence. The activity of the PDI domain mutants was examined in cells expressing mutant ALS proteins, SOD1, TDP-43 and FUS. The sequences for the three domain constructs are shown in Figure 4.4.

a domain construct

Start codon

<u>ATG</u>CTGCGCCGCGCTCTGCTGTGCCTGGCCGTGGCCGCCCTGGTGCGC — PDI signal sequence

BamHI ← GCC**GGATCC**GACGCCCCCGAGGAGGAGGACCACGTCCTGGTGCTGCG
GAAAAGCAACTTCGCGGAGGCGCTGGCGGCCCACAAGTACCTGCTGG
TGGAGTTCTATGCCCCTTGGTGTGGCCACTGCAAGGCTCTGGCCCCTG
AGTATGCCAAAGCCGCTGGGAAGCTGAAGGCAGAAGGTTCCGAGATC
AGGTTGGCCAAGGTGGACGCCACGGAGGAGTCTGACCTGGCCCAGC
AGTACGGCGTGCGCGGCTATCCCACCATCAAGTTCTTCAGGAATGGAG
ACACGGCTTCCCCCAAGGAATATACAGCTGGCAGAGAGGCTGATGACA
TCGTGAACTGGCTGAAGAAGCGCACGGGC**GGATCC**GGTAAGCCTATC — BamHI

V5 tag ← <u>CCTAACCCT</u>CTCCTCGGTCTCGATTCTACGAAAGATGAACTG<u>TAA</u>

KDEL   Stop codon

a' domain construct

Start codon

<u>ATG</u>CTGCGCCGCGCTCTGCTGTGCCTGGCCGTGGCCGCCCTGGTGCGC — PDI signal sequence

BamHI ← GCC**GGATCC**GTCAAGGTGCTTGTTGGGAAGAACTTTGAAGACGTGGC
TTTTGATGAGAAAAAAAAACGTCTTTGTGGAGTTCTATGCCCCATGGTGT
GGTCACTGCAAACAGTTGGCTCCCATTTGGGATAAACTGGGAGAGAC
GTACAAGGACCATGAGAACATCGTCATCGCCAAGATGGACTCGACTGC
CAACGAGGTGGAGGCCGTCAAAGTGCACAGCTTCCCCACACTCAAGT
TCTTTCCTGCCAGTGCCGACAGGACGGTCATTGATTACAACGGGGAAC
GCACGCTGGATGGTTTTAAGAAATTCCTGGAGAGCGGTGGCCAGGAT
GGGGCAGGG**GGATCC**GGTAAGCCTATCCCTAACCCTCTCCTCGGTCTC — BamHI
GATTCTACGAAAGATGAACTG<u>TAA</u> — V5 tag

KDEL   Stop codon

bb' domain construct

Start codon

<u>ATG</u>CTGCGCCGCGCTCTGCTGTGCCTGGCCGTGGCCGCCCTGGTGCGC — PDI signal sequence

BamHI ← GCC**GGATCC**GCCACCACCCTGCCTGACGGCGCAGCTGCAGAGTCCTT
GGTGGAGTCCAGCGAGGTGGCTGTCATCGGCTTCTTCAAGGACGTGG
AGTCGGACTCTGCCAAGCAGTTTTTGCAGGCAGCAGAGGCCATCGAT
GACATACCATTTGGGATCACTTCCAACAGTGACGTGTTCTCCAAATACC
AGCTCGACAAAGATGGGGTTGTCCTCTTTAAGAAGTTTGATGAAGGCC
GGAACAACTTTGAAGGGGAGGTCACCAAGGAGAACCTGCTGGACTTT
ATCAAACACAACCAGCTGCCCCTTGTCATCGAGTTCACCGAGCAGACA
GCCCCGAAGATTTTTGGAGGTGAAATCAAGACTCACATCCTGCTGTTC
TTGCCCAAGAGTGTGTCTGACTATGACGGCAAACTGAGCAACTTCAAA
ACAGCAGCCGAGAGCTTCAAGGGCAAGATCCTGTTCATCTTCATCGAC
AGCGACCACACCGACAACCAGCGCATCCTCGAGTTCTTTGGCCTGAAG
AAGGAAGAGTGCCCGGCCGTGCGCCTCATCACCCTGGAGGAGGAGAT
GACCAAGTACAAGCCCGAATCGGAGGAGCTGACGGCAGAGAGGATC
ACAGAGTTCTGCCACCGCTTCCTGGAGGGC**GGATCC**GGTAAGCCTATC — BamHI

V5 tag ← <u>CCTAACCCT</u>CTCCTCGGTCTCGATTCTACGAAAGATGAACTG<u>TAA</u>

KDEL   Stop codon

Figure 4.4: The sequences of the PDI *a*, *a'* and *bb'* domain constructs. The PDI domain constructs contain PDI's signal sequence at the N-terminus, the domain of interest in between two BamHI restriction recognition sites, followed by a V5 tag, PDI's KDEL ER-retention sequence and stop codon at the C-terminal.

4.3.2 Localisation of PDI domain mutants

To ensure that the individual PDI domain mutant proteins exhibited similar localisation to PDI, the localisation of the V5-tagged proteins was analysed in Neuro-2A cells using confocal microscopy. This was important to investigate because previous studies have shown that the localisation of PDI is important in its protective activity. Cells were transfected with either the PDI *a* domain, *a'* domain or *bb'* domain constructs for 24 h before immunocytochemistry using an anti-V5 tag antibody and an anti-calreticulin antibody to probe for ER-resident protein, calreticulin, was performed. All three PDI domain mutants co-localised with calreticulin in all transfected cells examined, indicating all three mutant proteins were expressed in the ER (Figure 4.5). This result was expected due to the presence of PDI's signal sequence and KDEL sequence, which target or retain proteins in the ER, respectively.
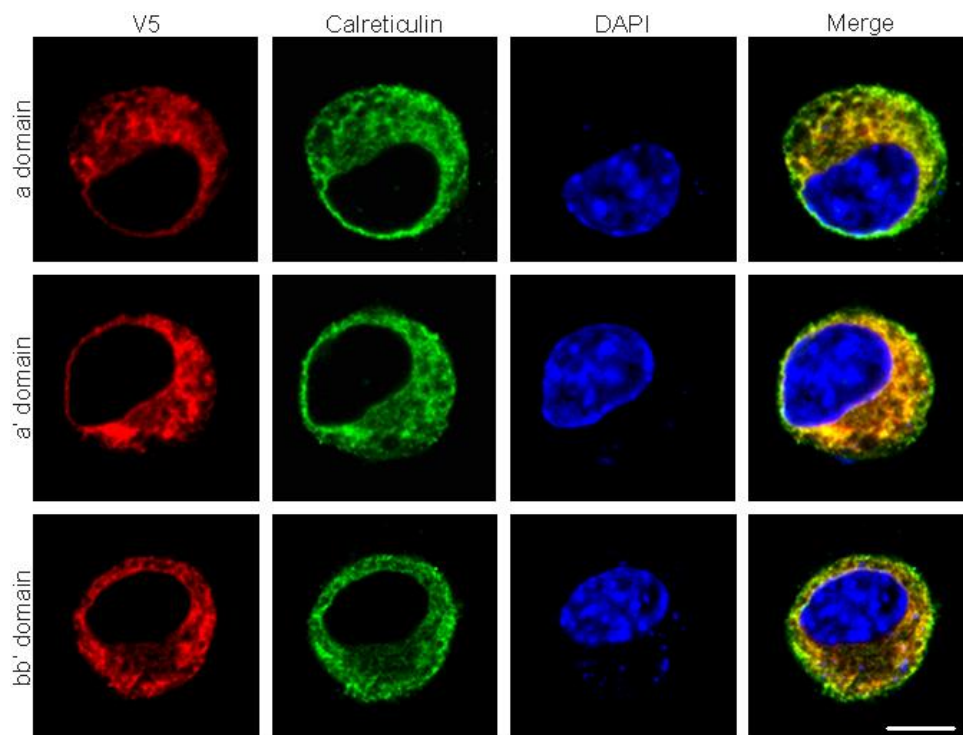
Figure 4.5: The PDI *a* domain, *a'* domain and *bb'* domain mutants are localised in the ER of Neuro-2A cells. Neuro-2A cells were transfected with pcDNA3.1 vectors containing either the PDI *a* domain, *a'* domain or *bb'* domain mutants tagged with V5 (left column; V5). After a 24 h transfection, cells were fixed and immunocytochemistry was performed using antibodies for the V5 tag and calreticulin (second column from left), and the nucleus was stained with Hoechst (third column). The yellow in the merge column (last column) illustrates co-localisation of the PDI domain mutants and calreticulin, demonstrating that these proteins are localised in the ER, as expected. Scale bar represents 30 µM.

The PDI domain mutants and their effect on mutant SOD1

The PDI domain mutants were first examined in Neuro-2A cells expressing mutant SOD1 A4V. Their activity on SOD1 inclusion formation, mutant SOD1-induced ER stress and apoptosis was investigated in the following experiments. In this section, the effect of SOD1's four cysteine residues on ER stress is also investigated. There is also an investigation into PDI's cellular location and its loss of active site on mutant SOD1-induced apoptosis.

4.3.3 PDI domain mutants are co-expressed in almost all cells expressing EGFP-SOD1.

The PDI domain mutants were first analysed in cells expressing mutant SOD1, therefore, the co-transfection efficiency of the PDI domain mutants and SOD1 was first examined in Neuro-2A cells. Cells were transfected with EGFP-SOD1 and either the PDI *a* domain, PDI *a'* domain or PDI *bb'* domain constructs for 72 h, before fixing and performing immunocytochemistry using an anti-V5 antibody and staining the nuclei with Hoechst. Co-transfection was verified by fluorescent microscopy, examining EGFP expression (green) from SOD1 and performing immunocytochemistry with an Alexa Fluor 568-tagged secondary antibody to detect the V5 tag (Figure 4.6). The overall transfection efficiency of SOD1 was approximately 75-80% in Neuro-2A cells when observed 72 h post transfection, similar to previous observations. For each of the three replicate experiments, fluorescent microscopy was used to examine at least 100 SOD1-expressing cells and these cells were further analysed for co-expression with the PDI domain mutant proteins. Quantification revealed that approximately 95% of SOD1 expressing cells also co-expressed the PDI *a* domain, 94% co-expressed the PDI *a'* domain, and 96% co-expressed the PDI *bb'* domain mutant. Therefore, it was assumed in all further experiments that detection of SOD1

153

expression reflected co-expression of both SOD1 and the PDI domain mutants when they were co-transfected and immunocytochemistry using a V5 antibody was not performed.
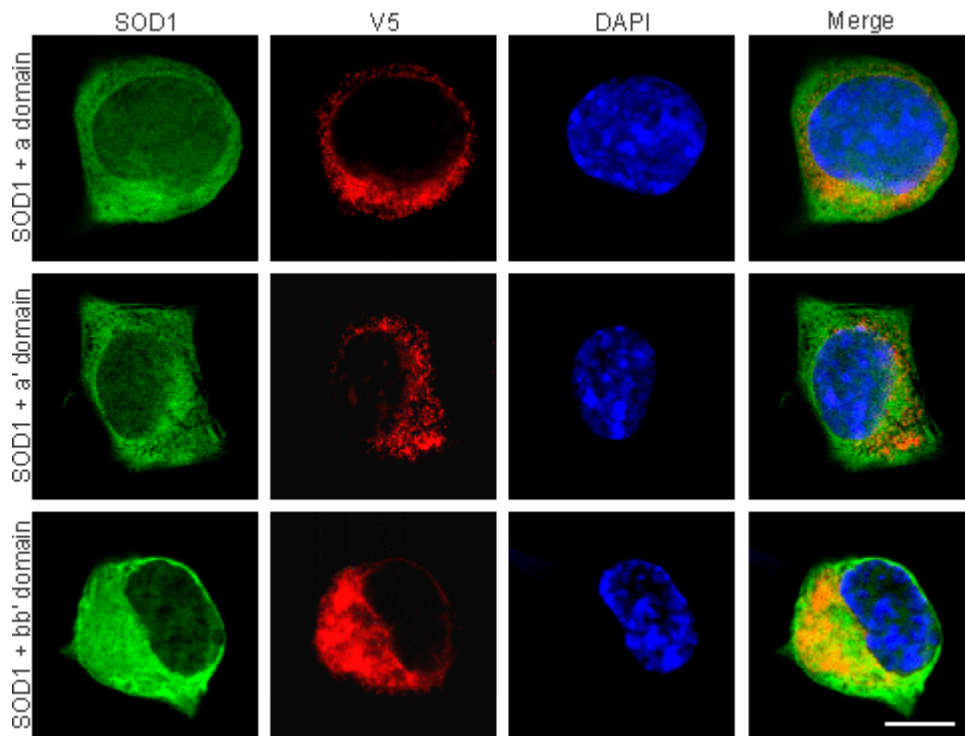
Figure 4.6: The PDI *a* domain, *a'* domain and *bb'* domain mutant proteins are co-expressed in almost all Neuro-2A cells co-transfected with EGFP-SOD1. Neuro-2A cells were transfected with SOD1 (left column) and either the PDI *a* domain, *a'* domain or *bb'* domain mutants (second column from the left; V5) for 72 h. Cells were fixed and immunocytochemistry was performed using an anti-V5 antibody and nuclei were stained with Hoechst (third column). The merge column demonstrates co-expression of each of the three domain mutants with SOD1 in the cells shown. Scale bar = 30 µM.

4.3.4 Expression of SOD1 and PDI domain mutants in Neuro-2A cells

Prior to examining the effect of the PDI domain mutants on mutant SOD1-induced cellular pathogenesis, Western blotting analysis was performed to ensure that transfection of each construct resulted in similar levels of mutant protein expression and to confirm that the expressed proteins were of the expected MW (Figure 4.7). Lysates were prepared from the following cell populations; GFP, wildtype SOD1 co-expressed with empty vector pcDNA3.1, and mutant SOD1 A4V co-expressed with either empty vector pcDNA3.1, wildtype PDI, PDI *a* domain, *a'* domain or *bb'* domain mutants. Immunoblotting using an anti-GFP antibody revealed that wildtype and mutant EGFP-SOD1 proteins were expressed at the expected size of 50 kDa, and GFP alone was expressed at 26 kDa. Wildtype SOD1 was expressed at higher levels compared to mutant SOD1 A4V, as expected. Wildtype PDI was detected at 62 kDa using an anti-V5 tag antibody, as expected. The PDI *a* domain mutant was detected at 15 kDa, the PDI *a'* domain mutant was detected at 12 kDa and the PDI *bb'* domain mutant was detected at 25 kDa using an anti-V5 tag antibody. All PDI proteins were expressed at similar levels. β-actin was used as a loading control and was detected using an anti-β-actin antibody at 40 kDa.

A
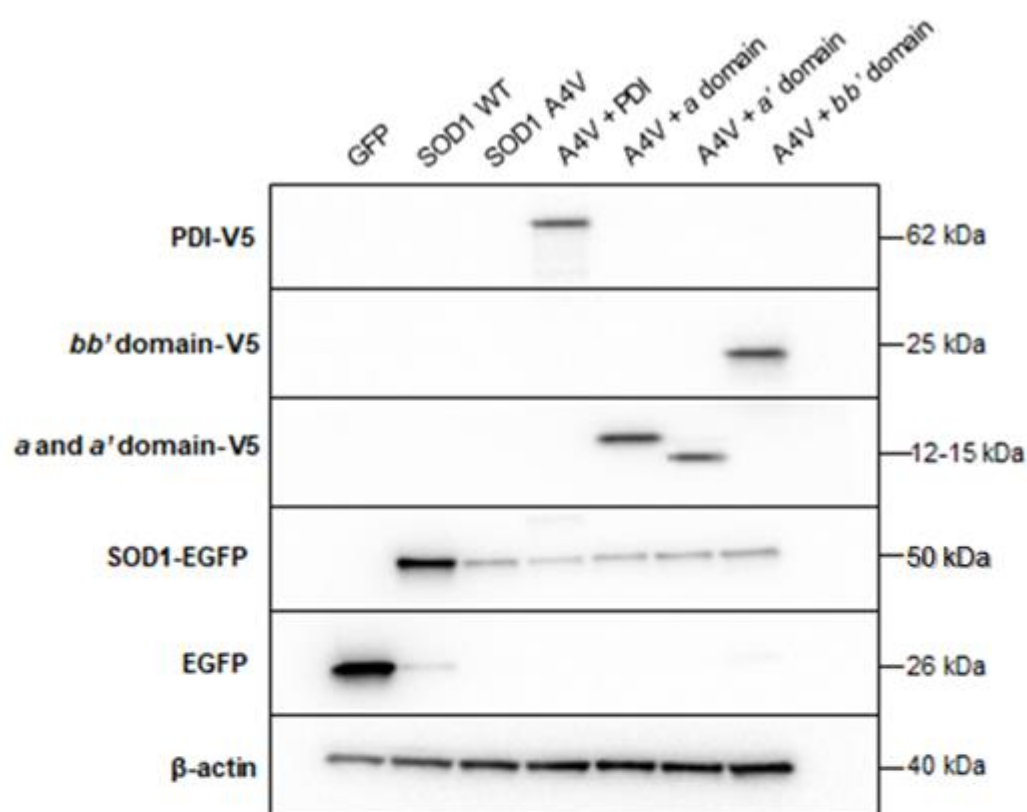
B
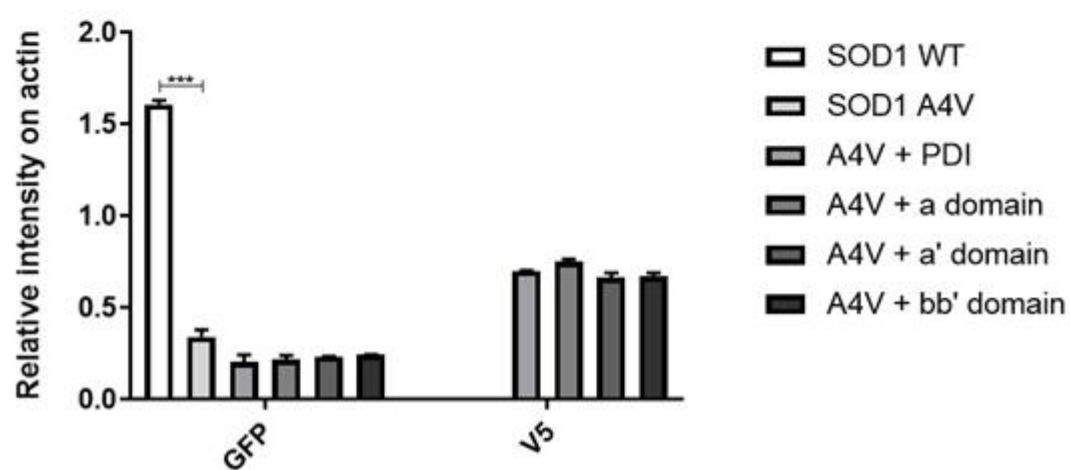
Figure 4.7: Protein expression of PDI domain constructs and EGFP-SOD1 in Neuro-2A cells. A) Western blotting analysis of cell lysates was performed and quantified to ensure that PDI domain mutant proteins were expressed at similar levels and were of the expected MW. Lysates examined were from cells expressing either GFP alone, wildtype SOD1 co-expressed with empty vector pcDNA3.1, and mutant SOD1 A4V co-expressed with either pcDNA3.1, PDI, the PDI *a* domain, *a'* domain or *bb'* domain. PDI was detected at 62 kDa as expected (PDI = 60 kDa, V5 tag = 2 kDa), whereas the *a* domain mutant was detected at 15 kDa, the *a'* domain mutant was detected at 12 kDa and the *bb'* domain mutant was detected at 25 kDa. Wildtype and mutant SOD1 were detected at 50 kDa (SOD1 = 18 kDa, GFP = 26 kDa) and GFP alone at 26 kDa. Loading control, β-actin was detected at 40 kDa. **B)** Quantification revealed that wildtype SOD1 had a significantly higher ($p < 0.001$) than mutant SOD1 A4V, as expected. Mutant SOD1 A4V was expressed at similar levels across all cell lysate populations. PDI and the PDI domain mutants were expressed at similar levels also. Lysates expressing GFP only were not included in quantification. N=3, Mean ± SEM, *** $p < 0.001$.

4.3.5 Overexpression of PDI's 'a' domains reduce mutant SOD1 inclusion formation

Previous studies in our laboratory have demonstrated that PDI overexpression in motor-neuron like cell lines significantly reduces the percentage of cells expressing mutant SOD1 inclusions [448]. It remains unclear, however, how PDI mediates its protective activity, whether it be via its disulphide interchange activity, facilitated by the *a* and *a'* domains, or by its chaperone function, mediated by the *b* domains with substrate binding capabilities. Thus, it was next investigated which specific domains of PDI are protective against mutant SOD1 inclusion formation in Neuro-2A cell lines.

Neuro-2A cells were transfected with constructs encoding empty pcDNA3.1 vector, GFP alone, wildtype SOD1 co-expressed with empty pcDNA3.1 vector, and mutant SOD1 A4V co-expressed with either pcDNA3.1, PDI, the *a* domain or the *bb'* domain mutants. SOD1 inclusion formation was analysed 72 h post-transfection because at this time-point maximal levels of mutant SOD1 inclusions and expression are observed. Immunocytochemistry was performed using an anti-V5 antibody to detect PDI and domain mutant expression, and cells were stained with Hoechst to clearly visualise the nuclei. At least 100 cells co-expressing mutant SOD1 A4V and the V5-tagged PDI proteins were examined and quantified for the presence of SOD1 inclusions (EGFP fluorescence) using fluorescence microscopy. Inclusions were categorised by prominent "clumps" of EGFP fluorescence in the cytoplasm of mutant SOD1 expressing cells (Figure 4.8 A). Low magnification images are also shown (Supplementary figure 5).

As expected, untransfected cells and cells expressing pcDNA3.1 or GFP did not bear any inclusions, and wildtype SOD1 expressing cells formed very few inclusions (1.7% ± 0.3). Conversely, significantly more cells expressing mutant SOD1 A4V with empty pcDNA3.1 vector ($p < 0.001$) displayed inclusions (25.3% ± 2.9), similar to previous results [265]. Co-

expression of wildtype PDI with mutant SOD1 A4V significantly reduced ($p < 0.001$) the

proportion of cells bearing mutant SOD1 inclusions to 12.8% ± 1.8, consistent with previous

results. Moreover, overexpression of the PDI *a* domain mutant in cells expressing mutant

SOD1 A4V resulted in significantly ($p < 0.01$) fewer cells with SOD1 inclusions (15.0%

±1.5). In fact, there was no significant difference to the cells co-expressing full-length PDI,

implying that PDI's *a* domain contributes to its protective activity against SOD1 inclusions.

Interestingly, when mutant SOD1 A4V was co-expressed with the *bb'* domain mutant, there

was no significant difference in the proportion of cells bearing inclusions when compared to

cells expressing mutant SOD1 A4V with empty vector (19.0% ±2.0). There was, however, a

significant increase ($p < 0.05$) compared to cells co-expressing mutant SOD1 A4V and full-

length PDI, implying that the *bb'* domains do not contribute to the protective activity (Figure

4.8 B). Hence, these data suggest that PDI's *a* domain, and therefore its disulphide

interchange activity, is responsible for preventing the formation of misfolded protein

inclusions formed by mutant SOD1. This result was confirmed using matched expression

levels in the cells displaying inclusions to ensure that the co-expression of mutant SOD1 A4V

with either PDI, the *a* domain mutant or the *bb'* domain mutant did not decrease its

expression levels (Supplementary figure 6).

Next, the *a* domain mutant was compared directly to the *a'* domain mutant, to examine

whether the *a'* domain had a similar protective effect to that of the *a* domain. Cells were

transfected with empty pcDNA3.1 vector, GFP, wildtype SOD1 co-expressed with

pcDNA3.1 and mutant SOD1 A4V co-expressed with either full-length PDI, the *a* domain

mutant or the *a'* domain mutant. Again, cells were fixed and immunocytochemistry was

performed using an anti-V5 antibody and nuclei stained with Hoechst. Similar to the studies

described above, cells expressing empty pcDNA3.1 vector, GFP alone and wildtype SOD1

did not form inclusions. As expected, there was a significant increase ($p < 0.001$) in inclusion

formation in cells expressing mutant SOD1 A4V (23.7% ± 1.5), and the proportion of cells

with inclusions was significantly decreased (p < 0.001) when PDI was co-expressed with

mutant SOD1 A4V (10.0% ± 1.0). Co-expression of the *a* domain with mutant SOD1 A4V

resulted in significantly fewer (p < 0.05) cells bearing SOD1 inclusions compared to cells

expressing mutant SOD1 A4V alone (15.3% ± 0.9). Moreover, when the *a'* domain mutant

was co-expressed with mutant SOD1 A4V, there was a significant reduction (p < 0.001) in

the proportion of cells forming SOD1 inclusions to 10.7% ± 2.0, compared to cells

expressing mutant SOD1 A4V alone (Figure 4.8 C). No differences were observed in the

proportion of cells forming inclusions in populations expressing *a* domain or *a'* domain

mutants, or full-length PDI, suggesting that either the PDI *a* or *a'* domain is sufficient to

prevent SOD1 inclusion formation.
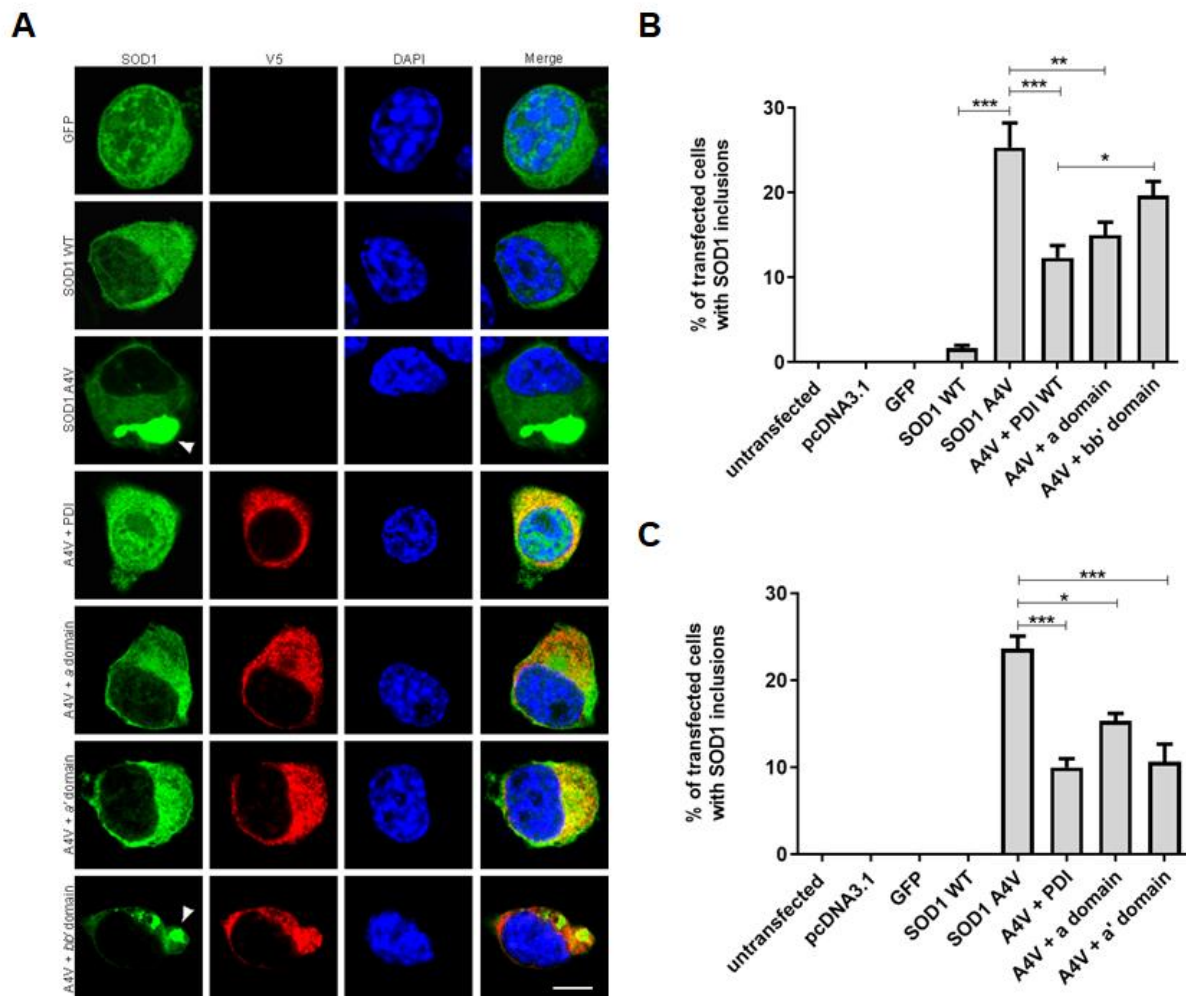
Figure 4.8: Overexpression of either the PDI *a* and *a'* domains reduces mutant SOD1 inclusion formation. A) Immunofluorescence images of Neuro-2A cells expressing GFP, wildtype SOD1 and mutant SOD1 A4V co-expressed with or without PDI, the *a* domain, *a'* domain or *bb'* domain. Cells expressing GFP and wildtype SOD1 did not present with inclusions (first and second panels; GFP, SOD1 WT). Conversely, more cells expressing mutant SOD1 A4V (third panel; SOD1 A4V) displayed SOD1 inclusions, as indicated by the white arrowhead (third panel, column one). When PDI (fourth panel; A4V + PDI), the *a* domain (fifth panel; A4V + *a* domain) or the *a'* domain (sixth panel; A4V + *a'* domain) were co-expressed with mutant SOD1 A4V, significantly fewer cells displayed SOD1 inclusions. However, when the *bb'* domain was co-expressed with mutant SOD1 A4V, there was no difference in the proportion of cells with SOD1 inclusions compared to mutant SOD1 A4V expressing cells. Scale bar = 20 µM. **B)** Quantification of Neuro-2A cells with SOD1 inclusion formation shown in A). There was a significant increase ($p < 0.001$) in the proportion of cells with SOD1 inclusions in cells expressing mutant SOD1 A4V, compared to cells expressing wildtype SOD1. A significant decrease in the proportion of cells bearing SOD1 inclusions was observed when mutant SOD1 A4V was co-expressed with either full-length PDI ($p < 0.001$) or the *a* domain mutant ($p < 0.01$). However, there was a significant increase in the proportion of cells co-expressing mutant SOD1 A4V with the *bb'* domain mutant ($p < 0.05$), compared to cells co-expressing mutant SOD1 A4V with PDI, indicating that the *bb'* domains are not protective. N=3, Mean ± SEM, * $p < 0.05$, ** $p < 0.01$, *** $p < 0.001$. **C)** Quantification of Neuro-2A cells with SOD1 inclusions in A). There was a significant increase ($p < 0.001$) in the proportion of cells with SOD1 inclusions in cells expressing mutant SOD1 A4V, compared to cells expressing wildtype SOD1, as expected. A significant decrease in the proportion of cells displaying mutant SOD1 inclusions was observed when mutant SOD1 A4V was co-expressed with either full-length PDI ($p < 0.001$),

the *a* domain mutant ($p < 0.05$) or the *a'* domain mutant ($p < 0.001$), compared to cells

expressing mutant SOD1 A4V with empty pcDNA3.1 vector. N=3, Mean ± SEM, * $p < 0.05$,

*** $p < 0.001$.

4.3.6 Overexpression of either the PDI 'a' or 'bb'' domain is protective against mutant SOD1 induced ER stress

Our laboratory previously demonstrated that SOD1 inclusion formation is linked to ER stress in motor neuron-like cell lines and that PDI inhibits ER stress in these cells [448]. Therefore, it was next examined which of the domain mutants inhibit ER stress induced by mutant SOD1. The activation of CHOP, indicated by nuclear immunoreactivity, was used as a marker for ER stress, as previous. Neuro-2A cells were transfected with empty pcDNA3.1 vector, GFP, wildtype SOD1 and mutant SOD1 A4V co-expressed with either pcDNA3.1, PDI, the *a* domain or *bb'* domain mutants. Cells were fixed 72 h after transfection, and immunocytochemistry was performed using an anti-CHOP antibody, where nuclear immunoreactivity to CHOP indicated its activation, as well as the induction of pro-apoptotic UPR (Figure 4.9 A). Nuclei were stained with Hoechst to clearly visualise the nucleus of each cell. Low magnification images are also shown (Supplementary figure 7).

Quantification revealed that less than 5% of untransfected cells or cells expressing either empty pcDNA3.1 vector or GFP only displayed nuclear immunoreactivity to CHOP, consistent with previous observations that these controls do not induce ER stress. Furthermore, only $8.0\% \pm 1.5$ of cells expressing wildtype SOD1 displayed CHOP activation, as expected. There was a significant increase ($p < 0.001$) in the proportion of cells displaying CHOP activation in cells expressing mutant SOD1 A4V ($26.7\% \pm 0.9$), compared to wildtype SOD1 expressing cells. In contrast, co-expression of PDI with mutant SOD1 A4V resulted in a significant decrease ($p < 0.001$) in the proportion of cells with CHOP activation ($11.3\% \pm 1.9$), consistent with previous studies [448]. Moreover, when the *a* domain mutant was co-expressed with mutant SOD1 A4V, there was also a significant decrease ($p < 0.001$) in the proportion of cells with activated CHOP ($9.0\% \pm 1.7$), compared to cells expressing mutant SOD1 A4V alone. This result implies that the *a* domain, and thus the disulphide interchange

activity of PDI, is important for the inhibition of ER stress induced by mutant SOD1. Interestingly, there was also a significant reduction ($p < 0.05$) in the proportion of cells with CHOP activation in populations co-expressing mutant SOD1 A4V and the *bb'* domain mutant (18.3% ± 2.0), suggesting that either, or both, of the *b* domains of PDI contribute to PDI's protective activity against ER stress. This result indicates that PDI's chaperone function contributes to this activity. However, there was also a significant difference in the proportion of CHOP activated cells between populations expressing the *bb'* domain mutant, compared to those expressing full-length PDI ($p < 0.05$), and the *a* domain mutant ($p < 0.01$), suggesting that the *a* domain makes a greater contribution than the *bb'* domains to PDI's protective effect against ER stress-induced apoptotic signalling, stimulated by mutant SOD1 in Neuro-2A cells (Figure 4.9 B).

Next, the protective activity of the *a'* domain of PDI was compared to that of the *a* domain in Neuro-2A cells. Cells were transfected with empty pcDNA3.1 vector, GFP only, wildtype SOD1 and mutant SOD1 A4V, co-expressed with either pcDNA3.1, PDI, the *a* domain mutant or the *a'* domain mutant. Similar to the results described above, less than 10% of untransfected cells or cells expressing either pcDNA3.1, GFP or wildtype SOD1 displayed CHOP activation. There was a significant increase ($p < 0.001$) in the proportion of cells with CHOP activation in populations expressing mutant SOD1 A4V, compared to wildtype SOD1, to 29.7% ± 1.5. However, there was a significant decrease ($p < 0.01$) in the proportion of mutant SOD1 expressing cells with CHOP activation when co-expressed wither either PDI or the *a* domain mutant (17.3% ± 0.9 and 15.7% ± 1.9, respectively). The proportion of cells displaying CHOP activation was also significantly reduced ($p < 0.05$) when the *a'* domain was co-expressed with mutant SOD1 A4V (20.3% ± 3.5), compared to cells expressing mutant SOD1 A4V with empty pcDNA3.1 vector. Moreover, there was no significant difference between cells expressing the *a'* domain to those expressing full-length PDI. These

results therefore imply that both the *a* and *a'* domains of PDI are protective against ER stress induced by mutant SOD1 (Figure 4.9 C).
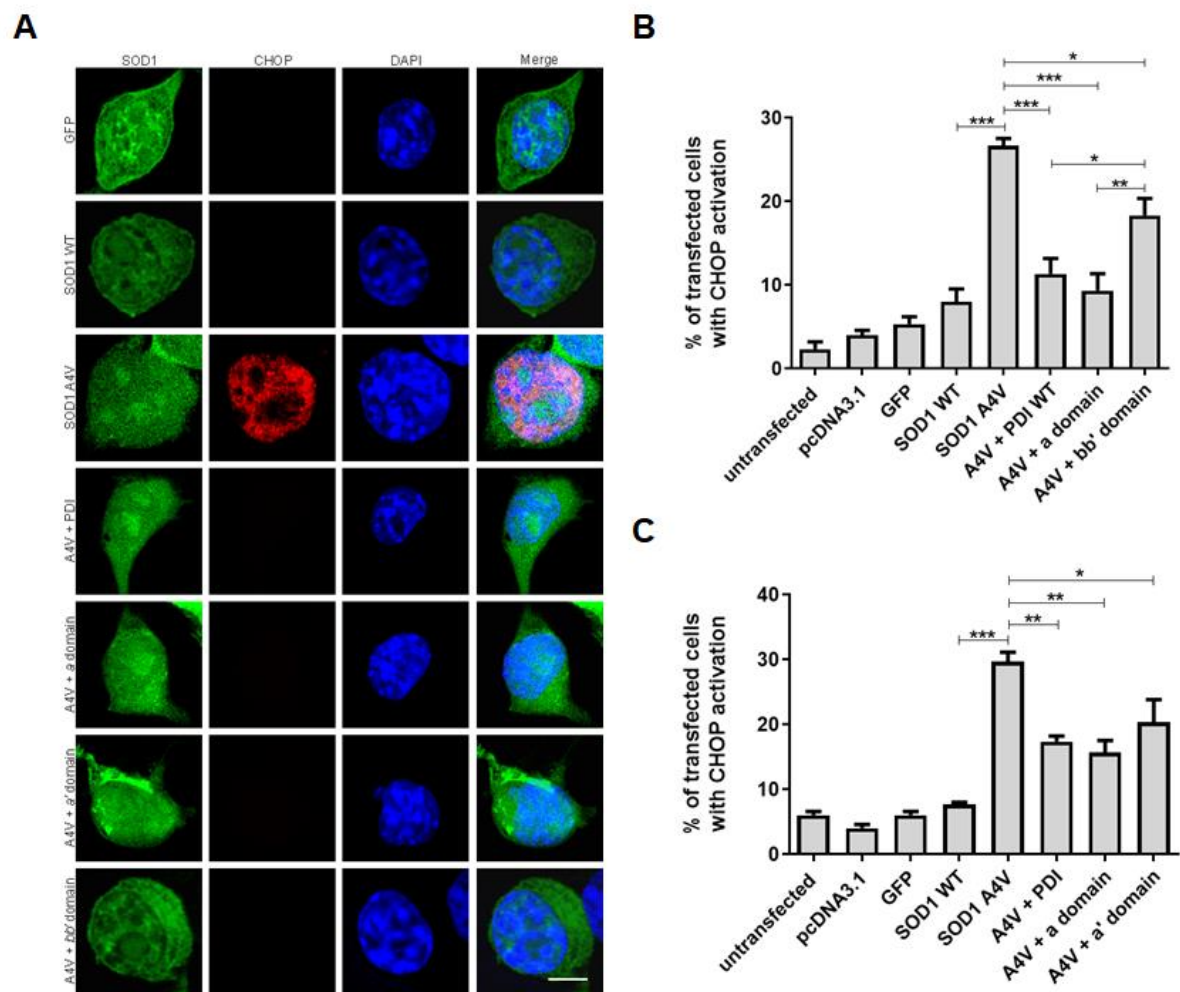
Figure 4.9: The overexpression of PDI's *a*, *a'* or *bb'* domains are protective against CHOP activation induced by mutant SOD1. A) Neuro-2A cells were transfected with GFP alone (first panel; GFP), wildtype SOD1 (second panel; SOD1 WT) or mutant SOD1 A4V, co-expressed with either empty pcDNA3.1 vector (third panel; SOD1 A4V), PDI (fourth panel; A4V + PDI), the *a* domain (fifth panel; A4V + *a* domain), *a'* domain (sixth panel; A4V + *a'* domain) or *bb'* domain mutants (seventh panel; A4V + *bb'* domain). Cells expressing GFP or wildtype SOD1 displayed little CHOP activation. Conversely, in cells expressing SOD1 A4V, nuclear immunoreactivity to CHOP was more commonly visualised (third panel, second column), as expected. However, when PDI, the *a* domain, *a'* domain or *bb'* domain mutants were co-expressed with mutant SOD1 A4V, the proportion of cells with CHOP activation was reduced. Scale bar = 20 µM. **B)** Quantification of cells in A) displaying nuclear immunoreactivity to CHOP, indicating CHOP activation. Very few untransfected cells or cells expressing pcDNA3.1, GFP or wildtype SOD1 displayed CHOP activation. There was a significant increase ($p < 0.001$) in the proportion of cells with CHOP activation in populations expressing mutant SOD1 A4V, compared to cells expressing wildtype SOD1. In comparison, significantly fewer ($p < 0.001$) cells co-expressing mutant SOD1 A4V with either PDI or the *a* domain mutant displayed CHOP activation, compared to those co-expressing mutant SOD1 A4V with empty pcDNA3.1 vector. Moreover, cells co-expressing mutant SOD1 A4V with the *bb'* domain mutant demonstrated a significant decrease ($p < 0.05$) in the proportion of cells with nuclear immunoreactivity to CHOP, however there was a significant difference in this proportion compared to cells co-expressing SOD1 A4V and PDI ($p < 0.05$) or the *a* domain ($p < 0.01$). N=3, Mean ± SEM, * $p < 0.05$, ** $p < 0.01$, *** $p < 0.001$. **C)** Quantification of the cells in A) displaying CHOP activation. There was a significant increase ($p < 0.001$) in the proportion of cells exhibiting CHOP activation in cells expressing mutant SOD1 A4V, compared to cells expressing wildtype SOD1, GFP alone or

empty pcDNA3.1 vector. Significantly fewer SOD1 A4V expressing cells displayed CHOP activation when either PDI ($p < 0.01$), the *a* domain ($p < 0.01$) or the *a'* domain ($p < 0.05$) were co-expressed, compared to cells expressing mutant SOD1 A4V alone. N=3, Mean $\pm$ SEM, * $p < 0.05$, ** $p < 0.01$, *** $p < 0.001$.

4.3.7 The effect of SOD1's cysteine residues on mutant SOD1 induced ER stress

ALS-associated mutant SOD1 forms disulphide-reduced monomers and high molecular weight oligomers containing non-native disulphide bonds [506, 511]. The following experiments examined the effect of mutating the four cysteine residues in SOD1 A4V to serines on induction of ER stress by mutant SOD1 A4V. For the purpose of this study, eight mutant constructs were previously generated in our laboratory, containing different combinations of the four cysteine residues in the mutant SOD1 A4V backbone. Serine was chosen to replace cysteine due to their structural similarity, but serine residues lack the ability to form disulphide bonds. These cysteine mutants are listed in Table 4.2 and the sites of their mutations are shown in Figure 4.10.

TABLE 4.2. SOD1 A4V cysteine mutants

1	A4V C6S
2	A4V C57S
3	A4V C111S
4	A4V C146S
5	A4V C57S C146S
6	A4V C6S C111S
7	A4V C57S C111S C146S
8	A4V QUAD

(Alanine 4)   (Cysteine 6)

ATG GCG ACG AAG GCC GTG TGC GTG CTG AAG GGC GAC GGC
CCA GTG CAG GGC ATC ATC AAT TTC GAG CAG AAG GAA AGT AAT
GGA CCA GTG AAG GTG TGG GGA AGC ATT AAA GGA CTG ACT
GAA GGC CTG CAT GGA TTC CAT GTT CAT GAG TTT GGA GAT AAT
(Cysteine 57)← ACA GCA GGC TGT ACC AGT GCA GGT CCT CAC TTT AAT CCT CTA
TCC AGA AAA CAC GGT GGG CCA AAG GAT GAA GAG AGG CAT
GTT GGA GAC TTG GGC AAT GTG ACT GCT GAC AAA GAT GGT GTG
GCC GAT GTG TCT ATT GAA GAT TCT GTG ATC TCA CTC TCA GGA
(Cysteine 111)← GAC CAT TGC ATC ATT GGC CGC ACA CTG GTG GTC CAT GAA AAA
GCA GAT GAC TTG GGC AAA GGT GGA AAT GAA GAA AGT ACA
AAG ACA GGA AAC GCT GGA AGT CGT TTG GCT TGT GGT GTA
(Cysteine 146)

Figure 4.10: Sequence of wildtype SOD1. ATG represents the start codon. The location of the A4V mutation is denoted in red, and the sites of the four cysteine residues which are mutated to serines are indicated in blue.

Previous studies have examined the effect of similar SOD1 mutations on SOD1 aggregation. These studies demonstrated that Cys-6 and Cys-111 play a role in the abnormal aggregation of SOD1 via non-native disulphide bonds [512]. Hence, the role of these cysteine residues on induction of ER stress by mutant SOD1 A4V was next examined. Prior to performing these experiments, Western blotting was performed to ensure similar levels of each cysteine mutant was expressed in Neuro-2A cells. Lysates from cells expressing SOD1 A4V and each cysteine mutant were prepared; A4V C6S, A4v C57S, A4V C111S, A4V C146S, A4V C57S C146S, A4V C6S C111S, A4V C57S C111S C146S and A4V QUAD, containing all four mutations. All A4V cysteine mutant proteins were detected at approximately 50 kDa using an anti-GFP antibody. Interestingly, mutant SOD1 A4V displayed lower expression levels compared to the SOD1 A4V cysteine mutants. Moreover, the C57S C111S C146S mutant displayed higher expression levels compared to the other cysteine mutant. β-actin was used as a loading control and was detected at 40 kDa, as expected (Figure 4.11).

A
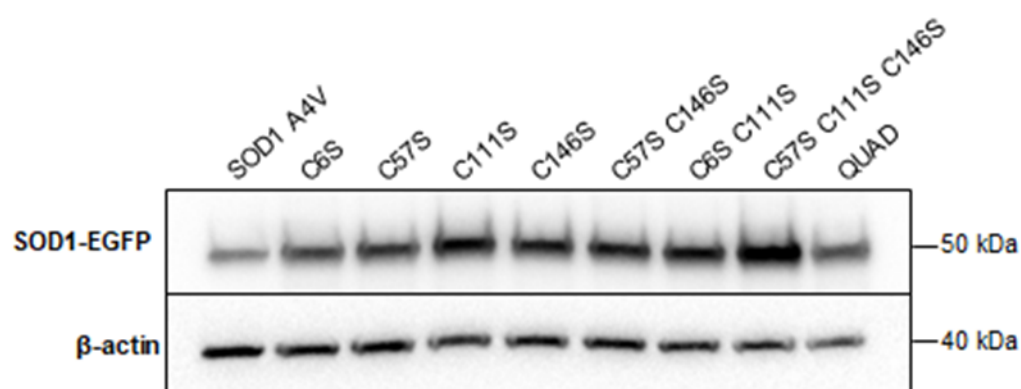
B
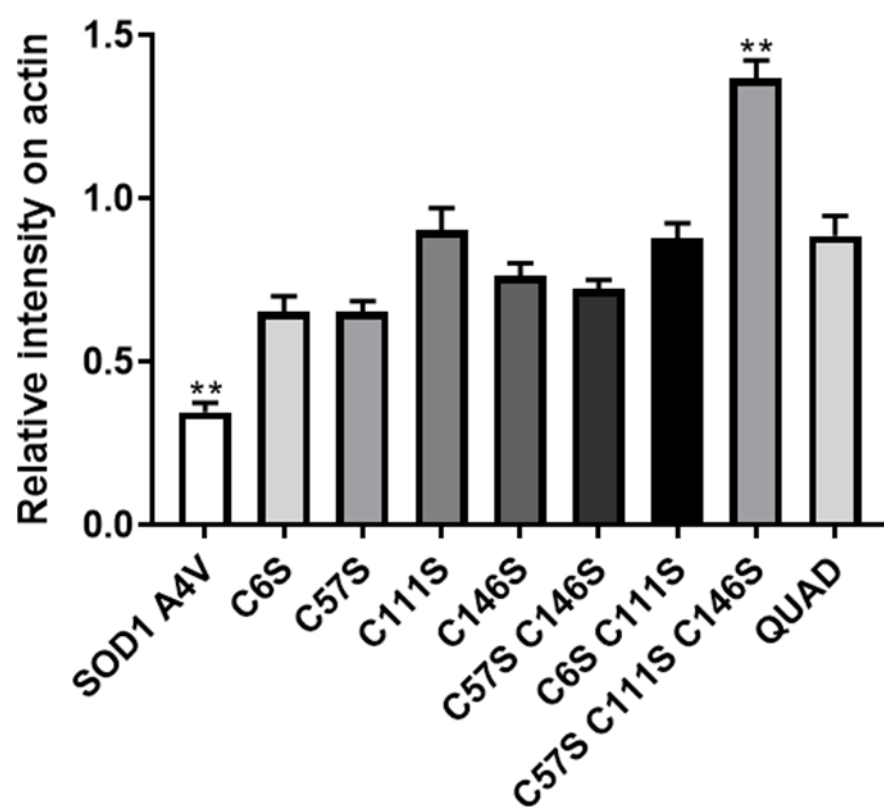
Figure 4.11: Protein expression of SOD1 A4V and SOD1 A4V cysteine mutation constructs. A) Western blotting analysis was performed to ensure that the A4V cysteine mutants were expressed to a similar degree and that they were of the expected size for SOD1-EGFP. All SOD1 proteins were detected at the expected size of 50 kDa using anti-GFP antibody. The loading control, β-actin was detected at 40 kDa. **B)** Quantification revealed that mutant SOD1 A4V was expressed at significantly lower levels ($p < 0.01$) than the SOD1 A4V cysteine mutants. The C57S C111S C146S cysteine mutant was expressed at significantly higher levels ($p < 0.01$) than the other SOD1 A4V cysteine mutants. Lysates expressing GFP only were not included in quantification. N=3, Mean ± SEM, ** $p < 0.01$.

4.3.8 Mutant SOD1 A4V Cysteine-111 is necessary to induce ER stress in Neuro-2A cells

It was next investigated whether the cysteine residues of mutant SOD1 A4V were involved in induction of ER stress, given that cysteine residues are involved in mutant SOD1 aggregation and that mutant SOD1 aggregation has been linked to the induction of ER stress. Two UPR markers were examined in cells expressing these mutants; XBP-1 and CHOP, as in Chapter 3.

XBP-1 was used to examine the IRE-1 pathway of the UPR, which is usually activated during the early, pro-survival stages of the UPR [393, 472]. As in Chapter 3, activation of the IRE1 pathway was indicated by nuclear immunoreactivity to XBP-1. Neuro-2A cells were transfected with either GFP (as a control), wildtype SOD1, mutant SOD1 A4V, and the eight mutant SOD1 A4V cysteine mutant constructs. After 72 h transfection, cells were fixed and immunocytochemistry was performed using an anti-XBP-1 antibody to determine whether XBP-1 was present within the cells' nucleus. Cells were also stained with Hoechst to visualise the nuclei (Figure 4.12 A).

In untransfected cells and cells expressing GFP or wildtype SOD1, less than 10% of cells displayed XBP-1 activation. There was a significant increase ($p < 0.01$) in the proportion of cells expressing mutant SOD1 A4V with XBP-1 activation (31.3% $\pm$ 2.4), compared to cells expressing GFP or wildtype SOD1, as expected. However, activation of XBP-1 was detected in a significantly decreased proportion of cells expressing the C111S mutant (16.0% $\pm$ 2.4), compared to mutant SOD1 A4V expressing cells ($p < 0.05$). Similarly, there was also a significant reduction in the proportion of cells with XBP-1 activation in populations expressing the C6S C111S mutant to 18.0% $\pm$ 1.5 of cells ($p < 0.05$), compared to mutant SOD1 A4V. Moreover, significantly fewer cells expressing the A4V QUAD mutant ($p < 0.05$) displayed XBP-1 activation (15.3% $\pm$ 2.0), compared to cells expressing mutant SOD1 A4V. However, there was no significant difference in the proportion of SOD1 A4V

expressing cells with nuclear XBP-1 immunoreactivity and cells expressing the other A4V cysteine mutants (Figure 4.12 B) Hence, these results indicate that mutation of either Cys-111, Cys-111 and Cys-6, or all four cysteines is protective against XBP-1 nuclear immunoreactivity, and hence ER stress induced by mutant SOD1 A4V.
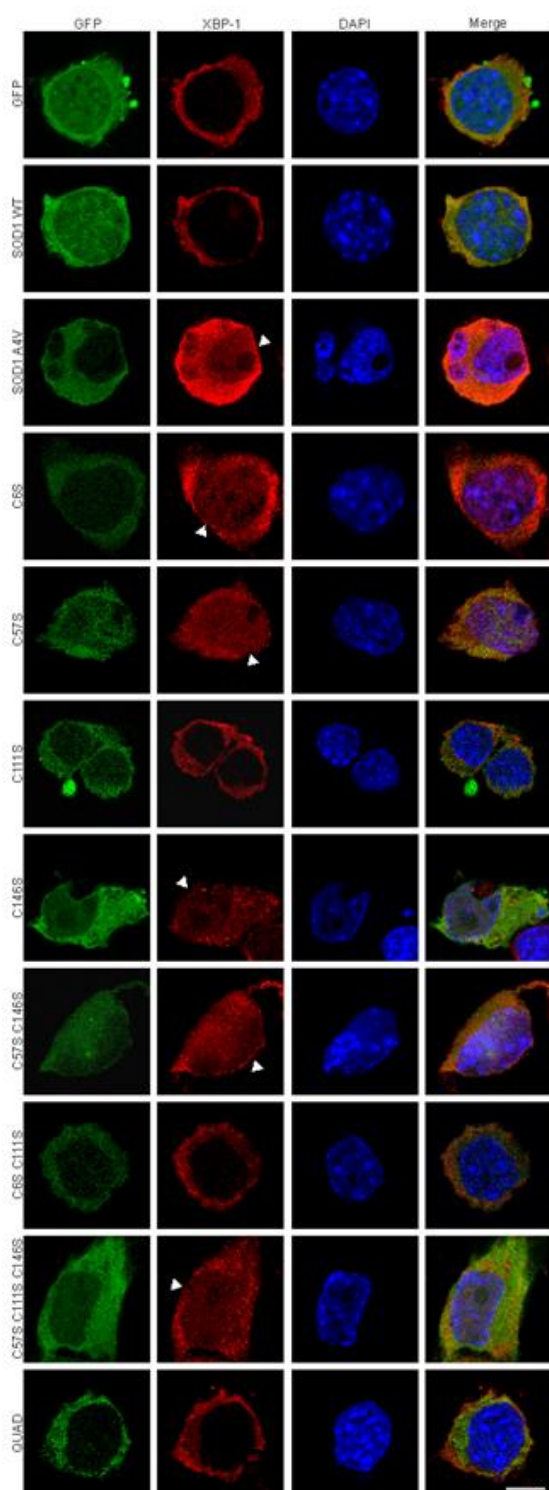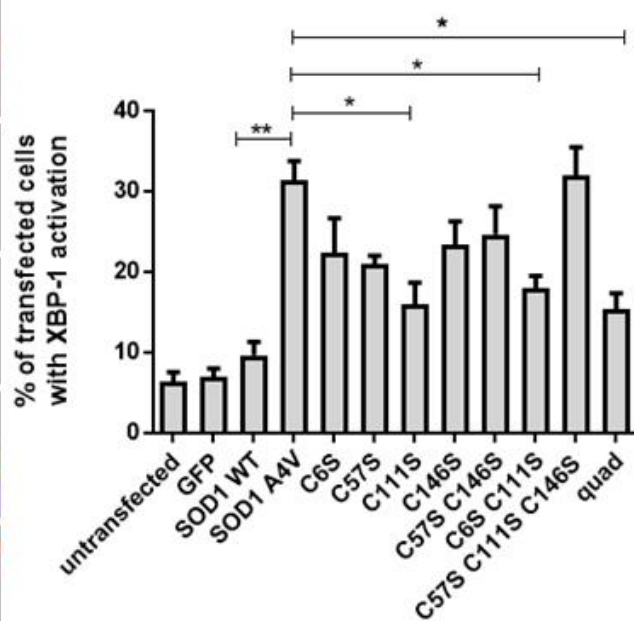
Figure 4.12: Mutating Cysteine-111 in mutant SOD1 A4V to serine is protective against XBP-1 activation. A) Immunocytochemistry images of Neuro-2A cells expressing GFP alone (first panel; GFP), wildtype SOD1 (second panel; SOD1 WT), mutant SOD1 A4V (third panel; SOD1 A4V), or A4V cysteine mutants (panels four to 11). Cells expressing GFP or wildtype SOD1 displayed little nuclear immunoreactivity to XBP-1, indicating activation. In contrast, more cells expressing mutant SOD1 A4V, C6S, C57S, C146S, C57S C146S, and C57S C111S C146S displayed nuclear immunoreactivity to XBP-1, as indicated by the white arrowhead (column two). However, fewer cells expressing C111S, C6S C111S, and QUAD exhibited XBP-1 activation. Scale bar = 20 µM. **B)** Quantification of the cells in A) displaying nuclear immunoreactivity to XBP-1. There was a significant increase ($p < 0.01$) in the proportion of cells with XBP-1 activation in mutant SOD1 A4V expressing cells, compared to cells expressing wildtype SOD1 and GFP, as expected. A significant decrease in the proportion of cells with XBP-1 activation was observed in populations expressing the A4V C111S mutant, the A4V C6S C111S mutant, or the A4V QUAD mutant ($p < 0.05$). N=3, Mean ± SEM, * $p < 0.05$, ** $p < 0.01$.

To confirm these results, a second marker of ER stress was examined in cells expressing SOD1 A4V cysteine mutants. CHOP is induced via the PERK pathway and is upregulated at the late pro-apoptotic phase of the UPR [562]. CHOP activation was detected by nuclear immunoreactivity following immunocytochemistry, indicating the activation of pro-apoptotic phases of the UPR. Cells were fixed 72 h after transfection, immunocytochemistry was performed using an anti-CHOP antibody and nuclei were stained with Hoechst, before examining cells for CHOP activation using fluorescent microscopy (Figure 4.13 A).

Quantification revealed that in untransfected cells, and cells expressing either GFP or wildtype SOD1, less than 5% of cells displayed nuclear immunoreactivity to CHOP. As expected, there was a significant increase ($p < 0.001$) in the proportion of cells with CHOP activation in populations expressing mutant SOD1 A4V (22.8% $\pm$ 1.8), compared to cells expressing wildtype SOD1. Similar to the XBP-1 results, there was a significant reduction ($p < 0.001$) in the proportion of cells with CHOP activation in cells expressing the A4V C111S mutant, compared to cells expressing mutant SOD1 A4V (8.0% $\pm$ 2.1). Also, significantly fewer cells expressing the A4V C6S C111S mutant ($p < 0.001$) or A4V QUAD mutant ($p < 0.01$) displayed nuclear immunoreactivity to CHOP (10.7% $\pm$ 2.7 and 12.7% $\pm$ 1.2, respectively), compared to mutant SOD1 A4V. Interestingly, significantly fewer cells ($p < 0.05$) expressing the A4V C57S C146S mutant displayed CHOP activation (14.0% $\pm$ 1.0). There was no significant difference in the proportion of cells with CHOP activation in the populations expressing the other mutant SOD1 A4V cysteine mutants and mutant SOD1 A4V itself (Figure 4.13 B).

178
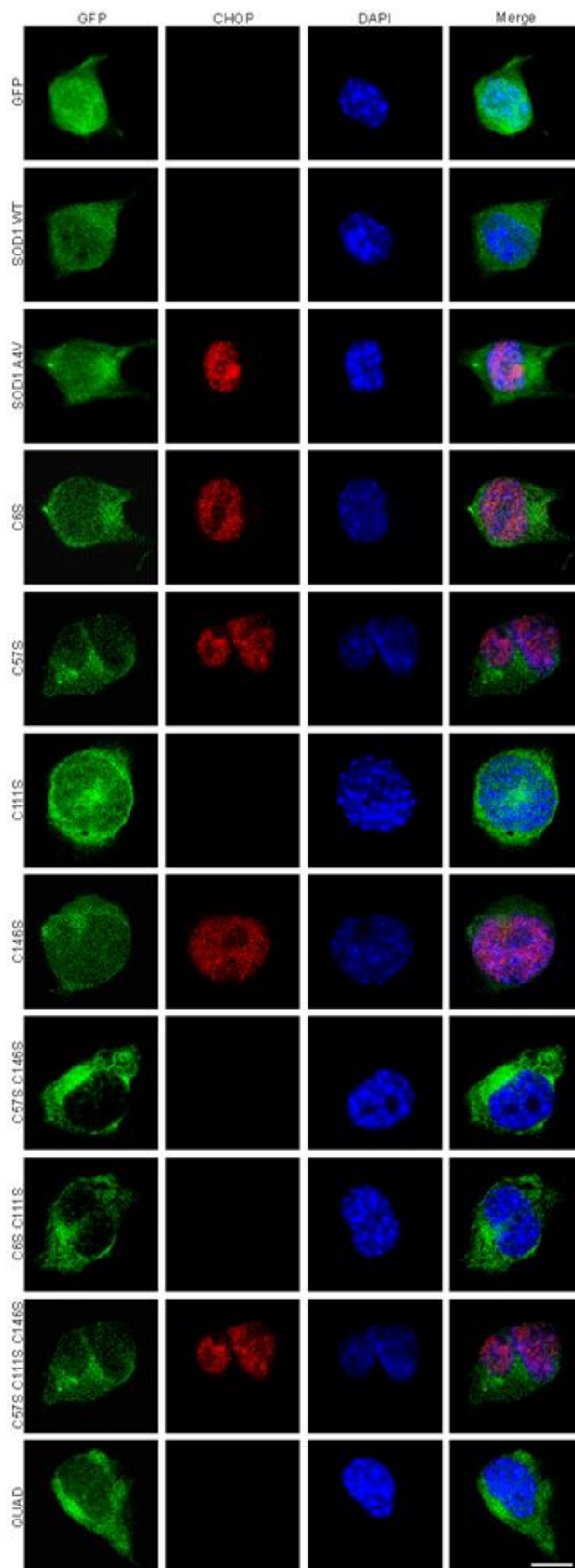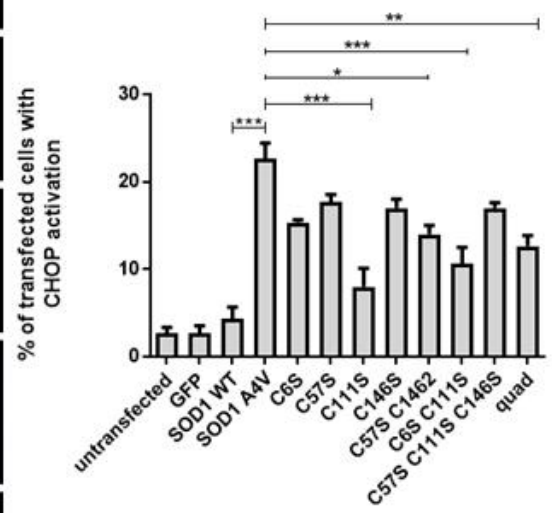
Figure 4.13: Mutating Cysteine-111 in mutant SOD1 A4V to serine is protective against CHOP activation. A) Neuro-2A cells were transfected with GFP alone (first panel; GFP), wildtype SOD1 (second panel; SOD1 WT), mutant SOD1 A4V (third panel; SOD1 A4V) or mutant SOD1 A4V cysteine mutants (panels fours to 11). Few cells expressing GFP or wildtype SOD1 displayed CHOP activation. Conversely, more cells expressing mutant SOD1 A4V exhibited CHOP immunoreactivity in the nucleus (third panel, second column). More cells expressing A4V cysteine mutants also displayed CHOP activation, except those expressing C111S (panel six), C57S C146S (panel eight), C6S C111S (panel nine) or QUAD (panel 11). Scale bar = 20 µM. **B)** Quantification of the cells in A) displaying nuclear immunoreactivity to CHOP, indicating activation. Less than 10% of untransfected cells and cells expressing either GFP or wildtype SOD1 displayed CHOP activation. There was a significant increase ($p < 0.001$) in the proportion of cells expressing mutant SOD1 A4V with CHOP activation, compared to those expressing wildtype SOD1. Significantly fewer cells expressing mutants C111S ($p < 0.001$), C6S C111S ($p < 0.001$), QUAD ($p < 0.01$) or C57S C146S displayed nuclear immunoreactivity to CHOP, compared to mutant SOD1 A4V. There was no significant difference in the proportion of cells exhibiting CHOP activation between the populations expressing the other cysteine mutants and cells expressing mutant SOD1 A4V. N=3, Mean ± SEM, * $p < 0.05$, ** $p < 0.01$, *** $p < 0.001$.

4.3.9 Overexpression of PDI's 'a' domains are protective against apoptosis induced by mutant SOD1

It has been previously demonstrated that mutant SOD1 inclusion formation is closely correlated with apoptosis [315] and that full length PDI prevents apoptosis induced by mutant SOD1 . [448]. Hence, next it was examined whether overexpression of the PDI domain mutants was protective against apoptosis induced by mutant SOD1, utilising nuclear condensation and morphology analysis as previous.

Neuro-2A cells were transfected for 72 h with empty pcDNA3.1 vector, GFP, wildtype SOD1 with pcDNA3.1, and mutant SOD1 A4V with either pcDNA3.1, PDI, the *a* domain or *bb'* domain mutants. Cells were fixed, immunocytochemistry was performed using an anti-V5 antibody to visualise PDI and the domain mutants, and stained with Hoechst to examine morphology of the nuclei. Nuclear morphology was examined in at least 100 transfected cells per experiment. Cells were considered apoptotic if the nucleus was condensed or fragmented (Figure 4.14 A).

Condensed nuclei were rarely present in untransfected cells or in cells expressing pcDNA3.1 (less than 5%). The proportion of cells with apoptotic nuclei was significantly higher ($p < 0.001$) in cells expressing mutant SOD1 A4V ($16.3\% \pm 0.3$), compared to cells expressing wildtype SOD1 ($5.0\% \pm 0.6$). However, significantly fewer apoptotic nuclei were observed in cells co-expressing mutant SOD1 A4V with either PDI ($9.7\% \pm 1.2$, $p < 0.05$), or the *a* domain mutant ($8.7\% \pm 1.5$, $p < 0.01$), suggesting that the *a* domain, and thus the disulphide interchange activity of PDI, is protective against mutant SOD1-induced apoptosis. In contrast, $15.3\% \pm 2.2$ of cells co-expressing mutant SOD1 A4V and the *bb'* domain exhibited condensed nuclei. This proportion of apoptotic nuclei was significantly higher ($p < 0.05$) than in SOD1 A4V expressing cells co-expressing either PDI or the *a* domain mutant, and was not

significantly different to cells expressing SOD1 A4V alone. These data therefore indicate that the *bb'* domain of PDI alone is not protective against mutant SOD1-induced apoptosis (Figure 4.14 B).

Next, it was examined whether the *a'* domain was also protective against mutant SOD1-induced apoptosis. Cells were transfected with empty pcDNA3.1 vector, GFP wildtype SOD1 with pcDNA3.1, and mutant SOD1 A4V with either pcDNA3.1, PDI, *a* domain or *a'* domain mutants. After fixing and immunocytochemistry with an anti-V5 antibody was performed, nuclei were stained with Hoechst to visualise condensation or fragmentation. As expected, very few untransfected cells or cells expressing pcDNA3.1, GFP or wildtype SOD1 exhibited nuclei condensation (less than 3% of cells). In contrast, a significantly higher ($p < 0.001$) proportion of cells expressing mutant SOD1 A4V displayed apoptotic nuclei (13.7% $\pm$ 1.5). There was a significant reduction in the proportion of cells with apoptotic nuclei, however, when mutant SOD1 A4V expressing cells were co-expressed with PDI (4.7% $\pm$ 0.9, $p < 0.001$), the *a* domain (7.7% $\pm$ 0.3, $p < 0.05$), and the *a'* domain mutants (6.0% $\pm$ 0.6, $p < 0.01$) (Figure 4.14 C). Hence both a domain and a' domain mutants are protective against mutant SOD1-induced apoptosis.

A

	SOD1	V5	DAPI	Merge
GFP				
SOD1 WT				
SOD1 A4V				
A4V + PDI				
A4V + a domain				
A4V + a' domain				
A4V + bb' domain				

B

% of transfected cells with nuclei condensation

untransfected, pcDNA3.1, GFP, SOD1 WT, SOD1 A4V, A4V + PDI WT, A4V + a domain, A4V + bb' domain

C

% of transfected cells with nuclei condensation

untransfected, pcDNA3.1, GFP, SOD1 WT, SOD1 A4V, A4V + PDI, A4V + a domain, A4V + a' domain

182
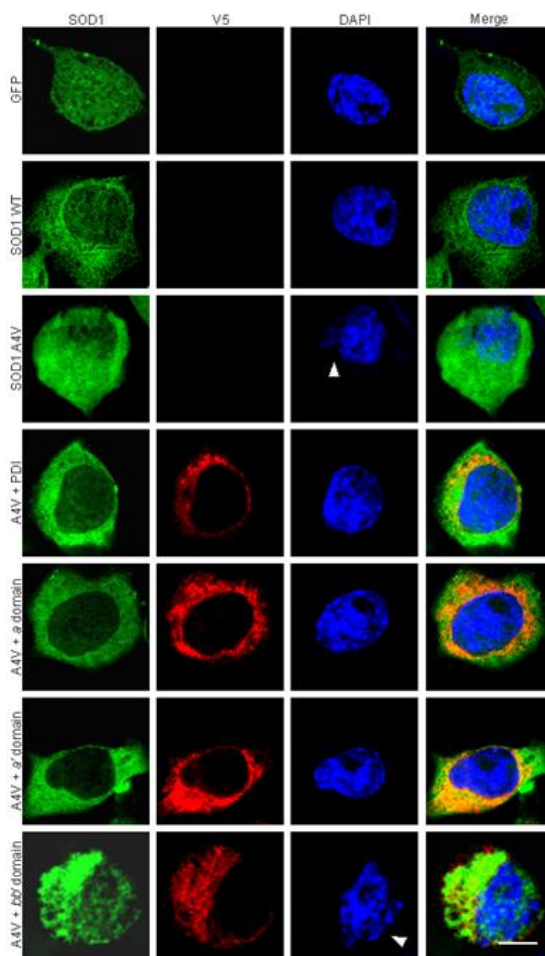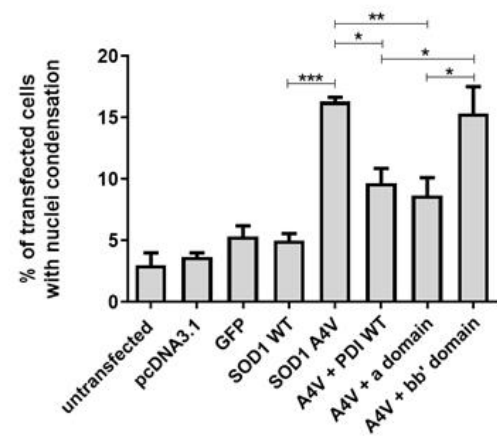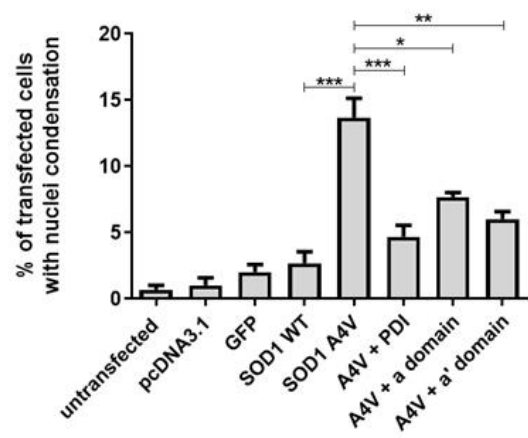
Figure 4.14: Overexpression of the PDI *a* and *a'* domain mutants inhibit mutant SOD1-induced apoptosis. A) Neuro-2A cells expressing GFP (first panel; GFP) or wildtype SOD1 (second panel; SOD1 WT) display few apoptotic nuclei, indicated by cells with regular morphology and size. In contrast, more cells expressing mutant SOD1 A4V (third panel; SOD1 A4V) exhibit irregular morphology, as indicated by the white arrowhead (third panel, column three). However, the proportion of cells with apoptotic nuclei is reduced in cells co-expressing mutant SOD1 A4V with either PDI (fourth panel; A4V + PDI), the *a* domain (fifth panel; A4V + *a* domain) and the *a'* domain mutants (sixth panel; A4V + *a'* domain). Cells co-expressing mutant SOD1 A4V and the *bb'* domain mutant (seventh panel; A4V + *bb'* domain) displayed a high proportion of apoptotic nuclei, as indicated by the white arrowhead (seventh panel, column three). Scale bar = 20 µM. **B)** Quantification of cells exhibiting apoptotic nuclei in A). There was a significant increase in the proportion of cells with condensed or fragmented nuclei in cells expressing mutant SOD1 A4V, compared to cells expressing wildtype SOD1 ($p < 0.001$). When PDI or the *a* domain mutant was co-expressed with mutant SOD1 A4V, however, there was a significant decrease in the proportion of cells with apoptotic nuclei ($p < 0.05$ and $p < 0.01$, respectively). There was a significant increase in the proportion of cells with apoptotic nuclei in mutant SOD1 A4V populations co-expressing the *bb'* domain, compared to SOD1 A4V cells expressing PDI or the *a* domain ($p < 0.05$). N=3, Mean ± SEM, * $p < 0.05$, ** $p < 0.01$, *** $p < 0.001$. **C)** Quantification of cells with apoptotic nuclei in A). There was a significant increase in the proportion of cells with apoptotic nuclei in mutant SOD1 A4V populations, compared to those expressing wildtype SOD1 ($p < 0.001$). However, a significant decrease in the proportion of cells with apoptotic nuclei was observed when mutant SOD1 A4V cells co-expressed PDI ($p < 0.001$), the *a* domain ($p < 0.05$) or the *a'* domain ($p < 0.01$). N=3, Mean ± SEM, * $p < 0.05$, ** $p < 0.01$, *** $p < 0.001$.

4.3.10 The effect of PDI QUAD and cytoplasmic PDI in Neuro-2A cells expressing mutant

SOD1

Analysing nuclei condensation and fragmentation as a measure of apoptosis is often criticised

for its subjective nature. Therefore, in the next set of studies, it was examined whether other

apoptotic assays demonstrated similar results to a nuclei condensation assay. These

experiments follow on from studies performed in the laboratory where PDI's chaperone

activity and localisation in the cytoplasm were assessed for any protective effect against

mutant SOD1-induced apoptosis (Parakh et al., 2017 in preparation). The study first involved

mutating the active site cysteines in PDI to serines (CGHC to SGHS). The construct bearing

the SGHS active site was termed PDI QUAD, and it has been previously established that

mutating cysteines to serines in the active site abolishes PDI's disulphide interchange

activity, leaving only the chaperone activity to function [502, 563]. The final two constructs

were designed so that PDI was localised in the cytoplasm. This was achieved by deleting the

signal sequence of PDI and the ER-retention signal (KDEL), by site-directed mutagenesis, in

both wildtype PDI and in the PDI QUAD mutant, resulting in cytoplasmic forms of both

proteins. These constructs, termed "Cytoplasmic wildtype PDI" and "Cytoplasmic PDI

QUAD", as well as PDI QUAD, have previously been investigated in our laboratory (Parakh

et al., 2017 in preparation). In these studies, PDI QUAD and both cytoplasmic PDI proteins

demonstrated a protective effect against apoptotic nuclei, indicating that the chaperone

activity of PDI, as well as PDI's localisation in the cytoplasm, is protective against apoptosis

induced by mutant SOD1. Hence, here, further studies were undertaken to verify the

protective effect of these proteins against apoptosis using three apoptotic assays.

First, the localisation of overexpressed PDI QUAD, cytoplasmic wildtype PDI and

cytoplasmic PDI QUAD proteins were analysed in Neuro-2A cells using confocal

microscopy. Cells were transfected with the PDI mutants for 24 h before performing

immunocytochemistry using a V5 antibody and a calreticulin antibody to probe for

calreticulin, an ER-resident protein. As expected, PDI QUAD co-localised with calreticulin in

all transfected cells, indicating that abolishment of the disulphide interchange activity does

not affect the localisation of PDI. As expected, cytoplasmic wildtype PDI and cytoplasmic

PDI QUAD did not co-localise with calreticulin, and both proteins were instead present in the

cytoplasm of transfected cells, confirming that by removing the signal sequence and KDEL,

PDI is excluded from the ER and becomes localised in cytoplasm (Figure 4.15).
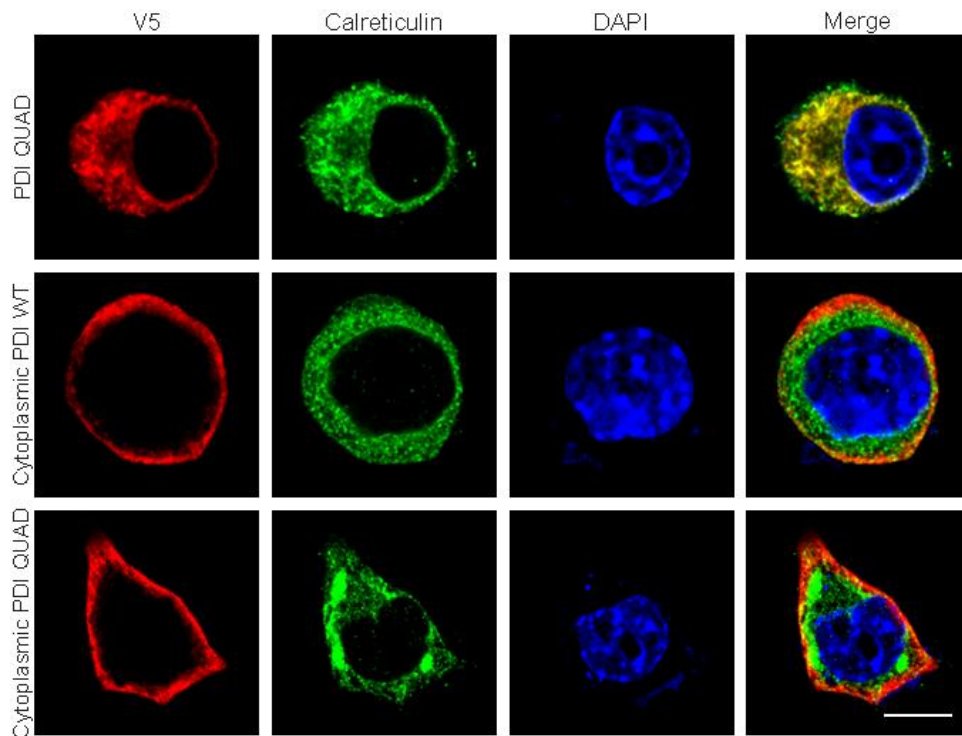
Figure 4.15: Localisation of PDI QUAD and cytoplasmic PDIs in Neuro-2A cells.

Neuro-2A cells were transfected with constructs encoding either PDI QUAD, cytoplasmic wildtype PDI or cytoplasmic PDI QUAD (left column). After a 24 h transfection, cells were fixed and immunocytochemistry was performed using antibodies for the V5 tag and calreticulin (second column), and the nucleus was stained with Hoechst (third column). PDI QUAD co-localised with calreticulin, as illustrated by the yellow signal in the merge panel (last column), indicating that PDI QUAD is localised in the ER. Both cytoplasmic wildtype PDI and cytoplasmic PDI QUAD did not co-localise with calreticulin, demonstrating that these proteins are expressed in the cytoplasm, instead of the ER. Scale bar represents 20 µM.

4.3.11 PDI QUAD and cytoplasmic PDIs are co-expressed in almost all cells transfected with SOD1.

Next, the co-transfection efficiency of PDI QUAD, cytoplasmic wildtype PDI and cytoplasmic PDI QUAD with mutant SOD1 was examined in Neuro-2A cells. Cells were transfected with one of the three PDI constructs and EGFP-SOD1 for 72 h, before fixing and performing immunocytochemistry using an anti-V5 antibody and staining with Hoechst to visualise the nuclei. Co-transfection was verified using fluorescent microscopy by examining EGFP expression (green) from SOD1 and performing immunocytochemistry with an Alexa Fluor 568-tagged secondary antibody to detect the V5 tags of PDI (Figure 4.16). The overall transfection efficiency of mutant SOD1 was found to be around 75-80% in Neuro-2A cells when observed 72 h post-transfection. For each of the three replicate experiments, fluorescent microscopy was utilised to examine at least 100 cells expressing mutant SOD1 and these cells were further analysed for co-expression with PDI QUAD, cytoplasmic wildtype PDI or cytoplasmic PDI QUAD. Quantification revealed that approximately 96% of SOD1 transfected cells also co-expressed PDI QUAD or cytoplasmic wildtype PDI. Furthermore, 95% of SOD1 expressing cells also co-expressed cytoplasmic PDI QUAD. Thus, it was assumed in all further experiments that the detection of SOD1 expression signified co-expression with the respective PDI proteins when they were co-transfected and immunocytochemistry using a V5 antibody was not performed.
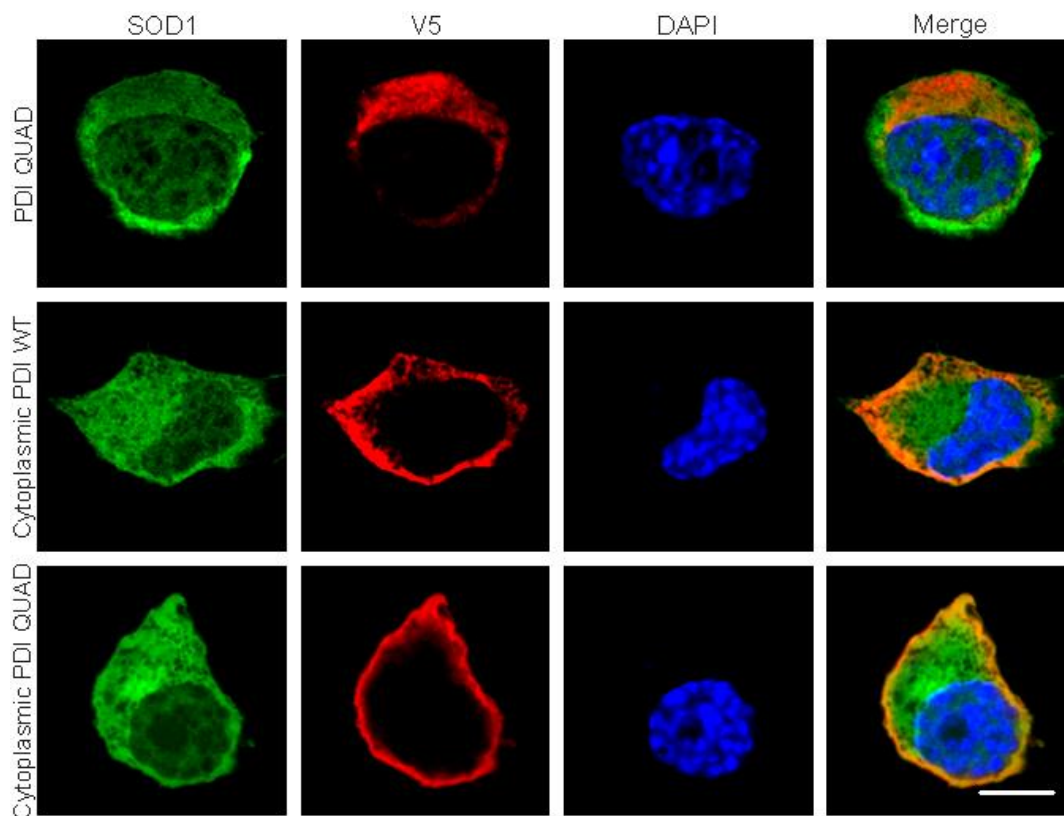
Figure 4.16: PDI QUAD, cytoplasmic wildtype PDI and cytoplasmic PDI QUAD are co-expressed in almost all Neuro-2A cells co-expressing EGFP-SOD1. Neuro-2A cells were transfected for 72 h with EGFP-SOD1 (left column) and PDI-V5 constructs (second column). Cells were fixed and immunocytochemistry was performed using an anti-V5 antibody. Nuclei were stained with Hoechst (third column). The merge column demonstrates co-expression of SOD1 and the respective PDI proteins in the cells shown. Scale bar = 20 µM.

4.3.12 Expression of SOD1 and PDI proteins in Neuro-2A cells

Prior to examining apoptosis using overexpressed mutant SOD1 and PDI constructs, Western blotting analysis was performed to ensure that the PDI proteins were expressed at the expected MW and similar levels of expression were obtained between groups (Figure 4.17). Cell lysates were prepared from the following groups; GFP alone, wildtype SOD1 co-expressed with empty pcDNA3.1 vector, and mutant SOD1 A4V co-expressed with either empty pcDNA3.1 vector, wildtype PDI, PDI QUAD, cytoplasmic wildtype PDI or cytoplasmic PDI QUAD. Immunoblotting revealed that wildtype and mutant EGFP-SOD1 proteins were expressed at the expected size of 50 kDa, and GFP alone was expressed at 26 kDa, using an anti-GFP antibody. Wildtype SOD1 was expressed at significantly higher levels than mutant SOD1 A4V, as expected. The PDI constructs were detected at 62 kDa using an anti-V5 tag antibody and shared similar expression levels. β-actin was used as a loading control and was detected using an anti-β-actin antibody at 40 kDa.

A
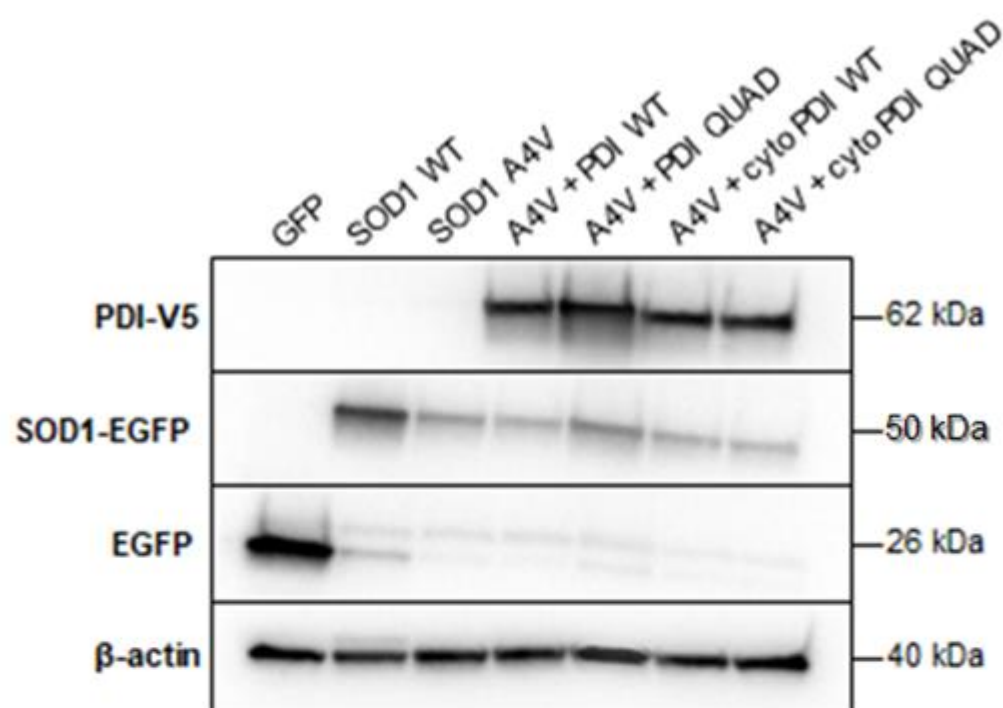
B
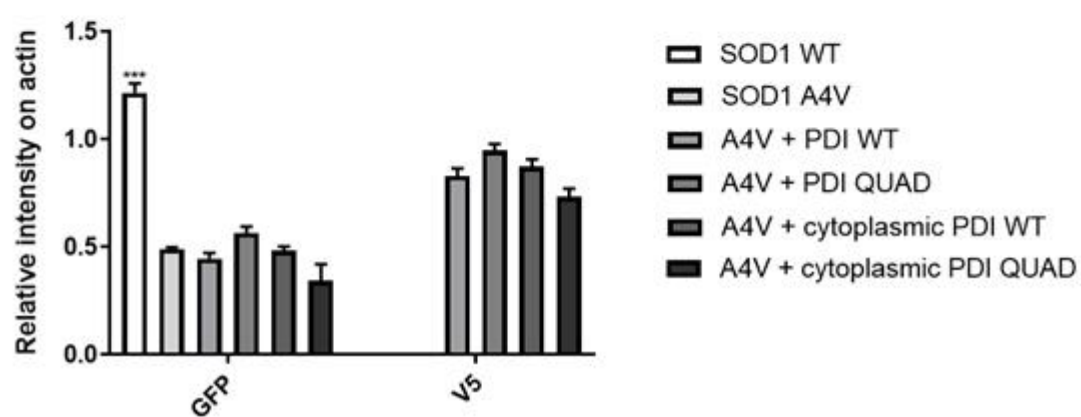
Figure 4.17: Protein expression of EGFP-SOD1 and wildtype PDI, PDI QUAD, and cytoplasmic PDIs in Neuro-2A cells. A) Western blotting of cell lysates and quantification was performed to ensure that the proteins were expressed at the correct size and with similar expression levels between groups. The lysates examined were GFP, wildtype SOD1 with empty pcDNA3.1 vector, and mutant SOD1 A4V with either empty pcDNA3.1 vector, wildtype PDI, PDI QUAD, cytoplasmic wildtype PDI, or cytoplasmic PDI QUAD. The PDI proteins were expressed at the expected size of 62 kDa (PDI = 60 kDa, V5 tag = 2 kDa). Wildtype and mutant SOD1 were expressed at 50 kDa (SOD1 = 18 kDa, GFP = 26kDa) and GFP was detected at 26 kDa. The loading control, β-actin, was detected at 40 kDa. **B)** Quantification revealed that wildtype SOD1 was expressed at significantly higher levels (p < 0.001) than mutant SOD1 A4V, as expected. Mutant SOD1 A4V was expressed similarly across all cell lysate populations, and PDI and the PDI domain mutants shared similar expression also. Lysates expressing GFP only were not included in quantification. N=3, Mean ± SEM, *** p < 0.001.

4.3.13 Overexpression of PDI QUAD, cytoplasmic wildtype PDI and cytoplasmic PDI QUAD are protective against SOD1 induced apoptosis.

Our laboratory has recently demonstrated that PDI is able to rescue cells from apoptosis induced by mutant SOD1. Moreover, previous studies observed that PDI's disulphide interchange activity was not required for protection against nuclei condensation and fragmentation (Parakh et al., 2017 in preparation). Previous reports demonstrate that PDI interacts with SOD1 in the cytoplasm, but it remained unknown whether a cytoplasmic-localised PDI would also be protective against apoptosis. Hence, next apoptosis was examined in cells co-expressing mutant SOD1 A4V with either PDI QUAD, cytoplasmic wildtype PDI and cytoplasmic PDI QUAD, using three separate assays; Bax activation, Bax recruitment to mitochondria and Caspase-3 activation.

First, Bax activation and its recruitment to mitochondria were examined. Upregulation of CHOP activates Bax, which results in the localisation of Bax to mitochondria [564]. Bax activation was examined by permeabilising the nuclear envelope with CHAPS buffer, hence nuclear immunoreactivity to Bax indicated Bax activation [315]. Bax recruitment was analysed by permeabilising the cell membrane with 0.1% (v/v) Triton-100 in PBS, so that Bax localisation to the mitochondria could be observed.

Neuro-2A cells were transfected with pcDNA3.1 empty vector, GFP, wildtype SOD1, and mutant SOD1 A4V with either pcDNA3.1 empty vector, or constructs encoding wildtype PDI, PDI QUAD, cytoplasmic wildtype PDI, or cytoplasmic PDI QUAD. After fixing and permeabilising the nuclear envelope with CHAPS buffer, immunocytochemistry was performed using an anti-Bax antibody, where nuclear immunoreactivity to Bax indicated its activation (Figure 4.18 A). Cells were also stained with Hoechst to visualise the nuclei.

Less than 10% of untransfected cells or cells expressing pcDNA3.1, GFP and wildtype SOD1 displayed Bax activation, as expected. A significantly greater ($p < 0.001$) proportion of cells expressing mutant SOD1 A4V displayed activation of Bax, indicating apoptosis (28.3% ± 4.7). This proportion of cells was significantly decreased ($p < 0.001$) when wildtype PDI was co-expressed with mutant SOD1 A4V (9.3% ± 1.5). However, when PDI QUAD was co-expressed with mutant SOD1 A4V, the proportion of cells with Bax activation was significantly reduced ($p < 0.05$) to 18.7% ± 0.7, although this proportion was significantly different ($p < 0.05$) to cells co-expressing wildtype PDI. A similar result was obtained in cells co-expressing SOD1 A4V with cytoplasmic PDI QUAD, where a significant decrease ($p < 0.05$) in the proportion of cells with Bax activation was observed compared to cells co-expressing mutant SOD1 A4V and empty pcDNA3.1 vector (18.7% ± 1.5), but this proportion was significantly different ($p < 0.05$) to cells co-expressing SOD1 A4V with wildtype PDI. When cells expressing mutant SOD1 A4V were co-expressed with cytoplasmic wildtype PDI, there was a significant decrease ($p < 0.01$) in the proportion of cells exhibiting nuclear immunoreactivity to Bax (15.0% ± 0.6), compared to cells co-expressing mutant SOD1 A4V and empty vector (Figure 4.18 B). Hence, these results imply that cytoplasmic PDI retains the protective activity of wildtype PDI. Moreover, these results demonstrate a protective activity for PDI's chaperone function against mutant SOD1-induced apoptosis. However, whilst PDI QUAD and cytoplasmic PDI QUAD were also protective, they did not retain the full protective capacity of wildtype PDI.

A

B

194
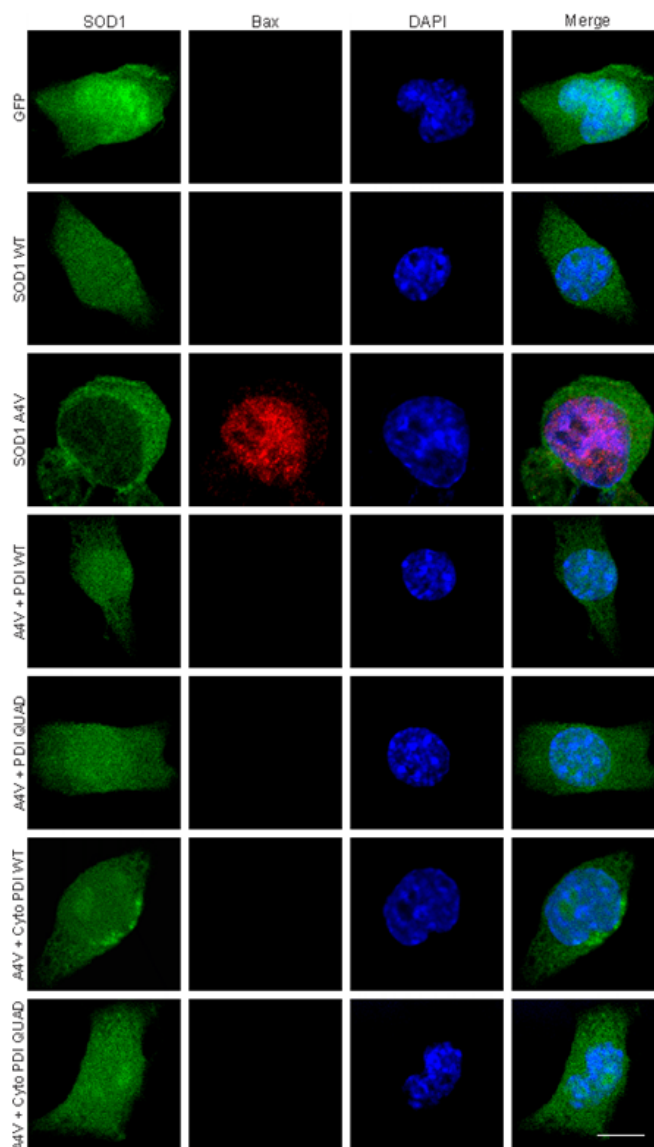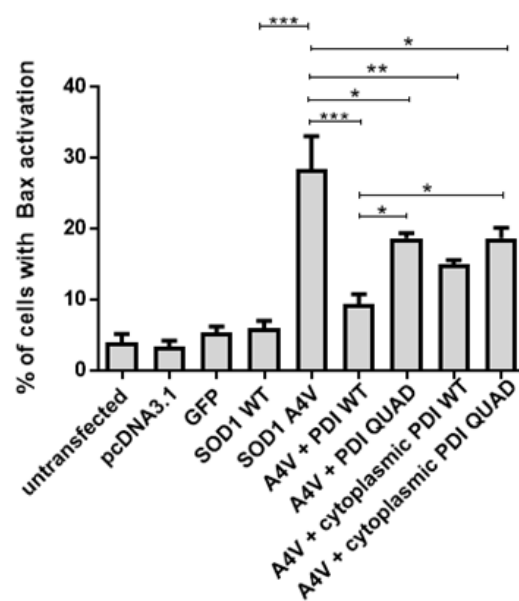
Figure 4.18: Overexpression of PDI QUAD, cytoplasmic wildtype PDI and cytoplasmic PDI QUAD are protective against Bax activation. A) Neuro-2A cells expressing GFP, wildtype SOD1 and mutant SOD1 A4V, with either pcDNA3.1, wildtype PDI, PDI QUAD, cytoplasmic wildtype PDI, or cytoplasmic PDI QUAD. Few cells expressing GFP or wildtype SOD1 displayed Bax activation (first two panels; GFP, SOD1 WT). Conversely, a larger proportion of cells expressing mutant SOD1 A4V (third panel; SOD1 A4V) demonstrated Bax activation, indicated by nuclear immunoreactivity of Bax (third panel, column two). When PDI, PDI QUAD, cytoplasmic wildtype PDI, or cytoplasmic PDI QUAD were co-expressed with mutant SOD1 A4V, fewer cells displayed Bax activation (panels 4-7). Scale bar = 20 μM. **B)** Quantification of the proportion of cells with Bax activation in A). A similar proportion of untransfected cells and cells expressing pcDNA3.1, GFP or wildtype SOD1 displayed Bax activation. There was a significant increase in the proportion of cells with Bax activation in mutant SOD1 A4V populations, compared to wildtype SOD1 populations ($p < 0.001$). The proportion of cells with Bax activation was significantly reduced when wildtype PDI ($p < 0.001$) or cytoplasmic wildtype PDI ($p < 0.01$) was co-expressed with mutant SOD1 A4V. The proportion of cells exhibiting Bax activation was also significantly decreased when SOD1 A4V expressing cells were co-expressed with either PDI QUAD or cytoplasmic PDI QUAD ($p < 0.05$). However, there were significantly more ($p < 0.05$) cells in these populations with Bax activation when compared to cells co-expressing mutant SOD1 A4V and wildtype PDI. N=3, Mean ± SEM, * $p < 0.05$, ** $p < 0.01$, *** $p < 0.001$.

Next, Bax recruitment to mitochondria was examined in cells transfected with pcDNA3.1, GFP, wildtype SOD1, and mutant SOD1 A4V with either pcDNA3.1 empty vector, wildtype PDI, PDI QUAD, cytoplasmic wildtype PDI or cytoplasmic PDI QUAD. After fixing and permeabilising the cell membrane with 0.1 % (v/v) Triton-100 in PBS, immunocytochemistry was performed using an anti-Bax antibody, where Bax localisation in the mitochondria indicated recruitment, and hence, that apoptosis was underway (Figure 4.19 A). Cells were stained with Hoechst to visualise the nuclei.

Less than 10% of untransfected cells, or cells expressing pcDNA3.1, GFP or wildtype SOD1, displayed Bax recruitment to mitochondria. There was a significant increase ($p < 0.001$) in the proportion of mutant SOD1 A4V expressing cells with Bax recruitment ($26.7\% \pm 2.7$) compared to those expressing wildtype SOD1. As expected, this proportion was significantly decreased ($p < 0.001$) when mutant SOD1 A4V expressing cells were co-expressed with wildtype PDI ($10.3\% \pm 0.9$). Moreover, this proportion also significantly decreased ($p < 0.01$) when cytoplasmic wildtype PDI was co-expressed with SOD1 A4V ($12.3\% \pm 1.5$). There was also a significant reduction ($p < 0.05$) in the proportion of cells with Bax recruitment to mitochondria when SOD1 A4V expressing cells were co-expressed with either PDI QUAD or cytoplasmic PDI QUAD ($18.3\% \pm 0.9$ and $19.3\% \pm 1.8$, respectively), compared to cells expressing mutant SOD1 A4V with empty pcDNA3.1 vector. Similar to Bax activation, there was also a significant difference ($p < 0.05$) in the proportion of cells with Bax recruitment in populations co-expressing mutant SOD1 A4V with either PDI QUAD or cytoplasmic PDI QUAD, and cells co-expressing mutant SOD1 A4V with wildtype PDI (Figure 4.19 B). These findings confirm that PDI localised in the cytoplasm is protective against apoptosis induced by mutant SOD1. They also suggest that the disulphide interchange activity of PDI is not required to rescue cells from apoptosis. However, as the QUAD mutants were not as

protective as wildtype PDI, these findings also imply that the disulphide interchange activity and chaperone activities both contribute to the protective functions of PDI against apoptosis.

A
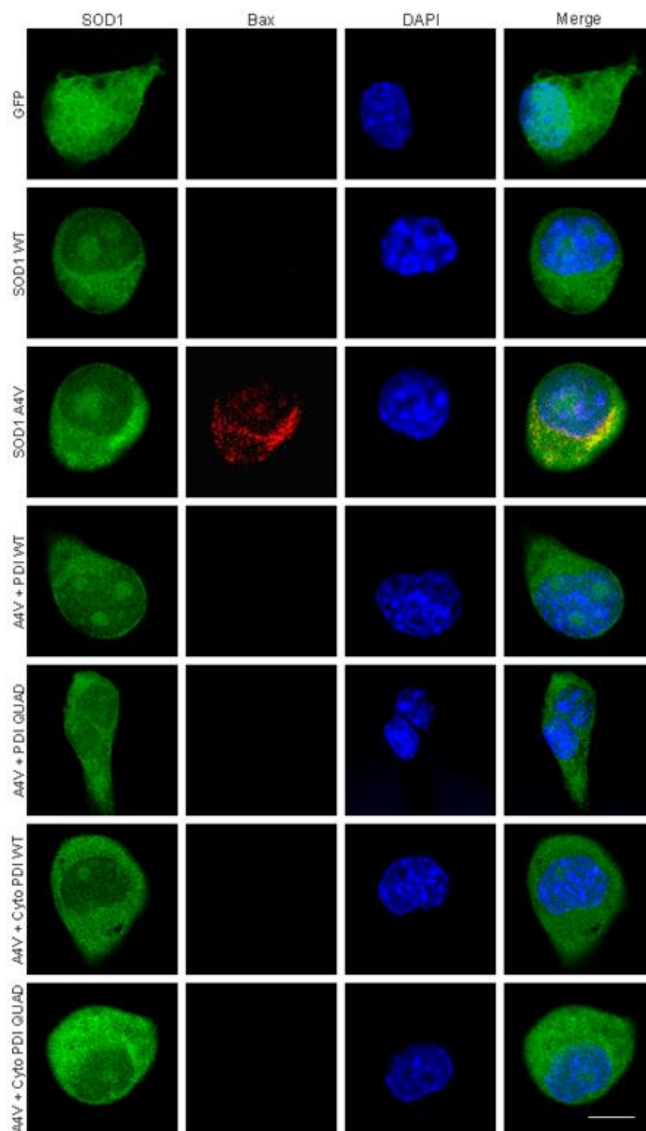
B
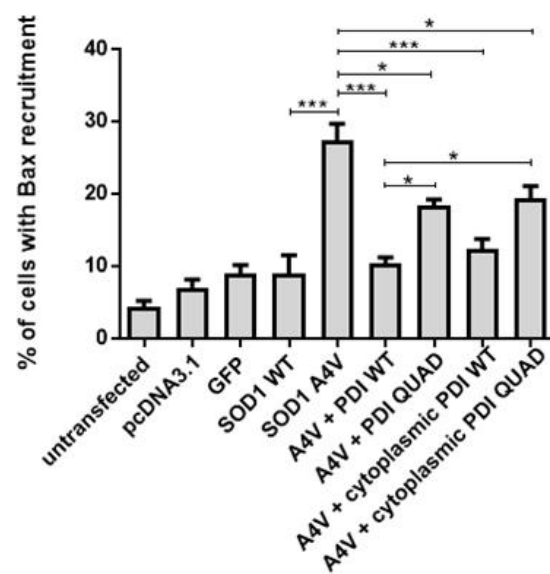
Figure 4.19: Overexpression of PDI QUAD, cytoplasmic wildtype PDI and cytoplasmic PDI QUAD are protective against Bax recruitment to the mitochondria. A) Immunofluorescence images of Neuro-2A cells expressing GFP, wildtype SOD1, and mutant SOD1 A4V, with either empty vector pcDNA3.1, wildtype PDI, PDI QUAD, cytoplasmic wildtype PDI or cytoplasmic PDI QUAD. Few cells expressing GFP or wildtype SOD1 displayed Bax recruitment to the mitochondria (first two panels; GFP, SOD1 WT), whereas a greater proportion of cells expressing mutant SOD1 A4V (third panel; SOD1 A4V) demonstrated Bax recruitment, indicated by Bax localisation in the mitochondria (third panel, column two). When wildtype PDI (fourth panel; A4V + PDI WT), PDI QUAD (fifth panel; A4V + PDI QUAD), cytoplasmic wildtype PDI (sixth panel; A4V + Cyto PDI WT) or cytoplasmic PDI QUAD (seventh panel; A4V + Cyto PDI QUAD) were co-expressed with mutant SOD1 A4V, fewer cells displayed Bax recruitment. Scale bar = 20 µM. **B)** Quantification of the proportion of SOD1 expressing cells with Bax recruitment in A). There was no significant difference in the proportion of cells with Bax recruitment between untransfected cells and cells expressing GFP, pcDNA3.1 and wildtype SOD1. There was a significant increase ($p < 0.001$) in the proportion of mutant SOD1 A4V expressing cells with Bax recruitment, compared to wildtype SOD1 expressing cells. The proportion of cells with Bax recruitment was significantly reduced when wildtype PDI or cytoplasmic wildtype PDI was co-expressed with mutant SOD1 A4V ($p < 0.001$). There was a slight but significant decrease in the proportion of cells with Bax recruitment in populations co-expressing mutant SOD1 A4V with either PDI QUAD or cytoplasmic PDI QUAD ($p < 0.05$), compared to cells co-expressing mutant SOD1 A4V with empty pcDNA3.1 vector. There was also a significant increase ($p < 0.05$) in the proportion of cells with Bax recruitment in these populations when compared to populations expressing mutant SOD1 A4V and wildtype PDI. N=3, Mean $\pm$ SEM, * $p < 0.05$, *** $p < 0.001$.

4.3.14 Overexpression of PDI QUAD and the cytoplasmic PDIs decrease Caspase-3
activation induced by mutant SOD1.

To confirm these findings, Caspase-3 activation was next examined in cells expressing mutant SOD1 with PDI proteins. Caspase-3 is induced following the activation of Bax and its recruitment to the mitochondria, therefore it is indicative of later stages of apoptosis. Neuro-2A cells were transfected with pcDNA3.1, GFP, wildtype SOD1, and mutant SOD1 A4V with either pcDNA3.1 empty vector, wildtype PDI, PDI QUAD, cytoplasmic wildtype PDI or cytoplasmic PDI QUAD. After fixing, immunocytochemistry was performed using an anti-cleaved Caspase-3 antibody, specific for the cleaved, or activated form, of Caspase-3. Nuclear immunoreactivity to Caspase-3 was indicative of its activation, hence induction of apoptosis (Figure 4.20 A). Cells were stained with Hoechst to visualise the nuclei.

Less than 10% of untransfected cells or cells expressing pcDNA3.1, GFP or wildtype SOD1 displayed Caspase-3 activation. In contrast, a significant increase ($p < 0.001$) in the proportion of mutant SOD1 A4V expressing cells with Caspase-3 activation was observed (25.0% $\pm$ 3.2). However, upon co-expression of mutant SOD1 A4V with wildtype PDI or cytoplasmic wildtype PDI, there was a significant decrease ($p < 0.001$) in the proportion of cells with Caspase-3 activation (12.3% $\pm$ 2.3 and 11.3% $\pm$ 1.7, respectively). There was also a slight but significant decrease ($p < 0.05$) in the proportion of cells with Caspase-3 activation in populations co-expressing mutant SOD1 A4V and either PDI QUAD or cytoplasmic PDI QUAD (17.3% $\pm$ 1.1 and 16.0% $\pm$ 1.2, respectively) (Figure 4.20 B). Now that is has been shown that the nuclei condensation assay of apoptosis produces similar results to other apoptotic assays, only nuclei condensation was assessed in further experiments of this chapter examining apoptosis.

A
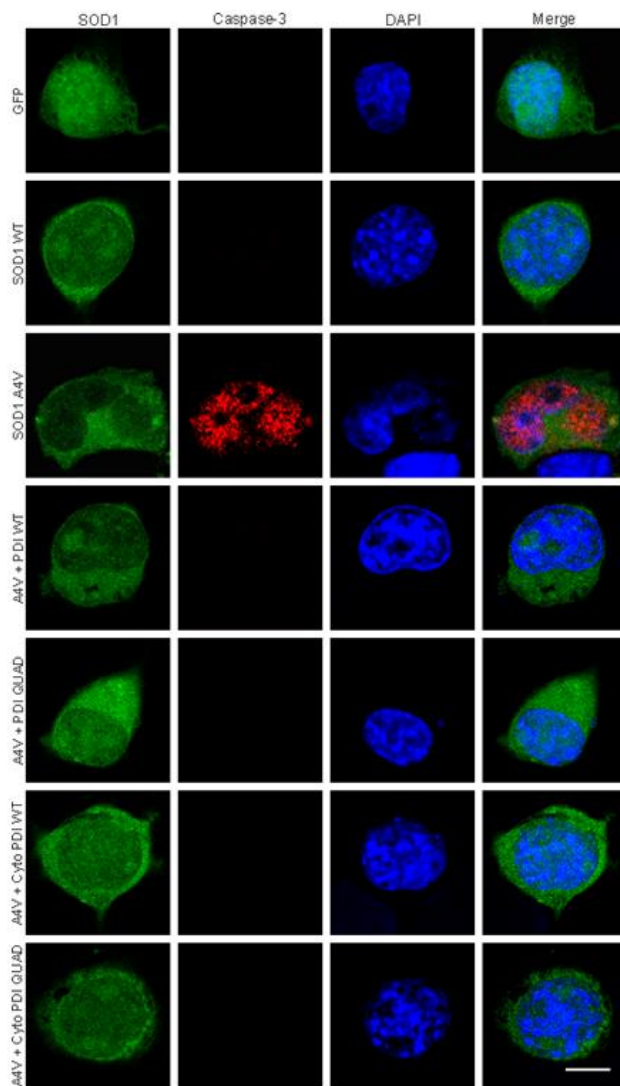
B
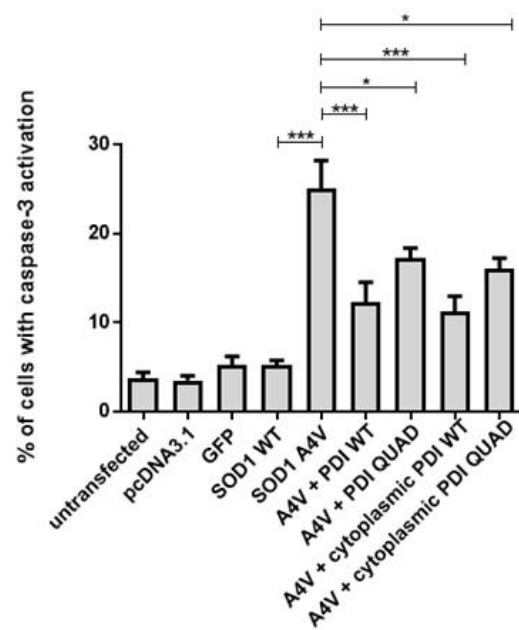
Figure 4.20: Overexpression of PDI QUAD, cytoplasmic wildtype PDI and cytoplasmic PDI QUAD inhibit Caspase-3 activation induced by mutant SOD1. A) Neuro-2A cells expressing GFP (first panel; GFP) or wildtype SOD1 (second panel; SOD1 WT) display low levels of Caspase-3 activation. In contrast, more cells expressing mutant SOD1 A4V (third panel; SOD1 A4V) demonstrate nuclear immunoreactivity to Caspase-3 (third panel, column two). However, the proportion of cells with Caspase-3 activation is reduced in mutant SOD1 A4V cells co-expressing wildtype PDI, PDI QUAD, cytoplasmic wildtype PDI, or cytoplasmic PDI QUAD (panels four to seven; A4V + PDI WT, A4V + PDI QUAD, A4V + Cyto PDI WT, A4V + Cyto PDI QUAD), compared to those expressing empty vector. Scale bar = 20 µM. **B**) Quantification of the proportion of cells with Caspase-3 activation in A). There was a significant increase in the proportion of cells with Caspase-3 activation in mutant SOD1 A4V populations, compared to those expressing wildtype SOD1, GFP or pcDNA3.1 ($p < 0.001$). There was a significant decrease, however, when mutant SOD1 A4V expressing cells were co-expressed with wildtype PDI ($p < 0.001$), PDI QUAD ($p < 0.05$), cytoplasmic wildtype PDI ($p < 0.001$) and cytoplasmic PDI QUAD ($p < 0.05$). N=3, Mean ± SEM, * $p < 0.05$, *** $p < 0.001$.

Investigation into the protective properties of PDI domain mutants in neuronal cells expressing mutant TDP-43.

The PDI domain mutants were next examined in Neuro-2A cells expressing mutant TDP-43 Q331K. Their activity on mutant TDP-43 mislocalisation to the cytoplasm and mutant TDP-43-induced ER stress was investigated in the following experiments.

4.3.15 PDI domain constructs are co-expressed in almost all cells transfected with TDP-43

It was next examined whether the PDI domain constructs were protective in cells expressing mutant TDP-43 induced. First, the co-transfection efficiency of the domain constructs and EGFP-TDP-43 was analysed in Neuro-2A cells. Cells were transfected for 72 h with EGFP-TDP-43 and either the PDI *a* domain, *a'* domain, or *bb'* domain mutants, before cells were fixed. Immunocytochemistry was then performed using an anti-V5 antibody and the nuclei were stained with Hoechst. Co-transfection was verified using fluorescence microscopy by examining EGFP expression (green) for TDP-43 and by performing immunocytochemistry using an Alexa Fluor 568-tagged secondary antibody, to detect the V5 tag of the domain mutants (Figure 4.21). The transfection efficiency of EGFP-TDP-43 was approximately 70-75% in Neuro-2A cells when observed 18 h post-transfection. For each of the three replicate experiments, at least 100 cells expressing TDP-43 were analysed using fluorescent microscopy and these cells were further examined for co-expression with the PDI domain mutants. Data was represented as mean ± standard error of the mean (SEM). Quantification revealed that approximately 97% of SOD1 transfected cells also co-expressed the PDI *a* domain, 94% also co-expressed the *a'* domain, and 96% also co-expressed the *bb'* domain. Thus, in all further experiments where TDP-43 and the domain mutants were co-transfected

and immunocytochemistry using a V5 antibody was not performed, it was assumed that detection of TDP-43 expression reflected co-expression of both TDP-43 and the domain mutants.
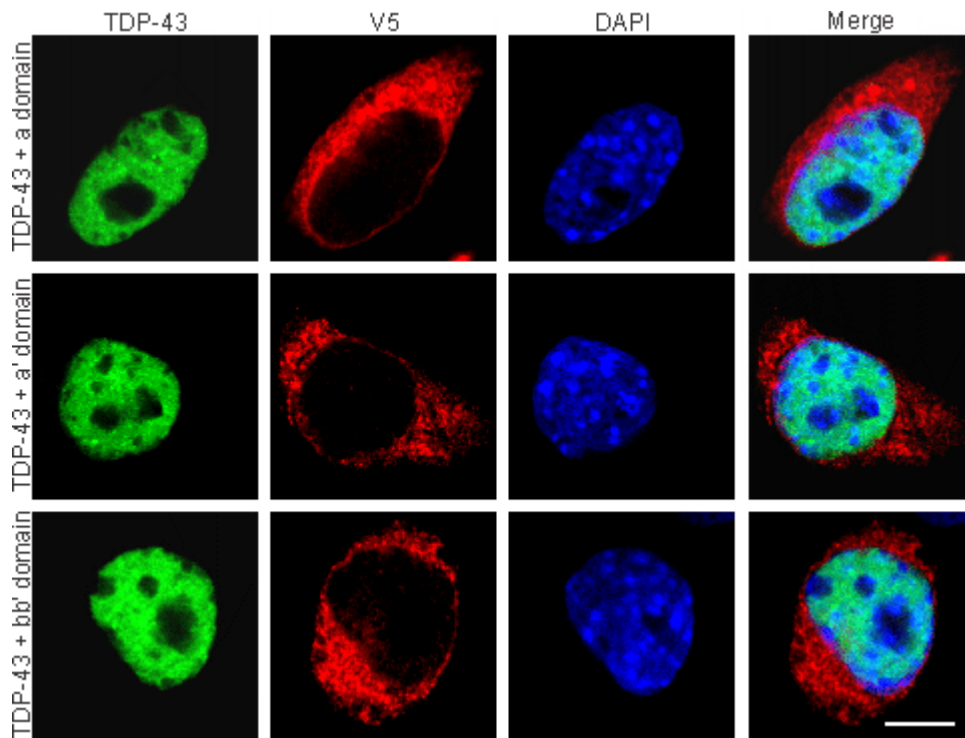
Figure 4.21: The PDI *a* domain, *a'* domain and the *bb'* domain are co-expressed in almost all Neuro-2A cells co-transfected with EGFP-TDP-43. Neuro-2A cells were transfected for 18 h with EGFP-TDP-43 (left column) with either the PDI *a* domain, *a'* domain or *bb'* domain (second column; V5). Cells were fixed and immunocytochemistry performed using an anti-V5 antibody, with nuclei stained with Hoechst (third column). The merge column indicates co-expression of the PDI domain mutants and TDP-43 in the shown cells. Scale bar = 30 µM.

4.3.16 Expression of TDP-43 and PDI domain mutants in Neuro-2A cells

Western blotting analysis was performed prior to examining cellular assays using the PDI domain mutants and TDP-43 in order to ensure that transfection of each mutant resulted in similar levels of expression and that the expressed proteins were of the expected size (Figure 4.22). Cell lysates were prepared from the following groups; GFP alone, wildtype TDP-43 co-expressed with pcDNA3.1, and mutant TDP-43 Q331K co-expressed with either pcDNA3.1, wildtype PDI, PDI *a* domain, *a'* domain or *bb'* domain. Immunoblotting revealed that wildtype and mutant TDP-43 were expressed at the expected size of 64 kDa (TDP-43 = 38 kDa, GFP = 26 kDa) and GFP was expressed at 26 kDa using an anti-GFP antibody. Wildtype TDP-43 was expressed at higher levels compared to mutant TDP-43 Q331K, as expected. PDI was detected in transfected cell lysates using an anti-V5 antibody at 62 kDa, whereas the *a* domain was detected at 15 kDa, the *a'* domain at 12 kDa and the *bb'* mutant at 25 kDa. All PDI proteins shared similar expression levels. β-actin was used as a loading control, detected using an anti-β-actin antibody (40 kDa).

A
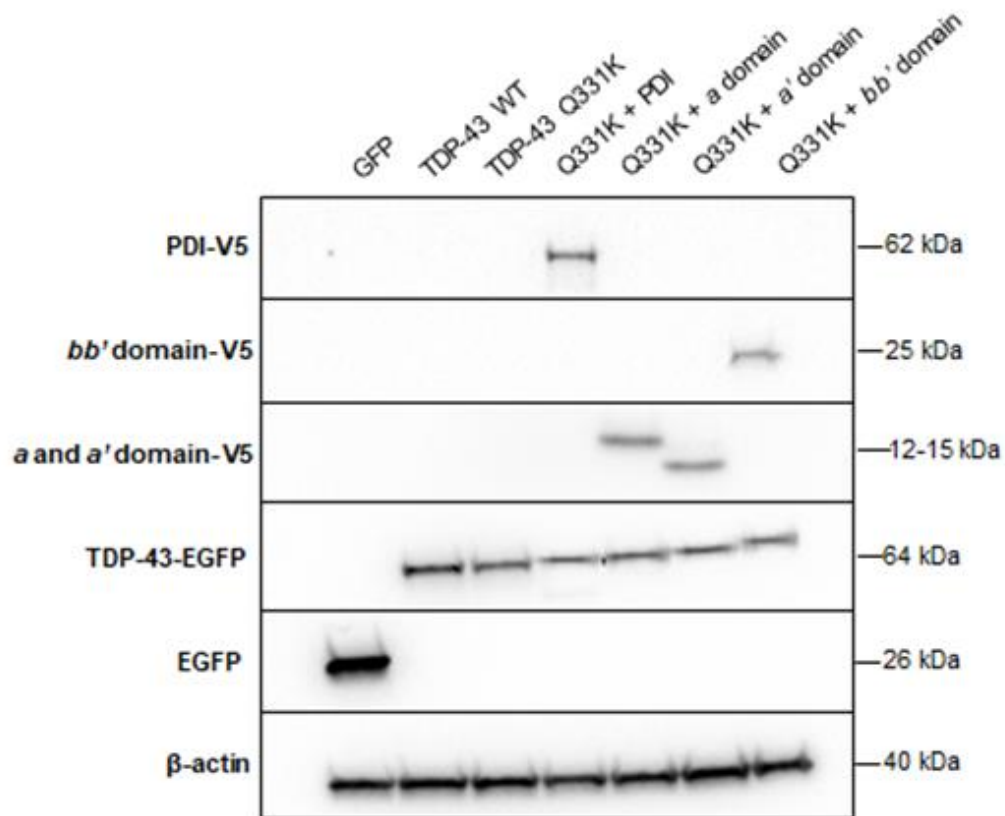
B
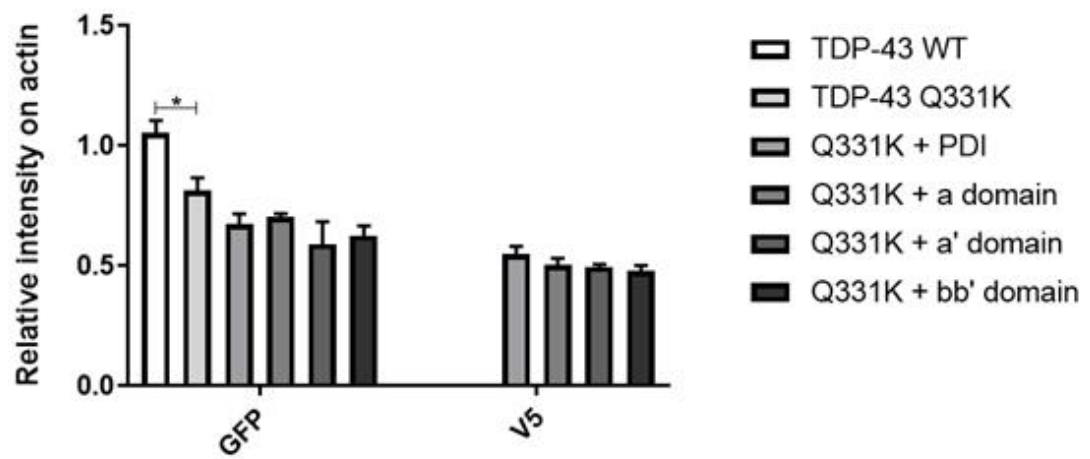
Figure 4.22: Protein expression of EGFP-TDP-43, full length PDI and the PDI domain mutants in Neuro-2A cells. A) Western blotting of cell lysates was performed and quantified to ensure that the proteins expressed were of the expected size and to verify that the expression level of each protein was similar between groups. Cell lysates examined were GFP alone, wildtype TDP-43 with empty pcDNA3.1 vector, and mutant TDP-43 Q331K with either empty pcDNA3.1 vector, full length PDI, the *a* domain, *a'* domain or *bb'* domain mutants. Wildtype and mutant TDP-43 were detected at 64 kDa and GFP was detected at 26 kDa as expected. The *a* domain mutant was detected at 15 kDa, whereas the *a'* domain mutant was expressed at 12 kDa, and *bb'* domain mutant at 25 kDa. β-actin was used as a loading control and was detected at 40 kDa. **B)** Quantification revealed that wildtype TDP-43 was expressed at significantly higher levels ($p < 0.05$) than mutant TDP-43 Q331K, as expected. Mutant TDP-43 Q331K shared similar expression levels across all cell lysate populations. Full length PDI and the PDI domain mutants were also expressed at similar expression levels. Lysates expressing GFP only were not included in quantification. N=3, Mean ± SEM, * $p < 0.05$.

4.3.17 Overexpression of PDI a or a' domain inhibits mutant TDP-43 mislocalisation to the cytoplasm

The mislocalisation of normally nuclear TDP-43 and FUS to the cytoplasm in ALS patient motor neurons is a common pathological trait shared by mutant versions of these proteins in ALS [469]. Interestingly, our laboratory has demonstrated that over expression of PDI in neuronal cells expressing mutant TDP-43 inhibits TDP-43 mislocalisation to the cytoplasm (Parakh et al., 2017 in preparation). It is unclear, however, which of PDI's functions is involved in this protective activity. Therefore, it was next investigated whether over expression of the *a* domains or *b* domains of PDI was protective against mutant TDP-43 mislocalisation to the cytoplasm in Neuro-2A cells.

Neuro-2A cells were transfected with empty pcDNA3.1 vector, GFP, wildtype TDP-43 with pcDNA3.1, and mutant TDP-43 Q331K with either pcDNA3.1, PDI, the *a* domain or *a'* domain mutants. TDP-43 localisation was analysed 18 h post-transfection because previous experiments performed in our laboratory demonstrated that TDP-43 display the maximal levels of mislocalisation to the cytoplasm [427]. Immunocytochemistry was not performed as it was assumed that EGFP-TDP-43 expression reflected co-expression with the V5-tagged mutants. However, DAPI staining using Hoechst was performed to visualise nuclei of the cells. Cells were examined for expression and localisation of TDP-43 using fluorescence microscopy, whereby at least 100 cells transfected with TDP-43 were analysed. TDP-43 was considered nuclear when it completely co-localised with the DAPI-stained nucleus. Conversely, TDP-43 was considered mislocalised when fluorescence was detected in both the nucleus and cytoplasm of TDP-43 expressing cells (Figure 4.23 A).

Wildtype TDP-43 was expressed in the cytoplasm in $5.3\% \pm 0.3$ of cells. Compared to wildtype TDP-43 expressing cells, there was a significant increase ($p < 0.001$) in the

proportion of cells displaying cytoplasmic TDP-43 in mutant TDP-43 Q331K expressing cells (17.0% ± 2.0). However, co-expression of PDI with mutant TDP-43 Q331K significantly reduced ($p < 0.01$) the proportion of cells with TDP-43 localisation in the cytoplasm to 7.7% ± 1.8, as expected. Similarly, there was a significant reduction ($p < 0.05$) in the proportion of cells with cytoplasmic expression of TDP-43 when the *a* domain was co-expressed with mutant TDP-43 (9.0% ± 0.6), revealing that the *a* domain is protective against TDP-43 mislocalisation. However, there was no significant decrease in the proportion of cells with cytoplasmic expression of TDP-43 in mutant TDP-43 Q331K populations co-expressing the *bb'* domain (14.0% ± 1.0), when compared to cells expressing mutant TDP-43 Q331K with empty pcDNA3.1 vector, although there was a significant difference ($p < 0.05$) compared to cells co-expressing mutant TDP-43 Q331K and PDI. Together these results suggest that the *b* domains of PDI are not protective against mutant TDP-43 mislocalisation to the cytoplasm (Figure 4.23 B). This result was confirmed using matched expression levels in the cells displaying mislocalised TDP-43 to ensure that the co-expression of mutant TDP-43 Q331K with either PDI, the *a* domain mutant or the *bb'* domain mutant did not decrease its expression levels (Supplementary figure 8).

Next, it was investigated whether the *a'* domain was also protective against mutant TDP-43 mislocalisation. Neuro-2A cells were transfected with empty pcDNA3.1 vector, GFP, wildtype TDP-43 with pcDNA3.1, and mutant TDP-43 with either pcDNA3.1, PDI, *a* domain or *a'* domain mutants for 18 h. Quantification revealed that there was a significant increase ($p < 0.001$) in the proportion of cells with cytoplasmic expression of TDP-43 in populations expressing mutant TDP-43 Q331K (14.7% ± 1.5), compared to cells expressing wildtype TDP-43 (1.7% ± 0.3) as expected. There was a significant reduction in the proportion of cells with cytoplasmic expression of TDP-43 when mutant TDP-43 Q331K expressing cells were also co-expressed with either PDI (5.3% ± 1.2, $p < 0.001$), the *a* domain (8.7% ± 0.9, $p <$

0.01) or *a'* domain mutants (4.7% ± 0.3, p < 0.001). Interestingly, there was a significant

difference (p < 0.05) in the proportion of cells with cytoplasmic localisation of TDP-43 in

populations expressing the *a* domain with those expressing the *a'* domain, suggesting that

the *a'* domain is more efficient in inhibiting the cytoplasmic localisation of TDP-43.,

However there were no differences in the proportion of cells with cytoplasmic expression of

TDP-43 in populations expressing either of the domain mutants to those expressing PDI

(Figure 4.23 C).
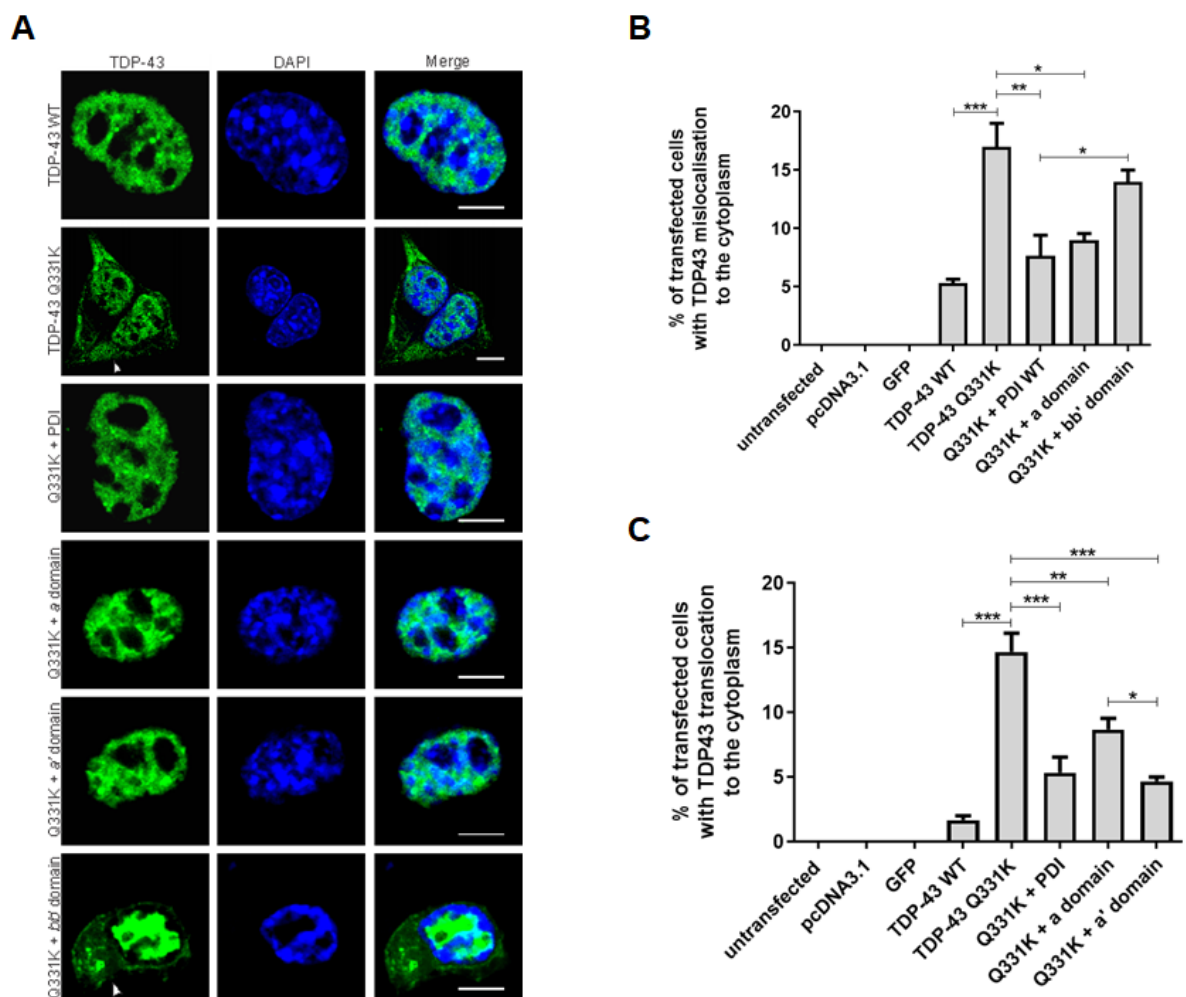
Figure 4.23: Overexpression of the PDI *a* and *a'* domains inhibits mutant TDP-43 mislocalisation to the cytoplasm. A) Immunofluorescence images of Neuro-2A cells expressing wildtype TDP-43 with empty pcDNA3.1 vector, and mutant TDP-43 Q331K co-expressing either pcDNA3.1, PDI, the *a* domain, *a'* domain or *bb'* domain. Cells expressing wildtype TDP-43 (first panel; TDP-43 WT) display mainly nuclear localisation of TDP-43, whereas more TDP-43 Q331K (second panel; TDP-43 Q331K) cells express TDP-43 in the cytoplasm, as indicated by the white arrowhead (second panel, first column). When mutant TDP-43 Q331K was co-expressed with PDI (third panel; Q331K + PDI), the *a* domain (fourth panel; Q331K + *a* domain) or the *a'* domain mutants (fifth panel; Q331K + *a'* domain), significantly fewer cells expressed TDP-43 in the cytoplasm. In comparison, more cells co-expressing mutant TDP-43 Q331K with the *bb'* domain mutant (sixth panel; Q331K + *bb'* domain) expressed TDP-43 in the cytoplasm, as indicated by the white arrowhead (sixth panel, first column). Scale bar = 20 µM. **B)** Quantification of cells with TDP-43 mislocalisation in A). There was a significant increase ($p < 0.001$) in the proportion of cells with TDP-43 mislocalisation in cells expressing mutant TDP-43 Q331K, compared to cells expressing wildtype TDP-43 as expected. A significant decrease in the proportion of cells with cytoplasmic TDP-43 was observed when mutant TDP-43 Q331K was co-expressed with either PDI ($p < 0.01$) or the *a* domain mutant ($p < 0.05$). However, there was a significant increase ($p < 0.05$) in the proportion of cells with cytoplasmic TDP-43 in populations co-expressing mutant TDP-43 Q331K and the *bb'* domain mutant, compared to cells co-expressing TDP-43 Q331K with PDI. N=3, Mean ± SEM, * $p < 0.05$, ** $p < 0.01$, *** $p < 0.001$. **C)** Quantification of cells with cytoplasmic TDP-43 in A). There was a significant increase ($p < 0.001$) in the proportion of cells with cytoplasmic localisation of TDP-43 in populations expressing mutant TDP-43 Q331K, compared to cells expressing wildtype TDP-43. A significant decrease in the proportion of cells with cytoplasmic TDP-43was observed

when mutant TDP-43 Q331K was co-expressed with either PDI ($p < 0.001$), the *a* domain ($p < 0.01$) or *a'* domain ($p < 0.001$) mutants. Also, there was a significantly higher ($p < 0.05$) proportion of cells with cytoplasmic localisation of TDP-43 in populations co-expressing the *a* domain and mutant TDP-43 Q331K, compared to those co-expressing the *a'* domain and TDP-43 Q331K. N=3, Mean $\pm$ SEM, * $p < 0.05$, ** $p < 0.01$, *** $p < 0.001$.

4.3.18 Overexpression of PDI's a domain, a' domain, or bb' domains are protective against mutant TDP-43 induced ER stress

Our laboratory has previously shown that the overexpression of mutant TDP-43 induces ER stress in neuronal cells compared to wildtype TDP-43 [427] and that PDI co-precipitates with mutant TDP-43 and is also upregulated in transgenic mutant TDP-43 mouse spinal cords [427]. More recently, our laboratory has demonstrated that the overexpression of PDI inhibits ER stress in Neuro-2A cells expressing mutant TDP-43, as detected by the activation of CHOP or XBP-1(Parakh et al., 2017 in preparation). Therefore, it was next investigated whether the domain mutants and hence which regions of PDI are responsible for the protective activity against ER stress.

Neuro-2A cells were transfected with empty pcDNA3.1 vector, GFP, wildtype TDP-43 with empty pcDNA3.1 vector, and mutant TDP-43 Q331K with either pcDNA3.1, PDI the *a* domain or *a'* domain mutant. After 72 h transfection, the cells were fixed and immunocytochemistry was performed using an anti-CHOP antibody to probe for nuclear immunoreactivity to CHOP, as previous. Cells were also stained with Hoechst to visualise the nuclei. Fluorescence microscopy was utilised to analyse at least 100 transfected cells, whereby nuclear immunoreactivity to CHOP indicated activation, and thus, induction of ER stress (Figure 4.24 A).

Quantification revealed very little CHOP activation in untransfected cells and cells transfected with empty pcDNA3.1 vector and GFP (less than 5% cells). Only 8.3% ± 0.9 of cells expressing wildtype TDP-431 displayed CHOP activation and as expected, significantly more cells expressing mutant TDP-43 Q331K displayed ($p < 0.001$) nuclear CHOP immunoreactivity (20.3% ± 0.7) in comparison. Similar to previous reports, there was a significant decrease ($p < 0.01$) in the proportion of cells with nuclear immunoreactivity to

CHOP when cells were co-expressed with PDI and mutant TDP-43 Q331K (9.3% ± 1.5), compared to cells expressing mutant TDP-43 Q331K alone. Similarly, significantly fewer cells co-expressing the *a* domain with mutant TDP-43 Q331K ($p < 0.01$) displayed CHOP activation (10.0% ± 3.2) compared to cells expressing mutant TDP-43 Q331K alone. Together these data indicate that the disulphide interchange activity of PDI is protective against ER stress induced by mutant TDP-43. Interestingly, significantly fewer cells co-expressing the *bb'* domain with TDP-43 Q331K displayed ($p < 0.001$) nuclear CHOP immunoreactivity (9.0% ± 1.0), suggesting that the chaperone function of PDI also contributes to inhibition of ER stress induced by mutant TDP-43 (Figure 4.24 B).

Next, the *a* and *a'* domain mutants were compared for their protective activity against mutant TDP-43 induced activation of CHOP. Neuro-2A cells were transfected with empty pcDNA3.1 vector, GFP, wildtype TDP-43 with pcDNA3.1, and TDP-43 Q331K with either pcDNA3.1, PDI, the *a* domain or *a'* domain mutants. Immunocytochemistry was performed using an anti-CHOP antibody to examine nuclear immunoreactivity of CHOP, indicative of its activation, and cells were stained with Hoechst to visualise the nuclei. As expected, there was little CHOP activation in untransfected cells and in cells expressing pcDNA3.1, GFP and wildtype SOD1 (less than 10%). There was a significant increase ($p < 0.001$) in the proportion of cells with CHOP activation in populations expressing mutant TDP-43 Q331K (23.7% ± 1.3), compared to cells expressing wildtype TDP-43 (8.0% ± 1.2). A significant decrease ($p < 0.001$) in the proportion of cells with CHOP activation was detected when mutant TDP-43 Q331K was co-expressed with either PDI (9.3% ± 1.7) or the *a* domain mutant (11.7% ± 0.3), compared to cells co-expressing empty pcDNA3.1 vector. There was also a significant reduction ($p < 0.05$) in the proportion of cells with CHOP activation when mutant TDP-43 Q331K was co-expressed with the *a'* domain mutant (16.3% ± 2.6). Hence these data imply that both *a* and a' domains exhibit protective activity against mutant TDP-

43-induced ER stress. However, significantly more (p < 0.05) cells expressing the a' domain displayed nuclear immunoreactivity to CHOP compared to those co-expressing PDI with TDP-43 Q331K, suggesting that the protective activity of the *a'* domain mutant may not be as effective as that of PDI (Figure 4.24 C).
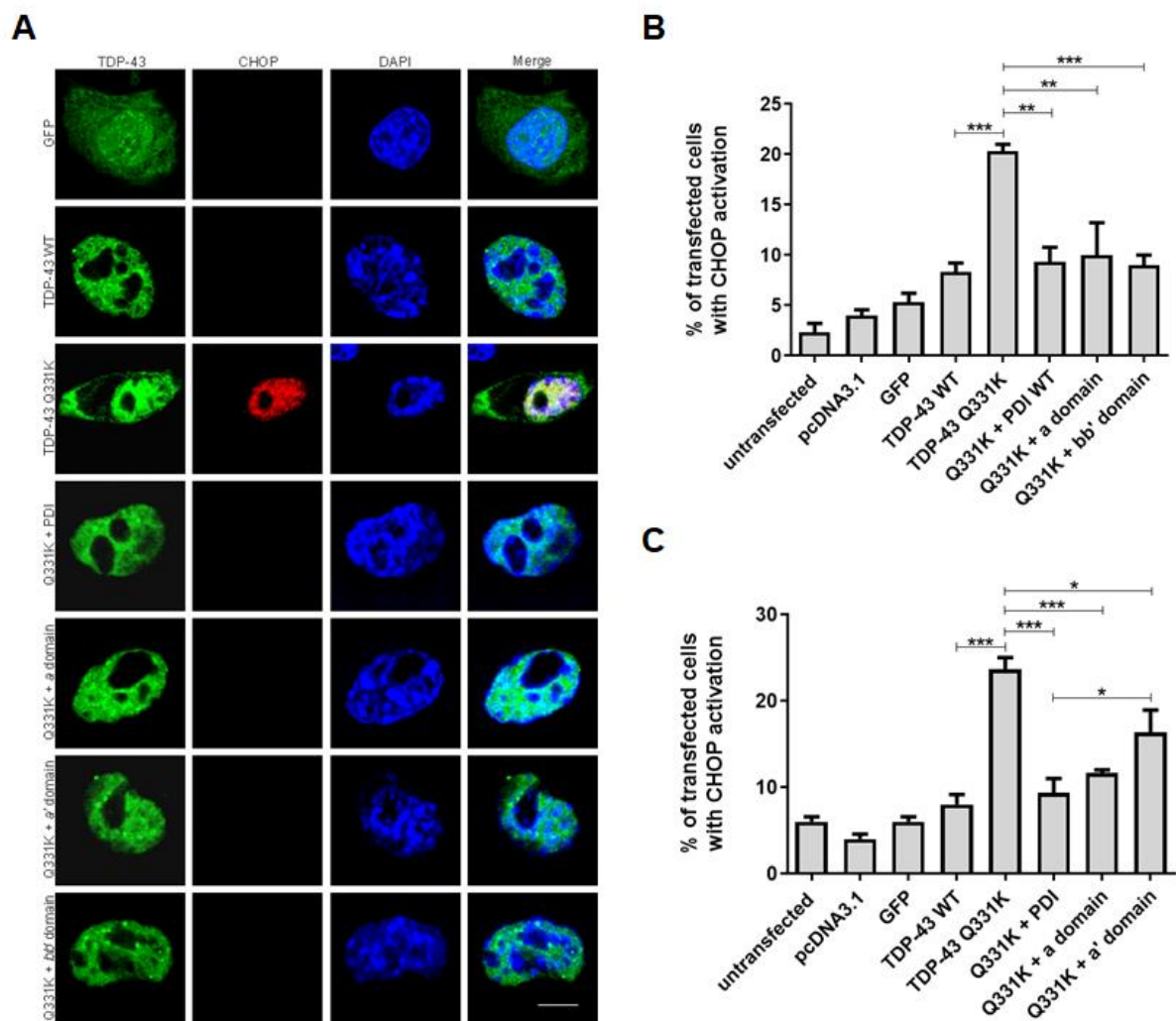
Figure 4.24: Overexpression of the *a domain*, *a' domain* or the *bb' domain* is protective against CHOP activation induced by mutant TDP-43. A) Immunofluorescence images of Neuro-2A cells expressing GFP alone, wildtype TDP-43, and mutant TDP-43 Q331K co-expressed with either pcDNA3.1, PDI, *a* domain, *a'* domain or *bb'* domain (first column), with or without nuclear immunoreactivity to CHOP (second column). The third column illustrates DAPI-stained nuclei and the fourth column depicts a merged image of the cell. Few cells expressing GFP or wildtype TDP-43 (first and second panel; GFP, TDP-43 WT) displayed CHOP activation. Conversely, more cells expressing mutant TDP-43 Q331K and pcDNA3.1 (third panel; TDP-43 Q331K) displayed CHOP activation, as indicated by red fluorescence in the nucleus (third panel, second column). However, when either PDI (fourth panel; Q331K + PDI), the *a* domain (fifth panel; Q331K + *a* domain), *a'* domain (sixth panel; Q331K + *a'* domain) or *bb'* domain (seventh panel; Q331K + *bb'* domain) mutants were co-expressed with TDP-43 Q331K, fewer cells displayed CHOP activation, indicating ER stress. Scale bar = 20 μM. **B)** Quantification of cells in A) with CHOP nuclear immunoreactivity. The proportion of cells with CHOP activation was significantly higher in populations expressing mutant TDP-43 Q331K, compared to wildtype TDP-43 ($p < 0.001$) as expected. However, significantly fewer cells displayed CHOP activation when PDI ($p < 0.01$), the *a* domain ($p < 0.01$) or the *bb'* domain ($p < 0.001$) was co-expressed with TDP-43 Q331K, implying that both the *a* and *bb'* domains are protective against mutant TDP-43-induced ER stress. N=3, Mean ± SEM, * $p < 0.05$, ** $p < 0.01$, *** $p < 0.001$. **C)** Quantification of the cells in A) with nuclear immunoreactivity to CHOP. The proportion of cells with CHOP activation was significantly higher in populations expressing mutant TDP-43 Q331K, compared to those expressing wildtype TDP-43 ($p < 0.001$). Significantly fewer cells with CHOP activation were present when PDI ($p < 0.001$), the *a* domain ($p < 0.001$) or the *a'* domain ($p < 0.05$) mutants, were co-expressed with TDP-43 Q331K. However, there was a

significant difference (p < 0.05) in the proportion of cells with CHOP activation between TDP-43 Q331K cells co-expressing PDI and those co-expressing the *a'* domain. N=3, Mean ± SEM, * p < 0.05, *** p < 0.001.

Investigation into the protective properties of PDI domain mutants in neuronal cells expressing mutant FUS

The PDI domain mutants were finally examined for protective effect in Neuro-2A cells expressing mutant FUS R521G. Their activity on mutant FUS mislocalisation to the cytoplasm and mutant FUS-induced ER stress were analysed in this section.

4.3.19 PDI domain mutants are co-expressed in almost all cells transfected with FUS

Finally, the PDI domain mutants were analysed for their protective activity against mutant FUS is. Similar to the SOD1 and TDP-43 experiments the co-transfection efficiency of FUS and the PDI domain mutants were first examined in Neuro-2A cells. Cells were transfected with mutant GFP FUS R521G and the PDI *a* domain, *a'* domain or *bb'* domain mutants for 72 h. Cells were fixed, immunocytochemistry using an anti-V5 antibody performed, and nuclei stained with Hoechst. Co-transfection was confirmed by analysing GFP expression (green) for FUS and performing immunocytochemistry with an Alexa Fluor 568-tagged secondary antibody to detect the V5 tag of the domain mutants (Figure 4.25). Upon observation at 72 h post transfection, the overall transfection efficiency of GFP FUS was approximately 80 % in Neuro-2A cells. For each of the three replicate experiments, at least 100 FUS expressing cells were visualised using fluorescent microscopy, and these cells were further analysed for co-expression with the PDI *a* domain, *a'* domain and *bb'* domain mutants. Quantification revealed that approximately 97 % of FUS expressing cells also co-expressed the PDI *a* domain, 94 % also co-expressed the *a'* domain, and 97 % also co-expressed the *bb'* domain mutants. Thus, in further experiments, it was assumed that FUS

expression reflected co-expression of both FUS and the PDI domain mutants when they were

co-transfected but immunocytochemistry using a V5 antibody was not performed.
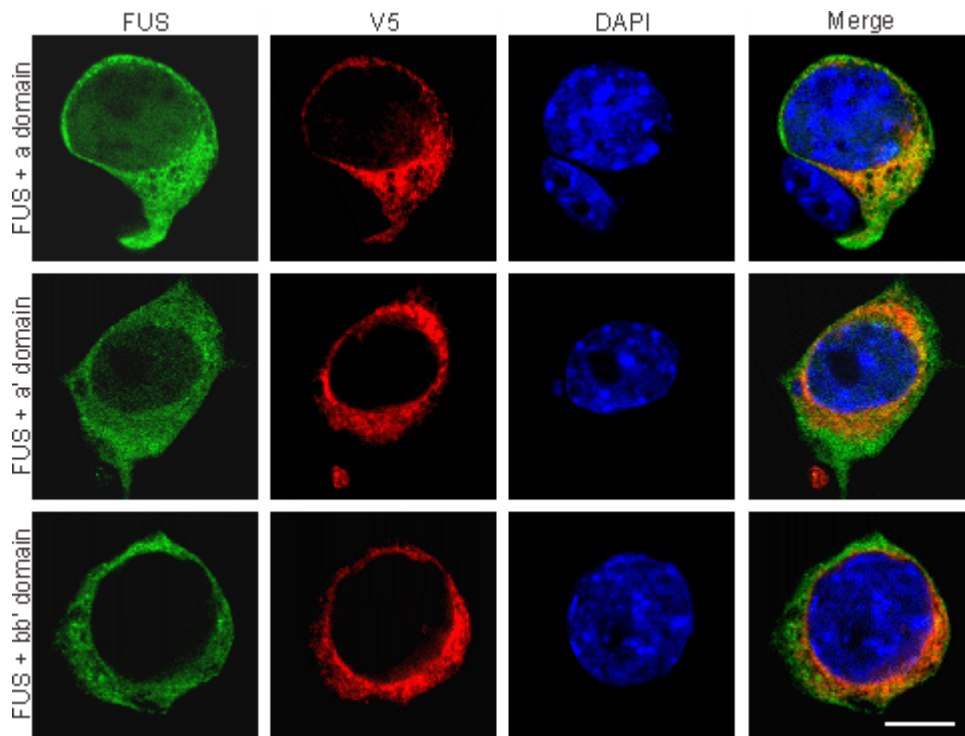
Figure 4.25: The PDI *a* domain, *a' * domain and *bb'* domain are co-expressed in almost all Neuro-2A cells co-expressing GFP FUS. Neuro-2A cells were transfected with GFP FUS (left column) and the PDI domain mutants (second column; V5) for 72 h. Cells were fixed, immunocytochemistry was performed using an anti-V5 antibody, and the nuclei were stained with Hoechst (third column). The merge column illustrates co-expression of the PDI domain mutants and FUS in the cells shown. Scale bar = 30 µM.

4.3.20 Expression of FUS and PDI domain mutants in Neuro-2A cells

Western blotting analysis was next undertaken to confirm that the expressed proteins were of the expected size and that transfection of each mutant resulted in comparable levels of protein expression (Figure 4.26). Cell lysates were prepared from the following groups; GFP alone, wildtype FUS co-expressed with pcDNA3.1, and mutant FUS R521G co-expressed with either pcDNA3.1, PDI, PDI *a* domain, *a'* domain or *bb'* domain mutants. Immunoblotting revealed that wildtype and mutant FUS GFP proteins were expressed at the expected size of 100 kDa, and GFP alone was expressed at 26 kDa, using an anti-GFP antibody. PDI was detected at 62 kDa, PDI *a* domain at 15 kDa, *a'* domain at 12 kDa and *bb'* domain at 25 kDa, using an anti-V5 tag antibody. β-actin was used as a loading control and was detected at 40 kDa using an anti-β-actin antibody.

A
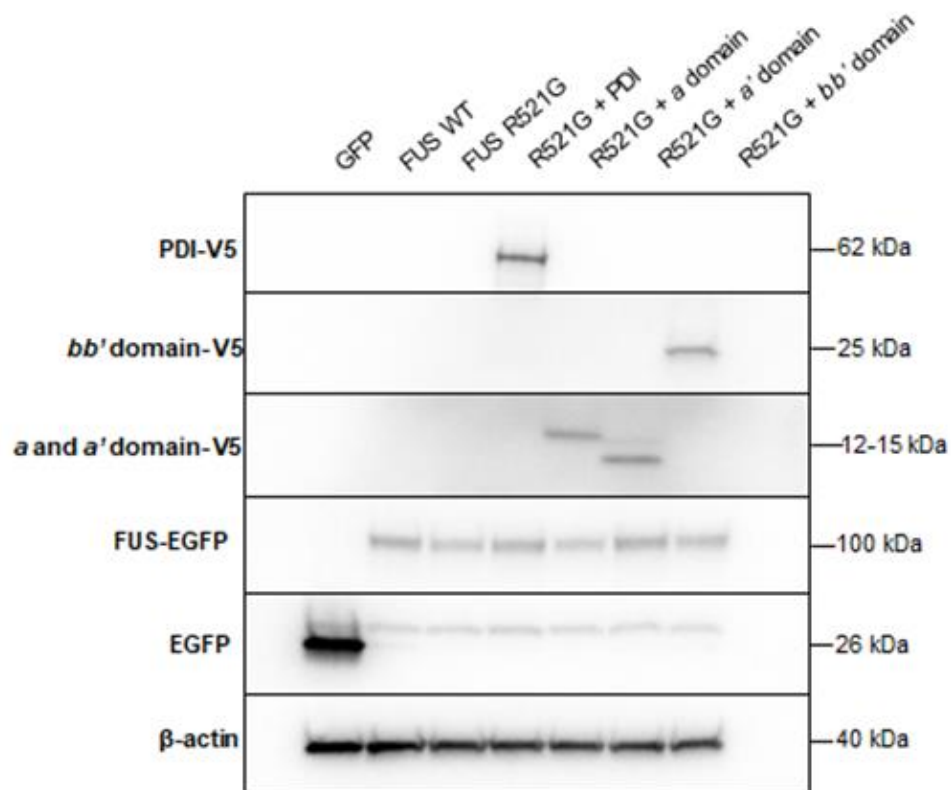
B
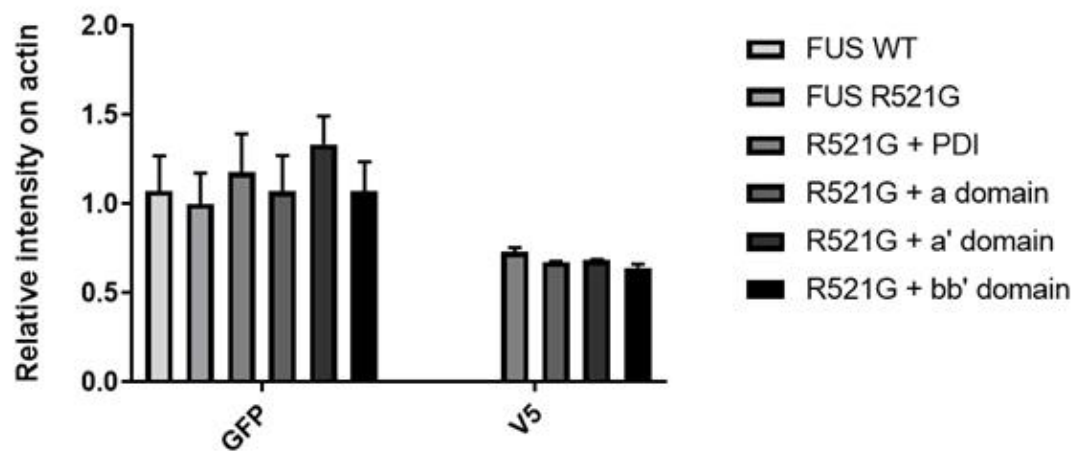
Figure 4.26: Protein expression of the PDI domain mutants and GFP FUS in Neuro-2A cells. A) Western blotting of cell lysates was performed and quantified to determine if protein expression levels were comparable between groups and to ensure that proteins were expressed at the expected size. Cell lysates examined were GFP alone, wildtype FUS with pcDNA3.1, and mutant FUS R521G with either pcDNA3.1, PDI, PDI *a* domain, *a'* domain or *bb'* domain mutants. PDI was detected at 62 kDa, the PDI *a* domain was detected at 15 kDa, the *a'* domain was detected at 12 kDa, and the *bb'* domain was detected at 25 kDa. Wildtype and mutant FUS were detected at 100 kDa (FUS = 74 kDa, GFP = 26 kDa) and GFP alone at 26 kDa. β-actin was used as a loading control and was expressed at 40 kDa. **B)** Quantification revealed that wildtype FUS and mutant FUS R521G shared similar expression levels. Similarly, full length PDI and the PDI domain mutants also demonstrated comparable levels of expression. Lysates expressing GFP only were not included in quantification. N=3, Mean ± SEM.

4.3.21 Overexpression of the 'a' or a' domains of PDI inhibits mutant FUS mislocalisation to the cytoplasm

Our laboratory has previously demonstrated that PDI colocalises with FUS in ALS cell lines and in ALS patient tissue [426]. Furthermore, more recent studies have shown that PDI overexpression is protective against mutant FUS mislocalisation to the cytoplasm in neuronal cell lines (Parakh et al., 2017 in preparation). Hence, the activity of PDI's *a* and *b* domains was next investigated to determine which regions of PDI are essential in preventing the cytoplasmic localisation of FUS.

Neuro-2A cells were transfected with empty pcDNA3.1 vector, GFP, wildtype FUS with pcDNA3.1, and mutant FUS R521G with either pcDNA3.1, PDI, the *a* domain or *bb'* domain mutants for 72 h. After fixing, cells were stained with Hoechst to visualise the nuclei. Immunocytochemistry was not performed as it was assumed that FUS expression reflected co-expression with the V5-tagged mutants, as determined in section 4.3.21. At least 100 transfected cells were examined for the localisation of FUS using fluorescence microscopy. FUS was considered cytoplasmic when fluorescence was detected only in the cytoplasm, and was considered nuclear when fluorescence was detected in both the nucleus and the cytoplasm (Figure 4.27 A). The reason that mislocalisation in mutant FUS expressing cells were categorised differently to mutant TDP-43 expressing cells is that a much higher percentage of cells were localised only in the cytoplasm compared to TDP-43. The R521G mutation of FUS is an aggressive form and studies have demonstrated that it is highly retained in the cytoplasm, characterised by a high proportion of insoluble FUS and a decrease in soluble nuclear FUS [137].

Quantification revealed that in populations expressing wildtype FUS, FUS was never localised in the cytoplasm. Conversely, 75.3% $\pm$ 5.2 of mutant FUS R521G populations

expressed cytoplasmic FUS. There was a significant decrease in the proportion of cells exhibiting cytoplasmic localisation when mutant FUS R521G populations were co-expressed with either PDI (56.0% ± 1.5, $p < 0.01$) or the *a* domain (54.3% ± 3.8, $p < 0.001$), compared to FUS R521G populations co-expressed with empty pcDNA3.1 vector. However, there was no significant difference in the proportion of cells with cytoplasmic localisation in populations co-expressing mutant FUS R521G with pcDNA3.1 to those co-expressing FUS R521G with the *bb'* domain (67.7% ± 2.6). A significant difference ($p < 0.05$) was observed in the proportion of cells co-expressing FUS R521G with the *a* domain and those co-expressing the *bb'* domain, suggesting that the *a* domain, and thus PDI's disulphide interchange activity, is required for inhibiting the cytoplasmic mislocalisation of FUS (Figure 4.27 B).

Next, the cytoplasmic localisation of FUS was examined in cells co-expressing the *a'* domain compared to those co-expressing the *a* domain. Neuro-2A cells were transfected with pcDNA3.1, GFP, wildtype FUS with pcDNA3.1, and mutant FUS R521G with either pcDNA3.1, PDI, the *a* domain or *a'* domain mutants. Quantification revealed that there was a significant increase ($p < 0.001$) in the proportion of mutant R521G cells displaying cytoplasmic FUS (88.3% ± 0.9), compared to cells expressing wildtype FUS (2.7% ± 1.3). Co-expression of PDI and mutant R521G resulted in significantly fewer ($p < 0.001$) cells with FUS mislocalisation to the cytoplasm, compared to those expressing mutant R521G alone (75.3% ± 0.9). Similarly, a significant decrease in the proportion of cells with cytoplasmic FUS was observed when mutant R521G was co-expressed with either the *a* domain (77.7% ± 1.2, $p < 0.01$), or the *a'* domain mutants (71.0% ± 2.3, $p < 0.001$), indicating that both PDI's *a* and a' domains inhibit the mislocalisation of FUS to the cytoplasm (Figure 4.27 C).

A

	FUS	DAPI	Merge
FUS			
FUS R521G			
R521G + PDI			
R521G + *a* domain			
R521G + *a'* domain			
R521G + *bb'* domain			

B
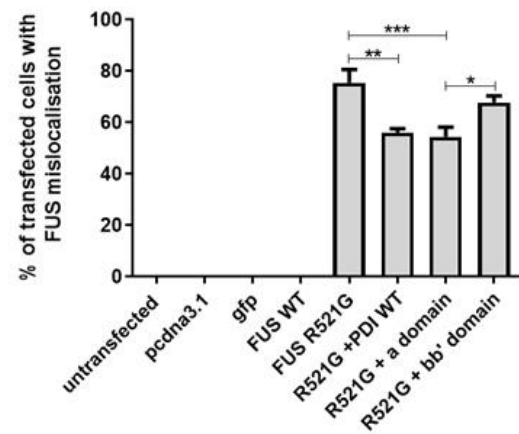
C
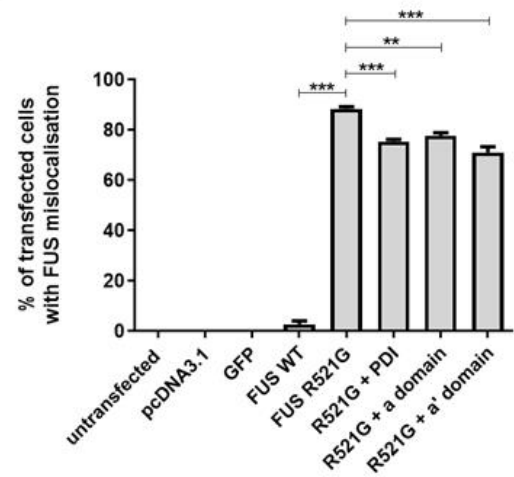
Figure 4.27: Overexpression of the PDI *a* and *a'* domains inhibits mutant FUS mislocalisation to the cytoplasm. A) Immunofluorescence images of Neuro-2A cells expressing wildtype FUS with empty pcDNA3.1 vector and mutant FUS R521G with either pcDNA3.1, PDI, the *a* domain, *a'* domain or *bb'* domain mutant (first column). DAPI-stained nuclei are illustrated in column two, and a merged image of the cell is shown in column three. Cells expressing wildtype FUS displayed nuclear localisation (first panel; FUS WT), whereas more cells expressing mutant R521G (second panel; FUS R521G) displayed cytoplasmic localisation of FUS, with no expression in the nucleus. When PDI, the *a* domain or *a'* domain mutants, were co-expressed with mutant FUS R521G (panels three – five; R521G + PDI, R521G + *a* domain, R521G + *a'* domain), fewer cells displayed FUS localisation in the cytoplasm, as indicated by expression in both the nucleus and cytoplasm. However, more cells co-expressing mutant FUS R521G and the *bb'* domain (sixth panel; R521G + *bb'* domain) displayed cytoplasmic FUS. Scale bar = 20 µM. **B)** Quantification of Neuro-2A cells with FUS mislocalisation in A). As expected, FUS was never expressed in the cytoplasm in populations expressing wildtype FUS, in contrast to the majority of cells expressing mutant FUS R521G. There was a significant decrease in the proportion of cells with cytoplasmic FUS when PDI ($p < 0.01$) and the *a* domain ($p < 0.001$) mutant were co-expressed with mutant R521G, compared to cells expressing mutant FUS R521G alone. Compared to cells co-expressing mutant FUS R521G and the *a* domain mutant, there was a significant increase ($p < 0.05$) in in the proportion of cells with cytoplasmic FUS when cells were co-expressing mutant R521G and the *bb'* domain mutant. N=3, Mean ± SEM, * $p < 0.05$, ** $p < 0.01$, *** $p < 0.001$. **C)** Quantification of Neuro-2A cells with FUS mislocalisation in A). There was a significant increase ($p < 0.001$) in the proportion of cells with cytoplasmic FUS in populations expressing mutant FUS R521G, compared to those expressing wildtype FUS. A significant decrease in the proportion of cells with cytoplasmic FUS was observed when

mutant FUS R521G cells were co-expressed with PDI (p < 0.001), the *a* domain (p < 0.01) or

a' domain mutants (p < 0.001). N=3, Mean ± SEM, ** p < 0.01, *** p < 0.001.

4.3.22 Overexpression of PDI's a domain, a' domain or bb' domains are protective against mutant FUS induced ER stress

Previously, our laboratory demonstrated that ER stress is triggered in cells expressing mutant FUS, and this is closely associated with FUS redistribution to the cytoplasm [426]. Moreover, recent studies have demonstrated that PDI overexpression is protective against FUS induced ER stress in neuronal cells (Parakh et al., 2017 in preparation). It is currently unclear, however, which PDI functions mediate this protective activity. Therefore, the PDI domain mutants were next examined for their effect on mutant FUS induced CHOP activation.

Neuro-2A cells were transfected with pcDNA3.1, GFP, wildtype FUS with pcDNA3.1, and mutant FUS R521G with either pcDNA3.1, PDI, the *a* domain or *bb'* domain mutants for 72 h. Immunocytochemistry was performed using an anti-CHOP antibody to detect immunoreactivity in the nucleus, indicating its activation, and thus induction of ER stress. At least 100 transfected were analysed using fluorescence microscopy (Figure 4.28 A).

Quantification revealed that few untransfected cells or cells expressing either pcDNA3.1, GFP or wildtype FUS displayed nuclear immunoreactivity to CHOP (less than 5%). There was a significant increase ($p < 0.001$) in the proportion of cells with CHOP activation in populations expressing mutant FUS R521G (19.3% $\pm$ 2.0), compared to those expressing wildtype FUS (1.7% $\pm$ 0.9) as expected. Significantly fewer ($p < 0.001$) cells with CHOP activation were detected when PDI was co-expressed with mutant FUS R521G (6.3% $\pm$ 0.3), compared to cells expressing mutant FUS R521G alone. Moreover, there was also a significant decrease ($p < 0.01$) in the proportion of cells with CHOP activation when either the a or bb' domain mutants was co-expressed with FUS R521G, to 9.0% $\pm$ 1.5 and 9.3% $\pm$ 2.0 cells respectively. These data therefore indicate that both the disulphide interchange

activity and chaperone function of PDI are protective against mutant FUS-induced ER stress (Figure 4.28 B).

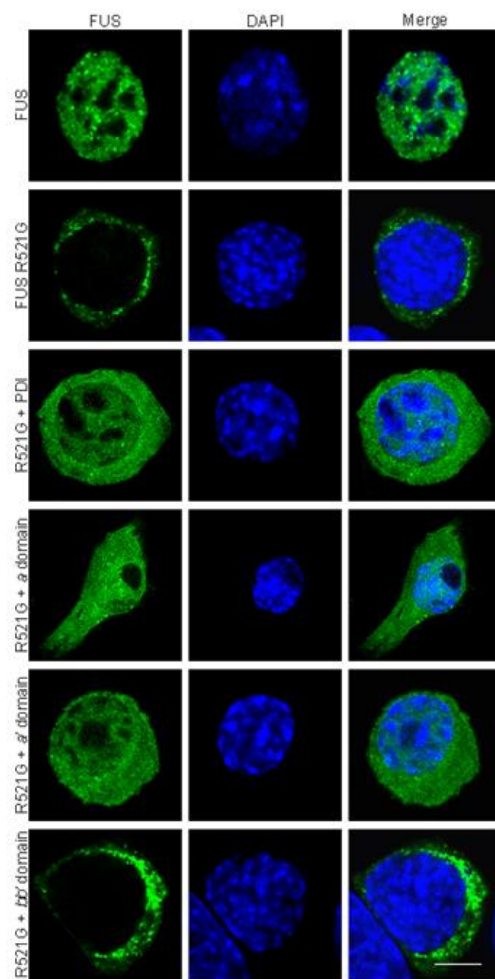Finally, the activity of the *a'* domain mutant against CHOP activation was compared to that of the *a* domain. Neuro-2A cells were transfected with pcDNA3.1, GFP, wildtype FUS and pcDNA3.1, and mutant FUS R521G with pcDNA3.1, PDI, the *a* domain or *a'* domain mutants. As expected, there was a significant increase ($p < 0.001$) in the proportion of cells displaying CHOP activation in populations expressing mutant FUS R521G ($27.7\% \pm 2.0$), compared to those expressing wildtype FUS ($8.3\% \pm 0.9$). Significantly fewer cells displayed CHOP activation when PDI or the *a* domain mutant was co-expressed with mutant FUS R521G ($13.0\% \pm 0.6$, $p < 0.001$ $17.7\% \pm 1.5$, $p < 0.01$ respectively). Similarly, there was a significant reduction ($p < 0.001$) in the proportion of cells with nuclear immunoreactivity to CHOP when the *a'* domain mutant was co-expressed with FUS R521G ($15.7\% \pm 0.9$) compared to those co-transfected with empty vector. Hence these data imply that both *a* and *a'* domains are protective against mutant FUS-induced ER stress (Figure 4.28 C).

A

	FUS	CHOP	DAPI	Merge
GFP				
FUS				
FUS R521G				
R521G + PDI				
R521G + a domain				
R521G + a' domain				
R521G + bb' domain				

B

C

230
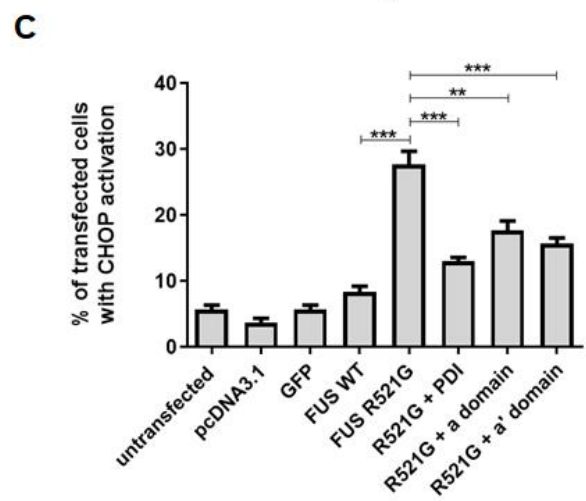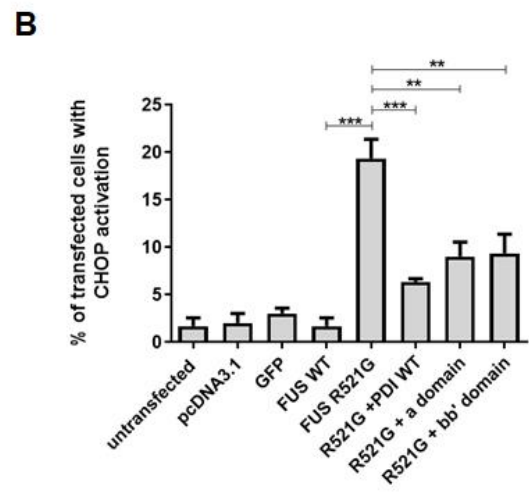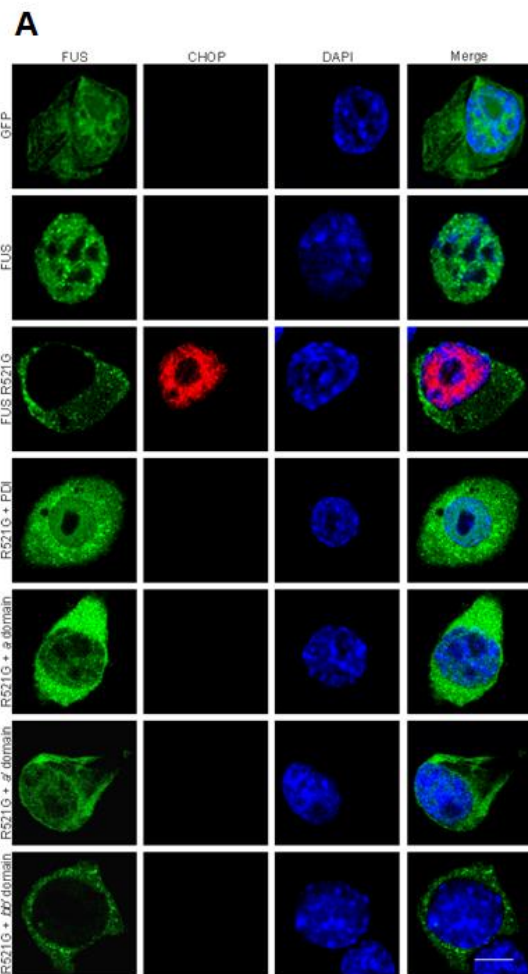
Figure 4.28: PDI's *a*, *a'* and *bb'* domains are protective against CHOP activation induced by mutant FUS. A) Immunofluorescence images of Neuro-2A cells expressing GFP (first panel; GFP) or wildtype FUS (second panel; FUS WT) reveal minimal levels of CHOP activation in these populations. In contrast, more cells expressing mutant FUS R521G (third panel; FUS R521G) exhibit CHOP activation, indicated by nuclear immunoreactivity (as shown in the third panel, column two). However, co-expression of mutant FUS R521G with PDI (fourth panel; R521G + PDI), the *a* domain (fifth panel; R521G + *a* domain), *a'* domain (sixth panel; R521G + *a'* domain) or *bb'* domain (seventh panel; R521G + *bb'* domain) resulted in fewer cells with CHOP activation. Scale bar = 20 µM. **B)** Quantification of cells with CHOP activation in A). Very few untransfected cells or cells expressing pcDNA3.1, GFP or wildtype FUS displayed nuclear immunoreactivity to CHOP. Significantly more cells ($p < 0.001$) expressing mutant FUS R521G displayed CHOP activation, however this proportion was significantly decreased when either PDI ($p < 0.001$), the *a* domain ($p < 0.01$) or the *bb'* domain ($p < 0.01$) mutant was co-expressed with FUS R521G. N=3, Mean ± SEM, ** $p < 0.01$, *** $p < 0.001$. **C)** Quantification of cells with CHOP activation in A). Significantly more cells ($p < 0.001$) expressing mutant FUS R521G displayed CHOP activation, compared to untransfected cells and populations expressing pcDNA3.1, GFP or wildtype FUS. There was a significant reduction in the proportion of cells with CHOP activation when PDI ($p < 0.001$), the *a* domain ($p < 0.01$) or the *a'* domain ($p < 0.01$) mutants were co-expressed with mutant FUS R521G. N=3, Mean ± SEM, ** $p < 0.01$, *** $p < 0.001$.

4.3.23 A summary of the protective activity of the PDI domain mutants

A summary of the protective effects of the PDI domain mutants against ALS-associated proteins, SOD1, TDP-43 and FUS, is shown in Table 4.3. The *a* and *a'* domains demonstrated a protective effect against all cellular mechanisms of pathogenesis across all three mutant proteins. The *bb'* domain mutant only elicited a protective effect against ER stress induced by either mutant SOD1, TDP-43 or FUS.

TABLE 4.3 The protective activities of the PDI domain mutants.

SOD1			
	Inclusion formation	**ER stress**	**Apoptosis**
a domain	✔	✔	✔
a' domain	✔	✔	✔
bb' domain	✘	✔	✘
TDP-43			
	TDP-43 mislocalisation		**ER stress**
a domain	✔		✔
a' domain	✔		✔
bb' domain	✘		✔
FUS			
	FUS mislocalisation		**ER stress**
a domain	✔		✔
a' domain	✔		✔
bb' domain	✘		✔

Investigation into the protective properties of eukaryotic DsbA and DsbC-like proteins in neuronal cells expressing mutant SOD1, TDP-43 and FUS.

DsbA and DsbC are prokaryotic proteins located in the periplasm, with properties similar to thioredoxin and PDI. DsbA functions as an oxidase, whilst DsbC is an isomerase but it can also function as a chaperone [492, 561]. In order to provide insights as to whether the oxidase or isomerase properties of PDI are protective in ALS, it was next investigated whether DsbA or DsbC are protective, similar to PDI and the domain mutants.

4.3.24 Sequences of newly synthesised DsbA and DsbC mutants

A BLAST search was initially performed to compare the nucleotide sequences of the Dsb protein, which revealed that the proteins were not similar in any way. To express these bacterial proteins in mammalian cells, constructs encoding DsbA and DsbC were synthesised. These constructs were codon-optimised, designed by adding PDI's signal sequence at the N-terminus of each Dsb protein and PDI's KDEL ER-retention signal at their C-terminus to ensure that DsbA and DsbC are expressed in the ER of a eukaryotic cell, similar to PDI. A V5 tag was also added to the C-terminus of both proteins so that visualisation was possible using an anti-V5 tag antibody. The cDNA encoding each protein was inserted into pcDNA3.1, a mammalian expression vector. The sequences of the newly synthesised Dsb proteins are illustrated in Figure 4.29.

DsbA construct

Start codon

ATGCTGCGCCGCGCTCTGCTGTGCCTGGCCGTGGCCGCCCTGGTGCG — PDI signal sequence

BamHI ← CGCCGGATCCGCGCAGTATGAAGATGGTAAACAGTACACTACCCTGG
AAAAACCGGTAGCTGGCGCGCCGCAAGTGCTGGAGTTTTTCTCTTTC
TTCTGCCCGCACTGCTATCAGTTTGAAGAAGTTCTGCATATTTCTGATA
ATGTGAAGAAAAAACTGCCGGAAGGCGTGAAGATGACTAAATACCAC
GTCAACTTCATGGGTGGTGACCTGGGCAAAGATCTGACTCAGGCATG
GGCTGTGGCGATGGCGCTGGGCGTGGAAGACAAAGTGACTGTTCCG
CTGTTTGAAGGCGTACAGAAAACCCAGACCATTCGTTCTGCTTCTGAT
ATCCGCGATGTATTTATCAACGCAGGTATTAAAGGTGAAGAGTACGAC
GCGGCGTGGAACAGCTTCGTGGTGAAATCTCTGGTCGCTCAGCAGGA
AAAAGCTGCAGCTGACGTGCAATTGCGTGGCGTTCCGGCGATGTTTG
TTAACGGTAAATATCAGCTGAATCCGCAGGGTATGGATACCAGCAATAT
GGATGTTTTTGTTCAGCAGTATGCTGATACAGTGAAATATCTGTCCGAG — DsbA

BamHI ← AAAAAAGGATCCGGTAAGCCTATCCCTAACCCTCTCCTCGGTCTCGATT → V5 tag
CTACGAAAGATGAACTGTAA

KDEL   Stop codon

DsbC construct

Start codon

ATGCTGCGCCGCGCTCTGCTGTGCCTGGCCGTGGCCGCCCTGGTGCGC — PDI signal sequence

BamHI ← GCCGGATCCGATGACGCGGCAATTCAACAAACGTTAGCCAAAATGGG
CATCAAAAGCAGCGATATTCAGCCCGCGCCTGTAGCTGGCATGAAGAC
AGTTCTGACTAACAGCGGCGTGTTGTACATCACCGATGATGGTAAACAT
ATCATTCAGGGGCCAATGTATGACGTTAGTGGCACGGCTCCGGTCAAT
GTCACCAATAAGATGCTGTTAAAGCAGTTGAATGCGCTTGAAAAAGAG
ATGATCGTTTATAAAGCGCCGCAGGAAAAACACGTCATCACCGTGTTTA
CTGATATTACCTGTGGTTACTGCCACAAACTGCATGAGCAAATGGCAGA
CTACAACGCGCTGGGGATCACCGTGCGTTATCTTGCTTTCCCGCGCCA
GGGGCTGGACAGCGATGCAGAGAAAGAAATGAAAGCTATCTGGTGTG
CGAAAGATAAAAACAAAGCGTTTGATGATGTGATGGCAGGTAAAAGC
GTCGCACCAGCCAGTTGCGACGTGGATATTGCCGACCATTACGCACTT
GGCGTCCAGCTTGGCGTTAGCGGTACTCCGGCAGTTGTGCTGAGCAAT — DsbC
GGCACACTTGTTCCGGGTTACCAGCCGCCGAAAGAGATGAAAGAATT
CCTCGACGAACACCAAAAAATGACCAGCGGTAAAGGATCCGGTAAGC → BamHI

V5 tag ← CTATCCCTAACCCTCTCCTCGGTCTCGATTCTACGAAAGATGAACTGTAA

KDEL   Stop codon

234

Figure 4.29: Design of constructs for expression of Dsb proteins, DsbA and DsbC, in mammalian cells. The Dsb mammalian constructs encode PDI's signal sequence at the N-terminus, the Dsb cDNA sequence cloned between two BamHI restriction recognition sites, followed by a V5 tag, PDI's KDEL ER-retention sequence and stop codon at the C-terminus. The new sequences were inserted into the backbone of the mammalian expression vector, pcDNA3.1.

4.3.25 Localisation of DsbA and DsbC-V5 mutants

To ensure the new constructs were capable of expressing Dsb-like proteins in mammalian cells, and to confirm that expression was ER-localised and hence that the PDI signal sequence and KDEL were functional, confocal microscopy was used to examine the localisation of the V5-tagged Dsb proteins in Neuro-2A cells. Cells were transfected with the DsbA and DsbC-like constructs for 24 h before immunocytochemistry was performed using an anti-V5 tag antibody to visualise Dsb expression, and an anti-calreticulin antibody to probe for the ER-resident protein, calreticulin. These results demonstrated that both DsbA and DsbC were expressed in Neuro-2A cells, and moreover, that DsbA and DsbC co-localised with calreticulin in all transfected cells examined, indicating that these proteins were localised within the ER, as desired (Figure 4.30).
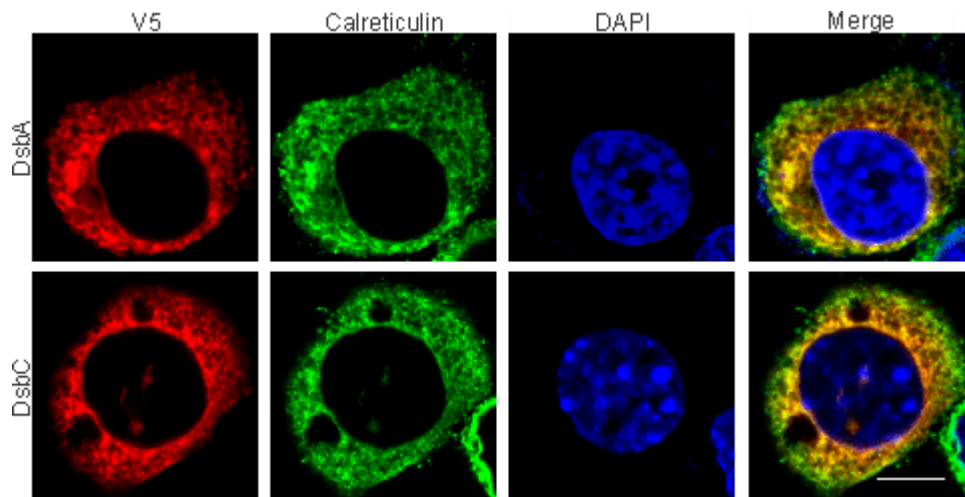
Figure 4.30: The DsbA and DsbC-like proteins are localised in the ER of Neuro-2A cells. Neuro-2A cells were transfected with a pcDNA3.1 vector encoding either DsbA or DsbC (left column). After a 24 h transfection, cells were fixed and immunocytochemistry was performed using antibodies for V5 tag and calreticulin (second column). The nuclei were stained with Hoechst (third column). The yellow in the merge column (last column) demonstrates co-localisation of the Dsbs with calreticulin, indicating that the DsbA and DsbC-like proteins are localised within in the ER of mammalian Neuro-2A cells. Scale bar represents 20 µM.

The Dsb-like eukaryotic proteins and their effect on mutant SOD1

DsbA and DsbC eukaryotic proteins were first examined in Neuro-2A cells expressing

mutant SOD1 A4V. Their activity on SOD1 inclusion formation, mutant SOD1-induced ER

stress and apoptosis was investigated in the following experiments.

4.3.26 DsbA and DsbC are co-expressed in almost all cells transfected with SOD1

First, the protective activity of the DsbA and DsbC-like proteins was examined in Neuro-2A

cells expressing mutant SOD1. However, firstly the co-transfection efficiency of the Dsb-like

proteins and SOD1 was investigated. Cells were transfected with EGFP-SOD1 and either

DsbA-V5 or DsbC-V5 constructs for 72 h, before fixing and performing

immunocytochemistry using an anti-V5 antibody and staining the nuclei with Hoechst. Co-

transfection was confirmed by fluorescence microscopy examining EGFP expression (green)

from SOD1 and performing immunocytochemistry with an Alexa Fluor 568-tagged

secondary antibody to detect the V5 tag of the Dsbs (Figure 4.31). Similar to the expressed

PDI proteins, the overall transfection efficiency of wildtype and mutant SOD1 was

approximately 75-80% when observed 72 h post-transfection in Neuro-2A cells. Fluorescent

microscopy was used to examine at least 100 SOD1-expressing cells for each of the three

replicate experiments. These cells were analysed further for co-expression with DsbA and

DsbC. Quantification revealed that approximately 96% of SOD1 expressing cells also co-

expressed DsbA and approximately 95% of SOD1 expressing cells also co-expressed DsbC.

Thus, in all further experiments, it was assumed that the observation of SOD1 expression

indicated co-expression of both SOD1 and the Dsb-like proteins, where SOD1 and Dsb

constructs were co-transfected and immunocytochemistry with an anti-V5 antibody was not

performed.
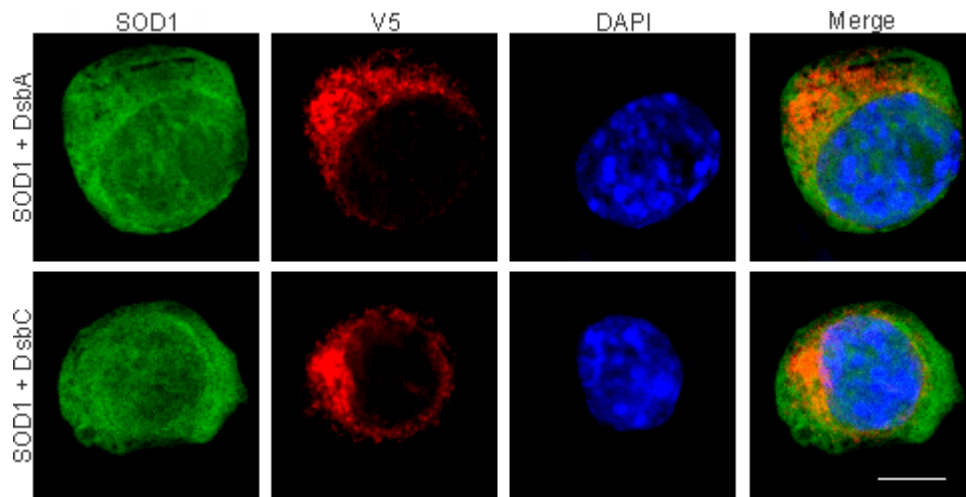
Figure 4.31: Mammalian DsbA-V5 and DsbC-V5 proteins are co-expressed in almost all Neuro-2A cells expressing EGFP-SOD1. Neuro-2A cells were transfected for 72 h with EGFP-SOD1 (left column) and either DsbA-V5 or DsbC-V5 (second column). Cells were fixed, immunocytochemistry was performed using an anti-V5 antibody, and nuclei were stained with Hoechst (third column). The merge column illustrates co-expression of DsbA and DsbC with SOD1 in the cell shown. Scale bar = 20 µM.

4.3.27 Expression of Dsb-like proteins and SOD1 in Neuro-2A cells

Prior to examining the protective activity of DsbA and DsbC in cells expressing mutant SOD1, Western blotting was undertaken to ensure the expressed proteins were of the expected MW, and to ensure that the transfection of each protein resulted in comparable levels of expression (Figure 4.32). Cell lysates were prepared from the following; GFP alone, wildtype SOD1 co-expressed with empty pcDNA3.1 vector, and mutant SOD1 A4V co-expressed with either pcDNA3.1, wildtype PDI, DsbA or DsbC-like proteins. Immunoblotting revealed that wildtype and mutant EGFP-SOD1 proteins were expressed at the expected MW of 50 kDa, and GFP alone was expressed at the expected MW of 26 kDa, utilising an anti-GFP antibody. Wildtype SOD1 displayed significantly higher expression levels ($p < 0.001$), compared to mutant SOD1 A4V, as expected. PDI was detected at 62 kDa using an anti-V5 antibody, as expected. Also using an anti-V5 antibody, DsbA-V5 was detected at 25 kDa and the two DsbC-V5 monomers were detected at around 30 kDa. DsbC was expressed at significantly higher ($p < 0.01$) levels than PDI and DsbA, although this could be due to the presence of two monomers. The loading control, β-actin, was detected using an anti- β-actin antibody (40 kDa).

A

B

241
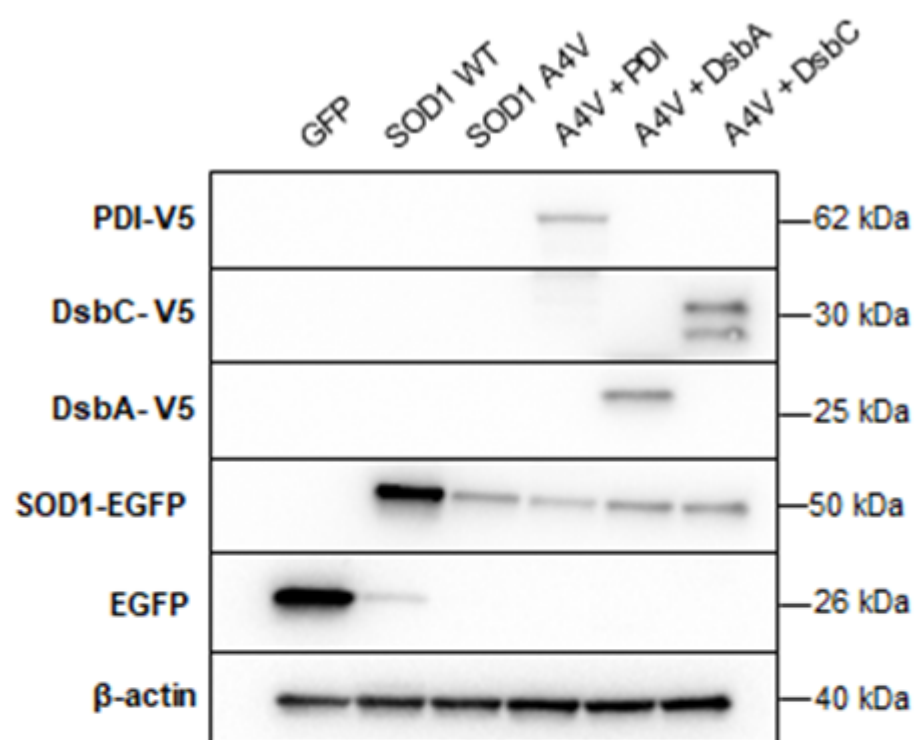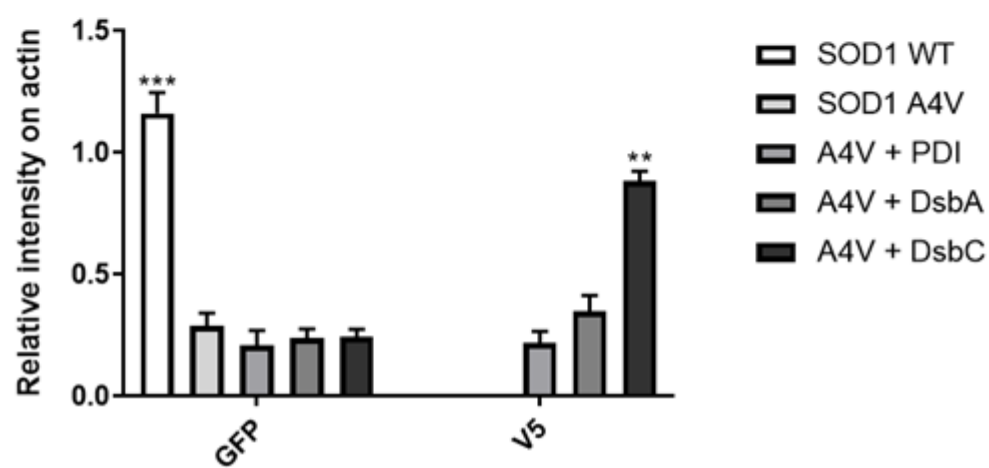
Figure 4.32: Expression of DsbA-V5 and DsbC-V5 proteins with EGFP-SOD1 in Neuro-2A cells. A) Western blotting of cell lysates and quantification was performed to ensure that the levels of protein expression were similar between groups and to confirm that proteins were expressed at their expected sizes. Cell lysates observed were GFP alone, wildtype SOD1 co-expressed with pcDNA3.1, and mutant SOD1 A4V co-expressed with either pcDNA3.1, PDI, DsbA or DsbC. PDI was detected at 62 kDa, whereas DsbA was detected at 25 kDa and DsbC was detected at 30 kDa. Two bands were detected for DsbC as this protein exists as a dimer. Wildtype and mutant EGFP-SOD1 were expressed at 50 kDa and EGFP alone was expressed at 26 kDa. β-actin, the loading control, was detected at 40 kDa. **B)** Quantification revealed that wildtype SOD1 was expressed at significantly higher ($p < 0.001$) levels than mutant SOD1 A4V. Mutant SOD1 A4V displayed comparable levels of expression across all cell lysate populations. DsbC expression was significantly higher than that of PDI and DsbA ($p < 0.01$). Lysates expressing GFP only were not included in quantification. N=3, Mean ± SEM, ** $p < 0.01$, *** $p < 0.001$.

4.3.28 Overexpression of DsbA inhibits mutant SOD1 inclusion formation

As discussed above, the presence of prominent misfolded, mutant SOD1 inclusions is a classical hallmark of mutant SOD1-associated ALS. The results of the studies obtained using the domain mutants demonstrated that the disulphide interchange activity of PDI is essential in inhibiting SOD1 inclusion formation in Neuro-2A cells. Therefore, it was next investigated whether DsbA, an oxidase, plays a similar role to PDI. Neuro-2A cells were transfected with empty pcDNA3.1 vector, GFP, wildtype SOD1 with pcDNA3.1, and mutant SOD1 A4V with either pcDNA3.1, PDI or DsbA-V5 for 72 h. Immunocytochemistry was performed using an anti-V5 antibody to detect the expression of PDI and DsbA, and cells were stained with Hoechst to visualise the nuclei. Fluorescent microscopy was used to quantify at least 100 co-transfected cells for the presence of SOD1 inclusions (EGFP fluorescence) (Figure 4.33 A).

A significant increase ($p < 0.001$) in the proportion of cells bearing SOD1 inclusions was observed in cells expressing mutant SOD1 A4V (37.0% ± 1.7), compared to cells expressing wildtype SOD1 (2.0% ± 1.2) consistent with previous observations. When PDI was also co-expressed with mutant SOD1 A4V, there was a significant reduction ($p < 0.001$) in the proportion of cells forming SOD1 inclusions, as expected (19.3% ± 1.2). Similarly, co-expression of mutant SOD1 A4V with DsbA resulted in a significant reduction ($p < 0.001$) in the proportion of cells with SOD1 inclusions (to 26.7% ± 1.3), compared to cells expressing mutant SOD1 A4V alone. These results therefore indicate that DsbA is able to inhibit e SOD1 inclusion formation similar to PDI. However, there was a significant increase ($p < 0.05$) in the proportion of cells bearing SOD1 inclusion in populations co-expressing SOD1 A4V and DsbA compared to those co-expressing SOD1 A4V and PDI, suggesting that whilst DsbA is protective, it is not as protective as PDI (Figure 4.33 B).

Next, the protective activity of DsbC, an isomerase, was investigated against mutant SOD1 inclusion formation. As well as its ability to isomerase disulphide bonds in proteins, DsbC also functions as a chaperone, hence it possesses similarities to the *bb'* domain mutant studied earlier in this chapter. Neuro-2A cells were transfected for 72 h with empty pcDNA3.1 vector, GFP, wildtype SOD1 with pcDNA3.1, and mutant SOD1 A4V with either pcDNA3.1, PDI or DsbC. Immunocytochemistry using an anti-V5 antibody was performed and DAPI-staining was implemented using Hoechst.

Quantification analysis of at least 100 co-transfected cells bearing SOD1 inclusions revealed a significant increase ($p < 0.001$) in the proportion of cells displaying SOD1 inclusions in mutant A4V expressing cells (25.3% ± 2.9), compared to wildtype SOD1 expressing cells (1.7% ± 0.3). As expected, there was a significant reduction ($p < 0.01$) in in the proportion of SOD1 inclusion-bearing cells when cells were co-expressed with PDI and mutant SOD1 A4V (12.7% ± 1.8), compared to cells expressing SOD1 A4V only. Interestingly, co-expression of DsbC and mutant SOD1 A4V did not alter the proportion of cells bearing SOD1 inclusions. In fact, there were significantly more ($p < 0.05$) SOD1 inclusions in these populations (22.3% ± 1.5), compared to cells co-expressing PDI and mutant SOD1 A4V, suggesting that DsbC is not protective against SOD1 inclusion formation (Figure 4.33 C).
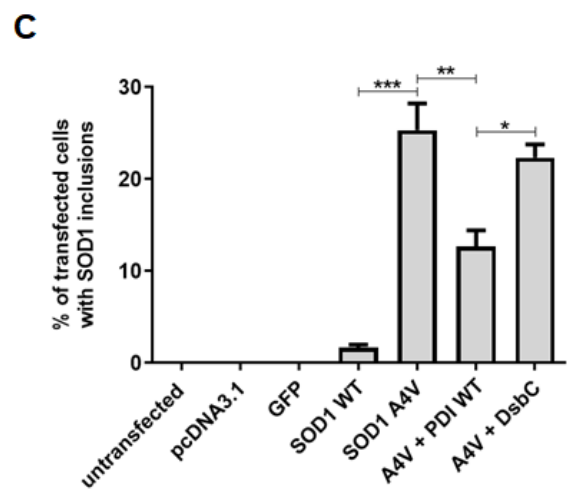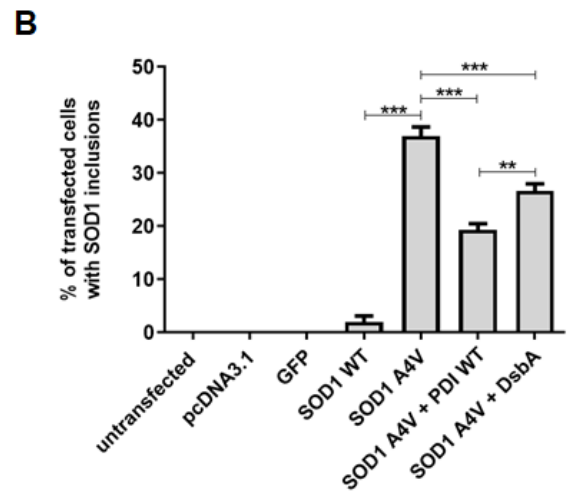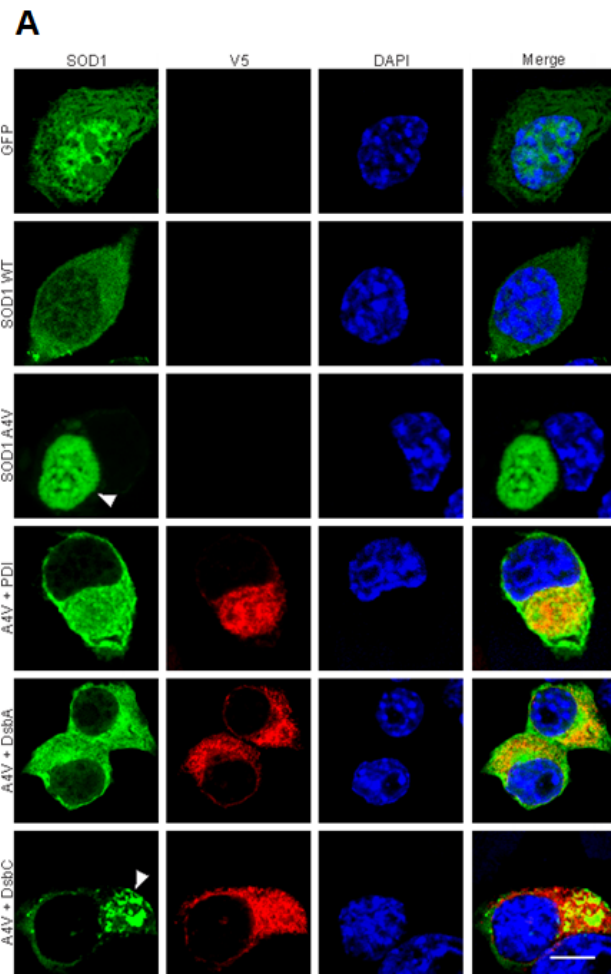
Figure 4.33: Overexpression of DsbA but not DsbC-like proteins inhibits mutant SOD1 inclusion formation. A) Immunofluorescence images of Neuro-2A cells expressing GFP (first panel; GFP), wildtype SOD1 with pcDNA3.1 (second panel; SOD1 WT), and mutant SOD1 A4V with either pcDNA3.1, PDI, DsbA or DsbC. Cells expressing GFP and wildtype SOD1 do not bear SOD1 inclusions. In contrast, a significant proportion of cells expressing mutant SOD1 A4V (third panel; SOD1 A4V) display SOD1 inclusions, as indicated by the white arrowhead (third panel, column one). However, co-expression of PDI or DsbA with mutant SOD1 A4V resulted in fewer cells forming SOD1 inclusions (fourth and fifth panel; A4V + PDI, A4V + DsbA). In contrast, more cells co-expressing DsbC and SOD1 A4V (sixth panel; A4V + DsbC) displayed SOD1 inclusions (sixth panel, column one). Scale bar = 20 µM. **B)** Quantification of cells bearing SOD1 inclusions in A). Very few cells expressing wildtype SOD1 displayed SOD1 inclusions. Significantly more ($p < 0.001$) cells expressing mutant SOD1 A4V formed SOD1 inclusions, however this proportion was significantly reduced ($p < 0.001$) when either PDI or DsbA were co-expressed. However, significantly fewer cells bore inclusions ($p < 0.01$) when PDI and SOD1 A4V were co-expressed, compared to populations co-expressing DsbA and SOD1 A4V. N=3, Mean ± SEM, ** $p < 0.01$, *** $p < 0.001$. Hence DsbA is protective against mutant SOD1 inclusion formation, but not to the same extent as PDI. **C)** Quantification of cells bearing SOD1 inclusions in A). There was a significant increase ($p < 0.001$) in the proportion of cells forming SOD1 inclusions in populations expressing mutant SOD1 A4V compared to cells expressing wildtype SOD1. Significantly fewer cells ($p < 0.01$) bore SOD1 inclusions when PDI was co-expressed with mutant SOD1 A4V as expected. However, significantly more cells ($p < 0.05$) displayed SOD1 inclusions when DsbC and SOD1 A4V were co-expressed, compared to cells co-expressing PDI and mutant SOD1 A4V and there was no difference in the proportion

of cells co-expressing DsbC with vector only. Hence DsbC is not protective against mutant SOD1 inclusion formation. N=3, Mean ± SEM, * $p < 0.05$, ** $p < 0.01$, *** $p < 0.001$.

4.3.29 DsbA and DsbC-like proteins are protective against mutant SOD1 induced ER stress

Next, the activity of DsbA and DsbC was examined against mutant SOD1-induced ER stress. CHOP activation was used as a marker for late-phase, apoptotic ER stress, as previous. Firstly, Neuro-2A cells were transfected with empty pcDNA3.1 vector, GFP, wildtype SOD1 with pcDNA3.1, and mutant SOD1 A4V with either pcDNA3.1, PDI or DsbA for 72 h. Immunocytochemistry was performed using an anti-CHOP antibody to examine nuclear immunoreactivity as previous. Cells were also stained with Hoechst to visualise the nuclei. Fluorescent microscopy was utilised to examine at least 100 co-transfected cells and quantification of the proportion of cells with nuclear immunoreactivity to CHOP was performed, indicating activation of CHOP, and thus, induction of ER stress (Figure 4.34 A).

Less than 10% of untransfected cells or cells expressing pcDNA3.1, GFP or wildtype SOD1, displayed nuclear immunoreactivity to CHOP. A significantly greater ($p < 0.001$) proportion of cells expressing mutant SOD1 A4V were found to be undergoing ER stress, indicated by CHOP activation (26.0% ± 1.7), compared to cells expressing wildtype SOD1 (7.0% ± 1.5). However, the proportion of cells displaying CHOP activation was significantly decreased ($p < 0.001$) when either PDI (11.3% ± 1.3) or DsbA (14.3% ± 0.7) was co-expressed with mutant SOD1 A4V, indicating that DsbA has a protective role against mutant SOD1-induced ER stress, similar to PDI (Figure 4.34 B).

Next, DsbC was examined for its protective activity against CHOP activation induced by mutant SOD1. Neuro-2A cells were transfected with empty pcDNA3.1 vector, GFP, wildtype SOD1 with pcDNA3.1, and mutant SOD1 A4V with either pcDNA3.1, PDI or DsbC for 72 h. Immunocytochemistry was performed using an anti-CHOP antibody and the nuclei were stained with Hoechst. CHOP nuclear immunoreactivity was then examined using fluorescent microscopy. Quantification revealed a significant increase ($p < 0.001$) in the proportion of

cells with CHOP activation in populations expressing mutant SOD1 A4V (27.7% ± 0.9),
compared to wildtype SOD1 expressing cells (8.0% ± 1.5). As expected, significantly fewer
(p < 0.001) cells displayed CHOP activation when SOD1 A4V cells were co-expressed with
PDI (11.3% ± 1.9). Interestingly, however, when cells co-expressed DsbC and mutant SOD1
A4V, there was a significant reduction (p < 0.001) in the proportion of cells exhibiting CHOP
activation (16.7% ± 1.9), compared to cells expressing mutant SOD1 A4V alone. Hence,
these data suggest that DsbC is also protective against ER stress induced by mutant SOD1,
revealing that the isomerase activity or chaperone function of DsbC is protective (Figure 4.34
C).
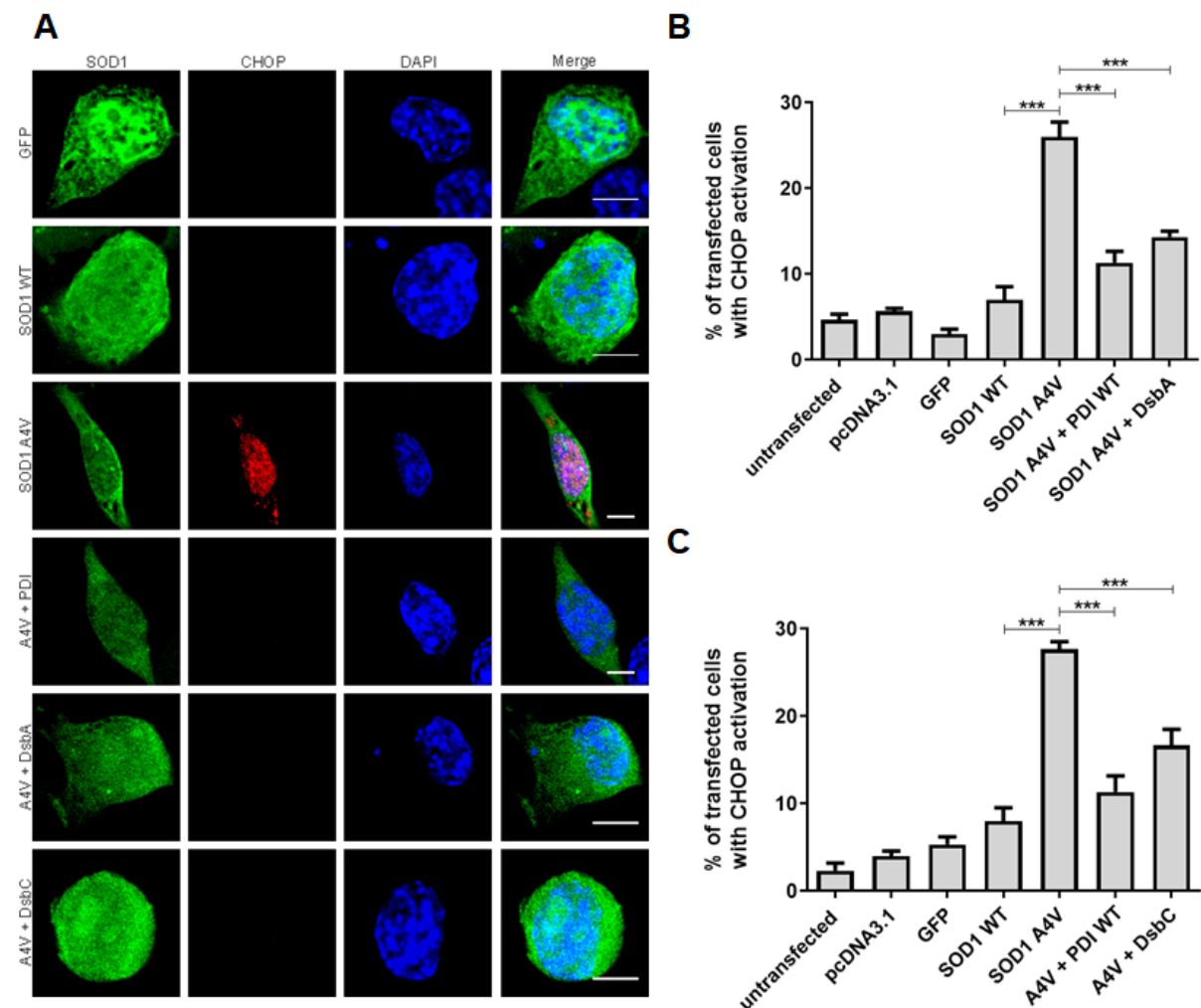
Figure 4.34: Overexpression of DsbA and DsbC-like proteins inhibits mutant SOD1 induced CHOP activation. A) Immunofluorescence images of cells expressing GFP, wildtype SOD1 with empty pcDNA3.1 vector, and mutant SDO1 A4V with either pcDNA3.1, PDI, DsbA or DsbC. Few cells expressing GFP (first panel; GFP) or wildtype SOD1 (second panel; SOD1 WT) display CHOP activation, whereas a greater proportion of cells expressing mutant SOD1 A4V (third panel; SOD1 A4V) demonstrate activation of CHOP, indicated by its nuclear immunoreactivity (third panel, column two). When PDI, DsbA or DsbC were co-expressed with mutant SOD1 A4V, fewer cells displayed CHOP activation (panels four – six; A4V + PDI, A4V + DsbA, A4V + DsbC). Scale bar = 20 µM. **B)** Quantification of the proportion of cells with CHOP activation in A). There was a significant increase in the proportion of mutant SOD1 A4V expressing cells with CHOP activation, compared to wildtype SOD1 expressing cells ($p < 0.001$) as expected. The proportion of cells with CHOP activation was significantly reduced when either PDI or DsbA were co-expressed with mutant SOD1 A4V ($p < 0.001$), and there was no significant difference between populations co-expressing PDI or DsbA. N=3, Mean ± SEM, *** $p < 0.001$. **C)** Quantification of the proportion of cells with CHOP activation in A). Significantly more cells expressing mutant SOD1 A4V displayed CHOP activation, compared to cells expressing wildtype SOD1 ($p < 0.001$). Co-expression of either PDI or DsbC with mutant SOD1 A4V resulted in a significant reduction in the proportion of cells with CHOP activation, compared to cells expressing SOD1 A4V alone ($p < 0.001$). N=3, Mean ± SEM, *** $p < 0.001$. There was no significant difference between populations co-expressing PDI or DsbA.

4.3.30 Overexpression of DsbA inhibits apoptosis induced by mutant SOD1

As these results indicated that both DsbA and DsbC were able to inhibit ER stress induced apoptotic signalling, it was next hypothesised that these proteins may also inhibit apoptotic cell death. Hence, it was next examined whether overexpression of DsbA or DsbC was protective against apoptosis induced by mutant SOD1. Neuro-2A cells were transfected for 72 h with empty pcDNA3.1 vector, GFP, wildtype SOD1 with pcDNA3.1, and mutant SOD1 A4V with either pcDNA3.1, PDI or DsbA. After fixing, immunocytochemistry was performed using an anti-V5 antibody to visualise PDI and DsbA, and the nuclei were stained with Hoechst. Fluorescent microscopy was utilised to examine at least 100 co-transfected cells for the presence of apoptotic nuclei. Nuclei of irregular, condensed or fragmented morphology were considered apoptotic as previous (Figure 4.35 A).

Apoptotic nuclei were rarely present in untransfected cells or cells expressing pcDNA3.1 and GFP (less than 5%) and in cells expressing wildtype SOD1, only $6.0\% \pm 0.6$ of cells displayed condensed nuclei as expected. Apoptotic nuclei were more common in cells expressing mutant SOD1 A4V ($19.0\% \pm 1.2$), compared to cells expressing wildtype SOD1 ($p < 0.001$) as previous. However, significantly fewer ($p < 0.05$) cells bearing apoptotic nuclei was observed in populations co-expressing either PDI ($13.0\% \pm 2.3$) or DsbA ($12.3\% \pm 1.2$) with mutant SOD1 A4V, indicating that DsbA overexpression is protective against mutant SOD1-induced apoptosis (Figure 4.35 B).

DsbC overexpression was next examined for its protective effect against apoptosis. Neuro-2A cells were transfected with empty pcDNA3.1 vector, GFP, wildtype SOD1 with pcDNA3.1, and mutant SOD1 A4V with either pcDNA3.1, PDI or DsbC for 72 h. After performing immunocytochemistry with an anti-V5 antibody and staining nuclei with Hoechst, at least 100 co-transfected cells were analysed for the presence of apoptotic nuclei. Quantification

revealed that untransfected cells or cells expressing pcDNA3.1, GFP and wildtype SOD1 had minimal apoptotic nuclei (less than 5%). There was a significant increase ($p < 0.001$) in the proportion of cells with apoptotic nuclei in cells expressing mutant SOD1 A4V (16.3% ± 0.3), compared to cells expressing wildtype SOD1 (5.0% ± 0.6) as expected. Significantly fewer ($p < 0.01$) cells presented with apoptotic nuclei when PDI was co-expressed with SOD1 A4V (9.7% ± 1.2), compared to cells expressing mutant SOD1 A4V alone as previous. However, there was no significant difference in the proportion of cells with apoptotic nuclei when DsbC was co-expressed with mutant SOD1 A4V (15.3% ± 1.8). A significant difference ($p < 0.05$) in the proportion of cells with apoptotic nuclei was detected between populations co-expressing PDI with those co-expressing DsbC, revealing that unlike DsbA, DsbC is not able to inhibit apoptosis induced by mutant SOD1 (Figure 4.35 C).
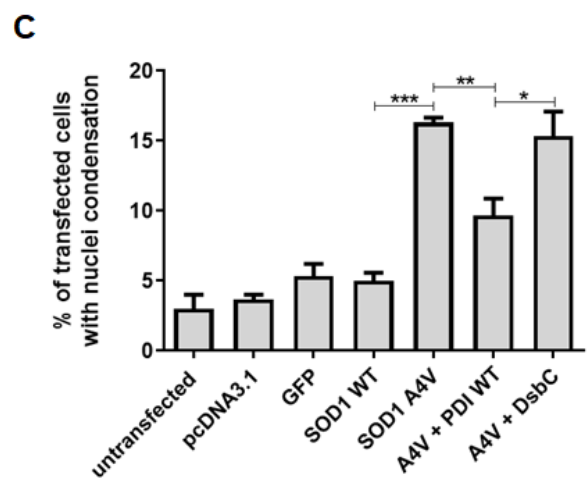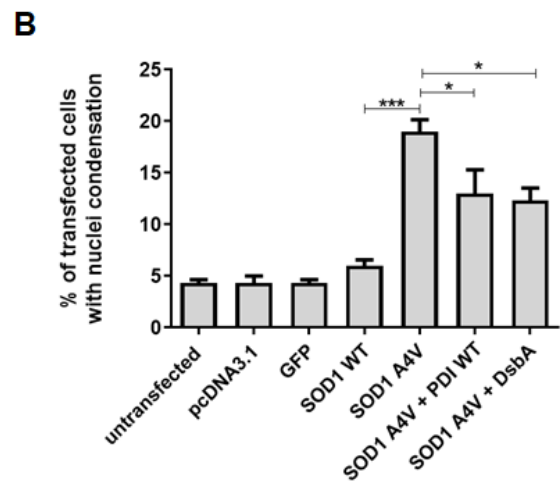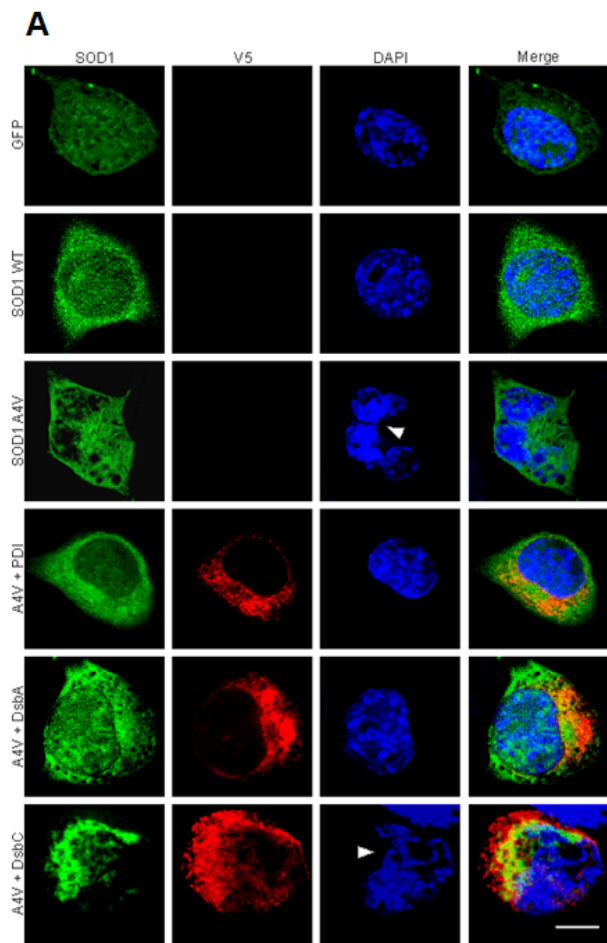
Figure 4.35: Overexpression of DsbA, but not DsbC, inhibits apoptosis induced by mutant SOD1. A) Immunofluorescence images of cells expressing GFP, wildtype SOD1 with pcDNA3.1, and mutant SOD1 A4V with either pcDNA3.1, PDI, DsbA or DsbC. Cells expressing GFP (first panel; GFP) and wildtype SOD1 (second panel; SOD1 WT) rarely exhibit apoptotic nuclei, indicated by cells with regular morphology and size. In contrast, more cells expressing mutant SOD1 A4V (third panel; SOD1 A4V) display apoptotic nuclei, as indicated by the white arrowhead (third panel, column three). The proportion of cells with apoptotic nuclei was reduced when PDI and DsbA were co-expressed with mutant SOD1 A4V (panels 4 -5; A4V + PDI, A4V + DsbA). However, more cells co-expressing DsbC and SOD1 A4V (sixth panel; A4V + DsbC) display apoptotic nuclei, indicated by the white arrowhead (sixth panel, column three). Scale bar = 20 µM. **B)** Quantification of cells exhibiting apoptotic nuclei in A). There was a significant increase in the proportion of cells with condensed nuclei in mutant SOD1 A4V populations, compared to those expressing wildtype SOD1 ($p < 0.001$) as expected. When PDI or DsbA were co-expressed with SOD1 A4V, however, there was a significant decrease in the proportion of cells with apoptotic nuclei ($p < 0.05$), indicating that DsbA is protective against mutant SOD1-induced apoptosis. N=3, Mean ± SEM, * $p < 0.05$, *** $p < 0.001$. **C)** Quantification of cells displaying apoptotic nuclei in A). Significantly more ($p < 0.001$) cells expressing mutant SOD1 A4V possessed apoptotic nuclei than cells expressing wildtype SOD1. When PDI was co-expressed with SOD1 A4V, there was a significant decrease ($p < 0.01$) in the proportion of cells with apoptotic nuclei, however no significant difference was observed when DsbC was co-expressed with SOD1 A4V, compared to cells expressing mutant SOD1 A4V alone. However, significantly fewer cells displayed apoptotic nuclei in cells co-expressing PDI with mutant SOD1 A4V, compared to those co-expressing DsbC and mutant SOD1 A4V ($p <$

0.05), revealing that DsbC is not protective against mutant SOD1-induced apoptosis. N=3,

Mean ± SEM, * $p < 0.05$, ** $p < 0.01$, *** $p < 0.001$.

Investigation into the protective properties of DsbA and DsbC-like eukaryotic proteins in neuronal cells expressing mutant TDP-43.

Eukaryotic DsbA and DsbC were next examined in Neuro-2A cells expressing mutant TDP-43 Q331K. Their activity on mutant TDP-43 mislocalisation to the cytoplasm and mutant TDP-43-induced ER stress was investigated in the following experiments.

4.3.31 DsbA and DsbC are co-expressed in almost all cells transfected with TDP-43

Next, the activity of DsbA and DsbC was analysed against mutant TDP-43. The co-transfection efficiency of the Dsb-like proteins and TDP-43 in Neuro-2A cells was first investigated. Cells were transfected with either DsbA or DsbC and EGFP-TDP-43 constructs for 18 h, before fixing and performing immunocytochemistry using an anti-V5 antibody. Cells were also stained with Hoechst to visualise the nuclei. Co-transfection was confirmed using fluorescent microscopy by examining EGFP expression (green) from TDP-43 and performing immunocytochemistry with an Alexa Fluor 568-tagged secondary antibody to detect the V5 tag for both DsbA and DsbC (Figure 4.36). The overall transfection efficiency of the TDP-43 constructs was approximately 70-75 % in Neuro-2A cells when examined 18 h post-transfection. For each of the three replicate experiments, fluorescent microscopy was used to visualise at least 100 cells transfected with TDP-43 and these cells were further analysed for co-expression with either DsbA or DsbC. Quantification revealed that approximately 97% of TDP-43 expressing cells also co-expressed either DsbA or DsbC. Hence, in all further experiments, it was assumed that detection of TDP-43 expression reflected co-expression of TDP-43 and either DsbA or DsbC when they were co-transfected and immunocytochemistry using a V5 antibody was not performed.
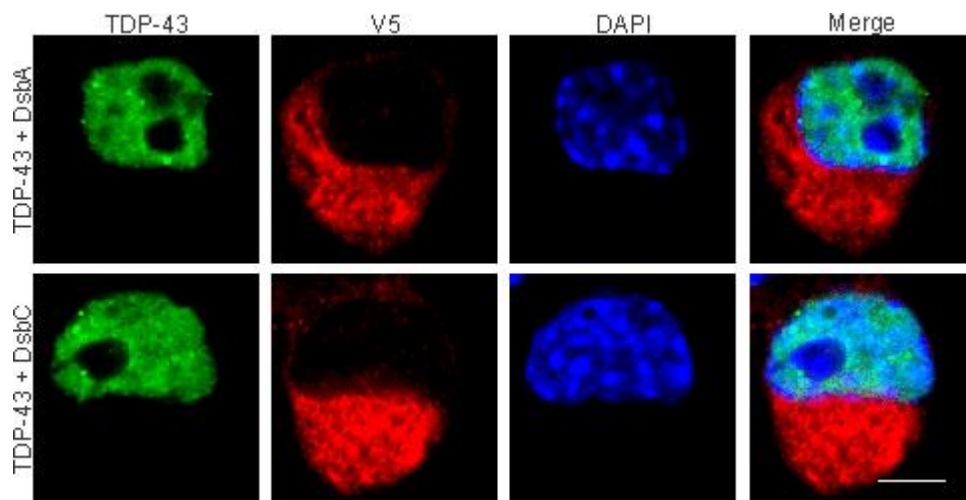
Figure 4.36: DsbA-V5 and DsbC-V5 are co-expressed in almost all Neuro-2A cells co-expressing EGFP-TDP-43. Neuro-2A cells were transfected for 18 h with constructs encoding EGFP-TDP-43 (left column) and either DsbA-V5 or DsbC-V5 (second column). Cells were fixed, immunocytochemistry was performed using an anti-V5 antibody and the nuclei were stained with Hoechst (third column). The merge column illustrates co-expression of the Dsb-like proteins and TDP-43 in the cells shown. Scale bar = 20 µM.

4.3.32 Expression of DsbA and DsbC-like proteins and TDP-43 in Neuro-2A cells

Prior to undertaking cellular assays using overexpressed TDP-43 and the mammalian Dsb proteins, control Western blotting was performed to ensure that each protein was expressed to a similar level and to verify that the expressed proteins were of the expected MW (Figure 4.37). Cell lysates were prepared from the following populations; GFP alone, wildtype TDP-43 co-expressed with empty pcDNA3.1 vector, and mutant TDP-43 Q331K co-expressed with either pcDNA3.1, PDI, DsbA or DsbC. Immunoblotting using an anti-GFP antibody revealed that wildtype and mutant EGFP-TDP-43 proteins were expressed at similar levels at the expected MW of 64 kDa, and GFP alone was expressed at the expected MW of 26 kDa. PDI was detected in cell lysates using an anti-V5 tag antibody (62 kDa), as well as DsbA (25 kDa) and DsbC (30 kDa). β-actin was used as a loading control, detected at 40 kDa using an anti-β-actin antibody.

A

B

259
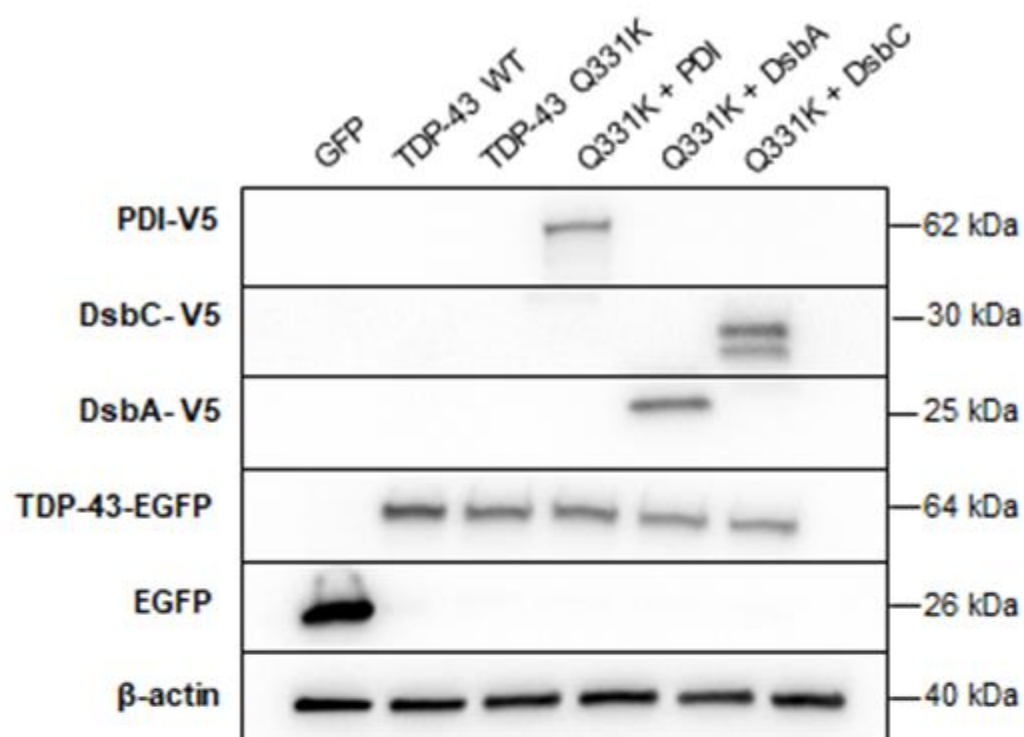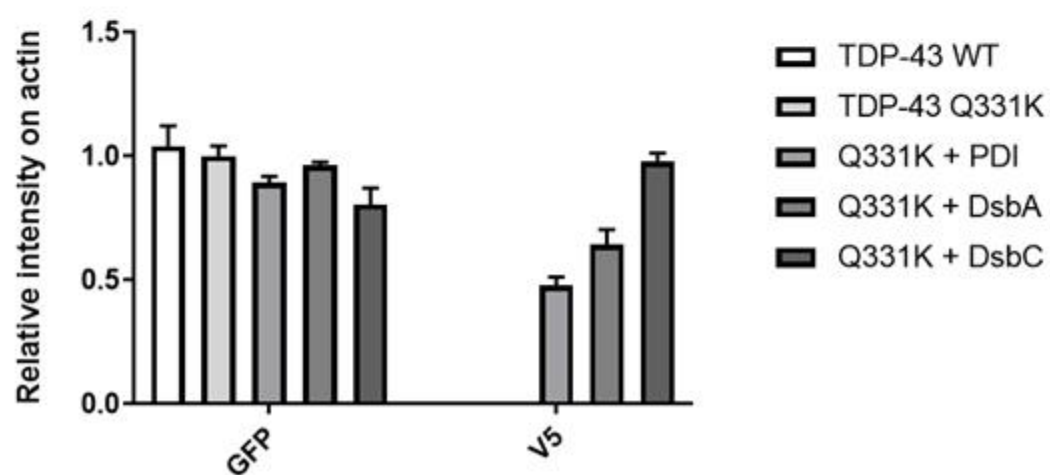
Figure 4.37: Protein expression of DsbA-V5, DsbC-V5-like proteins and EGFP-TDP-43 in Neuro-2A cells. A) Western blotting of cell lysates was performed and quantified to ensure that the proteins expressed were of similar expression levels between groups and that each was expressed at the expected MW. Cell lysates examined were GFP alone, wildtype TDP-43 co-expressed with empty pcDNA3.1 vector, and mutant TDP-43 Q331K co-expressed with either empty pcDNA3.1 vector, PDI, DsbA or DsbC. PDI was detected at 62kDa, DsbA was detected at 25 kDa and DsbC was detected at 35 kDa. Two bands were detected for DsbC as it is a dimer. Moreover, wildtype and mutant TDP-43 were expressed at 64 kDa, whereas GFP alone was detected at 26 kDa. β-actin was utilised as the loading control and was detected at 40 kDa. **B)** Quantification revealed that wildtype and mutant TDP-34 proteins were expressed at comparable levels. Similarly, PDI and the Dsb proteins were also shared similar expression levels. Lysates expressing GFP only were not included in quantification. N=3, Mean ± SEM.

4.3.33 Overexpression of DsbA and DsbC is protective against mutant TDP-43 mislocalisation to the cytoplasm

As TDP-43 mislocalises from the nucleus to the cytoplasm in ALS, it was first investigated whether DsbA and DsbC could prevent this, similar to PDI. Neuro-2A cells were transfected with empty pcDNA3.1 vector, GFP, wildtype TDP-43 with pcDNA3.1, and mutant TDP-43 Q331K with either pcDNA3.1, PDI or DsbA. Immunocytochemistry was not performed as it was assumed that TDP-43 expression reflected co-expression with PDI or the Dsbs, however, cells were stained with Hoechst to visualise nuclei. The cellular localisation of TDP-43 was analysed 18 h post-transfection using fluorescent microscopy because previous studies in our laboratory found that more TDP-43 was localised in the cytoplasm at this timepoint [427]. TDP-43 was considered to be nuclear when it completely localised with the DAPI-stained nucleus. Conversely, TDP-43 was considered to be cytoplasmic when fluorescence was detected in both the nucleus and the cytoplasm of TDP-43 expressing cells (Figure 4.38 A).

Wildtype TDP-43 was mislocalised to the cytoplasm in $4.0\% \pm 1.0$ of cells. In comparison, significantly more cells expressing mutant TDP-43 Q331K ($p < 0.001$) displayed mislocalisation, as expected ($17.3\% \pm 1.5$). When PDI was co-expressed with mutant TDP-43 Q331K there was a significant decrease ($p < 0.01$) in the proportion of cells with cytoplasmic TDP-43, compared to cells expressing mutant TDP-43 Q331K alone ($6.7\% \pm 1.7$). Moreover, co-expression of DsbA with TDP-43 Q331K also resulted in significantly fewer ($p < 0.01$) cells displaying cytoplasmic TDP-43($7.3\% \pm 1.9$), indicating that DsbA is protective against mutant TDP-43 mislocalisation to the cytoplasm (Figure 4.38 B).

Next it was examined whether DsbC was also protective against mutant TDP-43 mislocalisation to the cytoplasm. Neuro-2A cells were transfected with empty pcDNA3.1 vector, GFP, wildtype TDP-43 with pcDNA3.1, and mutant TDP-43 Q331K with either

pcDNA3.1, PDI or DsbC for 18 h. After fixing, DAPI-staining was performed using Hoechst to visualise the nuclei. 100 co-transfected cells were analysed with fluorescent microscopy and quantified according to whether TDP-43 was expressed in the cytoplasm. Quantification revealed a significant increase ($p < 0.001$) in the proportion of cells with cytoplasmic TDP-43 in mutant TDP-43 Q331K expressing populations (16.0% ± 2.6), compared to wildtype TDP-43 expressing cells (4.3% ± 1.2). Significantly fewer cells ($p < 0.05$) displayed TDP-43 mislocalisation when PDI was co-expressed with mutant TDP-43 Q331K (7.7% ± 1.8), compared to populations expressing TDP-43 Q331K only. Interestingly, there was also a significant reduction ($p < 0.01$) in the proportion of cells with cytoplasmic TDP-43 when DsbC was co-expressed with mutant TDP-43 Q331K (6.3% ± 1.3). These data reveal that DsbC, and therefore either its isomerase or chaperone activity, is protective against mutant TDP-43 mislocalisation to the cytoplasm (Figure 4.38 C).
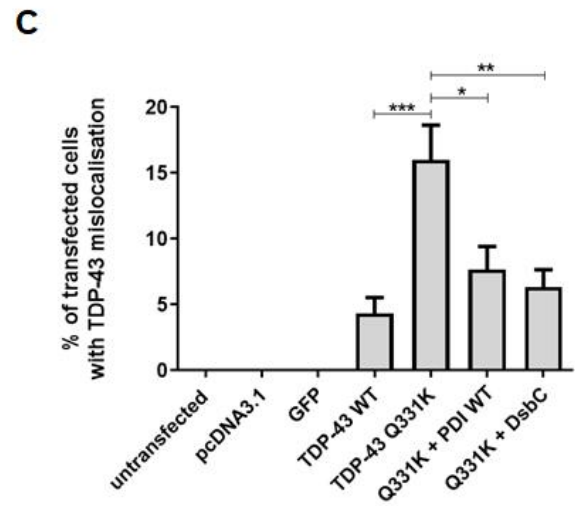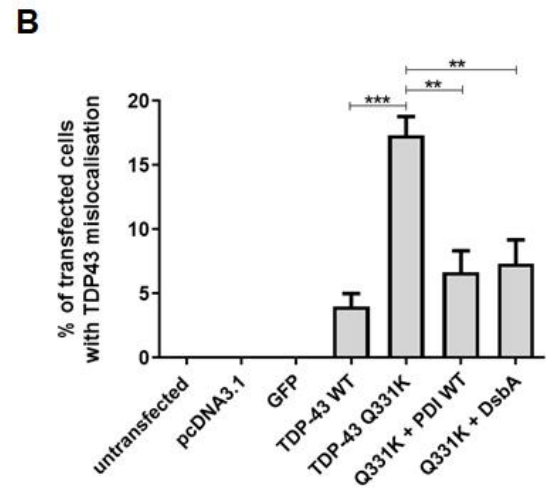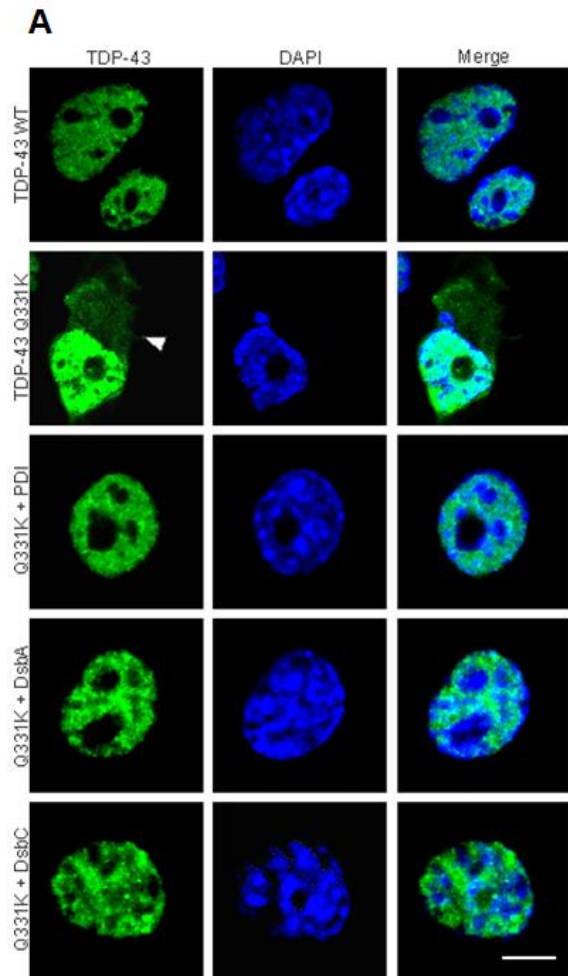
Figure 4.38: Overexpression of DsbA and DsbC is protective against mutant TDP-43 mislocalisation to the cytoplasm. A) Immunofluorescence images of Neuro-2A cells expressing wildtype TDP-43 with empty pcDNA3.1 vector and mutant TDP-43 Q331K with either pcDNA3.1, PDI, DsbA or DsbC (column one). Wildtype TDP-43 expressing cells (first panel; TDP-43 WT) displayed mainly nuclear localisation of TDP-43, which co-localised entirely with the DAPI-stained nuclei (column two), as demonstrated in the merge column. Conversely, more cells expressing mutant TDP-43 Q331K (second panel; TDP-43 Q331K) displayed mislocalisation to the cytoplasm, as indicated with the white arrowhead. However, when PDI, DsbA or DsbC (panels 3 – 5; Q331K + PDI, Q331K + DsbA, Q331K + DsbC) were co-expressed with mutant TDP-43 Q331K, significantly fewer cells displayed cytoplasmic TDP-43, Scale bar = 20 µM. **B)** Quantification of Neuro-2A cells with TDP-43 mislocalisation in A). There was a significant increase ($p < 0.001$) in the proportion of cells with mislocalisation of mutant TDP-43 Q331K, compared to wildtype TDP-43. A significant decrease ($p < 0.01$) in the proportion of cells with mislocalisation of TDP-43 was observed when mutant TDP-43 Q331K was co-expressed with either PDI or DsbA. N=3, Mean ± SEM, ** $p < 0.01$, *** $p < 0.001$. **C)** Quantification of Neuro-2A cells with cytoplasmic TDP-43 in A). Significantly more ($p < 0.001$) cells expressing mutant TDP-43 Q331K displayed cytoplasmic TDP-43, compared to cells expressing wildtype TDP-43. However, there was a significant decrease in the proportion of cells with cytoplasmic TDP-43 when mutant TDP-43 Q331K populations were co-expressed with PDI ($p < 0.05$) or DsbC ($p < 0.01$). N=3, Mean ± SEM, * $p < 0.05$, ** $p < 0.01$, *** $p < 0.001$.

4.3.34 Overexpression of DsbA, but not DsbC, is protective against ER stress induced by mutant TDP-43

As TDP-43 mislocalisation to the cytoplasm and ER stress are closely associated [427], it was next examined whether the DsbA and DsbC-like proteins were protective against the induction of ER stress, by activation of pro-apoptotic ER stress marker, CHOP. Neuro-2A cells were transfected with empty pcDNA3.1 vector, GFP, wildtype TDP-43 with pcDNA3.1, and mutant TDP-43 Q331K with either pcDNA3.1, PDI or DsbA for 18 h. After fixing, immunocytochemistry was performed using an anti-CHOP antibody to examine nuclear immunoreactivity, indicating CHOP activation as previous, and cells were stained with Hoechst to clearly visualise the nuclei. Fluorescent microscopy was utilised to analyse at least 100 co-transfected cells for nuclear immunoreactivity to CHOP (Figure 4.39 A).

Less than 10% of untransfected cells, or cells expressing either empty pcDNA3.1 vector, GFP alone or wildtype TDP-43 displayed nuclear immunoreactivity to CHOP. There was a significant increase ($p < 0.001$) in the proportion of cells displaying CHOP activation in cells expressing mutant TDP-43 Q331K (18.3% ± 1.9), compared to cells expressing wildtype TDP-43 (7.0% ± 1.5) consistent with previous observations (Walker et al., 2013). In contrast, co-expression of mutant TDP-43 Q331K with either PDI or DsbA resulted in a significant decrease ($p < 0.001$) in the proportion of cells with CHOP activation (6.7 % ± 1.3 and 9.7% ± 1.9, respectively), compared to cells expressing TDP-43 Q331K alone. Thus, these data demonstrate that DsbA is protective against mutant TDP-43 induced CHOP activation (Figure 4.39 B).

Next, it was examined whether DsbC was also protective against ER stress, similar to DsbA. Cells were transfected with empty pcDNA3.1 vector, GFP, wildtype TDP-43 with pcDNA3.1, and mutant TDP-43 Q331K with either pcDNA3.1, PDI or DsbC for 18 h before

immunocytochemistry was performed using an anti-CHOP antibody. Similar to the result in Figure 4.39 B, there was a significant increase ($p < 0.001$) in the proportion of cells with nuclear immunoreactivity to CHOP, in populations expressing mutant TDP-43 Q331K (20.3% $\pm$ 0.7), compared to those expressing wildtype TDP-43 (8.3% $\pm$ 0.9). As previous, significantly fewer cells ($p < 0.001$) co-expressing mutant TDP-43 Q331K and PDI displayed CHOP activation (9.3% $\pm$ 1.5). However, co-expression of DsbC with TDP-43 Q331K did not alter the proportion of cells with nuclear immunoreactivity to CHOP (16.0% $\pm$ 2.0), compared to cells expressing mutant TDP-43 Q331K alone, revealing that DsbC is not protective against ER stress induced by mutant TDP-43. Furthermore, a significant difference ($p < 0.05$) in the proportion of TDP-43 Q331K cells with CHOP activation was observed between populations co-expressing PDI to those co-expressing DsbC. Hence these data indicate that although DsbC is protective against ER stress induced by mutant SOD1, it is not protective against ER stress induced by mutant TDP-43 (Figure 4.39 C).
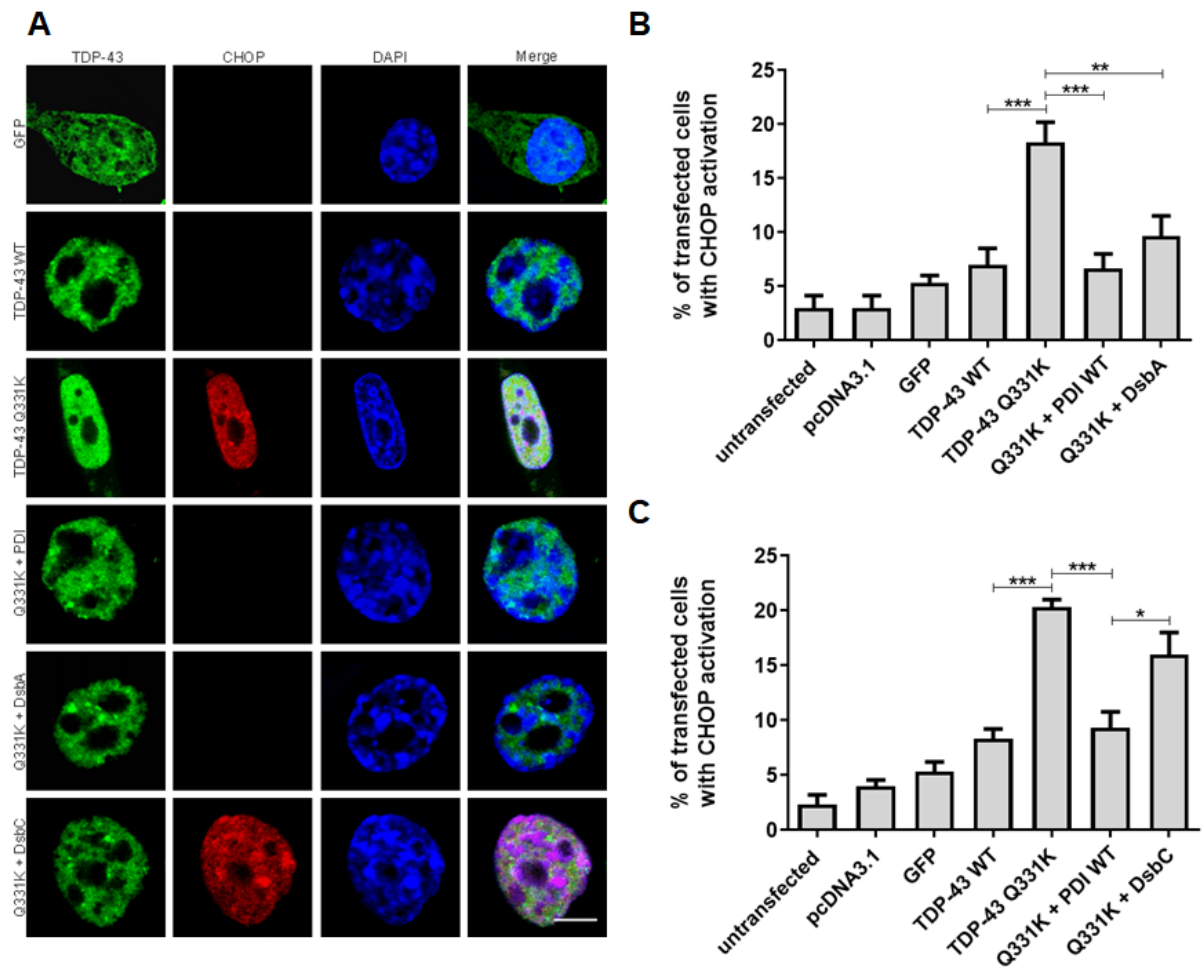
Figure 4.39: Overexpression of DsbA is protective against ER stress induced by mutant TDP-43. A) Immunofluorescence images of Neuro-2A cells expressing GFP, wildtype TDP-43 with pcDNA3.1, and mutant TDP-43 Q331K with either pcDNA3.1, PDI, DsbA or DsbC. Cells expressing GFP (first panel; GFP) or wildtype TDP-43 (second panel; TDP-43 WT) rarely display nuclear immunoreactivity to CHOP, indicating activation of ER stress. In contrast, in cells expressing mutant TDP-43 Q331K (third panel; TP-43 Q331K), CHOP nuclear immunoreactivity was more commonly visualised (third panel, second column). However, when PDI or DsbA were co-expressed with mutant TDP-43 Q331K, the proportion of cells with CHOP activation was reduced (fourth and fifth panel; Q331K + PDI, Q331K + DsbA). Conversely, there was no difference in the proportion of cells co-expressing DsbC and mutant TDP-43 Q331K (sixth panel; Q331K + DsbC) to those expressing DsbC with vector only. Scale bar = 20 µM. **B)** Quantification of cells in A) displaying CHOP activation. Very few untransfected cells and cells expressing pcDNA3.1, GFP or wildtype TDP-43 displayed nuclear CHOP immunoreactivity. There was a significant increase ($p < 0.001$) in the proportion of cells with CHOP activation in cells expressing mutant TDP-43 Q331K, compared to wildtype TDP-43, as previous. Significantly fewer cells displayed CHOP activation when PDI ($p < 0.001$) or DsbA ($p < 0.01$) was co-expressed with TDP-43 Q331K, compared to cells co-expressing the empty vector. N=3, Mean ± SEM, ** $p < 0.01$, *** $p < 0.001$. **C)** Quantification of cells in A) displaying CHOP activation. Significantly more ($p < 0.001$) cells expressing mutant TDP-43 Q331K displayed CHOP activation, compared to cells expressing wildtype TDP-43 or controls. A significant decrease ($p < 0.001$) in the proportion of cells with CHOP activation was observed in populations co-expressing PDI with mutant TDP-43 Q331K compared to those expressing vector only. However, there was a significant increase ($p < 0.05$) in the proportion of cells with CHOP activation in populations

co-expressing DsbC with TDP-43 Q331K, compared to cells co-expressing PDI withTDP-43

Q331K. N=3, Mean ± SEM, * $p < 0.05$, ** $p < 0.01$, *** $p < 0.001$.

Investigation into the protective properties eukaryotic DsbA and DsbC-like proteins in neuronal cells expressing mutant FUS.

DsbA and DsbC were finally examined for protective effect in Neuro-2A cells expressing mutant FUS R521G. Their activity on mutant FUS mislocalisation to the cytoplasm and mutant FUS-induced ER stress were analysed in this section.

4.3.35 DsbA and DsbC are co-expressed in almost all cells transfected with FUS

Firstly, the co-transfection efficiency of DsbA and DsbC with FUS was examined in Neuro-2A cells. Cells were transfected with constructs encoding GFP-FUS and either DsbA or DsbC for 72 h, before fixing. Immunocytochemistry was then performed using an anti-V5 antibody and the nuclei were stained with Hoechst. Co-expression of either DsbA or DsbC with GFP-FUS was confirmed using fluorescence microscopy by analysing GFP expression (green) from FUS and performing immunocytochemistry with an Alexa Fluor 568-tagged secondary antibody to detect the V5 tag for both DsbA and DsbC (Figure 4.40). The overall transfection efficiency of FUS was approximately 80% in Neuro-2A cells when observed 72 h post-transfection. Three replicate experiments were undertaken, whereby fluorescent microscopy was used to visualise at least 100 FUS expressing cells. These cells were further analysed for co-expression with either DsbA or DsbC. Quantification revealed that approximately 97% of FUS expressing cells also co-expressed DsbA and approximately 96% of FUS expressing cells also co-expressed DsbC. Thus, in all further experiments where FUS and the Dsbs were co-transfected and immunocytochemistry using a V5 antibody was not performed, it was assumed that detection of FUS reflected co-expression of both FUS and either DsbA or DsbC.
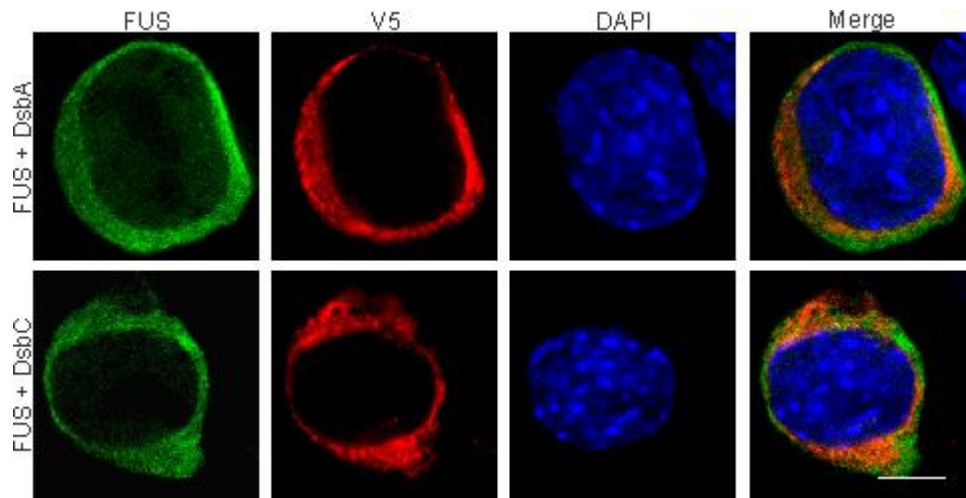
Figure 4.40: DsbA-V5 and DsbC-V5-like proteins are co-expressed in almost all Neuro-2A cells co-expressing GFP-FUS. Neuro-2A cells were transfected for 72 h with constructs encoding GFP-FUS (left column) and either DsbA-V5 or DsbC-V5 (second column). Cells were fixed, immunocytochemistry was performed using an anti-V5 antibody, and the nuclei were stained with Hoechst (third column). The merge column demonstrates co-expression of the Dsb-like proteins s with FUS in the cell shown. Scale bar = 20 µM.

4.3.36 Expression of DsbA and DsbC-like proteins and FUS in Neuro-2A cells

Western blotting was performed next to ensure that each protein was expressed to a similar efficiency s and to confirm that the DsbA and DsbC-like proteins were of the expected MW (Figure 4.41). Cell lysates were prepared from the following; GFP alone, wildtype FUS co-expressed with empty pcDNA3.1 vector, and mutant FUS R521G co-expressed with either empty pcDNA3.1 vector, PDI, DsbA or DsbC-like proteins. Immunoblotting showed that wildtype and mutant GFP-FUS were expressed at similar levels at 100 kDa, and GFP alone was expressed at 26 kDa, as expected, using an anti-GFP antibody. DsbA and DsbC were detected at 25 kDa and 30 kDa, respectively using an anti-V5 antibody. PDI was also detected using an anti-V5 antibody (62 kDa). The loading control, β-actin, was detected using an anti- β-actin antibody at 40 kDa.
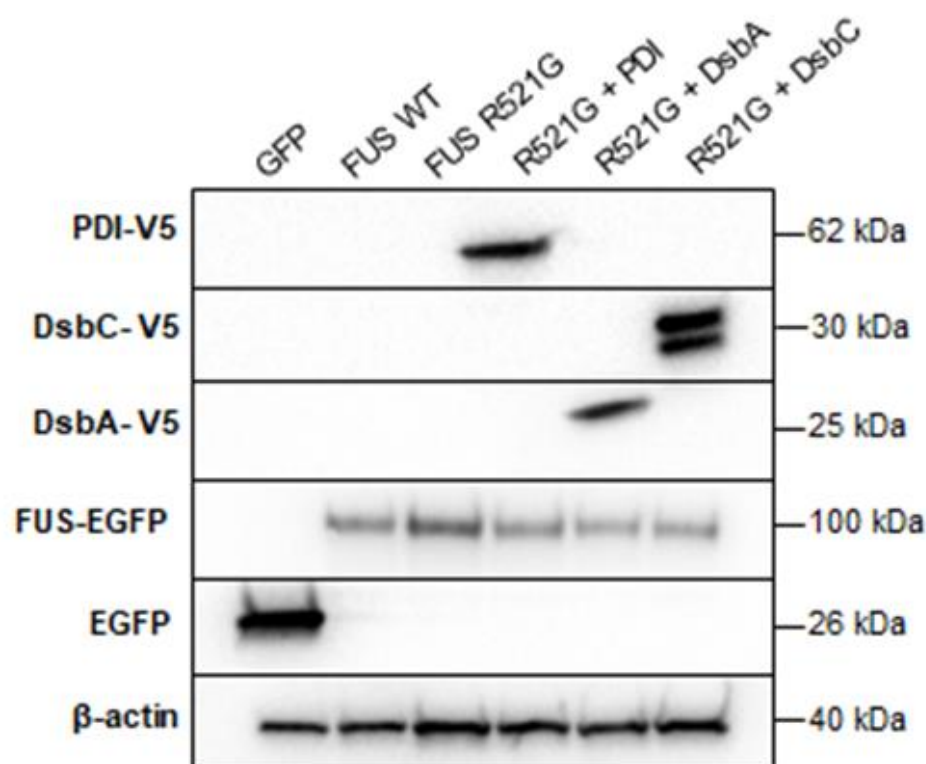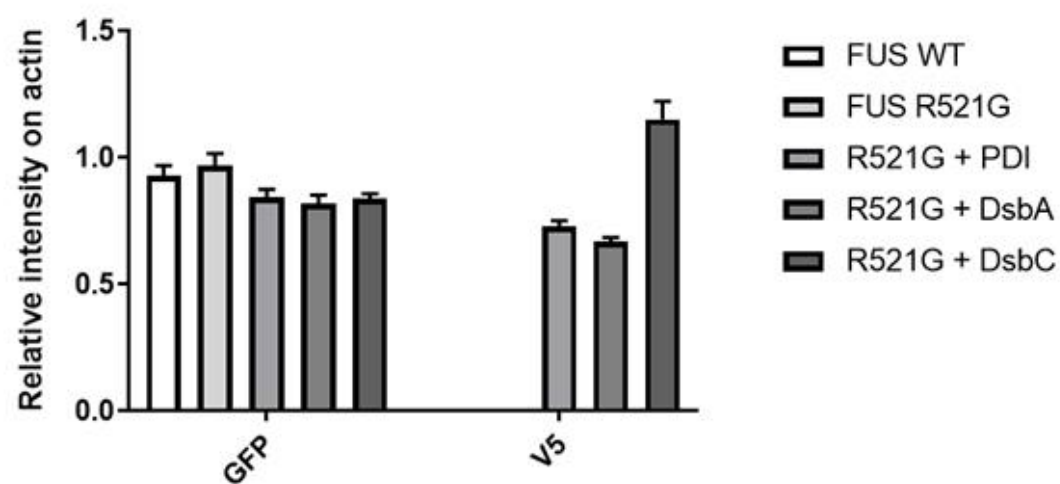
Figure 4.41: Expression of GFP-FUS with DsbA-V5 and DsbC-V5-like proteins in Neuro-2A cells. A) Western blotting of cell lysates and quantification was performed to ensure that the expressed proteins were the correct MW and that similar expression levels between proteins were observed. Cell lysates analysed were GFP alone, wildtype FUS with empty pcDNA3.1 vector, and mutant FUS R521G with either empty pcDNA3.1 vector, PDI, DsbA or DsbC. Wildtype and mutant FUS were detected at 100 kDa and GFP alone was detected at 26 kDa. DsbA was expressed at 25 kDa, DsbC was expressed at 30 kDa and PDI was detected at 62 kDa. The two bands detected for DsbC demonstrate that DsbC is a dimer. The loading control, β-actin, was detected at 40 kDa. **B)** Quantification revealed that wildtype FUS and mutant FUS R521G were expressed at similar levels. Moreover, mutant FUS R521G displayed similar expression across all cell lysate populations. DsbC appeared to have higher expression levels than PDI and DsbA, although this was not statistically significant. Lysates expressing GFP only were not included in quantification. N=3, Mean ± SEM.

4.3.37 Overexpression of DsbA mutant FUS mislocalisation to the cytoplasm

As previous studies have demonstrated that FUS mislocalises from the nucleus to the cytoplasm in ALS, it was next investigated whether the Dsb-like proteins were able to inhibit this process. First, Neuro-2A cells were transfected with empty pcDNA3.1 vector, GFP, wildtype FUS with pcDNA3.1, and mutant FUS R521G with either pcDNA3.1, PDI or DsbA. Immunocytochemistry was not performed as it was assumed that FUS expression reflected co-expression of both FUS and V5-tagged DsbA and DsbC. Cells were fixed and DAPI-stained using Hoechst to visualise the nuclei. The cellular localisation of FUS was analysed 72 h post-transfection using fluorescence microscopy to ensure maximal levels of protein expression, where at least 100 FUS expressing cells were examined. FUS was considered to be nuclear either when it completely co-localised with the DAPI-stained nucleus, or when it was localised within the nucleus and the cytoplasm, as the R521G mutation is quite aggressive. In contrast, FUS was considered cytoplasmic when fluorescence was only detected in the cytoplasm in FUS expressing cells (Figure 4.42 A).

Untransfected cells and cells expressing pcDNA3.1, GFP and wildtype FUS, did not display FUS localisation in the cytoplasm. In contrast, there was a significant increase ($p < 0.001$) in the proportion of cells with cytoplasmic FUS in populations expressing mutant FUS R521G (71.3% ± 2.9). However, there was a significant decrease in the proportion of cells with cytoplasmic FUS when either PDI ($p < 0.001$) or DsbA ($p < 0.01$) was co-expressed with mutant FUS R521G, compared to cells expressing FUS R521G with empty pcDNA3.1 vector (58.0% ± 1.5 and 59.0% ± 3.0, respectively). This data demonstrates a protective role for DsbA against mutant FUS mislocalisation to the cytoplasm (Figure 4.42 B).

Next, the protective activity of DsbC was examined against mutant FUS mislocalisation. Neuro-2A cells were transfected with empty pcDNA3.1 vector, GFP, wildtype FUS with

pcDNA3.1, or mutant FUS R521G with either pcDNA3.1, PDI or DsbC for 72 h. After fixing, cells were stained with Hoechst to visualise the nuclei and fluorescent microscopy was utilised to examine at least 100 FUS transfected cells. Quantification revealed that cytoplasmic FUS was never observed in populations expressing wildtype FUS. Conversely, there was a significant increase ($p < 0.001$) in the proportion of cells with cytoplasmic FUS in populations expressing mutant FUS R521G (75.3% $\pm$ 5.2) compared to wildtype FUS. As expected, co-expression of PDI with mutant FUS R521G resulted in a significant decrease ($p < 0.01$) in the proportion of cells with cytoplasmic FUS (56.0% $\pm$ 1.5), compared to cells expressing FUS R521G with empty pcDNA3.1 vector. However, co-expression of DsbC with FUS R521G resulted in a significant increase ($p < 0.05$) in the proportion of cells with cytoplasmic FUS (67.7% $\pm$ 3.2) compared to cells co-expressing PDI with mutant FUS, and this proportion was not significantly different to cells expressing vector only. Hence, these data indicate that DsbC is not protective against mutant FUS mislocalisation to the cytoplasm (Figure 4.42 C).
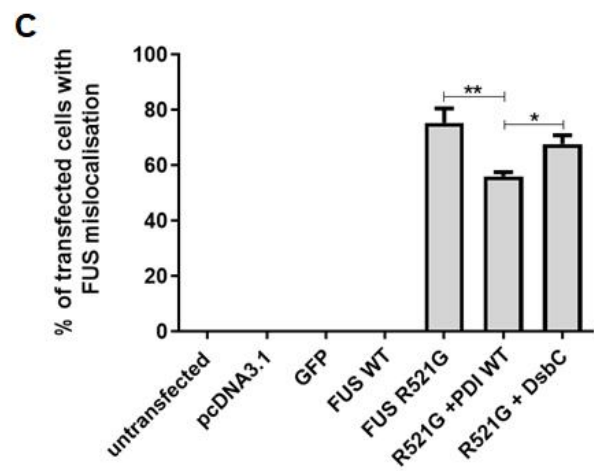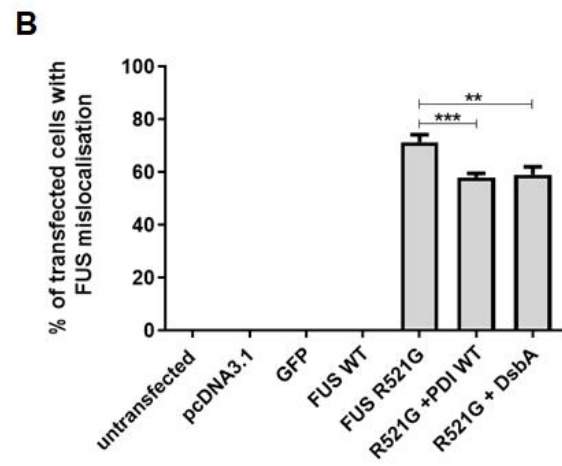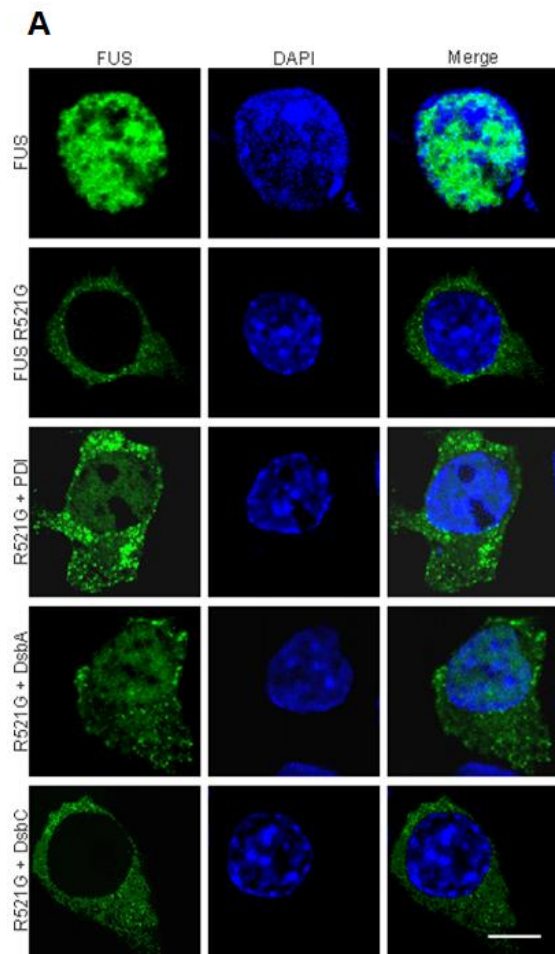
Figure 4.42: Overexpression of DsbA prevents mutant FUS mislocalisation to the cytoplasm. A) Immunofluorescence images of Neuro-2A cells expressing wildtype FUS with pcDNA3.1, or mutant FUS R521G with either pcDNA3.1, PDI, DsbA or DsbC (column one). DAPI stained nuclei are illustrated in column two, and a merged image of the cells is shown in column three. Cells expressing wildtype FUS (first panel; FUS WT) only displayed FUS co-localisation with the DAPI-stained nucleus, revealing that wildtype FUS is only ever expressed in the nucleus of Neuro-2A cells. In contrast, mutant FUS R521G (second panel; FUS R521G) was frequently observed in the cytoplasm, as indicated by no fluorescence in the DAPI-stained nucleus. However, when PDI or DsbA were co-expressed with mutant FUS R521G, significantly fewer cells displayed cytoplasmic FUS, as illustrated by the localisation of FUS in both the nucleus and cytoplasm (third and fourth panel; R521G + PDI, R521G + DsbA). In contrast, mutant FUS was present (fifth panel; R521G + DsbC) mostly in the cytoplasm when DsbC was co-expressed with R521G, similar to populations expressing mutant FUS R521G only. Scale bar = 20 µM. **B)** Quantification of Neuro-2A cells with FUS mislocalisation to the cytoplasm in A). Wildtype FUS was never found in the cytoplasm of Neuro2A cells, whereas mutant FUS R521G was expressed mostly in the cytoplasm. There was a significant decrease in the proportion of cells with cytoplasmic FUS when PDI ($p < 0.001$) or DsbA ($p < 0.01$) was co-expressed with mutant R521G. N=3, Mean ± SEM, ** $p < 0.01$, *** $p < 0.001$. **C)** Quantification of Neuro-2A cells with cytoplasmic FUS in B). A significant decrease ($p < 0.01$) in the proportion of cells with cytoplasmic FUS was observed in populations co-expressing PDI with mutant R521G, compared to those expressing mutant FUS R521G and pcDNA3.1. In comparison, there was no significant difference in the proportion of cells with cytoplasmic FUS in populations co-expressing DsbC with mutant R521G, compared to those co-expressing mutant FUS R521G with empty vector. Furthermore, there was a significant increase ($p < 0.05$) in the proportion of cells with

cytoplasmic FUS between populations co-expressing DsbC and FUS R521G compared to

those expressing PDI and FUS R521G. N=3, Mean $\pm$ SEM, * p < 0.05, ** p < 0.01.

4.3.38 Overexpression of DsbA and DsbC-like proteins is protective against ER stress induced by mutant FUS

Finally, the activity of DsbA and DsbC-like proteins was investigated against mutant FUS induced ER stress. The activation of CHOP was assessed by its nuclear immunoreactivity as above, to examine induction of the pro-apoptotic phase of the UPR. Neuro-2A cells were first transfected with empty pcDNA3.1 vector, GFP, wildtype FUS with pcDNA3.1, and mutant FUS R521G with either pcDNA3.1, PDI or DsbA for 72 h. After fixing, immunocytochemistry was performed using an anti-CHOP antibody and cells were stained with Hoechst to detect the nuclei. Fluorescence microscopy was utilised to examine at least 100 FUS transfected cells for ER stress, whereby nuclear immunoreactivity to CHOP was indicative of its activation (Figure 4.43 A).

Untransfected cells, or cells expressing pcDNA3.1, GFP and wildtype FUS rarely displayed CHOP activation (less than 5%). Conversely, significantly more ($p < 0.001$) cells expressing mutant FUS R521G displayed nuclear immunoreactivity to CHOP ($22.3\% \pm 1.8$), compared to those expressing wildtype FUS ($1.7\% \pm 0.9$). Co-expression of PDI with mutant FUS R521G resulted in a significant reduction ($p < 0.001$) in the proportion of cells with CHOP activation ($5.7\% \pm 0.3$), compared to those expressing mutant FUS R521G with empty pcDNA3.1 vector. Moreover, significantly fewer cells co-expressing DsbA with FUS R521G ($p < 0.001$) displayed CHOP activation compared to those expressing mutant FUS only. Hence these data imply that DsbA, and hence its oxidase activity, is protective against mutant FUS induced ER stress (Figure 4.43 B).

Finally, DsbC was examined for its protective activity against CHOP activation. Neuro-2A cells were transfected for 72 h with empty pcDNA3.1 vector, GFP, wildtype FUS with pcDNA3.1, and mutant FUS R521G with either pcDNA3.1, PDI, or DsbC. After

immunocytochemistry was performed using an anti-CHOP antibody, cells were examined for CHOP activation using fluorescence microscopy. Similar to the results presented in Figure 4.43 B, less than 5% of untransfected cells or cells expressing pcDNA3.1, GFP and wildtype FUS, exhibited nuclear immunoreactivity to CHOP. A significant increase ($p < 0.001$) in the proportion of cells with CHOP activation was observed in populations expressing mutant FUS R521G ($19.3\% \pm 2.0$), compared to those expressing wildtype FUS ($1.7\% \pm 0.9$). As expected, there was a significant decrease ($p < 0.001$) in the proportion of cells with CHOP activation when PDI was co-expressed with mutant FUS R521G ($6.3\% \pm 0.3$), compared to cells expressing mutant FUS R521G with empty pcDNA3.1 vector. Interestingly, co-expression of mutant FUS R521G with DsbC also resulted in a significant decrease ($p < 0.01$) in the proportion of cells with nuclear immunoreactivity to CHOP ($10.0\% \pm 2.5$) compared to FUS R521G cells co-expressing empty pcDNA3.1 vector. Hence, these data indicate that DsbC, and hence either its isomerase or chaperone activity, is also protective against mutant FUS induced-ER stress (Figure 4.43 C).
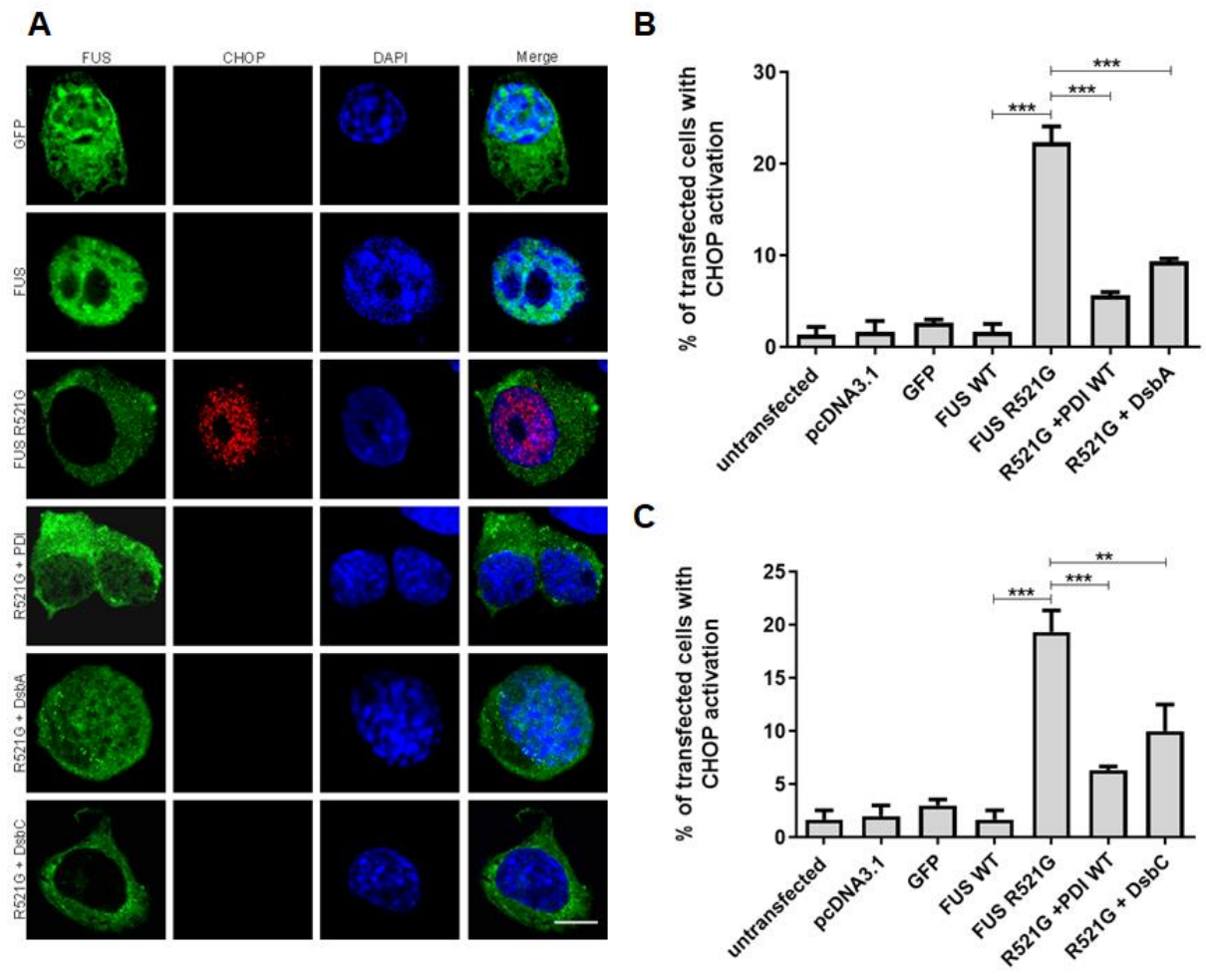
Figure 4.43: Overexpression of DsbA and DsbC is protective against ER stress-induced by mutant FUS. A) Immunofluorescence images of Neuro-2A cells expressing GFP, wildtype FUS with pcDNA3.1, and mutant FUS with either pcDNA3.1, PDI, DsbA or DsbC (column one), and immunocytochemistry to CHOP (column two). Cells expressing GFP (first panel; GFP) or wildtype FUS (second panel; FUS WT) rarely displayed nuclear immunoreactivity to CHOP, indicating activation. In contrast, more cells expressing mutant FUS R521G (third panel; FUS R521G) displayed nuclear immunoreactivity to CHOP, as indicated by red fluorescence in the nucleus (panel three, column two). However, when mutant FUS R521G was co-expressed with either PDI, DsbA or DsbC, fewer cells displayed CHOP activation. Scale bar = 20 µM. **B)** Quantification of cells in A) displaying CHOP activation. Very few untransfected cells and cells expressing pcDNA31, GFP or wildtype FUS displayed nuclear CHOP immunoreactivity as expected. There was a significant increase ($p < 0.001$) in the proportion of cells with CHOP activation in populations expressing mutant FUS R521G, compared to those expressing wildtype FUS. Significantly fewer ($p < 0.001$) mutant FUS R521G cells displayed CHOP activation when PDI or DsbA were co-expressed, compared to those co-expressing empty pcDNA3.1 vector. N=3, Mean ± SEM, *** $p < 0.001$. Hence DsbA is protective against mutant FUS-induced ER stress. **C)** Quantification of cells in A) displaying nuclear immunoreactivity to CHOP. There was a significant increase ($p < 0.001$) in the proportion of cells with CHOP activation in populations expressing mutant FUS R521G, compared to those expressing wildtype FUS, GFP or empty pcDNA3.1 vector alone. However, this proportion was significantly reduced when either PDI ($p < 0.001$) or DsbC ($p < 0.01$) was co-expressed with mutant FUS R521G. Hence DsbC is protective against mutant FUS-induced ER stress. N=3, Mean ± SEM, ** $p < 0.01$, *** $p < 0.001$.

4.3.39 A summary of the protective activity of the DsbA and DsbC-like proteins

A summary of the protective effects of the DsbA and DsbC-like proteins against ALS-associated proteins, SOD1, TDP-43 and FUS, is shown in Table 4.4. DsbA was protective against all cellular pathogenic mechanisms induced by all three mutant proteins, demonstrating an importance for oxidase activity. DsbC demonstrated protective properties against ER stress induced by either mutant SOD1 or FUS, and mutant TDP-43 mislocalisation to the cytoplasm.

TABLE 4.4. The protective activities of the DsbA and DsbC-like proteins.

SOD1			
	Inclusion formation	**ER stress**	**Apoptosis**
DsbA	✓	✓	✓
DsbC	✗	✓	✗
TDP-43			
	TDP-43 mislocalisation		**ER stress**
DsbA	✓		✓
DsbC	✓		✗
FUS			
	FUS mislocalisation		**ER stress**
DsbA	✓		✓
DsbC	✗		✓

4.4 Discussion

PDI is a molecular chaperone found primarily in the ER, which is upregulated during ER stress [437]. It is the prototype of a large family of chaperones which possess two distinct protein folding functions; firstly, PDI is an oxidoreductase, and thus, possesses disulphide interchange activity, in which disulphide bonds are oxidised (formed), reduced (broken down) and isomerised (rearranged). Secondly, PDI demonstrates general chaperone activity [438, 489]. Hence, PDI is an essential part of ER proteostasis, because it is able to facilitate the correct folding of misfolded proteins back into their native conformation. Previous studies have revealed a protective activity for PDI in ALS. Unfortunately, the exact mechanism of action of PDI's protective activity in ALS and other neurodegenerative diseases is poorly understood. Therefore, this chapter aimed to identify the specific requirements that enable the protective capabilities of PDI and to determine which of PDI's domains and therefore, which of its functions, are fundamental for this protective activity in cells expressing mutant ALS proteins, SOD1, TDP-43 and FUS. These experiments may then assist in the development of novel therapeutics based on PDI's activity and protective function.

It has been previously considered that PDI can prevent mutant SOD1 aggregation by modulating disulphide bonding, and thus utilise its disulphide interchange activity, since reports suggest a correlation between SOD1 aggregation and disulphide reduction/non-native cross-linking between SOD1's disulphide bonds [506, 510, 511, 565]. Previous studies have demonstrated that a non-native intermolecular disulphide bond between Cys-6 and Cys-111 residues of mutant SOD1 mediates high molecular weight aggregate formation because mutagenesis of Cys-6 and Cys-111 to serine reduces ALS-linked mutant SOD1 aggregation, and thus, inclusion formation and apoptosis [510, 512]. Hence, this study investigated whether the mutagenesis of the same cysteine residues in SOD1 to serines would also prevent induction of ER stress, as ER stress is becoming increasingly implicated in the cellular

pathogenesis in ALS. The results obtained in this study demonstrate a reduction in the proportion of cells with XBP-1 activation, indicative of early phase UPR induction, when mutants A4V C111S, A4V C6S C111S and A4V QUAD were expressed in Neuro-2A cells. This data is concurrent with previous reports which concluded that mutagenesis of the Cys-111 residue to serine inhibits SOD1 aggregation, inclusion formation and apoptosis [512], and studies which indicate that Cys-111 is a target for oxidation [566]. Similar results were obtained from the nuclear CHOP immunoreactivity studies, which examined ER stress induced apoptotic signalling. However, in contrast to the XBP-1 results, the A4V C57S C146S mutant was also protective against CHOP activation. It is interesting to note, however, that mutation of the A4V Cys-6 residue to serine was not protective against ER stress, and removing this cysteine would ensure that the non-native disulphide bond between Cys-6 and Cys-111 could not form. Previous studies have reported aggregation of mutant SOD1 upon C-6 mutagenesis, however [512]. Moreover, in this study, mutation of the A4V Cys-57 Cys-111 Cys-146 residues to serines did not alter the proportion of cells with either activated XBP-1 or CHOP, even though the Cys-111 residue is unable to cross link with Cys-6. These results imply that the mechanism triggering induction of ER stress by mutant SOD1 is more complex than just non-native disulphide bonding of mutant SOD1 cysteine residues. In fact, nuclear XBP-1 and CHOP activation, indicating induction of ER stress, can be detected in mutant SOD1 A4V expressing cells that do not bear inclusions. It is unusual however that expression of the A4V C57S C146S mutant did not alter the proportion of Neuro-2A cells with CHOP activation, since Cys-57 and Cys-146 are involved in formation of SOD1's disulphide bridge, hence mutating these residues to serine would effectively destabilise the SOD1 dimer. Interestingly, in our laboratory, all the cysteine mutations have also been generated in the wildtype SOD1 construct. Unpublished observations have demonstrated that these mutations in wildtype SOD1 do not form aggregates, suggesting that the Cys-to-Ser

mutations do not cause ALS-like gain of toxic functional properties. It is important to note however, that the role of disulphide cross-linking in the aggregation of mutant SOD1 has been disputed [513], therefore future studies will need to be undertaken to further investigate the role of SOD1's cysteine residues on mutant SOD1 aggregation, and now, ER stress. In future studies, it would also be interesting to examine whether PDI can inhibit induction of ER stress triggered by the SOD1 A4V cysteine mutants that induce the UPR; C6S, C57S, C146S, and C57S C111S C146S. A protective role for PDI in this instance would suggest that PDI does not need to interact with SOD1 via its disulphide bonds. Conversely, if PDI is not protective against ER stress induced by A4V SOD1 cysteine mutants, this would further strengthen the notion that PDI interacts with mutant SOD1, and therefore is protective via its disulphide interchange activity.

Previous studies undertaken in our laboratory have demonstrated that PDI's disulphide interchange activity is required for its protective activity against SOD1 inclusion formation, ER stress and ER-Golgi transport defects induced by mutant SOD1 (Parakh et al., 2017 in preparation). Based on these results, the active site cysteine residues are evidently fundamental for PDI function, in this case by binding to misfolded proteins and subsequently contributing to protein stabilisation [486]. Other studies have suggested that monomeric and oligomeric forms of misfolded SOD1 are toxic to motor neurons [567, 568]. For example, it has been demonstrated that mutations in SOD1 destabilise the SOD1 dimer to form monomers, and it is these unstable monomeric SOD1 proteins which cause aggregation [568]. Thus, future studies should be performed to examine PDI's effects on SOD1 monomer or oligomer formation, to further elucidate its mode of protection. One explanation for the protective functions of PDI is that it is able to stabilise the formation of the SOD1 dimer through its disulphide interchange activity, therefore preventing monomerisation or oligomerisation of misfolded SOD1, thus preventing the formation of inclusions.

Interestingly though, both the disulphide interchange activity and chaperone function of PDI were protective against mutant SOD1-induced apoptosis, whereby the PDI QUAD mutant, which contains only serine residues instead of cysteines in PDI's active sites, was found to decrease the proportion of cells with nuclei condensation and fragmentation in comparison to wildtype PDI (Parakh et al., 2017 in preparation). Previous studies have confirmed conclusively that removal of all four cysteine residues in PDI's active sites ablates the disulphide interchange activity [502, 563]; hence experiments to demonstrate that the QUAD mutant does not retain this function were not performed here. DNA fragmentation is considered a late marker of apoptosis, hence, it was also investigated here whether expression of the PDI QUAD mutant was also able to inhibit early apoptotic events; the activation of Bax, its recruitment to mitochondria, and the activation of cleaved Caspase-3 [315]. These results demonstrated that PDI QUAD mutant retained its protective activity against apoptosis using all three of these markers, confirming the DAPI condensation results, and demonstrating that the chaperone function of PDI is sufficient to rescue cells from apoptotic cell death. It remains unclear exactly how the chaperone activity is protective against mutant-SOD1 induced apoptosis when it is not protective against inclusion formation which was previously linked to apoptosis [315]. However, it could be speculated that the chaperone activity of PDI is triggered as a last resort to restore cellular proteostasis.

It is also important to note that cytoplasmic wildtype PDI and cytoplasmic PDI QUAD were also protective in decreasing the proportion of cells with activation and recruitment of Bax, and activation of Caspase-3. These data suggest that the cytoplasm is the cellular location where PDI is protective. The cytoplasmic PDI proteins were examined for their cellular location using confocal microscopy and they were found to be clearly absent in the ER, confirming their cytoplasmic expression. In fact, previous studies have shown that endogenous PDI is present in multiple non-ER locations, including the cytoplasm [450], and

it has been demonstrated that PDI is released into the cytoplasm during ER stress-induced apoptosis [569]. SOD1 is predominantly cytoplasmic and excluded from the ER [355], so it is plausible that PDI and SOD1 interact mainly in the cytoplasm. Cytoplasmic PDI may be protective due to an augmented availability of mutant SOD1 and other proteins linked to ALS in the cytoplasm compared to the ER. Consistent with this notion, pathological forms of TDP-43 and FUS are also present in the cytoplasm [145, 570] and our laboratory has recently demonstrated that cytoplasmic wildtype PDI is also protective against other cellular events linked to pathogenesis that occur in the cytoplasm, such as mislocalisation of TDP-43 and FUS from the nucleus, and defects in ER-Golgi transport (Parakh et al., 2017 in preparation). Therefore, together these data imply that PDI is most beneficial when available in the cytoplasm. A study by Yang and colleagues (2009) identified that reticulons, a family of ER membrane proteins, are important modulators of PDI subcellular localisation, and interestingly, deletion of reticulon-4A accelerates motor neuron degeneration in mutant SOD1 G93A mouse models [452], providing further evidence that the cellular location of PDI is relevant to disease *in vivo* in ALS.

Although previous studies have confirmed that PDI's chaperone activity can be isolated by mutating the cysteine residues on its active sites to remove the disulphide interchange activity, the individual domains of PDI are thought to play their own distinct roles in PDI's functions. The *a* and *a'* domains of PDI, which contain the CGHC active sites, are responsible for the disulphide interchange activity, whereas the *b* domains contain the substrate binding sites that are essential for PDI's chaperone function. These substrate binding sites are able to bind to the hydrophobic regions of misfolded proteins with high affinity, albeit broad specificity [495]. Hence, three PDI domain mutants (*a* domain, *a'* domain and *bb'* domain) were generated by removing the other domains. It is important to note that the constructs encoding these mutants were designed to retain PDI's signal sequence

and KDEL sequence to ensure that the native localisation of PDI was preserved. The ER - localisation of the domain mutants was confirmed using confocal microscopy, whereby each mutant co-localised with ER resident protein, calreticulin.

In this study, only the *a* and *a'* domains, possessing the disulphide interchange activity, were protective against mutant SOD1 inclusion formation, suggesting that the *b* domains, and thus the chaperone functions, are not protective. One possible reason for this is that the disulphide interchange activity of PDI is required for the oxidation, isomerisation and reduction of misfolded SOD1 disulphide bonds, in order to produce SOD1's native conformation. On the other hand, it is possible that the chaperone activity of PDI is in fact protective, however the *bb'* domain mutant alone is insufficient to elicit a protective response against inclusion formation. It has been previously demonstrated that complex reactions involving extensive conformational changes in substrate proteins require all of PDI's domains [487], implying that the chaperone activity of PDI alone is not protective against the formation of misfolded SOD1 proteins. Remarkably, however, the *bb'* domain, along with the *a* and *a'* domains, was protective against mutant SOD1-induced ER stress. This is an interesting result since the presence of SOD1 inclusions is closely associated with ER stress [429]. Previous reports, however, have demonstrated that induction of the UPR upregulates chaperones, including PDI [571]. Also, it may be that major conformational changes of substrate proteins are not required to inhibit ER stress, thus the *b* and *b'* domains alone are sufficient to elicit a protective response. It should be noted however, that there were significantly fewer mutant SOD1 expressing cells with ER stress when the *a* domain was over-expressed, compared to when the *bb'* domain was over-expressed, indicating that the *a* domain, and thus the disulphide interchange activity of PDI, is more efficient in preventing ER stress, compared to the chaperone function. This could be due to the fact that the disulphide interchange activity

of PDI is also protective against the formation of SOD1 inclusions, unlike the chaperone function, which would further contribute to the protective activity against the UPR.

Another interesting result obtained in this study was that only the *a* and *a'* domain mutants were protective against mutant SOD1-induced apoptotic cell death. It was initially hypothesised that the *bb'* domain mutant would also be protective against apoptosis, given that the PDI QUAD mutant, which possesses chaperone activity only, was in fact, protective. Again, perhaps the chaperone function of PDI still requires the presence of all domains to prompt a protective response against apoptosis, which would explain why the *bb'* domain mutant alone was unable to decrease the proportion of cells with apoptotic nuclei. These results, however, do highlight the importance of the *a* and *a'* domains, and thus the disulphide interchange activity of PDI, in restoring cellular proteostasis and thus ensuring cellular viability.

The *a*, *a'* and *bb'* domain mutants were also protective against mutant TDP-43-induced ER stress. Similar to the mutant SOD1 result, the chaperone function of PDI may be induced following ER stress, whereby an upregulation of ER chaperones occurs to alleviate the load of misfolded proteins, thus accounting for the protective activity of the *bb'* domain. Mutant TDP-43 also forms abnormal non-native disulphide bonds following oxidation, which eventually leads to aggregation, and subsequent activation of ER stress [572]. Therefore, the *a* and *a'* domains, or the disulphide interchange activity of PDI, may prevent the formation of these TDP-43 aggregates by refolding the non-native disulphide bonds, thus preventing activation of ER stress. TDP-43 aggregation may also be the reason why mutant TDP-43 remains mislocalised to the cytoplasm. Interestingly, only the *a* and *a'* domain mutants were able to inhibit TDP-43 mislocalisation to the cytoplasm, implying that only the disulphide interchange activity, and not the chaperone function, is protective. Further studies are necessary to elucidate the mechanism by which the *b* and *b'* domains of PDI were protective

against mutant TDP-43-induced ER stress, but have no protective effect against TDP-43 mislocalisation to the cytoplasm, especially since mislocalisation is associated with ER stress [427]. Perhaps mislocalisation of TDP-43 to the cytoplasm is triggered by an alternative mechanism, or perhaps the chaperone function of PDI requires the presence of all domains of PDI.

Similar findings were obtained from cells expressing mutant FUS R521G, where only the *a* and *a'* domains were protective against mutant FUS mislocalisation to the cytoplasm, but all three domain mutants, including *bb'*, were protective against ER stress. TDP-43 and FUS have similar functions and they share multiple DNA/RNA targets [573], therefore it is possible that PDI has a similar protective function against both proteins. The *bb'* domain mutant, and thus the chaperone function of PDI, was protective against ER stress induced by all three of the ALS-associated proteins examined here; SOD1, TDP-43 and FUS. These results suggest that the chaperone function of PDI plays an important role in the alleviation of ER stress following its upregulation via the UPR. However, the *a* and *a'* domains were protective against every cellular mechanism linked to pathogenesis investigated in this study, for each of the three mutant proteins, indicating that the disulphide interchange activity of PDI is imperative for its protective function. This makes sense as S-nitrosylation of PDI affects only its active site cysteine residues, but it ultimately compromises PDI's function. On the contrary, however, whilst SOD1 and TDP-43 aggregation is mediated via their cysteine residues, FUS aggregates are formed in stress granules that do not rely on cysteine residues. It is interesting, then, that the disulphide interchange activity is protective against mutant FUS pathogenesis. Therefore, future work should be performed to investigate the effect of PDI, and consequently the effect of the *a* and *a'* domain mutants, on stress granule formation, to further elucidate PDI's protective mechanisms against FUS aggregation.

Although the *a* and *a'* domains of PDI only share 33.6% homology [483], in this study their protective activities were found to be remarkably similar, indicating that the disulphide interchange activity relies predominantly on the identical CGHC active site. Interestingly, however, one previous study examining the PDI *a* and *a'* domains, concluded that the *a'* domain functions as a disulphide oxidase, whereas the *a* domain functions as a disulphide isomerase [574]. This variability between the functions of the two domains was linked to asymmetry in PDI's active sites, resulting from the substrate-independent enhanced rate of oxidation of the *a'* domain compared to the *a* domain, and the substrate-mediated inhibition of oxidation of the *a* domain [574]. The results obtained in this study demonstrate that there is a slight, but non-significant, decrease in the proportion of cells forming SOD1 inclusions, mutant SOD1-induced apoptosis, and mislocalisation of both TDP-43 and FUS to the cytoplasm when the *a'* domain was overexpressed, compared to the *a* domain, suggesting that the oxidase activity of PDI may be more protective against these properties. The *a* domain, and thus, the predicted isomerase activity of PDI, was found to be more protective against mutant SOD1 and TDP-43 induced ER stress than the *a'* domain, however, these results were not statistically significant. Therefore, further studies should include more sensitive assays to explore these findings further. Moreover, the protective effects of the *a* and *a'* domains relative to PDI were quite comparable in this study, however other studies report that disruption to one of PDI's active sites abolishes 50% of PDI's catalytic activity overall [502]. Again, further studies, utilising more sensitive assays, may be required to investigate the relative degree of protective activity of the *a* and *a'* domain mutants, in comparison to PDI, and to each other. However, these studies provide a good foundation for further drug design studies based on PDI's protective activity. Full length PDI, being a protein of 55 kDa, is undesirable to be used therapeutically, therefore isolating the protective properties of PDI and

using smaller proteins derived from PDI as a basis for designing potential therapeutics, may be beneficial.

Studies examining eukaryotic versions of DsbA and DsbC proteins can illustrate the importance of redox activity on the protective properties of PDI. DsbA is normally a monomer, which is responsible for oxidising disulphide bonds in prokaryotes [575], whereas DsbC is a normally dimeric protein, responsible for isomerising disulphide bonds. Furthermore, DsbC is also capable of chaperone activity because its V-shape 3D conformation contains a highly hydrophobic inner surface capable of binding substrate proteins [559]. Here, BLAST comparisons of DsbA and DsbC sequences revealed that these proteins do not share extensive homology with one another, nor do they share much similarity to PDI, other than possessing a CXXC thioredoxin-like active site (CPHC in DsbA and CGYC in DsbC). However, nonetheless, these differences, particularly in the two residues between the cysteines of the active sites, result in different redox properties of PDI, DsbA and DsbC, so that PDI is an oxidoreductase, DsbA is an oxidase and DsbC is an isomerase.

DsbA was protective in cells expressing mutant SOD1, TDP-43 or FUS, in that it was able to decrease the proportion of cells with SOD1 inclusions and mutant SOD1-induced apoptotic nuclei, as well as inhibit TDP-43 and FUS mislocalisation to the cytoplasm, and induction of ER stress. These results imply that the oxidase activity of DsbA, where it facilitates disulphide bond formation, is broadly protective. In prokaryotic cells, DsbA becomes re-oxidised via DsbB. The crystal structure of DsbB demonstrates that DsbB shares a core structure and is functionally analogous to Ero1p, the redox partner of PDI [576, 577]. Therefore, it is plausible that the DsbA-like protein expressed here can bind and become re-oxidised in the eukaryotic cells by Ero1p, allowing it to retain its native functionality. DsbC, on the other hand, displayed protective activity only against ER stress induced by mutant

SOD1 and FUS, and TDP-43 mislocalisation to the cytoplasm. DsbC is an intriguing protein, in that it's V-shaped 3D structure is similar to that of the *b* domains of PDI. In this respect, it is unknown whether the isomerase or chaperone activity of DsbC were protective against the cellular events identified here. However, the *bb'* domain mutant was not protective against TDP-43 mislocalisation to the cytoplasm, thus it could be speculated that the isomerase activity of PDI is of importance in maintain TDP-43's localisation in the nucleus. In contrast, however, it was evident from this study that the chaperone function of PDI, via the *bb'* domain mutant, plays a fundamental role in inhibiting ER stress induced by all three mutant proteins examined. These data therefore imply that DsbC's chaperone function may be responsible for inhibiting ER stress in this study. Moreover, the structure of DsbD, which is responsible for maintaining DsbC in its reduced form, has not yet been defined, hence the mechanism by which the DsbC-like protein examined here maintains its reduced form in the eukaryotic cell remains uncertain. Therefore, the chaperone function of DsbC seems a more plausible mechanism for the inhibition of ER stress observed here in eukaryotic cells, rather than the isomerase function.

Ultimately, the results obtained here, by analysing the protective activity of DsbA and DsbC, suggest that the redox activity is of particular importance for the protective function of oxidoreductase proteins in ALS, such as PDI. The results indicate that the oxidase activity is more protective than the isomerase activity, however it is important to note that DsbA does also possess isomerase capabilities [492, 549]. Whereas DsbC is implicated in the isomerisation of substrate proteins in prokaryotes, it is possible that the combined activity of DsbA and Ero1p in the Neuro-2A cells examined here allows DsbA to facilitate its oxidase function, as well as additional isomerase activity if required, which involves both oxidase and reductase activity. It would be beneficial then, in future, to analyse the protective activity of Thioredoxin in eukaryotic cells against ALS-associated mutant proteins. Thioredoxin is

highly homologous in structure to the *a* domain of PDI [578], despite being a reductase, thus it would be interesting to investigate whether it possesses the same protective capabilities as PDI's *a* domain, or whether its reductase activity would result in different protective activities. The redox potential of PDI and its consequential protective activity in ALS is explored further in Chapter 5.

In summary, this study reveals that the *a* and *a'* domains of PDI are fundamental for PDI's protective capabilities in ALS. The *a* and *a'* domains were found to be protective across all cellular mechanisms examined, induced by mutant SOD1, TDP-43 and FUS. These results indicate that the *a* and *a'* domains, responsible for the disulphide interchange activity, are a key feature in facilitating PDI's protective function against misfolded proteins in ALS. Thus, novel therapeutics based on the disulphide interchange activity, should be designed based on this domain. The chaperone function of PDI was shown to be protective against ALS-associated ER stress as well as SOD1-induced apoptosis, indicating that PDI may elicit its protective response through several different pathways simultaneously. This study also demonstrates the importance of the redox potential in oxidoreductase proteins such as PDI, hence further studies are warranted to better understand how the redox activity of PDI affects its role in ALS, and how differences in redox activity can mediate a change in activity.

Chapter 5: The Role of Redox Activity in the Protective Function of PDI

5.1 Introduction

As an oxidoreductase, PDI can act as an oxidase, reductase or isomerase in eukaryotic cells, thus catalysing oxidative protein folding in the ER. PDI can oxidise pairs of cysteines to form disulphide bonds, reduce cysteine pairs to break down disulphide bonds, or isomerase cysteines to rearrange incorrect disulphides into their correct pairings [489].

PDI is a member of the thioredoxin-like superfamily, and proteins of this family are characterised by the presence of one or more thioredoxin-like domains, that display sequence or structural similarity to thioredoxin [550]. Redox active members, including PDI, all possess a CXXC catalytic motif, in which the two amino acid residues between the cysteines have a fundamental role in determining the overall redox potential of the protein. PDI has a redox potential of -160 mV, allowing it to perform its oxidoreductase function [437]. Conversely, thioredoxin-like proteins can act solely as oxidants of thiols, such as DsbA [575], reductants of disulphide bonds, such as thioredoxin itself [579], or isomerases that shuffle non-native disulphide bonds, as for DsbC and DsbG [559, 580]. All the aforementioned thioredoxin-like proteins possess diverse redox potentials, which dictate their characteristic activities against substrates [489]. Interestingly, features other than the CXXC motif can influence redox activity, including the cis-proline loop, which is described subsequently in this chapter.

The experiments outlined in this chapter investigate the role of redox activity on PDI's protective function. This was examined by modulating specific features characteristic of thioredoxin-like proteins; the active site motif and the cis-proline loop. Studies investigating the redox properties of other thioredoxin-like proteins, including DsbA, DsbC and thioredoxin, have been previously performed. However, these studies have yet to be implemented on PDI.

5.1.1 The redox properties of thioredoxin-like proteins

Thioredoxin-like proteins all contain a structural motif, the thioredoxin fold. This fold is the core scaffold of this group of proteins, which possess the general motif $\beta_1\alpha_1\beta_2$-α_2-$\beta_3\beta_4\alpha_3$. The fold is incorporated into proteins that control the cellular redox environment [550]. However, thioredoxin-like proteins share no overall homology, except for the presence of the CXXC catalytic motif, which is located at the N-terminus of the first helix in the conserved thioredoxin fold, and a cis-proline loop, which precedes the $\beta_3\beta_4\alpha_3$ motif [489, 550]. The CXXC motif and cis-proline loop are distant in sequence, however they are closely adjacent in three-dimensional space within the thioredoxin fold. Thus, the CXXC motif and cis-proline loop together constitute the active site of these redox proteins [492].

The wide range of redox activities observed in thioredoxin-like proteins is postulated to be a consequence of modifications to the core scaffold, in particular the CXXC motif and cis-proline loop, which result in diverse redox properties. For example, the redox potential of the archetype of the family, thioredoxin, is highly reducing at -271 mV [581], whereas that of periplasmic DsbA is highly oxidising at -120 mV [582]. The redox potential of bacterial isomerases DsbC and DsbG, are both approximately -130 mV [559]. Thioredoxin-like proteins that participate in numerous thiol disulphide exchange reactions, including PDI, have intermediate redox potentials, and PDI possesses a redox potential of -160 mV [583].

The cis-proline loop plays a significant role in the stability and structure of thioredoxin-like proteins [584, 585], and it also contributes to substrate binding and release [552, 586, 587]. The cis-proline loop is also thought to be involved in decreasing the pKa of the N-terminal cysteine of the CXXC motif, by stabilising the negative charge of the thiolate [486, 559]. Furthermore, the cysteine pKa, and thus the catalytic activity of the protein, is influenced by the electrostatic nature of neighbouring residues, and in particular by the residues located

between the two active-site cysteines [505, 588]. Moreover, the side chain of the residue preceding the proline in the cis-proline loop is closely associated with the N-terminal cysteine of the CXXC motif, thus this residue has the potential to also be involved in hydrophobic interactions with this cysteine, thereby modulating its activity [492].

Variability in CXXC active site motifs, and the residue preceding proline in the cis-proline loops, is observed in thioredoxin-like proteins. PDI contains a CGHC active site motif in both it's *a* and *a'* domains, and a cis-proline loop of sequence GYP in it's *a* domain and a cis-proline loop of sequence SFP in it's a*'* domain [489]. The oxidase DsbA possesses an active site motif of CPHC and a cis-proline loop of sequence GVP. In contrast, isomerases DsbC and DsbG both have a conserved GTP cis-proline loop, however their active site motifs are CGYC and CPYC, respectively. The reductase thioredoxin contains a CGPC active site motif and a GIP cis-proline loop [492] (Figure 5.1).

A
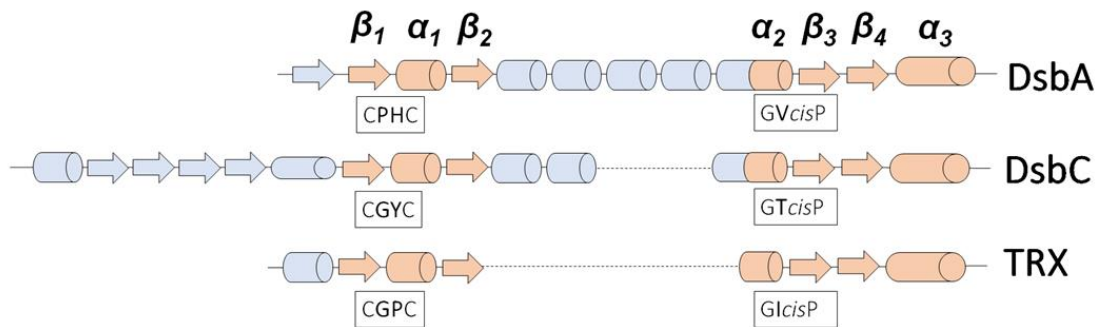
B
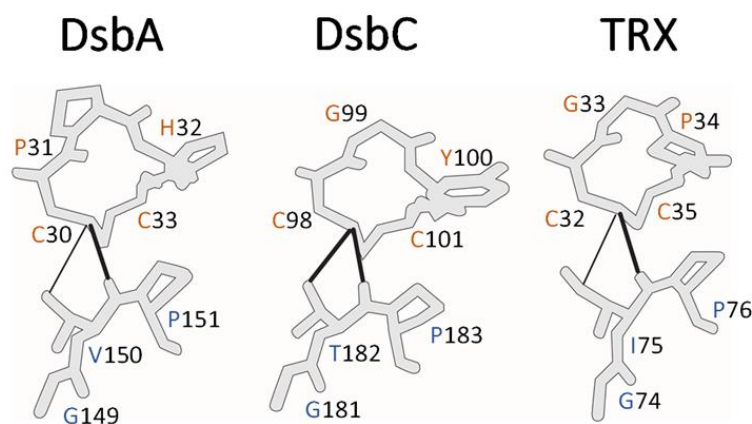
Figure 5.1: A schematic representation of thioredoxin-like proteins DsbA, DsbC and thioredoxin (TRX). A) A representation of the secondary structure elements of DsbA, DsbC and TRX. The thioredoxin fold is illustrated in pink/orange, and insertions in the thioredoxin fold are shaded in blue. The position of the CXXC active site motifs and cis-proline loops are indicated, with the differing residues contained within each protein in bold. DsbG has a similar secondary structure to DsbC, except that its active site motif is CPYC. **B)** A close-up of the active sites of DsbA, DsbC and TRX, demonstrating the close association of the catalytic CXXC motif and the cis-proline loop. Hydrogen bonds are represented by a black line [492].

5.1.2 Modulation of the CXXC motif and cis-proline loops in thioredoxin-like proteins

Studies investigating the redox potential of the strongly oxidising protein, DsbA, indicated that its redox properties could be modulated by replacing the residues between the two cysteines of the CXXC active site motif [589]. In these experiments, DsbA's CPHC active site motif was replaced with, CGHC similar to the oxidoreductase PDI, CPYC, similar to isomerase DsbG, or CGPC, as observed in the reductase thioredoxin. The results obtained demonstrated that all these CXXC variants were less oxidising that wildtype DsbA, and the resulting redox potentials were in the same order as the native proteins from which the active site sequence was obtained; DsbA > PDI > DsbG > thioredoxin [589]. In addition, mutating thioredoxin's CXXC active site motif to those of more oxidising proteins, resulted in a more oxidising redox potential for thioredoxin. Moreover, this impacted thioredoxin's ability to function as a reductase and its interaction with folding protein substrates [590].

More recent studies have investigated the role of the cis-proline loop in modulating the redox potential of thioredoxin-like proteins. When DsbA's GVP cis-proline loop is mutated to GTP, equivalent to that of DsbC and DsbG, interestingly, the redox potential of DsbA is substantially increased [492]. Thus, the presence of threonine within the cis-proline loop exerts a more oxidising influence than valine. Moreover, when thioredoxin's GIP cis-proline loop is substituted to any other residue, thioredoxin becomes more oxidising, therefore demonstrating that isoleucine has a strong reducing influence [492]. These results indicate that substituting the residue preceding the proline in the cis-proline loop of a thioredoxin-like protein to a threonine increases the oxidase activity, whereas substituting it to an isoleucine increases the reductase activity. It was also concluded in this study that the cis-proline loop has a strong influence on the redox properties of thioredoxin-like proteins, similar to the CXXC active site motif [492].

5.1.3 The generation of PDI redox mutants

Based on these previous studies defining the structural requirements that contribute to the redox potential of thioredoxin-like proteins, in this study mutations in PDI were designed to create a series of PDI redox mutants, either by altering the CGHC active site motif of PDI or its cis-proline loops.

The CXXC active site mutations were based on the oxidase, isomerase and reductase properties from the thioredoxin-like protein superfamily. Therefore, PDI's active site motif, in both it's *a* and *a'* domains, was replaced with; CPHC, the motif observed in the highly oxidising protein DsbA; CPYC, present in the isomerase DsbG; and CGPC, present in the strongly reducing protein, thioredoxin. It was predicted that upon mutation, PDI's redox activity would be modified to that of an oxidase, isomerase and reductase, respectively.

The cis-proline loop mutations were based on studies that reported that substituting the residue preceding the proline to threonine increases oxidising activity, whilst a substitution to isoleucine decreases oxidising activity. Therefore, PDI's *a* domain cis-proline loop was substituted from GYP to GTP, with the aim of making it more oxidising, or to GIP, with the aim of rendering it more reducing. Similarly, the *a'* domain cis-proline loop was exchanged from SFP to STP, which is predicted to enhance its oxidising ability, or to SIP, with the aim of enhancing its reducing activity.

 The seven proposed redox mutants are summarised in Table 5.1.

TABLE 5.1. PDI redox potential mutants

Variant name	Modification	Predicted outcome
CXXC active site mutants		
PDI CPHC	Modify both CXXC active site motifs in the *a* and *a'* domains from CGHC to CPHC	PDI becomes a stronger <u>oxidase</u> (forms disulphide bonds)
PDI CPYC	Modify both CXXC active site motifs in the *a* and *a'* domains from CGHC to CPYC	PDI acts as an <u>isomerase</u> (re-arranges disulphide bonds)
PDI CGPC	Modify both CXXC active site motifs in the *a* and *a'* domains from CGHC to CGPC	PDI becomes a stronger <u>reductase</u> (break down disulphide bonds)
Cis-proline loop mutants		
PDI GIP	Modify the *a* domain cis-proline loop from GYP to GIP	PDI becomes more <u>reducing</u>
PDI GTP	Modify the *a* domain cis-proline loop from GYP to GTP	PDI becomes more <u>oxidising</u>
PDI SIP	Modify the *a'* domain cis-proline loop from SFP to SIP	PDI becomes more <u>reducing</u>
PDI STP	Modify the *a'* domain cis-proline loop from SFP to STP	PDI becomes more <u>oxidising</u>

5.1.4 Aims of this chapter

In Chapter 4, it was demonstrated that PDI's *a* and *a'* domains were required for its protective function against cellular pathogenic mechanisms induced by mutant forms of SOD1, TDP-43 and FUS. These two domains contain PDI's active site, comprising a CGHC active motif, which is responsible for PDI's oxidoreductase function and hence, its disulphide interchange activity. As detailed above, other thioredoxin-like proteins also possess a CXXC active site motif, however they possess differing redox potentials. This was demonstrated in the studies outlined in Chapter 4 which investigated the activity of Dsb proteins, bearing differing redox potentials, on pathogenic mechanisms induced in ALS. DsbA, an oxidase with a CPHC active site motif, was consistently protective in these studies, whereas DsbC, an isomerase with a CGYC active site motif, was only protective in some instances. Hence, these findings indicate that the redox potential of PDI is important in determining its protective activity. Therefore, it was next hypothesised that alterations in PDI's active site motif would result in changes to PDI's redox potential, and thus, its protective function. Furthermore, as mutating the residue preceding the cis-proline loop of thioredoxin-like proteins also alters their redox potential and function [492], it was also hypothesised that alterations in PDI's cis-proline loop would also modify its function.

Therefore, the aim of the studies described in this chapter was to investigate the effect of mutating either the active site motifs or cis-proline loops of PDI, on its protective activity. To perform these studies, the CGHC active sites were modified in both the *a* and *a'* domains, the GYP cis-proline loop was modified in the *a* domain, and the SFP cis-proline loop mutant was modified in the *a'* domain, to create seven mutants of PDI. These studies aimed to investigate which of PDI's oxidoreductase properties (oxidase, isomerase or reductase activity) were essential for protective activity. Thus, it was predicted that these studies would highlight the importance of redox potential on modulating PDI's protective function.

5.2 Materials/Methods

5.2.1 Constructs used in this chapter

A pcDNA3.1 vector containing full-length PDI and a V5 tag was provided by Dr. Neil Bulleid, University of Glasgow, UK. This construct was used as the template for site-directed mutagenesis. Wildtype SOD1 and mutant SOD1 A4V constructs encoding EGFP-tagged human SOD1 at the C-terminus were previously described [265]. Wildtype TDP-43 and mutant TDP-43 Q331K constructs encoding EGFP-tagged human TDP-43 at the N-terminus was a gift from Professor Benjamin Wolozin, Boston University, USA, and GFP-tagged FUS (wildtype and mutant R521G) vectors were provided by Dr. Justin Yerbury, University of Wollongong, Australia. All DNA plasmids used in this chapter were verified by DNA sequencing before use.

5.2.2 Site-directed mutagenesis to generate redox mutants of PDI

Site-directed mutagenesis was performed to generate PDI redox mutants using the Q5 Site-Directed Mutagenesis Kit (New England Biolabs), according to the manufacturer's protocol. Primers for mutagenesis were designed using New England Biolabs' NEBaseChanger (available at http://www.nebasechanger.neb.com) and are shown in Table 5.2. Primers were dissolved at a stock concentration of 10 µM.

TABLE 5.2: Mutagenesis primers.

Primer name	Primer sequence
Redox active site mutants	
PDIa CPHC Forward	5'-CCCTTGGTGTCCCCACTGCAAG
PDIa CPHC Reverse	5'-GCATAGAACTCCACCAGC
PDIa' CPHC Forward	5'-CCCATGGTGTCCTCACTGCAAACAG
PDIa' CPHC Reverse	5'- GCATAGAACTCCACAAAG
PDIa CPYC Forward	5'- CCCTTGGTGTCCCTACTGCAAGGC
PDIa CPYC Reverse	5'- GCATAGAACTCCACCAGC
PDIa' CPYC Forward	5'-CCCATGGTGTCCTTACTGCAAACAGTTG
PDIa' CPYC Reverse	5'- GCATAGAACTCCACAAAG
PDIa CGPC Forward	5'-TGGTGTGGCCCCTGCAAGGCT
PDIa CGPC Reverse	5'-AGGGGCATAGAACTCCACC
PDIa' CGPC Forward	5'-TGGTGTGGTCcCTGCAAACAG
PDIa' CGPC Reverse	5'- TGGGGCATAGAACTCCAC
Cis-proline loop mutants	
PDI GIP Forward	5'- CGTGCGCGGCATTCCCACCATC
PDI GIP Reverse	5'- CCGTACTGCTGGGCCAGG
PDI GTP Forward	5'- CGTGCGCGGCACTCCCACCATCAAG
PDI GTP Reverse	5'- CCGTACTGCTGGGCCAGG
PDI SIP Forward	5'- AGTGCACAGCATCCCCACACTC
PDI SIP Reverse	5'- TTGACGGCCTCCACCTCG
PDI STP Forward	5'- AGTGCACAGCACCCCCACACTCAAG
PDI STP Reverse	5'- TTGACGGCCTCCACCTCG

Reactions were made up to a volume of 25 µL, containing 12.5 µL Q5 Hot Start High-Fidelity 2X Master Mix (1 X), 1.25 µL forward primer (0.5 µM), 1.25 µL reverse primer (0.5 µM), 1 µL template DNA (1-25 ng/µL), and 9.0 µL nuclease free H_2O. Reactions were cycled on a PCR thermal cycler under the following conditions (Table 5.3):

TABLE 5.3. Thermocycling conditions

	98°C	30 seconds
	98°C	10 seconds
25 cycles	50-72°C*	30 seconds
	72°C	30 seconds/kb plasmid length
	72°C	2 minutes

* The annealing temperature of the primers was determined using NEBaseChanger.

The PCR product was digested with the addition of 2 µL DpnI (New England Biolabs) and 3 µl CutSmart Buffer (New England Biolabs) with incubation at 37°C for 1 h. Reactions were transformed into NEB 5-alpha Competent E. coli cells, according to the manufacturer's protocol. Transformed cells were spread onto LB agar plates which were incubated overnight at 37°C. Single colonies were selected and inoculated into LB Broth containing the appropriate antibiotic the following day. Inoculations were incubated overnight in a shaking incubator at 37°C and 200 rpm, followed by small scale DNA plasmid production (section 2.2.5) the next day. DNA plasmid samples were quantified using a Nanodrop ND-1000 spectrophotometer. The presence of the desired mutation was confirmed by DNA sequencing.

5.3 Results

5.3.1 Sequences and sequencing results for point mutations

Once site-directed mutagenesis of PDI had been performed to generate the redox active site and cis-proline loop mutants, these constructs were sequenced to confirm the presence of each point mutation. The nucleotide and amino acid sequences of wildtype PDI, and the position of each mutation, are shown in Figure 5.2. The sequencing results confirmed that each point mutations, for both the active site redox mutants (Figure 5.3) and the cis-proline loop mutants (Figure 5.4), were present.

Nucleotide sequence of human PDI (1527 nucleotides)

```
ATG CTG CGC CGC GCT CTG CTG TGC CTG GCC GTG GCC GCC CTG GTG CGC GCC GAC GCC CCC GAG GAG GAG GAC
CAC GTC CTG GTG CTG CGG AAA AGC AAC TTC GCG GAG GCG CTG GCG GCC CAC AAG TAC CTG CTG GTG GAG TTC
TAT GCC CCT TGG TGT GGC CAC TGC AAG GCT CTG GCC CCT GAG TAT GCC AAA GCC GCT GGG AAG CTG AAG GCA
GAA GGT TCC GAG ATC AGG TTG GCC AAG GTG GAC GCC ACG GAG GAG TCT GAC CTG GCC CAG CAG TAC GGC GTG
CGC GGC TAT CCC ACC ATC AAG TTC TTC AGG AAT GGA GAC ACG GCT TCC CCC AAG GAA TAT ACA GCT GGC AGA
GAG GCT GAT GAC ATC GTG AAC TGG CTG AAG AAG CGC ACG GGC CCG GCT GCC ACC ACC CTG CCT GAC GGC GCA
GCT GCA GAG TCC TTG GTG GAG TCC AGC GAG GTG GGT GTC ATC TTC TTC AAG GAC GTG GAG TCG GAC TCT
GCC AAG CAG TTT TTG CAG GCA GCA GAG GCC ATC GAT GAC ATA CCA TTT GGG ATC ACT TCC AAC AGT GAC GTG
TTC TCC AAA TAC CAG CTC GAC AAA GAT GGG GTT GTC CTC TTT AAG AAG TTT GAT GAA GGC CGG AAC AAC TTT
GAA GGG GAG GTC ACC AAG GAG AAC CTG CTG GAC TTT ATC AAA CAC AAC CAG CTG CCC CTT GTC ATC GAG TTC
ACC GAG CAG ACA GCC CCG AAG ATT TTT GGA GGT GAA ATC AAG ACT CAC ATC CTG CTG TTC TTG CCC AAG AGT
GTG TCT GAC TAT GAC GGC AAA CTG AGC AAC TTC AAA ACA GCA GCC GAG AGC TTC AAG GGC AAG ATC CTG TTC
ATC TTC ATC GAC AGC GAC CAC ACC GAC AAC CAG CGC ATC CTC GAG TTC TTT GGC CTG AAG AAG GAA GAG TGC
CCG GCC GTG CGC CTC ATC ACC CTG GAG GAG GAG ATG ACC AAG TAC AAG CCC GAA TCG GAG GAG CTG ACG GCA
GAG AGG ATC ACA GAG TTC TGC CAC CGC TTC CTG GAG GGC AAA ATC AAG CCC CAC CTG ATG AGC CAG GAG CTG
CCG GAG GAC TGG GAC AAG CAG CCT GTC AAG GTG CTT GTT GGG AAG AAC TTT GAA GAC GTG GCT TTT GAT GAG
AAA AAA AAC GTC TTT GTG GAG TTC TAT GCC CCA TGG TGT GGT CAC TGC AAA CAG TTG GCT CCC ATT TGG GAT
AAA CTG GGA GAG ACG TAC AAG GAC CAT GAG AAC ATC GTC ATC GCC AAG ATG GAC TCG ACT GCC AAC GAG GTG
GAG GCC GTC AAA GTG CAC AGC TTC CCC ACA CTC AAG TTC TTT CCT GCC AGT GCC GAC AGG ACG GTC ATT GAT
TAC AAC GGG GAA CGC ACG CTG GAT GGT TTT AAG AAA TTC CTG GAG AGC GGT GGC CAG GAT GGG GCA GGG GAT
GAT GAC GAT CTC GAG GAG GCA GAG GAG CCA GAC ATG GAG GAA GAC GAT GAT CAG AAA GCT GTG
AAA GAT GAA CTG TAA
```

Translation of human PDI (508 amino acids)

```
MLRRALLCLAVAALVRADAPEEEDHVLVLRKSNFAEALAAHKYLLVEFYAPWCGHCKALAPEYAKAAGKL
KAEGSEIRLAKVDATEESDLAQQYGVRGYPTIKFFRNGDTASPKEYTAGREADDIVNWLKKRTGPAATTL
PDGAAAESLVESSEVAVIGFFKDVESDSAKQFLQAAEAIDDIPFGITSNSDVFSKYQLDKDGVVLFKKFD
EGRNNFEGEVTKENLLDFIKHNQLPLVIEFTEQTAPKIFGGEIKTHILLFLPKSVSDYDGKLSNFKTAAE
SFKGKILFIFIDSDHTDNQRILEFFGLKKEECPAVRLITLEEEMTKYKPESEELTAERITEFCHRFLEGK
IKPHLMSQELPEDWDKQPVKVLVGKNFEDVAFDEKKNVFVEFYAPWCGHCKQLAPIWDKLGETYKDHENI
VIAKMDSTANEVEAVKVHSFPTLKFFPASADRTVIDYNGERTLDGFKKFLESGGQDGAGDDDDLEDLEEA
EEPDMEEDDDQKAVKDEL
```

Figure 5.2: The nucleotide and amino acid sequences of wildtype human PDI.

The sequences highlighted in yellow represent the CGHC active sites of PDI's *a* and *a'*

domains, which are the site of the point mutations for the active site mutants. It is important

to note that both domains of the active site mutants contained the mutation. The sequences

highlighted in green demonstrate the GYP and SFP cis-proline loops of the *a* and *a'* domain,

respectively, as well as the site of the point mutations for the cis-proline loop mutants. Only

one cis-proline loop was mutated (either GYP or SFP) per mutation.
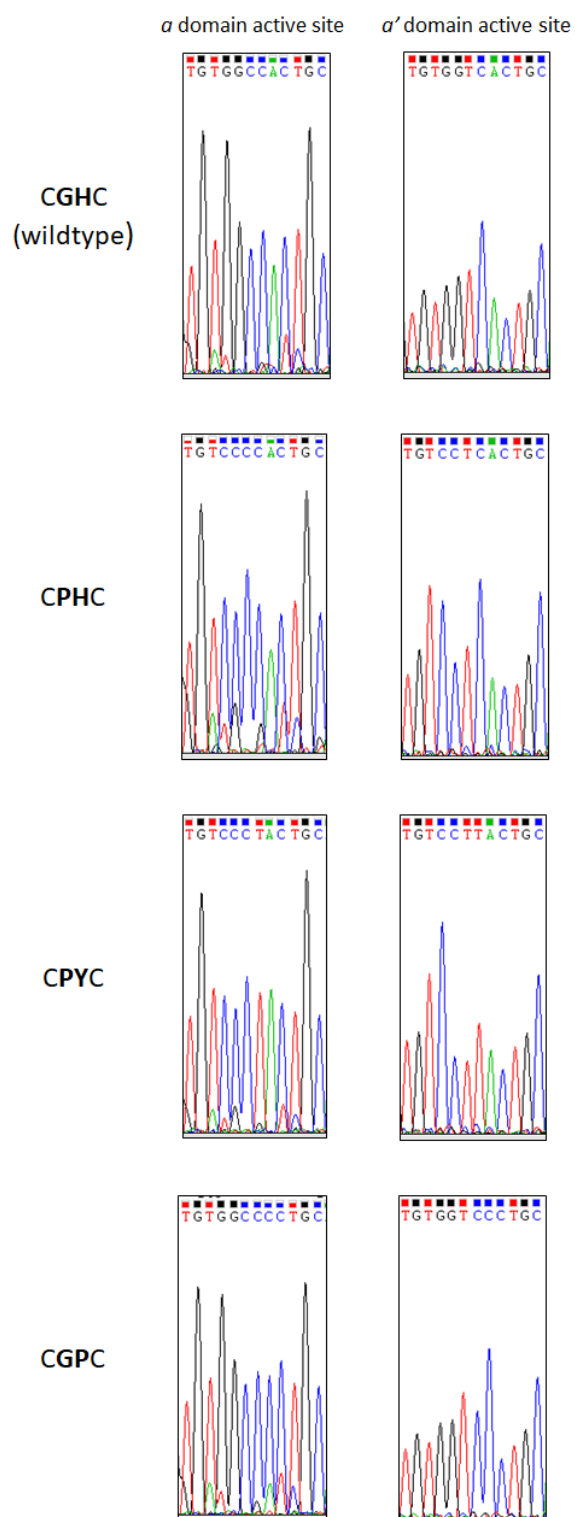
Figure 5.3: Sequencing of each active site mutant confirmed that each point mutations had been successfully incorporated into in the PDI-V5 tagged construct. The CGHC active sites in both of wildtype PDI's *a* and *a'* domains were mutated to CPHC, CPYC or CGPC, resulting in three redox active site mutants, termed 'CPHC, CPYC, and CGPC'.
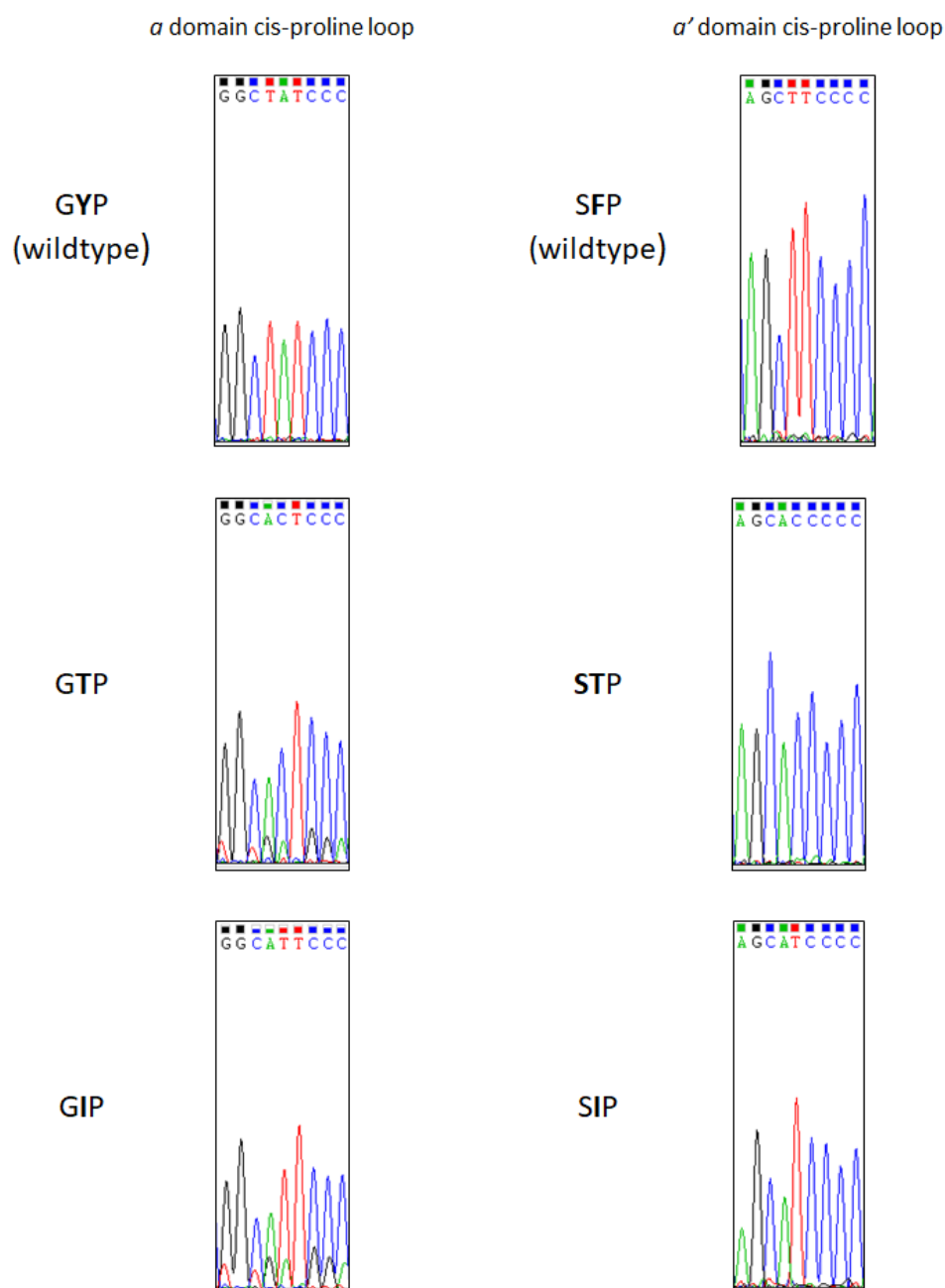
Figure 5.4: Sequencing of each cis-proline loop mutant confirmed that the appropriate point mutations had been successfully incorporated into each PDI construct. The cis-proline loops in PDI's *a* and *a'* domains were mutated separately, to create either the GTP or GIP mutant, in which the GYP cis-proline loop in wildtype PDI's *a* domain was mutated to GTP or GIP respectively, or to create either the STP or SIP mutant, in which the SFP cis-proline loop in wildtype PDI's *a'* domain was mutated to STP or SIP, respectively. Hence, in total four cis-proline loop PDI mutants were created.

5.3.2 Proof of a change in redox potential in redox mutants

The mutations were designed to modulate the redox activity of PDI and they were based on studies of thioredoxin-like proteins such as the Dsb family, which possess similar active site motifs. However, it has not been previously established that these mutations modulate the redox activity of PDI specifically. Hence, once the presence of each point mutation was confirmed for the redox mutants, it was first examined whether the redox potential of each mutant was altered by substitution of residues in either the active site or the cis-proline loops. To investigate the redox properties of the mutants, a cytoplasmic reduction-oxidation sensitive green fluorescent protein (cyto-roGFP) was utilised. Cyto-roGFP is a redox sensitive biosensor containing two cysteines in the beta barrel structure of GFP. When the two cysteine residues are oxidised and a disulphide is formed, cyto-roGFP exhibits GFP expression [591]. Hence, a cell fluoresces green when it has been oxidised. However, in a reducing environment, no GFP expression is observed. Therefore, if a redox mutant is more oxidising, more cells transfected with roGFP will exhibit GFP luminescence, compared to a reducing redox mutant, where fewer cells transfected with roGFP will produce a GFP signal.

Neuro-2A cells were transfected with either empty vector pcDNA3.1 alone (control), GFP alone (control), cyto-roGFP alone, or cyto-roGFP co-expressed with either empty vector pcDNA3.1, wildtype PDI, the active site mutants, CPHC, CPYC or CGPC, or the cis-proline loop mutants, GIP, GTP, SIP or STP for 18 h. Immunocytochemistry was performed using an anti-V5 antibody and nuclei were stained with Hoechst before examining cells using fluorescent microscopy. At least 100 cells expressing either wildtype PDI or the PDI mutants were examined and these cells were further analysed for cyto-roGFP expression (Figure 5.5 A).

Cells expressing cyto-roGFP alone or cyto-roGFP with empty vector pcDNA3.1 displayed low levels of roGFP expression (13.7% ± 4.3 and 13.3% ± 1.9, of transfected cells respectively). There was a significant increase ($p < 0.01$) in the proportion of cells with roGFP expression when wildtype PDI was co-expressed with cyto-roGFP (42.7% ± 2.3), compared to cells expressing cyto-roGFP with empty pcDNA3.1 vector, indicating that oxidation is taking place in the cell when PDI is expressed. Moreover, significantly more cells ($p < 0.01$) displayed roGFP expression when cyto-roGFP was co-expressed with the CPHC active site mutant (69.7% ± 2.3), compared to those co-expressing cyto-roGFP with wildtype PDI. This suggests that PDI is more oxidising when its active site is mutated from CGHC to CPHC active site, as hypothesised, consistent with our predictions. In contrast, there was a significant reduction ($p < 0.05$) in the proportion of cells with roGFP expression when cyto-roGFP was co-expressed with the CGPC active site mutant (18.0% ± 2.5), compared to when it was co-expressed with wildtype PDI. This result indicates that when PDI's active site is mutated to CGPC, it becomes more reducing than the native CGHC sequence, also consistent with our predictions. There was a decrease in the proportion of cells with roGFP expression when cells co-expressed cyto-roGFP and the CPYC active site mutant (26.0% ± 8.6), compared to cells co-expressing cyto-roGFP and PDI, however this reduction was not statistically significant. It was expected that wildtype PDI and CPYC would have similar levels of roGFP expression. Similarly, there was no statistical difference in the proportion of cells with roGFP expression between populations co-expressing cyto-roGFP with wildtype PDI and cells co-expressing cyto-roGFP with any of the cis-proline loop mutants; GIP (28.7% ± 3.2), GTP (54.7% ± 5.8), SIP (40.7% ± 1.8), and STP (45.3 % ± 2.6). However, there was a slight increase in the proportion of cells with roGFP expression when cyto-roGFP was co-expressed with GTP, compared to co-expression with wildtype PDI (Figure 5.5 B), as was expected, although this was not statistically significant. Whilst these

results did not display a statistical difference between the cis-proline loop mutants and wildtype PDI, this could be due to the sensitivity of the assay used.
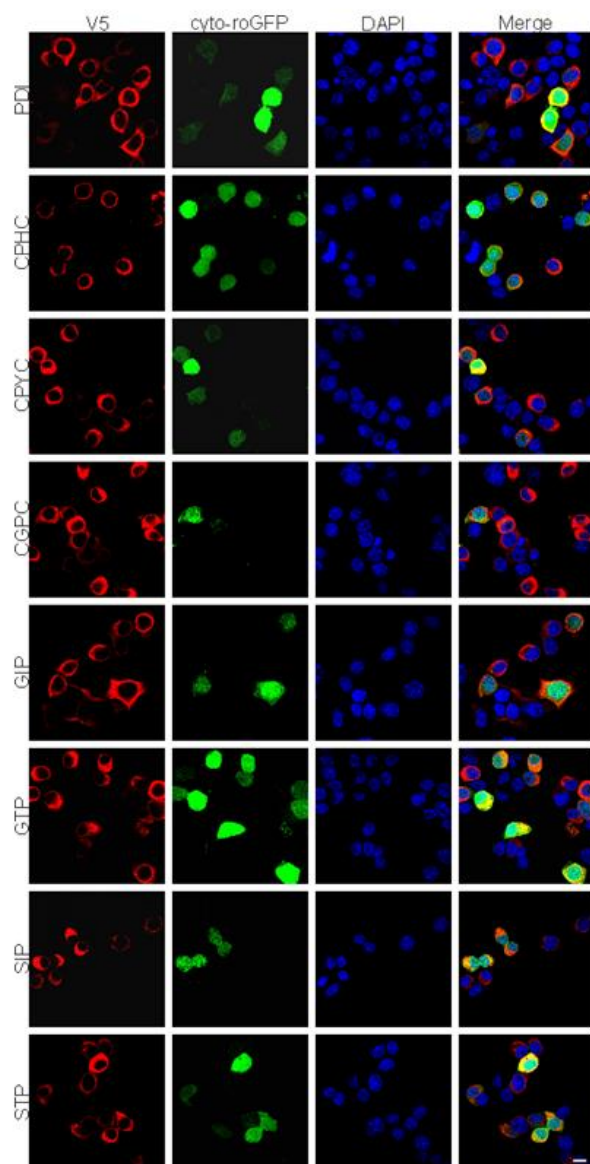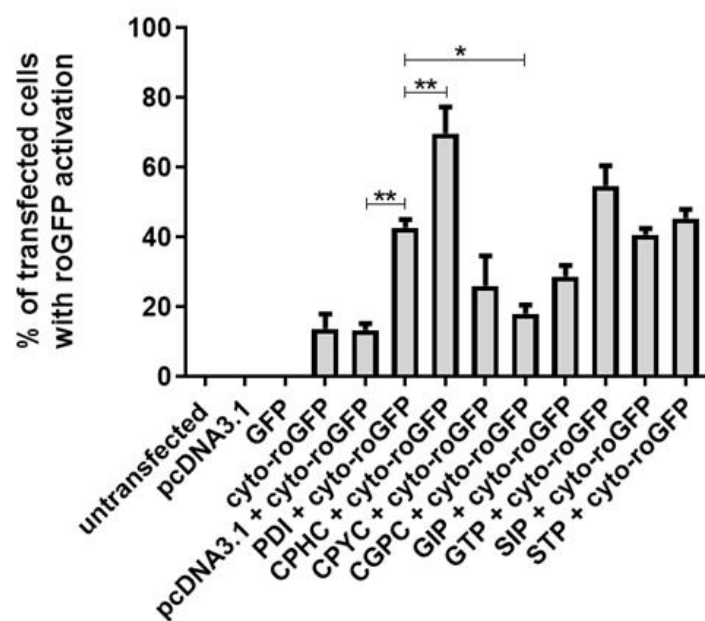
Figure 5.5: The active site mutants, but not the cis-proline loop mutants, alter the redox potential of PDI. A) Immunofluorescence images of Neuro-2A cells co-expressing either wildtype PDI, the PDI active site mutants or the PDI cis-proline loops mutants (column one), with cyto-roGFP (column two). The third column shows DAPI-stained nuclei and the fourth column depicts a merged image of the cell. A similar proportion of cells (approximately 50%) expressing either wildtype PDI (first panel; PDI), or the CPYC active site mutant (third panel; CPYC), SIP cis-proline loops mutant (seventh panel; SIP) or STP cis-proline loop mutant (eighth panel; STP) displayed roGFP expression. In contrast, more cells expressing either the CPHC active site mutant (second panel; CPHC) or the GTP cis-proline loop mutant (sixth panel; GTP) demonstrated roGFP expression. Conversely, fewer cells expressing either the CGPC active site mutant (fourth panel; CGPC) or the GIP cis-proline loop mutant (fifth panel; GIP) displayed roGFP expression. Scale bar = 30 µM. **B)** Quantification of Neuro-2A cells with roGFP expression in A). There was a significant increase ($p < 0.01$) in the proportion of cells displaying roGFP expression in cells co-expressing cyto-roGFP with wildtype PDI, compared to cells co-expressing cyto-roGFP with empty vector pcDNA3.1. Significantly more cells ($p < 0.01$) with roGFP expression were observed in populations co-expressing cyto-roGFP with the CPHC active site mutant, compared to those expressing wildtype PDI. In contrast, compared to cells expressing PDI, significantly fewer cells ($p < 0.05$) co-expressing cyto-roGFP with the CGPC active site mutant demonstrated roGFP expression. There were no significant differences observed between cells expressing wildtype PDI and those expressing either the CPYC active site mutant or any of the cis-proline loop mutants. N=3, Mean ± SEM, * $p < 0.05$, ** $p < 0.01$.

The redox active site mutants of PDI

The following section of this chapter focuses on the redox active site mutants which modify PDI's native CGHC active site to either CPHC, CPYC or CGPC. Based on previous studies [589, 592], it was postulated that through point mutations in the two amino acid residues between the cysteines of the active site, the redox potential of PDI would be shifted to be either more oxidising (demonstrated with the CPHC active site), isomerising (as in the CPYC active site) or reducing (observed in the CGPC active site). The activity of the redox active site mutants was analysed in cells expressing mutant ALS proteins; SOD1, TDP-43 and FUS.

5.3.3 Cellular localisation of the PDI redox active site mutants in Neuro-2A cells

Firstly, to ensure that the PDI redox active site mutants were still expressed within the ER, implying that they retained their native properties (except redox activity), the localisation of the V5-tagged PDI proteins was analysed in Neuro-2A cells using confocal microscopy. Cells were transfected with either the CPHC, CPYC or CGPC active site mutants for 24 h before immunocytochemistry using an anti-V5 tag antibody to visualise the mutants, and an anti-calreticulin antibody to probe for the ER-resident protein, calreticulin. It was hypothesised that all three active site mutants would still be retained in the ER due to the presence of PDI's signal sequence and KDEL sequence. Results demonstrated that all three active site mutants co-localised with calreticulin all transfected cells, indicating their localisation in the ER, as expected (Figure 5.6).
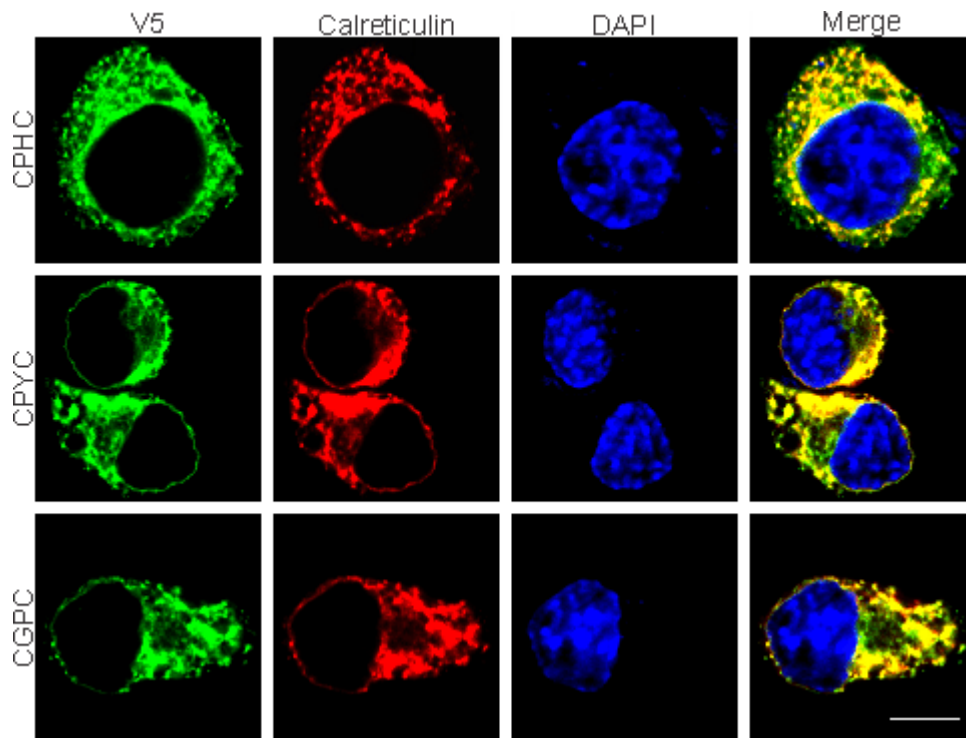
Figure 5.6: The CPHC, CPYC and CGPC active site mutants are localised within the ER of Neuro-2A cells. Neuro-2A cells were transfected with either the CPHC, CPYC or CGPC PDI active site mutants (first column; V5) for 24 h. Cells were fixed and immunocytochemistry performed using antibodies for V5 tag and calreticulin (second column; Calreticulin), and nuclei were stained using Hoechst (third column; DAPI). The yellow in the merge column (fourth column; Merge) illustrates co-localisation of each of the active site mutants with calreticulin, demonstrating that the active site mutants are localised within the ER. Scale bar = 30 µM.

Examining the protective effect of the PDI redox active site mutants in cells expressing mutant SOD1.

The protective effects of the PDI redox active site mutants was first analysed in Neuro-2A cells expressing mutant SOD1 A4V. Their activity against SOD1 inclusion formation, mutant SOD1-induced ER stress and apoptosis was investigated in the following experiments.

5.3.4 PDI redox active site mutants are co-expressed in almost all cells transfected with SOD1

Firstly, the co-transfection efficiency of the PDI active site mutants and SOD1 was examined in Neuro-2A cells. Cells were transfected with mutant EGFP-SOD1 and either the CPHC, CPYC, or CGPC active site mutant, for 72 h, before fixing and performing immunocytochemistry using an anti-V5 antibody. DAPI-staining was performed using Hoechst to visualise the nuclei. Co-transfection was verified by EGFP expression (green) from SOD1 and performing immunocytochemistry with an Alexa Fluor 568-tagged secondary antibody to detect the V5 tag of the PDI mutants (Figure 5.7). At 72 h post-transfection, the overall transfection efficiency of mutant SOD1 was found to be approximately 75-80% in Neuro-2A cells. For each of the three replicate experiments, fluorescent microscopy was used to examine at least 100 SOD1-expressing cells and these cells were further analysed for co-expression with the active site mutant proteins. Quantification revealed that approximately 96% of SOD1-expressing cells also co-expressed the CPHC active site mutant, 96% co-expressed the CPYC active site mutant, and 97% co-expressed the CGPC active site mutant. Therefore, in all further experiments, it was assumed that detection of SOD1 expression reflected co-expression of both SOD1 and the PDI active

site mutants when they were co-transfected and immunocytochemistry using a V5 antibody was not performed.
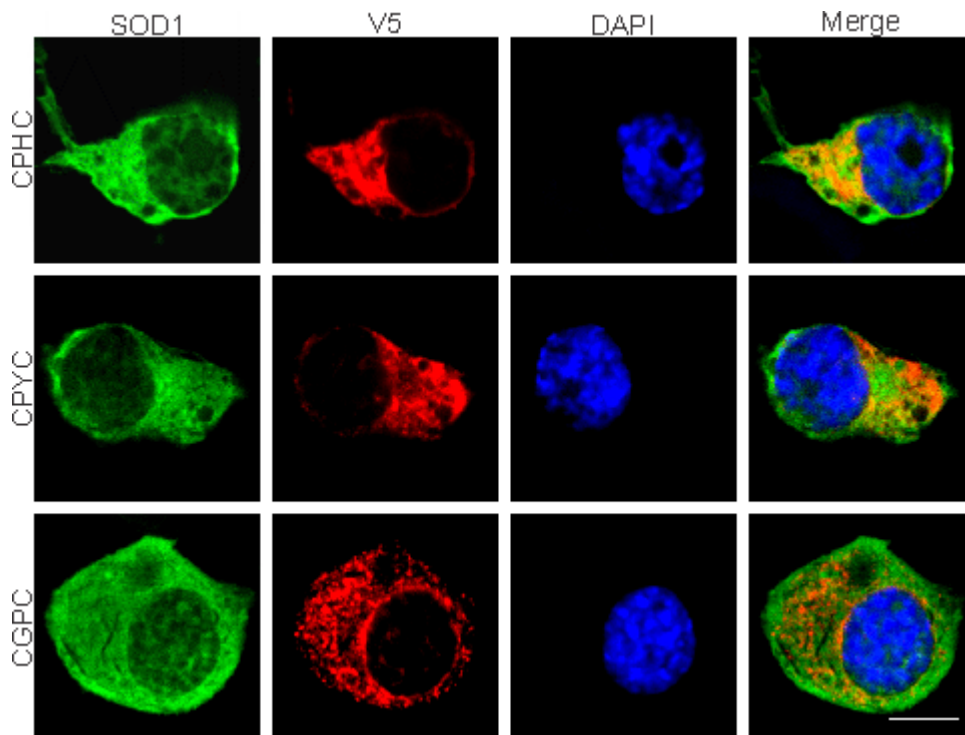
Figure 5.7: The CPHC, CPYC and CGPC active site mutants are co-expressed in almost all Neuro-2A cells co-transfected with EGFP-SOD1. Neuro-2A cells were transfected with SOD1 (first column; SOD1), and either the CPHC, CPYC, or CGPC active site mutants (second column; V5) for 72 h. Cells were fixed and immunocytochemistry was performed using an anti-V5 antibody and nuclei were stained with Hoechst (third column; DAPI). The merge column demonstrates co-expression of the three PDI active site mutants with SOD1. Scale bar = 30 μM.

5.3.5 Protein expression of SOD1 and the PDI active site mutants in Neuro-2A cells

Once localisation and expression of the redox active site mutants was established in Neuro-2A cells, Western blotting analysis was performed to ensure that the transfection of each protein resulted in similar expression levels and to confirm that the expressed proteins were of the expected MW (Figure 5.8). Cell lysates were prepared from the following cell populations; GFP alone, wildtype SOD1 co-expressed with empty vector pcDNA3.1, and mutant SOD1 A4V co-expressed with either empty vector pcDNA3.1, wildtype PDI, CPHC, CPYC, or CGPC active site mutants. Immunoblotting using an anti-GFP antibody revealed that wildtype and mutant EGFP-SOD1 proteins were expressed at the expected size of 50 kDa, and GFP alone was expressed at 26 kDa. Wildtype SOD1 was expressed at higher levels compared to mutant SOD1 A4V, as expected. Wildtype PDI and the PDI active site mutants were detected at 62 kDa using an anti-V5 antibody, and shared similar expression levels. β-actin was used as a loading control and was detected using an anti-β-actin antibody (40 kDa).
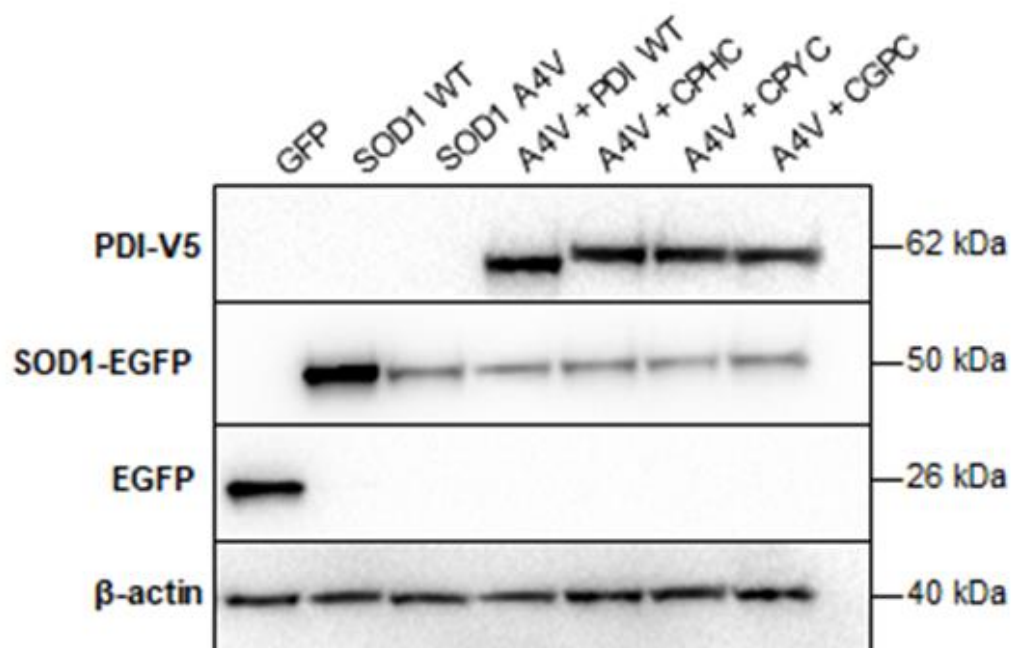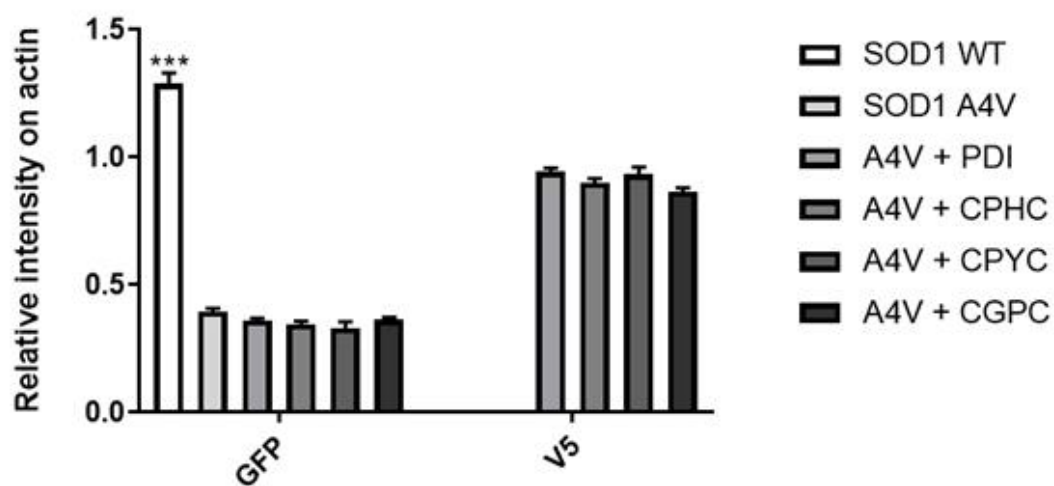
Figure 5.8: Protein expression of wildtype PDI, PDI active site mutants and EGFP-SOD1 proteins in Neuro-2A cells. A) Western blotting analysis of cell lysates was performed and quantified to ensure that PDI redox active site mutants were expressed at similar levels and were of the expected MW. Lysates examined were from cells expressing either GFP alone, wildtype SOD1 co-expressed with empty pcDNA3.1 vector, and mutant SOD1 A4V co-expressed with either empty pcDNA3.1 vector, wildtype PDI, or the CPHC, CPYC or CGPC active site mutants. PDI and the active site mutants were detected at 62 kDa, as expected (PDI = 60 kDa, V5 tag = 2 kDa). Wildtype and mutant SOD1 were detected at approximately 50 kDa, and GFP alone was detected at 26 kDa. β-actin was detected at 40 kDa. **B)** Quantification revealed that wildtype SOD1 was expressed at significantly higher levels ($p < 0.001$) compared to mutant SOD1 A4V, as expected. Mutant SOD1 A4V was expressed at similar levels across all cell lysate populations. PDI and the active site mutants were expressed at similar levels also. Lysates expressing GFP only were not included in quantification. N=3, Mean ± SEM, *** $p < 0.001$.

5.3.6 The oxidase and reductase activity of PDI is necessary to inhibit mutant SOD1 inclusion formation

Chapter 4 of this thesis previously demonstrated that PDI's disulphide interchange activity, mediated by it's *a* domains, was fundamental for PDI's protective function in preventing mutant SOD1 inclusion formation. The effect of the redox potential was also explored through experiments involving the Dsb proteins, where the oxidase, DsbA, was able to inhibit the formation of SOD1 inclusions in Neuro-2A cells. Hence, it was next investigated if modifying the redox potential of the CGHC active site in the *a* domain would alter PDI's capability to prevent SOD1 aggregation.

Neuro-2A cells were transfected with empty pcDNA3.1 vector, GFP alone, wildtype SOD1 co-expressed with empty pcDNA3.1 vector, and mutant SOD1 A4V co-expressed with either pcDNA3.1, wildtype PDI, or the CPHC, CPYC or CGPC active site mutants. Mutant SOD1 inclusion formation was analysed 72 h post-transfection to ensure maximal levels of protein aggregation and expression. After fixing, immunocytochemistry was performed using an anti-V5 antibody to detect expression of PDI and the active site mutants, and cells were stained with Hoechst to visualise the nuclei. For each of three replicate experiments, at least 100 cells co-expressing mutant SOD1 A4V and the V5-tagged proteins were examined and quantified for the presence of SOD1 inclusions (EGFP fluorescence) using fluorescence microscopy (Figure 5.9 A).

As expected, untransfected cells and cells expressing pcDNA3.1 or GFP did not bear any inclusions, and similarly, wildtype SOD1 expressing cells formed very few inclusions (1.0% $\pm$ 0.6). In contrast, significantly more cells (p < 0.001) expressing mutant SOD1 A4V with empty pcDNA3.1 vector displayed inclusions (32.7% $\pm$ 4.3), as expected. Consistent with previous results, co-expression of mutant SOD1 A4V with wildtype PDI significantly

reduced ($p < 0.01$) the proportion of cells bearing mutant SOD1 inclusions to 16.3% ± 0.9.

Moreover, overexpression of the CPHC active site mutant, which is predicted to possess oxidase activity, in cells expressing mutant SOD1 A4V resulted in significantly fewer ($p < 0.05$) cells with SOD1 inclusion formation (18.7% ± 1.9), compared to cells expressing mutant SOD1 A4V alone. Similarly, expression of the CGPC active site mutant, predicted to possess reductase activity, also significantly decreased ($p < 0.05$) the proportion of cells bearing SOD1 inclusions (19.7% ± 3.2). In contrast, in cells co-expressing the CPYC active site mutant, bearing predicted isomerase activity, and SOD1 A4V, there was no change in the proportion of cells with SOD1 inclusions (30.7% ± 5.2) compared to cells expressing mutant SOD1 A4V with empty pcDNA3.1 vector. Significantly more ($p < 0.05$) cells expressing the CPYC mutant displayed SOD1 inclusions compared to cells co-expressing wildtype PDI with mutant SOD1 A4V (Figure 5.9 B). These results suggest that the oxidase (formation of disulphide bonds) and reductase (break down of disulphide bonds) activities of PDI are required to prevent mutant SOD1 inclusion formation.

A

	SOD1	V5	DAPI	Merge
GFP				
SOD1 WT				
SOD1 A4V				
A4V + PDI				
A4V + CPHC				
A4V + CPYC				
A4V + CGPC				
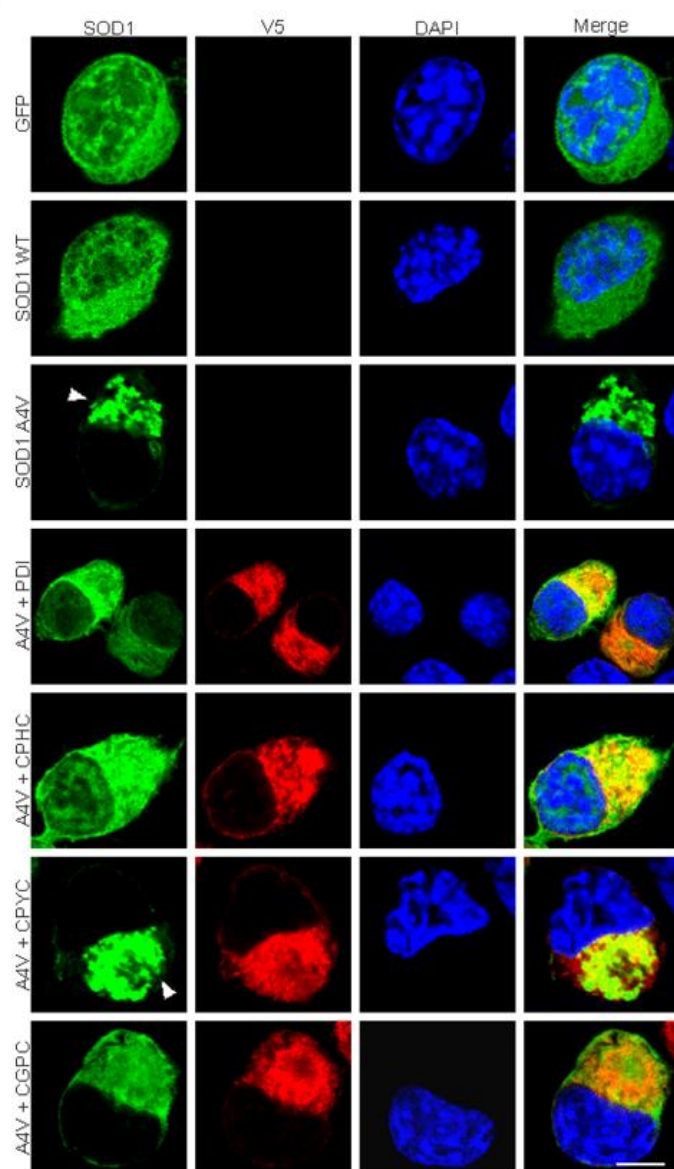
B
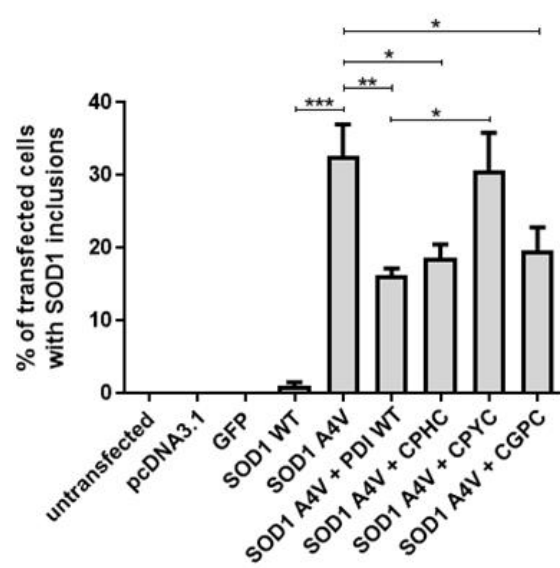
Figure 5.9: The oxidase and reductase activities of PDI prevent mutant SOD1 inclusion formation. A) Immunofluorescence images of Neuro-2A cells expressing GFP, wildtype SOD1 and mutant SOD1 A4V co-expressed with either empty pcDNA3.1 vector, wildtype PDI, or the CPHC, CPYC or CGPC active site mutants. Cells expressing GFP and wildtype SOD1 did not present with inclusions (first and second panels; GFP, SOD1 WT). In contrast, more cells expressing mutant SOD1 A4V (third panel; SOD1 A4V) displayed SOD1 inclusions, as indicated by the white arrowhead (third panel, column one). However, when PDI (fourth panel; A4V + PDI), the CPHC active site mutant (fifth panel; A4V + CPHC), or the CGPC active site mutant (seventh panel; A4V + CGPC) were co-expressed with mutant SOD1 A4V, significantly fewer cells displayed SOD1 inclusions. Conversely, when the CPYC active site mutant (sixth panel; A4V + CPYC) was co-expressed with mutant SOD1 A4V, there was no change in the proportion of cells bearing inclusions. Scale bar = 20 µM. **B)** Quantification of Neuro-2A cells bearing SOD1 inclusions in A). There was a significant increase ($p < 0.001$) in the proportion of cells with SOD1 inclusions in cells expressing mutant SOD1 A4V, compared to cells expressing wildtype SOD1. However, significantly fewer ($p < 0.01$) cells bore SOD1 inclusions in populations expressing SOD1 A4V with PDI. Similarly, a significant decrease ($p < 0.05$) in the proportion of cells bearing SOD1 inclusions was observed when either the CPHC or the CGPC active site mutants were co-expressed with mutant SOD1 A4V. Conversely, co-expression of the CPYC active site mutant did not prevent SOD1 inclusion formation, compared to cells expressing SOD1 A4V alone. Furthermore, significantly more cells ($p < 0.05$) bore SOD1 inclusions in populations co-expressing the CPYC active site mutant with mutant SOD1 A4V, compared to those co-expressing wildtype PDI and SOD1 A4V. N=3, Mean ± SEM, * $p < 0.05$, ** $p < 0.01$, *** $p < 0.001$.

5.3.7 The oxidase, reductase and isomerase activities of PDI are protective against ER stress induced by mutant SOD1

5.3.7.1 XBP-1 as a marker of early UPR induction

In Chapter 4, it was demonstrated that PDI's *a* and *b* domains alone were protective against induction of ER stress in Neuro-2A cells, implying that both the disulphide interchange and chaperone functions of PDI are protective in ALS. It was also shown that both DsbA and DsbC, an oxidase and isomerase respectively, were protective against ER stress induced by mutant SOD1. Thus, it was next investigated whether the active site mutants of PDI were also protective. The activation of XBP-1 was used as a marker for ER stress as previous, to examine the effect of the redox active site mutants on early UPR induction induced by mutant SOD1.

Neuro-2A cells were transfected for 72 h with empty pcDNA3.1 vector, GFP, wildtype SOD1 with empty pcDNA3.1 vector, and mutant SOD1 A4V co-expressed with either pcDNA3.1, wildtype PDI, or the CPHC, CPYC or CGPC active site mutants. After fixing the cells, immunocytochemistry was performed using an anti-XBP-1 antibody, where nuclear immunoreactivity to XBP-1 signified its activation, indicative of UPR induction (Figure 5.10 A). To clearly visualise the nucleus of each cell, DAPI-staining with Hoechst was also performed.

Quantification revealed that only approximately 10% of untransfected cells or cells expressing either empty pcDNA3.1 vector or GFP, exhibited nuclear immunoreactivity to XBP-1, indicating low levels of activation of ER stress in these cells. There was a slight, but insignificant increase in the proportion of cells with XBP-1 activation in populations expressing wildtype SOD1 with empty pcDNA3.1 vector (17.0% ± 2.6), consistent with

previous studies [119]. As expected, there was a significant increase ($p < 0.01$) in the proportion of cells with XBP-1 activation in populations expressing mutant SOD1 A4V with empty pcDNA3.1 vector (35.3% ± 3.5), compared to those expressing wildtype SOD1. However, when PDI was co-expressed with mutant SOD1 A4V, there was a significant reduction ($p < 0.01$) in the percentage of cells with activated XBP-1 (16.3% ± 2.0), consistent with previous studies [448]. Significantly fewer cells with XBP-1 activation were also observed when mutant SOD1 A4V was co-expressed with either the CPHC ($p < 0.01$, 19.0% ± 2.6), CPYC ($p < 0.05$, 19.7% ± 3.9) or CGPC ($p < 0.01$, 18.7% ± 3.2) active site mutants (Figure 5.10 B), but in each case, there was no significant difference to cells expressing wildtype PDI. These results suggest that wildtype PDI and the redox mutants were equally protective against induction of ER stress induced by mutant SOD1. Hence modifying PDI's active site redox potential does not further improve PDI's capability to inhibit early UPR induction.

A

	SOD1	XBP-1	DAPI	Merge
GFP				
SOD1 WT				
SOD1 A4V				
A4V + PDI				
A4V + CPHC				
A4V + CPYC				
A4V + CGPC				

B

333
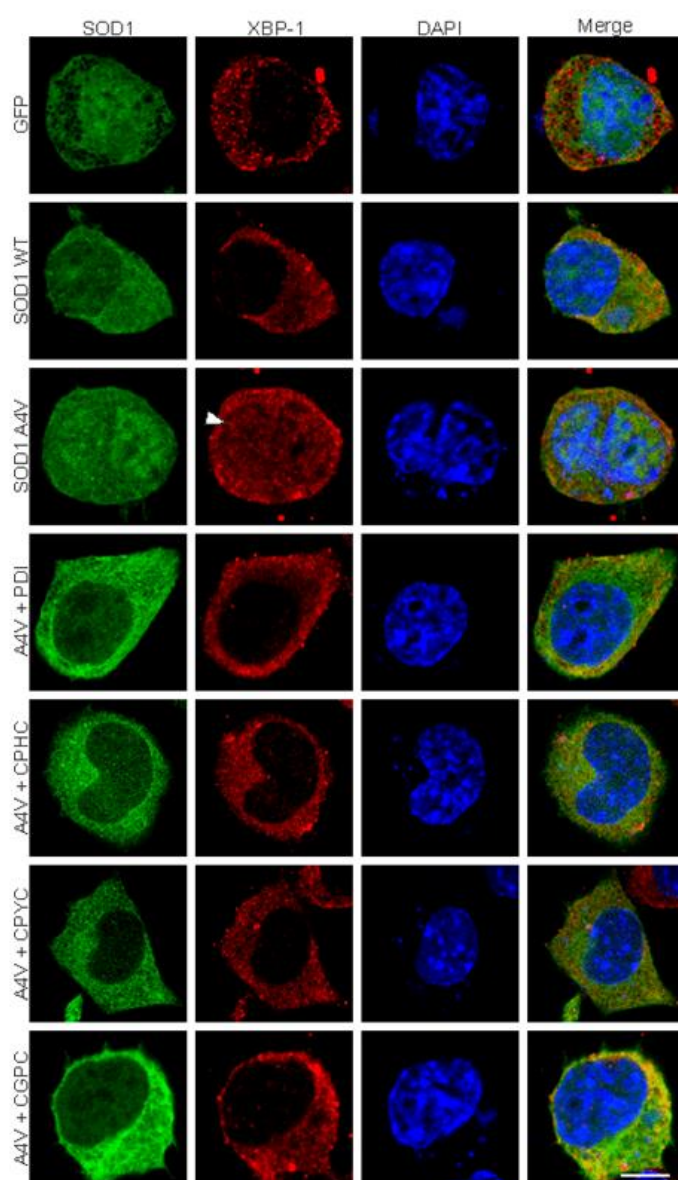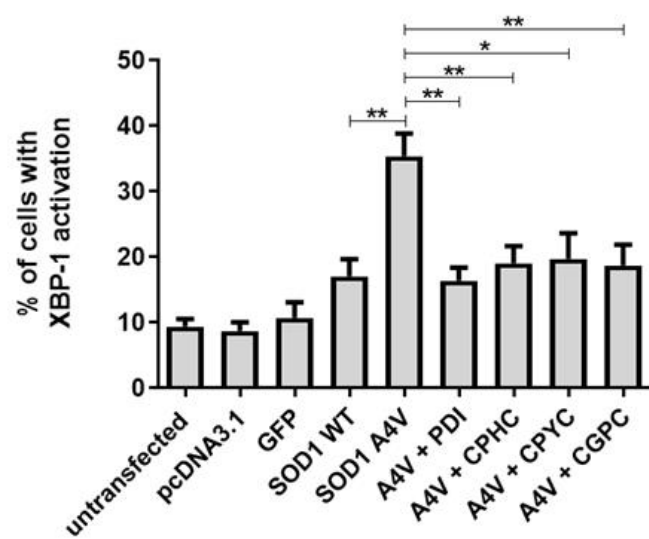
Figure 5.10: The oxidase, reductase and isomerase activities of PDI are protective against XBP-1 activation induced by mutant SOD1. A) Neuro-2A cells were transfected with GFP alone, wildtype SOD1 with empty pcDNA3.1 vector, and mutant SOD1 A4V with either pcDNA3.1, wildtype PDI, or the CPHC, CPYC or CGPC active site mutants. Cells expressing GFP or wildtype SOD1 displayed little XBP-1 activation (first and second panel; GFP, SOD1 WT). However, in cells expressing mutant SOD1 A4V (third panel; SOD1 A4V), nuclear immunoreactivity to XBP-1 was more commonly visualised, as indicated by the white arrowhead (third panel, second column). Co-expression of mutant SOD1 A4V with either wildtype PDI (fourth panel; A4V + PDI) or the active site mutants (panels five to seven; A4V + CPHC, A4V + CPYC, A4V + CGPC), resulted in a reduction in the proportion of cells displaying XBP-1 activation. Scale bar = 20 µM. **B)** Quantification of cells in A) displaying XBP-1 activation. Few untransfected cells or cells expressing pcDNA3.1, GFP or wildtype SOD1, displayed XBP-1 activation. There was a significant increase ($p < 0.01$) in the proportion of cells with XBP-1 activation in populations expressing mutant SOD1 A4V, compared to those expressing wildtype SOD1. Significantly fewer cells displayed XBP-1 activation, when either wildtype PDI ($p < 0.01$), or the CPHC ($p < 0.01$), CPYC ($p < 0.05$) or CGPC ($p < 0.01$) active site mutants, were co-expressed with mutant SOD1 A4V. N=3, Mean ± SEM, * $p < 0.05$, ** $p < 0.01$.

5.3.7.2 CHOP as a marker of the apoptotic phases of UPR

Next, to confirm the results obtained using XBP-1 nuclear immunoreactivity, that all three PDI redox active site mutants are protective against mutant SOD1-induced ER stress in Neuro-2A cells, another marker of ER stress was examined; CHOP. The activation of CHOP is also indicative of ER stress-induced apoptotic signalling; hence it was investigated whether the PDI active site mutants were able to inhibit the UPR's shift from pro-survival to pro-apoptosis within these cells. Neuro-2A cells were transfected with empty pcDNA3.1 vector, GFP alone, wildtype SOD1 with pcDNA3.1, and mutant SOD1 A4V with either pcDNA3.1, wildtype PDI, or the CPHC, CPYC, or CGPC active site mutants. Cells were fixed 72 h after transfection where immunocytochemistry was performed using an anti-CHOP antibody and nuclei were stained with Hoechst. Cells were analysed using fluorescent microscopy, whereby nuclear immunoreactivity to CHOP was indicative of its activation, as well as the induction of pro-apoptotic UPR (Figure 5.11 A), as in previous chapters.

Quantification revealed that less than 5% of untransfected cells or cells expressing empty pcDNA3.1 vector or GFP alone displayed CHOP activation, as expected. Similarly, only $5.0\% \pm 0.6$ of cells expressing wildtype SOD1 exhibited nuclear immunoreactivity to CHOP. A significant increase ($p < 0.001$) in the proportion of cells displaying CHOP activation was observed in mutant SOD1 A4V expressing cells ($19.0\% \pm 1.5$), compared to wildtype SOD1 expressing cells, consistent with previous studies. In contrast, significantly fewer ($p < 0.01$) cells displayed CHOP activation when PDI was co-expressed with mutant SOD1 A4V ($12.0\% \pm 1.2$), compared to cells expressing mutant SOD1 A4V alone. Similar to wildtype PDI, when either the CPHC, CPYC or CGPC active site mutants were co-expressed with SOD1 A4V, there was a significant reduction ($p < 0.05$) in the proportion of cells with nuclear immunoreactivity to CHOP ($12.7\% \pm 0.9$, $13.7\% \pm 1.2$ and $13.7\% \pm 1.5$, respectively), suggesting that the oxidase, reductase and isomerase activity of PDI are equally

protective against CHOP activation, and hence, ER stress-induced apoptotic signalling

(Figure 5.11 B). These results were therefore consistent with the findings obtained using

XBP-1 as a marker of ER stress.
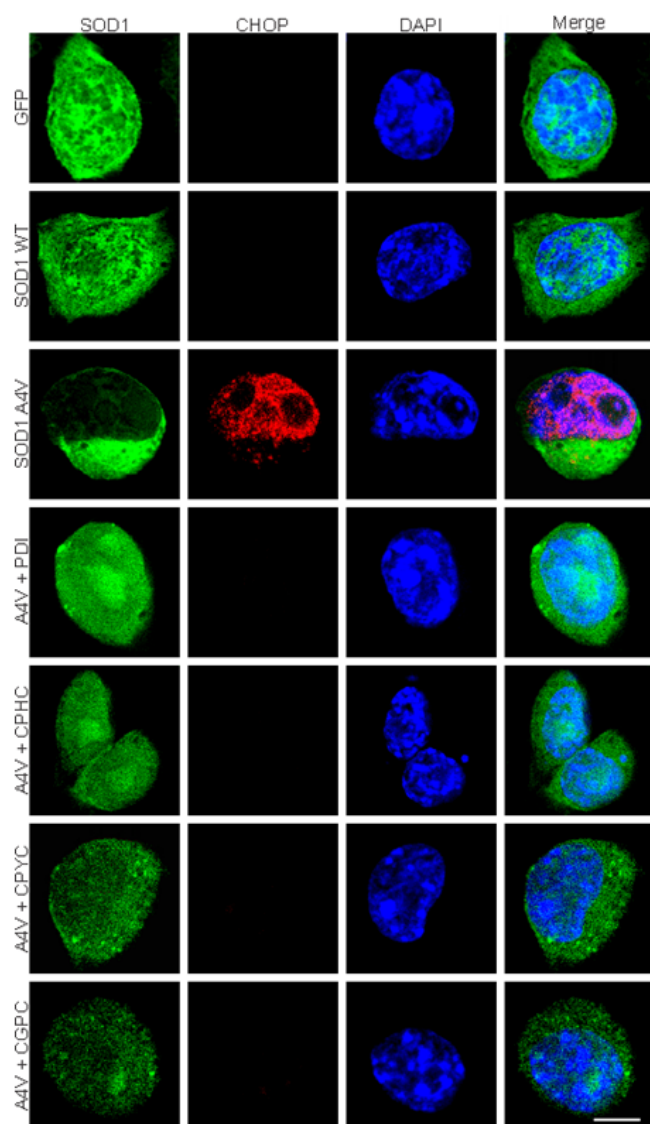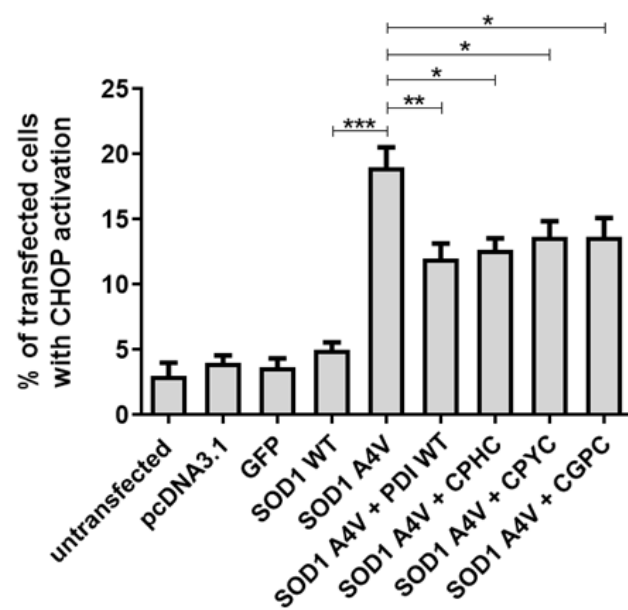
Figure 5.11: The oxidase, reductase and isomerase activities of PDI are protective against CHOP activation induced by mutant SOD1. A) Immunofluorescence images of Neuro-2A cells transfected with GFP, wildtype SOD1 with pcDNA3.1, and mutant SOD1 A4V with either pcDNA3.1, wildtype PDI, and the CPHC, CPYC and CGPC active site mutants. Cells expressing GFP alone or wildtype SOD1 (first and second panels; GFP, SOD1 WT) displayed little CHOP activation. In contrast, more mutant SOD1 A4V expressing cells (third panel; SOD1 A4V) displayed nuclear immunoreactivity to CHOP (third panel, column two). However, when PDI (fourth panel; A4V + PDI) or the PDI active site mutants (panels five to seven; A4V + CPHC, A4V + CPYC, A4V + CGPC) were co-expressed with mutant SOD1 A4V, the proportion of cells displaying CHOP activation was reduced. Scale bar = 20 µM. **B)** Quantification of the cells in A) displaying CHOP activation. Very few untransfected cells or cells expressing pcDNA3.1, GFP or wildtype SOD1 displayed nuclear immunoreactivity to CHOP, indicating activation. There was a significant increase ($p < 0.001$) in the proportion of cells with CHOP activation in mutant SOD1 A4V expressing cells, compared to wildtype SOD1 expressing cells. Significantly fewer ($p < 0.01$) cells expressing mutant SOD1 A4V exhibited CHOP activation when wildtype PDI was co-expressed. Similarly, there was a significant reduction ($p < 0.05$) in the proportion of cells displaying nuclear CHOP immunoreactivity when mutant SOD1 A4V expressing cells were co-expressed with either the CPHC, CPYC or CGPC active site mutants, and no significant differences were observed between these groups. N=3, Mean ± SEM, * $p < 0.05$, ** $p < 0.01$, *** $p < 0.001$.

5.3.8 The oxidase activity of PDI is protective against apoptosis induced by mutant SOD1

5.3.8.1 Nuclear condensation as a marker of apoptosis

Previous studies described in Chapter 4 of this thesis investigated the role of the individual domains of PDI in ALS and their subsequent protective functions. The results demonstrated that PDI's *a* domains, and therefore the disulphide interchange activity of PDI, was required to inhibit apoptosis induced by mutant SOD1. Moreover, other studies described in Chapter 4 demonstrated that the oxidase activity via DsbA was protective against apoptosis. Therefore, it was next examined whether the PDI active site mutants, and therefore modulation of the redox potential of PDI's active sites, plays a role in mediating this protective activity. To assess apoptosis, the condensation and morphology of cell nuclei were firstly analysed.

Neuro-2A cells were transfected with empty pcDNA3.1 vector, GFP alone, wildtype SOD1 with pcDNA3.1, and mutant SOD1 A4V with either pcDNA3.1, wildtype PDI, or the CPHC, CPYC, or CGPC active site mutants for 72 h. Immunocytochemistry was performed after fixing the cells using an anti-V5 antibody to visualise expression of PDI and the redox active site mutant proteins. Moreover, cells were stained with Hoechst to examine the morphology of nuclei. Nuclear morphology was analysed in at least 100 transfected cells per cell population using fluorescent microscopy and cells were considered apoptotic if the nucleus was condensed or fragmented, as in previous studies (Figure 5.12 A).

Condensed nuclei were rarely present in untransfected cells (4.0%) or in cells expressing pcDNA3.1, GFP or wildtype SOD1 (4.0%, 5.7% $\pm$ 0.7 and 6.0% $\pm$ 0.6, respectively). The proportion of cells with apoptotic nuclei was significantly higher (p < 0.001) in cells expressing mutant SOD1 A4V (16.3% $\pm$ 1.9), compared to cells expressing wildtype SOD1. However, significantly fewer apoptotic nuclei were observed when wildtype PDI was co-

expressed with mutant SOD1 A4V ($p < 0.05$, 10.0% ± 2.0) or the CPHC active site mutant ($p < 0.01$, 9.7% ± 1.2), suggesting that the oxidase activity of PDI is protective against apoptosis induced by mutant SOD1. In contrast, co-expression of the CPYC and CGPC active site mutants did not reduce the presence of apoptotic nuclei in cells expressing mutant SOD1 A4V (16.3% ± 0.3 and 17.3% ± 0.9, respectively). Moreover, the proportion of apoptotic nuclei was significantly higher in cells co-expressing SOD1 A4V with either CPYC ($p < 0.05$) or CGPC ($p < 0.01$), compared to those co-expressing PDI with mutant SOD1 A4V, implying that the isomerase and reductase activities of PDI are not protective against mutant SOD1-induced apoptosis (Figure 5.12 B).

A

	SOD1	V5	DAPI	Merge
GFP				
SOD1 WT				
SOD1 A4V				
A4V + PDI				
A4V + CPHC				
A4V + CPYC				
A4V + CGPC				
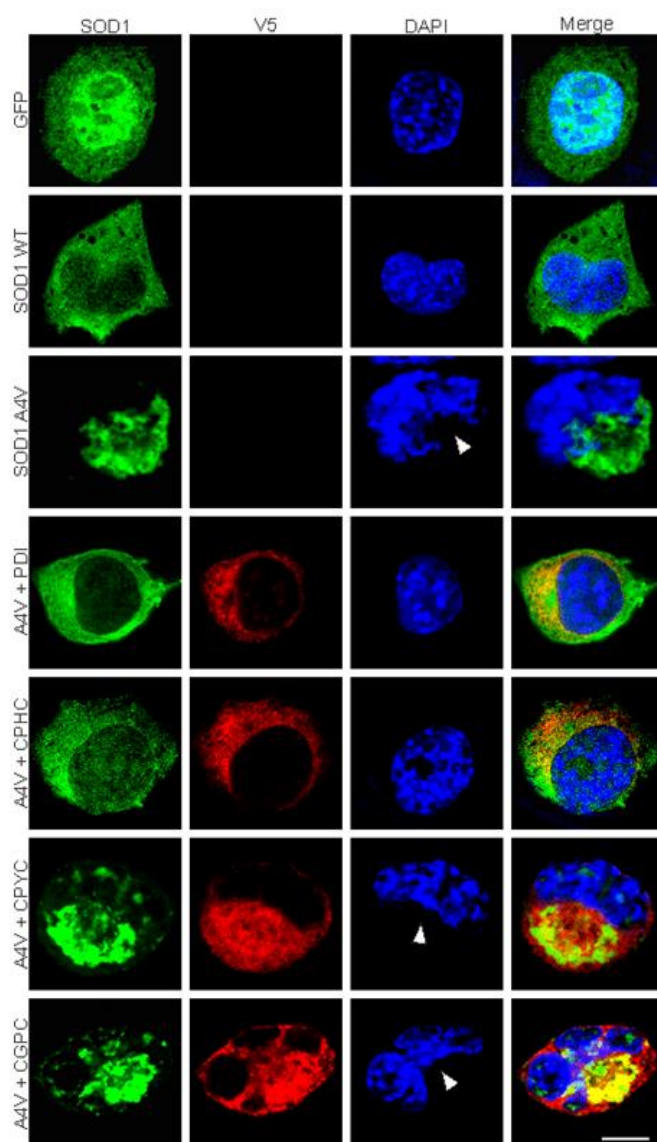
B
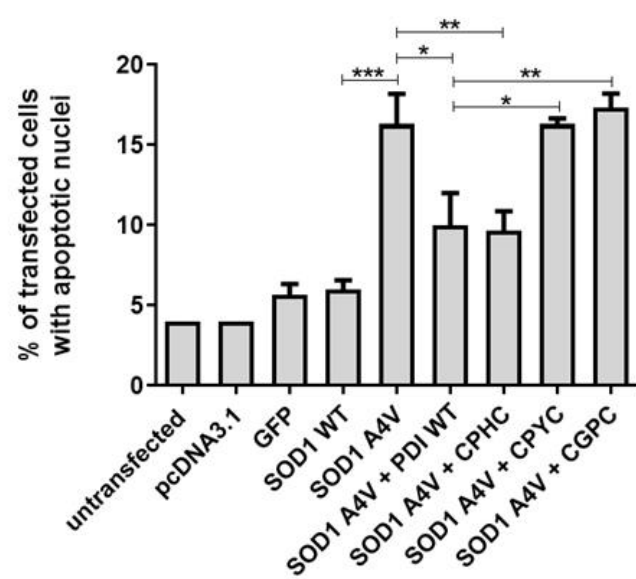
Figure 5.12: The oxidase activity of PDI is protective against nuclei condensation induced by mutant SOD1. A) Immunofluorescence images of Neuro-2A cells transfected with GFP, wildtype SOD1 with pcDNA3.1, and mutant SOD1 A4V with either pcDNA3.1, wildtype PDI, or the CPHC, CPYC, or CGPC active site mutants. Cells expressing GFP (first panel; GFP) or wildtype SOD1 (second panel; SOD1 WT) display nuclei of regular morphology and size. In contrast, more cells expressing mutant SOD1 A4V (third panel; SOD1 A4V) display apoptotic nuclei, indicated by condensed nuclei or irregular morphology, as shown by the white arrowhead (third panel, column three). However, the proportion of cells with apoptotic nuclei is reduced in populations co-expressing mutant SOD1 A4V with either wildtype PDI (fourth panel; A4V + PDI) or the CPHC active site mutant (fifth panel; A4V + CPHC). Cells co-expressing mutant SOD1 A4V with either the CPYC active site mutant (sixth panel; A4V + CPYC) or the CGPC active site mutant (seventh panel; A4V + CGPC) displayed more apoptotic nuclei, indicated by the white arrowheads. Scale bar = 20 µM. **B)** Quantification of cells displaying apoptotic nuclei in A). A significant increase in the proportion of apoptotic nuclei was observed in cells expressing mutant SOD1 A4V, compared to cells expressing wildtype SOD1 ($p < 0.001$). However, there was a significant decrease in the proportion of cells with apoptotic nuclei when mutant SOD1 A4V was co-expressed with either wildtype PDI ($p < 0.05$) or the CPHC active site mutant ($p < 0.01$). In contrast, significantly more cells with apoptotic nuclei were detected in populations co-expressing mutant SOD1 A4V with either the CPYC active site mutant ($p < 0.05$) or the CGPC active site mutant ($p < 0.01$), compared to cells co-expressing mutant SOD1 A4V and PDI. Hence these data indicate that these mutants are not protective against apoptosis, unlike the CPHC mutant. N=3, Mean ± SEM, * $p < 0.05$, ** $p < 0.01$, *** $p < 0.001$.

5.3.8.2 Caspase-3 as an early marker of apoptosis

To confirm these findings, another marker of apoptosis was examined, the activation of Caspase-3. Neuro-2A cells were transfected for 72 h with empty pcDNA3.1 vector, and constructs encoding GFP alone, wildtype SOD1 with pcDNA3.1, and mutant SOD1 A4V with either pcDNA3.1, wildtype PDI, or the CPHC, CPYC, or CGPC active site mutants. Cells were fixed and immunocytochemistry was performed using an anti-cleaved Caspase-3 antibody, where nuclear immunoreactivity to Caspase-3 was indicative of its activation, and moreover, of a cell undergoing apoptosis (Figure 5.13 A). Cells were also stained with Hoechst to clearly visualise the nuclei.

Less than 5% of untransfected cells or cells expressing either empty pcDNA3.1 vector or GFP displayed nuclear immunoreactivity to Caspase-3. Similarly, only 4.7% ± 1.2 cells expressing wildtype SOD1 demonstrated Caspase-3 activation. As expected, there was a significant increase ($p < 0.001$) in the proportion of cells displaying Caspase-3 activation when mutant SOD1 A4V was expressed (19.0% ± 1.5). However, when PDI was co-expressed with mutant SOD1 A4V, significantly fewer ($p < 0.01$) cells displayed Caspase-3 activation (10.7% ± 1.7), compared to cells expressing mutant SOD1 A4V alone. A similar significant decrease ($p < 0.001$) in the proportion of cells with Caspase-3 activation was also observed when the CPHC active site mutant was co-expressed with mutant SOD1 A4V (8.7% ± 0.3), compared to cells expressing mutant SOD1 A4V with empty pcDNA3.1 vector, suggesting that the active site mutant with predicted oxidase activity, CPHC, is protective against mutant SOD1-induced apoptosis, similar to PDI. Conversely, co-expression of mutant SOD1 A4V with either the CPYC active site mutant (15.3% ± 1.8) or the CGPC active site mutant (16.7% ± 1.2) did not alter the proportion of cells displaying Caspase-3 activation. Moreover, a significant difference ($p < 0.05$) in the proportion of cells with Caspase-3 activation was observed between mutant SOD1 A4V cells co-expressing PDI, and SOD1

A4V cells co-expressing the CGPC active site mutant. Furthermore, significantly fewer mutant SOD1 A4V cells co-expressing the CPHC active site mutant displayed Caspase-3 activation, compared to SOD1 A4V cells co-expressing either the CPYC active site mutant ($p < 0.05$) or the CGPC active site mutant ($p < 0.01$). These results demonstrate that the mutants with predicted isomerase activity, CPYC, and reductase activity, CGPC, are not protective against mutant SOD1-induced apoptosis (Figure 5.13 B). These results therefore confirm the results obtained using nuclei condensation as a marker of apoptosis. Hence, Caspase-3 activation was no longer utilised as an apoptotic marker in this chapter given that similar percentages of apoptosis was obtained using both markers.

A

|	SOD1	Caspase-3	DAPI	Merge
GFP				
SOD1 WT				
SOD1 A4V				
A4V + PDI				
A4V + CPHC				
A4V + CPYC				
A4V + CGPC				
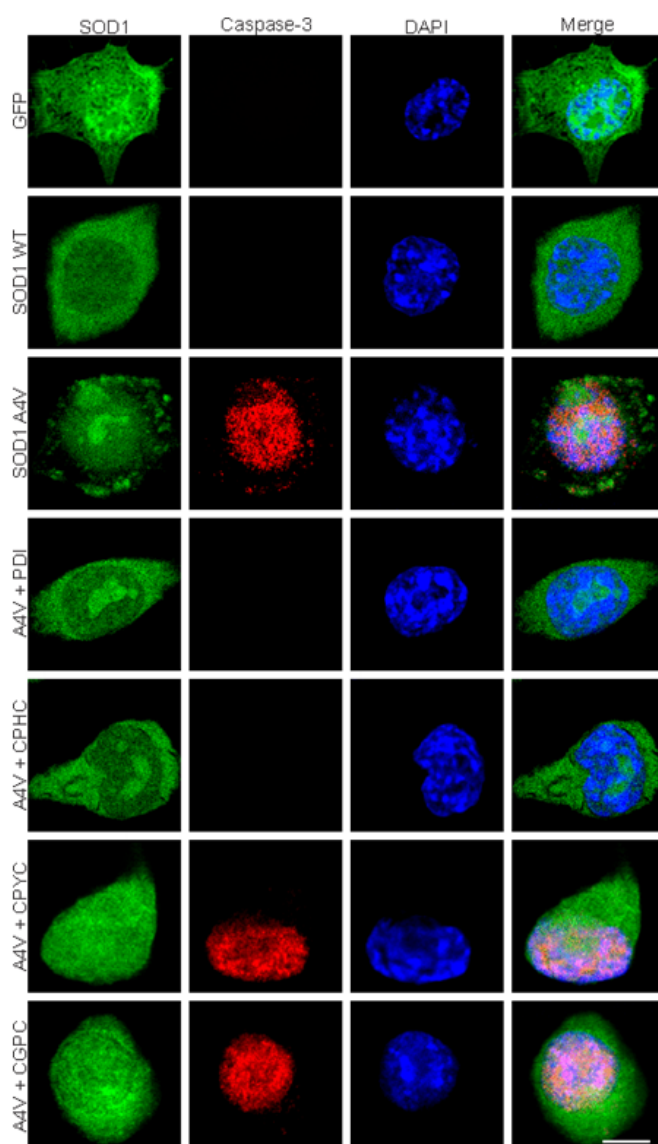
B
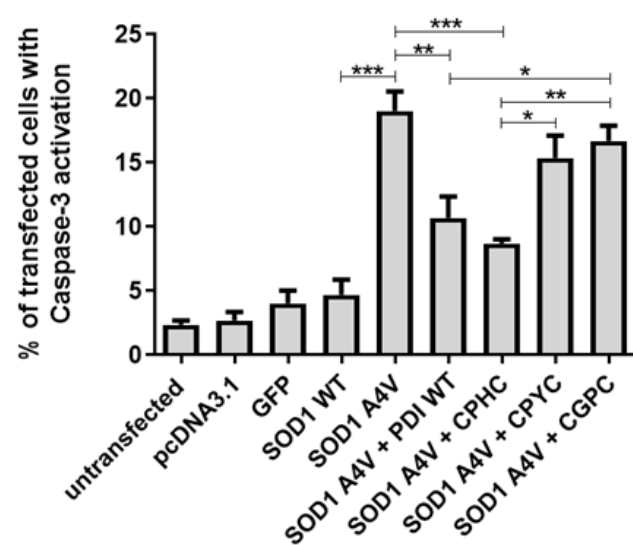
Figure 5.13: The oxidase activity of PDI is protective against Caspase-3 activation induced by mutant SOD1. A) Immunofluorescence images displaying Neuro-2A cells expressing GFP, wildtype SOD1 with pcDNA3.1, and mutant SOD1 A4V with either pcDNA3.1, PDI, or the CPHC, CPYC, or CGPC active site mutants. Few cells expressing GFP or wildtype SOD1 displayed Caspase-3 activation (first and second panels; GFP, SOD1 WT), whereas more cells expressing mutant SOD1 A4V (third panel; SOD1 A4V) demonstrated Caspase-3 activation, indicated by nuclear immunoreactivity to Caspase-3 (third panel, column two). When PDI or the CPHC active site mutant were co-expressed with mutant SOD1 A4V, fewer cells displayed Caspase-3 activation (fourth and fifth panels; A4V + PDI, A4V + CPHC) compared to mutant SOD1 A4V cells expressing empty vector. However, when mutant SOD1 A4V was co-expressed with either the CPYC or CGPC active site mutants (sixth and seventh panels; A4V + CPYC, A4V + CGPC), a similar proportion of cells with Caspase-3 activation was detected. Scale bar = 20 µM. **B)** Quantification of the proportion of cells with Caspase-3 activation in A). There was a significant increase in the proportion of mutant SOD1 A4V expressing cells with Caspase-3 activation, compared to the proportion of cells expressing wildtype SOD1 ($p < 0.001$). However, the proportion of cells with Caspase-3 activation was significantly reduced when PDI ($p < 0.01$) or the CPHC active site mutant ($p < 0.001$) were co-expressed with mutant SOD1 A4V compared to cells expressing mutant SOD1 A4V with empty vector. There was a significant increase in the proportion of SOD1 A4V expressing cells displaying Caspase-3 activation in populations co-expressing either the CPYC ($p < 0.05$) or the CGPC ($p < 0.01$) active site mutants compared to mutant SOD1 A4V cells co-expressing the CPHC active site mutant. Similarly, there was a significant increase in the proportion of Caspase-3 activated cells expressing mutant SOD1 A4V with the CGPC active site mutant, compared to cells expressing SOD1 A4V with PDI ($p < 0.05$.) N=3, Mean ± SEM, * $p < 0.05$, ** $p < 0.01$, *** $p < 0.001$.

Examining the protective effect of the PDI redox active site mutants in cells expressing mutant TDP-43

The PDI redox active site mutants were next analysed in Neuro-2A cells expressing mutant TDP-43 Q331K. Their activity on TDP-43 mislocalisation and mutant TDP-43-induced ER stress was investigated in the following experiments.

5.3.9 The redox active site mutants are co-expressed in almost all cells transfected with TDP-43

Firstly, the co-transfection efficiency of the active site mutants and TDP-43 was investigated by transfecting either the CPHC, CPYC or CGPC active site mutants with EGFP-TDP-43 Q331K for 18 h. Cells were fixed, immunocytochemistry was performed using an anti-V5 antibody, and cells were stained with Hoechst to visualise the nuclei. Co-transfection was confirmed by examining EGFP expression for TDP-43 using fluorescent microscopy, and by performing immunocytochemistry with an Alexa Fluor 568-tagged secondary antibody to detect the V5 tag on the active site mutants (Figure 5.14). The overall transfection efficiency of TDP-43 was approximately 70-75% 18 h post-transfection in Neuro-2A cells. For each of the three replicate experiments undertaken, at least 100 TDP-43 expressing cells were examined for co-expression with either the CPHC, CPYC or CGPC active site mutants using fluorescent microscopy. Quantification revealed that approximately 98% of TDP-43 expressing cells also co-expressed the CPHC active site mutant, 94% of TDP-43 expressing cells co-expressed the CPYC active site mutant, and 96% of TDP-43 expressing cells co-expressed the CGPC active site mutant. Therefore, it was assumed that the detection of TDP-43 expression reflected co-expression of both TDP-43 and the appropriate PDI active site

mutant in future experiments, where they were co-transfected and immunocytochemistry

using a V5 antibody was not performed.
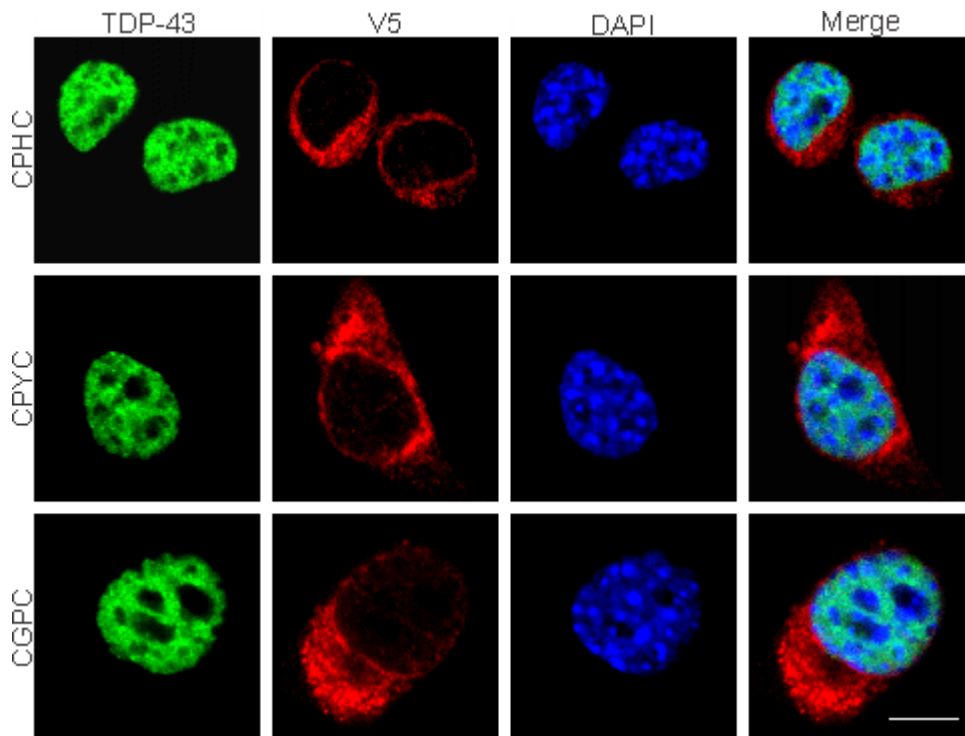
Figure 5.14: The CPHC, CPYC and CGPC redox active site mutants are co-expressed in almost all Neuro-2A cells co-transfected with EGFP-TDP-43. Neuro-2A cells were transfected with EGFP-TDP-43 (left column; TDP-43) and either the CPHC, CPYC or CGPC active site mutants (second column; V5) for 18 h. Cells were fixed, immunocytochemistry performed using an anti-V5 antibody and the nuclei stained with Hoechst (third column; DAPI). The merge column demonstrates co-expression of the active site mutants and TDP-43. Scale bar = 20 μM.

5.3.10 Expression of TDP-43 and redox active site mutants in Neuro-2A cells

Next, Western blotting analysis was performed to ensure that the transfection of each protein resulted in similar expression levels and to confirm that the expressed proteins were of the expected size (Figure 5.15). Cell lysates were prepared from the following cellular populations; GFP alone, wildtype TDP-43 co-expressing empty vector pcDNA3.1, and mutant TDP-43 Q331K co-expressing either pcDNA3.1, wildtype PDI, or the CPHC, CPYC or CGPC active site mutants. Immunoblotting revealed that wildtype and mutant EGFP-TDP-43 proteins were expressed at the expected size of 64 kDa, and GFP alone was expressed at the expected size of 26 kDa, using an anti-GFP antibody. Wildtype TDP-43 was expressed at higher levels compared to mutant TDP-43 Q331K, as expected. Wildtype PDI and the PDI active site mutants were detected in cell lysates at similar levels using an anti-V5 antibody at 62 kDa. β-actin was used as a loading control, detected at 40 kDa using an anti-β-actin antibody.

A

B

350
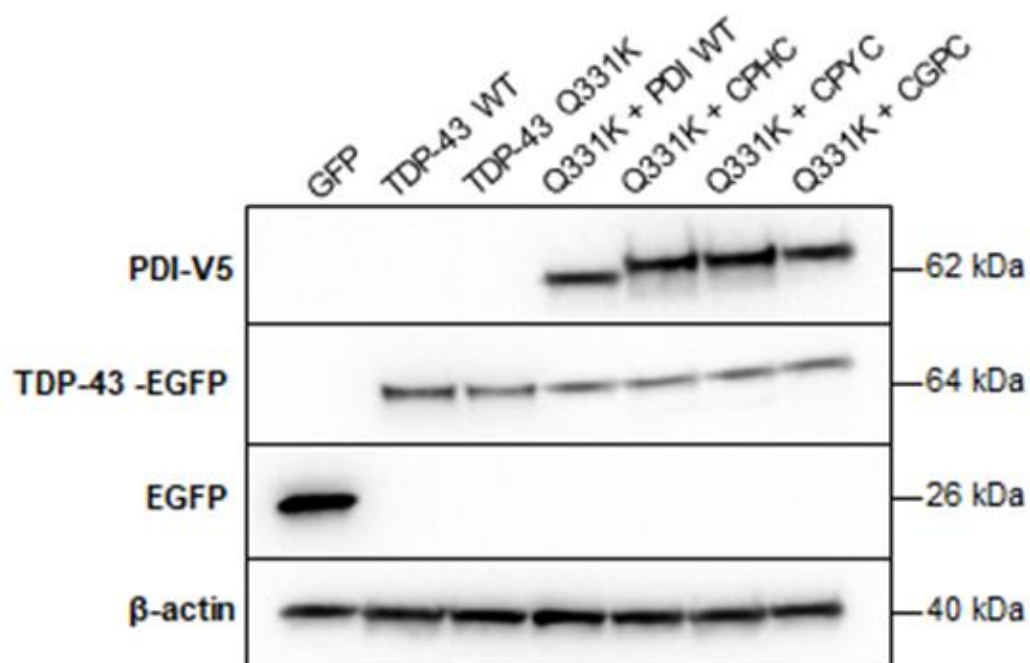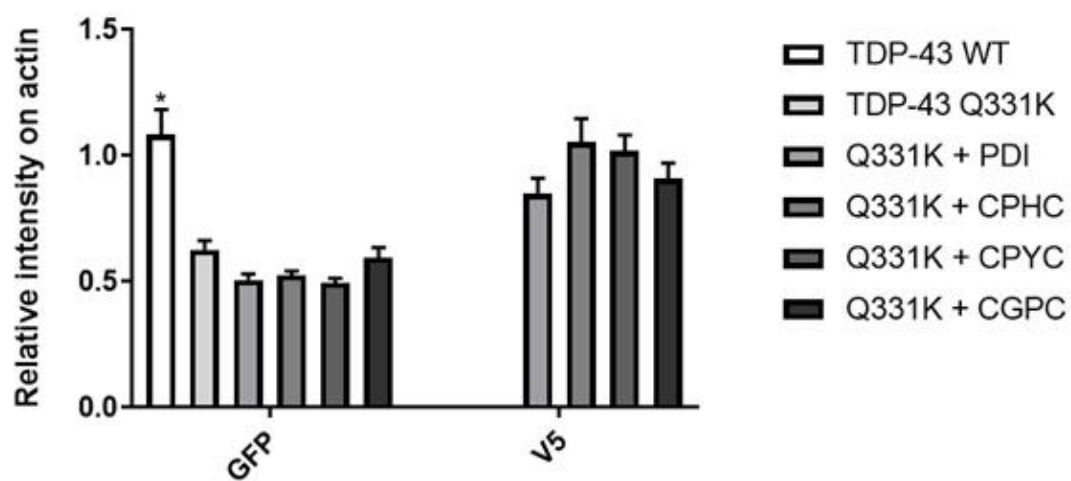
Figure 5.15: Protein expression of wildtype PDI, the PDI redox active site mutants and EGFP-TDP-43 proteins in Neuro-2A cells. A) Western blotting analysis was performed and quantified to ensure that the proteins expressed were of expected MW and to verify that the expression level of each protein was similar between groups. Cell lysates examined were GFP alone, wildtype TDP-43 with empty pcDNA3.1 vector, and mutant TDP-43 Q331K with either empty pcDNA3.1 vector, wildtype PDI, or the CPHC, CPYC or CGPC active site mutants. Wildtype and mutant TDP-43 were detected at 64 kDa (TDP-43 = 48 kDa, GFP = 26 kDa) and GFP was detected at 26 kDa, as expected. Wildtype PDI and the redox active site mutants were detected at 62 kDa and loading control, β-actin, was detected at 40 kDa. **B)** Quantification revealed that wildtype TDP-43 was expressed at significantly higher levels ($p < 0.05$) than mutant TDP-43 Q331K, as expected. Mutant TDP-43 Q331K shared similar expression levels across all cell lysate populations. Wildtype PDI and the active site mutants were also expressed at similar expression levels. Lysates expressing GFP only were not included in quantification. N=3, Mean ± SEM, * $p < 0.05$.

5.3.11 The oxidase and isomerase activity of PDI is necessary for preventing mutant TDP-43 mislocalisation to the cytoplasm

Previously in Chapter 4, it was demonstrated that the *a* domain of PDI was protective against mutant TDP-43 mislocalisation to the cytoplasm, suggesting that the disulphide interchange activity of PDI plays an important role in inhibiting TDP-43's translocation to the cytoplasm. Furthermore, other studies outlined in Chapter 4 examining the Dsb proteins revealed that both DsbA and DsbC, and hence the oxidase and isomerase activity respectively, prevented mutant TDP-43 mislocalisation to the cytoplasm. Therefore, next, the active site mutants of PDI were examined to investigate whether alterations in the redox potential of PDI modifies this protective activity.

Neuro-2A cells were transfected with empty pcDNA3.1 vector, GFP alone, wildtype SOD1 with pcDNA3.1, and mutant SOD1 A4V with either pcDNA3.1, wildtype PDI, or the CPHC, CPYC, or CGPC active site mutants. At 18 h post-transfection, cells were fixed and stained with Hoechst to clearly visualise the nuclei. Immunocytochemistry was not performed as it was assumed that EGFP-TDP-43 expression reflected co-expression with the V5-tagged proteins, as previously described in section 5.3.11. At least 100 TDP-43 expressing cells were examined for mislocalisation using fluorescent microscopy. TDP-43 was considered nuclear when it completely co-localised with the nucleus but was considered mislocalised when TDP-43 was detected in both the nucleus and the cytoplasm in EGFP-TDP-43 expressing cells (Figure 4.16 A).

Very few cells expressing wildtype TDP-43 displayed mislocalisation to the cytoplasm (1.0% $\pm$ 0.6). There was a significant increase ($p < 0.001$) in the proportion of cells displaying TDP-43 mislocalisation in populations expressing mutant TDP-43 Q331K with empty pcDNA3.1 vector (14.7% $\pm$ 1.2) compared to those expressing wildtype TDP-43, as expected. However,

co-expression of PDI with mutant TDP-43 Q331K significantly reduced ($p < 0.01$) the proportion of cells with TDP-43 mislocalisation (6.7% ± 1.7), compared to those expressing mutant TDP-43 Q331K alone, consistent with previous reports. Similarly, significantly fewer ($p < 0.05$) cells displayed TDP-43 mislocalisation to the cytoplasm when either the CPHC active site mutant (7.7% ± 0.3) or the CPYC active site mutant (8.3% ± 1.5) were co-expressed with mutant TDP-43, suggesting that both PDI's oxidase and isomerase activity are protective against mutant TDP-43 mislocalisation to the cytoplasm. Conversely, co-expression of the CGPC active site mutant with mutant TDP-43 Q331K did not reduce the proportion of cells with TDP-43 mislocalisation (11.3% ± 1.5), compared to cells expressing mutant TDP-43 Q331K alone. However, there was also no significant differences between the proportion of these cells with mutant TDP-43 mislocalisation and those expressing the other active site mutants or wildtype PDI, indicating that further studies may be warranted to elucidate the protective properties of the active site mutants (Figure 5.16 B).

A

B

354
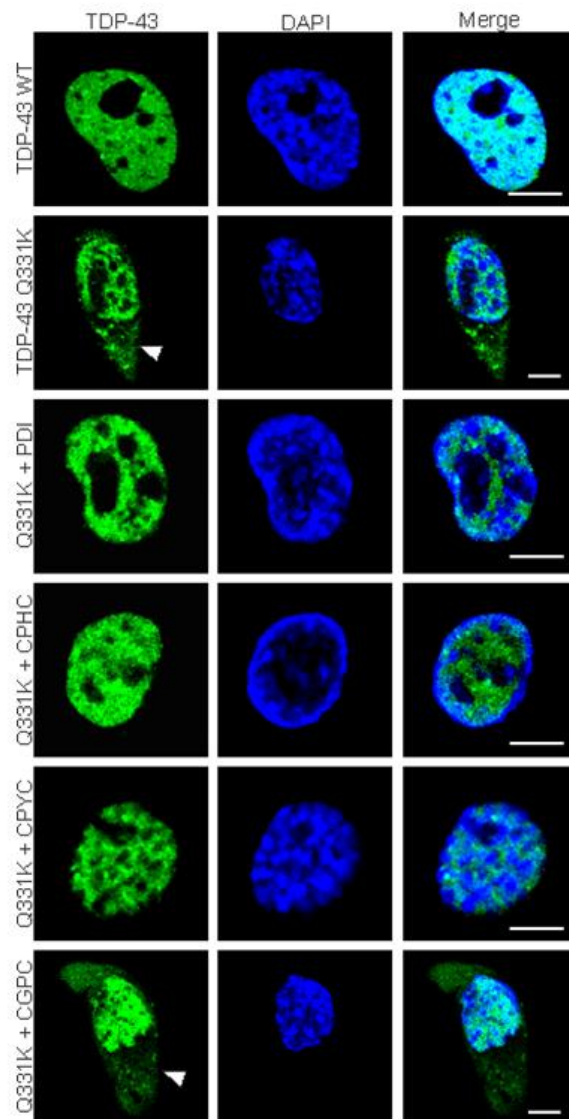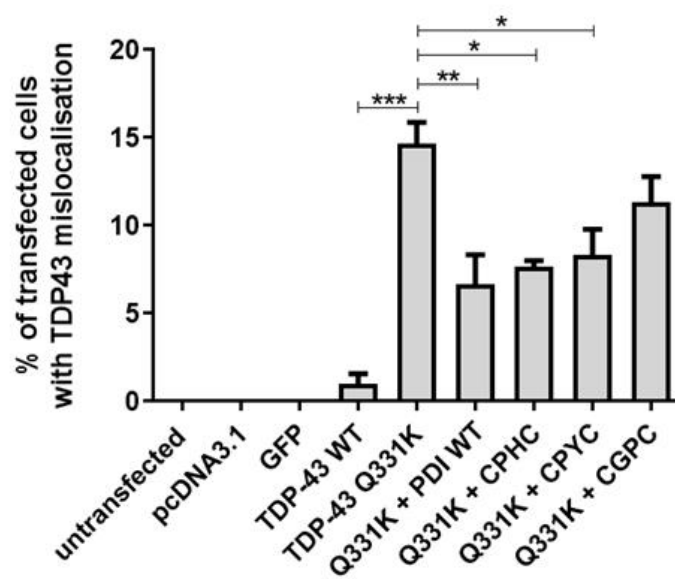
Figure 5.16: The oxidase and isomerase activities of PDI are protective against mutant TDP-43 mislocalisation to the cytoplasm. A) Immunofluorescence images of Neuro-2A cells expressing wildtype TDP-43 with pcDNA3.1, and mutant TDP-43 Q331K with either pcDNA3.1, wildtype PDI, or the CPHC, CPYC or CGPC active site mutants. Wildtype TDP-43 expressing cells (first panel; TDP-43 WT) displayed nuclear localisation of TDP-43, whereas more cells expressing mutant TDP-43 Q331K (second panel; TDP-43 Q331K) displayed cytoplasmic, mislocalised TDP-43, as indicated by the white arrowhead (second panel, first column). When mutant TDP-43 Q331K was co-expressed with PDI (third panel; Q331K + PDI), the CPHC active site mutant (fourth panel; Q331K + CPHC) or the CPYC active site mutant (fifth panel; Q331K + CPYC), fewer cells displayed TDP-43 mislocalisation. However, more cells co-expressing mutant TDP-43 Q331K with the CGPC active site mutant (sixth panel; Q331K + CGPC) displayed TDP-43 mislocalisation, as indicated by the white arrowhead (sixth panel, first column). Scale bar = 20 µM. **B)** Quantification of cells with TDP-43 mislocalisation in A). There was a significant increase ($p < 0.001$) in the proportion of cells with TDP-43 mislocalisation in mutant TDP-43 Q331K expressing cells, compared to wildtype TDP-43 expressing cells. However, this proportion was significantly decreased when mutant TDP-43 Q331K was co-expressed with either wildtype PDI ($p < 0.01$), the CPHC active site mutant ($p < 0.05$) or the CPYC active site mutant ($p < 0.05$). Co-expression of the CGPC active site mutant with TDP-43 Q331K did not reduce the proportion of cells exhibiting TDP-43 mislocalisation to the cytoplasm. N=3, Mean ± SEM, * $p < 0.05$, ** $p < 0.01$, *** $p < 0.001$.

5.3.12 The oxidase activity of PDI is protective against ER stress induced by mutant TDP-43

In Chapter 4, it was demonstrated that both the *a* and *b* domains of PDI, and hence both the disulphide interchange activity and chaperone function, were protective against mutant TDP-43-induced ER stress. Studies involving DsbA and DsbC explored how the redox potential of PDI modulates this protective activity, and they demonstrated that only the oxidase protein, DsbA, was able to inhibit the induction of mutant TDP-43-induced ER stress in Neuro-2A cells. Therefore, it was next investigated whether the active site mutants were protective against ER stress, to investigate how altering PDI's active site to modify its redox potential, also alters its protective activity. The activation of XBP-1 was examined in cells expressing mutant TDP-43-induced.

Neuro-2A cells were transfected with empty pcDNA3.1 vector, GFP alone, wildtype SOD1 with pcDNA3.1, and mutant SOD1 A4V with either pcDNA3.1, wildtype PDI, or the CPHC, CPYC, or CGPC active site mutants for 18 h. Cells were fixed, immunocytochemistry was performed using an anti-XBP-1 antibody to probe for XBP-1 activation, and cells were DAPI-stained with Hoechst. Fluorescent microscopy was utilised to analyse at least 100 TDP-43 expressing cells for activation of XBP-1 and hence ER stress, illustrated by nuclear immunoreactivity to XBP-1 (Figure 5.17 A).

Approximately 10% of untransfected cells, or cells expressing either empty pcDNA3.1 vector or GFP only, displayed XBP-1 activation. Similarly, few cells expressing wildtype TDP-43 exhibited XBP-1 activation (11.3% $\pm$ 1.9). In contrast, there was a significant increase ($p < 0.01$) in the proportion of cells displaying XBP-1 activation in populations expressing mutant TDP-43 Q331K (29.3% $\pm$ 1.8). However, co-expression of mutant TDP-43 with either wildtype PDI or the CPHC active site mutant resulted in a significant decrease ($p < 0.05$) in

the proportion of cells with XBP-1 activation ($14.0\% \pm 1.2$ and $15.0\% \pm 3.6$, respectively).

Co-expression of the CPYC and CGPC active site mutant did not decrease the proportion of

cells with XBP-1 activation in mutant TDP-43 Q331K expressing populations ($27.0\% \pm 5.0$

and $23.0\% \pm 2.6$, respectively), and a significant difference ($p < 0.05$) in this proportion was

observed between mutant TDP-43 Q331K cells co-expressing the CPYC active site mutant

and TDP-43 Q331K cells co-expressing wildtype PDI. These results demonstrate that the

CPHC active site mutant, with predicted oxidase activity, is protective against mutant TDP-

43-induced XBP-1 activation, similar to wildtype PDI (Figure 5.17 B).

A

TDP-43 | XBP-1 | DAPI | Merge

GFP

TDP-43 WT

TDP-43 Q331K

Q331K + PDI

Q331K + CPHC

Q331K + CPYC

Q331K + CGPC

B

% of transfected cells with XBP-1 activation

untransfected, pcDNA3.1, GFP, TDP-43 WT, TDP-43 Q331K, Q331K + PDI, Q331K + CPHC, Q331K + CPYC, Q331K + CGPC
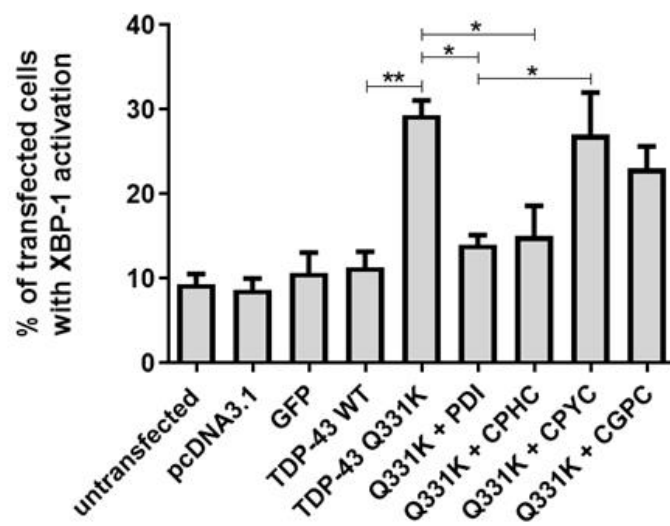
Figure 5.17: The oxidase activity of PDI is protective against XBP-1 activation induced by mutant TDP-43. A) Immunofluorescence images of Neuro-2A cells expressing GFP, wildtype TDP-43 with pcDNA3.1, and mutant TDP-43 Q331K with either pcDNA3.1, wildtype PDI or the CPHC, CPYC or CGPC active site mutants. Few cells expressing GFP alone or wildtype TDP-43 (first and second panels; GFP, TDP-43 WT) displayed nuclear XBP-1 immunoreactivity, and hence, XBP-1 activation. In contrast, more cells expressing mutant TDP-43 Q331K displayed XBP-1 activation (third panel; TDP-43 Q331K), as indicated by the white arrowhead (third panel, column two). However, when wildtype PDI or the CPHC active site mutant was co-expressed with mutant TDP-43 Q331K (fourth and fifth panels; Q331K + PDI, Q331K + CPHC), fewer cells displayed XBP-1 activation. Co-expression of TDP-43 Q331K with either the CPYC or CGPC active site mutants (sixth and seventh panels; Q331K + CPYC, Q331K + CGPC) did not reduce the proportion of cells with XBP-1 activation, indicated by the white arrowheads (column two, panels six and seven). Scale bar = 20 µM. **B)** Quantification of the cells in A) with XBP-1 activation. The proportion of cells with XBP-1 activation was significantly higher in cells expressing mutant TDP-43 Q331K, compared to cells expressing wildtype TDP-43 ($p < 0.01$) as expected. However, when either PDI or the CPHC active site mutant was co-expressed with mutant TDP-43 Q331K, significantly fewer cells ($p < 0.05$) displayed XBP-1 activation, implying that the CPHC oxidase active site mutant is protective against ER stress induced by mutant TDP-43 Q331K. Mutant TDP-43 Q331K cells co-expressing either the CPYC or CGPC active site mutants did not reduce the proportion of cells with XBP-1 nuclear immunoreactivity and significantly higher ($p < 0.05$) levels of XBP-1 activation was observed in TDP-43 Q331K cells co-expressing CPYC, compared to TDP-43 Q331K cells co-expressing wildtype PDI. N=3, Mean ± SEM, * $p < 0.05$, ** $p < 0.01$.

5.3.13 The oxidase activity is protective against CHOP activation induced by mutant TDP-43

The oxidase, isomerase and reductase active site mutants were all protective against ER stress induced by mutant SOD1, however only the oxidase was protective against mutant TDP-43 induced ER stress. To confirm this result, a second marker of ER stress, CHOP, was examined in cells co-expressing mutant TDP-43 and the active site mutants. Neuro-2A cells were transfected for 18 h with empty pcDNA3.1 vector, GFP alone, wildtype TDP-43 with pcDNA3.1, and mutant TDP-43 Q331K with either pcDNA3.1, wildtype PDI, or the CPHC, CPYC, or CGPC active site mutants. Immunocytochemistry was performed using an anti-CHOP antibody, where nuclear immunoreactivity to CHOP indicated the activation of pro-apoptotic UPR, similar to previous studies [448], and nuclei were stained with Hoechst (Figure 5.18 A).

Quantification revealed that untransfected cells and cells expressing either empty pcDNA3.1 vector or GFP alone displayed almost no nuclear immunoreactivity to CHOP, as expected. Similarly, only 7.0% ± 1.5 cells co-expressing wildtype TDP-43 and empty pcDNA3.1 vector exhibited CHOP activation. Compared to wildtype TDP-43 expressing cells, there was a significant increase ($p < 0.001$) in the proportion of cells co-expressing mutant TDP-43 Q331K and empty pcDNA3.1 vector displaying CHOP activation (17.0% ± 0.6) as expected. In contrast, co-expression of mutant TDP-43 Q331K with either wildtype PDI (6.7% ± 1.3) or the CPHC active site mutant (8.0% ± 1.2) resulted in a significant decrease ($p < 0.001$ and $p < 0.01$, respectively) in the proportion of cells with CHOP activation, compared to cells co-expressing mutant TDP-43 Q331K with empty vector, confirming that the CPHC oxidase active site mutant is protective against ER stress induced by mutant TDP-43. Co-expression of mutant TDP-43 Q331K with either the CPYC or CGPC active site mutant did not alter the proportion of cells displaying CHOP activation (12.7% ± 1.5 and 11.7% ± 1.5, respectively),

compared to cells co-expressing TDP-43 Q331K and empty vector. Moreover, significantly more cells ($p < 0.05$) expressing mutant TDP-43 Q331K and the CPYC active site mutant exhibited CHOP activation, compared to cells co-expressing TDP-43 Q331K and wildtype PDI (Figure 5.18 B). These results therefore confirm that the CPHC active site is protective against ER stress induced by mutant TDP-43, unlike the CPYC isomerase active site and the CGPC reductase active site mutants
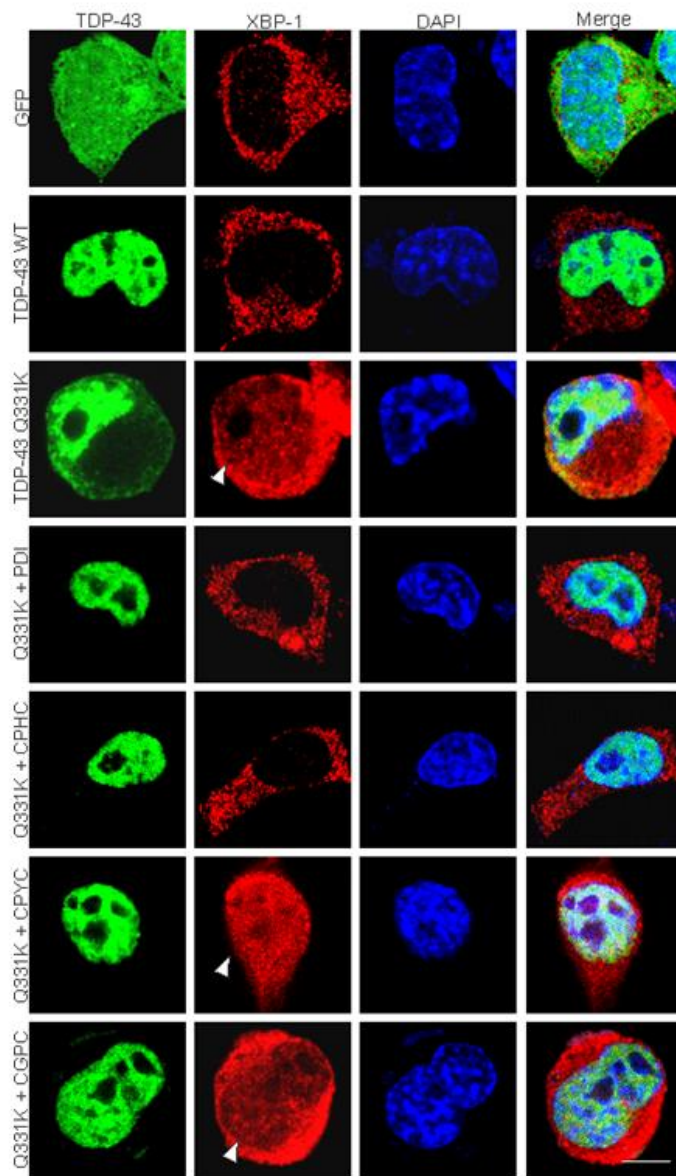
362
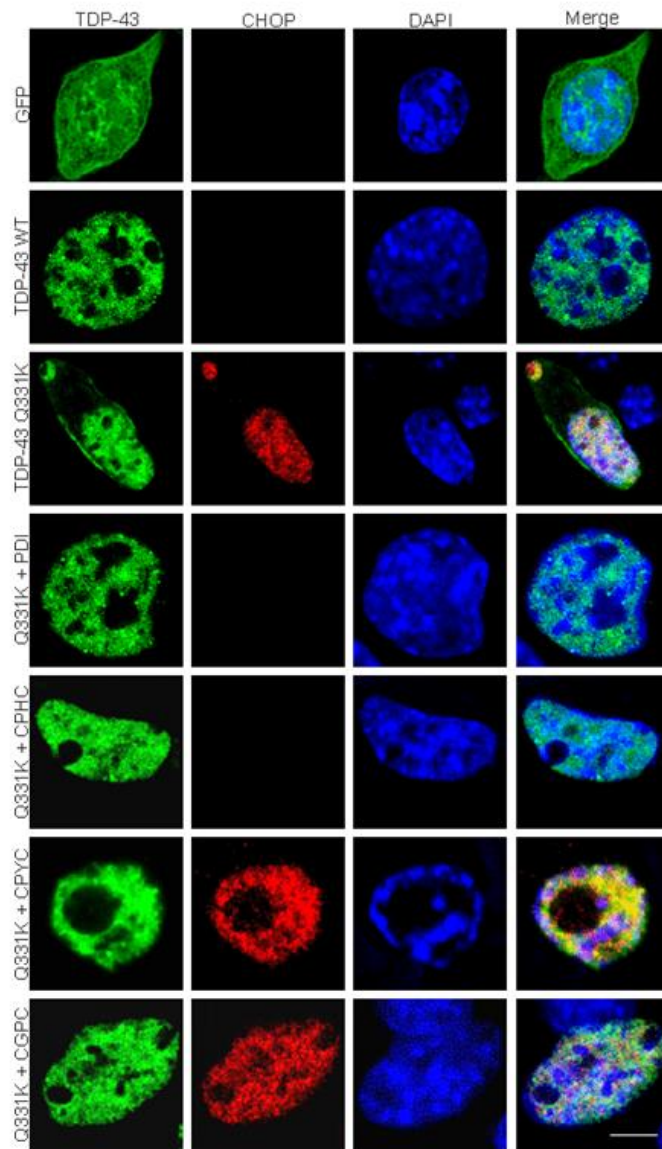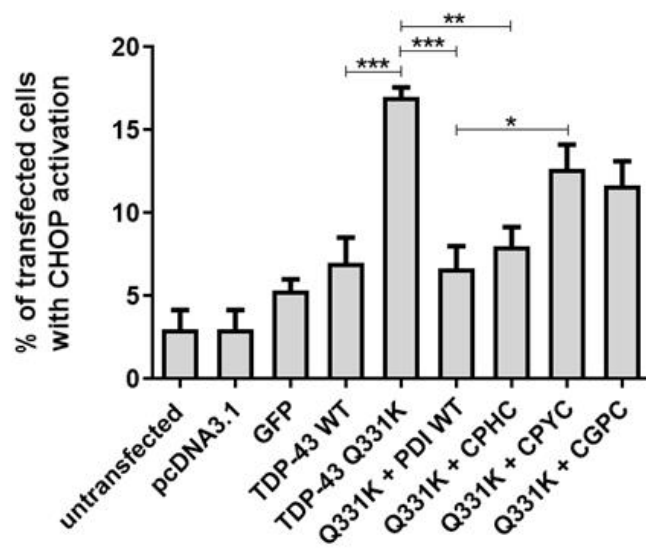
Figure 5.18: The oxidase activity of PDI is protective against CHOP activation induced by mutant TDP-43. A) Immunofluorescence images of Neuro-2A cells expressing GFP alone, wildtype TDP-43 with empty pcDNA3.1 vector, or mutant TDP-43 Q331K with either pcDNA3.1, wildtype PDI, or the CPHC, CPYC or CGPC active site mutants. Cells expressing either GFP alone (first panel; GFP) or wildtype TDP-43 (second panel; TDP-43 WT) rarely displayed nuclear immunoreactivity to CHOP, indicating activation. In contrast, more cells expressing mutant TDP-43 Q331K (third panel; TDP-43 Q331K) displayed nuclear immunoreactivity to CHOP (third panel, column two). Fewer cells exhibited CHOP activation when either wildtype PDI (fourth panel; Q331K + PDI) or the CPHC active site mutant (fifth panel; Q331K + CPHC) were co-expressed with TDP-43 Q331K. However, co-expression of either the CPYC or CGPC active site mutants with mutant TDP-43 Q331K (sixth and seventh panels; Q331K + CPYC, Q331K + CGPC) resulted in more cells with CHOP nuclear immunoreactivity (column two, sixth and seventh panels) compared to cells co-expressing wildtype PDI or the CPHC mutant. Scale bar = 20 µM. **B)** Quantification of the cells in A) with CHOP activation. Very few untransfected cells or cells expressing either empty pcDNA3.1 vector, GFP alone or wildtype TDP-43, displayed activation of CHOP. Significantly more cells ($p < 0.001$) expressing mutant TDP-43 Q331K demonstrated CHOP activation, compared to wildtype TDP-43 expressing cells. However, this proportion was significantly decreased when either wildtype PDI ($p < 0.001$) or the CPHC active site mutant ($p < 0.01$) was co-expressed with mutant TDP-43. Compared to TDP-43 Q331K cells co-expressing PDI, a significant increase ($p < 0.05$) in the proportion of cells with CHOP activation was observed when the CPYC active site was co-expressed with mutant TDP-43 Q331K. N=3, Mean ± SEM, * $p < 0.05$, ** $p < 0.01$, *** $p < 0.001$.

Examining the protective effect of the PDI redox active site mutants in cells expressing

mutant FUS

Finally, the PDI redox active site mutants were analysed in Neuro-2A cells expressing mutant

FUS R521G. Their protective activity against FUS mislocalisation and mutant FUS-induced

ER stress was investigated in the following experiments.

5.3.14 Redox active site mutants are co-expressed in almost all cells transfected with FUS

Firstly, as with the studies involving SOD1 and TDP-43, the co-transfection efficiency of the

PDI active site mutants and FUS was examined. Cells were transfected with GFP-FUS and

either the CPHC, CPYC, or CGPC active site mutants for 72 h, before fixing, and

immunocytochemistry using an anti-V5 antibody and DAPI-staining with Hoechst was

performed. Co-transfection was verified by examining the GFP expression of mutant FUS-

GFP using fluorescent microscopy and performing immunocytochemistry with an Alexa

Fluor 568-tagged secondary antibody to detect the V5 tags on the active site mutants (Figure

5.19). The overall transfection efficiency of mutant FUS was approximately 80% in Neuro-

2A cells when observed 72 h post-transfection. Three replicate experiments were undertaken,

where fluorescent microscopy was utilised to examine at least 100 FUS expressing cells.

These cells were analysed for co-expression with either the CPHC, CPYC or CGPC active

site mutants. Quantification revealed that approximately 96% of FUS expressing cells also

co-expressed the CPHC active site mutant, 94% of these cells co-expressed the CPYC active

site mutant, and 98% of cells co-expressed the CGPC active site mutant. Hence, in all further

experiments where FUS and the PDI active site mutants were co-transfected and

immunocytochemistry using an V5 antibody was not performed, it was assumed that

detection of FUS reflected co-expression of both FUS and either the CPHC, CPYC or CGPC active site mutants.
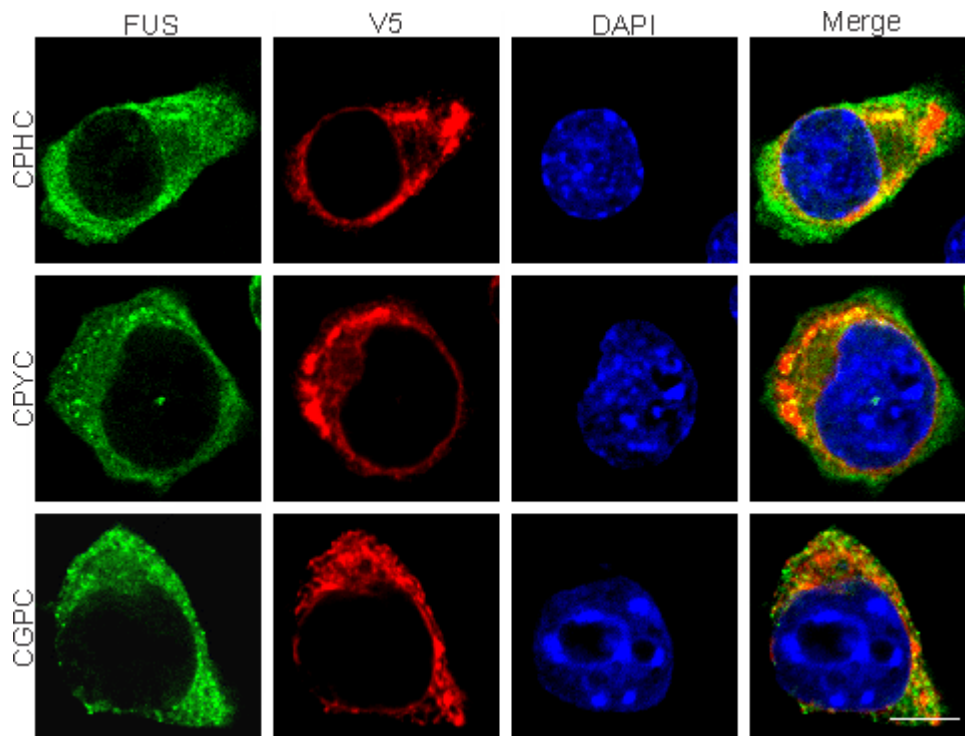
Figure 5.19: The CPHC, CPYC and CGPC active site mutants are co-expressed in almost all Neuro-2A cells co-transfected with GFP-FUS. Neuro-2A cells were transfected for 72 h with mutant GFP-FUS (left column; FUS) and either the CPHC, CPYC or CGPC active site mutants (second column; V5). Immunocytochemistry was performed using an anti-V5 antibody to visualise the PDI active site mutants, and the nuclei were stained with Hoechst (third column; DAPI). The merge column illustrates co-expression of the PDI active site mutants with FUS in the shown cells. Scale bar = 20 μM.

5.3.15 Expression of FUS and redox active site mutants in Neuro-2A cells

Western blotting analysis was next performed to ensure that the transfection of each protein resulted in similar expression levels and to verify that the expressed proteins were of the expected sizes (Figure 4.20). Cell lysates were prepared from the following populations; GFP alone, wildtype FUS co-expressed with empty vector pcDNA3.1, and mutant FUS R521G with either pcDNA3.1, wildtype PDI, or the CPHC, CPYC or CGPC active site mutants. Immunoblotting revealed that both wildtype and mutant GFP-FUS were expressed at 100 kDa as expected (FUS = 74 kDa, GFP = 26kDa) and GFP alone was expressed at 26 kDa using an anti-GFP antibody. Wildtype FUS was expressed at higher levels than mutant FUS R521G, as expected. Wildtype PDI and the PDI redox active site mutants were detected at approximately 62 kDa using an anti-V5 antibody. The loading control, β-actin, was detected using an anti-β-actin antibody (40 kDa).

A
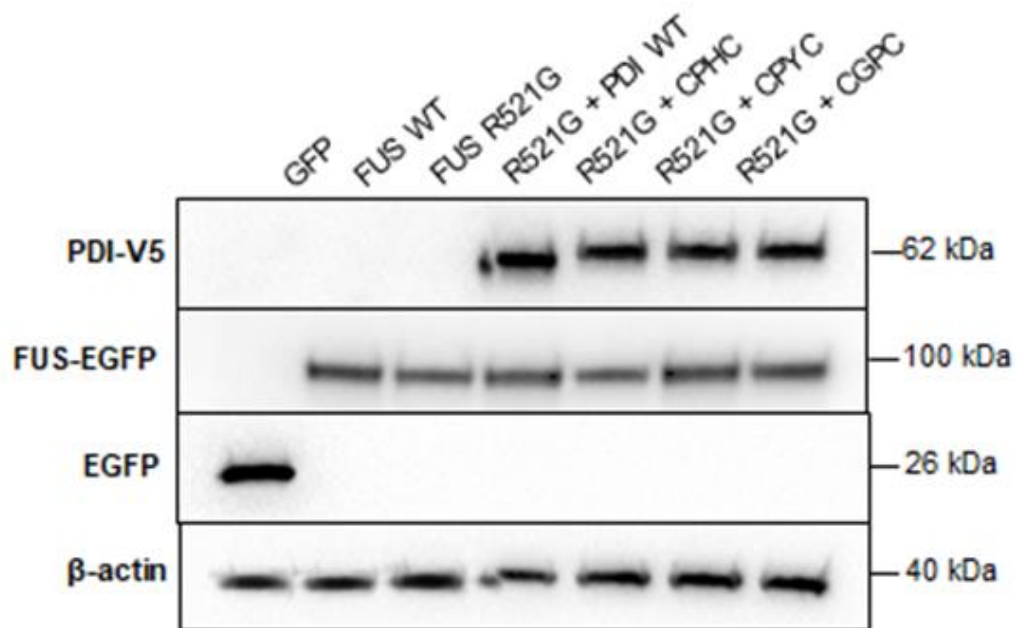
B
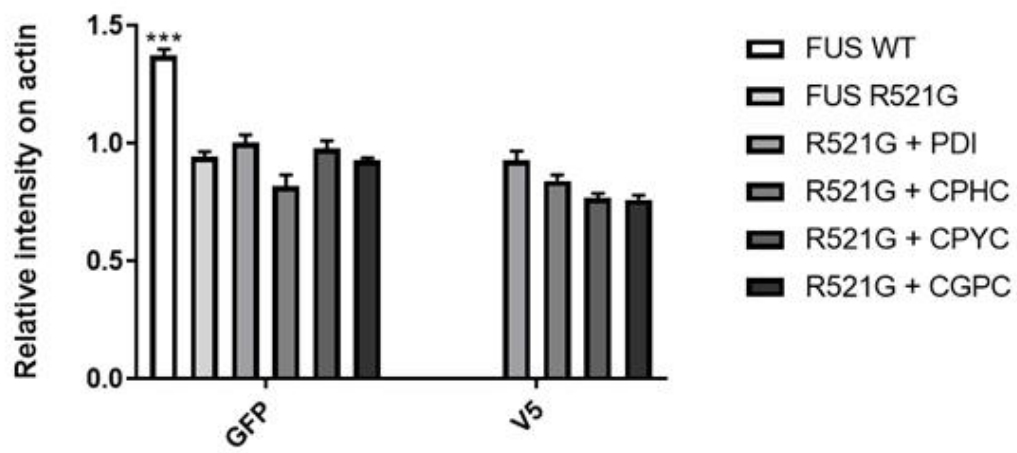
Figure 5.20: Protein expression of wildtype PDI, the PDI redox active site mutants and GFP-FUS proteins in Neuro-2A cells. A) Western blotting of cell lysates was performed and quantified to determine if protein expression levels were comparable between groups and to ensure that proteins were expressed at expected MW. Cell lysates examined were GFP alone, wildtype FUS with empty pcDN3.1, and mutant FUS R521G with either pcDNA3.1, wildtype PDI, or the CPHC, CPYC or CGPC active site mutants. PDI and active site mutants were detected at 62 kDa, wildtype FUS and mutant FUS R521G were detected at 100 kDa and GFP alone was detected at 26 kDa, as expected. β-actin was used as a loading control and was expressed at 40 kDa. **B)** Quantification revealed that wildtype FUS was expressed at significantly higher levels ($p < 0.05$) compared to mutant FUS R521G. Mutant FUS R521G shared similar expression levels across all cell lysates. Similarly, wildtype PDI and active site mutants also demonstrated comparable levels of expression. Lysates expressing GFP only were not included in quantification. N=3, Mean ± SEM, * $p < 0.05$.

5.3.16 The oxidase activity of PDI is necessary for preventing mutant FUS mislocalisation to the cytoplasm

Previous results obtained in Chapter 4 demonstrated that the *a* and a' domains, which are responsible for PDI's disulphide interchange activity, were both protective against mutant FUS mislocalisation to the cytoplasm. Furthermore, analysis of Dsb proteins, DsbA and DsbC, demonstrated that only DsbA, which possesses oxidase activity, was able to prevent FUS mislocalisation to the cytoplasm, in contrast to DsbC, the isomerase. Therefore, the redox active site mutants of PDI were next examined in Neuro-2A cells expressing mutant FUS to determine whether modulating the redox potential of PDI's *a* and a' domains altered the protective activity of PDI in preventing ALS-associated FUS mislocalisation to the cytoplasm.

Neuro-2A cells were transfected for 72 h with empty pcDNA3.1 vector, GFP alone, wildtype FUS with pcDNA3.1, and mutant FUS R521G with either pcDNA3.1, wildtype PDI, or the CPHC, CPYC, or CGPC active site mutants. Immunocytochemistry was not performed as it was assumed that detection of FUS expression also reflected co-expression with V5-tagged PDI proteins, previously determined in section 5.3.16. Fluorescent microscopy was utilised to examine the cellular location of FUS, following fixing and staining of the cells with Hoechst to visualise the nuclei. FUS was considered cytoplasmic when fluorescence was only detected in the cytoplasm but FUS was considered to be nuclear when it was localised in both the cytoplasm and nucleus, as previous, as well as when it localised solely in the nucleus (Figure 5.21 A). The reason that these cells were categorised differently to mutant TDP-43 is that a much higher percentage of cells were localised only in the cytoplasm compared to TDP-43. The R521G mutation of FUS is an aggressive form and studies have demonstrated that it is highly retained in the cytoplasm, characterised by a high proportion of insoluble FUS and a decrease in soluble nuclear FUS [137].

Untransfected cells, cells expressing empty pcDNA3.1 vector and those expressing GFP alone, were not expressing GFP-FUS and hence they were not included in the analysis. In wildtype FUS-GFP cells, FUS was expressed solely within the nucleus, and cytoplasmic localisation was never detected. Conversely, a high proportion of cells co-expressing mutant FUS R521G, with empty pcDNA3.1 vector, displayed cytoplasmic FUS mislocalisation (71.3% ± 2.9). However, co-expression of mutant FUS R521G with either wildtype PDI or the CPHC active site mutant resulted in a significant reduction ($p < 0.05$) in the proportion of cells expressing cytoplasmic FUS (55.7% ± 1.8 and 53.7% ± 4.3, respectively). This result implies that the oxidase activity of the CPHC active site mutant is protective against mutant FUS mislocalisation. In contrast, however, there was no difference in the proportion of cells with cytoplasmic FUS in populations co-expressing mutant FUS with either the CPYC or the CGPC active site mutants (60.3% ± 6.4 and 65.3% ± 2.4, respectively), compared to cells expressing mutant FUS R521G with empty pcDNA3.1 vector. Hence these data imply that the isomerase and reductase activity of PDI are not protective against mutant FUS mislocalisation to the cytoplasm (Figure 5.21 B).
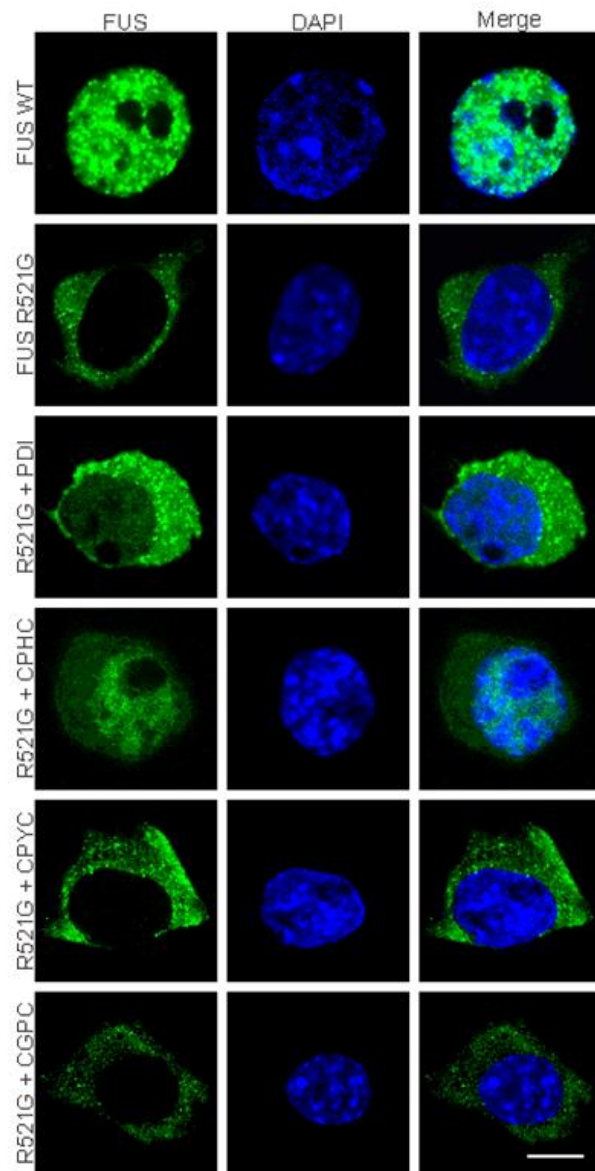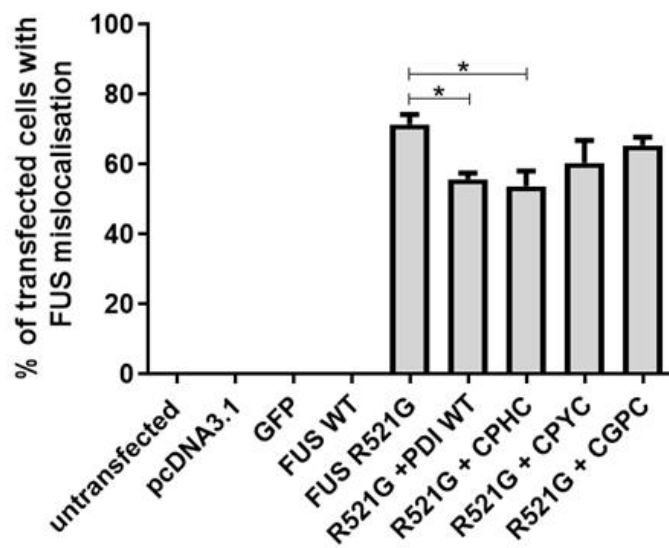
Figure 5.21: The oxidase activity of PDI prevents mutant FUS mislocalisation to the cytoplasm. A) Immunofluorescence images of Neuro-2A cells expressing wildtype FUS with empty pcDNA3.1 vector, and mutant FUS R521G with either pcDNA3.1, wildtype PDI or the CPHC, CPYC or CGPC active site mutants. Cells expressing wildtype FUS displayed only nuclear FUS localisation, demonstrated by complete co-localisation with the DAPI-stained nucleus (first panel; FUS WT). In contrast, more cells expressing mutant FUS R521G with empty vector demonstrated cytoplasmic localisation of FUS (second panel; FUS R521G). Similarly, FUS was localised primarily in the cytoplasm in mutant FUS R521G cells co-expressing either the CPYC or the CGPC active site mutants (fifth and sixth panels; R521G + CPYC, R521G + CGPC). However, fewer FUS R521G cells co-expressing either wildtype PDI or the CPHC active site mutant (third and fourth panels; R521G + PDI, R521G + CPHC), demonstrated FUS localisation in the cytoplasm. Scale bar = 20 µM. **B)** Quantification of Neuro-2A cells with FUS mislocalisation in A). FUS was expressed only in the nucleus in populations expressing wildtype FUS, and no cells with cytoplasmic FUS were detected. In contrast, most (71.3 %) cells expressing mutant FUS R521G displayed cytoplasmic localisation of FUS. A significant decrease ($p < 0.05$) in the proportion of cells with FUS mislocalisation to the cytoplasm was observed when either wildtype PDI or the CPHC active site mutant were co-expressed with mutant FUS R521G. However, no significant difference was observed in the proportion of FUS R521G cells co-expressing either the CPYC or the CGPC active site mutants. N=3, Mean ± SEM, * $p < 0.05$.

5.3.17 The oxidase, reductase and isomerase activity of PDI are protective against XBP-1 activation induced by mutant FUS

In the studies described in Chapter 4 both the oxidase activity of DsbA and the isomerase activity of DsbC were found to be protective against mutant FUS-induced ER stress. Hence, it was next examined whether the redox active site mutants of PDI were also protective against ER stress. Firstly, the activation of XBP-1 was used as a marker of ER stress in FUS expressing cells. Neuro-2A cells were transfected with empty pcDNA3.1 vector, GFP alone, wildtype FUS with pcDNA3.1, and mutant FUS R521G with either pcDNA3.1, wildtype PDI, or the CPHC, CPYC, or CGPC active site mutants for 72 h. After fixing, immunocytochemistry was performed using an anti-XBP-1 antibody, whereby XBP-1 nuclear immunoreactivity was indicative of its activation, and thus, UPR induction. DAPI-staining was performed with Hoechst to visualise the nuclei (Figure 5.22 A).

Quantification revealed that approximately 10% of untransfected cells or control cells expressing empty pcDNA3.1 vector or GFP alone, displayed XBP-1 activation. Similarly, cells expressing wildtype FUS exhibited little XBP-1 activation (12.0% ± 1.5). In contrast, there was a significant increase ($p < 0.001$) in the proportion of cells with XBP-1 activation in populations expressing mutant FUS R521G with empty pcDNA3.1 vector (35.7% ± 2.6), consistent with previous observations. As expected, a significant decrease ($p < 0.001$) in the proportion of cells with XBP-1 activation was observed when mutant FUS R521G was co-expressed with wildtype PDI (20.7% ± 2.3), compared to mutant FUS R521G cells co-expressed with empty vector. Similarly, significantly fewer mutant FUS R521G expressing cells demonstrated XBP-1 nuclear immunoreactivity when either of the active site mutants was co-expressed; CPHC ($p < 0.01$, 22.3% ± 1.2), CPYC ($p < 0.05$, 25.0% ± 2.6) or CGPC ($p < 0.01$, 23.3% ± 1.5). Hence these data imply that the oxidase, isomerase and reductase

activities of PDI are all protective against mutant FUS induced UPR induction (Figure 5.22
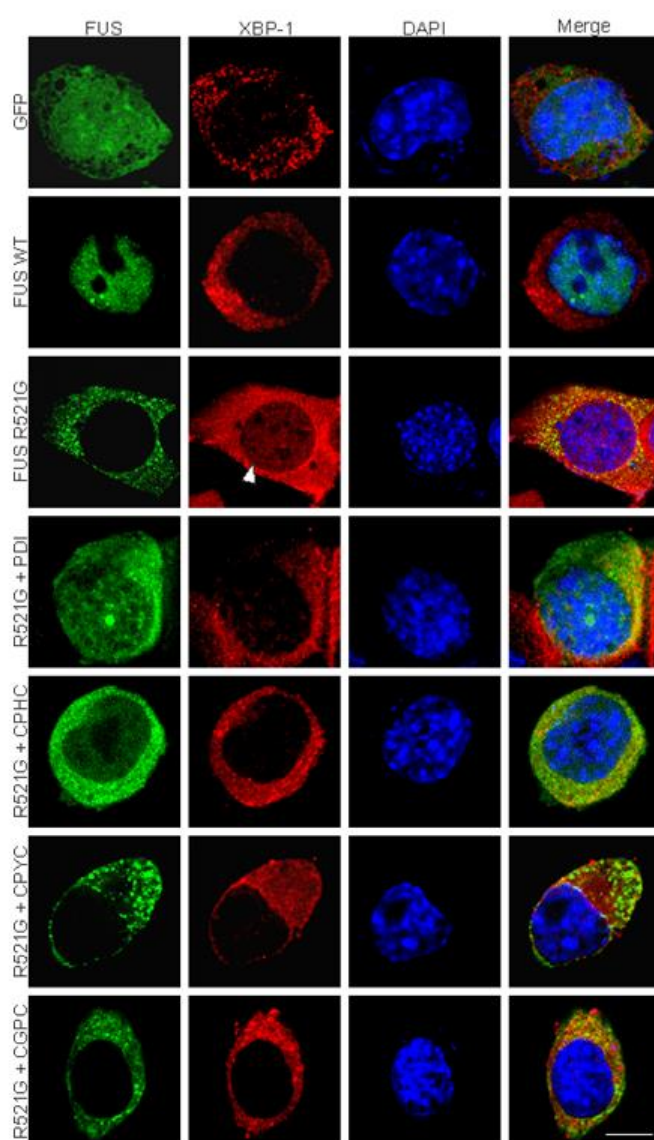
B).
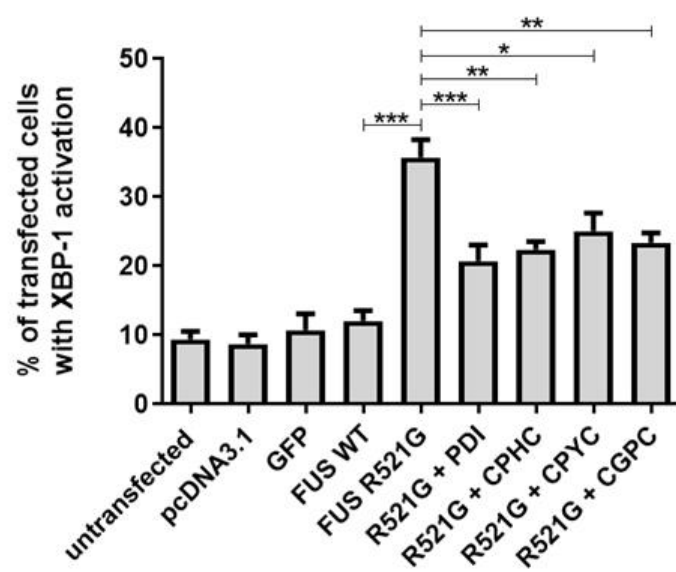
Figure 5.22: The oxidase, reductase and isomerase activities of PDI are protective against XBP-1 activation induced by mutant FUS. A) Immunofluorescence images of Neuro-2A cells expressing GFP alone, wildtype FUS with pcDNA3.1, and mutant FUS R521G with either pcDNA3.1, wildtype PDI or the CPHC, CPYC or CGPC active site mutants. Cells expressing either GFP alone or wildtype FUS (first and second panels; GFP, FUS WT) rarely displayed XBP-1 activation. Conversely, more cells expressing mutant FUS R521G (third panel; FUS R521G) demonstrated XBP-1 nuclear immunoreactivity, indicative of XBP-1 activation, as specified by the white arrowhead (third panel, column two). Co-expression of mutant FUS R521G with either wildtype PDI (fourth panel; R521G + PDI) or the redox active site mutants (panels five to seven; R521G + CPHC, R521G + CPYC, R521G + CGPC) resulted in fewer cells with XBP-1 activation. Scale bar = 20 µM. **B)** Quantification of the cells in A) with XBP-1 activation. There was a significant increase ($p < 0.001$) in the proportion of cells co-expressing mutant FUS R521G with empty vector, compared to cells co-expressing wildtype FUS with empty vector, as expected. Significantly fewer cells displayed XBP-1 activation when mutant FUS R521G was co-expressed with either wildtype PDI ($p < 0.001$), the CPHC active site mutant ($p < 0.01$), CPYC active site mutant ($p < 0.05$) or the CGPC active site mutant ($p < 0.01$). N=3, Mean ± SEM, * $p < 0.05$, ** $p < 0.01$, *** $p < 0.001$.

5.3.18 The oxidase, reductase and isomerase activities of PDI are protective against CHOP activation induced by mutant FUS

To confirm the XBP-1 findings that all three redox active site mutants were protective against mutant FUS induced ER stress, the activation of pro-apoptotic CHOP was analysed in Neuro-2A cells. Cells were transfected for 72 h with empty pcDNA3.1 vector, GFP alone, wildtype FUS with pcDNA3.1, and mutant FUS R521G with either pcDNA3.1, wildtype PDI, or the CPHC, CPYC, or CGPC active site mutants. Immunocytochemistry was performed using an anti-CHOP antibody to detect nuclear immunoreactivity to CHOP, indicating activation. Cells were also stained with Hoechst to visualise the nuclei and examined using fluorescent microscopy (Figure 5.23 A).

Less than 5% of untransfected cells or cells expressing either empty pcDNA3.1 vector or GFP displayed CHOP activation. Moreover, only $1.7\% \pm 0.9$ of cells expressing wildtype FUS demonstrated nuclear immunoreactivity to CHOP. Conversely, there was a significant increase ($p < 0.001$) in the proportion of cells with CHOP activation ($22.3\% \pm 1.8$) in populations expressing mutant FUS R521G, compared to those expressing wildtype FUS. Co-expression of PDI with mutant FUS R521G resulted in a significant reduction ($p < 0.001$) in the proportion of cells displaying CHOP activation ($5.7\% \pm 0.3$), compared to cells co-expressing mutant FUS R521G with empty vector. Moreover, significantly fewer cells ($p < 0.001$) displayed CHOP activation when mutant FUS R521G cells were co-expressed with either the CPHC ($4.7\% \pm 1.8$), CPYC ($8.0\% \pm 2.5$) or the CGPC ($7.7\% \pm 0.9$) active site mutants. Hence these results reveal that all three mutants were protective against ER stress induced by mutant FUS, thus confirming the results observed with XBP-1 (Figure 5.23 B). Furthermore, as very similar results were obtained whether XBP-1 or CHOP was used as a marker of ER stress, in experiments involving mutant SOD1, TDP-43 or FUS proteins, only

the activation of CHOP was used as an ER stress marker in the studies described in the

remainder of this Chapter.

A

	FUS	CHOP	DAPI	Merge
GFP				
FUS WT				
FUS R521G				
R521G + PDI				
R521G + CPHC				
R521G + CPYC				
R521G + CGPC				

B

379
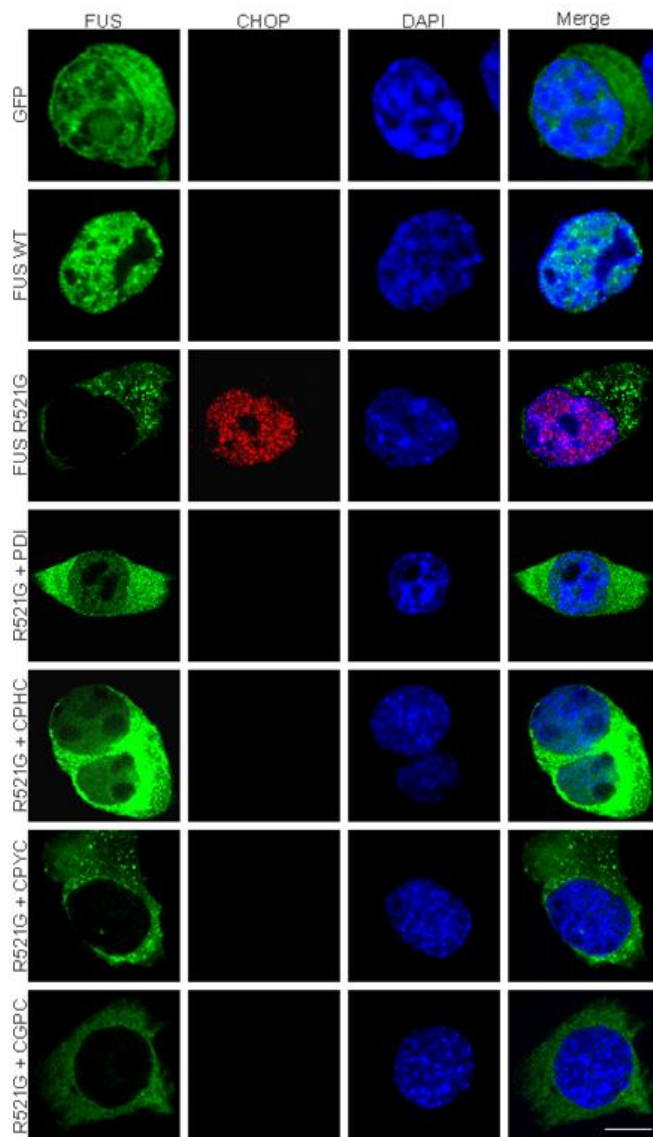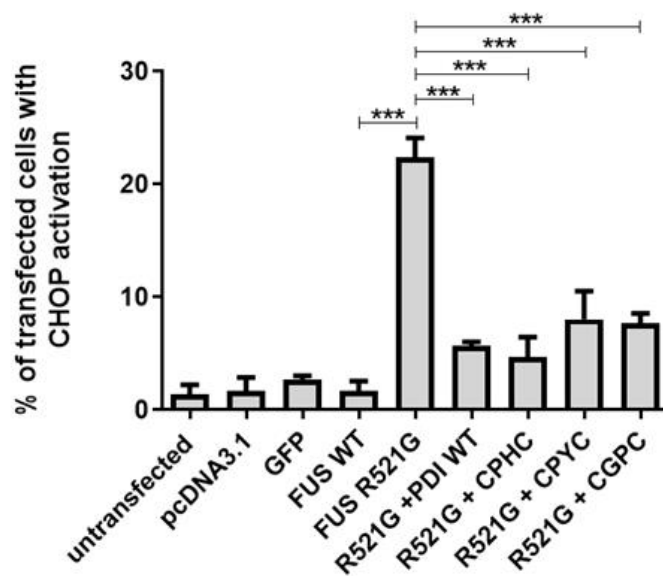
Figure 5.23: The oxidase, reductase and isomerase activities of PDI are protective against CHOP activation induced by mutant FUS. A) Immunofluorescence images of Neuro-2A cells expressing GFP, wildtype FUS with pcDNA.31, and mutant FUS R521G with either pcDNA3.1, wildtype PDI or the CPHC, CPYC or CGPC active site mutants. Cells expressing either GFP (first panel; GFP) or wildtype FUS (second panel; FUS WT) rarely displayed CHOP activation. In contrast, more cells expressing mutant FUS R521G (third panel; FUS R521G) demonstrated CHOP nuclear immunoreactivity (third panel, column two). However, co-expression of mutant FUS R521G with either wildtype PDI or each of the redox active site mutants (panels four to seven; R521G + PDI, R521G + CPHC, R521G + CPYC, R521G + CGPC), resulted in fewer cells displaying CHOP activation. Scale bar = 20 µM. **B)** Quantification of the cells in A) with CHOP activation. A significant increase ($p < 0.001$) in the proportion of cells with CHOP activation was observed when cells were co-expressed with mutant FUS R521G and empty pcDNA3.1 vector, compared to cells co-expressed with wildtype FUS and pcDNA3.1. However, there was a significant decrease ($p < 0.001$) in the proportion of mutant FUS R521G expressing cells displaying CHOP activation when either wildtype PDI, or the CPHC, CPYC or CGPC active site mutants were co-expressed. N=3, Mean ± SEM, *** $p < 0.001$.

5.3.19 A summary of the protective activity of the PDI redox active site mutants

A summary of the results obtained so far in this Chapter, examining the protective effects of the PDI redox active site mutants against ALS-associated proteins, SOD1, TDP-43 and FUS, is shown in Table 5.4. The CPHC active site mutant, with proposed oxidase activity, is protective against all cellular pathogenic mechanisms induced by mutant forms of SOD1, TDP-43 and FUS.

TABLE 5.4. The protective activities of the PDI redox active site mutants.

SOD1			
	Inclusion formation	**ER stress**	**Apoptosis**
CPHC (oxidase)	✓	✓	✓
CPYC (isomerase)	✗	✓	✗
CGPC (reductase)	✓	✓	✗
TDP-43			
	TDP-43 mislocalisation		**ER stress**
CPHC (oxidase)	✓		✓
CPYC (isomerase)	✓		✗
CGPC (reductase)	✗		✗
FUS			
	FUS mislocalisation		**ER stress**
CPHC (oxidase)	✓		✓
CPYC (isomerase)	✗		✓
CGPC (reductase)	✗		✓

The cis-proline loop mutants of PDI

The second half of this chapter focuses on studies involving a second set of PDI mutants, whereby the cis-proline loops of PDI were mutated to either GIP or GTP in the *a* domain, or SIP or STP in the *a'* domain. The rationale for this was based on previous studies of Dsb proteins which demonstrated that mutating the residue preceding the cis-proline in the cis-proline loop altered the redox potential of these proteins [492] Hence, it was postulated that a point mutation in the residue preceding the proline in the cis-proline loop of PDI would alter the redox potential of the *a* and *a'* domains, to be either more oxidising by substituting the residue for a threonine (mutants GTP and STP), or more reducing by substituting this residue to a isoleucine (mutants GIP and SIP). The roGFP expression assay demonstrated that there were no differences in oxidation levels between wildtype PDI and the cis-proline loop mutants, however, this could be due to the sensitivity of the assay utilised. The redox potential of these mutants was unable to be measured due to time constraints, however the experiments were performed anyway to investigate the role of the mutations. The activity of the cis-proline loop mutants was analysed in cells expressing mutant ALS proteins, SOD1, TDP-43 and FUS.

5.3.20 The localisation of the PDI cis-proline loop mutants in Neuro-2A cells

To ensure that mutations in the cis-proline loop did not alter the location of PDI, the localisation of the V5-tagged mutants was analysed using confocal microscopy in Neuro-2A cells. Cells were transfected with either the GIP, GTP, SIP or STP cis-proline loop mutants for 24 h before immunocytochemistry was performed, using an anti-V5 tag antibody to visualise the PDI mutants, and an anti-calreticulin antibody to probe for the ER-resident protein, calreticulin. These results illustrated that all four cis-proline loop mutants co-

localised with calreticulin in all transfected cells examined, indicating that mutations in PDI's

cis-proline loop did not alter PDI's ER localisation (Figure 5.24).
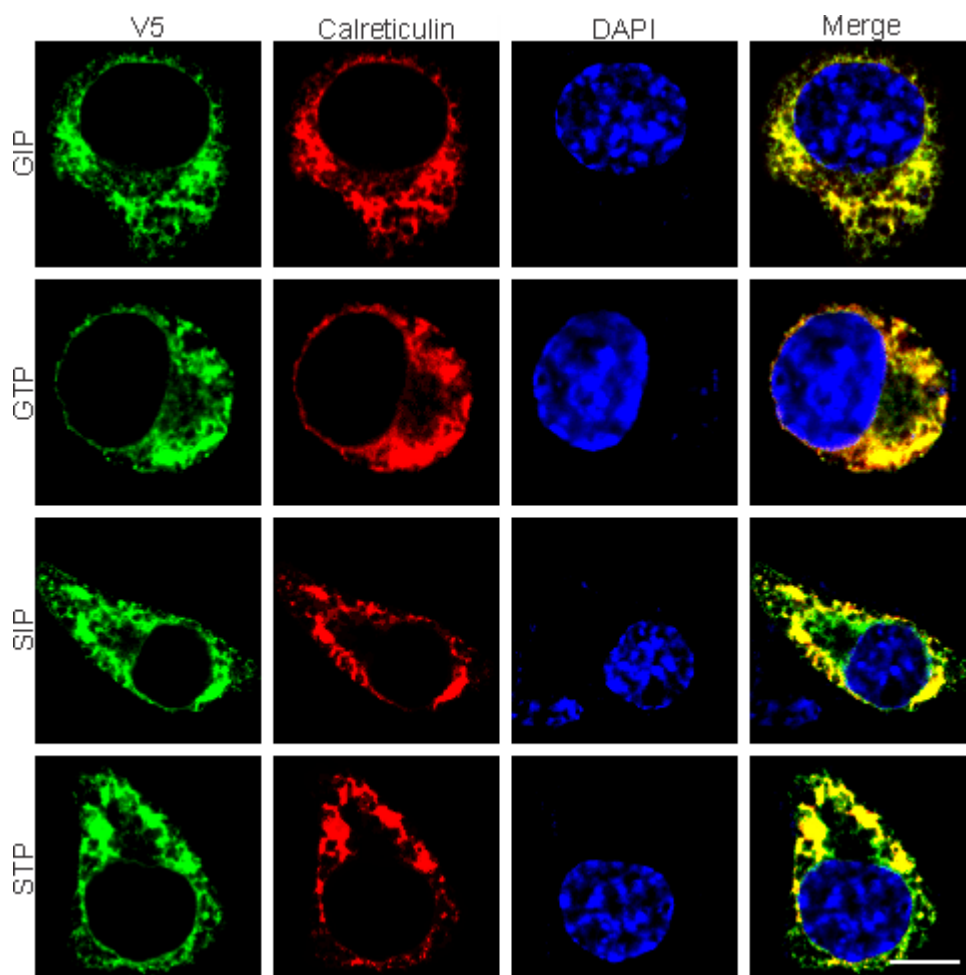
Figure 5.24: The PDI cis-proline loop mutants are localised in the ER of Neuro-2A cells.

Neuro-2A cells were transfected with either the V5-tagged GIP, GTP, SIP or STP cis-proline

loop mutant (left column; V5). At 24 h post-transfection, immunocytochemistry was

performed using antibodies for the V5 tag and calreticulin (second column; Calreticulin) and

the nuclei were stained with Hoechst (third column; DAPI). The yellow in the merge column

(last column; Merge) illustrates co-localisation of the mutants and calreticulin, indicating that

the PDI cis-proline loop mutants are localised within the ER of Neuro-2A cells. Scale bar =

20 μM.

Examining the protective effect of the PDI cis-proline loop mutants in cells expressing mutant SOD1

The PDI cis-proline loop mutants were first analysed in Neuro-2A cells expressing mutant SOD1 A4V. Their protective activities against SOD1 inclusion formation, mutant SOD1-induced ER stress and apoptosis, were investigated in the following experiments.

5.3.21 Cis-proline loop mutants are co-expressed in almost all cells transfected with SOD1

Firstly, the co-transfection efficiency of the cis-proline loop PDI mutants and SOD1 was examined. Cells were transfected with EGFP-SOD1 and either the GIP, GTP, SIP or STP cis-proline loop mutants for 72 h, before fixing and performing immunocytochemistry with an anti-V5 antibody, and DAPI-staining with Hoechst to visualise the nuclei. Co-transfection was verified by examining EGFP expression for mutant SOD1 and immunocytochemistry was performed with an Alexa Fluor 568-tagged secondary antibody to detect the V5 tag of the PDI mutants (Figure 5.25). The overall transfection efficiency of mutant SOD1 in Neuro-2A cells was approximately 75-80% when observed 72 h post-transfection. Fluorescent microscopy was utilised in three replicate experiments to observe at least 100 SOD1-expressing cells for co-expression with the cis-proline loop mutants. Quantification revealed that 95% of mutant SOD1 transfected cells also co-expressed GIP, 93% also co-expressed GTP, 97% also co-expressed SIP, and 97% also co-expressed STP. Therefore, in all further experiments where SOD1 and the cis-proline mutants were co-transfected and immunocytochemistry with an anti-V5 antibody was not performed, it was assumed that the observation of SOD1 expression illustrated co-expression of both SOD1 and the cis-proline loop mutants.
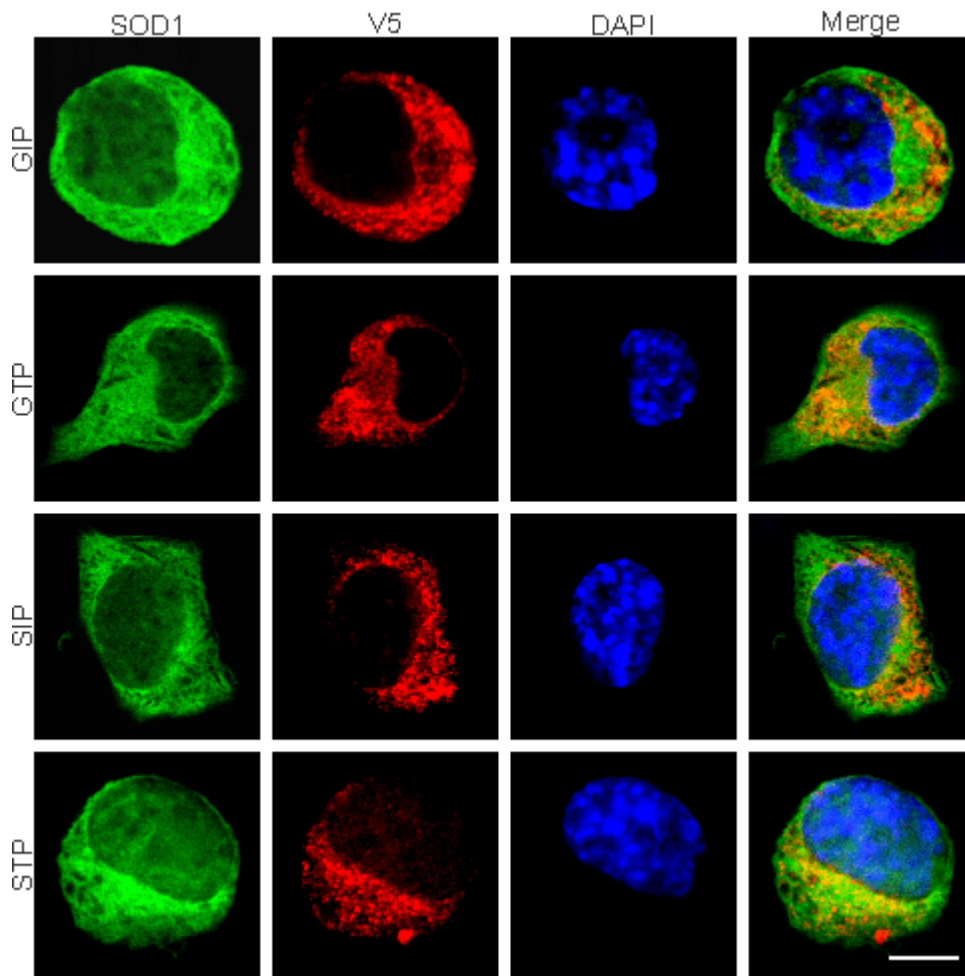
Figure 5.25: The PDI cis-proline loop mutants are co-expressed in almost all Neuro-2A cells co-transfected with EGFP-SOD1. Neuro-2A cells were transfected with EGFP-SOD1 (left column; SOD1) and either the GIP, GTP, SIP or STP cis-proline loop mutants (second column; V5) for 72 h. Immunocytochemistry was performed using an anti-V5 antibody, and nuclei were stained with Hoechst (third column; DAPI). The merge column depicts co-expression of the cis-proline loop mutants with SOD1 in the shown cells. Scale bar = 20 µM.

5.3.22 Expression of SOD1 and cis-proline loop mutants in Neuro-2A cells

Once the localisation and expression of the cis-proline loop mutants was established in Neuro-2A cells, Western blotting analysis was performed to ensure that the transfection of each protein resulted in similar levels of expression and to verify that the expressed proteins were of expected size (Figure 5.26). Cell lysates were prepared from the following populations; GFP alone, wildtype SOD1 co-expressed with empty vector pcDNA3.1, and mutant SOD1 A4V with either pcDNA3.1, wildtype PDI, GIP, GTP, SIP or STP cis-proline loop mutants. Western blotting revealed that wildtype and mutant EGFP-SOD1 proteins were expressed at the expected size of 50 kDa, and GFP alone was expressed at 26 kDa, using an anti-GFP antibody. Wildtype SOD1 was expressed at higher levels compared to mutant SOD1 A4V, as expected. Wildtype PDI and the PDI cis-proline loop mutants were detected at similar levels at approximately 62 kDa, using an anti-V5 antibody. β-actin was detected at 40 kDa using an anti-β-actin antibody, which was used as a loading control.

A
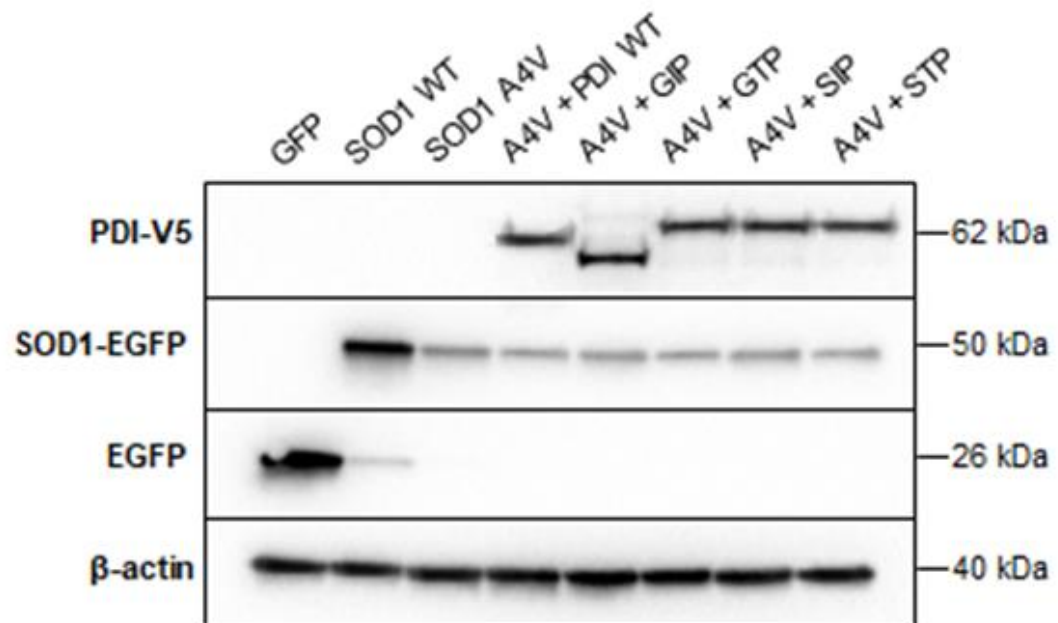
B
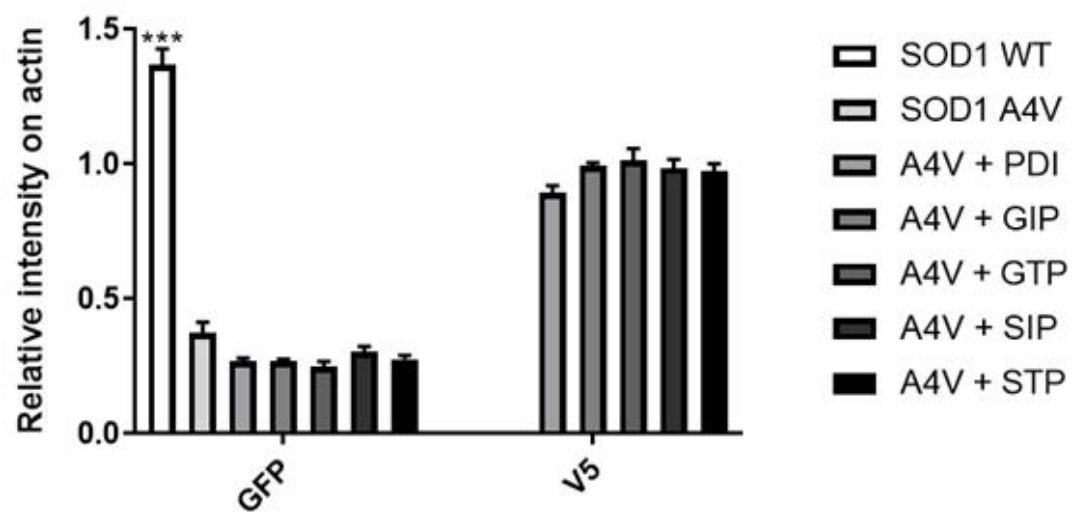
Figure 5.26: Protein expression of wildtype PDI, the PDI cis-proline loop mutants and EGFP-SOD1 proteins in Neuro-2A cells. A) Western blotting analysis was performed to ensure that the levels of protein expression were similar between groups and to confirm that proteins were expressed at their expected MW. Cell lysates observed were GFP alone, wildtype SOD1 co-expressed with empty pcDNA3.1 vector, and mutant SOD1 A4V co-expressed with either pcDNA3.1, wildtype PDI, or the GIP, GTP, SIP or STP cis-proline loop mutants. Wildtype PDI and the GTP, SIP or STP cis-proline loop mutants were detected at 62 kDa, whereas GIP was expressed at around 60 kDa. Wildtype SOD1 and mutant SOD1 A4V were expressed at 50 kDa and GFP alone was detected at 26 kDa. The loading control, β-actin, was detected at 40 kDa. **B)** Quantification revealed that wildtype SOD1 was expressed at significantly higher ($p < 0.001$) levels, compared to mutant SOD1 A4V. Mutant SOD1 A4V was expressed similarly across all cell lysate populations. Wildtype PDI and the cis-proline loop mutants also shared similar expression levels. Lysates expressing GFP only were not included in quantification. N=3, Mean ± SEM, *** $p < 0.001$.

5.3.23 The GTP, SIP and STP cis-proline loop mutants prevent SOD1 inclusion formation in Neuro-2A cells

The results obtained investigating the activity of the redox active site mutants on SOD1 inclusion formation demonstrated that both PDI's oxidase and reductase activity inhibit the formation of inclusions. The protective activities of the PDI cis-proline loop mutants were next analysed, to determine whether alterations in the redox potential through modifications to these regions in either the *a* or *a'* domain, also impact on PDI's protective activity against SOD1 aggregation. Neuro-2A cells were transfected with empty pcDNA3.1 vector, GFP, wildtype SOD1 with pcDNA3.1, and mutant SOD1 A4V with either pcDNA3.1, wildtype PDI or the GIP, GTP, SIP or STP cis-proline loop mutants for 72 h. Immunocytochemistry was performed using an anti-V5 antibody to detect expression of PDI proteins, and cells were stained with Hoechst to visualise the nuclei. Fluorescent microscopy was utilised to quantify at least 100 co-transfected cells for the presence of SOD1 inclusions (Figure 5.27 A).

As expected, no inclusions were formed in untransfected cells or control cells expressing, empty pcDNA3.1 vector, GFP only, or wildtype SOD1. However, in contrast, inclusions were detected in 23.0% ± 1.5 of cells co-expressing mutant SOD1 A4V with empty pcDNA3.1 vector. A significant decrease in the proportion of cells with inclusions ($p < 0.001$) was observed when wildtype PDI was co-expressed with mutant SOD1 A4V (10.3% ± 1.3), compared to cells co-expressing mutant SOD1 A4V with empty pcDNA3.1 vector. Similarly, there was also a significant reduction ($p < 0.001$) in the proportion of cells displaying SOD1 inclusions when mutant SOD1 A4V was co-expressed with either the GTP (11.7% ± 1.5), SIP (10.7% ± 2.7) or the STP (9.7% ± 2.0) cis-proline loop mutants. In contrast however, there was no change in the proportion of cells forming inclusions when SOD1 A4V was co-expressed the GIP cis-proline loop mutant (18.0% ± 1.2), compared to cells co-expressing mutant SOD1 A4V and pcDNA3.1. Moreover, significantly more ($p <$

0.05) cells co-expressing SOD1 A4V and the GIP cis-proline loop mutant displayed inclusions, compared to cells co-expressing SOD1 A4V and wildtype PDI (Figure 5.27 B). Hence the GTP, SIP or STP cis-proline loop mutants, but not the GIP mutant, are protective against mutant SOD1 inclusion formation. These results therefore demonstrate that rendering the cis-proline loop in the *a* domain to become more oxidising (GTP) retains its protective activity against mutant SOD1 inclusion formation, whereas altering it to become more reducing (GIP) inhibits this protective activity. Interestingly, modifying the cis-proline loop in the *a'* domain, to render it either more oxidising (STP) or more reducing (SIP), does not alter PDI's protective function. This suggests that the activity of the *a* domain is imperative for the protective function of PDI, rather than the *a'* domain.

A

B

391
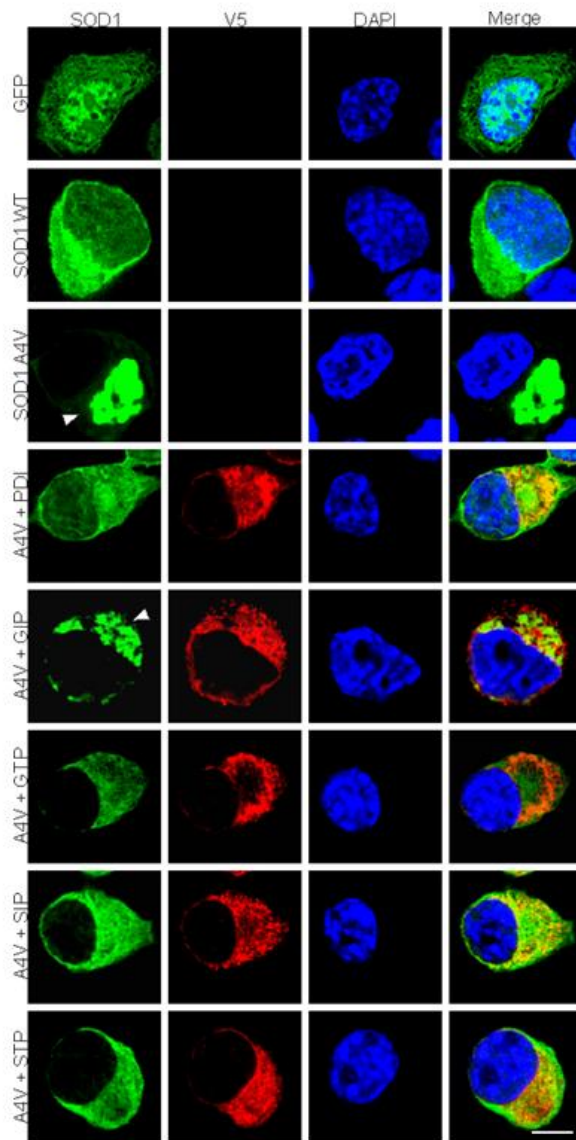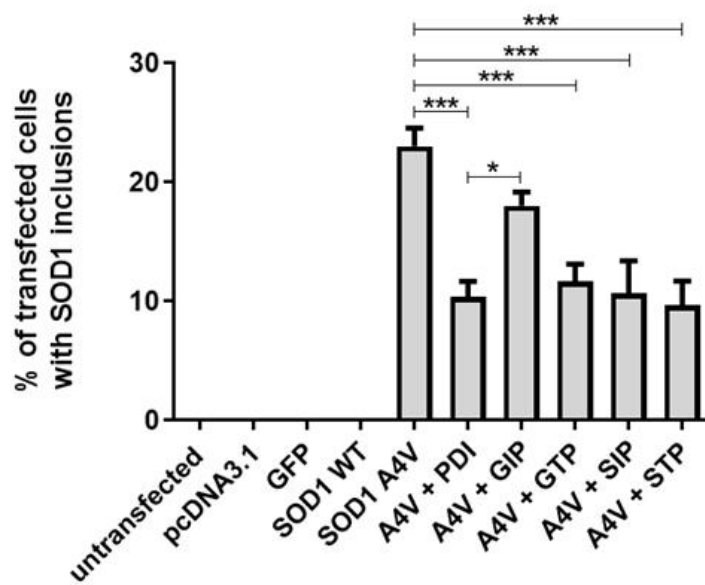
Figure 5.27: The GTP, SIP and STP cis-proline loop mutants inhibit SOD1 inclusion formation in Neuro-2A cells. A) Immunofluorescence images of Neuro-2A cells expressing GFP, wildtype SOD1 with empty pcDNA3.1 vector, or mutant SOD1 A4V with either pcDNA3.1, PDI or the GIP, GTP, SIP or STP cis-proline loop mutants. Cells expressing either GFP (first panel; GFP) or wildtype SOD1 with pcDNA3.1 (second panel; SOD1 WT) do not form SOD1 inclusions. In contrast, more cells expressing mutant SOD1 A4V with pcDNA3.1 (third panel; SOD1 A4V) form SOD1 inclusions, as indicated by the white arrowhead (third panel, first column). However, fewer mutant SOD1 A4V cells form SOD1 inclusions when co-expressed with either wildtype PDI (fourth panel; A4V + PDI), or the GTP, SIP or STP cis-proline loop mutants (panels six to eight; A4V + GTP, A4V + SIP, A4V + STP). In contrast, more cells co-expressing mutant SOD1 A4V and the GIP cis-proline loop mutant exhibited SOD1 inclusions (fifth panel; A4V + GIP), as indicated by the white arrowhead (fifth panel, first column). Scale bar = 20 µM. **B)** Quantification of the cells in A) forming SOD1 inclusions. Control cells expressing GFP only or wildtype SOD1 did not form inclusions, however significantly more cells expressing mutant SOD1 A4V formed SOD1 inclusions, as expected. A significant reduction ($p < 0.001$) in the proportion of cells displaying SOD1 inclusions was observed when mutant SOD1 A4V was co-expressed with either wildtype PDI, or the GTP, SIP or STP cis-proline loop mutants, but not the GIP mutant. Significantly more ($p < 0.05$) cells formed SOD1 inclusions when the GIP cis-proline loop mutant was co-expressed with mutant SOD1 A4V, compared to when wildtype PDI was co-expressed with SOD1 A4V. N=3, Mean ± SEM, * $p < 0.05$, *** $p < 0.001$.

5.3.24 The GTP, SIP and STP cis-proline loop mutants are protective against ER stress induced by mutant SOD1 in Neuro-2A cells

All three redox active site mutants of PDI (predicted oxidase, reductase and isomerase activities) were protective against mutant SOD1-induced ER stress. Therefore, it was next examined whether changes in redox potential modulated by the cis-proline loop mutants alters the protective activity of PDI. Neuro-2A cells were transfected with empty pcDNA3.1 vector, GFP, wildtype SOD1 with pcDNA3.1, and mutant SOD1 A4V with either pcDNA3.1, wildtype PDI or the GIP, GTP, SIP or STP cis-proline loop mutants for 72 h. After fixing, immunocytochemistry was performed using an anti-CHOP antibody to examine nuclear immunoreactivity, indicative of its activation. DAPI-staining with Hoechst was also performed to visualise the nuclei and fluorescent microscopy was utilised to determine the proportion of cells with CHOP activation, and thus, induction of pro-apoptotic ER stress signalling (Figure 5.28 A).

Very few untransfected cells, or cells expressing empty pcDNA3,1 vector, GFP or wildtype SOD1 displayed nuclear immunoreactivity to CHOP, signifying low levels of ER stress in these cells. A significantly greater ($p < 0.001$) proportion of cells co-expressing mutant SOD1 A4V with pcDNA3.1 were undergoing ER stress, indicated by CHOP activation ($30.0\% \pm 1.5$), compared to cells expressing wildtype SOD1 and pcDNA3.1 ($7.7\% \pm 0.3$). However, the proportion of cells displaying CHOP activation was significantly decreased ($p < 0.001$) when either PDI ($17.7\% \pm 0.9$), the GTP ($16.7\% \pm 0.3$), SIP ($14.7\% \pm 0.9$), or STP ($18.0\% \pm 1.2$) cis-proline loop mutants were co-expressed with mutant SOD1 A4V. In contrast, differences in the proportion of cells with CHOP activation was observed when the GIP cis-proline loop mutant was co-expressed with mutant SOD1 A4V ($26.0\% \pm 3.5$), compared to cells co-expressing mutant SOD1 with empty vector. Furthermore, there was a significant difference ($p < 0.05$) in the proportion of these cells with CHOP activation compared to cells

co-expressing wildtype PDI and mutant SOD1 A4V (Figure 5.28 B). These results demonstrate that, similar to the results obtained for inclusion formation, a more oxidising (GTP) cis-proline loop in the *a* domain retains PDI's protective activity against ER stress, whilst a more reducing (GIP) cis-proline loop in the *a* domain results in a loss of this protective activity. In contrast, changes to the cis-proline loop in the *a'* domain, either more oxidising (STP) or reducing (SIP), do not alter PDI's capability to inhibit induction of ER stress in mutant SOD1 expressing cells.

A
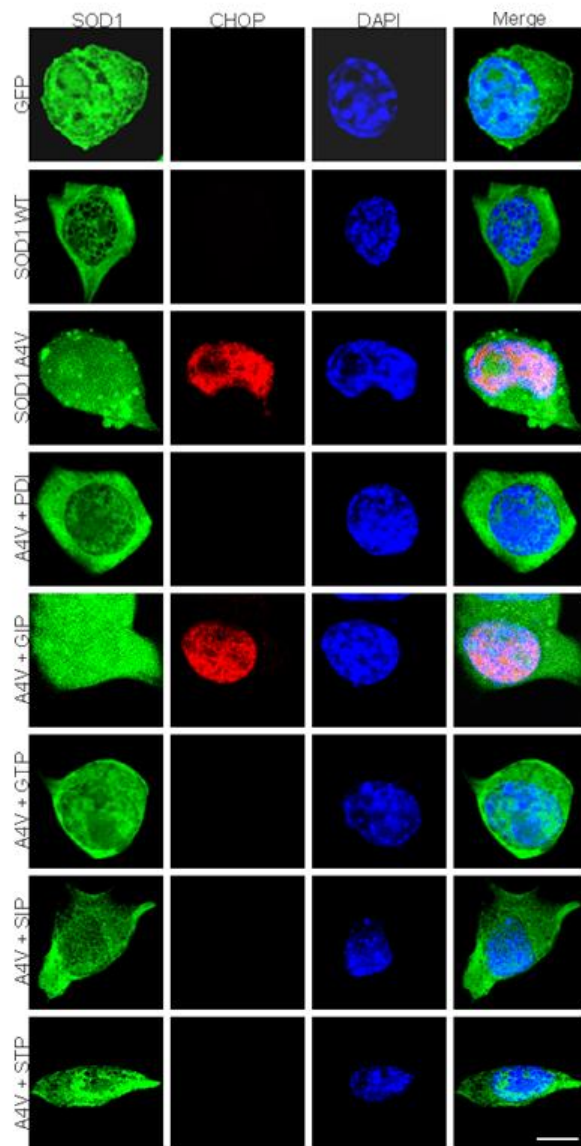
B
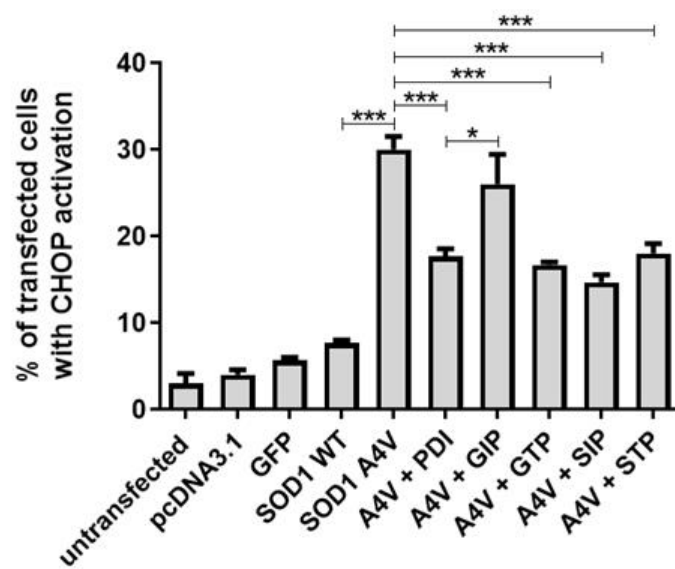
Figure 5.28: The GTP, SIP and STP cis-proline loop mutants are protective against ER stress induced by mutant SOD1 in Neuro-2A cells. A) Immunofluorescence images of Neuro-2A cells expressing GFP, wildtype SOD1 with empty pcDNA3.1 vector, or mutant SOD1 A4V with either pcDNA3.1, PDI, or the GIP, GTP, SIP or STP cis-proline loop mutants. Few cells expressing GFP (first panel; GFP) or wildtype SOD1 (second panel; SOD1 WT) were undergoing ER stress, indicated by nuclear immunoreactivity to CHOP, whereas a greater proportion of cells expressing mutant SOD1 A4V (third panel; SOD1 A4V) displayed CHOP activation (third panel, column two). The proportion of cells with CHOP activation did not alter when the GIP cis-proline loop mutant was co-expressed with mutant SOD1 A4V (fifth panel; A4V + GIP). However, when wildtype PDI (fourth panel; A4V + PDI) or the GTP, SIP or STP cis-proline loop mutants (panels six to eight; A4V + GTP, A4V + SIP, A4V + STP) were co-expressed with mutant SOD1 A4V, fewer cells displayed CHOP activation. Scale bar = 20 µM. **B)** Quantification of the proportion of cells with CHOP activation in A). A significant increase ($p < 0.001$) in the proportion of mutant SOD1 A4V expressing cells with CHOP activation was observed, compared to wildtype SOD1 expressing cells, as expected. However, this proportion of cells with CHOP activation was significantly reduced ($p < 0.001$) when either PDI, or the GTP, SIP or STP cis-proline loop mutants, were co-expressed with mutant SOD1 A4V. Significantly more cells ($p < 0.05$) co-expressing mutant SOD1 A4V and the GIP cis-proline loop mutant displayed CHOP activation compared to cells co-expressing mutant SOD1 A4V and wildtype PDI. N=3, Mean ± SEM, * $p < 0.05$, *** $p < 0.001$.

5.3.25 The GTP, SIP and STP cis-proline loop mutants inhibit induction of apoptosis induced by mutant SOD1 in Neuro-2A cells

As the results above indicated that the GTP, SIP and STP cis-proline loop mutants were capable of inhibiting ER stressed induced apoptotic signalling, it was next hypothesised that these mutants would be able to inhibit apoptotic cell death, whereas the GIP cis-proline loop mutant would not. Hence, it was next examined whether the overexpression of the cis-proline loop mutants were protective against apoptosis induced by mutant SOD1.

Neuro-2A cells were transfected with empty pcDNA3.1 vector, GFP, wildtype SOD1 with pcDNA3.1, and mutant SOD1 A4V with either pcDNA3.1, wildtype PDI or the GIP, GTP, SIP or STP cis-proline loop mutants for 72 h. Immunocytochemistry was performed after fixing, using an anti-V5 antibody to detect expression of PDI and the cis-proline loop mutants. DAPI-staining was performed using Hoechst, as the presence of apoptotic nuclei was used as a maker for cell apoptosis. Irregular, condensed or fragmented nuclei was considered apoptotic and these were examined utilising fluorescent microscopy (Figure 5.29 A).

Apoptotic nuclei were rarely observed in untransfected cells or cells expressing empty pcDNA3.1 vector or GFP (less than 5%), and cells expressing wildtype SOD1 only displayed apoptotic nuclei in 2.0% $\pm$ 0.6 of cells. There was a significant increase ($p < 0.001$) in the proportion of cells with apoptotic nuclei in populations co-expressing mutant SOD1 A4V with empty pcDNA3.1 vector (12.0% $\pm$ 0.6), compared to those expressing wildtype SOD1 with empty pcDNA3.1 vector. However, significantly fewer cells bearing apoptotic nuclei were observed in populations co-expressing mutant SOD1 A4V with either wildtype PDI ($p < 0.01$, 5.3% $\pm$ 1.5), or the GTP ($p < 0.05$, 6.0% $\pm$ 0.6), SIP ($p < 0.05$, 6.3% $\pm$ 1.3) or STP ($p < 0.01$, 5.3% $\pm$ 0.3) cis-proline loop mutants. There was no significant decrease in the

proportion of cells co-expressing mutant SOD1 A4V with the GIP cis-proline loop mutant, displaying apoptotic nuclei (9.0% ± 1.0) compared to cells expressing mutant SOD1 A4V with empty pcDNA3.1 vector (Figure 5.29 B). These results demonstrate that a more reducing cis-proline loop in the *a* domain (GIP) ensues a loss of protective activity of PDI, whereas a more oxidising cis-proline loop (GTP) retains this activity. Moreover, altering the *a'* domain active site to be either more oxidising (STP) or more reducing (SIP) does not alter PDI's protective activity against mutant SOD1 induced apoptosis.

A
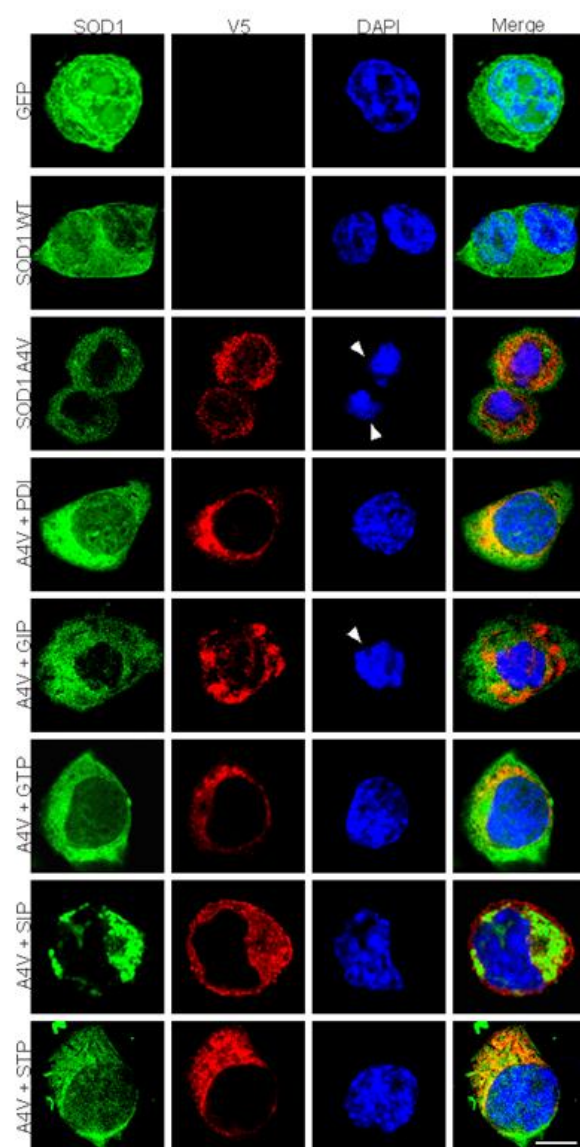
B
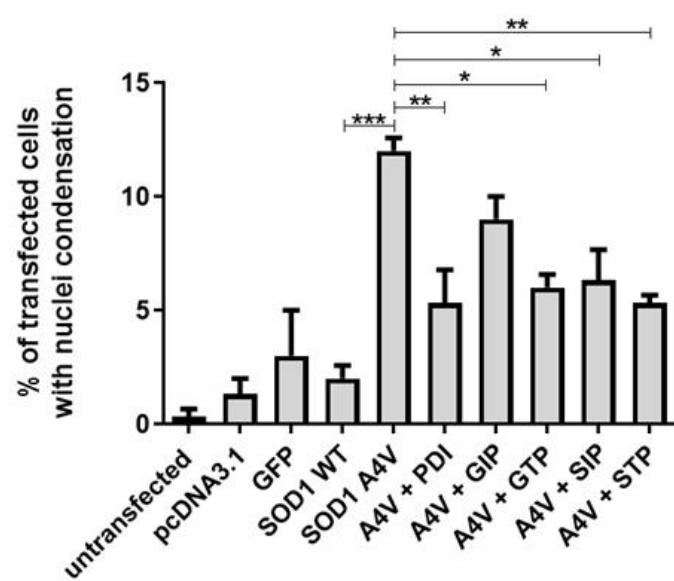
Figure 5.29: The GTP, SIP and STP cis-proline loop mutants inhibit apoptosis induced by mutant SOD1 in Neuro-2A cells. A) Immunofluorescence images of Neuro-2A cells expressing GFP, wildtype SOD1, or mutant SOD1 A4V with either empty pcDNA3.1 vector, PDI, or the GIP, GTP, SIP or STP cis-proline loop mutants. Cells expressing GFP or wildtype SOD1 rarely present with apoptotic nuclei (first and second panels; GFP, SOD1 WT), however, apoptotic nuclei were more common in cells expressing mutant SOD1 A4V (third panel; SOD1 A4V), as indicated by the white arrowhead, pointing to condensed nuclei (third panel, column three). The proportion of cells with apoptotic nuclei was reduced when PDI (fourth panel; A4V + PDI) or the GTP, SIP or STP cis-proline loop mutants were co-expressed with mutant SOD1 A4V (panels six to eight; A4V + GTP, A4V + SIP, A4V + STP). In contrast, more cells co-expressing the GIP cis-proline loop and SOD1 A4V (fifth panel; A4V + GIP) display apoptotic nuclei, as indicated by the white arrowhead (fifth panel, column three). Scale bar = 20 µM. **B)** Quantification of cells displaying apoptotic nuclei in A). There was a significant increase ($p < 0.001$) in the proportion of cells with apoptotic nuclei in mutant SOD1 A4V populations, compared to populations expressing wildtype SOD1. A significant decrease in the proportion of cells with apoptotic nuclei was observed when mutant SOD1 A4V was co-expressed with wildtype PDI ($p < 0.01$), the GTP cis-proline loop mutant ($p < 0.05$), SIP cis-proline loop mutant ($p < 0.05$) or the STP cis-proline loop mutant ($p < 0.01$). N=3, Mean ± SEM, * $p < 0.05$, ** $p < 0.01$, *** $p < 0.001$.

Examining the protective effect of the PDI cis-proline loop mutants in cells expressing

mutant TDP-43

The protective activities of the PDI cis-proline loop mutants were next analysed in Neuro-2A cells expressing mutant TDP-43 Q331K. Their activity against TDP-43 mislocalisation to the cytoplasm and mutant TDP-43-induced ER stress was investigated in the following experiments.

5.3.26 Cis-proline loop mutants are co-expressed in almost all cells transfected with TDP-43

First, the co-transfection efficiency of the PDI cis-proline loop mutants and TDP-43 was investigated in Neuro-2A cells. Cells were transfected with mutant EGFP-TDP-43 and either the GIP, GTP, SIP, or STP cis-proline loop mutants for 18 h, before immunocytochemistry was performed using an anti-V5 antibody, and cells were stained with Hoechst to visualise the nuclei. Co-transfection was confirmed by examining EGFP expression for TDP-43 and performing immunocytochemistry with an Alexa Fluor 568-tagged secondary antibody to detect the V5 tags for the cis-proline loop mutants (Figure 5.30). The overall transfection efficiency of TDP-43 was approximately 70-75% in Neuro-2A cells when examined 18 h post-transfection. Fluorescent microscopy allowed the visualisation of at least 100 mutant TDP-43 expressing cells, and for each of the three replicate experiments performed, these cells were further analysed for co-expression with the cis-proline loop mutants. Quantification revealed that approximately 97% of cells expressing mutant TDP-43 also co-expressed GIP, 94% also co-expressed GTP, 98% also co-expressed SIP, and 97% also co-expressed STP. Therefore, in further experiments where TDP-43 and the cis-proline loops were co-transfected and immunocytochemistry using a V5 antibody was not performed, it

was assumed that TDP-43 expression also reflected co-expression with either the GIP, GTP, SIP or STP cis-proline loop mutants.
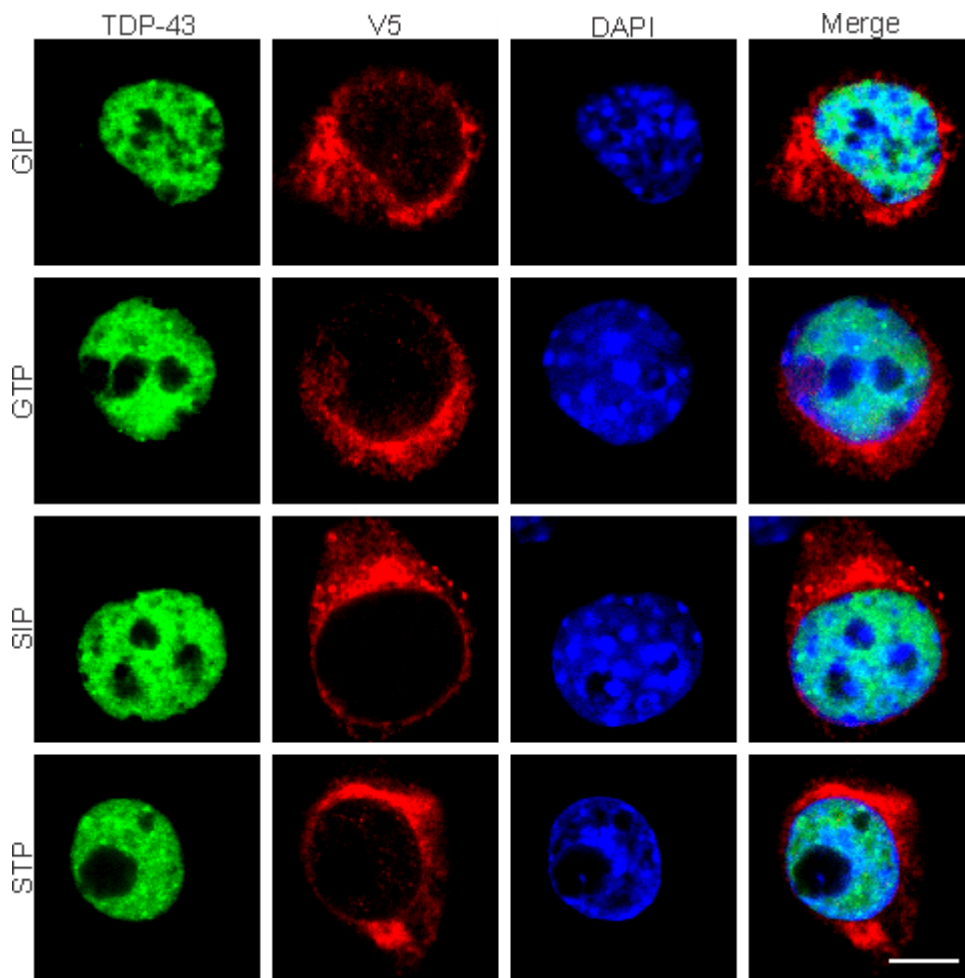
Figure 5.30: The PDI cis-proline loops are co-expressed in almost all Neuro-2A cells co-transfected with EGFP-TDP-43. Neuro-2A cells were transfected with EGFP-TDP-43 (left column; TDP-43) and either the GIP, GTP, SIP or STP cis-proline loop mutants (second column; V5) for 18 h. Cells were fixed, immunocytochemistry was performed using an anti-V5 antibody, and the nuclei were stained with Hoechst (third column; DAPI). The merge column demonstrates co-expression of the cis-proline loop mutants and TDP-43 in the shown cells. Scale bar = 20 µM.

5.3.27 Expression of TDP-43 and cis-proline loop mutants in Neuro-2A cells

Once localisation and co-expression of the cis-proline loop mutants with TDP-43 was established in Neuro-2A cells, Western blotting analysis was performed to ensure that the transfection of each protein resulted in similar levels of expression and that the expressed proteins were of the expected size (Figure 5.31). Cell lysates were prepared from the following cell populations; GFP alone, wildtype TDP-43 co-expressed with empty vector pcDNA3.1, and mutant TDP-43 Q331K with either pcDNA3.1, wildtype PDI, GIP, GTP, SIP or STP cis-proline loop mutants. Immunoblotting revealed that wildtype and mutant EGFP-TDP-43 were expressed at 64 kDa, as expected, with similar expression levels across all cell lysate populations, and GFP was expressed at 26 kDa, using an anti-GFP antibody. Wildtype PDI and the PDI cis-proline loop mutants were detected in transfected cell lysates using an anti-V5 antibody at approximately 62 kDa. The loading control, β-actin, was detected using an anti-β-actin antibody at 40 kDa.

A
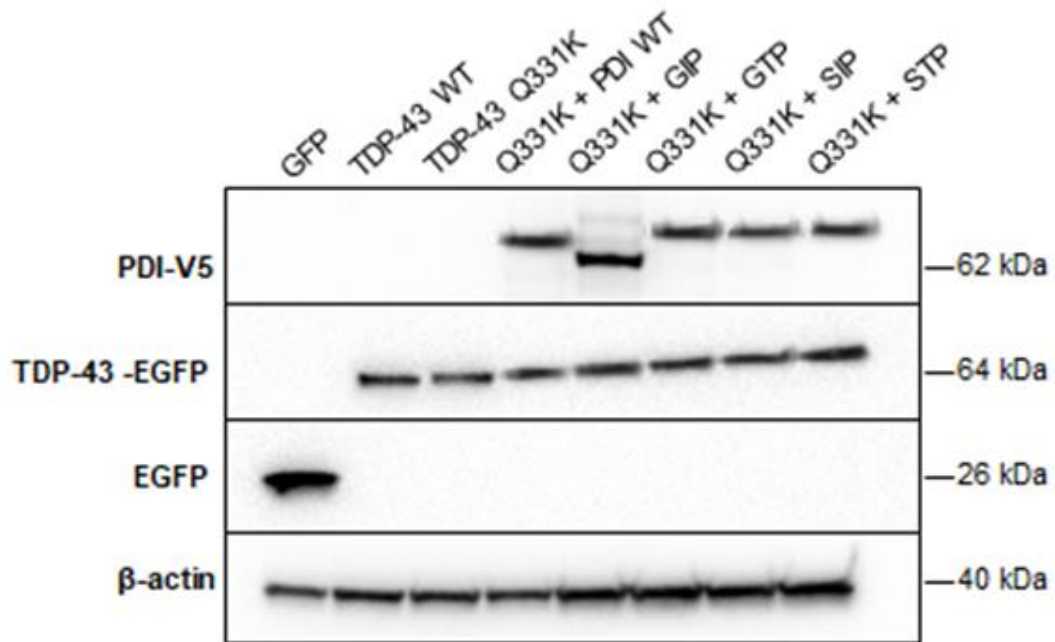
B
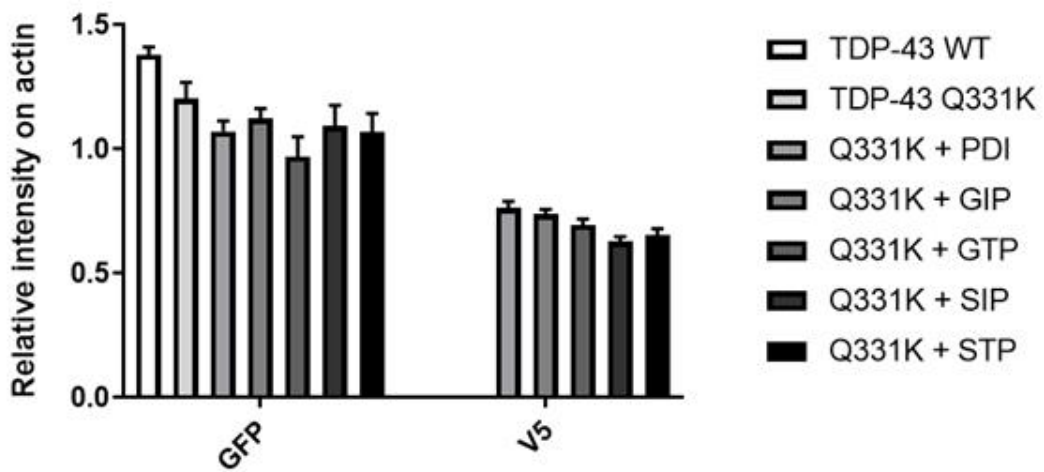
Figure 5.31: Protein expression of wildtype PDI, the PDI cis-proline loop mutants and EGFP-TDP-43 proteins in Neuro-2A cells. A) Western blotting of cell lysates was performed and quantified to ensure that the proteins expressed were of similar expression levels between groups and that each was at expressed at the expected MW. Cell lysates examined were GFP alone, wildtype TDP-43 with empty pcDNA3.1 vector, and mutant TDP-43 Q331K with either pcDNA3.1, wildtype PDI, or the GIP, GTP, SIP or STP cis-proline loop mutants. Wildtype TDP-43 and mutant TDP-43 Q331K were detected at 64 kDa, whereas GFP alone was detected at 26 kDa. Wildtype PDI and the GTP, SIP and STP cis-proline loop mutants were expressed at 62 kDa, however the GIP cis-proline loop mutant was expressed at 60 kDa. β-actin was detected at 40 kDa. **B)** Quantification revealed similar expression levels between wildtype TDP-43 and mutant TDP-43 Q331K between all cell lysate populations. Likewise, PDI and the cis-proline loop mutants shared similar levels of expression also. Lysates expressing GFP only were not included in quantification. N =3, Mean ± SEM.

5.3.28 The GTP, SIP and STP cis-proline loop mutants are protective against mutant TDP-43 mislocalisation to the cytoplasm

The results described in section 5.3.13 demonstrated that the oxidase and isomerase active site mutants (CPHC and CPYC, respectively) were protective against mutant TDP-43 mislocalisation to the cytoplasm, however the reductase active site mutant (CGPC) was not. Hence, it was next examined whether the *a* and *a'* domain cis-proline loops mutations alter PDI's ability to prevent mislocalisation to the cytoplasm in Neuro-2A cells expressing mutant TDP-43.

Neuro-2A cells were transfected with empty pcDNA3.1 vector, GFP, wildtype TDP-43 with pcDNA3.1, and mutant TDP-43 Q331K with either pcDNA3.1, wildtype PDI or the GIP, GTP, SIP or STP cis-proline loop mutants for 18 h. After fixing, DAPI-staining was performed using Hoechst to visualise the nuclei. Immunocytochemistry was not performed as it was assumed that detection of TDP-43 expression reflected co-expression with the V5-tagged proteins, as described above. The cellular localisation of TDP-43 was analysed using fluorescent microscopy. TDP-43 was considered to be nuclear when it completely localised in the DAPI-stained nucleus. In contrast, TDP-43 was considered to be cytoplasmic when fluorescence was detected in both the nucleus and the cytoplasm of TDP-43 expressing cells (Figure 5.32 A).

Wildtype TDP-43 was mislocalised to the cytoplasm in 2.3% ± 0.9 transfected cells. In contrast, there was a significant increase ($p < 0.001$) in the proportion of cells with TDP-43 mislocalisation to the cytoplasm in cells expressing mutant TDP-43 Q331K with empty pcDNA3.1 vector (23.3% ± 1.8). However, co-expression of mutant TDP-43 Q331K with either wildtype PDI (11.3% ± 2.7), or the GTP (11.0% ± 3.0), SIP (11.3% ± 1.3) or STP (11.3% ± 3.5) cis-proline loop mutants, resulted in a significant decrease ($p < 0.05$) in the

proportion of cells with mutant TDP-43 mislocalisation to the cytoplasm. Conversely, co-expression of mutant TDP-43 Q331K with the GIP cis-proline loop mutant (19.3% ± 2.9) did not reduce the proportion of cells with cytoplasmic TDP-43, compared to cells co-expressing mutant TDP-43 Q331K with empty vector (Figure 5.32 B). These results demonstrate that the predicted, more oxidising cis-proline loop in the *a* domain retains PDI's protective activity, however, the predicted more reducing cis-proline loop, results in a loss of protective activity. However, the more oxidising or reducing cis-proline loop in the *a'* domain of PDI does not alter PDI's protective activity.

A

	TDP-43	DAPI	Merge
TDP-43 WT			
TDP-43 Q331K			
Q331K + PDI			
Q331K + GIP			
Q331K + GTP			
Q331K + SIP			
Q331K + STP			
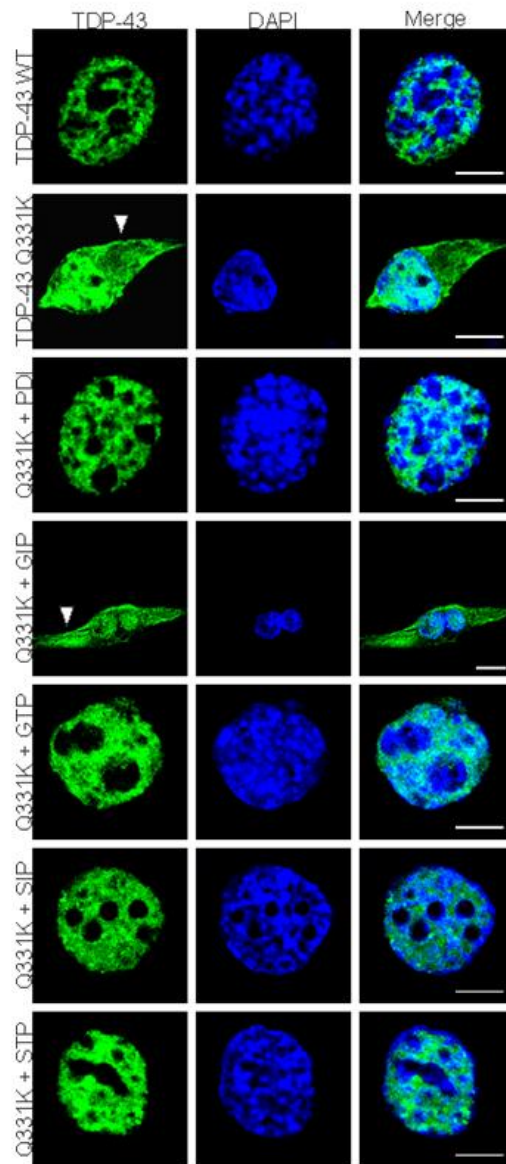
B
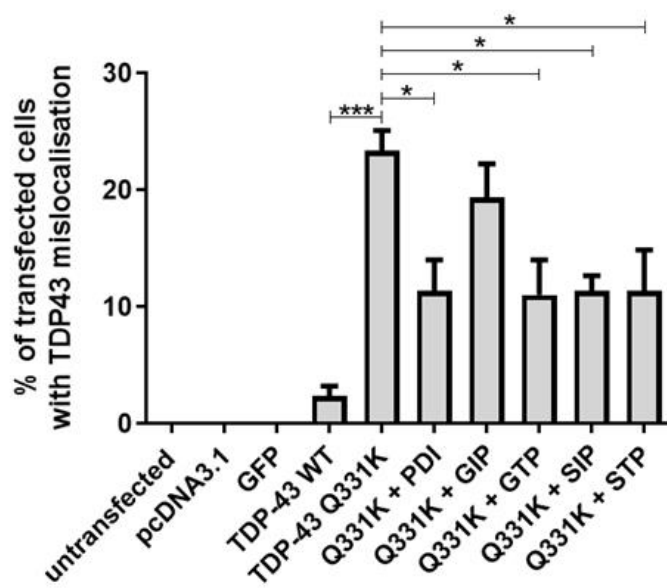
Figure 5.32: The GTP, SIP and STP cis-proline loop mutants are protective against mutant TDP-43 mislocalisation to the cytoplasm. A) Immunofluorescence images of Neuro-2A cells expressing wildtype TDP-43 and mutant TDP-43 Q331K with either empty pcDNA3.1 vector, wildtype PDI, or the GIP, GTP, SIP or STP cis-proline loop mutants. In cells expressing wildtype TDP-43 (first panel; TDP-43 WT), TDP-43 is expressed only in the nucleus, with no mislocalisation to the cytoplasm, however, in contrast, more cells expressing mutant TDP-43 Q331K (second panel; TDP-43 Q331K) display mislocalisation to the cytoplasm, as indicated by the white arrowhead (third panel, column one). Co-expression of mutant TDP-43 Q331K with wildtype PDI (third panel; Q331K + PDI) or cis-proline mutants, GTP, SIP or STP (panels five to seven; Q331K + GTP, Q331K + SIP, Q331K + STP), results in fewer cells with cytoplasmic TDP-43 compared to cells expressing mutant TDP-43 Q331K with empty vector. Conversely, co-expression of mutant TDP-43 Q331K with the GIP cis-proline loop mutant (fourth panel; Q331K + GIP) does not change the proportion of cells with cytoplasmic TDP-43, as indicated by the white arrowhead (fourth panel, column one). Scale bar = 20 µM. **B)** Quantification of the cells in A) with TDP-43 mislocalisation to the cytoplasm. A significant increase ($p < 0.001$) in the proportion of cells with TDP-43 mislocalisation was observed in populations co-expressing mutant TDP-43 Q331K with empty pcDNA3.1 vector, compared to cells co-expressing wildtype TDP-43 with empty pcDNA3.1 vector. Significantly fewer ($p < 0.05$) cells displayed TDP-43 mislocalisation to the cytoplasm when mutant TDP-43 Q331K expressing cells also co-expressed wildtype PDI or the GTP, SIP or STP cis-proline loop mutants. N=3, Mean ± SEM, * $p < 0.05$, *** $p < 0.001$.

5.3.29 The GIP, GTP, SIP and STP cis-proline loop mutants are protective against mutant TDP-43 induced ER stress

Previous studies in Chapter 4 demonstrated that the oxidase DsbA was protective against mutant TDP-43 induced ER stress, whilst the isomerase, DsbC, was not. Moreover, earlier in this chapter, in section 5.3.15, it was demonstrated that only the oxidase active site mutant (CPHC) was able to decrease the proportion of cells with ER stress in populations expressing mutant TDP-43. These results suggest that the oxidase activity of PDI is important for its protective activity against mutant TDP-43-induced ER stress. Therefore, it was next examined whether the predicted differences in redox potential in the cis-proline loops of PDI, would also modify its protective activity.

Neuro-2A cells were transfected with empty pcDNA3.1 vector, GFP, wildtype TDP-43 with pcDNA3.1, and mutant TDP-43 Q331K with either pcDNA3.1, wildtype PDI or the GIP, GTP, SIP or STP cis-proline loop mutants for 18 h. After fixing, immunocytochemistry was performed using an anti-CHOP antibody, and cells were stained with Hoechst to visualise the nuclei. Fluorescent microscopy was utilised to analyse at least 100 co-transfected cells for nuclear immunoreactivity to CHOP, indicative of its activation, and thus, induction of ER stress-induced apoptotic signalling (Figure 5.33 A).

Quantification revealed that less than 10% of untransfected cells, or cells expressing either empty pcDNA3.1 vector, GFP or wildtype TDP-43, displayed nuclear immunoreactivity to CHOP. In contrast, a significant increase ($p < 0.001$) in the proportion of cells displaying CHOP activation was observed in populations expressing mutant TDP-43 Q331K ($24.0\% \pm 1.5$), compared to cells expressing wildtype TDP-43 ($8.3\% \pm 1.2$). As expected, there was a significant reduction ($p < 0.001$) in the proportion of cells with CHOP activation in cells co-expressing mutant TDP-43 Q331K with wildtype PDI ($10.7\% \pm 0.7$), compared to cells co-

expressing mutant TDP-43 Q331K with empty pcDNA3.1 vector. Similar to previous results, co-expression of the GTP (16.0% ± 2.0), SIP (16.3% ± 1.2) or STP (12.7% ± 1.2) cis-proline loop mutants with mutant TDP-43 Q331K, resulted in a significant decrease ($p < 0.01$ and $p < 0.001$) in the proportion of cells displaying CHOP activation, in comparison to cells co-expressing mutant TDP-43 Q331K and empty pcDNA3.1 vector. Interestingly, significantly fewer ($p < 0.001$) cells co-expressing TDP-43 Q331K and the GIP cis-proline loop mutant (14.0% ± 0.6) also displayed CHOP activation (Figure 5.33 B). These results suggest that alterations in the cis-proline loop mutants in PDI's *a* and *a'* domains do not affect PDI's protective activity against ER stress in cells expressing mutant TDP-43.

A

| | TDP-43 | CHOP | DAPI | Merge |

GFP
TDP-43 WT
TDP-43 Q331K
Q331K + PDI
Q331K + GIP
Q331K + GTP
Q331K + SIP
Q331K + STP

B

412
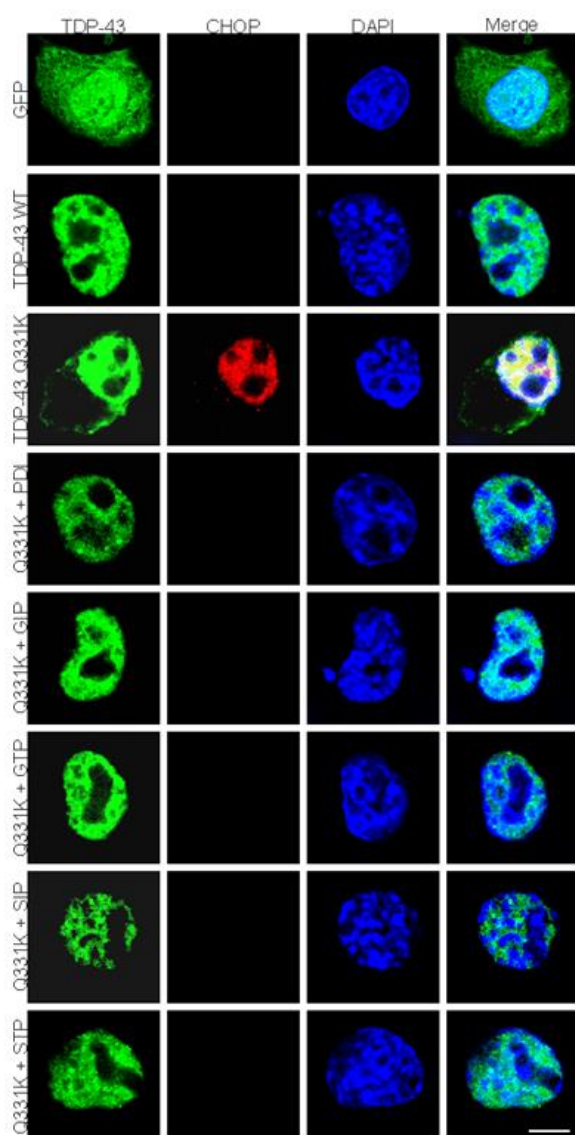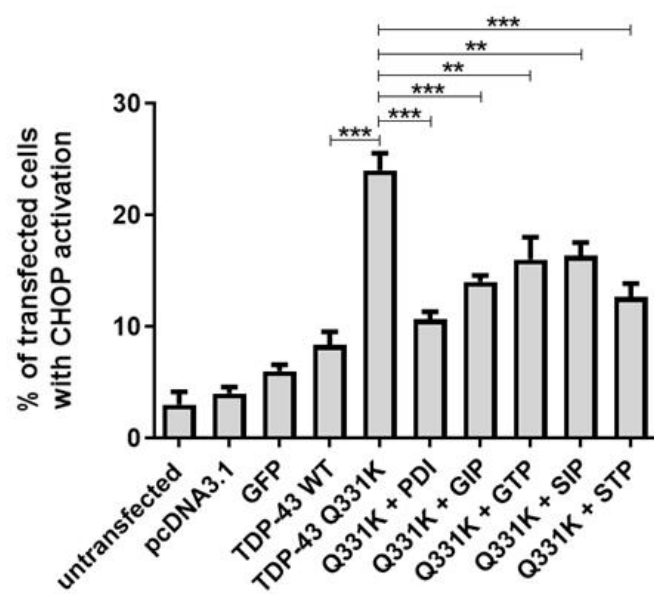
Figure 5.33: The GIP, GTP, SIP and STP cis-proline loop mutants are protective against mutant TDP-43-induced ER stress. A) Immunofluorescence images of Neuro-2A cells expressing GFP, wildtype TDP-43 and mutant TDP-43 Q331K with either empty pcDNA3.1 vector, wildtype PDI, or the GIP, GTP, SIP or STP cis-proline loop mutants. Few cells expressing GFP or wildtype TDP-43 (first and second panel; GFP, TDP-43 WT) displayed CHOP activation. Conversely, more cells expressing mutant TDP-43 Q331K (third panel; TDP-43 Q331K) were undergoing ER stress, indicated by nuclear immunoreactivity to CHOP (third panel, column two). A decrease in the proportion of cells with CHOP activation was observed in cells co-expressing mutant TDP-43 Q331K with either wildtype PDI (fourth panel; Q331K + PDI), or one of the cis-proline loop mutants (panels five to eight; Q331K + GIP, Q331K + GTP, Q331K + SIP, Q331K + STP). Scale bar = 20 µM. **B)** Quantification of the cells in A) displaying CHOP activation. Significantly more cells ($p < 0.001$) co-expressing mutant TDP-43 Q331K and pcDNA3.1 displayed CHOP activation, compared to cells co-expressing wildtype TDP-43 and pcDNA3.1. However, a significant decrease in the proportion of cells with CHOP activation was observed when mutant TDP-43 Q331K expressing cells also co-expressed wildtype PDI ($p < 0.001$), or the cis-proline loop PDI mutants; GIP ($p < 0.001$), GTP ($p < 0.01$), SIP ($p < 0.01$) or STP ($p < 0.001$). N=3, Mean ± SEM, ** $p < 0.01$, *** $p < 0.001$.

Examining the protective activity of the PDI cis-proline loop mutants in cells expressing

mutant FUS

Finally, the PDI cis-proline loop mutants were analysed in Neuro-2A cells expressing mutant

FUS R521G. Their protective activity against FUS mislocalisation to the cytoplasm and

mutant FUS-induced ER stress, was investigated in the following experiments.

5.3.30 The cis-proline loop mutants are co-expressed in almost all cells transfected with

FUS

Prior to performing the cellular assays, the co-transfection efficiency of the cis-proline loop

mutants with FUS was analysed in Neuro-2A cells. Cells were transfected with mutant GFP-

FUS and either the GIP, GTP, SIP or STP cis-proline loop mutants for 72 h, before

immunocytochemistry with an anti-V5 antibody and staining of the nuclei with Hoechst was

performed. Co-transfection was confirmed by examining GFP expression for FUS and

performing immunocytochemistry with an Alexa Fluor 568-tagged secondary antibody to

detect the V5 tag of the cis-proline loop PDI mutants (Figure 5.34). The overall transfection

efficiency of mutant FUS was approximately 80% in Neuro-2A cells when observed 72 h

post-transfection. Fluorescent microscopy was utilised to examine at least 100 cells

expressing FUS and these cells were further analysed for co-expression with the cis-proline

loop mutants. For each of the three replicate experiments, quantification revealed that

approximately 96% of mutant FUS expressing cells also co-expressed GIP, 95% also co-

expressed GTP, 98% also co-expressed SIP, and 96% also co-expressed STP. Thus, in all

further experiments, it was assumed that the detection of FUS reflected co-expression of both

FUS and the cis-proline loop PDI mutants when they were co-transfected but

immunocytochemistry using a V5 antibody was not performed.
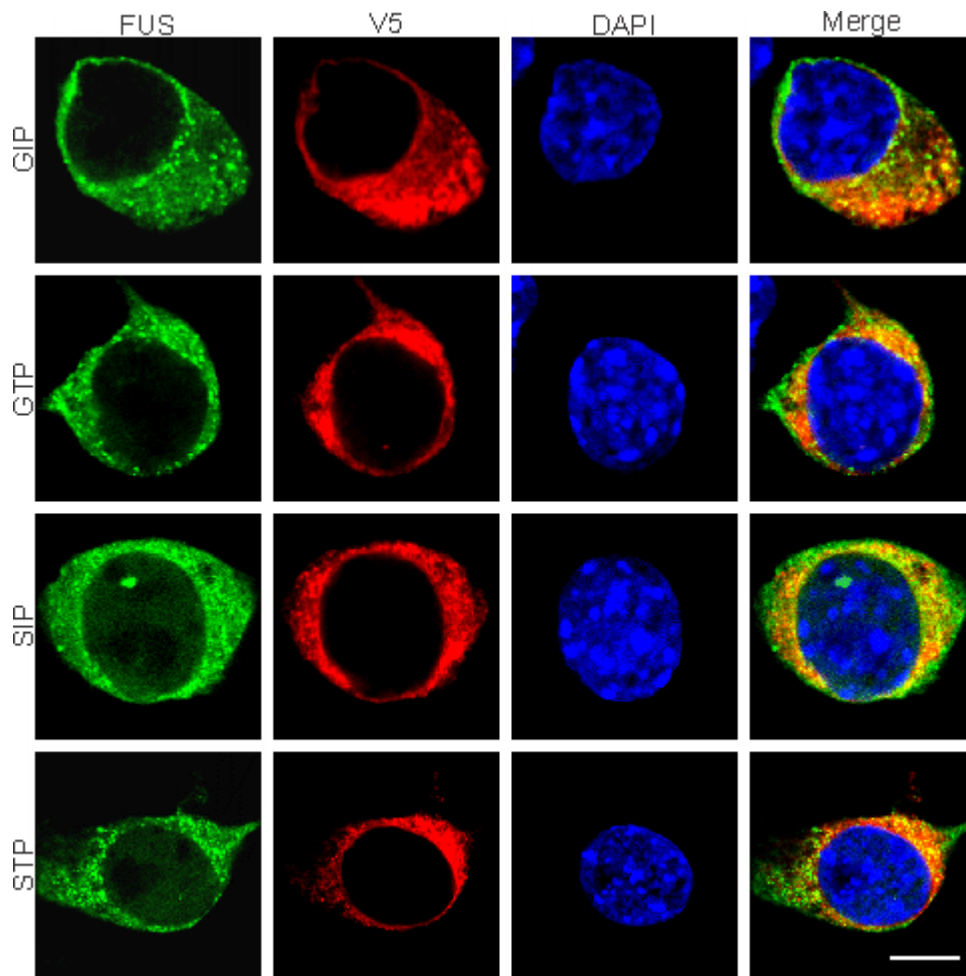
Figure 5.34: The cis-proline loop mutants are co-expressed in almost all Neuro-2A cells co-transfected with mutant GFP-FUS. Neuro-2A cells were transfected for 72 h with GFP-FUS (left column; FUS) and either the GIP, GTP, SIP or STP cis-proline loop mutants (second column; V5). Cells were fixed, immunocytochemistry was performed using an anti-V5 antibody, and the nuclei were stained using Hoechst (third column; DAPI). The merge column depicts co-expression of the cis-proline loop mutants with FUS in the shown cells. Scale bar = 20 µM.

5.3.31 Expression of FUS and cis-proline loop mutants in Neuro-2A cells

Once the localisation and expression of the cis-proline loops was established in Neuro-2A cells expressing mutant FUS, Western blotting analysis was undertaken to confirm that expressed proteins were of the expected size and that the transfection of each protein resulted in comparable levels of expression (Figure 5.35). Cell lysates were prepared from the following cell populations; GFP alone, wildtype FUS co-expressed with empty vector pcDNA3.1, and mutant FUS R521G with either pcDNA3.1, wildtype PDI, or the GIP, GTP, SIP or STP cis-proline loop mutants. Immunoblotting revealed that wildtype and mutant GFP-FUS were detected at the expected size of 100 kDa, and GFP alone was expressed at 26 kDa, using an anti-GFP antibody. Wildtype FUS was expressed at higher levels compared to mutant FUS R521G in some cell lysate populations, however, differences in expression levels are expected between wildtype and mutant forms of the protein. Wildtype PDI and the PDI cis-proline loop mutants were detected at approximately 62 kDa using an anti-V5 antibody and displayed similar expression levels. The β-actin loading control was detected at 40 kDa using an anti-β-actin antibody.

A

B

417
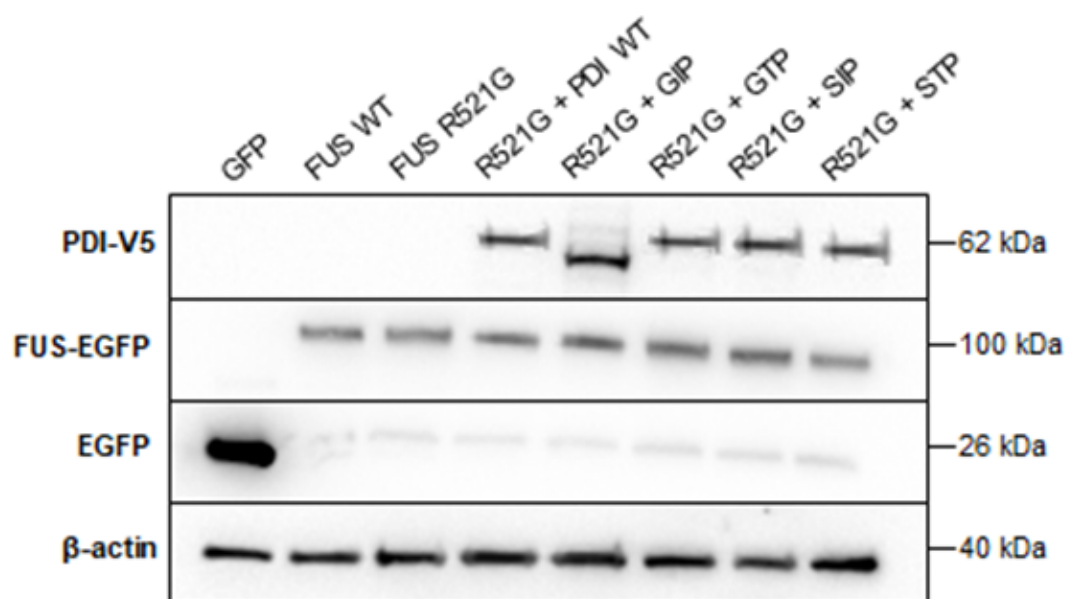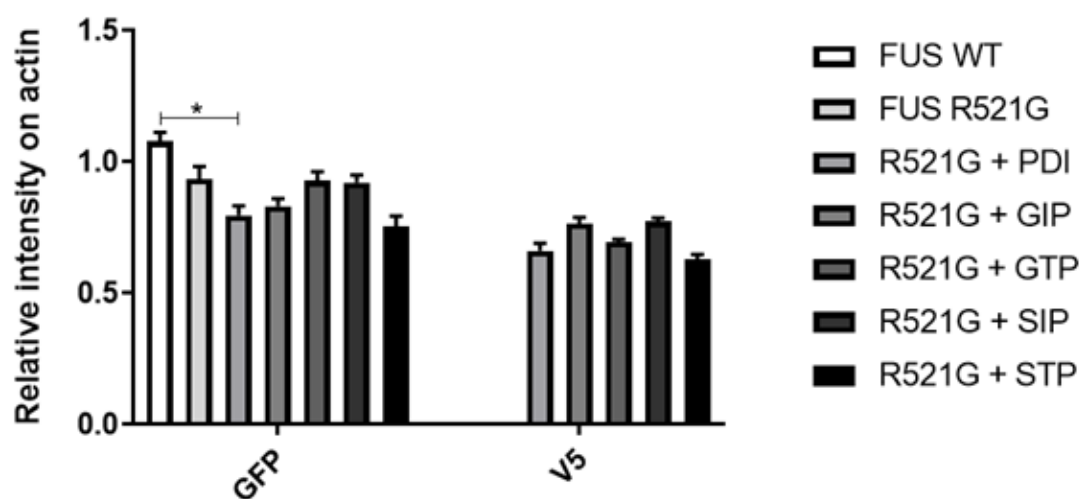
Figure 5.35: Protein expression of wildtype PDI, the PDI cis-proline loop mutants and GFP-FUS proteins in Neuro-2A cells. A) Western blotting of cell lysates was performed to ensure that the expressed proteins were the correct MW and that similar expression levels between proteins were observed. Cell lysates analysed were GFP alone, wildtype FUS with empty pcDNA3.1 vector, and mutant FUS R521G with either pcDNA3.1, wildtype PDI, or the GIP, GTP, SIP or STP cis-proline loop mutants. Wildtype and mutant FUS were detected at 100 kDa and GFP alone was detected at 26 kDa. Wildtype PDI and the GTP, SIP and STP cis-proline loop mutants were expressed at 62 kDa, as expected, however the GIP cis-proline loop mutant was detected at approximately 60 kDa. The loading control, β-actin, was detected at 40 kDa. **B)** Quantification revealed that wildtype FUS was expressed at significantly higher (p < 0.05) levels compared to mutant FUS R521G in some cell lysate populations. However, mutant FUS R521G displayed similar expression levels across all cell lysate populations. Wildtype PDI and the GIP, GTP, SIP and STP cis-proline loop mutants also displayed similar expression levels. Lysates expressing GFP only were not included in quantification. N=3, Mean ± SEM, * p < 0.05.

5.3.32 The GTP and SIP cis-proline loop mutants inhibit mutant FUS mislocalisation to the cytoplasm.

In Chapter 4, studies examining the Dsb proteins, DsbA and DsbC, demonstrated that the oxidase DsbA was able to prevent mutant FUS mislocalisation to the cytoplasm, whereas the isomerase, DsbC, could not. Furthermore, earlier in this chapter in section 5.3.18, it was determined that the CPHC oxidase mutant was the only active site mutant protective against FUS mislocalisation, implying an important role for the oxidase function in mediating the protective activity of PDI. Hence, it was next examined whether the cis-proline loop mutants were protective against FUS mislocalisation to the cytoplasm.

Neuro-2A cells were transfected with empty pcDNA3.1 vector, GFP, wildtype FUS with pcDNA3.1, and mutant FUS R521G with either pcDNA3.1, wildtype PDI or the GIP, GTP, SIP or STP cis-proline loop mutants for 72 h. After fixing, DAPI-staining was performed using Hoechst to visualise the nuclei. Immunocytochemistry was not performed because it was assumed that detection of FUS expression reflected co-expression of FUS with V5-tagged proteins, as determined in section 5.3.32. Fluorescent microscopy was utilised to analyse at least 100 FUS expressing cells for mislocalisation to the cytoplasm. Due to the aggressive nature of the R521G mutation, FUS was considered to be nuclear when it was expressed only in the nucleus, or when it was expressed in both the nucleus and cytoplasm. In contrast, FUS was considered to be cytoplasmic when it was only detected in the cytoplasm of FUS expressing cells (Figure 5.36 A).

Untransfected cells and cells expressing either empty pcDNA3.1 vector or GFP were excluded from analysis as they did not express FUS. Very few cells expressing wildtype FUS possessed cytoplasmic FUS (3.0% ± 1.5). In contrast, a significantly greater ($p < 0.001$) proportion of cells expressing mutant FUS R521G displayed FUS mislocalisation to the

cytoplasm (90.0% ± 0.6), compared to cells expressing wildtype FUS. Co-expression of

wildtype PDI (71.0% ± 2.1) or the GTP (72.7% ± 6.1) or SIP (70.7% ± 6.2) cis-proline loop

mutants with mutant FUS R521G, resulted in a significant decrease (p < 0.05) in the

proportion of cells with cytoplasmic FUS, compared to mutant FUS R521G cells expressing

empty pcDNA3.1 vector. When mutant FUS R521G was co-expressed with the GIP (78.0% ±

6.1), or the STP cis-proline loop mutant (79.0% ± 0.6), there was no change in the proportion

of cells with cytoplasmic FUS compared to cells expressing empty vector. These results

demonstrate that only the GTP and SIP cis-proline loop mutants were protective against

mutant FUS mislocalisation to the cytoplasm (Figure 5.36 B).

A

B

421
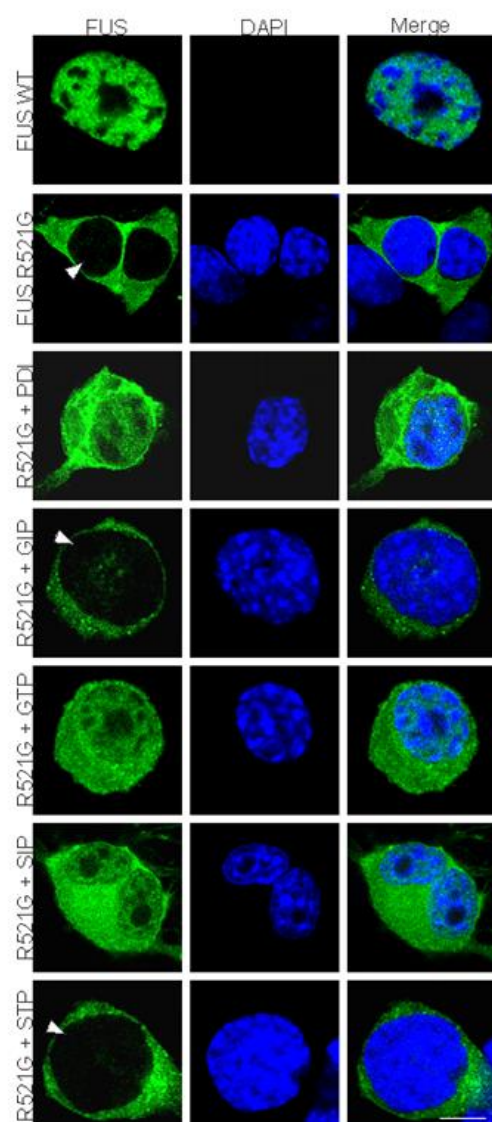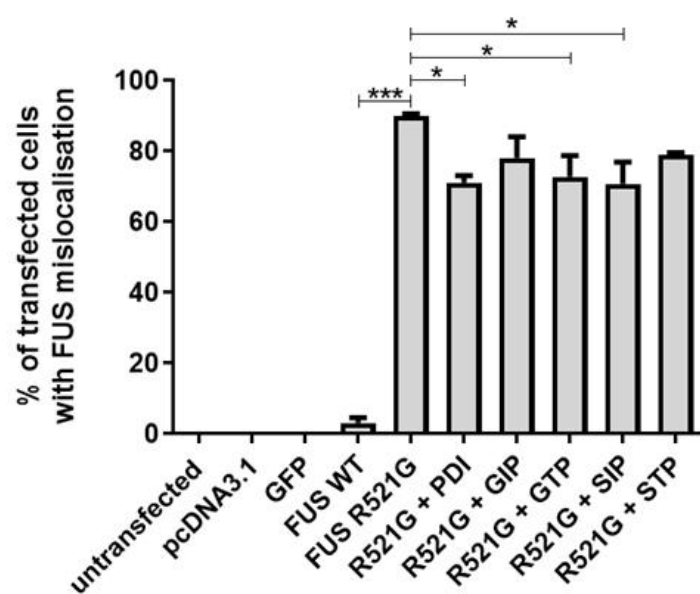
Figure 5.36: The GTP and SIP cis-proline loop mutants inhibit mutant FUS mislocalisation to the cytoplasm. A) Immunofluorescence images of Neuro-2A cells expressing wildtype FUS, or mutant FUS with either empty pcDNA3.1 vector, wildtype PDI, or the GIP, GTP, SIP or STP cis-proline loop mutants. Cells expressing wildtype FUS displayed only nuclear localisation of FUS (first panel; FUS WT), whereas cells expressing mutant FUS R521G mainly display cytoplasmic FUS (second panel; FUS R521G), as indicated by the white arrowhead (second panel, column one). Co-expression of mutant FUS R521G with either wildtype PDI (third panel; R521G + PDI) or cis-proline loop mutants, GTP and SIP (panels five and six; R521G + GTP, R521G + SIP), resulted in localisation of FUS in both the nucleus and the cytoplasm. Conversely, co-expression with either the GIP cis-proline loop mutant or STP cis-proline loop mutant (panels four and seven; R521G + GIP, R521G + STP) resulted in mainly cytoplasmic FUS. Scale bar = 20 µM. **B)** Quantification of cells in A) with FUS mislocalisation to the cytoplasm. A significant increase ($p < 0.001$) in the proportion of mutant FUS R521G expressing cells with FUS mislocalisation to the cytoplasm was observed, compared to wildtype FUS expressing cells. In contrast, significantly fewer ($p < 0.05$) cells exhibited FUS mislocalisation when mutant FUS R521G cells co-expressed either wildtype PDI or the GTP or SIP cis-proline loop mutants, but not the STP or GIP mutants. N=3, Mean ± SEM, * $p < 0.05$, *** $p < 0.001$.

5.3.33 The GTP and SIP cis-proline loop mutants are protective against ER stress induced by mutant FUS

Finally, the protective activity of the cis-proline loop mutants was examined against mutant FUS-induced ER stress. The oxidase, reductase and isomerase active site mutants of PDI were all protective against ER stress in cells expressing mutant FUS, implying that all three redox activities are important for PDI's protective function, or alternatively, that the chaperone capabilities of PDI are protective. Thus, modifications in the cis-proline loops of PDI were examined for differences in protective activity to further elucidate how this activity is mediated.

Neuro-2A cells were transfected with empty pcDNA3.1 vector, GFP, wildtype FUS with pcDNA3.1, and mutant FUS R521G with either pcDNA3.1, wildtype PDI or the GIP, GTP, SIP or STP cis-proline loop mutants for 72 h. After fixing, immunocytochemistry was performed using an anti-CHOP antibody to examine CHOP activation, a marker of ER stress induced apoptotic signalling as previous. Cells were also stained with Hoechst to visualise nuclei before fluorescent microscopy was utilised to analyse at least 100 FUS expressing cells for nuclear immunoreactivity to CHOP (Figure 5.37 A).

Very few untransfected cells or cells expressing empty pcDNA3.1 vector, GFP or wildtype FUS, presented with CHOP activation (less than 10%). In contrast, a significant increase ($p < 0.001$) in the proportion of cells displaying CHOP nuclear immunoreactivity was observed in populations expressing mutant FUS R521G with empty pcDNA3.1 vector (27.7% ± 2.0), compared to cells expressing wildtype FUS with empty vector (9.0% ± 0.6). Significantly fewer ($p < 0.001$) mutant FUS R521G expressing cells presented with CHOP activation when either wildtype PDI (13.7% ± 0.3), the GTP cis-proline loop mutant (12.0% ± 1.2) or the SIP cis-proline loop mutant (11.3% ± 2.0) was co-expressed, compared to mutant FUS R521G

co-expressing empty vector. A significant increase in the proportion of cells with CHOP activation was observed when either the GIP cis-proline loop mutant (21.7% ± 2.2, p < 0.05) or the STP cis-proline loop mutant (29.7% ± 1.5, p < 0.001) was co-expressed with mutant FUS R521G (Figure 5.37 B), compared to cells co-expressing mutant FUS R521G and PDI. Similar to the FUS mislocalisation data, these results indicated that only the GTP and SIP cis-proline loops are protective against mutant FUS induced ER stress. Both of these results indicate that altering the *a'* domain cis-proline loop can modify PDI's protective activity against mutant FUS-induced pathogenic cellular mechanisms.

A

	FUS	CHOP	DAPI	Merge
GFP				
FUS WT				
FUS R521G				
R521G + PDI				
R521G + GIP				
R521G + GTP				
R521G + SIP				
R521G + STP				
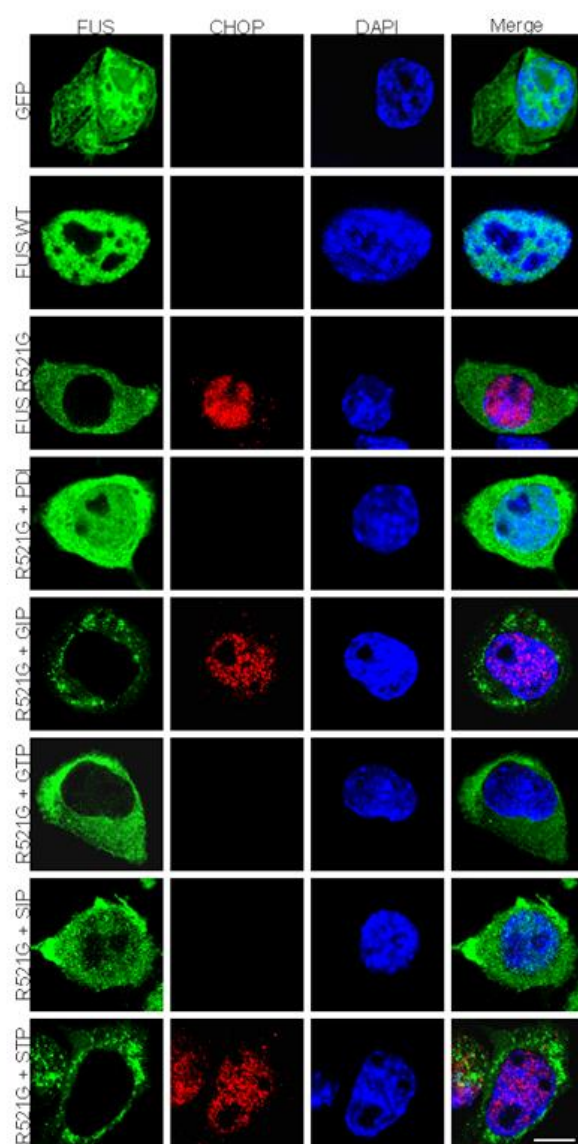
B
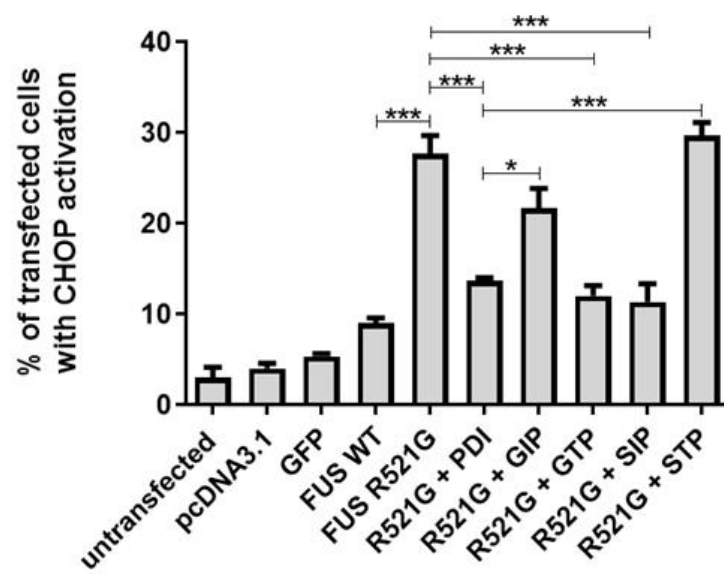
Figure 5.37: The GTP and SIP cis-proline loop mutants are protective against ER stress induced by mutant FUS. A) Immunofluorescence images of Neuro-2A cells expressing GFP, wildtype FUS, or mutant FUS R521G with either empty pcDNA3.1 vector, wildtype PDI or the GIP, GTP, SIP, or STP cis-proline loop mutants. Cells expressing GFP (first panel; GFP) or wildtype FUS (second panel; FUS WT) rarely display CHOP activation. Conversely, more cells expressing mutant FUS R521G (third panel; FUS R521G) display nuclear immunoreactivity to CHOP (third panel, column two). Fewer cells exhibit CHOP activation when mutant FUS R521G is co-expressed with either wildtype PDI (fourth panel; R521G + PDI) or the GTP (sixth panel; R521G + GTP) or SIP (seventh panel; R521G + SIP) cis-proline loop mutants. In contrast, cells co-expressing mutant FUS R521G with either the GIP or STP cis-proline loop mutants display more cells with CHOP activation (panels five and eight; R521G + GIP, R521G + STP), indicated by its nuclear immunoreactivity (column two, panels five and eight). Scale bar = 20 µM. **B)** Quantification of the cells in A) with CHOP activation. A significant increase ($p < 0.001$) in the proportion of cells with CHOP activation was observed in populations expressing mutant FUS R521G compared to cells expressing wildtype FUS. However, there was a significant decrease ($p < 0.001$) in the proportion of cells with CHOP activation when either wildtype PDI, the GTP cis-proline loop mutant, or the SIP cis-proline loop mutant, were co-expressed with mutant FUS R521G. Compared to cells co-expressing wildtype PDI and mutant FUS R521G, significantly more mutant FUS R521G cells co-expressing either the GIP cis-proline loop mutant ($p < 0.05$) or the STP cis-proline loop mutant ($p < 0.001$), displayed CHOP activation. N=3, Mean ± SEM, * $p < 0.05$, *** $p < 0.001$.

5.3.34 A summary of the protective activities of the PDI cis-proline loop mutants examined in this Chapter

A summary illustrating the results obtained in the Chapter, demonstrating the protective effects of each of the cis-proline loop mutants against ALS-associated proteins, SOD1, TDP-43 and FUS, is shown in Table 5.5.

TABLE 5.5. The protective activity of the PDI cis-proline loop mutants.

SOD1			
	Inclusion formation	**ER stress**	**Apoptosis**
GIP (*a* domain – reducing)	✘	✘	✘
GTP (*a* domain – oxidising)	✔	✔	✔
SIP (*a'* domain – reducing)	✔	✔	✔
STP (*a'* domain – oxidising)	✔	✔	✔
TDP-43			
	TDP-43 mislocalisation		**ER stress**
GIP (*a* domain – reducing)	✘		✔
GTP (*a* domain – oxidising)	✔		✔
SIP (*a'* domain – reducing)	✔		✔
STP (*a'* domain – oxidising)	✔		✔
FUS			
	FUS mislocalisation		**ER stress**
GIP (*a* domain – reducing)	✘		✘
GTP (*a* domain – oxidising)	✔		✔
SIP (*a'* domain – reducing)	✔		✔
STP (*a'* domain – oxidising)	✘		✘

5.4 Discussion

In Chapter 4, it was demonstrated that the *a* and *a'* domains are necessary for PDI's protective activity against mutant ALS proteins, SOD1, TDP-43 and FUS, in neuronal cell lines. This finding is consistent with previous studies in our laboratory which revealed that PDI's disulphide interchange activity, mediated by the CGHC active sites located in the *a* and *a'* domains, was important for its protective function in ALS (Parakh et al., 2017 in preparation). Moreover, Chapter 4 investigated the protective activities of eukaryotic versions of Dsb proteins, DsbA (oxidase) and DsbC (isomerase), in neuronal cell lines expressing ALS-associated SOD1, TDP-43 or FUS. These results demonstrated that the oxidase protein DsbA retains the protective activity of PDI against all the mechanisms of pathogenesis examined in this study, induced by mutant SOD1, TDP-43 and FUS. In contrast the isomerase protein DsbC, was only protective against a selection of these mechanisms. Thus, these results imply that the redox potential of PDI, mediated by the active sites of thioredoxin-like proteins, play an important role in mediating the protective capabilities of disulphide interchange activity in ALS.

As PDI is capable of acting as an oxidase, reductase and isomerase, predictions were made as to which of these redox activities are necessary for facilitating PDI's protective function. Therefore, redox active site mutants based on other specific oxidase, reductase and isomerase thioredoxin-like proteins, were designed to determine if alterations in the active site redox potential modify the protective effect of PDI in ALS. This work was based on previous studies which investigated the importance of the active site in thioredoxin-like proteins, where the DsbA active sites were mutated to that of PDI, DsbG and thioredoxin [589]. The study found that DsbA lost its oxidase activity when its active site motifs were mutated to that of PDI (CGHC), DsbG (CPYC) or thioredoxin (CGPC) [589]. In this study, following on from the results obtained in Chapter 4, the CPHC active site mutant was designed, based on

our current knowledge of DsbA proteins. DsbA is highly oxidising, with a redox potential of -120 mV [492], compared to PDI which has an intermediate redox potential, of -160 mV [593]. Therefore, it was hypothesised that mutation of the PDI active site from CGHC to CPHC would allow PDI to function more like an oxidase. The CPYC active site was based on the active site of DsbG, an isomerase and general chaperone, with 24% sequence homology and redox properties similar to that of DsbC [559]. Therefore, it was proposed that mutation of the active site from CGHC to CPYC would make PDI more isomerising. In contrast, the CGPC active site mutant was reminiscent of Thioredoxin's active site. Thioredoxin is a highly reducing protein with a redox potential of -271 mV [581], thus, it was postulated that PDI would act more like a reductase when it possesses this active site.

The experiment undertaken using cyto-roGFP to analyse roGFP expression when co-transfected with the redox active site mutants provided evidence to support the proposed redox activities of the active site mutants. The CPHC active site mutant demonstrated significantly higher levels of roGFP expression than wildtype PDI, suggesting that more roGFP was being oxidised in these experiments, as hypothesised. In comparison, less roGFP expression was observed when the CGPC active site mutant was expressed compared to wildtype PDI, indicating less oxidation and thus, more reduction. In fact, roGFP expression levels in cells expressing the mutant CGPC active site mutant were similar to those observed when only empty pcDNA3.1 vector was expressed, indicative of the reducing environment of the cytoplasm. In cells expressing the CPYC active site mutant, similar levels of roGFP expression to wildtype PDI were detected, as expected, since the redox potential of DsbG is between that of DsbA and thioredoxin [559]. It should be noted, however, that due to time restrictions, it was not possible to perform experiments that allow calculation of the precise redox potential of each active site mutant. Hence, future studies should be conducted to confirm the actual redox potential of these active site mutants, and thus, verify the results

obtained in this study, that the more oxidising PDI is, the more protective it is. Redox potential can be measured by incubation of the mutants in degassed redox buffers containing various concentrations of GSH/GSSG [492, 594].

A change in redox potential evidently altered the protective activity of PDI in these studies. The CPHC oxidase and CGPC reductase active site mutants were protective against mutant SOD1 inclusion formation, whereas the CPYC isomerase active site mutant was not protective. It is possible that the reductase activity of PDI is involved in the breakdown of misfolded disulphide bonds in aggregated, misfolded proteins, including mutant SOD1, whereas the oxidase activity is responsible for the formation of new correctly folded disulphide bonds in these proteins, such asSOD1. Previous studies have concluded that PDI's isomerisation capabilities are required for rearranging disulphide bonds in misfolded proteins [477], whereas others describe isomerisation as repeated bouts of oxidation and reduction [505]. Consistent with these findings, in Chapter 4, DsbA (oxidase) was found to be protective against SOD1 inclusion formation, whereas DsbC (isomerase) was not protective, demonstrating a consistency in these results.

Interestingly, when assessing the effect of the redox active site mutants on mutant SOD1-induced apoptosis, only the CPHC oxidase mutant was protective. This result is in accordance with the results obtained in Chapter 4, where only DsbA demonstrated a protective effect against apoptosis, and DsbC was not protective. It is possible that a more oxidising form of PDI is more effective than wildtype PDI in ensuring the correct formation of disulphide bonds in proteins, therefore maintaining proteostasis in the cell and preventing apoptosis. This result is interesting however, because previous studies undertaken in our laboratory (Parakh et al., 2017 in preparation) and studies performed in Chapter 4, demonstrated that the PDI QUAD mutant was protective against apoptosis, indicating that PDI's chaperone activity is protective against this property. Therefore, it is possible that a

change in redox potential of PDI alters substrate binding in the active sites, preventing the binding of mutant SOD1. These results demonstrate that PDI's protective activity against apoptosis is complex and further studies will need to be undertaken to fully understand the mechanisms involved.

Upon investigation of mutant SOD1-induced ER stress, all three redox active site mutants were found to be protective. These results suggest that the oxidase, reductase and isomerase activities of PDI are all able to inhibit ER stress induced by mutant SOD1 in Neuro-2A cells. Similarly, studies investigating the effect of DsbA and DsbC against mutant SOD1-induced ER stress in Chapter 4 demonstrated a protective effect for both the oxidase and isomerase Dsb proteins. However, it is important to note that DsbC does have chaperone capabilities, similar to PDI. In fact, studies investigating the protective activities of PDI's individual domains in Chapter 4, demonstrated that as well as the *a* and *a'* domains, the *b* domains of PDI also elicited a protective effect, implying that the chaperone function is also protective against mutant SOD1-induced ER stress. Therefore, it may be that PDI's chaperone activity is involved in protection against ER stress, instead of PDI's disulphide interchange activity, thus, the redox potential of PDI would bear no difference on whether PDI was protective or not. This is unlike SOD1 inclusion formation where only the *a* and *a'* domains of PDI, and therefore the disulphide interchange activity, were protective against the formation of inclusions.

A similar result was obtained when examining ER stress induced by mutant FUS. As in cells expressing mutant SOD1, all three redox active site mutants were protective, indicating that either PDI's oxidase, reductase and isomerase activities are all protective, or conversely, that the chaperone function of PDI is protective. DsbA and DsbC were also both protective against ER stress induced by mutant FUS, demonstrating that proteins of different redox potentials are able to restore ER proteostasis in response to the expression of misfolded

protein. This could also point to a protective activity for DsbC's chaperone function. Furthermore, studies described in chapter 4 analysing the effects of PDI's individual domains demonstrated that the *a, a'* and *b* domains of PDI were all protective against mutant FUS-induced ER stress, suggesting that either disulphide interchange activity or chaperone activity of PDI are capable of alleviating ER dysfunction. In contrast, only the CPHC active site mutant was able to inhibit mutant FUS mislocalisation to the cytoplasm in Neuro-2A cells, indicating that PDI's oxidase activity is required for this function. In accordance with this result, it was interesting to note that in Chapter 4, DsbA was also protective against mislocalisation of FUS, however DsbC was not. Again, it is possible that a more oxidising form of PDI can ensure the correct formation of disulphide bonds, and it may be less prone to errors compared to wildtype PDI.

The results obtained when analysing the effect of the PDI active site mutants on TDP-43 mislocalisation were different to those obtained with FUS. Both the CPHC and CPYC, or the oxidase and isomerase, active site mutants, were able to restore TDP-43's localisation in the nucleus. In contrast, the CGPC reductase mutant was not able to do this. TDP-43 inclusions are present in motor neurons of almost all ALS patients [62, 129], indicating that TDP-43 is incorrectly folded in ALS. Therefore, it is possible that the isomerase activity of PDI is essential for this protective function, as well as its oxidase activity, in order to rearrange disulphide bonds in misfolded proteins to form correctly folded, stable proteins. Furthermore, both DsbA and DsbC were protective against mutant TDP-43 mislocalisation to the cytoplasm in Chapter 4, further verifying a protective role for the PDI oxidase and isomerase activity. Interestingly, however, only the CPHC active site mutant was protective against mutant TDP-43-induced ER stress. This is quite different from the results obtained when investigating ER stress induced by mutant forms of SOD1 and FUS, because all redox active site mutants were able to inhibit ER stress in these cells. Similarly, however, DsbA was able

to inhibit ER stress induced by mutant TDP-43, whereas the isomerase DsbC was not. It is interesting to note that the *b* domains of PDI were protective against ER stress, implying that PDI's chaperone function may be involved in this ability. It may therefore be that changes to the redox potential of the active site of PDI alter its binding to TDP-43. The substrates which specifically bind to PDI will not necessarily bind to other PDI family members, so changes in PDI's active site may alter its broad specificity.

However, these results demonstrate a very important and widespread function for PDI's oxidase activity against misfolded proteins in ALS. The CPHC oxidase active site mutant was protective against all mechanisms of pathogenesis investigated across all three ALS-associated mutant proteins, similar to wildtype PDI. Oxidised PDI exists in an open state conformation compared to reduced PDI, resulting in more exposed hydrophobic areas, and a larger cleft with potential for substrate binding [501]. In addition, although the active sites of thioredoxin-like proteins are the main factor determining redox potential, previous studies have demonstrated that other factors can also determine the redox potential, such as the cis-proline loop [492]. Similar studies on the role of the intervening residues in the CXXC motif on the redox potential of PDI itself have however, not been performed.

The cis-proline loop is closely associated with the active site of thioredoxin-like proteins, and it has been shown to play a vital role in determining redox potential, protein structure and stability, and substrate binding and release [492]. Moreover, previous studies have demonstrated that substituting the residue preceding the proline can significantly alter these properties [492]. PDI has two cis-proline loops; one in the *a* domain (GYP) and the other in the *a'* domain (SFP). Following the study of Ren and colleagues (2009) in the role of the residue preceding the proline on redox potential, it was postulated that by substituting tyrosine in the *a* domain cis-proline loop to a threonine (GTP), PDI would become more oxidising, whereas substituting this tyrosine with an isoleucine (GIP), would render it more

433

reducing. Similarly, when substituting phenylalanine in the *a'* domain cis-proline loop with threonine (STP), it was predicted that PDI would become more oxidising, whilst a substitution of this phenylalanine with isoleucine (SIP) should make it more reducing. Upon examining roGFP expression in Neuro-2A cells co-expressing the cis-proline loop mutants, no significant difference in roGFP expression was observed compared to wildtype PDI. However, this may be because only one of the two cis-proline loops of PDI (*a* and *a'* domain) was mutated each time in these mutants, while the other remained native. These studies revealed a trend for the GTP cis-proline loop to be more oxidising compared to the native cis-proline loop, as expected, however this was not statistically significant. A more sensitive assay is necessary in future studies to assess and verify the redox potential of these cis-proline loops mutants. Furthermore, other future studies would involve the creation of additional mutants in which the cis-proline loops are modified in both the a and a' domains together, or alternatively, the a or a' domain mutant alone should be expressed with its cis-proline loop mutated.

In Neuro-2A cells expressing mutant SOD1, the GTP cis-proline loop mutant (located in the *a* domain) was protective against inclusion formation, ER stress and apoptosis. These results are consistent with those described previously in this thesis which suggest that a more oxidising form of PDI is effective in preventing the formation of SOD1 inclusions, mutant SOD1-induced ER stress and apoptosis. The results obtained with the GIP cis-proline loop mutant are consistent with this notion, as this mutant was not protective effect against mutant SOD1-induced pathogenic mechanisms, implying that a more reducing cis-proline loop results in a loss of the protective activity of PDI. Interestingly, the SIP and STP cis-proline loop mutants, which contain substitutions on the *a'* domain of PDI, were equally protective as wildtype PDI. Hence these data imply that a more oxidising or reducing *a'* domain cis-proline loop does not impact on its protective activity.

Similar results were obtained when assessing the protective activity of the cis-proline loop mutants against mutant TDP-43. The presence of an oxidising cis-proline loop in the *a* domain of PDI resulted in protective activity against TDP-43 mislocalisation, whereas a predicted more reducing cis-proline loop mutant was not protective. In contrast, the presence of either an oxidising or a reducing cis-proline loop in the *a'* domain still retained PDI's protective ability against mislocalisation of TDP-43 to the cytoplasm. An exception was noted when investigating the effects of the cis-proline loops on mutant TDP-43-induced ER stress, as the GIP mutant was found to be also protective. It is possible that this protective activity is due to PDI's chaperone function, although this remains unlikely, as PDI's chaperone function had no effect against ER stress induced by TDP-43 for the active site mutants. It is possible that mutation of the cis-proline loop from GYP to GIP allows effective substrate binding of TDP-43 to PDI, thus PDI is able to retain its activity. Regardless, the results obtained here imply that the protective activity of PDI is mediated primarily by PDI's *a* domain. Alterations to the cis-proline loop of PDI's *a'* domain did not modify PDI's protective activity, whereas mutation of the *a* domain cis-proline loop did alter PDI's protective activity. Therefore, it is possible in the full-length PDI protein, the protective activity lies primarily in the *a* domain. The *a'* domain mutant was found to be protective on its own in the studies outlined in Chapter 4, however, it is possible that the presence of the *a* domain acts as a secondary active site and is not necessarily required. Moreover, previous studies have concluded that the *a* domain of PDI acts as an oxidase, whereas the *a'* domain possesses more isomerase activity [574], further supporting the notion that the oxidase activity of PDI is essential for PDI's protective function.

Similar results were obtained when examining mechanisms of pathogenesis induced by mutant FUS, except that the presence of the STP cis-proline loop mutant resulted in PDI not being protective against mislocalisation of FUS to the cytoplasm and induction of ER stress.

This result is interesting as the STP cis-proline loop mutant is proposed to be more oxidising, compared to the native SFP cis-proline loop of the *a'* domain. Moreover, it is puzzling that alterations to the *a'* domain cis-proline loop did not alter the protective activity of PDI in cells expressing either mutant SOD1 or TDP-43, but it did alter the activity against mutant FUS. These differences in the protective activity of PDI, resulting from the presence of the cis-proline loop mutations, may be due to alterations in substrate binding when the STP cis-proline loop mutant is present. It is therefore possible that mutant FUS can no longer bind to the STP cis-proline loop mutant of PDI, thus PDI can no longer exert its protective effect.

In future studies, the cis-proline loop should be mutated in the individual *a* and *a'* domain proteins used in Chapter 4. This way, the effect of the different cis-proline loops of each domain can be assessed for protective activity individually. It would therefore be interesting to examine the resultant activity of the *a* and *a'* domain mutants upon mutagenesis of the cis-proline loops. These studies may also provide different results to those obtained using the full length PDI cis-proline loop mutants, and they may reveal additional insights into how modifying the redox potential of PDI can modify its activity. Therefore, *a* and *a'* domain proteins, containing mutations in the cis-proline loop, should be co-expressed with cyto-roGFP to provide insights into the redox potential of these proteins. It would be predicted that a significant difference in roGFP activity may be observed in these analyses. Assessing the domains of PDI individually would also provide more information into whether the *a'* domain is still functional when it contains the cis-proline loop mutations, once the *a* domain is no longer present. Future studies should also be undertaken to measure the actual redox potential of both the active site mutants and the cis-proline loop mutants as described above. Due to time constraints, redox potential measurements were unable to be performed here, however, they should be undertaken as the next stage in this study so that precise measurements of the redox potential can be determined and correlated precisely with the

protective activity of PDI. The fact that the experiments did reveal differences in the protective activity for the PDI mutants implies that these mutants do differ in redox potential, however this was not shown specifically. It would also be interesting to examine the redox potential of PDI when active site mutations are combined with alterations to the cis-proline loops, for example, an oxidising active site with a reducing cis-proline loop, and vice versa. Finally, it would also be important to perform some *in silico* analysis, such as molecular modelling, to ascertain that these mutations have not altered the protein's native conformation, resulting in its unfolding or dysfunction. Biophysical studies using purified proteins would also need to be performed to ensure that they are correctly folded and functioning as predicted.

In summary, this chapter provides insights into the importance of PDI's redox potential on its protective activity against misfolded proteins associated with ALS. It was demonstrated that the oxidase activity was protective against every cellular mechanism examined, in cells expressing ALS-associated forms of either mutant SOD1, TDP-43 or FUS. These data imply that the formation of disulphide bonds is an important function necessary for the protective activity in PDI in ALS. Furthermore, results obtained using the cis-proline loop mutants suggest that the *a* domain is more important in determining PDI's protective activity, compared to the *a'* domain. It was also shown in this Chapter that there are a number of factors that determine the protective effects of PDI, other than the *a* domain, such as the precise sequence of active site residues, and the cis-proline loop located in the *a* domain, which is also considered to be part of the active site of PDI.

Chapter 6: The Role of PDI and its Redox Activity in FUS-Linked ALS

6.1 Introduction

Over 46 mutations in FUS are currently associated with ALS and these mutations account for approximately 4% of fALS and 1% of sALS cases [8]. FUS has been well-studied in ALS, and recently, studies in our laboratory have demonstrated that PDI is protective against mutant FUS mislocalisation to the cytoplasm and mutant FUS-induced ER stress and ER-Golgi transport defects (Parakh et al., 2017 in preparation), suggesting that PDI is protective against mutant FUS in ALS.

The studies performed in Chapters 4 and 5 have highlighted key mechanisms by which PDI mediates its protective activity. Specifically, in Chapter 5, it was concluded that the oxidase activity of PDI, (involving the formation of disulphide bonds), is imperative for its protective function. In this chapter, the experiments performed further investigate the oxidase activity of wildtype PDI for one particular protein linked to ALS, mutant FUS mutant, R521G, which is responsible for an aggressive form of ALS [137]. Moreover, the protective activity of a PDI mimetic, BMC, and two novel PDI variants, D292N and R300H, are explored.

6.1.1 BMC: a PDI mimetic

-(±)-trans-1,2-Bis(2-mercaptoacetamido) cyclohexane (BMC) is a 262 Da synthetic dithiol which contains two hydrogen-sulphide bonds. It is designed to mimic the activity of PDI and is based on the CGHC motif, allowing it to mimic the disulphide interchange activity [595]. Previous studies have demonstrated that BMC can assist in the oxidation and isomerisation of disulphide bonds *in vitro* and it also accelerates protein folding during the production of recombinant proteins [595, 596]. Moreover, BMC has similar pKa and reduction potential to the CGHC active site motifs of PDI, suggesting that BMC is an efficient catalyst of disulphide oxidation and isomerisation [596]. However, unlike PDI, BMC cannot bind to protein substrates, and it is therefore not substrate specific [490].

A previous study from our group demonstrated a reduction in the formation of mutant SOD1 inclusions and in the levels of SDS-insoluble mutant SOD1, in a dose-dependent manner, in cells treated with BMC, indicating that BMC is able to mimic the protective effects of PDI on mutant SOD1 aggregation [448]. Moreover, unpublished studies performed have demonstrated that BMC is protective against ER-Golgi transport defects and ER stress in neuronal cells expressing mutant SOD1, TDP-43 and FUS, and it is also protective against the mislocalisation of mutant TDP-43 and mutant FUS. Unfortunately, however, BMC is highly insoluble and is predicted to be unable to cross the BBB, rendering it unsuitable for therapeutic use (unpublished observations). However, since treatment of neuronal cells with BMC emulates PDI overexpression utilising disulphide interchange activity, it is postulated whether BMC exerts this protective function primarily through its oxidase activity or isomerase activity.

6.1.2 PDI variants, D292N and R300H

As discussed briefly in Chapter 3, section 3.1.1, exome sequencing and a candidate gene approach identified 16 missense variants in the PDI and ERp57 genes (nine in PDI and seven in ERp57). These missense variants were overrepresented in ALS cases compared to controls, indicating that they may act as risk factors or phenotypic modifiers through gain- and loss-of-function mechanisms [444]. Moreover, it was reported that, overall, these variants were present in 1-2% of all fALS and 1% of all sALS cases analysed [444], similar to the frequencies of other ALS-linked gene variants [4].

Two variants in the PDI gene, D292N and R300H, have been studied in detail since their initial identification. Both variants are present within the substrate binding *b'* domain of PDI and modelling studies predict that these mutations perturb the binding of substrate proteins [441, 444]. However, significant or obvious structural alterations are not observed in these variants, suggesting that they confer functional changes in PDI, rather than structural modifications [441]. Interestingly, the aspartate residue that is removed in the D292N variant has previously been shown to control accessibility to the substrate binding site [597], indicating that the variant may impede substrate accessibility. Moreover, the R300H variant also perturbs redox-dependent substrate binding and accessibility to the catalytic active site [444]. Interestingly, different proteolytic patterns around the x-linker region of the D292N and R300H variants have been observed, compared to wildtype PDI [441]. Indeed, the x-linker region of PDI can adopt several conformations which determine the accessibility of substrates to the substrate binding site of the *b'* domain [597]. It was predicted that conformation of the D292N variant displays blocking of the x-linker region to the binding pocket, however the predicted conformation of the R300H displays an opposite effect, even though the R300H variant demonstrates a decrease in catalytic activity, compared to wildtype PDI [441].

Investigations in zebrafish have previously demonstrated that a large fraction of embryos expressing the R300H variant displayed a distinct shortening of the axis and tail curvature, which are features characteristic of zebrafish models of ALS. Similarly, axonal morphology was also impaired, resulting in reduced length and increased branching. Furthermore, synapse formation was also disrupted in these animals [441]. These results imply that expression of these variants disrupt motor neuron connectivity and function in zebrafish. Interestingly, defects observed in neurons were associated with motor behavioural defects, implying that the expression of R300H produces a phenotype characteristic of ALS zebrafish models. Moreover, the effect of PDI on neurite outgrowth in neuronal cells and human motor neurons was inhibited when the PDI variants were expressed, suggesting that the variants inhibit neurite outgrowth [441]. Conversely, however, the expression of R300H in zebrafish did not lead to motor neuron loss [441].

Interestingly, the PDI D292N and R300H variants do not induce cell toxicity or ER stress in neuronal cell lines and primary motor neuron cultures [441], despite ER stress being implicated as an early pathogenic mechanism in ALS [255]. Furthermore, ER morphology and protein secretion via the secretory pathway is retained upon expression of the variants, indicative of normal ER homeostasis in the cells [441]. Together these findings imply that D292N and R300H are not causative of ALS, but may be a risk factor for disease. The author of this thesis co-authored a review article discussing the PDI variants and PDI's novel roles in the nervous system [598]. The reader is directed to this review for more information.

6.1.3 Aims of this chapter

The studies in Chapters 4 and 5 have predicted an important role for oxidase activity in mediating PDI's protective function. In Chapter 4, oxidase DsbA was consistently protective against pathogenic mechanisms induced by ALS, compared to isomerase DsbC which was only protective in some instances. Moreover, studies examining the PDI active site mutants in Chapter 5 also demonstrated that a predicted oxidising active site motif or cis-proline loop was consistently protective against cellular disease processes, in comparison to predicted reducing or isomerising mutants.

In order to probe the role of redox activity in PDI's protective function in more detail, one specific ALS-associated protein was selected for further study, and FUS was chosen because it has not been as well studied as SOD1 or TDP-43. Therefore, the oxidase activities of wildtype PDI, BMC and PDI variants, D292N and R300H, were investigated in Neuro-2A cells expressing mutant FUS R521G. The studies in this chapter involve examining the function of each PDI protein, or PDI mimetic, on mutant FUS-induced pathogenic mechanisms, upon ablation of oxidase activity. It was hypothesised that ablation of oxidase activity would render the PDI proteins and BMC non-functional. These experiments were consequently confirmed by the use of cyto-roGFP to examine the oxidase activity of wildtype PDI, PDI R300H and PDI QUAD. Thus, it was predicted that these studies would verify the importance of the oxidase activity on PDI's protective function.

6.2 Materials/Methods

6.2.1 Constructs used in this chapter

A pcDNA3.1 vector containing full-length PDI and a V5 tag was provided by Dr. Neil Bulleid, University of Glasgow, UK. GFP FUS (wildtype and R521G) vectors were a gift from Dr. Justin Yerbury, University of Wollongong, Australia, and wildtype FUS and mutant FUS R521G constructs encoding hemagglutinin (HA)-tagged human FUS at the N-terminus were provided by Dr. Dorothee Dormann, Munich University, Germany. Mutant PDI D292N and R300H were a kind gift from Professor Claudio Hetz, University of Chile, Chile. The PDI QUAD mutant was generated by a Masters student, utilising site-directed mutagenesis. The cyto-roGFP construct was a gift from Paul Schumacker (Addgene plasmid #49435). The DNA plasmids used in this chapter were verified by DNA sequencing before use.

6.2.2 BSO administration

Cells transfected with FUS WT and R521G were treated with Buthionine sulfoximine (BSO) to reduce levels of glutathione, resulting in diminished oxidation. 75 µM BSO was administered into transfected cells 24 h post transfection for a total of 48 h. Cells were fixed 72 h post transfection and an immunofluorescence assay was performed before analysis of BSO's effect on PDI's activity under a Zeiss AxioImager epifluorescence microscope. BSO was stored at a stock solution of 100 mM at -20°C.

6.2.3 Cell culture treatment with BMC

Treatment with PDI mimetic, -(±)-trans-1,2-Bis(2-mercaptoacetamido) cyclohexane (BMC) (Toronto Research Chemicals), was administered to cells at a concentration of 25 µM approximately 5 h post transfection with FUS WT and R521G constructs. BMC was stored at a stock solution of 100 mM in DMSO at -20°C. Cells transfected with FUS constructs were also administered with DMSO alone to act as a control. Cells were fixed 72 h post transfection and an immunofluorescence assay was performed before analysis of BMC's effect on FUS mislocalisation, ER stress and inclusion formation under a Zeiss AxoImager epifluorescence microscope.

6.3 Results

6.3.1 Protein expression of PDI and FUS are not altered after administration of BSO in Neuro-2A cells

Chapter 5 of this thesis previously demonstrated that PDI's oxidase activity was imperative for its protective function. To further confirm this finding, the use of a specific redox inhibitor, BSO, was administered into Neuro-2A cells expressing mutant FUS R521G and PDI. BSO inhibits intracellular glutathione synthesis by inhibition of the enzyme γ-glutamyl-cysteine synthetase [599]. One of glutathione's functions is to modulate a redox environment in the ER lumen that maintains PDI in an active form for oxidation [600], and in the presence of glutathione, PDI accelerates its oxidation of disulphide bonds, but not isomerisation [601]. Therefore, it was predicted that the administration of BSO would inhibit PDI's oxidase activity, and thus, its protective activity.

First, Western blotting analysis was performed to ensure that BSO did not alter or diminish the protein expression of PDI, and wildtype and mutant FUS (Figure 6.1). Cell lysates were prepared from the following cell populations; GFP alone, wildtype FUS with either empty pcDNA3.1 vector or PDI, with and without BSO administration, and mutant FUS R521G with either empty pcDNA3.1 vector or PDI, with and without BSO administration. Immunoblotting using an anti-GFP antibody revealed that wildtype and mutant FUS-GFP proteins were expressed at the expected size of 100 kDa with similar levels of expression. GFP alone was expressed at 26 kDa, as expected. Wildtype PDI was detected at 62 kDa using an anti-V5 antibody, and expression levels were constant across cell lysate populations. These results indicate that the administration of BSO does not alter protein expression. β-actin was used as a loading control and was detected using an anti-β-actin antibody (40 kDa).

A

B

449
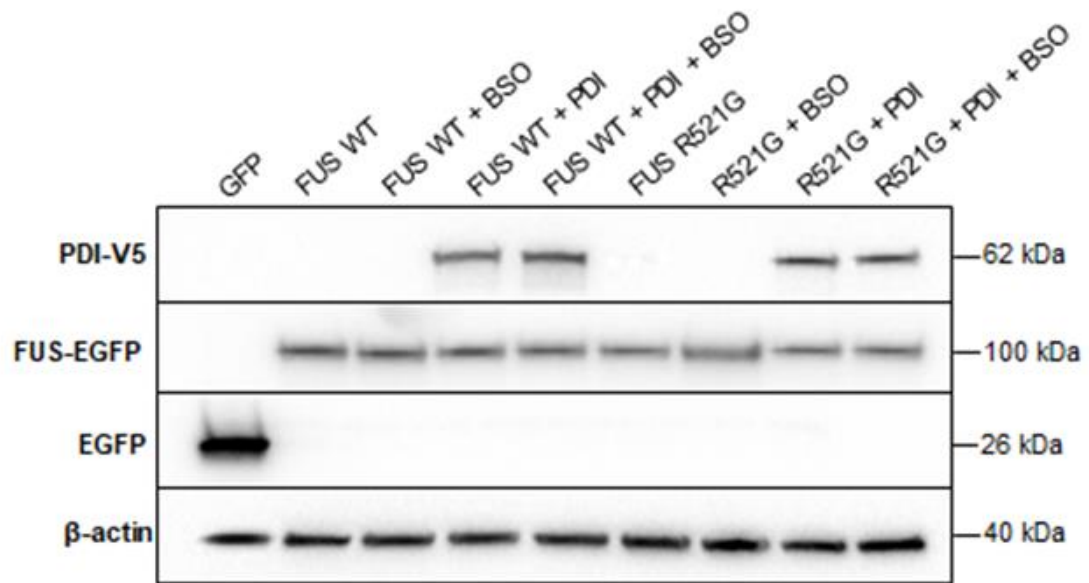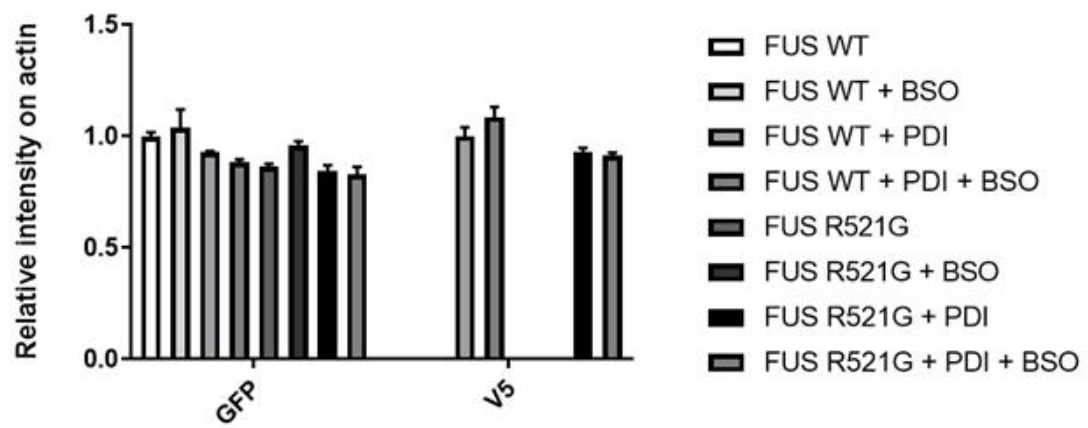
Figure 6.1: Protein expression of PDI and GFP-FUS proteins in Neuro-2A cells, with and without BSO administration. A) Western blotting analysis of cell lysates was performed to ensure that PDI and GFP-FUS proteins were expressed at similar levels and were of expected MW. Lysates examined were from cells expressing either GFP alone, wildtype FUS co-expressed with either pcDNA3.1 or PDI, with exposure to BSO or no exposure, or mutant FUS R521G co-expressed with either pcDNA3.1 or PDI, with and without BSO exposure. PDI was detected at 62 kDa (PDI = 60 kDa, V5 tag = 2 kDa). Wildtype and mutant FUS were detected at 100 kDa (FUS = 74 kDa, GFP = 26 kDa), and GFP alone was detected at 26 kDa. β-actin was expressed at 40 kDa. **B)** Quantification revealed that BSO did not alter protein expression levels upon administration. Wildtype FUS and mutant FUS R521G-expressing cells were expressed at similar levels, and the expression levels of PDI remained constant across cell lysate populations. Lysates expressing GFP only were not included in quantification. N = 3, Mean ± SEM.

6.3.2 The administration of BSO impedes PDI's ability to inhibit mutant FUS mislocalisation to the cytoplasm

The effect of BSO on PDI's activity was first investigated in Neuro-2A cells expressing wildtype and mutant FUS by examining FUS mislocalisation to the cytoplasm. Neuro-2A cells were transfected with GFP alone, wildtype FUS co-expressed with either empty pcDNA3.1 vector or PDI, and mutant FUS R521G co-expressed with either empty pcDNA3.1 vector or PDI. Transfected cells were both exposed and not treated with BSO to examine the effects of BSO administration. Cells were fixed after 72 h and immunocytochemistry was performed using an anti-V5 antibody to visualise V5-tagged PDI. Cells were also DAPI-stained with Hoechst to view the nuclei. Fluorescent microscopy was utilised to examine the cellular location of FUS, whereby FUS was considered cytoplasmic when fluorescence was only detected in the cytoplasm, but was considered nuclear when it was localised in both the cytoplasm and nucleus, as in previous chapters of this thesis (Figure 6.2 A).

Untransfected cells and cells expressing GFP alone were not included in the analysis because they did not express GFP-FUS. In wildtype FUS expressing cells, whether co-expressed with PDI or exposed to BSO, or not, less than 5% of cells demonstrated a cytoplasmic localisation of FUS. Conversely, a high proportion of cells co-expressing mutant FUS R521G with empty pcDNA3.1 vector displayed cytoplasmic FUS mislocalisation (93.5% ± 1.2), and this proportion did not change upon administration of BSO (91.8% ± 1.7). As expected, co-expression of mutant FUS R521G with PDI resulted in a significant reduction ($p < 0.001$) in the proportion of cells expressing cytoplasmic FUS (75.5% ± 3.8). However, upon administration of BSO to cells co-expressing mutant FUS R521G and PDI, significantly more ($p < 0.001$) cells expressed cytoplasmic FUS (94.23% ± 2.3), compared to FUS R521G and PDI co-expressing cells without BSO administration. These data indicate that in cells treated

with BSO, PDI loses it protective activity against FUS mislocalisation to the cytoplasm

(Figure 6.2 B).

A

	FUS	V5	DAPI	Merge
FUS WT				
FUS WT + BSO				
FUS WT + PDI				
FUS WT + PDI + BSO				
FUS R521G				
FUS R521G + BSO				
R521G + PDI				
R521G + PDI + BSO				

B

453
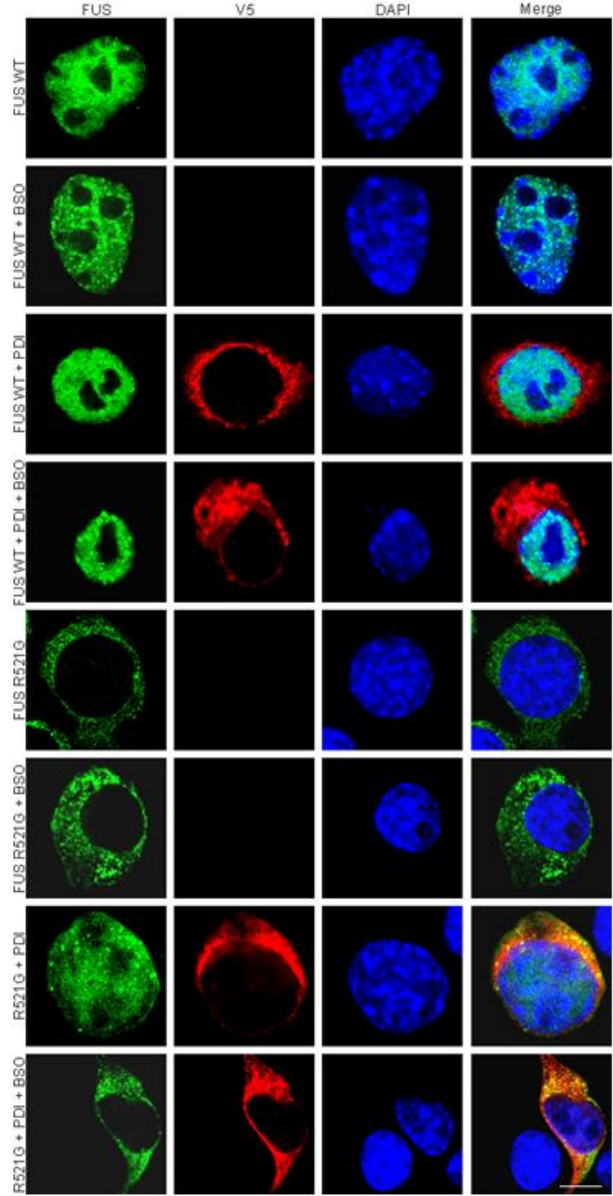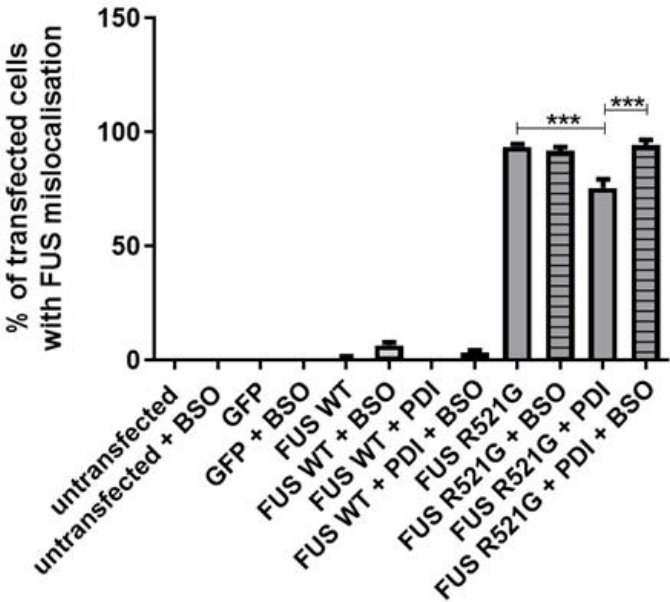
Figure 6.2: The administration of BSO inhibits PDI's ability to inhibit mutant FUS mislocalisation to the cytoplasm. A) Immunofluorescence images of Neuro-2A cells expressing wildtype FUS with either empty pcDNA3.1 vector or PDI (with or without BSO), and mutant FUS R521G with either pcNDA3.1 or PDI (with or without BSO). Cells expressing wildtype FUS displayed nuclear FUS localisation, demonstrated by complete co-localisation with the DAPI-stained nucleus (panels 1-4; FUS WT, FUS WT + BSO, FUS WT + PDI, FUS WT + PDI + BSO). In contrast, almost all cells expressing mutant FUS R521G with empty vector demonstrated cytoplasmic localisation of FUS (panels five and six; FUS R521G, FUS R521G + BSO). However, fewer FUS R521G cells co-expressing PDI (panel seven; R521G + PDI) displayed cytoplasmic FUS, demonstrated by localisation in both the nucleus and cytoplasm (panel seven, column one). Conversely, when BSO was administered to cells co-expressing mutant FUS R521G and PDI (panel eight; R521G + PDI + BSO), more cells demonstrated cytoplasmic FUS mislocalisation. Scale bar = 30 µM. **B)** Quantification of Neuro-2A cells with FUS mislocalisation in A). FUS was typically expressed in the nucleus in populations expressing wildtype FUS. In contrast, most cells expressing mutant FUS R521G with empty vector displayed cytoplasmic localisation of FUS, with or without BSO. A significant decrease ($p < 0.001$) in the proportion of cells with FUS mislocalisation to the cytoplasm was observed when PDI was co-expressed with mutant FUS R521G. However, the proportion of FUS R521G and PDI co-expressing cells with FUS mislocalisation was significantly increased ($p < 0.001$) when BSO was administered to cells. N=3, Mean ± SEM, *** $p < 0.001$.

6.3.3 The administration of BSO impedes PDI's ability to inhibit CHOP activation induced by mutant FUS

It was next examined whether BSO would impede PDI's protective activity against ER stress induced by mutant FUS. Only one marker for ER stress was utilised in these studies, based on the consistency of results obtained between different ER stress markers in Chapters 3, 4 and 5 and due to time constraints. However, ideally another marker of ER stress should be investigated to confirm these results in future experiments. For this study, the activation of CHOP was used to examine late, pro-apoptotic UPR induction. Neuro-2A cells were transfected with GFP alone, wildtype FUS with either empty pcDNA3.1 vector or PDI, and mutant FUS R521G with either pcDNA3.1 or PDI, with and without BSO administration. Cells were fixed 72 h after transfection, and immunocytochemistry was performed using an anti-CHOP antibody to detect nuclear immunoreactivity to CHOP, indicative of activation. Cells were also stained with Hoechst to visualise the nuclei and examined using fluorescent microscopy (Figure 6.3 A).

Less than 10% of untransfected cells or cells expressing GFP, with or without BSO administration, displayed activation of CHOP, as expected. Moreover, wildtype FUS expressing cells only displayed CHOP activation in 5.3% ± 0.3 of cells without BSO, and 11.0% ± 1.0 of cells with BSO. The proportion of cells with CHOP activation was also similar in wildtype FUS expressing cells when PDI was co-expressed. In contrast, there was a significant increase (p < 0.001) in the proportion of cells with nuclear immunoreactivity to CHOP in populations expressing mutant FUS R521G with empty pcDNA3.1 vector (22.0% ± 1.5), compared to those expressing wildtype FUS, as previous. This proportion did not alter in these cells when BSO was administered (18.3% ± 2.6). As expected, co-expression of PDI with mutant FUS R521G resulted in a significant reduction (p < 0.001) in the proportion of cells displaying CHOP activation (7.7% ± 1.2), compared to cells co-expressing mutant FUS

R521G with empty vector. However, administration of BSO to cells co-expressing PDI and mutant FUS R521G resulted in significantly more cells ($p < 0.01$) with nuclear immunoreactivity to CHOP (17.3% $\pm$ 1.5), compared to these cells without BSO treatment, indicating that BSO impedes PDI's ability to utilise its oxidase activity to inhibit ER stress induced by mutant FUS (Figure 6.3 B).

A

B

457
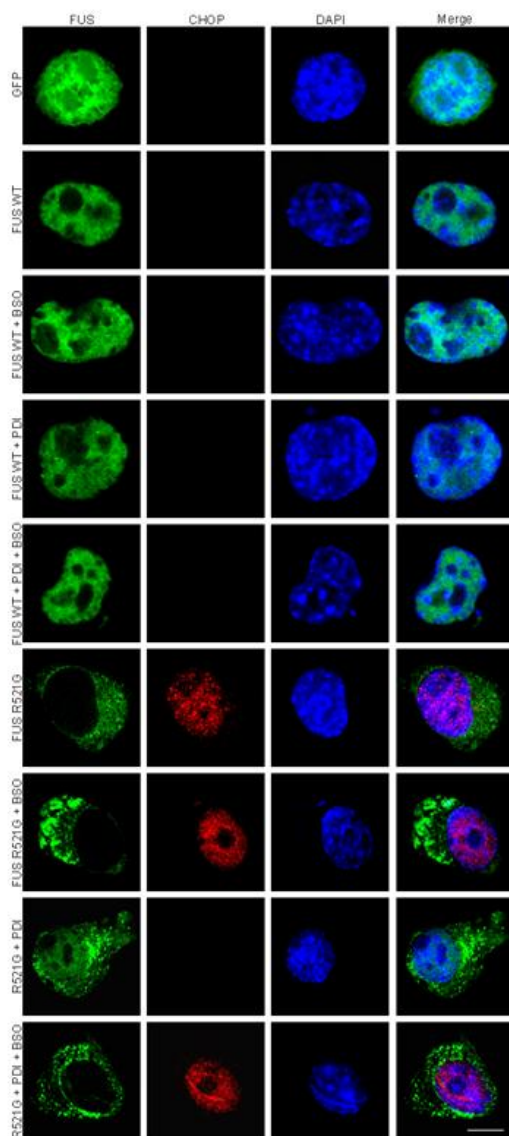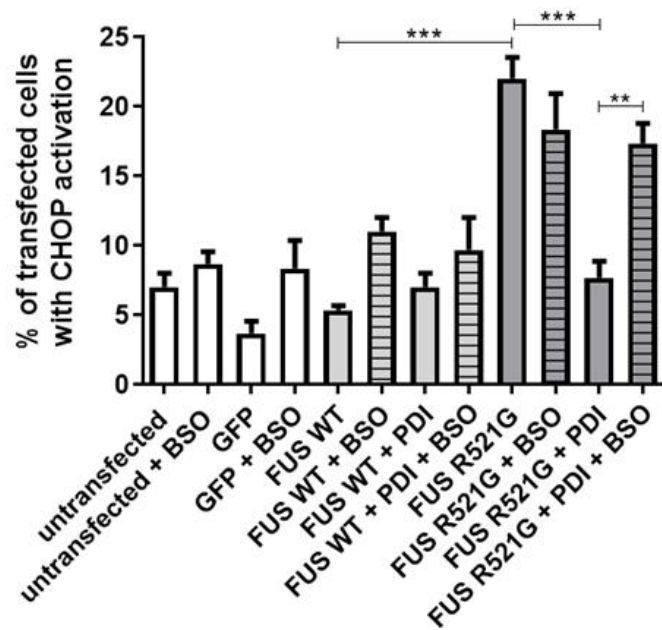
Figure 6.3: The administration of BSO impedes PDI's ability to inhibit CHOP activation induced by mutant FUS. A) Immunofluorescence images of Neuro-2A cells expressing GFP, wildtype FUS with either empty pcDNA3.1 vector or PDI (with and without BSO), and mutant FUS R521G with either pcDNA3.1 or PDI (with and without BSO). Cells expressing GFP (first panel; GFP) or wildtype FUS (panels two to five; FUS WT, FUS WT + BSO, FUS WT + PDI, FUS WT + PDI + BSO) rarely displayed CHOP activation. In contrast, more cells expressing mutant FUS R521G (panels six and seven; FUS R521G, FUS R521G + BSO) demonstrated CHOP nuclear immunoreactivity (panels six and seven, column two). Co-expression of mutant FUS R521G with PDI (panel eight; R521G + PDI) resulted in fewer cells displaying CHOP activation. However, the administration of BSO to cells co-expressing FUS R521G and PDI (panel nine; R521G + PDI + BSO) resulted in an increase in the proportion of cells with CHOP activation. Scale bar = 20 µM. **B)** Quantification of the cells in A) with CHOP activation. A significant increase ($p < 0.001$) in the proportion of cells with CHOP activation was observed when cells were co-expressed with mutant FUS R521G and empty pcDNA3.1 vector, compared to cells co-expressed with wildtype FUS and pcDNA3.1. There was a significant decrease ($p < 0.001$) in the proportion of mutant FUS R521G expressing cells displaying CHOP activation when PDI was co-expressed. However, when BSO was administered to cells co-expressing FUS R521G and PDI, significantly more cells ($p < 0.01$) displayed CHOP nuclear immunoreactivity, compared to these cells without BSO treatment. N=3, Mean ± SEM, ** $p < 0.01$, *** $p < 0.001$.

6.3.4 The administration of BSO impedes PDI's ability to inhibit mutant FUS inclusion formation

In previous studies performed in Chapter 4 and 5, the presence of inclusions was observed in the cytoplasm of cells expressing mutant FUS R521G, however they were not previously quantified in these experiments. Mutant FUS inclusions in Neuro-2A cells are observed as punctate structures in the cytoplasm. Moreover, the activity of PDI on mutant FUS inclusion formation has not been described previously in our laboratory. Hence, in these studies, mutant FUS inclusions were quantified, and the activity of PDI against the formation of these inclusions was investigated. Furthermore, the administration of BSO to in these cells was analysed for its effect on FUS inclusion formation.

Neuro-2A cells were transfected for 72 h with GFP alone, wildtype FUS with either empty pcDNA3.1 vector or PDI, and mutant FUS R521G with either pcDNA3.1 or PDI. These cell populations were both exposed and not exposed to BSO. After fixing, immunocytochemistry was performed using an anti-V5 antibody to detect the expression of V5-tagged PDI, and nuclei were stained with Hoechst. For each of three replicate experiments, at least 100 cells co-expressing FUS proteins and PDI were examined for the presence of FUS inclusions (GFP fluorescence) utilising fluorescent microscopy (Figure 6.4 A).

Untransfected cells and cells expressing GFP alone did not express GFP-FUS, and hence were not included in the analysis. Wildtype FUS cells, co-expressing either pcDNA3.1 or PDI, did not form inclusions. Interestingly though, upon BSO treatment, inclusions were occasionally observed in cells co-expressing wildtype FUS with either pcDNA3.1 or PDI, typically within the nucleus (9.3% ± 1.1 and 6.3% ± 1.3, respectively). Conversely, a high proportion of cells co-expressing mutant FUS R521G with empty pcDNA3.1 vector displayed FUS inclusions, with (22.0% ± 3.2) or without BSO administration (19.0% ± 1.4).

Co-expression of PDI with mutant FUS R521G resulted in a significant reduction ($p < 0.05$) in the proportion of cells bearing inclusions (11.5% $\pm$ 1.6), indicating that PDI is able to inhibit mutant FUS inclusion formation in Neuro-2A cells. However, upon BSO administration to cells co-expressing PDI and mutant FUS R521G, a significant increase ($p < 0.001$) in the proportion of cells with inclusions was observed (23.3% $\pm$ 1.8), compared to these cells without BSO treatment, implying that BSO impedes PDI's oxidase activity, and thus, its ability to inhibit FUS inclusion formation (Figure 6.4 B).

A

B

461
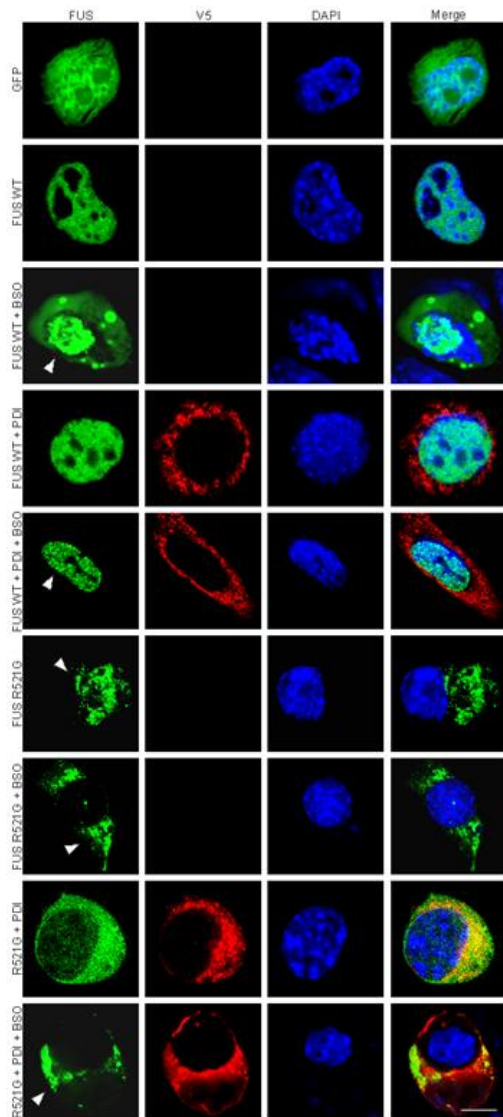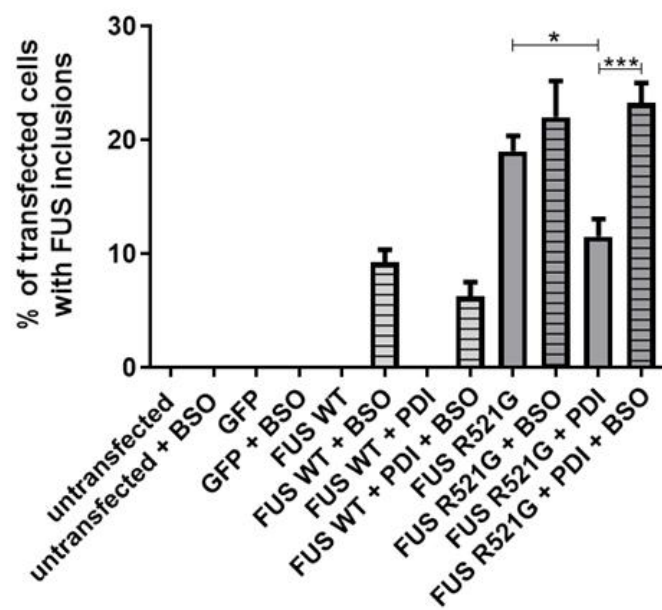
Figure 6.4: The administration of BSO impedes PDI's ability to inhibit mutant FUS inclusion formation. A) Immunofluorescence images of Neuro-2A cells expressing GFP, wildtype FUS with either pcDNA3.1 or PDI (with and without BSO), and mutant FUS R521G with either pcDNA3.1 or PDI (with and without BSO). Cells expressing GFP or wildtype FUS did not present with inclusions (panels one, two and four; GFP, FUS WT, FUS WT + PDI). In contrast, upon BSO treatment in cells expressing wildtype FUS, inclusions were observed (panels three and five; FUS WT + BSO, FUS WT + PDI + BSO), sometimes as a large prominent inclusion body (panel three, column 1), but usually as structures resembling paraspeckles (panel five, column 1) within the nucleus, indicated by the white arrowheads. More cells expressing mutant FUS R521G (panels six and seven; FUS R521G, FUS R521G + BSO) displayed FUS inclusions within the cytoplasm, as indicated by the white arrowheads (column one). Conversely, when PDI was co-expressed with mutant FUS R521G, fewer cells displayed FUS inclusions (panel eight; R521G + PDI). However, when BSO was administered to cells co-expressing PDI and FUS R521G, an increase in the proportion of cells with inclusions was observed (panel nine: R521G + PDI + BSO), as indicated by the white arrowhead (panel nine, column one). Scale bar = 20 µM. **B)** Quantification of Neuro-2A cells bearing FUS inclusions in A). No cells expressing wildtype FUS displayed inclusions. However, upon BSO administration, an increase in the proportion of wildtype FUS-expressing cells with inclusions was observed. There was a significant increase ($p < 0.001$) in the proportion of cells with FUS inclusions in cells expressing mutant FUS R521G, compared to cells expressing wildtype FUS. However, significantly fewer ($p < 0.05$) cells bore FUS inclusions in populations co-expressing PDI with mutant FUS R521G. Conversely, a significant increase ($p < 0.001$) in the proportion of cells with FUS inclusions was observed when BSO was administered to cells co-expressing PDI and mutant FUS

R521G, compared to these cells without BSO administration. N=3, Mean ± SEM, * $p < 0.05$,

*** $p < 0.001$.

6.3.5 The administration of BSO impedes the ability of BMC to inhibit mutant FUS mislocalisation to the cytoplasm

The next set of experiments investigated the effect of BSO on the PDI mimic, BMC. BMC mimics the disulphide interchange activity of PDI and possesses similar oxidoreductase properties [595]. Moreover, BMC has previously demonstrated protective activity against mutant FUS-induced ER stress and mislocalisation (Parakh et al., 2017 in preparation), therefore it was speculated whether BSO could inhibit the activity of BMC, similar to the way it inhibited PDI's function. The effect of BSO on BMC was first investigated in Neuro-2A cells expressing wildtype and mutant FUS by analysing FUS mislocalisation to the cytoplasm.

Neuro-2A cells were transfected for 72 h with GFP alone, wildtype FUS and mutant FUS R521G. Wildtype FUS and mutant FUS R521G were either co-expressed with empty pcDNA3.1 vector or PDI, or treated 5 h post-transfection with either DMSO (as a control) or BMC (with and without BSO administration). After fixing, nuclei were DAPI-stained with Hoechst and subsequently analysed using fluorescent microscopy for FUS mislocalisation to the cytoplasm. As previous, FUS was considered cytoplasmic when it was only detected in the cytoplasm, and was considered nuclear when it was expressed in both the nucleus and the cytoplasm of FUS expressing cells (Figure 6.5 A).

Untransfected cells and cells expressing GFP were excluded from analysis as they did not express FUS. Cells expressing wildtype FUS rarely displayed cytoplasmic FUS. In contrast, a significantly greater ($p < 0.001$) proportion of cells expressing mutant FUS R521G co-transfected with empty vector or treated with DMSO displayed FUS mislocalisation to the cytoplasm ($93.5\% \pm 1.2$ and $94.0\% \pm 1.6$, respectively), compared to cells expressing wildtype FUS. Co-expression of PDI with FUS R521G resulted in a significant decrease ($p <$

0.001) in the proportion of cells with cytoplasmic FUS (75.5% ± 3.8), compared to cells co-expressing FUS R521G with empty vector, as expected. Moreover, treatment of mutant FUS R521G expressing cells with BMC also significantly reduced (p < 0.01) the proportion of cells with mislocalisation (85.0% ± 1.1), however significantly more (p < 0.01) cells with cytoplasmic FUS were detected in these populations, compared to FUS R521G expressing cells with PDI. Interestingly, when BSO was administered to FUS R521G expressing cells with BMC treatment, a significant increase (p < 0.01) in the proportion of cells with FUS mislocalisation was observed (94.8% ± 1.7), compared to BMC treated cells expressing mutant FUS R521G without BSO treatment (Figure 6.5 B). These results indicate that BSO impedes BMC's ability to inhibit mutant FUS mislocalisation to the cytoplasm.
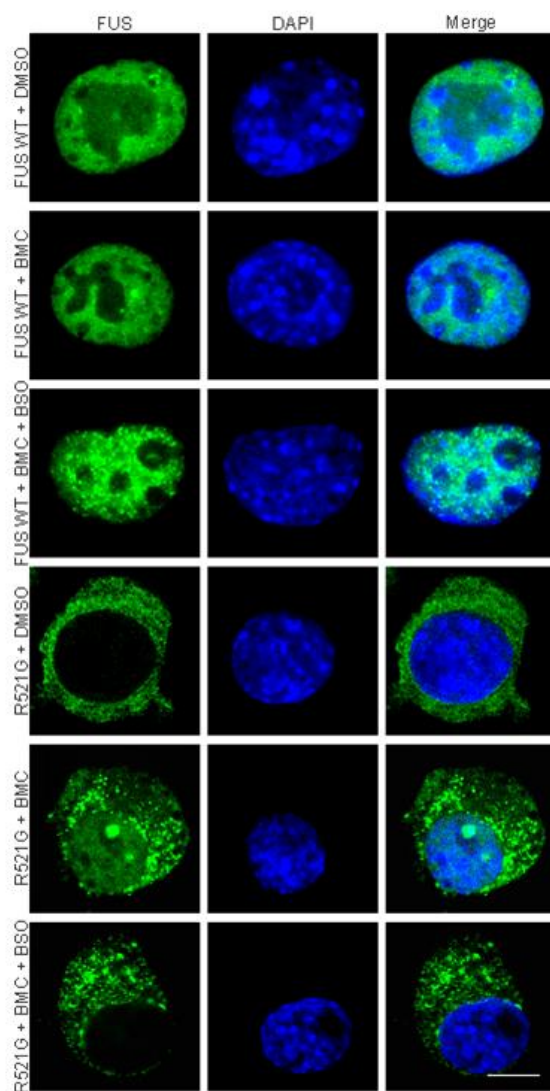
Figure 6.5: The administration of BSO impedes the ability of BMC to inhibit mutant FUS mislocalisation to the cytoplasm. A) Immunofluorescence images of Neuro-2A cells expressing wildtype FUS with treatment of either DMSO or BMC (with and without BSO), and mutant FUS R521G with treatment of either DMSO or BMC (with and without BSO). Cells expressing wildtype FUS displayed only nuclear localisation of FUS (panels 1-3; FUS WT + DMSO, FUS WT + BMC, FUS WT + BMC + BSO). Cells expressing mutant FUS R521G and treated with DMSO (panel four; R521G + DMSO) displayed mainly cytoplasmic FUS. In contrast, when mutant FUS R521G expressing cells were treated with BMC (panel five; R521G + BMC), fewer cells displayed FUS mislocalisation, as indicated by localisation of FUS in both the nucleus and cytoplasm (panel five, column one). However, BSO administration to FUS R521G expressing cells treated with BMC (panel six; R521G + BMC + BSO) resulted in mainly cytoplasmic FUS. Scale bar = 20 µM. **B)** Quantification of cells in A) with FUS mislocalisation to the cytoplasm. A significant increase ($p < 0.001$) in the proportion of mutant FUS R521G expressing cells with FUS mislocalisation to the cytoplasm was observed, compared to wildtype FUS expressing cells. In contrast, significantly fewer cells exhibited FUS mislocalisation when mutant FUS R521G cells were either co-expressed with PDI ($p < 0.001$) or treated with BMC ($p < 0.01$), compared to mutant FUS R521G expressing cells treated with DMSO. However, significantly more ($p < 0.01$) FUS R521G cells displayed FUS mislocalisation when treated with BMC, compared to when co-expressed with PDI. Moreover, significantly more ($p < 0.01$) BMC treated FUS R521G expressing cells displayed FUS mislocalisation when BSO was administered, compared to BMC treated FUS R521G expressing cells without BSO administration. N=3, Mean ± SEM, ** $p < 0.01$, *** $p < 0.001$.

6.3.6 The administration of BSO impedes the ability of BMC to inhibit CHOP activation induced by mutant FUS

Next, the effect of BSO on BMC's protective activity against mutant FUS induced ER stress was investigated. Neuro-2A cells were transfected for 72 h with GFP alone, wildtype FUS and mutant FUS R521G. Wildtype FUS and mutant FUS R521G were either co-expressed with empty pcDNA3.1 vector or PDI, or treated 5 h post-transfection with either DMSO (as a control) or BMC (with and without BSO administration). After fixing, immunocytochemistry was performed using an anti-CHOP antibody to examine CHOP activation. Cells were also stained with Hoechst to visualise the nuclei before fluorescent microscopy was used to analyse at least 100 FUS expressing cells for nuclear immunoreactivity to CHOP (Figure 6.6 A).

Less than 10% of untransfected cells, or cells expressing GFP, or wildtype FUS with either DMSO, PDI or BMC, presented with CHOP activation. In contrast, a significant increase ($p < 0.001$) in the proportion of cells displaying CHOP nuclear immunoreactivity was observed in populations expressing mutant FUS R521G with either empty pcDNA3.1 vector or treated with DMSO (22.0% $\pm$ 1.5 and 20.0% $\pm$ 1.2, respectively), compared to cells expressing wildtype FUS with either empty vector or DMSO (5.0% $\pm$ 0.6 and 7.7% $\pm$ 1.9, respectively). Significantly fewer ($p < 0.001$) mutant FUS R521G expressing cells presented with CHOP activation when either PDI was co-expressed (7.7% $\pm$ 1.2), or BMC was administered (9.7% $\pm$ 1.9), as expected. However, when BSO was administered to FUS R521G expressing cells treated with BMC, there was a significant increase ($p < 0.05$) in the proportion of cells exhibiting CHOP activation (16.7% $\pm$ 1.9), compared to BMC treated FUS R521G expressing cells without BSO administration (Figure 6.6 B). Hence these data indicate that BSO impedes BMC's protective activity against mutant FUS-induced ER stress.

A

B

469
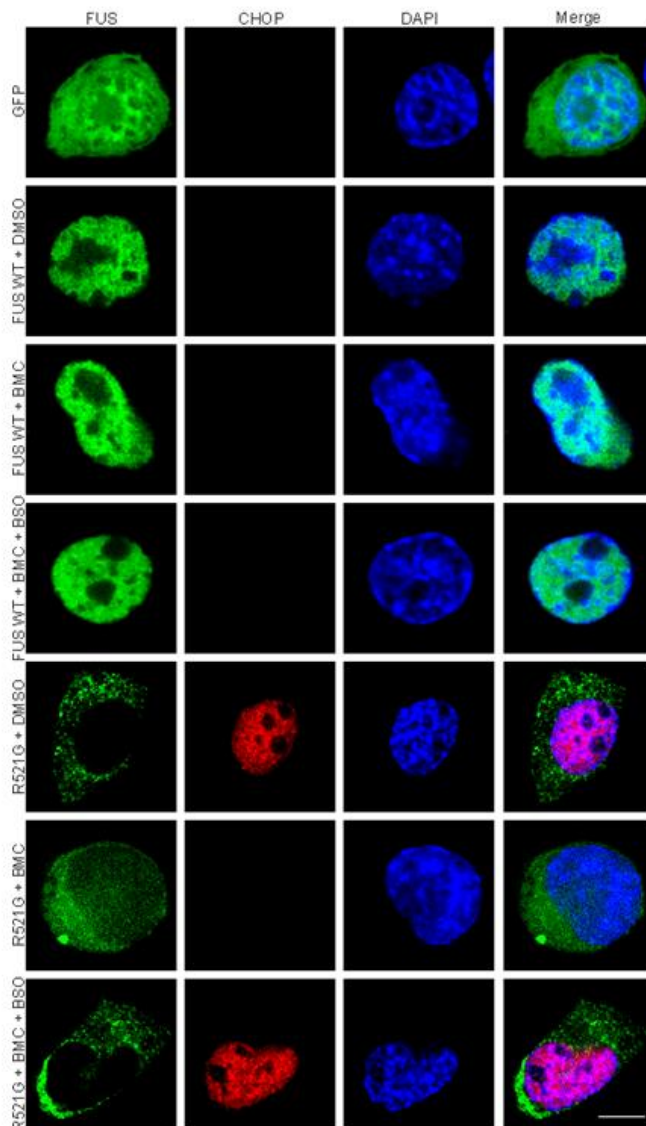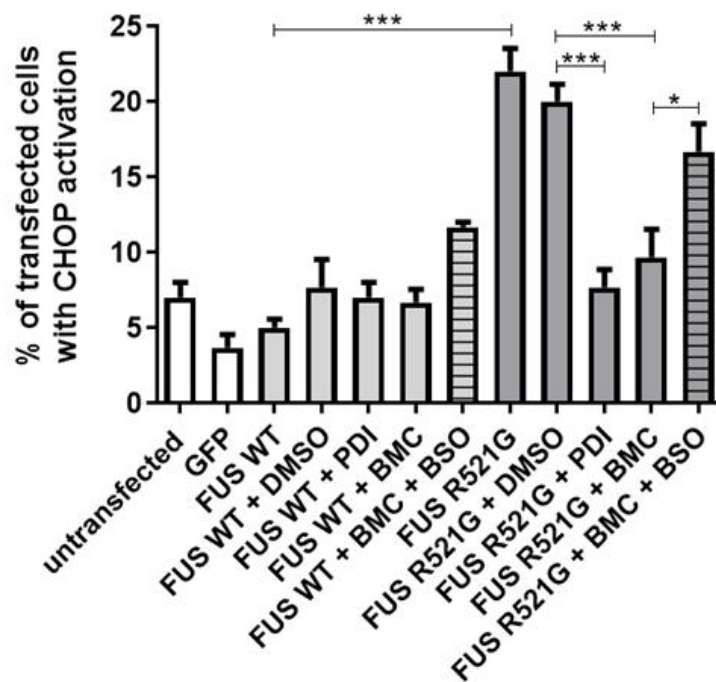
Figure 6.6: The administration of BSO impedes the ability of BMC to inhibit CHOP activation induced by mutant FUS. A) Immunofluorescence images of Neuro-2A cells expressing GFP, wildtype FUS with treatment of either DMSO or BMC (with and without BSO), and mutant FUS R521G with treatment of either DMSO or BMC (with and without BSO). Cells expressing GFP (first panel; GFP) or wildtype FUS (panels 2-4; FUS WT + DMSO, FUS WT + BMC, FUS WT + BMC + BSO) rarely display CHOP activation. Conversely, more cells expressing mutant FUS R521G with DMSO treatment (panel five; R521G + DMSO) display nuclear immunoreactivity to CHOP (fifth panel, column two). Fewer cells exhibit CHOP activation when mutant FUS R521G is treated with BMC (panel six; R521G + BMC), however, when BMC treated FUS R521G expressing cells are exposed to BSO, more cells display CHOP activation (panel seven; R521G + BMC + BSO), indicated by its nuclear immunoreactivity (panel seven, column two). **B)** Quantification of the cells in A) with CHOP activation. A significant increase ($p < 0.001$) in the proportion of cells with CHOP activation was observed in populations expressing mutant FUS R521G compared to cells expressing wildtype FUS. However, there was a significant decrease ($p < 0.001$) in the proportion of FUS R521G expressing cells with CHOP activation when either PDI was co-expressed, or BMC was administered. In contrast, significantly more ($p < 0.05$) BMC treated FUS R521G expressing cells displayed CHOP activation when they were exposed to BSO. N=3, Mean ± SEM, * $p < 0.05$, *** $p < 0.001$.

6.3.7 The administration of BSO impedes the ability of BMC to inhibit mutant FUS inclusion formation

As PDI was demonstrated to be protective against mutant FUS inclusion formation (section 6.3.4), it was finally investigated whether BMC is also protective, as this has not yet been previously shown and if so, whether BSO could also impede this function. To examine this, Neuro-2A cells were transfected with GFP alone, wildtype FUS and mutant FUS R521G. Wildtype FUS and mutant FUS R521G were either co-expressed with empty pcDNA3.1 vector or PDI, or treated 5 h post-transfection with either DMSO (as a control) or BMC (with and without BSO administration). After 72 h, cells were fixed and nuclei were stained with Hoechst before fluorescent microscopy was utilised to examine and quantify at least 100 FUS-expressing cells for the presence of FUS inclusions (Figure 6.7 A).

Untransfected cells and cells expressing GFP were excluded from analysis as they did not express FUS. As expected, cells expressing wildtype FUS did not bear any inclusions, however, interestingly, when BSO was administered to wildtype FUS expressing cells, a small proportion of cells displayed inclusions in the nucleus (5.25% $\pm$ 0.5). Compared to wildtype FUS expressing cells, significantly more cells ($p < 0.001$) expressing mutant FUS R521G, with either empty pcDNA3.1 vector or DMSO treatment, displayed inclusions (18.0% $\pm$ 1.1 and 15.8% $\pm$ 1.1, respectively), as expected. Co-expression of mutant FUS R521G with PDI significantly reduced the proportion of cells bearing FUS inclusions to 11.5% $\pm$ 1.6, compared to mutant FUS R521G expressing cells with either empty vector ($p < 0.001$) or with DMSO treatment ($p < 0.05$). Similarly, BMC treatment to cells expressing mutant FUS R521G also significantly reduced ($p < 0.001$) the proportion of cells bearing inclusions (8.8% $\pm$ 0.6), indicating that BMC is able to inhibit mutant FUS inclusion formation. Upon BSO administration to BMC treated cells expressing mutant FUS R521G, significantly more ($p < 0.001$) cells displayed FUS inclusions (16.8% $\pm$ 1.4), compared to

these cells without BSO administration (Figure 6.7 B), implying that BSO impedes BMC's

protective activity against mutant FUS inclusion formation.

A
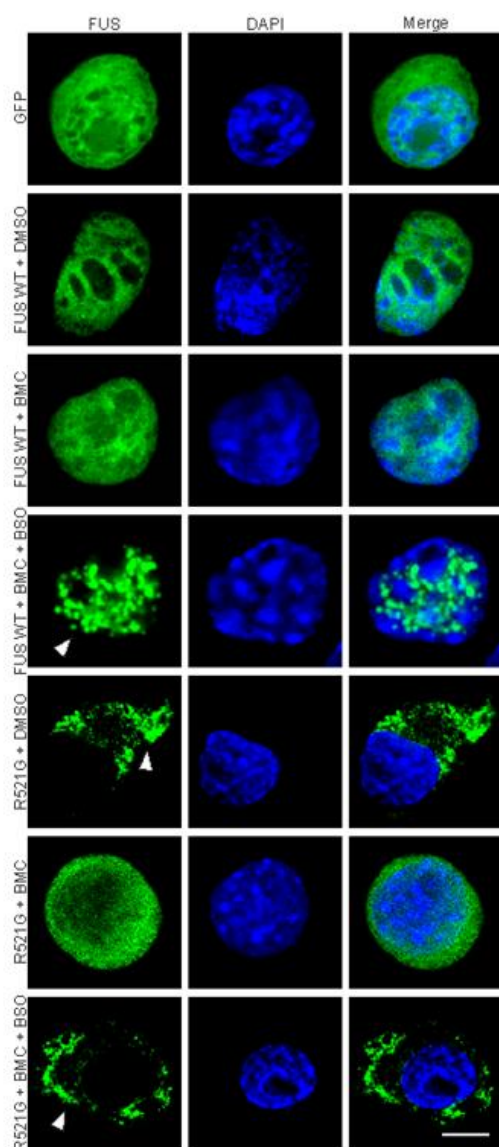
B

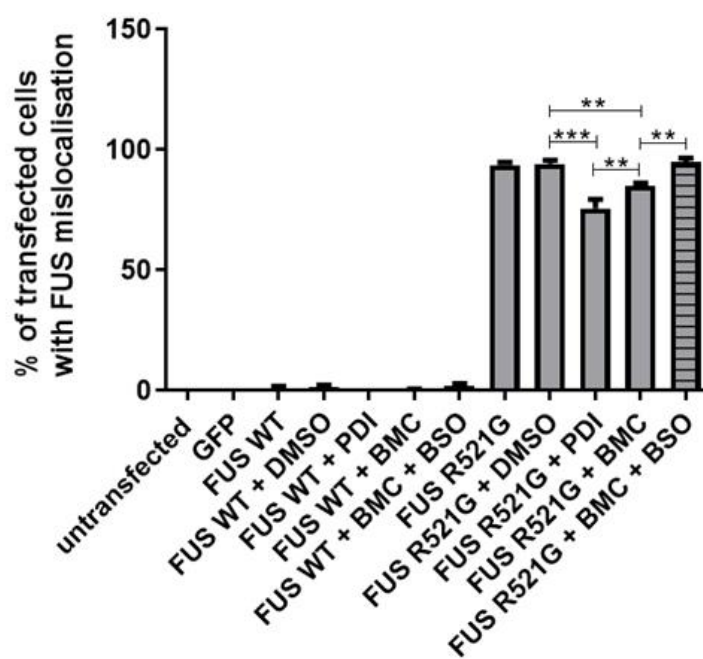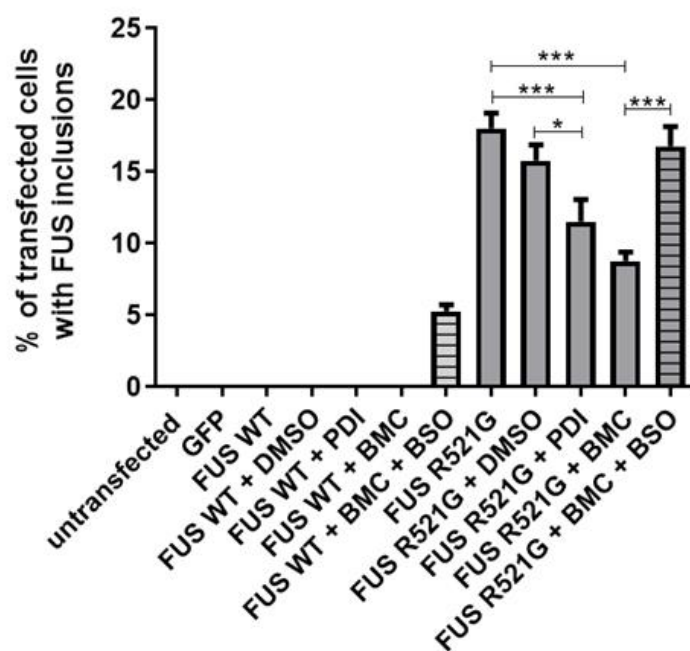**Figure 6.7: The administration of BSO impedes the ability of BMC to inhibit mutant FUS inclusion formation. A)** Immunofluorescence images of Neuro-2A cells expressing GFP, wildtype FUS with treatment of either DMSO or BMC (with and without BSO), and mutant FUS R521G with treatment of either DMSO or BMC (with and without BSO). Cells expressing GFP (first panel; GFP) or wildtype FUS (panels two and three; FUS WT + DMSO, FUS WT + BMC) did not present with inclusions. However, when wildtype FUS expressing cells were exposed to BSO (panel four; FUS WT + BMC + BSO), a small proportion of cells displayed inclusions within the nucleus, as indicated by the white arrowhead (fourth panel, column one). More cells expressing mutant FUS R521G with DMSO treatment (panel five; R521G + DMSO) displayed FUS inclusions in the cytoplasm, as indicated by the white arrowhead (panel five, column one). Conversely, when mutant FUS R521G expressing cells were treated with BMC (panel six; R521G + BMC), fewer cells displayed inclusions, however, when BSO was administered to these cells (panel seven; R521G + BMC + BSO), a greater proportion of cells presented with inclusions. Scale bar = 20 µM. **B)** Quantification of Neuro-2A cells bearing FUS inclusions in A). There was a significant increase ($p < 0.001$) in the proportion of cells with FUS inclusions in cells expressing mutant FUS R521G, compared to cells expressing wildtype FUS. A significant decrease in the proportion of cells with FUS inclusions was observed when PDI was co-expressed ($p < 0.05$), or BMC was administered ($p < 0.001$), to cells expressing mutant FUS R521G, compared to DMSO treated cells expressing mutant FUS R521G. Conversely, significantly more ($p < 0.001$) cells displayed inclusions in BMC treated FUS R521G expressing cells exposed to BSO, compared to those without exposure to BSO. N=3, Mean ± SEM, * $p < 0.05$, *** $p < 0.001$.

6.3.8 Cellular localisation of PDI variants, D292N and R300H, in Neuro-2A cells

The next set of experiments of this chapter focuses on the activity of PDI variants, D292N and R300H on mutant FUS cellular pathogenic mechanisms, including mislocalisation to the cytoplasm, ER stress and inclusion formation, and whether they still possess a protective function, similar to wildtype PDI. Furthermore, it was hypothesised that these mutations do not alter the protective function of PDI via its oxidase activity, thus the effect of BSO administration on these variants were also investigated.

Firstly, to ensure that PDI variants D292N and R300H were expressed within the ER, like wildtype PDI, the localisation of the V5-tagged PDI proteins were analysed in Neuro-2A cells using confocal microscopy. Cells were transfected with either the D292N or R300H variant for 24 h before immunocytochemistry using an anti-V5 tag antibody to visualise the mutants, and an anti-calreticulin antibody to probe for the ER-resident protein, calreticulin. These results demonstrated that both D292N and R300H variants were co-localised with calreticulin in all transfected cells, indicating their localisation in the ER, as expected (Figure 6.8), and that the mutations do not alter their subcellular distribution of PDI.
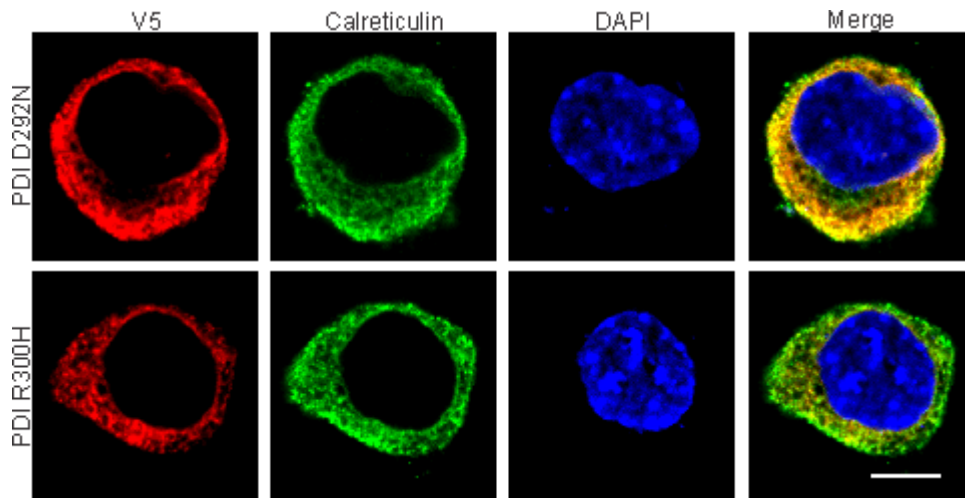
Figure 6.8: The PDI variants D292N and R300H are localised within the ER of Neuro-2A cells. Neuro-2A cells were transfected with either the D292N or R300H PDI variants (first column; V5) for 24 h. Cells were fixed and immunocytochemistry performed using antibodies for V5 tag and calreticulin (second column; Calreticulin), and nuclei were stained using Hoechst (third column; DAPI). The yellow in the merge column (fourth column; Merge) illustrates co-localisation of both D292N and R300H variants with calreticulin, demonstrating that the PDI variants, D292N and R300H, are localised within the ER. Scale bar = 20 μM.

6.3.9 PDI D292N and PDI R300H are co-expressed in almost all cells transfected with FUS

Firstly, the co-transfection efficiency of the PDI variants and mutant FUS was examined in Neuro-2A cells. Cells were transfected with mutant FUS R521G and either PDI D292N or PDI R300H for 72, before fixing and performing immunocytochemistry using an anti-V5 antibody. DAPI-staining was performed using Hoechst to visualise the nuclei. Co-transfection was verified by GFP fluorescence from FUS and performing immunocytochemistry with an Alexa Fluor 568-tagged secondary antibody to detect the V5 tag of the PDI variants (Figure 6.9). At 72 h post-transfection, the overall transfection efficiency of mutant FUS was found to be approximately 75-80% in Neuro-2A cells. For each of the three replicate experiments, fluorescent microscopy was used to examine at least 100 FUS-expressing cells and these cells were further analysed for co-expression with the PDI variants, D292N and R300H. Quantification revealed that approximately 97% of FUS-expressing also co-expressed PDI D292N, and 96% co-expressed PDI R300H. Therefore, in all further experiments, it was assumed that detection of FUS expression reflected co-expression of both FUS and the PDI variants when they were co-transfected and immunocytochemistry using a V5 antibody was not performed.
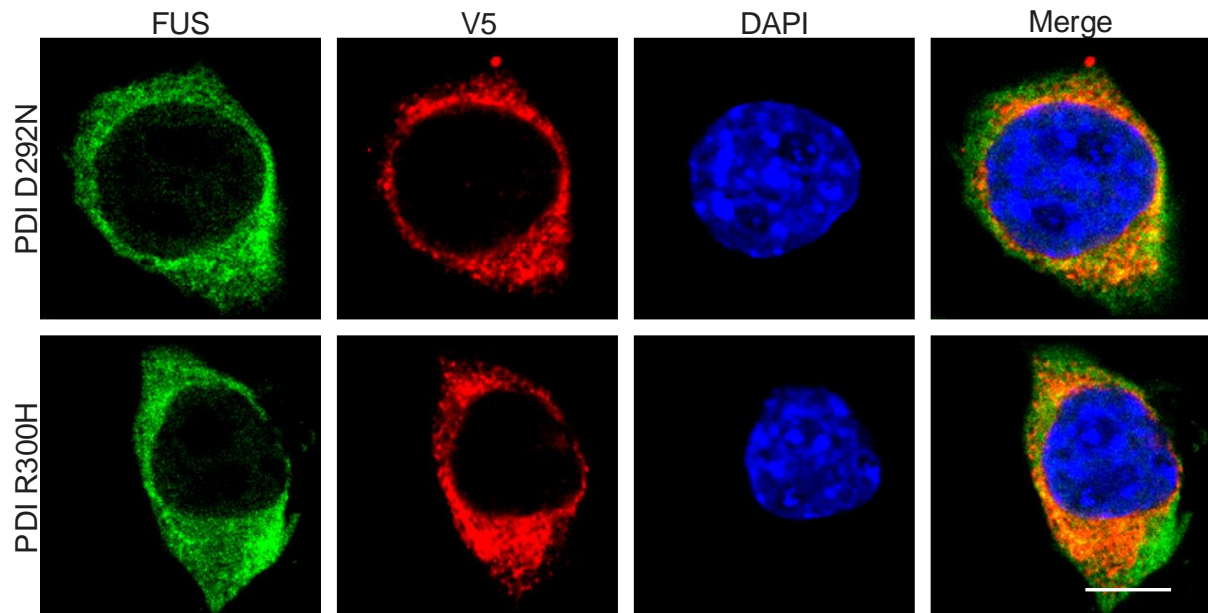
Figure 6.9: The PDI D292N and R300H variants are co-expressed in almost all Neuro-2A cells co-transfected with mutant GFP-FUS. Neuro-2A cells were transfected with mutant FUS (first column; FUS), and either PDI D292N or PDI R300H (second column; V5) for 72 h. Cells were fixed and immunocytochemistry was performed using an anti-V5 antibody and nuclei were stained with Hoechst (third column; DAPI). The merge column demonstrates co-expression of the PDI variants, D292N and R300H, with mutant FUS. Scale bar = 30 μM.

6.3.10 Protein expression of FUS and the PDI variants, D292N and R300H, in Neuro-2A cells

Once localisation and expression of the PDI variants was established in Neuro-2A cells, Western blotting analysis was performed to ensure that the transfection of each protein resulted in similar expression levels and to confirm that the expressed proteins were of the expected MW (Figure 6.10). Cell lysates were prepared from the following cell populations; GFP alone, wildtype FUS co-expressed with either empty pcDNA3.1 vector, wildtype PDI, PDI D292N or PDI R300H, and mutant FUS R521G co-expressed with either empty pcDNA3.1, wildtype PDI, PDI D292N or PDI R300H. Immunoblotting using an anti-GFP antibody revealed that wildtype and mutant FUS proteins were expressed at the expected size of 100 kDa, and were expressed at similar levels across cell lysate populations. Moreover, GFP alone was expressed at 26 kDa. Wildtype PDI and the PDI variants were detected at 62 kDa using an anti-V5 antibody, and were expressed at similar levels. β-actin was used as a loading control and was detected using an anti-β-actin antibody at 40 kDa.
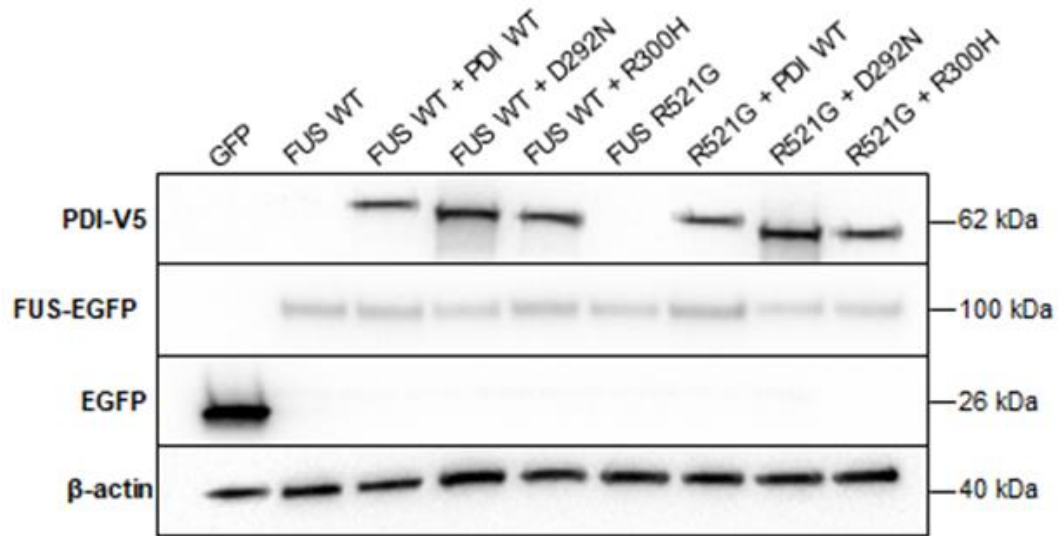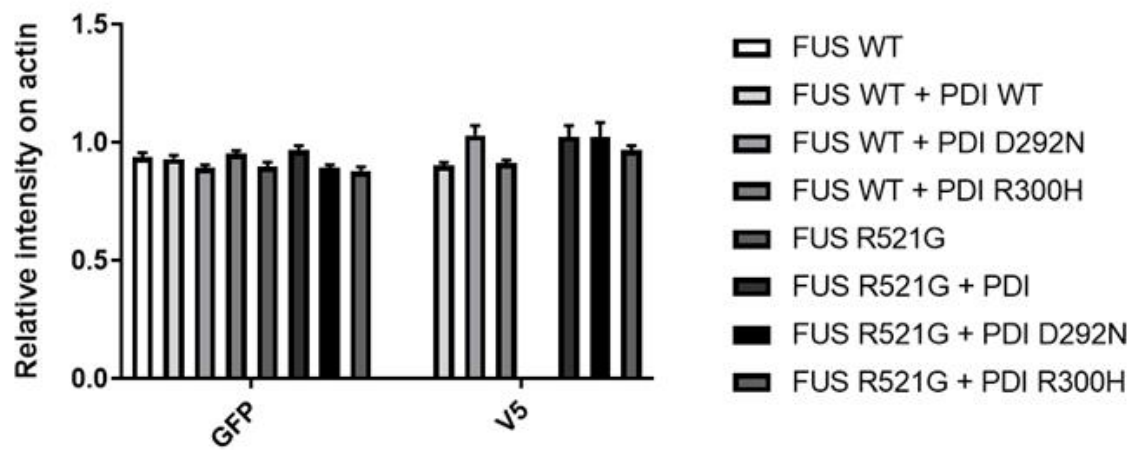
Figure 6.10: Protein expression of FUS and the PDI variants, D292N and R300H, in Neuro-2A cells. A) Western blotting analysis of cell lysates was performed and quantified to ensure that FUS proteins the PDI variants were expressed at similar levels and were of the expected MW. Lysates examined were from cells expressing either GFP alone, wildtype FUS co-expressed with either empty pcDNA3.1 vector, wildtype PDI, PDI D292N or PDI R300H, and mutant FUS R521G co-expressed with either empty pcDNA3.1 vector, wildtype PDI, PDI D292N or PDI R300H. Wildtype PDI and the PDI variants were detected at 62 kDa, as expected (PDI = 60 kDa, V5 = 2 kDa). Wildtype and mutant FUS R521G were detected at 100 kDa, and GFP alone was detected at 26 kDa. β-actin was detected at 40 kDa. **B)** Quantification revealed that wildtype and mutant FUS were expressed at similar levels across all cell lysate populations. PDI proteins were also expressed at similar levels. Lysates expressing GFP only were not included in the quantification. N = 3, Mean ± SEM.

6.3.11 PDI D292N and R300H are protective against mutant FUS mislocalisation to the cytoplasm, however, their function is perturbed when BSO is administered

The PDI variants, D292N and R300H, were first examined in Neuro-2A cells expressing mutant FUS to determine whether they could inhibit FUS mislocalisation to the cytoplasm. Neuro-2A cells were transfected with GFP alone, wildtype FUS with either pcDNA3.1, wildtype PDI, PDI D292N or PDI R300H, and mutant FUS R521G with either pcDNA3.1, wildtype PDI, PDI D292N or PDI R300H. After 72 h, cells were fixed and immunocytochemistry was performed using an anti-V5 antibody to detect expression of V5-tagged PDI proteins. Cells were stained with Hoechst to visualise the nuclei and fluorescent microscopy was utilised to examine the cellular location of FUS (Figure 6.11 A).

Untransfected cells and cells expressing GFP alone were excluded in the analysis as they did not express GFP-FUS. In wildtype FUS cells, FUS was expressed within the nucleus and was rarely detected in the cytoplasm ($1.0\% \pm 0.7$). Conversely, a high proportion of cells co-expressing mutant FUS R521G with empty pcDNA3.1 vector displayed mislocalisation to the cytoplasm ($93.5\% \pm 1.2$). However, a significant decrease ($p < 0.001$) in the proportion of cells with cytoplasmic FUS was observed when wildtype PDI was co-expressed with mutant FUS R521G ($75.5\% \pm 3.8$), compared to cells co-expressing mutant FUS R521G with empty vector. Moreover, compared to FUS R521G expressing cells with empty vector, significantly fewer displayed cytoplasmic FUS when either PDI D292N ($p < 0.001$, $80.8\% \pm 1.4$) or PDI R300H ($p < 0.05$, $85.5\% \pm 1.7$) were co-expressed with mutant FUS R521G, indicating that the PDI variants still retain their protective activity against FUS mislocalisation to the cytoplasm. Interestingly, however, a significant increase ($p < 0.01$) in the proportion of cells with FUS mislocalisation was observed in cells co-expressing FUS R521G and PDI R300H, compared to cells co-expressing FUS R521G and wildtype PDI, suggesting that the

protective activity of PDI R300H may not be as effective as that of wildtype PDI (Figure 6.11 B).

Next, the PDI variants were analysed for their protective activity against FUS mislocalisation upon administration of BSO. As expected, a high proportion of cells expressing mutant FUS R521G with empty pcDNA3.1 vector displayed cytoplasmic FUS (93.5% $\pm$ 1.2), compared to cells expressing wildtype FUS. Significantly fewer mutant FUS R521G expressing cells displayed mislocalisation when either PDI D292N ($p < 0.001$, 80.8% $\pm$ 1.4) or PDI R300H ($p < 0.01$, 85.5% $\pm$ 1.7) were co-expressed. However, upon administration of BSO to cells co-expressing FUS R521G and PDI D292N, a significant increase ($p < 0.001$) in the proportion of cells with FUS mislocalisation was observed (94.3% $\pm$ 2.5), compared to these cells without exposure to BSO. Similarly, when BSO was administered to FUS R521G cells co-expressing PDI R300H, significantly more ($p < 0.01$) cells displayed cytoplasmic FUS (93.8% $\pm$ 0.5), compared to these cells without BSO administration (Figure 6.11 C). These findings suggest that the loss of oxidase activity in the PDI variants, due to exposure to BSO, results in a loss of protective function.

A

	FUS	V5	DAPI	Merge
FUS WT				
FUS WT + PDI WT				
FUS WT + D292N				
FUS WT + R300H				
FUS R521G				
R521G + PDI WT				
R521G + D292N				
R521G + D292N + BSO				
R521G + R300H				
R521G + R300H + BSO				

B

% of transfected cells with FUS mislocalisation

C

% of transfected cells with FUS mislocalisation

484
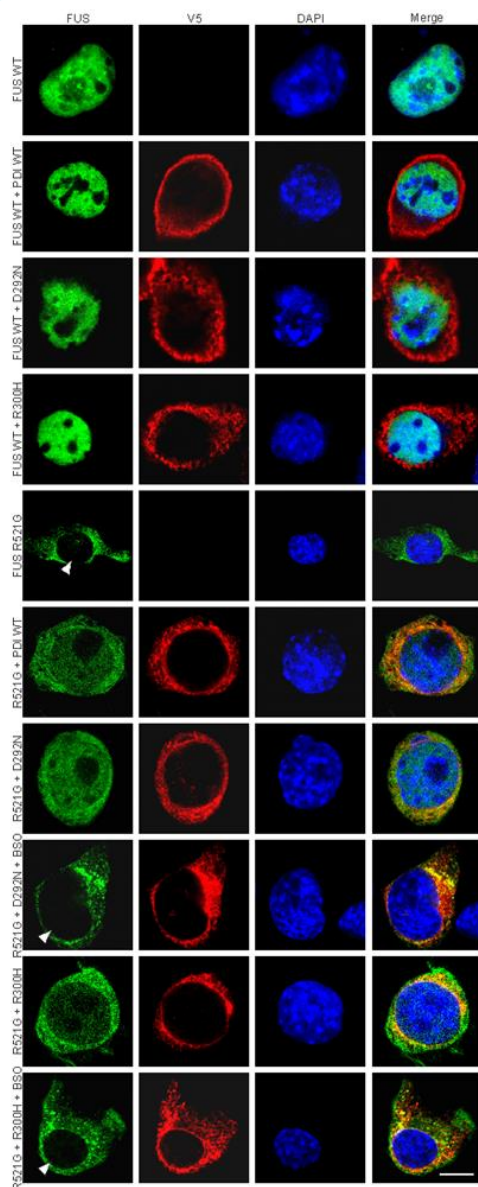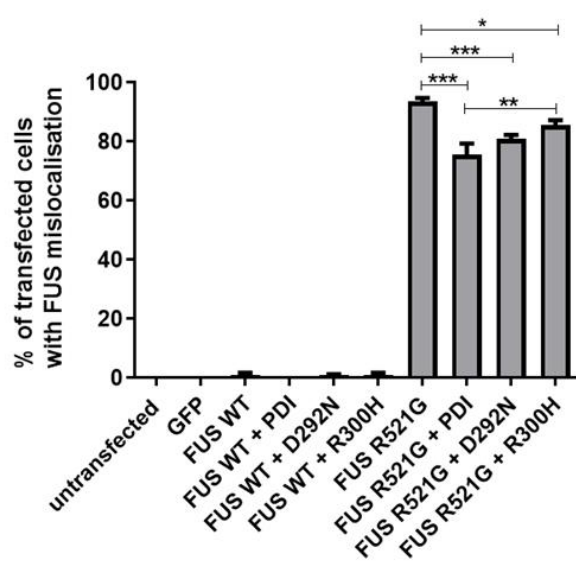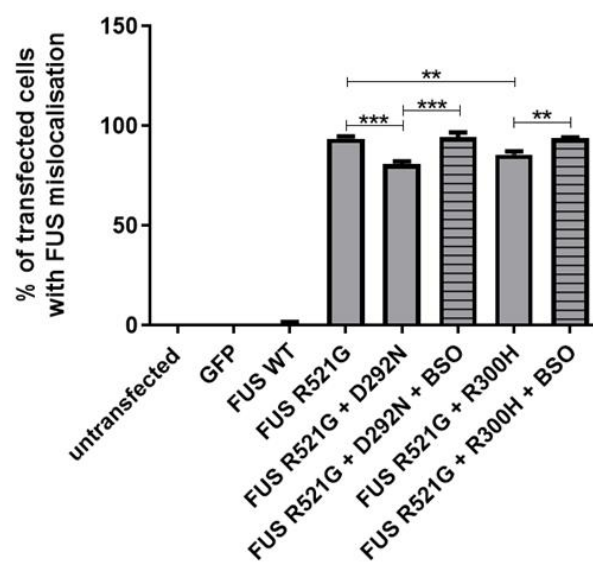
Figure 6.11: PDI D292N and R300H are protective against mutant FUS mislocalisation to the cytoplasm, however, their function is perturbed when BSO is administered. A) Immunofluorescence images of Neuro-2A cells expressing wildtype FUS with either pcDNA3.1, wildtype PDI, PDI D292N or PDI R300H, and mutant FUS R521G with either pcDNA3.1, wildtype PDI, PDI D292N (with and without BSO) and PDI R300H (with and without BSO). Cells expressing wildtype FUS (panels 1-4; FUS WT, FUS WT + PDI WT, FUS WT + D292N, FUS WT + R300H) displayed localisation within the DAPI-stained nucleus. In contrast, mutant FUS R521G (panel five; FUS R521G) was frequently observed in the cytoplasm, as indicated by no fluorescence in the nucleus. However, when wildtype PDI, PDI D292N or PDI R300H were co-expressed with mutant FUS R521G, fewer cells displayed cytoplasmic FUS, as illustrated by the localisation of FUS in both the nucleus and cytoplasm (panel six, seven and nine; R521G + PDI WT, R521G + D292N, R521G + R300H). Upon BSO administration to FUS R521G cells co-expressing PDI D292N and PDI R300H, more cells displayed cytoplasmic FUS (panels eight and ten; R521G + D292N + BSO, R521G + R300H + BSO). Scale bar = 20 μM. **B)** Quantification of Neuro-2A cells with FUS mislocalisation to the cytoplasm in A). Wildtype FUS was never found in the cytoplasm of Neuro-2A cells, whereas FUS R521G was expressed mostly in the cytoplasm. There was a significant decrease in the proportion of cells with cytoplasmic FUS when wildtype PDI ($p < 0.001$), PDI D292N ($p < 0.001$) or PDI R300H ($p < 0.05$) were co-expressed with mutant FUS R521G. Significantly more ($p < 0.01$) FUS R521G cells displayed mislocalisation when co-expressed with PDI R300H, compared to FUS R521G cells co-expressed with wildtype PDI. N=3, Mean ± SEM, * $p < 0.05$, ** $p < 0.01$, *** $p < 0.001$. **C)** A significant decrease in the proportion of mutant FUS R521G expressing cells with mislocalisation was observed in populations co-expressing either PDI D292N ($p < 0.001$) or PDI R300H ($p < 0.01$), compared to those expressing mutant FUS R521G and

485

empty vector. A significant increase (p < 0.001) in the proportion of cells with FUS

mislocalisation was observed when cells co-expressing FUS R521G and PDI D292N were

exposed to BSO, compared to these cells without exposure to BSO. Similarly, significantly

more (p < 0.01) cells displayed mislocalisation when BSO was administered to FUS R521G

populations co-expressing PDI R300H, compared to these cells without BSO administration.

N=3, Mean ± SEM, ** p < 0.01, *** p < 0.001.

6.3.12 PDI D292N and R300H are protective against CHOP activation induced by mutant FUS, however their protective activity is perturbed upon BSO administration

The activity of PDI D292N and PDI R300H was next investigated against mutant FUS-induced ER stress. Neuro-2A cells were transfected for 72 h with GFP alone, wildtype FUS with either pcDNA3.1, wildtype PDI, PDI D292N or PDI R300H, and mutant FUS R521G with either pcDNA3.1, wildtype PDI, PDI D292N or PDI R300H. After fixing, immunocytochemistry was performed using an anti-CHOP antibody and cells were stained with Hoechst to detect the nuclei. Fluorescence microscopy was utilised to examine at least 100 FUS transfected cells for ER stress, whereby nuclear immunoreactivity to CHOP was indicative of its activation (Figure 6.12 A).

Untransfected cells, or cells expressing either GFP alone or wildtype FUS rarely displayed CHOP activation (less than 10%). Conversely, significantly more (p < 0.001) cells expressing mutant FUS R521G and empty pcDNA3.1 vector displayed nuclear immunoreactivity to CHOP (22.0% ± 1.5), compared to those expressing wildtype FUS and empty pcDNA3.1 vector (5.0% ± 0.6). Co-expression of either wildtype PDI (7.7% ± 1.2), PDI D292N (8.0% ± 3.1) or PDI R300H (10.0% ± 1.8) with mutant FUS R521G resulted in a significant reduction (p < 0.001) in the proportion of cells with CHOP activation, compared to those expressing mutant FUS R521G with empty vector (Figure 6.12 B). Hence, these data imply that PDI D292N and R300H are protective against mutant FUS-induced ER stress.

Next, the PDI variants were analysed for their protective activity against ER stress induced by mutant FUS upon administration of BSO. Significantly more (p < 0.001) cells expressing mutant FUS R521G and pcDNA3.1 displayed CHOP activation (22.0% ± 1.5), compared to cells expressing wildtype FUS (5.0% ± 0.6). However, this proportion of FUS R521G populations with CHOP activation was significantly reduced (p < 0.001) when either PDI

D292N (8.0% ± 3.1) or PDI R300H (10.0% ± 1.8) were co-expressed. Administration of BSO to cells co-expressing mutant FUS R521G and PDI D292N resulted in a significant increase ($p < 0.05$) in the proportion of cells with nuclear immunoreactivity to CHOP (16.0% ± 1.5), compared to these cells without BSO. Similarly, when BSO was administered to FUS R521G cells co-expressed with PDI R300H, significantly more ($p < 0.05$) cells displayed CHOP activation (15.3% ± 0.9), compared to these cells without exposure to BSO (Figure 6.12 C). These results suggest that BSO perturbs the protective activity of the PDI variants against mutant FUS-induced ER stress.

489
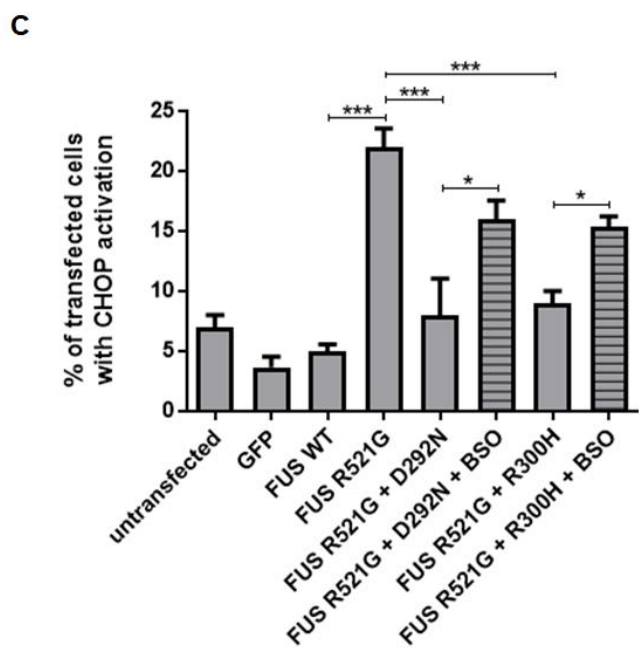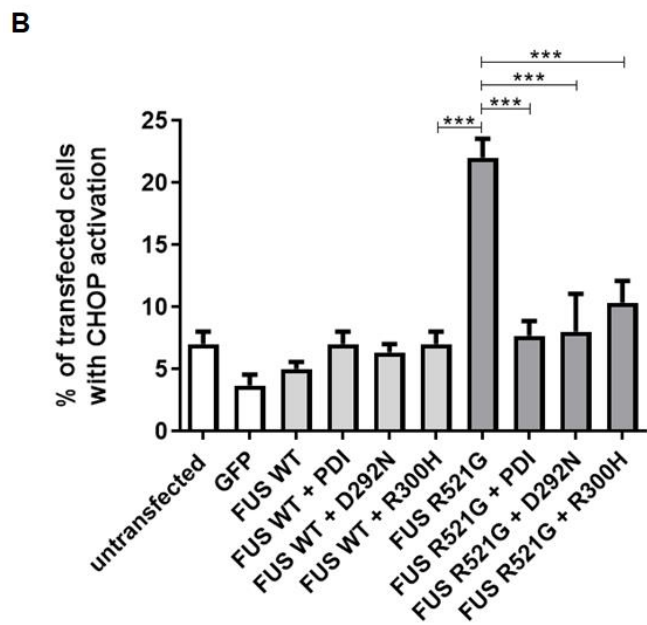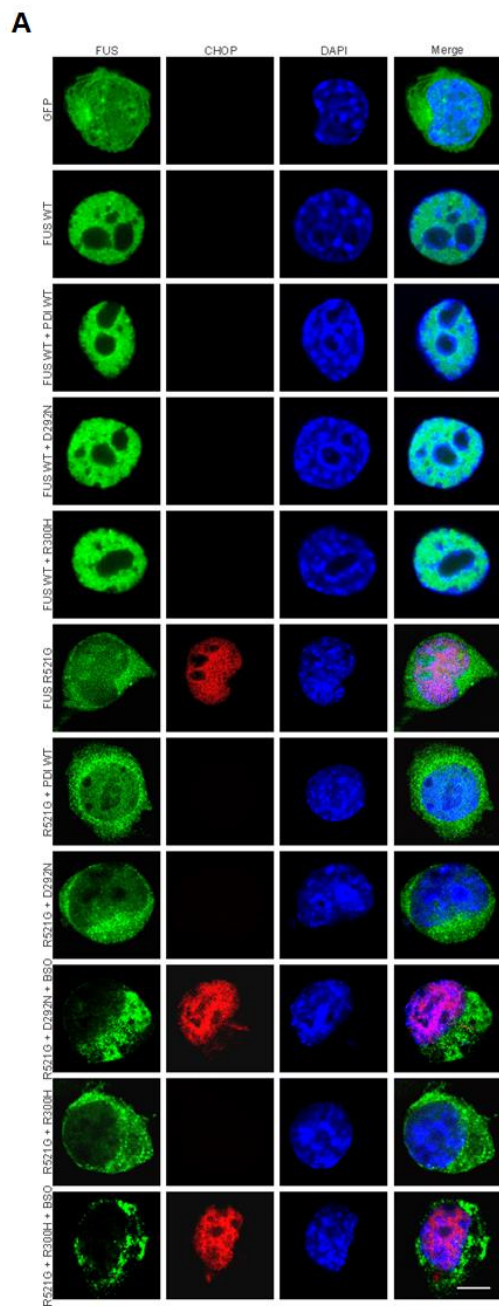
Figure 6.12: PDI D292N and R300H are protective against CHOP activation induced by mutant FUS, however their protective activity is perturbed upon BSO administration.

A) Immunofluorescence images of Neuro-2A cells expressing GFP, wildtype FUS with either pcDNA3.1, wildtype PDI, PDI D292N or PDI R300H, and mutant FUS R521G with either pcDNA3.1, wildtype PDI, PDI D292N (with and without BSO) and PDI R300H (with and without BSO). Cells expressing GFP (first panel; GFP) or wildtype FUS (panels 2-5; FUS WT, FUS WT + PDI WT, FUS WT + D292N, FUS WT + R300H) rarely displayed nuclear immunoreactivity to CHOP. In contrast, more cells expressing mutant FUS R521G (sixth panel; FUS R521G) displayed nuclear immunoreactivity to CHOP, as indicated by the red fluorescence in the nucleus (panel six, column two). However, when mutant FUS R521G was co-expressed with either wildtype PDI, PDI D292N or PDI R300H (panels seven, eight and ten; R521G + PDI WT, R521G + D292N, R521G + R300H), fewer cells displayed CHOP activation. Upon BSO administration to mutant FUS R521G cells co-expressing either PDI D292N or PDI R300H (panels nine and eleven; R521G + D292N + BSO, R521G + R300H + BSO), more cells displayed CHOP activation, as indicated by nuclear immunoreactivity (panels nine and eleven, column two). Scale bar = 20 µM. **B)** Quantification of cells in A) displaying CHOP activation. Very few untransfected cells and cells expressing GFP or wildtype FUS displayed CHOP activation. There was a significant increase ($p < 0.001$) in the proportion of cells with CHOP activation in populations expressing mutant FUS R521G, compared to those expressing wildtype FUS, as expected. Significantly fewer ($p < 0.001$) mutant FUS R521G cells displayed CHOP activation, when wildtype PDI, PDI D292N or PDI R300H were co-expressed, compared to those co-expressing pcDNA3.1 vector. N=3, Mean ± SEM, *** $p < 0.001$. **C)** There was a significant increase ($p < 0.001$) in the proportion of cells with CHOP activation in populations expressing mutant FUS R521G, compared to those expressing wildtype FUS. However, this proportion was significantly

reduced ($p < 0.001$) when PDI D292N or PDI R300H was co-expressed with mutant FUS R521G. When FUS R521G cells co-expressing PDI D292N were exposed to BSO, there was a significant increase ($p < 0.05$) in the proportion of cells with CHOP activation, compared to these cells without BSO. A similar result was observed in FUS R521G cells co-expressing PDI R300H upon BSO administration, in that significantly more ($p < 0.05$) cells displayed CHOP nuclear immunoreactivity, compared to FUS R521G cells co-expressing PDI R300H without BSO exposure. N=3, Mean $\pm$ SEM, * $p < 0.05$, *** $p < 0.001$.

6.3.13 PDI D292N and R300H inhibit mutant FUS inclusion formation, however, their function is perturbed when BSO is administered

Finally, it was investigated whether PDI variants, D292N and R300H, were protective against mutant FUS inclusion formation, similar to PDI. Furthermore, if protective, it was examined whether BSO inhibits the function of the variants by perturbing oxidase activity. Neuro-2A cells were transfected with GFP alone, wildtype FUS with either pcDNA3.1, wildtype PDI, PDI D292N or PDI R300H, and mutant FUS R521G with either pcDNA3.1, wildtype PDI, PDI D292N or PDI R300H. After 72 h, cells were fixed, immunocytochemistry was performed using an anti-V5 antibody to detect the expression of the V5-tagged PDI proteins, and nuclei were stained with Hoechst. Fluorescent microscopy was used to quantify at least 100 co-transfected cells for the presence of FUS inclusions (Figure 6.13 A).

Untransfected cells and cells expressing GFP were excluded from analysis as they do not express FUS. Wildtype FUS expressing cells did not form inclusions. Conversely, a high proportion of cells expressing mutant FUS R521G with empty pcDNA3.1 vector displayed inclusions ($18.0\% \pm 1.1$). When PDI was co-expressed with mutant FUS R521G, there was a significant reduction ($p < 0.001$) in the proportion of cells forming FUS inclusions ($11.0\% \pm 1.4$), as expected. Moreover, a significant decrease ($p < 0.001$) in the proportion of cells bearing FUS inclusions was observed in FUS R521G populations co-expressing either PDI D292N ($8.3\% \pm 0.5$) or PDI R300H ($8.0\% \pm 2.1$), indicating that the PDI variants retain their protective activity against mutant FUS inclusion formation (Figure 6.13 B).

Next, the activities of the PDI variants were analysed against mutant FUS inclusion formation upon administration of BSO. As expected, a significant decrease ($p < 0.001$) in the proportion of cells bearing FUS inclusions was observed when mutant FUS R521G populations were co-expressed with either PDI D292N ($8.3\% \pm 0.5$) or PDI R300H ($7.3\% \pm 1.4$), compared to

when they were co-expressed with empty pcDNA3.1 vector (18% $\pm$ 1.1). However, upon BSO administration to FUS R521G cells co-expressing PDI D292N, significantly more ($p <$ 0.05) cells displayed inclusions (13.5% $\pm$ 1.8), compared to these cells that weren't exposed to BSO. Similarly, a significant increase ($p < 0.05$) in the proportion of cells bearing inclusions was observed in FUS R521G cells co-expressing PDI R300H once treated with BSO (11.8% $\pm$ 0.5), compared to these cells that weren't treated with BSO. Interestingly, however, cells co-expressing mutant FUS R521G and D292N, and exposed to BSO, still displayed significantly fewer ($p < 0.05$) FUS inclusions, compared to cells expressing mutant FUS R521G and empty vector. Similarly, mutant FUS R521G cells co-expressing PDI R300G and treated with BSO also displayed significantly fewer ($p < 0.01$) inclusions, compared to mutant FUS R521G expressing cells (Figure 6.13 C). These data suggest that a loss of oxidase activity results in the inhibition of the PDI variants' protective function. However, they also suggest that the loss of PDI oxidase activity is not as detrimental compared to a mutant FUS R521G expressing cell without PDI expression.
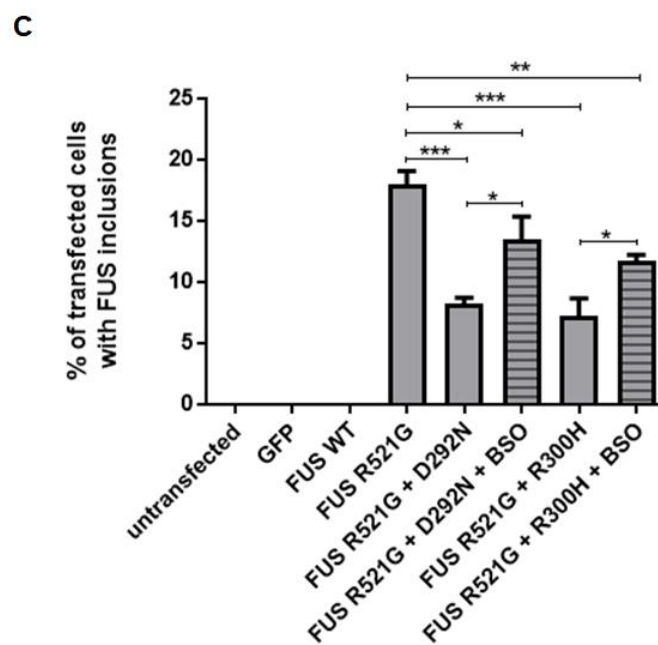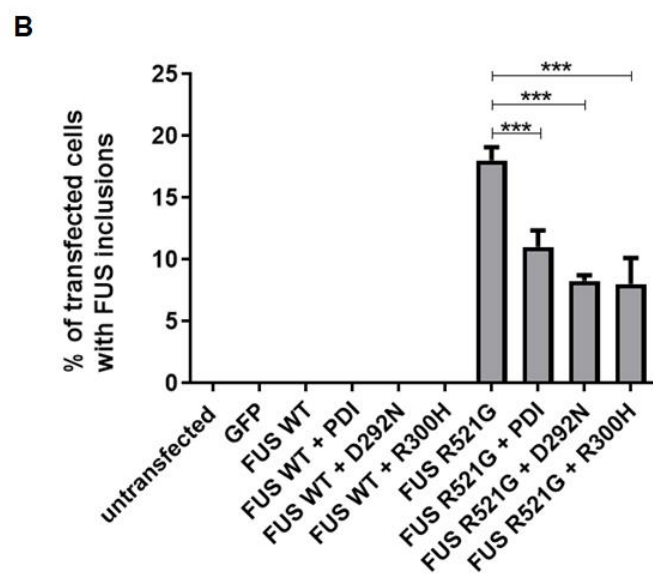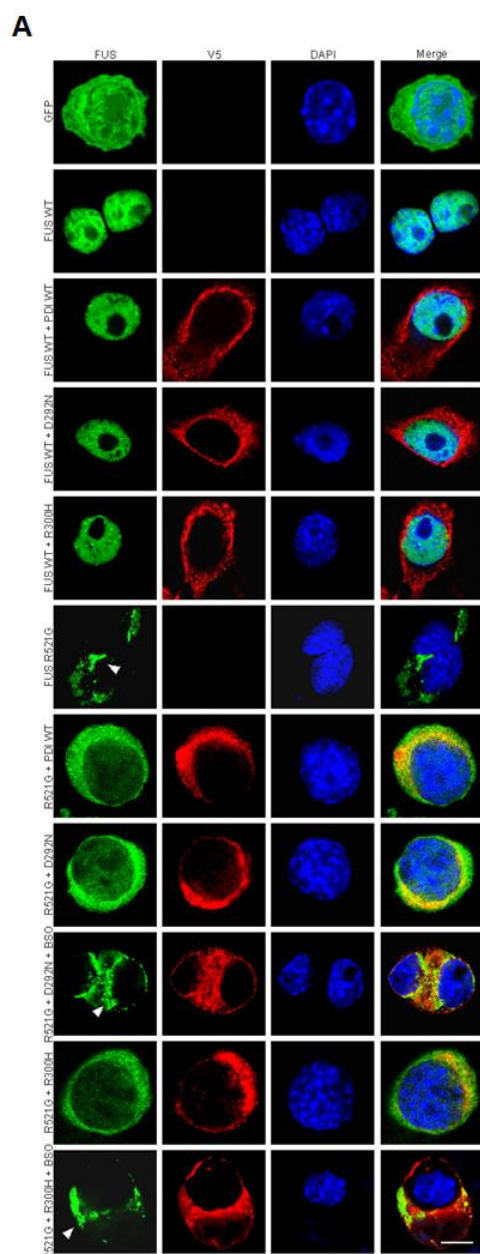
Figure 6.13: PDI D292N and R300H inhibit mutant FUS inclusion formation, however, their protective function is perturbed when BSO is administered. A) Immunofluorescence images of Neuro-2A cells expressing GFP, wildtype FUS with either pcDNA3.1, wildtype PDI, PDI D292N or PDI R300H, and mutant FUS R521G with either pcDNA3.1, wildtype PDI, PDI D292N (with and without BSO) and PDI R300H (with and without BSO). Cells expressing GFP (first panel; GFP) or wildtype FUS (panels 2-5; FUS WT, FUS WT + PDI WT, FUS WT + D292N, FUS WT + R300H) do not bear inclusions. In contrast, a greater proportion of cells expressing mutant FUS R521G (sixth panel; FUS R521G) display FUS inclusions, as indicated by the white arrowhead (sixth panel, column one). However, co-expression of either wildtype PDI, PDI D292N or PDI R300H with mutant FUS R521G resulted in fewer cells forming FUS inclusions (panels seven, eight and ten; R521G + PDI WT, R521G + D292N, R521G + R300H). Conversely, when BSO was administered to FUS R521G cells co-expressing either PDI D292N or PDI R300H, more cells displayed inclusions (panels nine and eleven; R521G + D292N + BSO, R521G + R300H + BSO). Scale bar = 20 μM. **B)** Quantification of cells bearing FUS inclusions in A). Cells expressing GFP or wildtype FUS do not bear inclusions. Significantly more ($p < 0.001$) cells expressing mutant FUS R521G formed FUS inclusions, however this proportion was significantly reduced ($p < 0.001$) when either wildtype PDI, PDI D292N or PDI R300H were co-expressed. N=3, Mean ± SEM, *** $p < 0.001$. **C)** A significant decrease ($p < 0.001$) in the proportion of cells bearing inclusions was observed when either PDI D292N or PDI R300H were co-expressed with mutant FUS R521G, compared to cells expressing mutant FUS R521G and empty vector. However, significantly more ($p < 0.05$) cells formed inclusions when BSO was administered to mutant FUS R521G cells co-expressed with either PDI D292N or PDI R300H, compared to these cells without BSO administration. FUS R521G cells co-expressing either PDI D292N or PDI R300H and subject to BSO exposure still

formed significantly fewer ($p < 0.05$ and $p < 0.01$, respectively) inclusions, compared to mutant FUS R521G expressing cells with empty vector. N=3, Mean ± SEM, * $p < 0.05$, ** $p < 0.01$, *** $p < 0.001$.

6.3.14 Overexpression of wildtype PDI and PDI R300H increases the expression of cyto-roGFP, indicating an increase in oxidase activity.

The BSO studies performed in this Chapter complement the results described in Chapter 5 which revealed that PDI's oxidase activity is fundamental for its protective function. To further confirm this notion, experiments utilising cyto-roGFP (as used in Chapter 5) in cells co-expressing FUS and PDI proteins were performed to analyse the levels of oxidation in Neuro-2A cells. As cyto-roGFP fluoresces green when it has been oxidised, HA-tagged FUS proteins, which fluoresce red, rather than GFP-tagged FUS, were used in these experiments. HA_FUS was also co-transfected with wildtype PDI, PDI QUAD (in which disulphide interchange activity has been ablated) and the PDI variant, R300H. From the results obtained in this Chapter, it would be expected that cell populations expressing wildtype PDI or PDI R300H would display higher expression of roGFP activation, indicative of more oxidase activity occurring in the cell.

As various PDI proteins and new versions of FUS proteins were utilised in this study, Western blotting analysis was first performed to ensure that each protein was expressed to a similar level and to verify that the expressed proteins were of the expected MW. Cell lysates were prepared from the following populations; wildtype FUS co-expressed with either empty pcDNA3.1 vector or wildtype PDI, and mutant FUS R521G co-expressed with either wildtype PDI, PDI QUAD or PDI R300H. Immunoblotting using an anti-HA antibody revealed that wildtype and mutant HA-FUS proteins were expressed at similar levels at the expected MW of 65 kDa. PDI proteins were detected in cell lysates using an anti-V5 antibody (62 kDa), and demonstrated similar expression levels. β-actin was used as a loading control, detected at 40 kDa using an anti-β-actin antibody (Figure 6.14 A and B).

Neuro-2A cells were then transfected with GFP alone, pcDNA3.1, wildtype PDI, wildtype

FUS with either pcDNA3.1 or wildtype PDI, and mutant FUS R521G with either pcDNA3.1,

wildtype PDI, PDI QUAD or PDI R300H. All populations were also co-transfected with

cyto-roGFP to determine the levels of oxidation occurring within the cells. After 72, cells

were fixed and the nuclei were stained with Hoechst before examining cells using fluorescent

microscopy. At least 100 cells expressing FUS were examined and these cells were further

analysed for cyto-roGFP expression (Figure 6.14 C).

Cells expressing cyto-roGFP alone or cyto-roGFP with empty vector pcDNA3.1 displayed

low levels of roGFP expression (approximately 10% of cells). There was a significant

increase ($p < 0.001$) in the proportion of cells with roGFP expression when wildtype PDI was

co-expressed with cyto-roGFP (27.0% $\pm$ 1.5), compared to cells expressing cyto-roGFP with

empty pcDNA3.1 vector (10.3% $\pm$ 1.4), indicating that oxidation is taking place in the cell

when PDI is expressed. Interestingly, when cells were transfected with wildtype and mutant

FUS proteins, roGFP expression was considerably increased. A significant increase ($p <$

0.01) in the proportion of cells with roGFP expression was observed when wildtype PDI was

co-expressed with wildtype FUS (75.0% $\pm$ 4.6), compared to when empty pcDNA3.1 vector

was co-expressed with wildtype FUS (61.7% $\pm$ 1.7). Similarly, PDI co-expression with

mutant FUS R521G demonstrated significantly higher ($p < 0.05$) levels of roGFP expression

(76.0% $\pm$ 2.1), compared to FUS R521G expressing cells with empty vector (65.0% $\pm$ 1.0), as

expected. There was no statistical difference in the proportion of FUS R521G populations co-

expressing PDI QUAD (58.0% $\pm$ 3.5), compared to FUS R521G expressing cells with empty

vector, indicating that PDI QUAD is not oxidising cyto-roGFP in these cells, thus confirming

the lack of disulphide interchange activity of this mutant. Moreover, roGFP expression in

FUS R521G populations co-expressing PDI QUAD was significantly lower ($p < 0.001$) than

roGFP expression observed in FUS R521G populations co-expressing wildtype PDI.

Interestingly, although there was an increase in the proportion of cells with roGFP expression, similar levels of roGFP expression (67.0% ± 1.2) were observed in FUS R521G populations co-expressing PDI R300H, compared to those cells co-expressing empty vector. Hence these data imply that PDI R300H is not utilising its oxidase activity in these cells. However, no statistical difference was observed in the proportion of these cells with roGFP expression compared to cells co-expressing FUS R521G and wildtype PDI either, suggesting that its activity is still similar to that of PDI's (Figure 6.14 D).

500
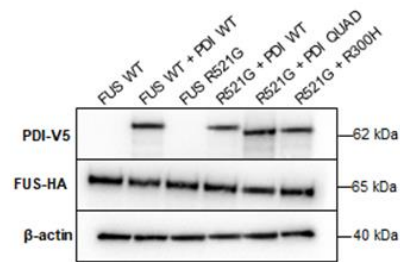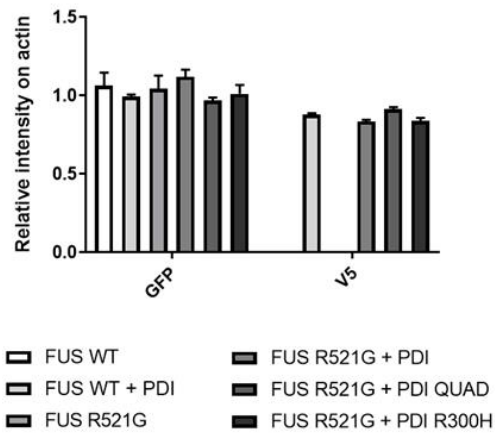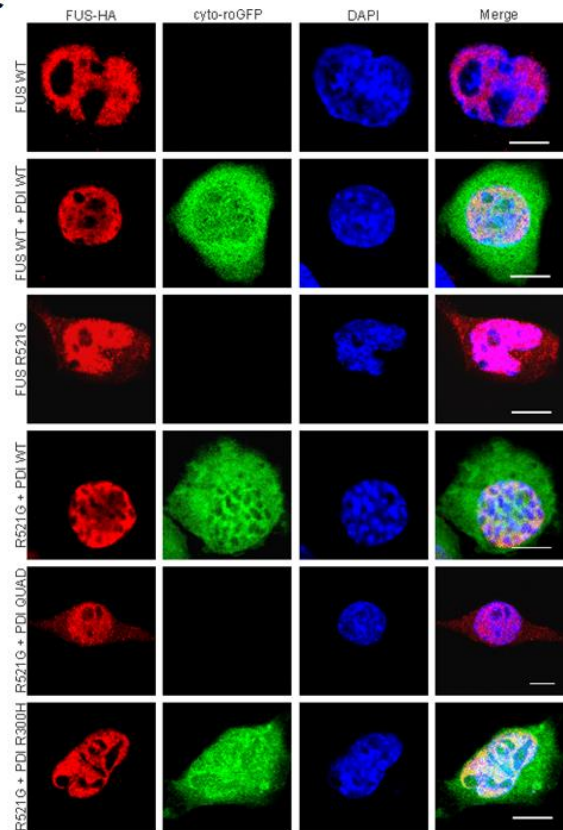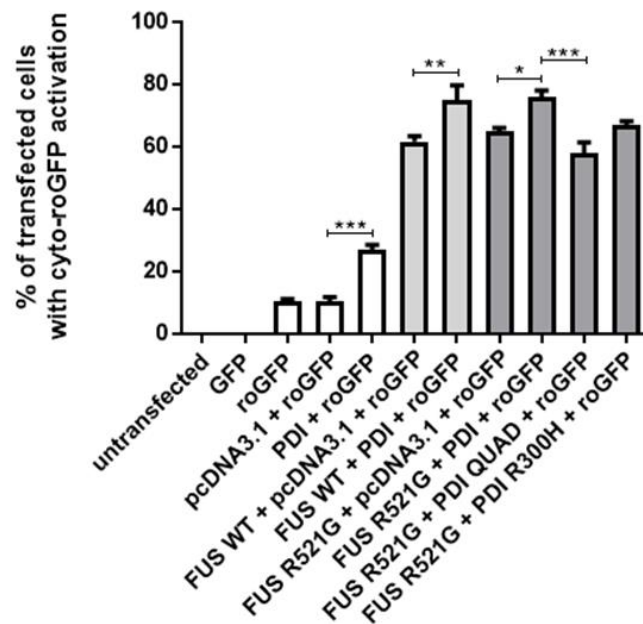
Figure 6.14: Overexpression of wildtype PDI and PDI R300H increases the proportion of cells with expression of cyto-roGFP, indicating an increase in oxidase activity. A) Western blotting of cell lysates was performed to ensure that the proteins expressed were of similar expression levels between groups and that each was expressed at the expected MW. Cell lysates examined were wildtype FUS co-expressed with either empty pcDNA3.1 vector or wildtype PDI, and mutant FUS R521G co-expressed with either wildtype PDI, PDI QUAD or PDI R300H. PDI proteins were detected at 62 kDa and HA-FUS proteins were detected at 65 kDa, as expected. β-actin was used as the loading control and was detected at 40 kDa. **B)** Quantification revealed that wildtype and mutant HA-FUS proteins were expressed at similar levels. Similarly, wildtype PDI, PDI QUAD and PDI R300H also displayed similar expression. N=3, Mean ± SEM. **C)** Immunofluorescence images of Neuro-2A cells co-expressing cyto-roGFP with wildtype FUS and either pcDNA3.1 or wildtype PDI, or mutant FUS R521G and either pcDNA3.1, wildtype PDI, PDI QUAD or PDI R300H. Populations expressing wildtype FUS display more cells with roGFP expression when co-expressed with wildtype PDI, as indicated by green fluorescence (second panel, column two), compared to when co-expressed with empty vector. Similarly, when mutant FUS R521G expressing cells are co-expressed with either wildtype PDI or PDI R300H, more display roGFP expression compared to mutant FUS R521G expressing cells with empty vector (panels four and six, column two). However, no differences in the proportion of cells with roGFP expression are observed when mutant FUS R521G is co-expressed with PDI QUAD. Scale bar = 20 µM. **D)** Quantification of Neuro-2A cells with roGFP expression in A). There was a significant increase ($p < 0.001$) in the proportion of cells displaying roGFP expression in cells co-expressing cyto-roGFP with wildtype PDI, compared to cells co-expressing cyto-roGFP with empty pcDNA3.1 vector. Significantly more cells ($p < 0.01$) with roGFP expression were observed in populations co-expressing wildtype FUS and wildtype PDI, compared to those

co-expressing wildtype FUS and empty vector. Similarly, significantly more cells (p < 0.05) displayed roGFP expression when observed in mutant FUS R521G populations co-expressing wildtype PDI, compared to co-expressing empty vector. There were no statistical differences observed between mutant FUS R521G populations co-expressing empty vector and FUS R521G populations co-expressing either PDI QUAD or PDI R300H. Moreover, roGFP expression was significantly higher (p < 0.001) in FUS R521G populations co-expressing wildtype PDI, compared to populations co-expression PDI QUAD. N=3, Mean ± SEM, * p < 0.05, ** p < 0.01, *** p < 0.001.

6.3.15 The administration of BSO decreases the proportion of cells with cyto-roGFP when co-expressed wildtype PDI or PDI R300H

Finally, to confirm that roGFP expression reflects the cellular redox environment, roGFP expression levels were examined when BSO was administered to cells expressing wildtype PDI, PDI QUAD and PDI R300H. Therefore, the same experiment was performed here as described above, except that BSO was added. At 72 h post-transfection, cells were fixed, stained with Hoechst to visualise the nuclei, and at least 100 FUS expressing cells were examined using fluorescent microscopy for roGFP expression (Figure 6.15 A).

As previous, expression of wildtype PDI significantly increased ($p < 0.01$) the proportion of cells with roGFP expression (27.0% ± 1.5), compared to cells expressing pcDNA3.1, however a significant decrease ($p < 0.01$) in this proportion was observed when BSO was administered (7.7% ± 0.3). When examining wildtype PDI co-expression with wildtype FUS, significantly fewer ($p < 0.001$) cells displayed roGFP expression when exposed to BSO (55.7% ± 6.9), compared to these cells without BSO (75.0% ± 4.6). Similarly, BSO administration to cells co-expressing wildtype PDI and mutant FUS R521G resulted in a significant decrease ($p < 0.001$) in the proportion of cells with roGFP expression (54.0% ± 3.5, compared to cells co-expressing wildtype PDI and mutant FUS R521G with no BSO (77.0% ± 1.5). These findings therefore suggest that the increase in roGFP expression observed when PDI is overexpressed is a result of its oxidase activity, because roGFP expression is decreased upon oxidation inhibition by BSO. Furthermore, a significant decrease ($p < 0.05$) in the proportion of cells with roGFP expression was observed when BSO was administered to cells co-expressing mutant FUS R521G and PDI R300H (53.0% ± 4.0), compared to these cells without BSO administration (67.0% ± 1.2). These results imply that PDI R300H does indeed possess oxidase activity, as roGFP expression is decreased upon exposure to BSO. As expected, BSO administration to FUS R521G populations co-

expressing PDI QUAD did not alter the proportion of cells with roGFP expression (56.3% ± 0.3), compared to cells not treated with BSO (58.0% ± 3.5), indicating that PDI QUAD mutant does not possess oxidase activity (Figure 6.15 B), as expected.

To confirm that BSO did not alter FUS or PDI protein expression in cells upon its administration, Western blotting analysis was performed and quantified to ensure that each protein was expressed at similar levels and at the expected MW. Immunoblotting using an anti-HA antibody revealed that wildtype and mutant HA-FUS proteins were expressed at similar levels at the expected MW of 65 kDa. Moreover, the PDI proteins were detected at 62 kDa, using an anti-V5 tag antibody, with similar expression levels, suggesting that administration of BSO did not alter protein expression in this experiment (Figure 6.15 C).

A

B

C

505

Figure 6.15: The administration of BSO decreases the proportion of cells with cyto-roGFP expression when co-expressed wildtype PDI and PDI R300H.

A) Immunofluorescence images of Neuro-2A cells co-expressing cyto-roGFP with wildtype FUS and either pcDNA3.1 or wildtype PDI (with and without BSO), or mutant FUS R521G and either pcDNA3.1, wildtype PDI, PDI QUAD or PDI R300H (with and without BSO). When wildtype PDI is co-expressed with wildtype FUS, more cells display roGFP expression, as indicated by green fluorescence (column two), compared to cells expressing wildtype FUS alone. However, when BSO is administered to cells co-expressing wildtype FUS and wildtype PDI, fewer cells display roGFP expression (see panels 1-3). A similar pattern is observed when wildtype PDI (see panels 4-6) or PDI R300H (see panels 9-10) are co-expressed with mutant FUS R521G, and then subsequently exposed to BSO. When mutant FUS R521G cells are co-expressed with PDI QUAD, there is no difference in roGFP expression compared to cells expressing mutant FUS R521G alone, and this proportion of cells is not altered upon BSO administration (see panels 7-8). **B)** Quantification of Neuro-2A cells with roGFP expression in A). Significantly fewer cells ($p < 0.001$) display roGFP expression when BSO is administered to cells co-expressing PDI with either wildtype FUS or mutant FUS R521G, compared to these cells without BSO treatment. Similarly, a significant decrease ($p < 0.05$) in the proportion of cells co-expressing mutant FUS R521G and PDI R300H with roGFP expression is observed upon administration of BSO, compared to these cells without BSO. BSO did not alter roGFP expression levels in cells co-expressing mutant FUS R521G and PDI QUAD. N=3, Mean ± SEM, * $p < 0.05$, *** $p < 0.001$. **C)** Western blotting analysis was performed to ensure that BSO administration did not alter protein expression. Wildtype and mutant HA-FUS proteins demonstrated similar levels of expression and were detected at 65 kDa. Moreover, PDI proteins, detected at 62 kDa, also displayed similar expression, indicating that administration of BSO did not reduce or alter the

expression of protein across cell populations. Loading control, β-actin, was detected at 40 kDa. Quantification is not shown.

6.4 Discussion

Chapters 4 and 5 of this thesis demonstrate that the oxidase activity of PDI is important for its function. In Chapter 4, the oxidase DsbA was consistently protective against cellular pathogenic mechanisms induced by ALS proteins, SOD1, TDP-43 and FUS. Moreover, the mutants with predicted oxidase activity generated in Chapter 5 were also consistently protective against ALS cellular disease processes, compared to the predicted reductase and isomerase redox mutants, suggesting that oxidase activity is the key feature mediating PDI's protective function. Therefore, this hypothesis was examined further by focussing on one ALS-associated protein in particular: FUS. The protective activity of wildtype PDI, PDI variants, D292N and R300H, as well as PDI mimetic, BMC, were examined in studies utilising mutant FUS-expressing Neuro-2A cells.

The results of this chapter confirm the importance of the redox and oxidase activities of PDI. Upon administration of BSO, which changes the cellular redox properties so that oxidation is ablated, wildtype PDI was unable to prevent mutant FUS mislocalisation to the cytoplasm, the formation of FUS inclusions, or the induction of ER stress induced by mutant FUS. These findings imply that without it's oxidase activity, PDI loses its protective function against mutant FUS in Neuro-2A cells. These results therefore complement the findings observed in Chapter 5 where an oxidising active site motif or cis-proline loop in PDI was protective against ALS cellular processes.

Similar results were observed when cells expressing mutant FUS were treated with BMC. As demonstrated previously in our laboratory, BMC is protective against pathogenic mechanisms induced by mutant forms of SOD1, TDP-43 and FUS. However, upon BSO administration in this study, BMC lost its protective effect against mutant FUS, indicating that, it too, is reliant on oxidase properties. Treatment of cells with BMC is able to emulate

the protective activity of PDI overexpression in neuronal cells by mimicking the disulphide interchange activity of PDI. From the results obtained in this study, it can be suggested that BMC functions similarly to PDI, and it primarily relies on its oxidase activity to elicit a protective response. It is important to note, however, that BMC is not substrate specific in the same way that PDI is, therefore it could be possible that BMC treatment may be creating a more reducing cellular environment, which in turn, facilitates efficient oxidation and isomerisation by endogenous PDI, which thrives on a reducing environment for activity [504]. Thus, it is possible that BSO is also preventing BMC from inducing the appropriate cellular (reducing) environment, similar to how it prevents reducing conditions by inhibiting glutathione synthesis.

An interesting observation from this study was that PDI variants, D292N and R300H, were protective against mutant FUS mislocalisation, the formation of FUS inclusions and ER stress. These variants previously displayed major detrimental effects in the nervous system and on neuromuscular connectivity in zebrafish [441], therefore it would be expected that these mutations would impede PDI's protective activity. However, previous studies have demonstrated that ER homeostasis is not perturbed, and cell toxicity is not induced, by the D292N and R300H variants [441], thus the results obtained here are consistent with those findings. It is puzzling, however, that ER homeostasis is not perturbed by the PDI variants, given that PDI is central to this process and several misfolded proteins linked to ALS trigger the UPR and ER dysfunction. It is important to note, however, that these PDI mutations are present in the *b'* domain of PDI, and the important *a* domain is left intact. Moreover, the variants appear to perturb substrate binding, and thus, chaperone function, rather than PDI's disulphide interchange activity. Therefore, PDI's oxidase activity should still be retained in these variants and its protective activity against mutant FUS is reminiscent of this. Moreover, upon BSO administration, both D292N and R300H variants lost their protective activity,

similar to wildtype PDI, implying that the oxidase activities of these variants are also fundamental for protective function. If additional PDI variants are detected in the future in ALS patients, it would be interesting to examine whether they are present within the *a* domain, and moreover, whether this would perturb protective activity in neuronal cells. Indeed, one of the identified ERp57 variants contains a mutation in the *a'* domain [444].

In this chapter, mutant FUS inclusions were quantified for the first time in this thesis, demonstrating that PDI was able to inhibit their formation. The formation of inclusions in cells expressing wildtype FUS have not been commonly observed in these cell model studies in our laboratory. However, upon BSO administration, inclusions and paraspeckle-like structures were sporadically detected within the nucleus. Paraspeckles are ribonucleoprotein bodies found in the interchromatin space of mammalian cell nuclei. They are RNA-protein structures formed by the interaction between a long non-coding RNA, NEAT1 [602]. Indeed, FUS is a major constituent of paraspeckles [603] and paraspeckle formation has been reported in motor neurons of ALS patient spinal cords [604]. Glutathione is an important antioxidant in cells, capable of preventing damage to cellular organelles caused by ROS [605]. Therefore, it is possible that upon BSO administration, which depletes glutathione, there is an increase in ROS inducing oxidative stress, and this results in the formation of these paraspeckles. Hence, future studies should explore how paraspeckles are induced in cells expressing FUS and how they are implicated in ALS. Interestingly, though, an increase in inclusion-like structures was only observed in cells expressing wildtype FUS, and the proportion of mutant FUS R521G expressing cells forming inclusions remained the same, with or without BSO administration, suggesting that these cells are already subject to oxidative stress.

Finally, to confirm that PDI utilises its oxidase activity in mutant FUS expressing cells, studies examining roGFP expression were performed. The roGFP construct fluoresces green

once it has been oxidised, hence an increase in roGFP expression is evident of increased cellular oxidation conditions, whereas a decrease in roGFP expression is reminiscent of a decline in cellular oxidation. As expected, more wildtype or mutant FUS cells displayed roGFP expression when PDI was co-expressed, indicating that roGFP is becoming oxidised under these conditions due to the presence of PDI. Conversely, when PDI QUAD was co-expressed with mutant FUS, no increase in the proportion of cells with roGFP expression was observed. This result was expected because previous studies have established that the PDI QUAD mutant does not possess disulphide interchange activity [502, 563], and thus, it cannot oxidise proteins. Interestingly, a decrease in the proportion of cells with roGFP expression was observed when BSO was administered to cells co-expressing mutant FUS with either wildtype PDI or PDI R300H. These findings indicate that BSO inhibits the oxidase activity of both PDI proteins, as observed by fewer cells with roGFP expression. Thus, this confirms that BSO ablates oxidase activity in this study. In contrast, the administration of BSO did not decrease the proportion of cells with roGFP expression in mutant FUS populations co-expressing PDI QUAD. Again, this was to be expected due to the absence of disulphide interchange activity in the PDI QUAD mutant. Therefore, alterations in roGFP expression were confirmed as either being due to an increase in oxidation when expression of roGFP was augmented, or a decrease in oxidation when its expression was diminished.

Some caveats in this study should be mentioned and future experiments are therefore warranted to address these issues. Firstly, roGFP expression was assessed in these studies by simply quantifying cells that exhibited expression. However, another, more widely used method to assess roGFP expression is to examine the ratios of fluorescence from excitation at 400 nm and 485 nm, because roGFP has two fluorescence excitation maxima at 400 nm (oxidised form) and 485 nm (reduced form) [606]. Hence, the results obtained in this study examining roGFP expression should be confirmed by this alternative method in the future.

Furthermore, because glutathione is depleted in cells with BSO, it is unknown whether these cells are exposed to higher levels of oxidative stress. This could be evident by the observation that wildtype FUS-expressing cells form inclusions and possible paraspeckle-like structures in the nucleus. However, control cell populations treated with BSO did not display any obvious cellular defects or cell death, suggesting that this is probably not the case, or that higher concentrations are required than those used here. Finally, there are limitations in using this cell culture model system, as the assay used may not be sensitive enough to detect whether there are other factors influencing PDI's protective activity, such as its chaperone function, or the isomerase and reductase activities which were found to be protective against mutant FUS-induced ER stress in Chapter 5.

In summary, this chapter confirms the importance of the oxidase activity for PDI's protective function against the cellular mechanisms examined here, as it was demonstrated that PDI and BMC lost these protective functions once their oxidase activities had been inhibited. Moreover, this study demonstrated that PDI variants, D292N and R300H, were still protective against mutant FUS-induced pathogenic mechanisms, even though they have detrimental effects on the nervous system in zebrafish models. The studies described in this thesis indicate that this protective activity is most likely due to the presence of the mutation being localised in the *b'* domain of PDI, and thus, the oxidase activity, mediated by the *a* domain, is still retained. This is supported by the results obtained here that demonstrated that both PDI variants lost their protective activities when BSO impeded their oxidase capabilities. Therefore, in conclusion, the oxidase activity of PDI is protective against mutant FUS-induced ALS. These studies should now be performed in cells expressing other ALS-associated proteins, such as SOD1, TDP-43 or Cyclin F.

Chapter 7: Peptides Based on PDI's Active Site are Protective in Neuronal Cells Expressing Mutant SOD1

7.1 Introduction

Therapeutic strategies that modulate ER stress are rapidly becoming an attractive target for ALS, and the ALS-Therapy Development Institute now lists seven compounds that target the UPR. However, it is possible that strategies based on PDI may provide more specific benefits rather than targeting ER stress itself. Protein misfolding is a common phenomenon of most proteins, therefore in neurodegenerative diseases associated with misfolded proteins, approaches that prevent protein aggregation may be particularly beneficial. Moreover, PDI is protective against a number of cellular pathogenic mechanisms observed in ALS, induced by multiple ALS-linked mutant proteins, suggesting that a therapeutic agent based on PDI's activity may be effective in multiple forms of ALS.

PDI is also an appealing therapeutic and novel target as it has dual functions. Indeed, all ER chaperones are essential for maintaining ER proteostasis by refolding aberrantly folded proteins, and thus preventing the formation of protein aggregates. However, PDI is both a chaperone and an oxidative foldase, and it has distinctive properties which make it an effective catalyst, such as conformational flexibility, broad substrate specificity and the ability to differentiate between unfolded and partially folded proteins, in contrast to other chaperones, which do not possess these properties [496]. Moreover, PDI can also refold proteins that do not contain disulphide bonds [607].

BMC, a small molecular mimic of PDI's disulphide interchange activity, was previously observed to enhance native protein folding and the secretion of recombinant proteins in yeast and bacterial cultures [595, 596]. Furthermore, in ALS cell models expressing mutant SOD1, BMC treatment inhibited the formation of SOD1 inclusions, indicating that BMC is able to reproduce the protective activity of PDI on SOD1 aggregation [448]. These studies provide further evidence that a therapeutic PDI mimic could be an effective treatment in ALS.

The studies performed in this doctoral thesis aimed to characterise the protective mechanisms of PDI, in particular, which domains and redox properties of the protein are responsible for its protective effect against ALS cellular pathogenesis. These studies were undertaken with the ultimate aim of designing novel therapeutic peptides based on PDI's protective properties. Preliminary cell culture experiments investigating the effect of linear peptides mimicking PDI's activity, which were designed based on the outcomes of the results obtained in Chapters 4 and 5, are described in this final chapter.

7.1.1 The use of peptides as therapeutics

Peptides currently only represent 2% of the drug market, however this market is constantly growing. Peptides represent a unique class of pharmaceutical agents that are molecularly similar to small molecules as well as proteins, yet they are biochemically and therapeutically distinct from both. Peptides have some advantages when compared to small molecules in that they are known to exhibit high binding affinity and excellent target specificity, whilst bearing low toxicity [608].

Another advantage of using peptides for therapeutic intervention is that they closely mimic normal cellular pathways, essentially acting as "replacement therapies" that supplement mechanisms in which endogenous levels are compromised. An example of this is the isolation and first therapeutic use of insulin in the 1920s for diabetics with inadequate production of the hormone [609] and later the purification of adrenocorticotrophic hormone (ACTH) from livestock pituitary glands to treat endocrine disorders in human patients. Unfortunately, however, typically naturally occurring peptides have poor absorption, distribution, metabolism, and excretion properties [610].

The utilisation of peptides evolved in the second half of the 20th century with the feasibility of chemically synthesising peptides. Examples of synthetic peptides include oxytocin and vasopressin [611]. Synthetic peptides have improved properties compared to naturally occurring peptides and they are much more stable [610]. Furthermore, cyclisation of linear peptides is one strategy to improve their stability for therapeutic applications. Moreover, the discovery of cell-penetrating peptides offers an exciting approach for delivering drugs to intracellular targets, as these peptides are capable of crossing the cell membrane and can carry many different therapeutic agents to cells, such as small molecules, plasmid DNA, siRNA, therapeutic proteins, viruses and various nanoparticles [612].

In 2017, information for 484 therapeutic peptides currently exists [613]. Of these, 68 peptides had been approved, however eight were subsequently withdrawn, therefore there are currently 60 approved therapeutic peptides in the United States, Europe and/or Japan. 155 of these peptides are currently in active clinical development with just under half in Phase 2 studies. Unfortunately, the remaining 261 peptide programs were terminated prior to approval [613]. Nevertheless, the cumulative number of approved peptides has progressively increased, with 13 peptide approvals occurring from the start of 2010 to the beginning of 2017 [613].

7.1.2 Linear peptides based on PDI's protective activity

Previous, unpublished studies in our laboratory, have provided evidence to suggest that PDI is protective against multiple cellular pathogenic events and against several misfolded proteins associated with ALS, such as SOD1, TDP-43 and FUS, as well as *in vivo* against motor performance and axonopathy in zebrafish models of ALS. The studies described in Chapter 3 of this doctoral thesis provide additional evidence that PDI is protective against

mutant forms of a novel ALS/FTD-associated protein, Cyclin F. Hence, these findings provide further evidence that PDI is broadly protective in ALS, although it should be noted that validation experiments in rodent models of disease has not yet been performed. Nonetheless, protein aggregation and ER stress are proposed to be early pathogenic events in ALS, suggesting that they are a fundamental process in causing motor neuron degeneration, rather than a secondary effect. These disease processes are common amongst many diverse types of ALS, and they are relevant in sporadic disease. Therefore, peptide therapeutics based on PDI's protective activity may be broadly applicable to all ALS, not just familial forms.

PDI, in its full native form, is too large to be delivered efficiently to the brain of ALS patients. Hence, experiments to investigate and characterise the protective mechanisms and domains of PDI were performed in this study. Previous studies in our laboratory have already shown that PDI's disulphide interchange activity, or oxidoreductase function, rather than its chaperone capabilities, is necessary for PDI's protective function (Parakh et al., 2017 in preparation). Experiments performed in Chapter 4 of this doctoral thesis confirmed this result, as it was demonstrated that the *a* and *a'* domains of PDI were much more protective than the *b* domains. Indeed, the *a* domains of PDI, containing the catalytic CGHC active sites, are the key mediators for PDI's disulphide interchange activity, as the cysteines in the active site facilitate disulphide bonding with substrate proteins. Therefore, it was decided to design novel peptides to mimic PDI's activity that are primarily be based on PDI's *a* and *a'* domains.

The studies outlined in Chapter 4, examining the Dsb proteins, suggested that the redox potential of thioredoxin-like proteins plays a key role in their protective activity in ALS, as it was demonstrated that the oxidase Dsb (DsbA) was protective against all cellular pathogenic mechanisms examined, in contrast to the isomerase Dsb (DsbC). Therefore, it was postulated whether modification in PDI's active sites, which are predicted to alter its redox potential,

would affect PDI's protective activity. In Chapter 5, the results obtained demonstrated that mutating PDI's active site to modulate its redox properties, resulted in variations in its protective activity, and in some instances, PDI's protective effect was lost. These results highlighted that PDI's oxidase activity is important in ALS, as this activity demonstrated a protective effect across all mutant proteins and all cellular mechanisms observed, compared to the reductase or isomerase activity. These results also verified that the active sites of PDI's *a* and *a'* domains were imperative for its protective function, as alterations in the active site can ablate this activity. Therefore, it was concluded that therapeutic peptides mimicking PDI's activity, based on its active sites and oxidase activity, may be protective in ALS.

Further studies performed in Chapter 5 also established that modulating PDI's cis-proline loop can affect its activity. In particular, the cis-proline loop of the *a* domain was necessary for this activity, as modifying this loop altered PDI's activity. Altering the cis-proline loop in the *a'* domain however, did not alter PDI's activity in most instances, suggesting that it is not essential for protective function. Therefore, one therapeutic peptide was designed to contain an additional proline residue, to mimic PDI's cis-proline loop in the *a* domain, whilst another peptide was designed without this residue.

7.1.3 The design of linear peptides, CGHC4 and CGHC5.

The design of the CGHC4 and CGHC5 linear peptides, 35 amino acids in length, was based on a naturally occurring α-hairpinin anti-microbial plant peptide, EcAMP1 [614]. This peptide possesses a two anti-parallel α-helices, with an intervening loop region and four naturally occurring cysteine residues [615]. The CGHC4 peptide was designed to contain the CGHC active site, within the loop region of EcAMP1. The four native cysteine residues of EcAMP1 were replaced with serines, to prevent them from interfering with the cysteines of

the CGHC sequence, and hence the redox potential. The CGHC5 peptide was designed in the

same way, except that it also incorporated a proline residue, five residues downstream of the

CGHC active site, in order to introduce a kink in the helix, reminiscent of PDI's cis-proline

loop. Flanking residues of the EcAMP1 peptide were replaced with a sequence to allow

cyclisation of these linear peptides in the future, using the vacuolar processing enzyme (VPE)

system [610], as used by collaborators Marilyn Anderson and Mark Bleackley. Figure 7.1

illustrates how the CGHC active site and proline sequences were incorporated into EcAMP1,

to create the novel peptides CGHC4 and CHGC5.
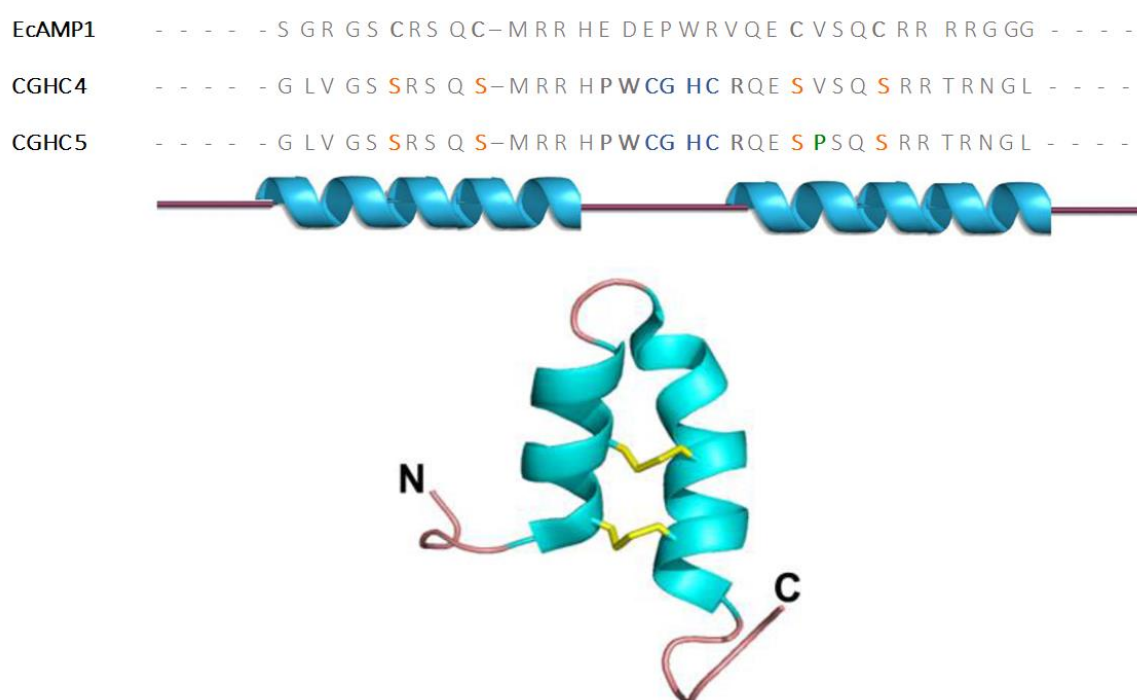
Figure 7.1: A schematic representation of the CGHC4 and CGHC5 peptides based on the α-hairpinin peptide, EcAMP1. The sequences for EcAMP1, CGHC4 and CGHC5 are shown above the peptide structure. The sequence in the loop region of EcAMP1 was replaced with the CGHC active site of PDI's *a* domain for both CGHC4 and CGHC5 (shown in blue). The native cysteine residues of EcAMP1 were also substituted to serines to prevent interference with the active site (shown in orange). In the CGHC5 peptide, a proline residue was inserted in place of the normal valine residue at this position, to introduce a kink into the helix, thus mimicking the cis-proline loop (shown in green). Flanking residues were replaced with a cyclisation sequence so that these linear peptides could be cyclised in the future using the VPE system. The 3D structure of the EcAMP1 peptide is also illustrated. The CGHC4 and CGHC5 peptides would not contain the disulphide bonds (yellow) due to the removal of cysteine residues.

7.1.4 Aims of this chapter

This doctoral thesis has characterised and identified the properties of PDI which are essential

for its protective activity, at least *in vitro*. Based on these results, two novel, linear peptides

based on PDI were synthesised. The aim of the studies outlined in this chapter was to

investigate whether these two peptides are protective against SOD1 inclusion formation, ER

stress and cell toxicity in neuronal cell lines expressing mutant SOD1. These preliminary

studies would therefore provide some evidence to determine whether these peptides are

functional or not, and if so, if they exert a protective effect similar to PDI. If protective,

further studies need to be performed in the future, to optimise the properties of these peptides,

so they can be developed as potential therapeutics for ALS in the future.

7.2 Materials/Methods

7.2.1 Administration of peptides into Neuro-2A cells

Peptides were dissolved in Milli Q water to a stock concentration of 1 mM, aliquoted and stored at -20°C. Upon treatment of cells, peptides were administered at varying concentrations from 10 µg/mL to 100 µg/mL, approximately 5 h post transfection with SOD1 A4V-EGFP constructs (section 2.3.3). Cells were fixed 72 h after transfection, and immunocytochemistry was performed (section 2.4.2) to analyse the effect of the peptides on cellular mechanisms linked to ALS.

7.3 Results

7.3.1 The expression of mutant SOD1 A4V does not alter upon administration of linear peptides.

The experiments described below in sections 7.3.2 to 7.3.4 examined the effect of two linear peptides, CGHC4 and CGHC5, that mimic the active site of PDI, on SOD1 inclusions, ER stress and apoptosis induced by mutant SOD1 A4V. SOD1 A4V was nominated as the ALS-associated mutant to assess as this accounts for a considerable proportion of familial ALS cases and presents as an aggressive form of disease within Neuro-2A cells. Prior to these immunocytochemistry based assays, control western blotting experiments were performed to ensure that the administration of the peptides did not alter or diminish the expression of mutant SOD1 A4V (Figure 7.2). Cell lysates were obtained for each experimental group. Wildtype SOD1 and mutant SOD1 A4V were detected at 50 kDa, as expected, using an anti-GFP antibody. Moreover, the peptides did not significantly alter mutant SOD1 A4V expression, when compared to SOD1 A4V expressing cells without peptide treatment. However, when CGHC4 was administered at 25 µg/mL and CGHC5 was administered at 10 µg/mL, SOD1 expression did appear to diminish (Figure 7.1 B). GFP was detected in GFP expressing cells at the expected size of 26 kDa using an anti-GFP antibody. β-actin was used as a loading control and was detected at 40 kDa utilising an anti-β-actin antibody.

A
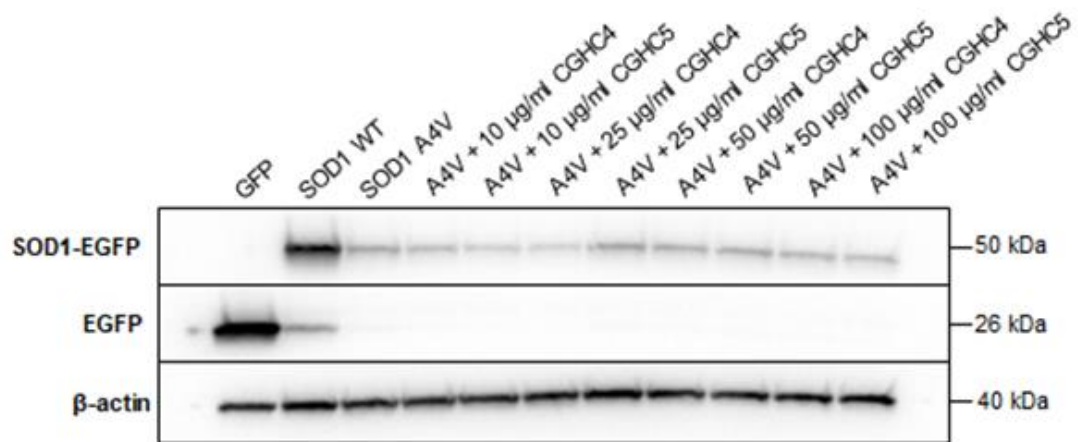
B
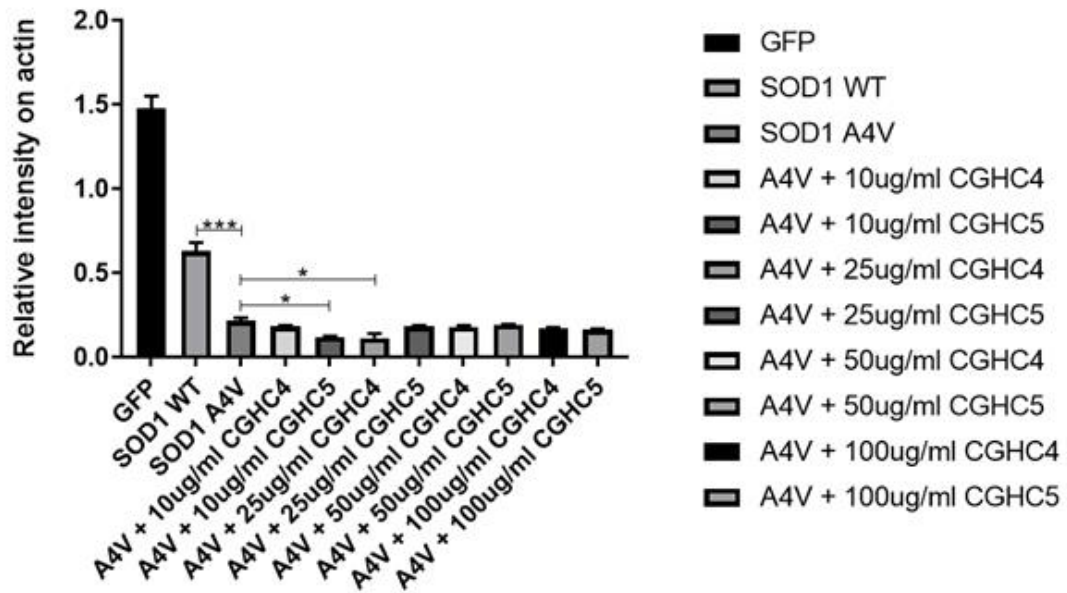
Figure 7.2: Protein expression of SOD1 A4V after linear peptide administration in Neuro-2A cells. A) Cell lysates for each experimental group were obtained and western blotting analysis was performed to ensure that expression of mutant SOD1 A4V-EGFP was produced at the expected size and its expression was not altered. GFP was detected at 26 kDa and wildtype SOD1 and mutant SOD1 A4V were detected at 50 kDa (SOD1 = 19 kDa, GFP = 26 kDa). The loading control, β-actin, was detected at 40 kDa. **B)** Quantification of western blotting analysis revealed that CGHC4 administration at 25 µg/mL and CGHC5 administration at 10 µg/mL resulted in less SOD1 expression compared to mutant SOD1 A4V expression without peptide treatment. At other varying concentrations, however, both CGHC4 and CGHC5 administration did not alter mutant SOD1 expression.

7.3.2 The administration of linear peptides mimicking the PDI active site results in a dose dependent inhibition of mutant SOD1 inclusion formation.

To analyse whether the linear peptides based on PDI's active sites were protective against mutant SOD1 A4V, it was first examined whether both the peptides were able to inhibit SOD1 inclusion formation in Neuro-2A cells.

CGHC4 and CGHC5 were administered to Neuro-2A cells at varying concentrations from 10 µg/mL to 100 µg/mL five hours after transfection with mutant SOD1 A4V. SOD1 inclusion formation was analysed 72 h post transfection after cells were fixed and stained with Hoechst to visualise the nuclei. Mutant SOD1 A4V expressing cells were examined for the formation of inclusions using fluorescence microscopy where at least 100 cells were examined per group. The frequency of cells bearing inclusions were quantified (Figure 7.3 A). Untransfected cells and cells expressing EGFP alone or wildtype SOD1 formed no inclusions (0%), as expected. Conversely, 24.6% ± 0.9 of cells expressing SOD1 A4V without peptide treatment did form inclusions, consistent with previous observations. Interestingly, cells exposed to 10 µg/mL of either CGHC4 or CGHC5 demonstrated a significant reduction ($p < 0.01$ and $p < 0.001$) in SOD1 inclusion formation to 13.3% ± 1.2 and 12.0% ± 1.0, respectively. Across all experimental groups, there appeared to be a dose dependent decrease in the percentage of cells forming inclusions (Figure 7.3 B). Cells in which 100 µg/mL of either CGHC4 or CGHC5 were administered displayed a significant decrease in inclusions to 8.7% ± 1.8 and 6.7% ± 0.3 respectively, compared to SOD1 A4V transfected cells with no peptide treatment ($p < 0.001$) (Figure 7.3 C).
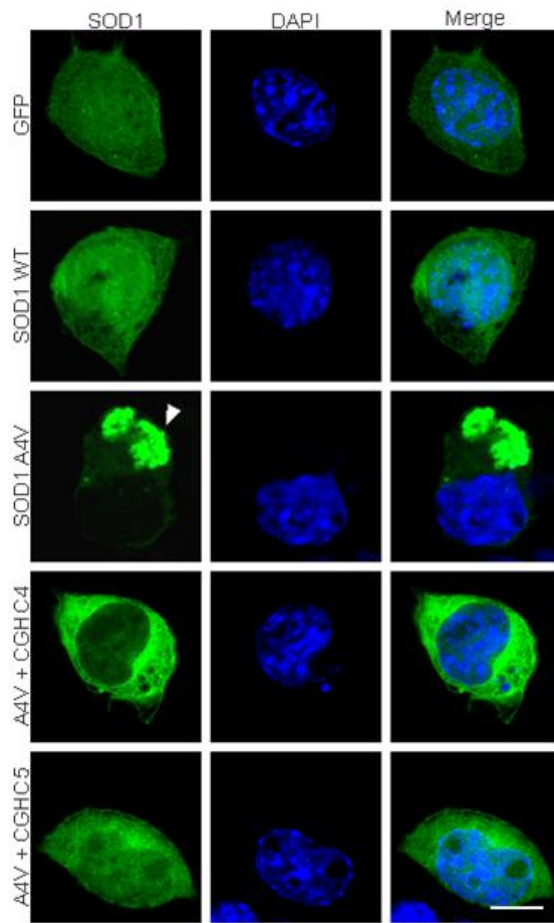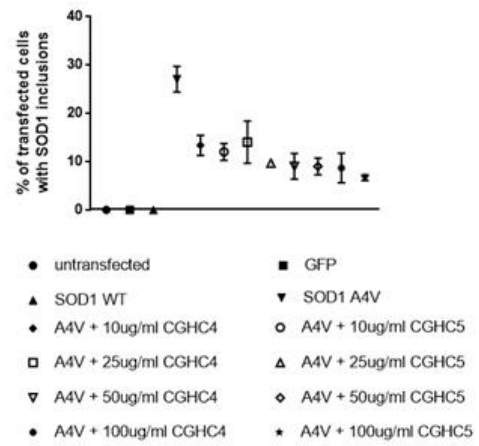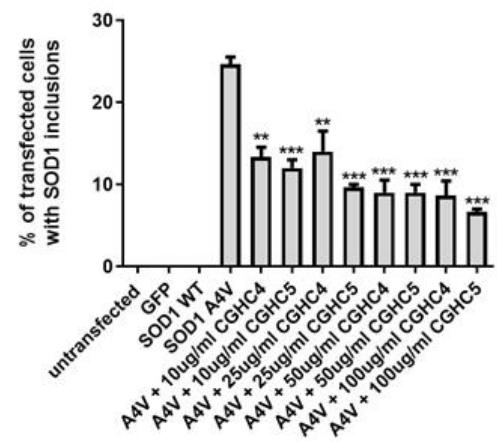
Figure 7.3: The administration of linear peptides, CGHC4 and CGHC5, results in a dose dependent decrease in mutant SOD1 inclusion formation. A) Immunofluorescence images of Neuro-2A cells expressing GFP (first panel; GFP), wildtype SOD1 (second column; SOD1 WT), and SOD1 A4V with or without either CGHC4 or CGHC5 peptide administration. Cells expressing GFP or wildtype SOD1 did not form SOD1 inclusions. A high proportion of cells expressing mutant SOD1 A4V without peptide treatment (third panel; SOD1 A4V) displayed SOD1 inclusions, as indicated by the white arrowhead, consistent with previous observations. When cells expressing mutant SOD1 A4V were exposed to CGHC4 and CGHC5 peptides (fourth and fifth panel; A4V + CGHC4, A4V + CGHC5), less cells formed inclusions. Scale bar = 30 µM. **B)** There was a dose dependent decrease in the proportion of cells forming inclusions in cells expressing mutant SOD1 A4V treated with the CGHC4 and CGHC5 peptides, compared to SOD1 A4V expressing cells without peptide administration. **C)** Quantification of cells in A) forming mutant SOD1 A4V inclusions. Untransfected cells, and cells expressing GFP or wildtype SOD1, did not display SOD1 inclusions, as expected. Conversely, there was a significant increase of SOD1 inclusions in cells expressing mutant SOD1 A4V, compared to cells expressing wildtype SOD1. However, the proportion of cells with SOD1 inclusions significantly decreased when either CGHC4 or CGHC5 was administered to mutant SOD1 A4V expressing cells, at all concentrations ($p < 0.01$, $p < 0.001$). N=3, Mean ± SEM, ** $p < 0.01$, *** $p < 0.001$.

7.3.3 The administration of linear peptides, CGHC4 and CGHC5, decreases CHOP activation induced by mutant SOD1.

Next, it was examined whether the PDI active site linear peptides were protective against ER stress, using CHOP activation as a marker of ER stress-induced pro-apoptotic signalling.

Cells expressing mutant SOD1 A4V were administered with CGHC4 and CGHC5, at a range of concentrations, five hours post-transfection. Cells were fixed 72 h after transfection and immunocytochemistry was performed using an anti-CHOP antibody. Cells were stained with Hoechst to visualise nuclei. Cells were examined using fluorescence microscopy and at least 100 transfected cells were counted and analysed for nuclear immunoreactivity to CHOP, indicating activation (Figure 7.4 A).

Quantification revealed that few untransfected cells and cells expressing GFP or wildtype SOD1 displayed CHOP activation (4.7% ± 0.3 and 5.0% ± 1.2, respectively). As expected, there was a significant increase ($p < 0.001$) in the proportion of cells expressing mutant SOD1 A4V with nuclear immunoreactivity to CHOP to 19.3% ± 1.9, compared to wildtype SOD1. However, when cells expressing mutant SOD1 A4V were exposed to either CGHC4 or CGHC5 peptides, there was a reduction in the percentage of cells with nuclear immunoreactivity to CHOP. At 10, 25 and 50 µg/mL, CGHC4 significantly reduced the proportion of cells displaying CHOP activation to approximately 10% ($p < 0.01$). At the highest concentration examined, 100 µg/mL, this proportion was further reduced to 7.7% ± 1.5 of cells with activated CHOP ($p < 0.001$). CGHC5 demonstrated a protective effect at 10 µg/mL, where the percentage of mutant SOD1 A4V expressing cells was reduced to 11.3% ± 1.7 ($p < 0.05$), however, this result could be due to less SOD1 expression. Furthermore, CGHC5 demonstrated no significant protective effect at 25 and 50 µg/mL, although a trend was evident. At 100 µg/mL, the protective effect of CGHC5 was significant; CHOP

activation in mutant SOD1 A4V expressing cells was reduced to 10.7% ± 1.3 ($p < 0.05$)

(Figure 7.4 B).

A
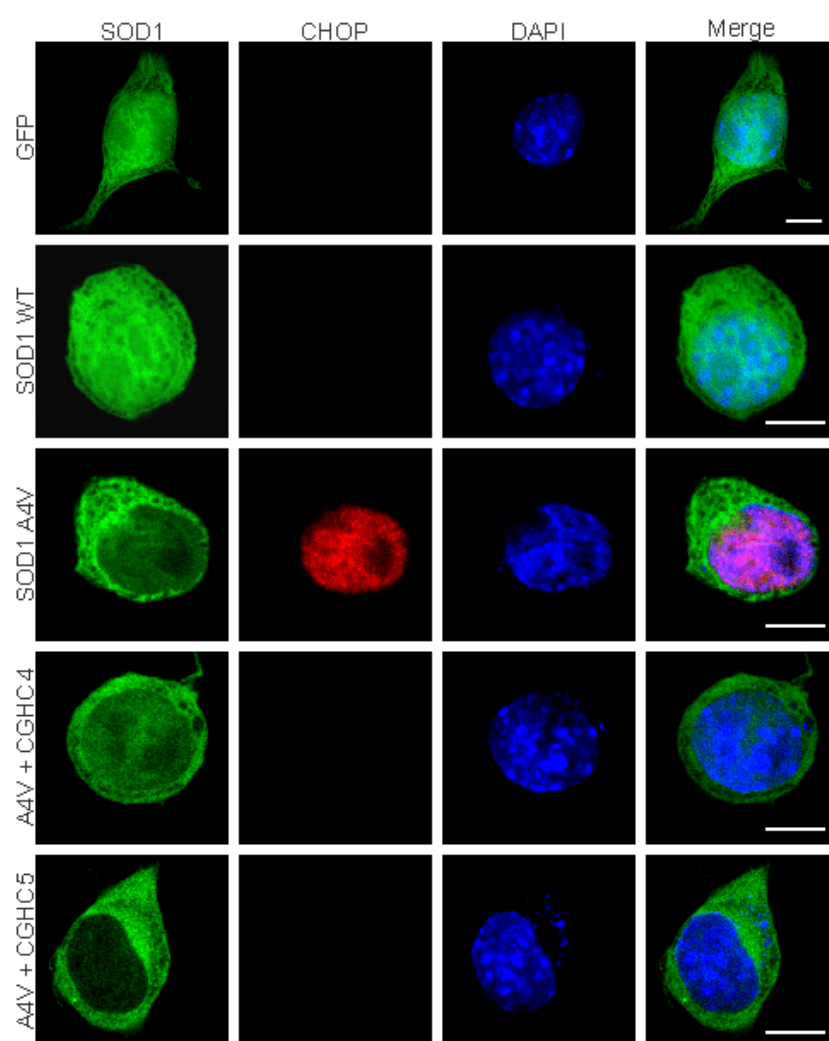
B
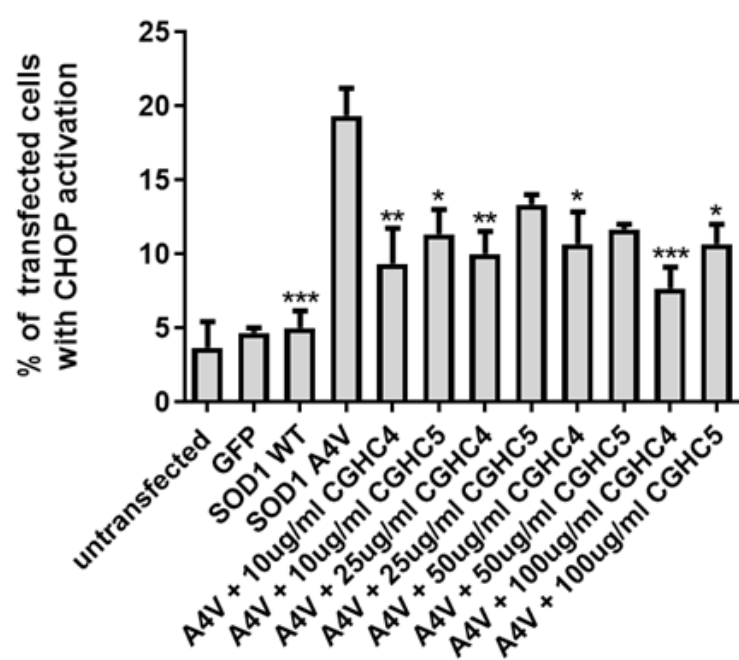
Figure 7.4: The administration of linear peptides, CGHC4 and CGHC5, decreases CHOP activation induced by mutant SOD1. A) Few neuro-2A cells expressing GFP (first panel; GFP) or wildtype SOD1 (second panel; SOD1 WT) displayed CHOP activation. As expected, cells expressing mutant SOD1 A4V (third panel; SOD1 A4V) displayed more CHOP activation, as indicated by red fluorescence in the nucleus (third panel, second column). However, when CGHC4 or CGHC5 were administered to mutant SOD1 A4V expressing cells, fewer cells displayed nuclear immunoreactivity to CHOP, indicating activation (fourth and fifth panels; A4V + CGHC4, A4V + CGHC5). Scale bar = 30 µM. **B)** Quantification of the cells in A) with CHOP nuclear immunoreactivity. The proportion of cells with CHOP activation was significantly lower in cells expressing wildtype SOD1 and GFP, compared to cells expressing mutant SOD1 A4V ($p < 0.001$). When CGHC4 was administered to mutant SOD1 A4V expressing cells, there was a decrease in the proportion of cells exhibiting CHOP activation across all concentrations (10 µg/mL and 25 µg/mL = $p < 0.01$, 50 µg/mL = $p < 0.05$, 100 µg/mL = $p < 0.001$). Similarly, there was a decrease in the proportion of cells with CHOP activation when exposed to CGHC5 at 10 µg/mL and 100 µg/mL ($p < 0.01$ and $p < 0.05$, respectively). N=3, Mean ± SEM, * $p < 0.05$, ** $p < 0.01$, *** $p < 0.001$.

7.3.4 The administration of linear peptides, CGHC4 and CGHC5, inhibits mutant SOD1 induced nuclei condensation, indicative of apoptosis.

It was next examined whether the CGHC4 and CGHC5 linear peptides were protective against apoptotic cell death induced by mutant SOD1. To determine this, nuclei condensation and fragmentation was observed by microscopy, which was indicative of a cell in late-phase apoptosis.

Neuro-2A cells were transfected with GFP, wildtype SOD1 or mutant SOD1 A4V, where cells expressing mutant SOD1 A4V were exposed to varying concentrations of CGHC4 and CGHC5 linear peptides. After 72 h, cells were fixed and the nuclei stained with Hoechst. The nuclei of transfected cells were examined and scored using fluorescence microscopy, whereby apoptosis was recorded if nuclei were condensed, fragmented or presented an irregular morphology (Figure 7.5 A).

Few untransfected cells and cells expressing GFP and wildtype SOD1 possessed condensed nuclei (less than 5%), indicating that GFP alone and wildtype SOD1 do not induce apoptosis, as expected. There was a significant increase in the proportion of cells undergoing apoptosis in mutant SOD1 A4V expressing cells (18.7% $\pm$ 0.9), compared to cells expressing wildtype SOD1 ($p < 0.001$), consistent with previous studies [265]. Upon administration of CGHC4 to SOD1 A4V expressing cells, there was a significant reduction in the proportion of cells with nuclei condensation, however this decrease did not appear to be dose dependent. An average of 10% of mutant SOD1 A4V expressing cells displayed nuclei condensation or fragmentation upon CGHC4 administration across all doses ($p < 0.01$). Administration of CGHC5 also displayed a significant decrease in apoptosis compared to mutant SOD1 A4V expressing cells without peptide treatment. At 10 and 25 µg/mL, there was a significant reduction in cells with apoptotic nuclei to 12.0% ($p < 0.05$). At 50 µg/mL, this proportion

decreased to 8.3% ± 0.7 (p < 0.001), and at 100 µg/mL, the proportion of cells with apoptotic

nuclei further decreased to 5.7% ± 0.3 (p < 0.001). Overall, this data suggests that linear

peptides based on PDI's active site are protective against apoptotic cell death induced by

mutant SOD1 (Figure 7.5 B).

A

	SOD1	DAPI	Merge
GFP			
SOD1 WT			
SOD1 A4V			
A4V + CGHC4			
A4V + CGHC5			

B

536
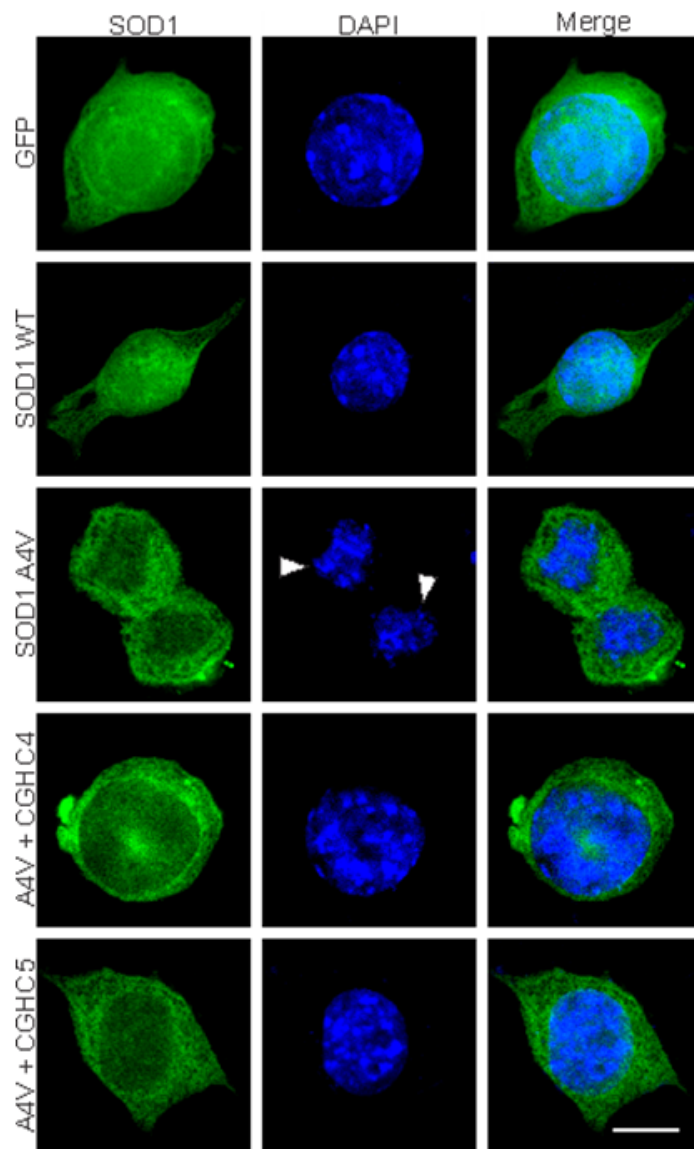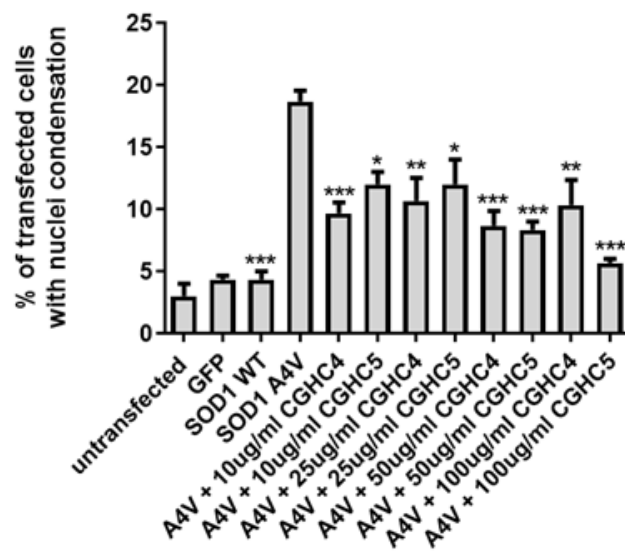
Figure 7.5: The administration of linear peptides, CGHC4 and CGHC5, reduces the proportion of cells with mutant SOD1 induced nuclei condensation, indicative of apoptosis. A) Neuro-2A cells expressing GFP (first panel; GFP) or wildtype SOD1 (second panel; SOD1 WT) exhibit few apoptotic nuclei. More cells expressing mutant SOD1 A4V (third panel; SOD1 A4V) possess condensed nuclei, indicating apoptosis, shown by the white arrowheads (third panel, column two). However, there is a decrease in the proportion of cells with nuclei condensation when mutant SOD1 A4V expressing cells are treated with CGHC4 and CGHC5 (fourth and fifth panel; A4V + CGHC4, A4V + CGHC5). Scale bar = 30 µM. **B)** Quantification of cells in A) displaying apoptotic nuclei. There was a significant increase in the proportion of cells with condensed or fragmented nuclei in cells expressing mutant SOD1 A4V, compared to untransfected cells, or cells expressing GFP or wildtype SOD1 ($p < 0.001$). When SOD1 A4V expressing cells were treated with peptides CGHC4 and CGHC5, at varying concentrations, there was a significant decrease in the proportion of apoptotic nuclei. N=3, Mean ± SEM, * $p < 0.05$, ** $p < 0.01$, *** $p < 0.001$.

7.4 Discussion

The aim of the studies described in this chapter was to investigate whether peptides designed to mimic the active site of PDI were protective in cell culture models. The peptides were designed based on findings obtained from the characterisation of PDI's protective activity in ALS, presented in the previous chapters of this thesis. Specifically, the peptides were based on PDI's CGHC active site in its *a* domain, where its disulphide interchange activity, or redox activity, is located. The experiments performed in this short study aimed to examine the effect of two linear peptides, termed CGHC4 and CGHC5, in preliminary cell culture studies against mutant SOD1. CGHC4 contained the CGHC active site, whilst CGHC5 contained a proline residue to mimic PDI's cis-proline loop, in addition to the CGHC active site. Linear peptides were analysed for their effects in mutant SOD1 expressing cells, specifically against mutant SOD1 inclusion formation, ER stress and apoptosis.

On the whole, these experiments demonstrated a beneficial effect of these peptides on mutant SOD1 expressing cells. There was a statistically significant decrease in the formation of SOD1 inclusions when both CGHC4 and CGHC5 were administered at only 10 µg/mL, and this proportion decreased further at higher concentrations of each peptide. However, it is important to note that at 10 µg/mL, CGHC5 caused a loss of SOD1 expression and a similar result was observed when CGHC4 was administered at 25 µg/mL. It is unknown why this reduction in SOD1 expression resulted, or whether this loss of SOD1 expression was due to experimental error in the transfection of mutant SOD1 A4V. Hence, future experiments should be undertaken to determine if modulating the concentration of these peptides alter the expression levels of SOD1. Regardless, the decrease observed in the proportion of cells bearing SOD1 inclusions is consistent with the results obtained in chapter 4, where expression of the PDI *a* domain constructs resulted in a protective effect against inclusion formation in cells expressing mutant SOD1. This result further strengthens the notion that the

a domain of PDI, and more importantly, the disulphide interchange activity, is imperative for its protective activity. It also demonstrates that the peptides, similar to PDI, are able to reduce protein misfolding, an important pathological hallmark in ALS. Protein misfolding is a common property of most proteins, even those without mutations, therefore peptides which prevent protein aggregation may be valuable against other misfolded proteins, such as those associated with other neurodegenerative diseases.

The CGHC4 and CGHC5 linear peptides were also able to reduce the proportion of cells with CHOP activation in cells expressing mutant SOD1, indicating that both peptides may also be protective against ER stress, although additional markers of ER stress were not examined due to time constraints. This effect was not dose-dependent as expected, although this could be a limitation of the cell culture assay. Therapeutic strategies targeting ER stress are becoming an appealing therapeutic target for ALS, with seven compounds targeting the UPR currently being examined for their therapeutic potential, according to the ALS Therapy Development Institute (ALS-TDI). Indeed, ER stress is proposed to play a fundamental role in ALS pathogenesis. However, strategies based on PDI's activity may provide more specific benefits, rather than just targeting the UPR. A reduction in the proportion of cells with CHOP activation also implies that there are fewer pro-apoptotic cells in populations treated with peptide, and this notion is further strengthened when analysing the effects of CGHC4 and CGHC5 specifically on apoptosis. At varying concentrations, both linear peptides were capable of reducing the proportion of mutant SOD1 expressing cells exhibiting condensed or fragmented nuclei, consistent with an apoptotic cell. However, additional apoptotic assays should be performed to confirm these findings. Ultimately, an effective therapeutic agent for ALS needs to prevent the death of neuronal cells, therefore this preliminary result demonstrating that the peptides can inhibit apoptosis is promising. It is important to note, however, that these results did not follow the typical sigmoidal shape expected of a dose

response curve, thus future experimentation will have to be undertaken, or perhaps more data points are needed between 0 to 10 µg/mL of peptide to ascertain the sigmoidal shape. If there does not seem to be a dose response in future experiments, it may imply that the peptide could have multiple targets.

It is interesting to note that both CGHC4 and CGHC5 exhibit much the same protective activity, despite the fact that only CGHC5 possesses the proline residue, reminiscent of PDI's cis-proline loop. The studies outlined in Chapter 5, analysing the effects of mutating PDI's cis proline loop, indicated that this loop did contribute to the protective activity in the *a* domain, because mutating the loop did perturb some activities. However, this study showed that CGHC4, the peptide without the proline, still retains a protective effect.

A previous study by Liu and colleagues (2013) examined the effect of a peptide disulphide they designed based on PDI, with the sequence RKCGCFF. As in the peptides designed in this study, this peptide contained two cysteine residues, albeit with only one residue between them, instead of two, and it did not contain a proline residue. Interestingly, this peptide was able to facilitate protein refolding and it was found to be more effective than oxidised glutathione [491]. It is therefore possible that the cis-proline loop only plays a role in substrate binding, rather than being involved in the disulphide interchange activity of PDI. However, previous studies examining the cis-proline loop of Dsb proteins have demonstrated that mutating a single residue of the cis-proline loop can also modify the redox properties of thioredoxin-like proteins, as well as altering its ability to interact with substrates [492]. It would be interesting in future studies therefore, to examine whether the linear peptides are protective when administered to cells expressing other ALS mutant proteins, such as mutant forms of TDP-43, FUS or Cyclin F.

It would also be interesting to design additional novel linear peptides utilising the CPHC oxidase active site, instead of the native CGHC sequence. When PDI's active site was mutated to CPHC, as described in Chapter 5 of this thesis, PDI still retained its protective activity, whereas mutating the active site to CPYC or CGPC was only protective in some instances. These results demonstrate that PDI's oxidase activity is important for its protective function. No significant differences were observed in the protective activity detected between native PDI and the novel "oxidase" forms of PDI, although it should be noted that this may be a limitation of the sensitivity of the assays used here. Hence, it is tempting to speculate that a peptide with the CPHC active site would still be as effective as the peptide containing CGHC, or it may be even more protective. Future studies should explore this notion.

Ultimately, however, there is a need to determine whether the protective effect of these peptides translates to ALS animal models. In future studies, these peptides should be cyclised and examined in zebrafish models of ALS, to determine if they can improve the axonopathy, induction of apoptosis, and impairment of motor function in these models. If effective, these peptides should then be analysed for their protective effect by administration to mutant SOD1 and TDP-43 transgenic mouse models of ALS, such as the recently described NEFH mice expressing cytoplasmically localised wildtype TDP-43 [616].

In future studies, it should also be examined if these peptides are able to cross the blood brain barrier (BBB). There are currently more than 30 BBB shuttle peptides available [617] and nanoparticles or exosomes can also be used in order to increase permeability to the BBB [618]. Hence, there are multiple options that could be examined in future studies if the peptides described in this Chapter cannot access the brain. Future experiments should also be undertaken in consideration of evidence implying that PDI becomes apoptotic when ER proteostasis cannot be resolved (reviewed in Parakh and Atkin [619]). These pro-apoptotic functions of PDI are not fully understood and thus need to be investigated if effective

therapeutic strategies based on PDI are to be designed. In models of Huntington's disease and Alzheimer's disease, PDI inhibitors were previously found to be protective [620], suggesting that inhibiting the harmful effects of PDI can sometimes also be beneficial therapeutically. Therefore, the switch from the protective functions to the detrimental activity of PDI need to be fully defined before effective therapeutic strategies based on the protein can be fully realised.

Peptides currently only represent 2% of the drug market, however this market is growing rapidly. Peptides have some advantages when compared to small molecules; they are known to exhibit high binding affinity and excellent target specificity, whilst bearing low toxicity [608]. Moreover, synthetic peptides, such as the peptides used in this study, have improved properties compared to natural peptides because they are much more stable [610], and cyclisation can further improve their stability.

The development of novel therapeutics in treating ALS is imperative given that there are currently few therapeutic options. The aim of the studies outlined in this chapter was to obtain preliminary evidence to determine whether novel therapeutic peptides based on the activity of PDI can be developed in the future. Whilst studies from our laboratory show that PDI is protective, it cannot be used as a drug as it is too large to be effectively delivered through the BBB. Moreover, the findings of previous chapters of this thesis reveal the disulphide interchange activity of PDI is fundamental for its protective activity, and this is reliant on the CGHC active site located in the *a* domain. This suggests that only this small region, mimicked in the peptides described in this Chapter, is responsible for PDI's protective activity against several ALS-associated proteins in cellular studies. Hence this study provides promising preliminary evidence that these peptides have further potential as novel therapeutic agents in ALS, although there are many future studies that need to be performed, as outlined further in the concluding chapter of this thesis.

Chapter 8: General Discussion

8.1 Summary of the main findings of this thesis

The findings reported in this thesis highlight the mechanisms by which PDI modulates its protective activity against cellular processes linked to ALS. In neuronal cell culture models, PDI was protective against mutant forms of a novel ALS/FTD-associated protein, Cyclin F. PDI was capable of inhibiting mutant Cyclin F mislocalisation to the cytoplasm, ER stress induction, impairment to the UPS and apoptosis. Hence, although Cyclin F is structurally and functionally different to the more well-studied ALS proteins, SOD1, TDP-43 and FUS, PDI was still able to elicit a protective response against these common cellular pathogenic mechanisms of ALS. Whilst extensive studies of the efficacy of PDI *in vivo* in rodents are currently underway, and need to be completed to ascertain its true potential in ALS, these results imply that therapeutics based on PDI's protective function may be beneficial in ALS. Given the considerable genetic and pathological overlap between ALS and FTD, it is also possible that the protective functions of PDI may also be applicable in FTD. Thus, an intensive study into the protective mechanisms mediated by PDI was performed to determine the specific properties of PDI that are necessary to elicit a protective response. It is possible that PDI is not protective against other cellular mechanisms associated with ALS, such as those processes related to RNA dysfunction. However, in terms of mechanisms linked to proteostasis and ER homeostasis, the evidence obtained by our group and others suggests that PDI is broadly protective, and should therefore be examined further as a possible therapeutic target.

Studies analysing the effect of co-expression of the individual domains of PDI with mutant proteins linked to ALS demonstrated that the *a* and *a'* domains are fundamental for PDI's protective activity, because they both were protective against all pathogenic mechanisms induced by mutant SOD1, TDP-43 and FUS that were examined in this study. Previous studies undertaken in our laboratory have revealed the importance of PDI's disulphide

interchange activity, rather than its chaperone function, in these protective effects (Parakh et al., 2017 in preparation). The findings obtained in this study are consistent with the previous results obtained from our laboratory, because the disulphide interchange activity of PDI requires the CXXC active site motif located within the *a* and *a'* domains. Therefore, studies investigating the relationship between the redox activity and the CXXC active site motif were performed to investigate how the redox characteristics of PDI modulate its protective activity. Whilst the roGFP results do not fully permit analysis of the precise redox properties of PDI, they do provide an indication of these characteristics. The results obtained demonstrated that an active site motif that is predicted to be more oxidising was protective against all pathogenic mechanisms examined in cells expressing mutant SOD1, TDP-43 or FUS, whereas motifs that were predicted to be either isomerising or reducing were only protective against mutant SOD1 and FUS induced ER stress, and mutant TDP-43 mislocalisation. Moreover, studies involving expression of bacterial Dsb proteins in eukaryotic cell culture, DsbA and DsbC, were subsequently performed and the redox properties of these proteins have been extensively characterised. These studies confirmed that the oxidising thioredoxin-like protein, DsbA, demonstrated much more protective capabilities than the isomerising DsbC. In fact, the oxidase DsbA demonstrated a protective effect against all the pathogenic mechanisms observed, induced by mutant SOD1, TDP-43 and FUS, similar to wildtype PDI. The isomerase, DsbC, was protective only against mutant SOD1 and FUS-induced ER stress, as well as mutant TDP-43 mislocalisation; results that were consistent with those obtained from the study of the CXXC active site mutants. These results together indicate that it is the oxidase activity of PDI that is essential for its protective functions in ALS. Furthermore, studies examining the effect of PDI's cis-proline loop demonstrated that it also plays a role in modulating protective function, and they provided additional evidence that the oxidase activity of PDI is protective in ALS. The results obtained revealed that mutations that were

predicted to enhance the oxidising activity of the cis-proline loop within the *a* domain, retained the protective activity of PDI. However, mutations that were predicted to enhance the reducing activity of the *a* domain cis-proline loop, inhibited PDI's protective activity. Interestingly, no alterations in PDI's activity were observed when the *a'* domain cis-proline loop was modified to become either more oxidising or reducing, suggesting that PDI's *a* domain and its oxidase activity is the key feature mediating PDI's protective function. These results therefore confirm that the oxidising activity of PDI is protective against ALS cellular mechanisms.

The oxidase activity of PDI was further investigated in cells expressing mutant FUS in Chapter 6. Upon ablation of PDI's oxidase activity, PDI lost its protective function against mutant FUS-induced pathogenic mechanisms. This was further confirmed in cells treated with the PDI mimetic, BMC, whereby BMC's protective activity was subsequently diminished once its oxidase capabilities were inhibited. Furthermore, this study demonstrated that PDI variants, D292N and R300H, are also protective against mutant FUS cellular mechanisms, including FUS mislocalisation, ER stress and the formation of inclusions. Moreover, the protective activities of the variants were inhibited upon disruption of the cellular redox conditions and ablation of oxidase activity by BSO, suggesting that these mutations in PDI do not affect disulphide interchange activity, and furthermore, their oxidase capabilities. The mutations in these mutants are located in the substrate binding *b'* domain, thus, these results further confirm that the *a* domains possess the protective properties of PDI.

Finally, based on the results obtained in this doctoral thesis, linear peptides based on PDI's protective features were synthesised. Preliminary studies investigating the effect of these peptides in neuronal cells expressing mutant SOD1 were performed. These experiments demonstrated that the peptides were protective against mutant SOD1 inclusion formation, ER stress and apoptosis. Since, the completion of the experimental work for this thesis, it has

also been demonstrated by another member of our laboratory that cyclised versions of CGHC4 and CGHC5 are also protective against the same processes in cells expressing mutant SOD1. These results suggest that therapeutic agents based on PDI's protective mechanisms may be beneficial in ALS and hence they should be explored in the future. A summary of all the main results obtained in this study, which demonstrate PDI's protective mechanisms against misfolded proteins linked to ALS, are presented in Table 8.1.

TABLE 8.1: A summary of the PDI characteristics investigated and the results obtained.

Mutant protein	SOD1 inclusion formation	SOD1-induced ER stress	SOD1-induced apoptosis	TDP-43 mislocalisation	TDP-43-induced ER stress	FUS mislocalisation	FUS-induced ER stress
PDI domain mutants							
a domain	✓	✓	✓	✓	✓	✓	✓
a' domain	✓	✓	✓	✓	✓	✓	✓
bb' domain	✗	✓	✗	✗	✓	✗	✓
PDI redox active site mutants							
CPHC (oxidase)	✓	✓	✓	✓	✓	✓	✓
CPYC (isomerase)	✗	✓	✗	✓	✗	✗	✓
CGPC (reductase)	✓	✓	✗	✗	✗	✗	✓
PDI cis-proline loop mutants							
GIP (*a* domain - reducing)	✗	✗	✗	✗	✓	✗	✗
GTP (*a* domain - oxidising)	✓	✓	✓	✓	✓	✓	✓
SIP (*a'* domain - reducing)	✓	✓	✓	✓	✓	✓	✓
STP (*a'* domain - oxidising)	✓	✓	✓	✓	✓	✗	✗
Dsb mutants							
DsbA (oxidase)	✓	✓	✓	✓	✓	✓	✓
DsbC (isomerase)	✗	✓	✗	✓	✗	✗	✓
Linear peptides							
CGHC 4	✓	✓	✓	NA	NA	NA	NA
CGHC 5	✓	✓	✓	NA	NA	NA	NA

8.1.1 PDI is protective against ALS-associated mutant Cyclin F

The findings detailed in Chapter 3 reveal that PDI has broader activity in ALS than previously recognised, because PDI was protective in cells expressing mutant S621G cyclin F. This mutation is associated with both ALS and FTD [89]; hence this is the first time that PDI has been shown to be protective against a mutation that causes FTD, implying that PDI may also be relevant therapeutically to FTD. ALS and FTD are associated with the accumulation of misfolded proteins that have the propensity to aggregate in the cytoplasm, resulting in the induction of ER stress and apoptosis. Previous studies undertaken in our laboratory have demonstrated that PDI is able to inhibit these cellular pathogenic mechanisms induced by mutant forms of ALS proteins, SOD1, TDP-43 and FUS [448](Parakh et al., 2017 in preparation). Here, neuronal cell culture models were used to demonstrate that PDI was also protective against mutant Cyclin F; a novel ALS/FTD associated protein with structural and functional disparities compared to other well-studied ALS associated proteins. In future studies these findings should be validated in additional disease models, such as IPSC-derived motor neurons or in vivo.

Interestingly, recent studies in our laboratory have shown that mutant Cyclin F ALS-associated mutant, S621G, perturbs ER homeostasis and induces similar cellular mechanisms to that of other proteins implicated ALS, such as its mislocalisation from the nucleus to the cytoplasm, induction of ER stress, inhibition of ER-Golgi transport, impairment of UPS, and thus, apoptosis (Ragagnin et al., 2017 in preparation). These results imply that common disease mechanisms are present in ALS, triggered by diverse mutant proteins. In Chapter 3, the overexpression of PDI in Neuro-2A cells expressing mutant Cyclin F S621G was found to be protective against Cyclin F mislocalisation to the cytoplasm, ER stress, UPS impairment, and apoptosis, similar to the observations obtained previously in cells expressing mutant SOD1, TDP-43 or FUS. However, the mechanisms that mediate this protective activity have

been unclear until now. Moreover, it is interesting to consider why PDI is protective in ALS cell models, as demonstrated here, but not in ALS patients where it is upregulated. One possible explanation for this is post-translational modification of PDI in ALS patients. In conditions of elevated stress, PDI is S-nitrosylated, therefore inhibiting PDI's normally protective function during disease states. S-nitrosylation may compromise both PDI's oxidoreductase and chaperone activities, further exacerbating protein misfolding and ER stress, and thus dysregulating proteostasis, creating a vicious cycle. Hence, overexpressing PDI in cell culture models may compensate for the loss of endogenous PDI caused by S-nitrosylation, therefore overcoming the cellular defects induced by mutant ALS proteins, such as Cyclin F. This notion supports the idea that therapeutic agents based on PDI's activity may be beneficial in ALS, by utilising a PDI mimic to compensate for the loss of PDI function in patients.

However, a number of confounding questions need to be considered, such as how the overexpression of PDI inhibits mutant Cyclin F mislocalisation from the nucleus to the cytoplasm? Whilst the PDI family of proteins are generally considered to be located in the ER, PDI re-distributes away from the ER in punctate vesicular structures, mediated by reticulon proteins, where it possesses higher enzymatic activity [475]. Moreover, PDI has been detected in other sub-organelles, such as the cytoplasm, nucleus and extracellular space [450], and previous studies from our group and others have suggested that the proteins that misfold in ALS are not associated with the ER, further suggesting that PDI exerts its protective activity away from the ER. Hence together these data imply that PDI interacts with Cyclin F in the cytoplasm. Consistent with this notion, in Chapter 4 of this thesis, cytoplasmic only PDI was found to inhibit apoptosis induced by mutant SOD1, as assessed by three separate apoptosis assays (Bax activation, Bax recruitment to mitochondria, and Caspase-3 activation), indicating that PDI prevents toxicity from a cytoplasmic localisation.

It should be noted that we cannot rule out the possibility that PDI did not alter its cellular localisation away from the cytoplasm following co-transfection with SOD1, but these findings are consistent with our previous studies.

It remains unknown if mutant Cyclin F induces ER stress from the ER or the cytoplasm, and additional studies are underway in our group to examine this. Our laboratory previously demonstrated that ER-Golgi impairment precedes ER stress induced by mutant Cyclin F (Ragagnin et al., 2017 in preparation), implying inhibition of transport activates ER stress. Unfortunately, in the current study, the protective activity of PDI against inhibition of ER-Golgi transport was not investigated. Therefore, further studies are warranted to elucidate both whether PDI is protective against inhibition of ER-Golgi transport, and the mechanisms by which ER stress is induced by mutant Cyclin F.

Protein misfolding is a normal physiological event in most proteins, even those that do not bear mutations. Misfolded proteins can display their normally folded hydrophobic regions at their surface, which can result in the accumulation of misfolded proteins into aggregates. PDI has unique properties which make it an effective chaperone in these instances, such as conformational flexibility, broad substrate specificity and the ability to differentiate between unfolded and partially folded proteins. Moreover, PDI possesses oxidoreductase capabilities, allowing it to oxidise, isomerise or reduce disulphide bonds, whereas other chaperones, such as heat shock proteins, do not. In addition, PDI can direct misfolded proteins to ERAD, thereby reducing protein aggregation. Interestingly, misfolded Cyclin F or Cyclin F inclusions were not detected in this study, even in cells that did not co-express PDI. Previous studies have demonstrated that mutant Cyclin F S621G impedes ERAD (Ragagnin et al., 2017 in preparation), therefore it is surprising that Cyclin F aggregation or inclusion formation was not observed. It is possible that Cyclin F oligomers were present in this study, however these are not detected by light microscopy, and assays to identify the formation of

smaller cyclin F aggregates were not performed due to time constrains. Therefore, further studies should be performed to investigate whether Cyclin F inclusions are associated with ALS/FTD. Studies of human ALS tissues bearing Cyclin F mutations are currently underway in our group, however, at the moment only a limited number of patient samples are available. As mutant Cyclin F impairs ERAD, it may also be predicted that PDI overexpression inhibits this process, and further studies should therefore be performed to investigate this possibility.

Several overall caveats of this study should be mentioned, and additional future experiments need to be performed to address these issues. The studies performed in this thesis all involved the use of cell culture models overexpressing mutant proteins linked to ALS. Although these studies provide some information regarding the protective activity of PDI against mutant proteins, it will be necessary to further investigate the role of PDI against mutant Cyclin F *in vivo*, given the limitations of utilising neuroblastoma cell lines to model post-mitotic neurons. It would therefore be beneficial to repeat these studies in primary neuron cultures or IPSC-derived motor neurons, which more closely mimic the physiological state of motor neurons in ALS patients, to validate the results observed. Similar experiments performed in mixed cultures of neurons and glial cells would also be informative, given that ALS is thought to be non-cell autonomous. Moreover, mutant Cyclin F S621G zebrafish are available in our group, which develop an axonopathy and impaired motor performance [465]. Indeed, we have also shown that PDI rescues a similar axonopathy and impaired motor performance in zebrafish expressing ALS-associated mutant SOD1 A4V (Laird et al., unpublished 2017). Therefore, it would be interesting to examine whether PDI has a similar protective effect in these zebrafish. In addition, validation of these findings in rodent disease models would provide compelling evidence that PDI is protective in ALS. Together these experiments would further strengthen the findings obtained in Chapter 3.

8.1.2 The protective domains of PDI that mediate protective activity

In order to develop therapeutic agents based on PDI's protective activity, it is first necessary to determine the specific requirements and key characteristics of PDI that render it protective. Full length PDI, being a protein of considerable size (55kDa) is unlikely to be effective as a drug itself as it is too large to penetrate the BBB. Thus, identifying the exact protective mechanisms or properties of PDI, and then developing a therapeutic agent that can mimic this property, is essential. With this as an overarching aim, Chapter 4 of this thesis described a detailed study to determine which of PDI's domains were fundamental for its protective activity in cells expressing mutant ALS proteins, SOD1, TDP-43 and FUS.

Three PDI domain mutants were generated; an *a* domain mutant, *a'* domain mutant and *bb'* domain mutant. The *a* and *a'* domains of PDI, which contain the CGHC active site motifs, are responsible for PDI's oxidoreductase, or disulphide interchange, activity, whereas the *b* domains of PDI contain the substrate binding sites that are utilised for PDI's chaperone function. Although the chaperone activity can be isolated by mutating the active site cysteine residues of PDI to inhibit the disulphide interchange activity, the individual domains of PDI are thought to perform their own distinct functions. Hence this approach, to investigate the individual domains of PDI, was also investigated in this study.

The *a* and *a'* domains were able to inhibit mutant SOD1 inclusion formation, implying that the disulphide interchange activity performs this function. One possible reason for this is that this activity facilitates the oxidation, reduction and isomerisation of misfolded SOD1 disulphide bonds, in order to retain SOD1's native conformation. It has been previously suggested that PDI can prevent mutant SOD1 aggregation by modulating disulphide bonding, since previous reports suggest a correlation between SOD1 aggregation and the formation of non-native disulphide bonds [506, 510, 565]. In Chapter 4, the effect of mutating SOD1's

cysteine residues on the induction of ER stress was described. These results demonstrated a reduction in the proportion of cells with ER stress when the Cys-111 residue was mutated to a serine. The removal of this cysteine residue would prevent the formation of a non-native disulphide bond between Cys-6 and Cys-111 in SOD1, which has been previously implicated in mediating mutant SOD1 aggregation [512]. Therefore, it is possible that PDI prevents the formation of this non-native disulphide bond, by utilising its disulphide interchange activity to either form the correct disulphide in SOD1 (Cys-57 - Cys-146), or to break down and re-arrange any incorrect disulphides (involving residues at Cys-6 or Cys-111), thus preventing monomerisation, which is implicated as a precursor to aggregation [104], or oligomerisation of misfolded SOD1. In future studies it would be interesting to examine whether PDI can inhibit the induction of ER stress by mutant SOD1 proteins containing mutations in cysteine residues, that are still capable of triggering the UPR. A protective role for PDI in this instance would imply that PDI does not need to interact with SOD1 via its disulphide bonds. However, if PDI is not protective, this would further strengthen the notion that PDI interacts with mutant SOD1, and therefore demonstrates a protective effect via its disulphide interchange activity.

Interestingly, in this study, the *bb'* domain mutant also demonstrated a protective effect against induction of ER stress by mutant SOD1, TDP-43 and FUS, indicating that PDI's chaperone function is protective against triggering of ER stress. Upon UPR induction, ER chaperones including PDI are upregulated to alleviate the load of misfolded proteins. Hence the chaperone activity of PDI may perform a generalized response against protein misfolding here and this could account for the protective activity of the *bb'* domain mutant. In contrast, the *a* and *a'* domain mutants may be protective against ER stress by a different mechanism, by preventing the formation of mutant protein aggregates by refolding non-native disulphide bonds, thus inhibiting the activation of ER stress.

It is also interesting to note that only the *a* and *a'* domain mutants were capable of preventing mutant TDP-43 and FUS mislocalisation to the cytoplasm, implying that only the disulphide interchange activity is protective for this function. Further studies are therefore warranted to elucidate the mechanism by which the *bb'* domain mutant was protective against ER stress induced by mutant forms of TDP-43 and FUS, yet there was no protective effect against their mislocalisation. This again implies that the *bb'* domain mutant, and hence the chaperone activity of PDI, may perform a generalised role against the load of misfolded proteins in the ER, rather than against misfolded TDP-43 or FUS specifically. Alternatively, it is possible that the *a* and *a'* domain mutants prevent the induction of ER stress by preventing the mislocalisation of TDP-43 and FUS to the cytoplasm, from where evidence points to ER stress being induced, and returning these proteins to the nucleus, from where they are unlikely to be capable of triggering the UPR. It is also possible that mislocalisation of TDP-43 and FUS to the cytoplasm is triggered by an alternative, unknown mechanism, which the *a* and *a'* domain mutants are protective against, but the bb' domain mutants are not. Another explanation is that the chaperone function of PDI requires the presence of all domains of PDI, rather than just the two *b* domains.

In contrast to the bb' domains, the *a* and *a'* domains were protective against every cellular mechanism linked to pathogenesis investigated in this study. This included mutant SOD1-induced apoptosis, indicating a fundamental role for these domains in preventing neurotoxicity. Furthermore, these results confirm that the disulphide interchange activity of PDI is imperative for its protective function. S-nitrosylation of PDI affects only the active site cysteine residues of the *a* and *a'* domain, but ultimately compromises all of PDI's function, thus implying that S-nitrosylation, and hence the integrity of the CGHC active site motif, may have an important role in the pathogenesis of ALS.

8.1.3 The role of redox potential in mediating PDI's protective activity

As PDI is capable of acting as an oxidase, reductase and isomerase, and the results obtained in Chapter 4 demonstrated that PDI's *a* and *a'* domains mediate its protective function, it was hypothesised in Chapter 5 whether redox potential contributes to PDI's protective function. Mutants were designed with modifications in either the active site motifs or cis-proline loops of PDI, in both the *a* and *a'* domains. These mutations were predicted to alter PDI's redox properties, and thus, alter its protective activity. These studies demonstrated that when PDI's active site was mutated to that of the oxidase DsbA (CPHC), PDI retained its protective function against all cellular mechanisms of pathogenesis investigated, induced by all proteins examined. These results were consistent with the studies described in Chapter 4 investigating the activity of a eukaryotic version of DsbA, which was also broadly protective against mutant SOD1, TDP-43 and FUS, strengthening the notion that the oxidase activity, responsible for the formation of disulphide bonds, is imperative for its protective function.

Assessing the role of the active site PDI mutants on the formation of mutant SOD1 inclusions demonstrated that the CPHC oxidase and CGPC reductase mutants were both protective, indicating the importance of both the formation and break down of disulphide bonds in preventing mutant SOD1 aggregation. The isomerase mutant, CPYC, was not protective, which was consistent with the results obtained with the eukaryotic version of the isomerase DsbC. Interestingly, all three active site mutants (with predicted oxidase, reductase and isomerase activities) were able to inhibit activation of the UPR in cells expressing mutant SOD1 or FUS, suggesting that all three redox activities are protective against ER stress. Similarly, and consistent with these results, DsbC inhibited ER stress induced by mutant SOD1 and FUS, in addition to DsbA. An alternative explanation is that the protective activity by all three redox active site mutants is due to PDI's chaperone function. This is consistent with the results obtained from studies of the *bb'* domain mutant which was protective against

ER stress induced by all three mutant proteins. It is interesting to note however, that only the CPHC oxidase mutant and DsbA were protective against ER stress induced by mutant TDP-43, whereas the other active site mutants and DsbC were not. Dissimilarities between TDP-43 and FUS were also observed in studies examining their mislocalisation to the cytoplasm, whereby only the CPHC oxidase active site mutant was protective for mutant FUS, but both the CPHC oxidase and isomerase CPYC active site mutants were protective for mutant TDP-43. Remarkably, the same pattern was observed in studies of the Dsb proteins, where both DsbA and DsbC were protective against mutant TDP-43 mislocalisation, but only DsbA was protective against the mislocalisation of mutant FUS. The consistency in these results implies that the redox potential of the active site motif does indeed modulate the function of PDI.

Interestingly, similar results were obtained when examining mutant SOD1-induced apoptosis in Chapters 4 and 5. Only the proteins with predicted oxidase activity were protective; the CPHC active site mutant and the oxidase DsbA. It is possible that a more oxidising form of PDI is better than wildtype PDI at forming the correct disulphide bonds in proteins, therefore maintaining cellular proteostasis and preventing apoptosis. This result is interesting however, because previous studies undertaken in our laboratory (Parakh et al., 2017 in preparation) and those described in Chapter 4, demonstrated that the PDI QUAD mutant was protective against apoptosis, indicating that PDI's chaperone activity retains its protective effect. This mutant has all active site cysteine residues removed, so its disulphide interchange activity is absent. Hence this suggests that PDI uses its chaperone function for its protective activity against apoptosis. Nascent and misfolded proteins may primarily bind to cysteine residues within the active site of PDI, before opting to bind with the weaker, hydrophobic forces of the *b* domains in later stages of protein folding. However, this finding implies that S-nitrosylated PDI is also protective against apoptosis, but this has not been reported before. However, it is possible that S-nitrosylation results in conformation changes in PDI, which impacts on its

chaperone function. Alternatively, a change in the redox potential of PDI may alter substrate binding in its active site, thus preventing the binding of mutant SOD1. Moreover, the results in Chapter 4 show that the *b* domains of PDI were not effective in inhibiting apoptosis induced by mutant SOD1, suggesting that only the disulphide interchange activity via the *a* and *a'* domains is protective. Alternatively, however, as all the domains of PDI have been previously shown to be necessary for its chaperone activity [487], it is possible that there are very specific structural requirements for the chaperone activity that are missing in the bb' domain mutant. Therefore, it is difficult to pinpoint the exact mechanism by which PDI is protective against apoptosis and the results obtained here demonstrate that this activity is quite complex. It also remains a possibility that the results obtained in these experiments may either be a consequence of a general redox alteration, or of the interaction between the PDI mutants and other proteins. It could be that a ligand to PDI is the active agent that is sequestered by the addition of PDI and other PDI-like agents. This notion is warranted based on the observation that PDI's natural function as a chaperone is not the factor that is mediating its protective activity against mutant ALS proteins. Further studies are therefore required to fully elucidate the mechanisms involved.

The studies investigating the effect of the mutations in the cis-proline loops provided additional insights into the mechanisms of protection of PDI. Firstly, these results demonstrated that mutations that aim to enhance the oxidising activity of the cis-proline loop in the *a* domain retained PDI's protective activity, whereas mutations that were predicted to enhance the reducing activity were not protective. These findings suggest that modifying the cis-proline loop in the a domain is sufficient to alter PDI's function. Moreover, they are consistent with the other studies performed in this thesis implying that PDI's oxidase activity is necessary for its protective activity. Interestingly, however, modifying the cis-proline loop of PDI's *a'* domain did not alter PDI's protective function against mutant SOD1 and TDP-43,

suggesting that the protective activity contributed by the cis-proline loop is mediated primarily by its *a* domain. The *a'* domain alone was found to be protective in the domain mutant studies described in Chapter 4, which at first appears contradictory. However, it is possible that when the *a* domain is present alongside the *a'* domain, as in full-length PDI, the *a* domain drives the disulphide interchange activity and the *a'* domain acts only as a secondary active site and is not necessarily required.

Future experiments examining the effect of the redox activity of PDI on its protective activity in ALS are warranted. In particular, the redox potential of each redox mutant needs to be specifically measured using established methods [492]. Due to time constraints, these studies were unable to be performed, therefore the redox properties of the mutants examined in this study are only predicted. The different results obtained for each mutant and the consistency of the overall findings, demonstrating that those mutants that are predicted to enhance the oxidase activity retained all of the protective activities of wildtype PDI, implies that variabilities in the redox potential of each mutant was present, although this needs to be confirmed experimentally. In addition, in future studies, the cis-proline loop mutations should be incorporated into the *a* and *a'* domain mutants used in Chapter 4, to assess the activity of PDI's cis-proline loops individually, without the presence of the intact cis-proline loop in the other disulphide interchange domain (*a* or *a'*).

8.1.4 The role of inhibiting oxidation on PDI's protective activity against mutant FUS

The results obtained in Chapter 6 reiterate the importance of the oxidase activity in mediating PDI's protective function. Upon oxidase ablation, due to cellular exposure to BSO, wildtype PDI was unable to inhibit mutant FUS mislocalisation to the cytoplasm, inclusion formation or ER stress induced by mutant FUS, indicating that PDI is non-functional when the cellular

redox conditions are altered so that it is less likely to be oxidising. Interestingly, similar results were obtained when examining PDI mimetic, BMC. It is known that BMC emulates PDI's disulphide interchange activity, however it was unknown if BMC primarily relies on its oxidase or isomerase activities. Based on the results observed, it could be suggested that the oxidase activity of BMC plays a key role in mediating its protection, similar to PDI. Moreover, this idea is consistent with the findings that inhibiting PDI's oxidase activity renders the protein non-functional. As a major catalyst for disulphide bond formation in the ER, PDI's oxidase activity is necessary to ensure that nascent proteins are correctly folded, thus preventing disturbances in ER homeostasis. As endogenous PDI in ALS cell lines is most likely S-nitrosylated, dysfunction in ER homeostasis is inevitable without the availability of overexpressed PDI to form disulphide bonds in nascent proteins to compensate. Furthermore, it would be interesting to examine the activity of the oxidase CPHC active site mutant or DsbA upon oxidase ablation by BSO treatment, and this should be investigated in future studies. In addition, further studies should now be performed to examine the activity of PDI, upon oxidase ablation, on other ALS-associated proteins, including SOD1 and TDP-43.

An interesting finding described in Chapter 6 was that PDI variants, D292N and R300H, were protective against mutant FUS-induced pathogenic mechanisms, even though they have been reported to cause detrimental effects to neurons in zebrafish models [441]. However, previous studies have shown that these variants do not induce ER stress or cell toxicity [441], consistent with the results obtained in this chapter. An explanation for why the D292N and R300H variants do not cause disturbances to ER homeostasis, even though ER stress is considered to be an important disease mechanism in ALS, is because their mutations lie in the substrate binding *b'* domain. Thus, these variants most likely cause inhibition of chaperone function. As investigated in Chapter 4, the *b* domains of PDI are not essential for PDI's

protective activity. In fact, the *a* domains in these variants remain functionally intact, and studies performed in Chapter 4 suggest that this is the most important region for mediating PDI's protection. Therefore, the disulphide interchange activity, and more specifically, the oxidase activity, of these variants are functional, and still able to elicit a protective response. Oxidase activity ablation, due to BSO administration, perturbed the protective activity of the D292N and R300H variants, demonstrating that these variants are protective via their oxidase capabilities, similar to PDI. Future analysis into additional variants should assess whether mutations are present in the *a* domain, and these variants should be examined for their activity.

Finally, it was demonstrated that PDI was protective against mutant FUS inclusion formation in these studies. Future studies investigating the activity of the PDI domain mutants, PDI active site mutants and PDI cis-proline loop mutants, on mutant FUS inclusion formation should now be performed to elucidate the protective mechanisms that prevent the formation of mutant FUS inclusions. Indeed, the reductase activity of PDI was protective against mutant SOD1 inclusion formation, as well as its oxidase activity, so it would be interesting in future studies to determine if PDI's reductase activity plays a role against FUS inclusion formation also.

8.1.5 Peptide therapeutics based on PDI's protective mechanisms

The final chapter of this thesis investigated the activity of linear peptides that were designed based on the findings obtained in this doctoral work concerning PDI's protective mechanisms. In the previous chapters, it was deduced that: 1) PDI's *a* and *a'* domains were protective against pathogenic mechanisms induced by mutant SOD1, TDP-43 and FUS; 2) specific redox activities of PDI-like proteins contribute to its protective function, contained

with the CGHC active site motif. This CGHC active site motif was conserved in the peptides that were designed as it is responsible for facilitating PDI's oxidoreductase activity; and 3) the role of PDI's cis-proline loop was partially investigated for the first time in this thesis, hence two peptides, one without a proline and one with, termed CGHC4 and CGHC5 respectively, were synthesised.

Preliminary studies were described here in which CGHC4 and CGHC5 were administered into neuronal cell lines expressing mutant SOD1. The results demonstrated that both CGHC4 and CGHC5 peptides were protective against mutant SOD1 inclusion formation, ER stress activation and apoptosis, indicating that the characteristics of PDI identified throughout this PhD project were necessary for the protective function. In future studies, it would be interesting to administer CGHC4 and CGHC5 into cells expressing mutant forms of TDP-43, FUS and Cyclin F, to analyse if these peptides are protective against other ALS-associated proteins. Ultimately, however, there is a necessity to determine whether these peptides are protective in ALS animal models. Thus, the next phase of experiments should entail administering either the linear versions, or newly created cyclised version, into zebrafish models of ALS.

Therapeutic strategies that target ER stress may be beneficial in ALS, but the studies described in this thesis imply that PDI uses different mechanisms in its protective activity. Therapeutic agents based on PDI should now be examined in detail. Indeed, PDI is upregulated in ALS patients, but is subsequently S-nitrosylated [254, 448], thus a pharmacological agent which compensates for PDI's loss of function may be beneficial in the treatment of disease. Treatment of the PDI mimic, BMC, in ALS cell models, results in a reduction in the proportion of cells forming SOD1 inclusions [448], suggesting that replicating the protective activity of PDI is at least beneficial against SOD1 aggregation.

However, further studies into what mediates the switch from a protective PDI to a harmful PDI are warranted if therapeutics based on PDI are to be designed to target ALS.

8.2 Concluding remarks

ALS is a devastating, late-onset neurodegenerative disorder, characterised at the cellular level by protein misfolding and aggregation. Moreover, the induction of ER stress has been recently implicated as a key mechanism of pathogenesis. During ER stress, PDI is upregulated and has the ability to restore proteostasis by utilising its oxidoreductase or chaperone functions, and thus plays an important role in protein quality control and in the restoration of ER homeostasis. Moreover, novel roles for PDI have been described in the nervous system, such as in neurite outgrowth and synapse connectivity. PDI has already been demonstrated to be protective against mutant forms of ALS proteins, SOD1, TDP-43 and FUS. In this PhD thesis, overexpression of PDI was shown to be protective against a novel protein linked to ALS and FTD, Cyclin F, demonstrating its broad activity against an array of proteins. Moreover, the work described in this thesis has aimed to characterise the protective mechanisms and properties of PDI that mediate its protection. Thus, these mechanisms are now better understood. Taken together, these findings have been utilised to design therapeutics based on these protective mechanisms of PDI, and will hopefully lead to the advancement of an effective treatment in the near future for this crippling disease.

References

1.   Brown, R.H. and A. Al-Chalabi, *Amyotrophic Lateral Sclerosis.* New England Journal of Medicine, 2017. **377**(2): p. 162-172.
2.   Robberecht, W. and T. Philips, *The changing scene of amyotrophic lateral sclerosis.* Nat Rev Neurosci, 2013. **14**(4): p. 248-64.
3.   Wolf, J., et al., *Causes of death in amyotrophic lateral sclerosis: Results from the Rhineland-Palatinate ALS registry.* Der Nervenarzt, 2017.
4.   Turner, M.R., et al., *Controversies and priorities in amyotrophic lateral sclerosis.* Lancet Neurol, 2013. **12**(3): p. 310-22.
5.   Bensimon, G., et al., *A controlled trial of riluzole in amyotrophic lateral sclerosis.* New England Journal of Medicine, 1994. **330**(9): p. 585-591.
6.   Miller, R.G., J. Mitchell, and D.H. Moore, *Riluzole for amyotrophic lateral sclerosis (ALS)/motor neuron disease (MND).* The Cochrane Library, 2012.
7.   Mora, J.S., *Edaravone for treatment of early-stage ALS.* The Lancet Neurology, 2017. **16**(10): p. 772.
8.   Renton, A.E., A. Chiò, and B.J. Traynor, *State of play in amyotrophic lateral sclerosis genetics.* Nature neuroscience, 2014. **17**(1): p. 17-23.
9.   Corcia, P., et al., *Genetics of amyotrophic lateral sclerosis.* Revue Neurologique, 2017. **173**(5): p. 254-262.
10.   Majounie, E., et al., *Frequency of the C9orf72 hexanucleotide repeat expansion in patients with amyotrophic lateral sclerosis and frontotemporal dementia: a cross-sectional study.* The Lancet Neurology, 2012. **11**(4): p. 323-330.
11.   Bozzoni, V., et al., *Amyotrophic lateral sclerosis and environmental factors.* Functional Neurology, 2016. **31**(1): p. 7-19.
12.   Perri, E.R., et al., *The Unfolded Protein Response and the Role of Protein Disulfide Isomerase in Neurodegeneration.* Front Cell Dev Biol, 2015. **3**: p. 80.
13.   Chio, A., et al., *Global epidemiology of amyotrophic lateral sclerosis: a systematic review of the published literature.* Neuroepidemiology, 2013. **41**(2): p. 118-130.
14.   Cronin, S., O. Hardiman, and B.J. Traynor, *Ethnic variation in the incidence of ALS A systematic review.* Neurology, 2007. **68**(13): p. 1002-1007.
15.   Gordon, P.H., et al., *Incidence of amyotrophic lateral sclerosis among American Indians and Alaska natives.* JAMA neurology, 2013. **70**(4): p. 476-480.
16.   Kiernan, M.C., et al., *Amyotrophic lateral sclerosis.* Lancet, 2011. **377**(9769): p. 942-55.
17.   Manjaly, Z.R., et al., *The sex ratio in amyotrophic lateral sclerosis: a population based study.* Amyotrophic Lateral Sclerosis, 2010. **11**(5): p. 439-442.
18.   Niccoli, T., L. Partridge, and A.M. Isaacs, *Ageing as a risk factor for ALS/FTD.* Human Molecular Genetics, 2017.
19.   Statland, J.M., et al., *Primary lateral sclerosis.* Neurologic clinics, 2015. **33**(4): p. 749.
20.   Diamanti, L., et al., *Genetics of ALS and correlations between genotype and phenotype in ALS—A focus on Italian population*, in *Current Advances in Amyotrophic Lateral Sclerosis*. 2013, InTech.
21.   Liewluck, T. and D.S. Saperstein, *Progressive muscular atrophy.* Neurologic clinics, 2015. **33**(4): p. 761-773.
22.   Kühnlein, P., et al., *Diagnosis and treatment of bulbar symptoms in amyotrophic lateral sclerosis.* Nature clinical practice Neurology, 2008. **4**(7): p. 366-374.

23. Ravits, J.M. and A.R. La Spada, *ALS motor phenotype heterogeneity, focality, and spread Deconstructing motor neuron degeneration.* Neurology, 2009. **73**(10): p. 805-811.

24. Tard, C., et al., *Clinical features of amyotrophic lateral sclerosis and their prognostic value.* Revue Neurologique, 2017.

25. Wijesekera, L.C. and P.N. Leigh, *Amyotrophic Lateral Sclerosis.* Orphanet Journal of Rare Diseases, 2009. **4**(3).

26. Newall, A.R., R. Orser, and M. Hunt, *The control of oral secretions in bulbar ALS/MND.* Journal of the Neurological Sciences, 1996. **139, Supplement**(0): p. 43-44.

27. Chiò, A., et al., *Early symptom progression rate is related to ALS outcome A prospective population-based study.* Neurology, 2002. **59**(1): p. 99-103.

28. Fujimura-Kiyono, C., et al., *Onset and spreading patterns of lower motor neuron involvements predict survival in sporadic amyotrophic lateral sclerosis.* J Neurol Neurosurg Psychiatry, 2011. **82**(11): p. 1244-1249.

29. Corcia, P., et al., *Respiratory onset in an ALS family with L144F SOD1 mutation.* Journal of Neurology, Neurosurgery & Psychiatry, 2010: p. jnnp. 2009.197558.

30. Llado, J., et al., *Degeneration of respiratory motor neurons in the SOD1 G93A transgenic rat model of ALS.* Neurobiol Dis, 2006. **21**(1): p. 110-8.

31. Körner, S., et al., *Interaction of physical function, quality of life and depression in Amyotrophic lateral sclerosis: characterization of a large patient cohort.* BMC neurology, 2015. **15**(1): p. 84.

32. Ferrari, R., et al., *FTD and ALS: a tale of two diseases.* Current Alzheimer research, 2011. **8**(3): p. 273-294.

33. Burrell, J.R., et al., *Motor Neuron dysfunction in frontotemporal dementia.* Brain, 2011. **134**(9): p. 2582-2594.

34. Turner, M.R., et al., *Genetic screening in sporadic ALS and FTD.* Journal of Neurology, Neurosurgery &amp; Psychiatry, 2017.

35. Shahheydari, H., et al., *Protein Quality Control and the Amyotrophic Lateral Sclerosis/Frontotemporal Dementia Continuum.* Frontiers in molecular neuroscience, 2017. **10**.

36. Pupillo, E., et al., *Trauma and amyotrophic lateral sclerosis: a case–control study from a population-based registry.* European journal of neurology, 2012. **19**(12): p. 1509-1517.

37. Armon, C., *Smoking may be considered an established risk factor for sporadic ALS.* Neurology, 2009. **73**(20): p. 1693-1698.

38. Fang, F. and W. Ye, *Smoking may be considered an established risk factor for sporadic ALS.* Neurology, 2010. **74**(23): p. 1927-1929.

39. Gallo, V., et al., *Smoking and risk for amyotrophic lateral sclerosis: analysis of the EPIC cohort.* Annals of neurology, 2009. **65**(4): p. 378-385.

40. Duncan, M.W., et al., *2-Amino-3-(methylamino)-propanoic acid (BMAA) in cycad flour An unlikely cause of amyotrophic lateral sclerosis and parkinsonism-dementia of Guam.* Neurology, 1990. **40**(5): p. 767-767.

41. Banack, S.A., T.A. Caller, and E.W. Stommel, *The cyanobacteria derived toxin beta-N-methylamino-L-alanine and amyotrophic lateral sclerosis.* Toxins, 2010. **2**(12): p. 2837-2850.

42. Murch, S., et al., *Occurrence of β-methylamino-l-alanine (BMAA) in ALS/PDC patients from Guam.* Acta Neurologica Scandinavica, 2004. **110**(4): p. 267-269.

43. Pablo, J., et al., *Cyanobacterial neurotoxin BMAA in ALS and Alzheimer's disease.* Acta Neurologica Scandinavica, 2009. **120**(4): p. 216-225.

44.   Dunlop, R.A., et al., *The non-protein amino acid BMAA is misincorporated into human proteins in place of L-serine causing protein misfolding and aggregation.* PloS one, 2013. **8**(9): p. e75376.

45.   Belli, S. and N. Vanacore, *Proportionate mortality of Italian soccer players: is amyotrophic lateral sclerosis an occupational disease?* European journal of epidemiology, 2005. **20**(3): p. 237-242.

46.   Valenti, M., et al., *Amyotrophic lateral sclerosis and sports: a case–control study.* European journal of neurology, 2005. **12**(3): p. 223-225.

47.   Abel, E.L., *Football increases the risk for Lou Gehrig's disease, amyotrophic lateral sclerosis.* Perceptual and motor skills, 2007. **104**(3_suppl): p. 1251-1254.

48.   Chiò, A., et al., *ALS in Italian professional soccer players: the risk is still present and could be soccer-specific.* Amyotrophic lateral sclerosis, 2009. **10**(4): p. 205-209.

49.   Julien, J.-P., *Amyotrophic lateral sclerosis: unfolding the toxicity of the misfolded.* Cell, 2001. **104**(4): p. 581-591.

50.   Chen, H., et al., *Head injury and amyotrophic lateral sclerosis.* American journal of epidemiology, 2007. **166**(7): p. 810-816.

51.   Sutedja, N.A., et al., *Exposure to chemicals and metals and risk of amyotrophic lateral sclerosis: a systematic review.* Amyotrophic Lateral Sclerosis, 2009. **10**(5-6): p. 302-309.

52.   McGuire, V., et al., *Occupational exposures and amyotrophic lateral sclerosis. A population-based case-control study.* American Journal of Epidemiology, 1997. **145**(12): p. 1076-1088.

53.   Horner, R.D., et al., *Occurrence of amyotrophic lateral sclerosis among Gulf War veterans.* Neurology, 2003. **61**(6): p. 742-749.

54.   Håkansson, N., et al., *Neurodegenerative diseases in welders and other workers exposed to high levels of magnetic fields.* Epidemiology, 2003. **14**(4): p. 420-426.

55.   Zhou, H., et al., *Association between extremely low-frequency electromagnetic fields occupations and amyotrophic lateral sclerosis: a meta-analysis.* PLoS One, 2012. **7**(11): p. e48354.

56.   Verma, A. and J.R. Berger, *ALS syndrome in patients with HIV-1 infection.* Journal of the neurological sciences, 2006. **240**(1): p. 59-64.

57.   Alfahad, T. and A. Nath, *Retroviruses and amyotrophic lateral sclerosis.* Antiviral research, 2013. **99**(2): p. 180-187.

58.   Rosen, D.R., et al., *Mutations in Cu/Zn superoxide dismutase gene are associated with familial amyotrophic lateral sclerosis.* Nature, 1993. **362**(6415): p. 59-62.

59.   Renton, A.E., et al., *A hexanucleotide repeat expansion in C9ORF72 is the cause of chromosome 9p21-linked ALS-FTD.* Neuron, 2011. **72**(2): p. 257-268.

60.   DeJesus-Hernandez, M., et al., *Expanded GGGGCC hexanucleotide repeat in noncoding region of C9ORF72 causes chromosome 9p-linked FTD and ALS.* Neuron, 2011. **72**(2): p. 245-256.

61.   Forsberg, K., et al., *Novel antibodies reveal inclusions containing non-native SOD1 in sporadic ALS patients.* PLoS one, 2010. **5**(7): p. e11552.

62.   Neumann, M., et al., *Ubiquitinated TDP-43 in frontotemporal lobar degeneration and amyotrophic lateral sclerosis.* Science, 2006. **314**(5796): p. 130-3.

63.   Deng, H.X., et al., *FUS-immunoreactive inclusions are a common feature in sporadic and non-SOD1 familial amyotrophic lateral sclerosis.* Annals of neurology, 2010. **67**(6): p. 739-748.

64.   Mori, K., et al., *The C9orf72 GGGGCC repeat is translated into aggregating dipeptide-repeat proteins in FTLD/ALS.* Science, 2013. **339**(6125): p. 1335-1338.

65.   Vance, C., et al., *Mutations in FUS, an RNA processing protein, cause familial amyotrophic lateral sclerosis type 6.* Science, 2009. **323**(5918): p. 1208-1211.

66.   Deng, H.-X., et al., *Mutations in UBQLN2 cause dominant X-linked juvenile and adult-onset ALS and ALS/dementia.* Nature, 2011. **477**(7363): p. 211-215.

67.   Johnson, J.O., et al., *Exome sequencing reveals VCP mutations as a cause of familial ALS.* Neuron, 2010. **68**(5): p. 857-864.

68.   Fecto, F., et al., *SQSTM1 mutations in familial and sporadic amyotrophic lateral sclerosis.* Archives of neurology, 2011. **68**(11): p. 1440-1446.

69.   Maruyama, H., et al., *Mutations of optineurin in amyotrophic lateral sclerosis.* Nature, 2010. **465**(7295): p. 223-226.

70.   Wu, C.-H., et al., *Mutations in the profilin 1 gene cause familial amyotrophic lateral sclerosis.* Nature, 2012. **488**(7412): p. 499-503.

71.   Nishimura, A.L., et al., *A mutation in the vesicle-trafficking protein VAPB causes late-onset spinal muscular atrophy and amyotrophic lateral sclerosis.* The American Journal of Human Genetics, 2004. **75**(5): p. 822-831.

72.   Johnson, J.O., et al., *Mutations in the Matrin 3 gene cause familial amyotrophic lateral sclerosis.* Nature neuroscience, 2014. **17**(5): p. 664.

73.   Smith, B.N., et al., *Exome-wide rare variant analysis identifies TUBA4A mutations associated with familial ALS.* Neuron, 2014. **84**(2): p. 324-331.

74.   Münch, C., et al., *Point mutations of the p150 subunit of dynactin (DCTN1) gene in ALS.* Neurology, 2004. **63**(4): p. 724-726.

75.   Figlewicz, D.A., et al., *Variants of the heavy neurofilament subunit are associated with the development of amyotrophic lateral sclerosis.* Human molecular genetics, 1994. **3**(10): p. 1757-1761.

76.   Gros-Louis, F., et al., *A frameshift deletion in peripherin gene associated with amyotrophic lateral sclerosis.* Journal of Biological Chemistry, 2004. **279**(44): p. 45951-45956.

77.   Yang, Y., et al., *The gene encoding alsin, a protein with three guanine-nucleotide exchange factor domains, is mutated in a form of recessive amyotrophic lateral sclerosis.* Nature genetics, 2001. **29**(2): p. 160-165.

78.   Chow, C.Y., et al., *Deleterious variants of FIG4, a phosphoinositide phosphatase, in patients with ALS.* The American Journal of Human Genetics, 2009. **84**(1): p. 85-88.

79.   Parkinson, N., et al., *ALS phenotypes with mutations in CHMP2B (charged multivesicular body protein 2B).* Neurology, 2006. **67**(6): p. 1074-1077.

80.   Chen, Y.-Z., et al., *DNA/RNA helicase gene mutations in a form of juvenile amyotrophic lateral sclerosis (ALS4).* The American Journal of Human Genetics, 2004. **74**(6): p. 1128-1135.

81.   Greenway, M., et al., *A novel candidate region for ALS on chromosome 14q11. 2.* Neurology, 2004. **63**(10): p. 1936-1938.

82.   Orlacchio, A., et al., *SPATACSIN mutations cause autosomal recessive juvenile amyotrophic lateral sclerosis.* Brain, 2010: p. awp325.

83.   Mitchell, J., et al., *Familial amyotrophic lateral sclerosis is associated with a mutation in D-amino acid oxidase.* Proceedings of the National Academy of Sciences, 2010. **107**(16): p. 7556-7561.

84.   Freischmidt, A., et al., *Haploinsufficiency of TBK1 causes familial ALS and fronto-temporal dementia.* Nature neuroscience, 2015. **18**(5): p. 631-636.

85.   Kim, H.J., et al., *Mutations in prion-like domains in hnRNPA2B1 and hnRNPA1 cause multisystem proteinopathy and ALS.* Nature, 2013. **495**(7442): p. 467-473.

86.   Belzil, V.V., et al., *Genetic analysis of SIGMAR1 as a cause of familial ALS with dementia.* European Journal of Human Genetics, 2013. **21**(2): p. 237-239.

87.   Elden, A.C., et al., *Ataxin-2 intermediate-length polyglutamine expansions are associated with increased risk for ALS.* Nature, 2010. **466**(7310): p. 1069-1075.

88.   Simpson, C.L., et al., *Variants of the elongator protein 3 (ELP3) gene are associated with motor neuron degeneration.* Human molecular genetics, 2008. **18**(3): p. 472-481.

89.   Williams, K.L., et al., *CCNF mutations in amyotrophic lateral sclerosis and frontotemporal dementia.* Nature communications, 2016. **7**.

90.   Johnson, J.O., et al., *Mutations in the CHCHD10 gene are a common cause of familial amyotrophic lateral sclerosis.* Brain, 2014. **137**(12): p. e311-e311.

91.   Takahashi, Y., et al., *ERBB4 mutations that disrupt the neuregulin-ErbB4 pathway cause amyotrophic lateral sclerosis type 19.* The American Journal of Human Genetics, 2013. **93**(5): p. 900-905.

92.   Ticozzi, N., et al., *Paraoxonase gene mutations in amyotrophic lateral sclerosis.* Annals of neurology, 2010. **68**(1): p. 102-107.

93.   Smith, B.N., et al., *Mutations in ANXA11 cause familial and sporadic amyotrophic lateral sclerosis.* amyotrophic lateral sclerosis, 2014. **17**(5): p. 664-6.

94.   Brenner, D., et al., *NEK1 mutations in familial amyotrophic lateral sclerosis.* Brain, 2016. **139**(5): p. e28-e28.

95.   Hand, C.K., et al., *Compound heterozygous D90A and D96N SOD1 mutations in a recessive amyotrophic lateral sclerosis family.* Annals of neurology, 2001. **49**(2): p. 267-271.

96.   Andersen, P.M., et al., *Amyotrophic lateral sclerosis associated with homozygosity for an Asp90Ala mutation in CuZn-superoxide dismutase.* Nature genetics, 1995. **10**(1): p. 61-66.

97.   Forsberg, K., *Misfolded superoxide dismutase-1 in sporadic and familial Amyotrophic Lateral Sclerosis.* 2011, Umeå Universitet.

98.   Valentine, J.S., P.A. Doucette, and S. Zittin Potter, *Copper-zinc superoxide dismutase and amyotrophic lateral sclerosis.* Annu. Rev. Biochem., 2005. **74**: p. 563-593.

99.   Pardo, C.A., et al., *Superoxide dismutase is an abundant component in cell bodies, dendrites, and axons of motor neurons and in a subset of other neurons.* Proceedings of the National Academy of Sciences, 1995. **92**(4): p. 954-958.

100.   Crapo, J.D., et al., *Copper, zinc superoxide dismutase is primarily a cytosolic protein in human cells.* Proceedings of the National Academy of Sciences, 1992. **89**(21): p. 10405-10409.

101.   Urushitani, M., et al., *Chromogranin-mediated secretion of mutant superoxide dismutase proteins linked to amyotrophic lateral sclerosis.* Nature neuroscience, 2006. **9**(1): p. 108.

102.   Jacobsson, J., et al., *Superoxide dismutase in CSF from amyotrophic lateral sclerosis patients with and without CuZn-superoxide dismutase mutations.* Brain, 2001. **124**(7): p. 1461-1466.

103.   Zetterström, P., et al., *Misfolded superoxide dismutase-1 in CSF from amyotrophic lateral sclerosis patients.* Journal of neurochemistry, 2011. **117**(1): p. 91-99.

104.   Rakhit, R., et al., *Monomeric Cu, Zn-superoxide dismutase is a common misfolding intermediate in the oxidation models of sporadic and familial amyotrophic lateral sclerosis.* Journal of Biological Chemistry, 2004. **279**(15): p. 15499-15504.

105.   Tiwari, A. and L.J. Hayward, *Familial amyotrophic lateral sclerosis mutants of copper/zinc superoxide dismutase are susceptible to disulfide reduction.* Journal of Biological Chemistry, 2003. **278**(8): p. 5984-5992.

106.   Anzai, I., et al., *A misfolded dimer of Cu/Zn-superoxide dismutase leading to pathological oligomerization in amyotrophic lateral sclerosis.* Protein Science, 2017. **26**(3): p. 484-496.

107. Kerman, A., et al., *Amyotrophic lateral sclerosis is a non-amyloid disease in which extensive misfolding of SOD1 is unique to the familial form.* Acta neuropathologica, 2010. **119**(3): p. 335-344.

108. Ling, S.-C., M. Polymenidou, and D.W. Cleveland, *Converging mechanisms in ALS and FTD: disrupted RNA and protein homeostasis.* Neuron, 2013. **79**(3): p. 416-438.

109. Shibata, N., et al., *Intense superoxide dismutase-1 immunoreactivity in intracytoplasmic hyaline inclusions of familial amyotrophic lateral sclerosis with posterior column involvement.* Journal of neuropathology and experimental neurology, 1996. **55**(4): p. 481-490.

110. Reaume, A.G., et al., *Motor neurons in Cu/Zn superoxide dismutase-deficient mice develop normally but exhibit enhanced cell death after axonal injury.* Nature genetics, 1996. **13**(1): p. 43-47.

111. Borchelt, D.R., et al., *Superoxide dismutase 1 subunits with mutations linked to familial amyotrophic lateral sclerosis do not affect wild-type subunit function.* Journal of Biological Chemistry, 1995. **270**(7): p. 3234-3238.

112. Carrì, M.T., et al., *Impaired copper binding by the H46R mutant of human Cu, Zn superoxide dismutase, involved in amyotrophic lateral sclerosis.* FEBS letters, 1994. **356**(2-3): p. 314-316.

113. Nagai, M., et al., *Rats expressing human cytosolic copper–zinc superoxide dismutase transgenes with amyotrophic lateral sclerosis: associated mutations develop motor neuron disease.* Journal of Neuroscience, 2001. **21**(23): p. 9246-9254.

114. Zhang, F., et al., *Interaction between familial amyotrophic lateral sclerosis (ALS)-linked SOD1 mutants and the dynein complex.* Journal of Biological Chemistry, 2007. **282**(22): p. 16691-16699.

115. Bunton-Stasyshyn, R.K., et al., *SOD1 function and its implications for amyotrophic lateral sclerosis pathology: new and renascent themes.* The Neuroscientist, 2015. **21**(5): p. 519-529.

116. Bosco, D.A., et al., *Wild-type and mutant SOD1 share an aberrant conformation and a common pathogenic pathway in ALS.* Nat Neurosci, 2010. **13**(11): p. 1396-403.

117. Rotunno, M.S. and D.A. Bosco, *An emerging role for misfolded wild-type SOD1 in sporadic ALS pathogenesis.* Frontiers in cellular neuroscience, 2013. **7**.

118. Guareschi, S., et al., *An over-oxidized form of superoxide dismutase found in sporadic amyotrophic lateral sclerosis with bulbar onset shares a toxic mechanism with mutant SOD1.* Proceedings of the National Academy of Sciences, 2012. **109**(13): p. 5074-5079.

119. Sundaramoorthy, V., et al., *Extracellular wildtype and mutant SOD1 induces ER–Golgi pathology characteristic of amyotrophic lateral sclerosis in neuronal cells.* Cellular and Molecular Life Sciences, 2013. **70**(21): p. 4181-4195.

120. Liu, H.-N., et al., *Targeting of monomer/misfolded SOD1 as a therapeutic strategy for amyotrophic lateral sclerosis.* Journal of Neuroscience, 2012. **32**(26): p. 8791-8799.

121. Turner, B.J. and K. Talbot, *Transgenics, toxicity and therapeutics in rodent models of mutant SOD1-mediated familial ALS.* Progress in Neurobiology, 2008. **85**(1): p. 94-134.

122. Winton, M.J., et al., *Disturbance of nuclear and cytoplasmic TAR DNA-binding protein (TDP-43) induces disease-like redistribution, sequestration, and aggregate formation.* Journal of Biological Chemistry, 2008. **283**(19): p. 13302-13309.

123. Buratti, E., et al., *TDP-43 binds heterogeneous nuclear ribonucleoprotein A/B through its C-terminal tail an important region for the inhibition of cystic fibrosis transmembrane conductance regulator exon 9 splicing.* Journal of Biological Chemistry, 2005. **280**(45): p. 37572-37584.

124.   Corcia, P., et al., *Phenotype and genotype analysis in amyotrophic lateral sclerosis with TARDBP gene mutations.* Neurology, 2012. **78**(19): p. 1519-1526.

125.   Sreedharan, J., et al., *TDP-43 mutations in familial and sporadic amyotrophic lateral sclerosis.* Science, 2008. **319**(5870): p. 1668-72.

126.   Colombrita, C., et al., *TDP-43 is recruited to stress granules in conditions of oxidative insult.* Journal of Neurochemistry, 2009. **111**(4): p. 1051-1061.

127.   Dewey, C.M., et al., *TDP-43 aggregation in neurodegeneration: are stress granules the key?* Brain research, 2012. **1462**: p. 16-25.

128.   Arai, T., et al., *TDP-43 is a component of ubiquitin-positive tau-negative inclusions in frontotemporal lobar degeneration and amyotrophic lateral sclerosis.* Biochemical and biophysical research communications, 2006. **351**(3): p. 602-611.

129.   Mackenzie, I.R., et al., *Pathological TDP-43 distinguishes sporadic amyotrophic lateral sclerosis from amyotrophic lateral sclerosis with SOD1 mutations.* Ann Neurol, 2007. **61**(5): p. 427-34.

130.   Zhang, Y.-J., et al., *Aberrant cleavage of TDP-43 enhances aggregation and cellular toxicity.* Proceedings of the National Academy of Sciences, 2009. **106**(18): p. 7607-7612.

131.   Igaz, L.M., et al., *Enrichment of C-terminal fragments in TAR DNA-binding protein-43 cytoplasmic inclusions in brain but not in spinal cord of frontotemporal lobar degeneration and amyotrophic lateral sclerosis.* The American journal of pathology, 2008. **173**(1): p. 182-194.

132.   Nonaka, T., et al., *Truncation and pathogenic mutations facilitate the formation of intracellular aggregates of TDP-43.* Human molecular genetics, 2009. **18**(18): p. 3353-3364.

133.   Arnold, E.S., et al., *ALS-linked TDP-43 mutations produce aberrant RNA splicing and adult-onset motor neuron disease without aggregation or loss of nuclear TDP-43.* Proceedings of the National Academy of Sciences, 2013. **110**(8): p. E736-E745.

134.   Wang, W., et al., *The inhibition of TDP-43 mitochondrial localization blocks its neuronal toxicity.* Nature medicine, 2016.

135.   Wang, W., et al., *Motor-coordinative and cognitive dysfunction caused by mutant TDP-43 could be reversed by inhibiting Its mitochondrial localization.* Molecular Therapy, 2017. **25**(1): p. 127-139.

136.   Alami, N.H., et al., *Axonal transport of TDP-43 mRNA granules is impaired by ALS-causing mutations.* Neuron, 2014. **81**(3): p. 536-543.

137.   Kwiatkowski, T.J., Jr., et al., *Mutations in the FUS/TLS gene on chromosome 16 cause familial amyotrophic lateral sclerosis.* Science, 2009. **323**(5918): p. 1205-8.

138.   Belzil, V., et al., *Mutations in FUS cause FALS and SALS in French and French Canadian populations.* Neurology, 2009. **73**(15): p. 1176-1179.

139.   Van Langenhove, T., et al., *Genetic contribution of FUS to frontotemporal lobar degeneration.* Neurology, 2010. **74**(5): p. 366-371.

140.   Blair, I.P., et al., *FUS mutations in amyotrophic lateral sclerosis: clinical, pathological, neurophysiological and genetic analysis.* Journal of Neurology, Neurosurgery & Psychiatry, 2009: p. jnnp. 2009.194399.

141.   Yang, S., et al., *Fused in sarcoma/translocated in liposarcoma: a multifunctional DNA/RNA binding protein.* The international journal of biochemistry & cell biology, 2010. **42**(9): p. 1408-1411.

142.   Dormann, D., et al., *ALS-associated fused in sarcoma (FUS) mutations disrupt Transportin-mediated nuclear import.* EMBO J, 2010. **29**(16): p. 2841-57.

143.   Fujii, R. and T. Takumi, *TLS facilitates transport of mRNA encoding an actin-stabilizing protein to dendritic spines.* Journal of cell science, 2005. **118**(24): p. 5755-5765.

144.   Dormann, D. and C. Haass, *Fused in sarcoma (FUS): an oncogene goes awry in neurodegeneration.* Molecular and Cellular Neuroscience, 2013. **56**: p. 475-486.

145.   Bosco, D.A., et al., *Mutant FUS proteins that cause amyotrophic lateral sclerosis incorporate into stress granules.* Human molecular genetics, 2010. **19**(21): p. 4160-4175.

146.   Murakami, T., et al., *ALS/FTD mutation-induced phase transition of FUS liquid droplets and reversible hydrogels into irreversible hydrogels impairs RNP granule function.* Neuron, 2015. **88**(4): p. 678-690.

147.   Soo, K., et al., *ALS-associated mutant FUS inhibits macroautophagy which is restored by overexpression of Rab1.* Cell death discovery, 2015. **1**: p. 15030.

148.   Neumann, M., et al., *A new subtype of frontotemporal lobar degeneration with FUS pathology.* Brain, 2009. **132**(11): p. 2922-2931.

149.   Seelaar, H., et al., *Frequency of ubiquitin and FUS-positive, TDP-43-negative frontotemporal lobar degeneration.* Journal of neurology, 2010. **257**(5): p. 747-753.

150.   Mackenzie, I.R., et al., *Atypical frontotemporal lobar degeneration with ubiquitin-positive, TDP-43-negative neuronal inclusions.* Brain, 2008. **131**(5): p. 1282-1293.

151.   Levine, T.P., et al., *The product of C9orf72, a gene strongly implicated in neurodegeneration, is structurally related to DENN Rab-GEFs.* Bioinformatics, 2013. **29**(4): p. 499-503.

152.   Sullivan, P.M., et al., *The ALS/FTLD associated protein C9orf72 associates with SMCR8 and WDR41 to regulate the autophagy-lysosome pathway.* Acta neuropathologica communications, 2016. **4**(1): p. 51.

153.   Farg, M.A., et al., *C9ORF72, implicated in amytrophic lateral sclerosis and frontotemporal dementia, regulates endosomal trafficking.* Human molecular genetics, 2014. **23**(13): p. 3579-3595.

154.   Taylor, J.P., R.H. Brown Jr, and D.W. Cleveland, *Decoding ALS: from genes to mechanism.* Nature, 2016. **539**(7628): p. 197-206.

155.   Belzil, V.V., et al., *Reduced C9orf72 gene expression in c9FTD/ALS is caused by histone trimethylation, an epigenetic event detectable in blood.* Acta neuropathologica, 2013. **126**(6): p. 895-905.

156.   Sellier, C., et al., *Loss of C9ORF72 impairs autophagy and synergizes with polyQ Ataxin-2 to induce motor neuron dysfunction and cell death.* The EMBO journal, 2016. **35**(12): p. 1276-1297.

157.   Koppers, M., et al., *C9orf72 ablation in mice does not cause motor neuron degeneration or motor deficits.* Annals of neurology, 2015. **78**(3): p. 426-438.

158.   Lee, Y.-B., et al., *Hexanucleotide repeats in ALS/FTD form length-dependent RNA foci, sequester RNA binding proteins, and are neurotoxic.* Cell reports, 2013. **5**(5): p. 1178-1186.

159.   Zhang, Y.-J., et al., *Aggregation-prone c9FTD/ALS poly (GA) RAN-translated proteins cause neurotoxicity by inducing ER stress.* Acta neuropathologica, 2014. **128**(4): p. 505-524.

160.   Zhang, K.Y., et al., *Ubiquilin 2: A component of the ubiquitin–proteasome system with an emerging role in neurodegeneration.* The international journal of biochemistry & cell biology, 2014. **50**: p. 123-126.

161.   Synofzik, M., et al., *Screening in ALS and FTD patients reveals 3 novel UBQLN2 mutations outside the PXX domain and a pure FTD phenotype.* Neurobiology of aging, 2012. **33**(12): p. 2949. e13-2949. e17.

162.   Seok Ko, H., et al., *Ubiquilin interacts with ubiquitylated proteins and proteasome through its ubiquitin-associated and ubiquitin-like domains.* FEBS letters, 2004. **566**(1-3): p. 110-114.

163.   N'Diaye, E.N., et al., *PLIC proteins or ubiquilins regulate autophagy-dependent cell survival during nutrient starvation.* EMBO reports, 2009. **10**(2): p. 173-179.

164.   Williams, K.L., et al., *UBQLN2/ubiquilin 2 mutation and pathology in familial amyotrophic lateral sclerosis.* Neurobiology of aging, 2012. **33**(10): p. 2527. e3-2527. e10.

165.   Meyer, H., M. Bug, and S. Bremer, *Emerging functions of the VCP/p97 AAA-ATPase in the ubiquitin system.* Nature cell biology, 2012. **14**(2): p. 117.

166.   Vij, N., *AAA ATPase p97/VCP: cellular functions, disease and therapeutic potential.* Journal of cellular and molecular medicine, 2008. **12**(6a): p. 2511-2518.

167.   Watts, G.D., et al., *Inclusion body myopathy associated with Paget disease of bone and frontotemporal dementia is caused by mutant valosin-containing protein.* Nature genetics, 2004. **36**(4): p. 377.

168.   Song, C., Q. Wang, and C.-C.H. Li, *ATPase activity of p97-valosin-containing protein (VCP) D2 mediates the major enzyme activity, and D1 contributes to the heat-induced activity.* Journal of Biological Chemistry, 2003. **278**(6): p. 3648-3655.

169.   Weihl, C.C., et al., *Inclusion body myopathy-associated mutations in p97/VCP impair endoplasmic reticulum-associated degradation.* Human molecular genetics, 2005. **15**(2): p. 189-199.

170.   Nowis, D., E. McConnell, and C. Wójcik, *Destabilization of the VCP-Ufd1-Npl4 complex is associated with decreased levels of ERAD substrates.* Experimental cell research, 2006. **312**(15): p. 2921-2932.

171.   Nakano, T., et al., *Expression of ubiquitin-binding protein p62 in ubiquitin-immunoreactive intraneuronal inclusions in amyotrophic lateral sclerosis with dementia: analysis of five autopsy cases with broad clinicopathological spectrum.* Acta neuropathologica, 2004. **107**(4): p. 359-364.

172.   Zatloukal, K., et al., *p62 Is a common component of cytoplasmic inclusions in protein aggregation diseases.* The American journal of pathology, 2002. **160**(1): p. 255-263.

173.   Gal, J., et al., *p62 accumulates and enhances aggregate formation in model systems of familial amyotrophic lateral sclerosis.* Journal of Biological Chemistry, 2007. **282**(15): p. 11068-11077.

174.   Teyssou, E., et al., *Mutations in SQSTM1 encoding p62 in amyotrophic lateral sclerosis: genetics and neuropathology.* Acta Neuropathologica, 2013. **125**(4): p. 511-522.

175.   Fifita, J.A., et al., *A novel amyotrophic lateral sclerosis mutation in OPTN induces ER stress and Golgi fragmentation in vitro.* Amyotrophic Lateral Sclerosis and Frontotemporal Degeneration, 2017. **18**(1-2): p. 126-133.

176.   Nagabhushana, A., et al., *Regulation of endocytic trafficking of transferrin receptor by optineurin and its impairment by a glaucoma-associated mutant.* BMC cell biology, 2010. **11**(1): p. 4.

177.   Sundaramoorthy, V., et al., *Defects in optineurin-and myosin VI-mediated cellular trafficking in amyotrophic lateral sclerosis.* Human molecular genetics, 2015. **24**(13): p. 3830-3846.

178.   Filimonenko, M., et al., *Functional multivesicular bodies are required for autophagic clearance of protein aggregates associated with neurodegenerative disease.* The Journal of cell biology, 2007. **179**(3): p. 485-500.

179.   Cox, L.E., et al., *Mutations in CHMP2B in lower motor neuron predominant amyotrophic lateral sclerosis (ALS).* PloS one, 2010. **5**(3): p. e9872.

180. Blair, I.P., et al., *CHMP2B mutations are not a common cause of familial or sporadic amyotrophic lateral sclerosis.* Journal of Neurology, Neurosurgery & Psychiatry, 2008. **79**(7): p. 849-850.

181. Sharma, S., et al., *Triggering the interferon antiviral response through an IKK-related pathway.* Science, 2003. **300**(5622): p. 1148-1151.

182. Pilli, M., et al., *TBK-1 promotes autophagy-mediated antimicrobial defense by controlling autophagosome maturation.* Immunity, 2012. **37**(2): p. 223-234.

183. Wild, P., et al., *Phosphorylation of the autophagy receptor optineurin restricts Salmonella growth.* Science, 2011. **333**(6039): p. 228-233.

184. Cirulli, E.T., et al., *Exome sequencing in amyotrophic lateral sclerosis identifies risk genes and pathways.* Science, 2015. **347**(6229): p. 1436-1441.

185. Gijselinck, I., et al., *Loss of TBK1 is a frequent cause of frontotemporal dementia in a Belgian cohort.* Neurology, 2015. **85**(24): p. 2116-2125.

186. Le Ber, I., et al., *TBK1 mutation frequencies in French frontotemporal dementia and amyotrophic lateral sclerosis cohorts.* Neurobiology of aging, 2015. **36**(11): p. 3116. e5-3116. e8.

187. Moore, A.S. and E.L. Holzbaur, *Dynamic recruitment and activation of ALS-associated TBK1 with its target optineurin are required for efficient mitophagy.* Proceedings of the National Academy of Sciences, 2016. **113**(24): p. E3349-E3358.

188. Richter, B., et al., *Phosphorylation of OPTN by TBK1 enhances its binding to Ub chains and promotes selective autophagy of damaged mitochondria.* Proceedings of the National Academy of Sciences, 2016. **113**(15): p. 4039-4044.

189. Korac, J., et al., *Ubiquitin-independent function of optineurin in autophagic clearance of protein aggregates.* J Cell Sci, 2013. **126**(2): p. 580-592.

190. Pensato, V., et al., *TUBA4A gene analysis in sporadic amyotrophic lateral sclerosis: identification of novel mutations.* Journal of neurology, 2015. **262**(5): p. 1376-1378.

191. Gentil, B.J., M. Tibshirani, and H.D. Durham, *Neurofilament dynamics and involvement in neurological disorders.* Cell and tissue research, 2015. **360**(3): p. 609-620.

192. Rooke, K., et al., *Analysis of the KSP repeat of the neurofilament heavy subunit in familial amyotrophic lateral sclerosis.* Neurology, 1996. **46**(3): p. 789-790.

193. Brettschneider, J., et al., *Axonal damage markers in cerebrospinal fluid are increased in ALS.* Neurology, 2006. **66**(6): p. 852-856.

194. Mizusawa, H., et al., *Focal accumulation of phosphorylated neurofilaments within anterior horn cell in familial amyotrophic lateral sclerosis.* Acta neuropathologica, 1989. **79**(1): p. 37-43.

195. Leung, C.L., et al., *A pathogenic peripherin gene mutation in a patient with amyotrophic lateral sclerosis.* Brain Pathology, 2004. **14**(3): p. 290-296.

196. Corrado, L., et al., *A novel peripherin gene (PRPH) mutation identified in one sporadic amyotrophic lateral sclerosis patient.* Neurobiology of aging, 2011. **32**(3): p. 552. e1-552. e6.

197. Xiao, S., et al., *An aggregate-inducing peripherin isoform generated through intron retention is upregulated in amyotrophic lateral sclerosis and associated with disease pathology.* Journal of Neuroscience, 2008. **28**(8): p. 1833-1840.

198. Robertson, J., et al., *A neurotoxic peripherin splice variant in a mouse model of ALS.* The Journal of cell biology, 2003. **160**(6): p. 939-949.

199. Teuling, E., et al., *Motor neuron disease-associated mutant vesicle-associated membrane protein-associated protein (VAP) B recruits wild-type VAPs into endoplasmic reticulum-derived tubular aggregates.* Journal of Neuroscience, 2007. **27**(36): p. 9801-9815.

200. Anagnostou, G., et al., *Vesicle associated membrane protein B (VAPB) is decreased in ALS spinal cord.* Neurobiology of aging, 2010. **31**(6): p. 969-985.

201. Tsuda, H., et al., *The Amyotrophic Lateral Sclerosis 8 Protein VAPB Is Cleaved, Secreted, and Acts as a Ligand for Eph Receptors.* Cell, 2008. **133**(6): p. 963-977.

202. Gkogkas, C., et al., *VAPB interacts with and modulates the activity of ATF6.* Human molecular genetics, 2008. **17**(11): p. 1517-1526.

203. Peretti, D., et al., *Coordinated lipid transfer between the endoplasmic reticulum and the Golgi complex requires the VAP proteins and is essential for Golgi-mediated transport.* Molecular biology of the cell, 2008. **19**(9): p. 3871-3884.

204. Puls, I., et al., *Mutant dynactin in motor neuron disease.* Nature genetics, 2003. **33**(4): p. 455-456.

205. Laird, F.M., et al., *Motor neuron disease occurring in a mutant dynactin mouse model is characterized by defects in vesicular trafficking.* Journal of Neuroscience, 2008. **28**(9): p. 1997-2005.

206. Farrer, M.J., et al., *DCTN1 mutations in Perry syndrome.* Nature genetics, 2009. **41**(2): p. 163-165.

207. Otomo, A., et al., *ALS2, a novel guanine nucleotide exchange factor for the small GTPase Rab5, is implicated in endosomal dynamics.* Human molecular genetics, 2003. **12**(14): p. 1671-1687.

208. Otomo, A., et al., *ALS2/alsin deficiency in neurons leads to mild defects in macropinocytosis and axonal growth.* Biochemical and biophysical research communications, 2008. **370**(1): p. 87-92.

209. Kunita, R., et al., *The Rab5 activator ALS2/alsin acts as a novel Rac1 effector through Rac1-activated endocytosis.* Journal of Biological Chemistry, 2007. **282**(22): p. 16599-16611.

210. Lai, C., et al., *Amyotrophic lateral sclerosis 2-deficiency leads to neuronal degeneration in amyotrophic lateral sclerosis through altered AMPA receptor trafficking.* Journal of neuroscience, 2006. **26**(45): p. 11798-11806.

211. Kanekura, K., et al., *Alsin, the product of ALS2 gene, suppresses SOD1 mutant neurotoxicity through RhoGEF domain by interacting with SOD1 mutants.* Journal of Biological Chemistry, 2004. **279**(18): p. 19247-19256.

212. Hadano, S., et al., *Loss of ALS2/Alsin exacerbates motor dysfunction in a SOD1H46R-expressing mouse ALS model by disturbing endolysosomal trafficking.* PLoS One, 2010. **5**(3): p. e9805.

213. Michell, R.H., et al., *Phosphatidylinositol 3, 5-bisphosphate: metabolism and cellular functions.* Trends in biochemical sciences, 2006. **31**(1): p. 52-63.

214. Chow, C.Y., et al., *Mutation of FIG4 causes neurodegeneration in the pale tremor mouse and patients with CMT4J.* Nature, 2007. **448**(7149): p. 68.

215. Smith, B.N., et al., *Mutations in the vesicular trafficking protein annexin A11 are associated with amyotrophic lateral sclerosis.* Science translational medicine, 2017. **9**(388): p. eaad9157.

216. Salton, M., et al., *Involvement of Matrin 3 and SFPQ/NONO in the DNA damage response.* Cell Cycle, 2010. **9**(8): p. 1568-1576.

217. Kenna, K.P., et al., *NEK1 variants confer susceptibility to amyotrophic lateral sclerosis.* Nature Genetics, 2016. **48**(9): p. 1037-1042.

218. Pelegrini, A.L., et al., *Nek1 silencing slows down DNA repair and blocks DNA damage-induced cell cycle arrest.* Mutagenesis, 2010. **25**(5): p. 447-454.

219. Chen, Y., et al., *Nek1 kinase functions in DNA damage response and checkpoint control through a pathway independent of ATM and ATR.* Cell Cycle, 2011. **10**(4): p. 655-663.

220. van Rheenen, W., et al., *Genome-wide association analyses identify new risk variants and the genetic architecture of amyotrophic lateral sclerosis.* Nature Genetics, 2016. **48**(9): p. 1043-1048.

221. Fang, X., et al., *The NEK1 interactor, C21ORF2, is required for efficient DNA damage repair.* Acta biochimica et biophysica Sinica, 2015. **47**(10): p. 834-841.

222. Suraweera, A., et al., *Senataxin, defective in ataxia oculomotor apraxia type 2, is involved in the defense against oxidative DNA damage.* The Journal of cell biology, 2007. **177**(6): p. 969-979.

223. Suraweera, A., et al., *Functional role for senataxin, defective in ataxia oculomotor apraxia type 2, in transcriptional regulation.* Human molecular genetics, 2009. **18**(18): p. 3384-3396.

224. Zhao, Z.-h., et al., *A novel mutation in the senataxin gene identified in a Chinese patient with sporadic amyotrophic lateral sclerosis.* Amyotrophic Lateral Sclerosis, 2009. **10**(2): p. 118-122.

225. Alzu, A., et al., *Senataxin associates with replication forks to protect fork integrity across RNA-polymerase-II-transcribed genes.* Cell, 2012. **151**(4): p. 835-846.

226. Sebastia, J., et al., *Angiogenin protects motoneurons against hypoxic injury.* Cell death and differentiation, 2009. **16**(9): p. 1238.

227. Subramanian, V., B. Crabtree, and K.R. Acharya, *Human angiogenin is a neuroprotective factor and amyotrophic lateral sclerosis associated angiogenin variants affect neurite extension/pathfinding and survival of motor neurons.* Human molecular genetics, 2007. **17**(1): p. 130-149.

228. Crabtree, B., et al., *Characterization of human angiogenin variants implicated in amyotrophic lateral sclerosis.* Biochemistry, 2007. **46**(42): p. 11810-11818.

229. Conforti, F., et al., *A novel Angiogenin gene mutation in a sporadic patient with amyotrophic lateral sclerosis from southern Italy.* Neuromuscular Disorders, 2008. **18**(1): p. 68-70.

230. Paubel, A., et al., *Mutations of the ANG gene in French patients with sporadic amyotrophic lateral sclerosis.* Archives of neurology, 2008. **65**(10): p. 1333-1336.

231. Greenway, M.J., et al., *ANG mutations segregate with familial and'sporadic'amyotrophic lateral sclerosis.* Nature genetics, 2006. **38**(4): p. 411.

232. Gellera, C., et al., *Identification of new ANG gene mutations in a large cohort of Italian patients with amyotrophic lateral sclerosis.* Neurogenetics, 2008. **9**(1): p. 33-40.

233. Seilhean, D., et al., *Accumulation of TDP-43 and α-actin in an amyotrophic lateral sclerosis patient with the K17I ANG mutation.* Acta neuropathologica, 2009. **118**(4): p. 561-573.

234. Cronin, S., et al., *Elevated serum angiogenin levels in ALS.* Neurology, 2006. **67**(10): p. 1833-1836.

235. Paul, P. and J. de Belleroche, *Experimental approaches for elucidating co-agonist regulation of NMDA receptor in motor neurons: therapeutic implications for amyotrophic lateral sclerosis (ALS).* Journal of pharmaceutical and biomedical analysis, 2015. **116**: p. 2-6.

236. Sasabe, J., et al., *d-Serine is a key determinant of glutamate toxicity in amyotrophic lateral sclerosis.* The EMBO journal, 2007. **26**(18): p. 4149-4159.

237. Sasabe, J., et al., *D-amino acid oxidase controls motoneuron degeneration through D-serine.* Proceedings of the National Academy of Sciences, 2012. **109**(2): p. 627-632.

238. Bannwarth, S., et al., *A mitochondrial origin for frontotemporal dementia and amyotrophic lateral sclerosis through CHCHD10 involvement.* Brain, 2014. **137**(8): p. 2329-2345.

239. Teyssou, E., et al., *Genetic analysis of CHCHD10 in French familial amyotrophic lateral sclerosis patients.* Neurobiology of aging, 2016. **42**: p. 218. e1-218. e3.

240. Chaussenot, A., et al., *Screening of CHCHD10 in a French cohort confirms the involvement of this gene in frontotemporal dementia with amyotrophic lateral sclerosis patients.* Neurobiology of aging, 2014. **35**(12): p. 2884. e1-2884. e4.

241. Perrone, F., et al., *Investigating the role of ALS genes CHCHD10 and TUBA4A in Belgian FTD-ALS spectrum patients.* Neurobiology of aging, 2017. **51**: p. 177. e9-177. e16.

242. Woo, J.-A., et al., *Loss of function CHCHD10 mutations in cytoplasmic TDP-43 accumulation and synaptic integrity.* Nature Communications, 2017. **8**.

243. Costa, L.G., et al., *Modulation of paraoxonase (PON1) activity.* Biochemical pharmacology, 2005. **69**(4): p. 541-550.

244. Slowik, A., et al., *Paraoxonase gene polymorphisms and sporadic ALS.* Neurology, 2006. **67**(5): p. 766-770.

245. Hayashi, T. and T.-P. Su, *Sigma-1 receptor chaperones at the ER-mitochondrion interface regulate Ca 2+ signaling and cell survival.* Cell, 2007. **131**(3): p. 596-610.

246. Vollrath, J., et al., *Loss of function of the ALS protein SigR1 leads to ER pathology associated with defective autophagy and lipid raft disturbances.* Cell death & disease, 2014. **5**(6): p. e1290.

247. Bernard-Marissal, N., et al., *Dysfunction in endoplasmic reticulum-mitochondria crosstalk underlies SIGMAR1 loss of function mediated motor neuron degeneration.* Brain, 2015. **138**(4): p. 875-890.

248. Van Damme, P., et al., *Expanded ATXN2 CAG repeat size in ALS identifies genetic overlap between ALS and SCA2.* Neurology, 2011. **76**(24): p. 2066-2072.

249. Daoud, H., et al., *Association of long ATXN2 CAG repeat sizes with increased risk of amyotrophic lateral sclerosis.* Archives of neurology, 2011. **68**(6): p. 739-742.

250. Chen, S., et al., *Genetics of amyotrophic lateral sclerosis: an update.* Mol Neurodegener, 2013. **8**(1): p. 28.

251. Daoud, H., et al., *Exome sequencing reveals SPG11 mutations causing juvenile ALS.* Neurobiology of aging, 2012. **33**(4): p. 839. e5-839. e9.

252. Martin, E., et al., *Spatacsin and spastizin act in the same pathway required for proper spinal motor neuron axon outgrowth in zebrafish.* Neurobiology of disease, 2012. **48**(3): p. 299-308.

253. Carr, F., *Selective vulnerability.* Nature Reviews Neuroscience, 2015. **16**(3).

254. Atkin, J.D., et al., *Endoplasmic reticulum stress and induction of the unfolded protein response in human sporadic amyotrophic lateral sclerosis.* Neurobiol Dis, 2008. **30**(3): p. 400-7.

255. Saxena, S., E. Cabuy, and P. Caroni, *A role for motoneuron subtype-selective ER stress in disease manifestations of FALS mice.* Nat Neurosci, 2009. **12**(5): p. 627-36.

256. Hetz, C. and B. Mollereau, *Disturbance of endoplasmic reticulum proteostasis in neurodegenerative diseases.* Nat Rev Neurosci, 2014. **15**(4): p. 233-249.

257. Lindholm, D., H. Wootz, and L. Korhonen, *ER stress and neurodegenerative diseases.* Cell Death Differ, 2006. **13**(3): p. 385-92.

258. Soto, C., *Unfolding the role of protein misfolding in neurodegenerative diseases.* Nature Reviews: Neuroscience, 2003. **4**(1): p. 49-60.

259. Wolozin, B., *Regulated protein aggregation: stress granules and neurodegeneration.* Molecular Neurodegeneration, 2012. **7**: p. 56.

260. Al-Chalabi, A., et al., *The genetics and neuropathology of amyotrophic lateral sclerosis.* Acta Neuropathol, 2012. **124**(3): p. 339-52.

261. Piao, Y.S., et al., *Neuropathology with clinical correlations of sporadic amyotrophic lateral sclerosis: 102 autopsy cases examined between 1962 and 2000.* Brain pathology, 2003. **13**(1): p. 10-22.

262. Furukawa, Y., *Pathological roles of wild-type cu, zn-superoxide dismutase in amyotrophic lateral sclerosis.* Neurology research international, 2012. **2012**.

263. Bruijn, L.I., et al., *ALS-linked SOD1 mutant G85R mediates damage to astrocytes and promotes rapidly progressive disease with SOD1-containing inclusions.* Neuron, 1997. **18**(2): p. 327-38.

264. Watanabe, M., et al., *Histological evidence of protein aggregation in mutant SOD1 transgenic mice and in amyotrophic lateral sclerosis neural tissues.* Neurobiology of disease, 2001. **8**(6): p. 933-941.

265. Turner, B.J., et al., *Impaired extracellular secretion of mutant superoxide dismutase 1 associates with neurotoxicity in familial amyotrophic lateral sclerosis.* J Neurosci, 2005. **25**(1): p. 108-17.

266. Wang, Q., et al., *Protein aggregation and protein instability govern familial amyotrophic lateral sclerosis patient survival.* PLoS biology, 2008. **6**(7): p. e170.

267. Prudencio, M., et al., *Variation in aggregation propensities among ALS-associated variants of SOD1: correlation to human disease.* Human molecular genetics, 2009. **18**(17): p. 3217-3226.

268. Van Deerlin, V.M., et al., *TARDBP mutations in amyotrophic lateral sclerosis with TDP-43 neuropathology: a genetic and histopathological analysis.* The Lancet Neurology, 2008. **7**(5): p. 409-416.

269. Mackenzie, I.R., et al., *Dipeptide repeat protein pathology in C9ORF72 mutation cases: clinico-pathological correlations.* Acta neuropathologica, 2013. **126**(6): p. 859-879.

270. Mackenzie, I.R., P. Frick, and M. Neumann, *The neuropathology associated with repeat expansions in the C9ORF72 gene.* Acta neuropathologica, 2014. **127**(3): p. 347-357.

271. Majcher, V., et al., *Autophagy receptor defects and ALS-FTLD.* Molecular and Cellular Neuroscience, 2015. **66**: p. 43-52.

272. Deng, H.-X., et al., *Differential involvement of optineurin in amyotrophic lateral sclerosis with or without SOD1 mutations.* Archives of neurology, 2011. **68**(8): p. 1057-1061.

273. Hortobágyi, T., et al., *Optineurin inclusions occur in a minority of TDP-43 positive ALS and FTLD-TDP cases and are rarely observed in other neurodegenerative disorders.* Acta neuropathologica, 2011. **121**(4): p. 519-527.

274. De Vos, K.J. and M. Hafezparast, *Neurobiology of axonal transport defects in motor neuron diseases: Opportunities for translational research?* Neurobiology of Disease, 2017.

275. Frey, D., et al., *Early and selective loss of neuromuscular synapse subtypes with low sprouting competence in motoneuron diseases.* Journal of Neuroscience, 2000. **20**(7): p. 2534-2542.

276. Williamson, T.L. and D.W. Cleveland, *Slowing of axonal transport is a very early event in the toxicity of ALS? linked SOD1 mutants to motor neurons.* Nature neuroscience, 1999. **2**(1).

277. Fischer, L.R., et al., *Amyotrophic lateral sclerosis is a distal axonopathy: evidence in mice and man.* Experimental neurology, 2004. **185**(2): p. 232-240.

278. Okada, Y., et al., *The neuron-specific kinesin superfamily protein KIF1A is a uniqye monomeric motor for anterograde axonal transport of synaptic vesicle precursors.* Cell, 1995. **81**(5): p. 769-780.

279. Hirano, A., et al., *Fine structural observations of neurofilamentous changes in amyotrophic lateral sclerosis.* Journal of Neuropathology & Experimental Neurology, 1984. **43**(5): p. 461-470.

280. Hirano, A., et al., *Fine structural study of neurofibrillary changes in a family with amyotrophic lateral sclerosis.* Journal of Neuropathology & Experimental Neurology, 1984. **43**(5): p. 471-480.

281. Rouleau, G.A., et al., *SOD1 mutation is assosiated with accumulation of neurofilaments in amyotrophic lateral scelaries.* Annals of neurology, 1996. **39**(1): p. 128-131.

282. Sasaki, S. and M. Iwata, *Ultrastructural study of synapses in the anterior horn neurons of patients with amyotrophic lateral sclerosis.* Neuroscience letters, 1996. **204**(1): p. 53-56.

283. Corbo, M. and A.P. Hays, *Peripherin and neurofilament protein coexist in spinal spheroids of motor neuron disease.* Journal of Neuropathology & Experimental Neurology, 1992. **51**(5): p. 531-537.

284. Hirokawa, N., S. Niwa, and Y. Tanaka, *Molecular motors in neurons: transport mechanisms and roles in brain function, development, and disease.* Neuron, 2010. **68**(4): p. 610-638.

285. Tateno, M., et al., *Mutant SOD1 impairs axonal transport of choline acetyltransferase and acetylcholine release by sequestering KAP3.* Human molecular genetics, 2008. **18**(5): p. 942-955.

286. Štalekar, M., et al., *Proteomic analyses reveal that loss of TDP-43 affects RNA processing and intracellular transport.* Neuroscience, 2015. **293**: p. 157-170.

287. Volkening, K., et al., *Tar DNA binding protein of 43 kDa (TDP-43), 14-3-3 proteins and copper/zinc superoxide dismutase (SOD1) interact to modulate NFL mRNA stability. Implications for altered RNA processing in amyotrophic lateral sclerosis (ALS).* Brain research, 2009. **1305**: p. 168-182.

288. Li, Y.R., et al., *Stress granules as crucibles of ALS pathogenesis.* J Cell Biol, 2013. **201**(3): p. 361-372.

289. Liu-Yesucevitz, L., et al., *ALS-linked mutations enlarge TDP-43-enriched neuronal RNA granules in the dendritic arbor.* Journal of Neuroscience, 2014. **34**(12): p. 4167-4174.

290. Corona, J.C., L.B. Tovar-y-Romo, and R. Tapia, *Glutamate excitotoxicity and therapeutic targets for amyotrophic lateral sclerosis.* Expert opinion on therapeutic targets, 2007. **11**(11): p. 1415-1428.

291. van Cutsem, P., et al., *Excitotoxicity and amyotrophic lateral sclerosis.* Neurodegenerative diseases, 2005. **2**(3-4): p. 147-159.

292. Bellingham, M.C., *A review of the neural mechanisms of action and clinical efficiency of riluzole in treating amyotrophic lateral sclerosis: what have we learned in the last decade?* CNS Neurosci Ther, 2011. **17**(1): p. 4-31.

293. Eisen, A., *Amyotrophic lateral sclerosis—evolutionary and other perspectives.* Muscle & nerve, 2009. **40**(2): p. 297-304.

294. Vucic, S. and M.C. Kiernan, *Utility of transcranial magnetic stimulation in delineating amyotrophic lateral sclerosis pathophysiology.* Handbook of clinical neurology, 2013. **116**: p. 561-575.

295. Williams, K.L., et al., *Pathophysiological insights into ALS with C9ORF72 expansions.* J Neurol Neurosurg Psychiatry, 2013: p. jnnp-2012-304529.

296. Carvalho, M.d., *Pathophysiological significance of fasciculations in the early diagnosis of ALS.* Amyotrophic Lateral Sclerosis and Other Motor Neuron Disorders, 2000. **1**(sup1): p. S43-S46.

297.   Plaitakis, A., E. Constantakakis, and J. Smith, *The neuroexcitotoxic amino acids glutamate and aspartate are altered in the spinal cord and brain in amyotrophic lateral sclerosis.* Annals of neurology, 1988. **24**(3): p. 446-449.

298.   Spreux-Varoquaux, O., et al., *Glutamate levels in cerebrospinal fluid in amyotrophic lateral sclerosis: a reappraisal using a new HPLC method with coulometric detection in a large cohort of patients.* Journal of the neurological sciences, 2002. **193**(2): p. 73-78.

299.   Shaw, P.J., et al., *CSF and plasma amino acid levels in motor neuron disease: elevation of CSF glutamate in a subset of patients.* Neurodegeneration, 1995. **4**(2): p. 209-216.

300.   Rothstein, J.D., et al., *Selective loss of glial glutamate transporter GLT-1 in amyotrophic lateral sclerosis.* Annals of neurology, 1995. **38**(1): p. 73-84.

301.   Guo, H., et al., *Increased expression of the glial glutamate transporter EAAT2 modulates excitotoxicity and delays the onset but not the outcome of ALS in mice.* Human molecular genetics, 2003. **12**(19): p. 2519-2532.

302.   Cozzolino, M., et al., *Mitochondrial dynamism and the pathogenesis of Amyotrophic Lateral Sclerosis.* Frontiers in cellular neuroscience, 2015. **9**.

303.   Carrì, M.T., N. D'Ambrosi, and M. Cozzolino, *Pathways to mitochondrial dysfunction in ALS pathogenesis.* Biochemical and biophysical research communications, 2017. **483**(4): p. 1187-1193.

304.   Jaarsma, D., et al., *CuZn superoxide dismutase (SOD1) accumulates in vacuolated mitochondria in transgenic mice expressing amyotrophic lateral sclerosis-linked SOD1 mutations.* Acta neuropathologica, 2001. **102**(4): p. 293-305.

305.   Pickles, S., et al., *ALS-linked misfolded SOD1 species have divergent impacts on mitochondria.* Acta neuropathologica communications, 2016. **4**(1): p. 43.

306.   Ferri, A., et al., *Familial ALS-superoxide dismutases associate with mitochondria and shift their redox potentials.* Proceedings of the National Academy of Sciences, 2006. **103**(37): p. 13860-13865.

307.   Cozzolino, M., et al., *Oligomerization of mutant SOD1 in mitochondria of motoneuronal cells drives mitochondrial damage and cell toxicity.* Antioxidants & redox signaling, 2009. **11**(7): p. 1547-1558.

308.   Magrané, J., et al., *Mutant SOD1 in neuronal mitochondria causes toxicity and mitochondrial dynamics abnormalities.* Human molecular genetics, 2009. **18**(23): p. 4552-4564.

309.   Igoudjil, A., et al., *In vivo pathogenic role of mutant SOD1 localized in the mitochondrial intermembrane space.* Journal of Neuroscience, 2011. **31**(44): p. 15826-15837.

310.   Wang, W., et al., *The ALS disease-associated mutant TDP-43 impairs mitochondrial dynamics and function in motor neurons.* Human molecular genetics, 2013. **22**(23): p. 4706-4719.

311.   Stoica, R., et al., *ER–mitochondria associations are regulated by the VAPB–PTPIP51 interaction and are disrupted by ALS/FTD-associated TDP-43.* Nature communications, 2014. **5**.

312.   Jaiswal, M.K. and B.U. Keller, *Cu/Zn superoxide dismutase typical for familial amyotrophic lateral sclerosis increases the vulnerability of mitochondria and perturbs Ca2+ homeostasis in SOD1G93A mice.* Molecular pharmacology, 2009. **75**(3): p. 478-489.

313.   Barrett, E.F., J.N. Barrett, and G. David, *Dysfunctional mitochondrial Ca2+ handling in mutant SOD1 mouse models of fALS: integration of findings from motor neuron somata and motor terminals.* Frontiers in cellular neuroscience, 2014. **8**.

314. Carrì, M.T., et al., *Expression of a Cu, Zn superoxide dismutase typical of familial amyotrophic lateral sclerosis induces mitochondrial alteration and increase of cytosolic Ca2+ concentration in transfected neuroblastoma SH-SY5Y cells.* FEBS letters, 1997. **414**(2): p. 365-368.

315. Soo, K.Y., et al., *Recruitment of mitochondria into apoptotic signaling correlates with the presence of inclusions formed by amyotrophic lateral sclerosis-associated SOD1 mutations.* Journal of neurochemistry, 2009. **108**(3): p. 578-590.

316. Soo, K.Y., et al., *Bim links ER stress and apoptosis in cells expressing mutant SOD1 associated with amyotrophic lateral sclerosis.* PLoS One, 2012. **7**(4): p. e35413.

317. Labbadia, J., et al., *Mitochondrial stress restores the heat shock response and prevents proteostasis collapse during aging.* Cell reports, 2017. **21**(6): p. 1481-1494.

318. McKee, A.E., et al., *A genome-wide in situ hybridization map of RNA-binding proteins reveals anatomically restricted expression in the developing mouse brain.* BMC developmental biology, 2005. **5**(1): p. 14.

319. Kapeli, K., F.J. Martinez, and G.W. Yeo, *Genetic mutations in RNA-binding proteins and their roles in ALS.* Human Genetics, 2017: p. 1-22.

320. Ugras, S.E. and J. Shorter, *RNA-binding proteins in amyotrophic lateral sclerosis and neurodegeneration.* Neurology research international, 2012. **2012**.

321. Scotter, E.L., H.-J. Chen, and C.E. Shaw, *TDP-43 proteinopathy and ALS: Insights into disease mechanisms and therapeutic targets.* Neurotherapeutics, 2015. **12**(2): p. 352-363.

322. Sun, S., et al., *ALS-causative mutations in FUS/TLS confer gain and loss of function by altered association with SMN and U1-snRNP.* Nature communications, 2015. **6**: p. 6171.

323. Igaz, L.M., et al., *Dysregulation of the ALS-associated gene TDP-43 leads to neuronal death and degeneration in mice.* The Journal of clinical investigation, 2011. **121**(2): p. 726.

324. Wils, H., et al., *TDP-43 transgenic mice develop spastic paralysis and neuronal inclusions characteristic of ALS and frontotemporal lobar degeneration.* Proceedings of the National Academy of Sciences, 2010. **107**(8): p. 3858-3863.

325. Wu, L.-S., W.-C. Cheng, and C.-K.J. Shen, *Targeted depletion of TDP-43 expression in the spinal cord motor neurons leads to the development of amyotrophic lateral sclerosis-like phenotypes in mice.* Journal of Biological Chemistry, 2012. **287**(33): p. 27335-27344.

326. Bentmann, E., *Stress granule recruitment and deposition of proteins of the FET family and TDP-43 in ALS and FTD.* 2014, lmu.

327. La Spada, A.R. and J.P. Taylor, *Repeat expansion disease: progress and puzzles in disease pathogenesis.* Nature reviews. Genetics, 2010. **11**(4): p. 247.

328. Moseley, M. and I.Y. Zu T, *Bidirectional expression of CUG and CAG expansion transcripts and intranu-Double the Trouble: Bidirectional Expression of the SCA8 CAG.* CTG Expansion Mutation—Evidence for RNA and Protein Gain of Function Effects. **50**: p. 983.

329. Zu, T., et al., *Non-ATG–initiated translation directed by microsatellite expansions.* Proceedings of the National Academy of Sciences, 2011. **108**(1): p. 260-265.

330. Wen, X., et al., *Antisense proline-arginine RAN dipeptides linked to C9ORF72-ALS/FTD form toxic nuclear aggregates that initiate in vitro and in vivo neuronal death.* Neuron, 2014. **84**(6): p. 1213-1225.

331. Boillée, S., C.V. Velde, and D.W. Cleveland, *ALS: a disease of motor neurons and their nonneuronal neighbors.* Neuron, 2006. **52**(1): p. 39-59.

332. Turner, B.J., et al., *Dismutase-competent SOD1 mutant accumulation in myelinating Schwann cells is not detrimental to normal or transgenic ALS model mice.* Human molecular genetics, 2009. **19**(5): p. 815-824.

333. Miller, T.M., et al., *Gene transfer demonstrates that muscle is not a primary target for non-cell-autonomous toxicity in familial amyotrophic lateral sclerosis.* Proceedings of the National Academy of Sciences, 2006. **103**(51): p. 19546-19551.

334. Yamanaka, K., et al., *Mutant SOD1 in cell types other than motor neurons and oligodendrocytes accelerates onset of disease in ALS mice.* Proceedings of the National Academy of Sciences, 2008. **105**(21): p. 7594-7599.

335. Beers, D.R., et al., *Wild-type microglia extend survival in PU. 1 knockout mice with familial amyotrophic lateral sclerosis.* Proceedings of the National Academy of Sciences, 2006. **103**(43): p. 16021-16026.

336. Wang, L., D.H. Gutmann, and R.P. Roos, *Astrocyte loss of mutant SOD1 delays ALS disease onset and progression in G85R transgenic mice.* Human molecular genetics, 2010. **20**(2): p. 286-293.

337. Gowing, G., et al., *Ablation of proliferating microglia does not affect motor neuron degeneration in amyotrophic lateral sclerosis caused by mutant superoxide dismutase.* Journal of Neuroscience, 2008. **28**(41): p. 10234-10244.

338. Di Giorgio, F.P., et al., *Non–cell autonomous effect of glia on motor neurons in an embryonic stem cell–based ALS model.* Nature neuroscience, 2007. **10**(5): p. 608.

339. Haidet-Phillips, A.M., et al., *Astrocytes from familial and sporadic ALS patients are toxic to motor neurons.* Nature biotechnology, 2011. **29**(9): p. 824-828.

340. Ramesh, N. and U.B. Pandey, *Autophagy Dysregulation in ALS: When Protein Aggregates Get Out of Hand.* Frontiers in Molecular Neuroscience, 2017. **10**.

341. Tian, F., et al., *In vivo optical imaging of motor neuron autophagy in a mouse model of amyotrophic lateral sclerosis.* Autophagy, 2011. **7**(9): p. 985-992.

342. Hetz, C., et al., *XBP-1 deficiency in the nervous system protects against amyotrophic lateral sclerosis by increasing autophagy.* Genes & development, 2009. **23**(19): p. 2294-2306.

343. Crippa, V., et al., *The small heat shock protein B8 (HspB8) promotes autophagic removal of misfolded proteins involved in amyotrophic lateral sclerosis (ALS).* Human molecular genetics, 2010. **19**(17): p. 3440-3456.

344. Li, L., X. Zhang, and W. Le, *Altered macroautophagy in the spinal cord of SOD1 mutant mice.* Autophagy, 2008. **4**(3): p. 290-293.

345. Morimoto, N., et al., *Increased autophagy in transgenic mice with a G93A mutant SOD1 gene.* Brain research, 2007. **1167**: p. 112-117.

346. Sasaki, S., *Autophagy in spinal cord motor neurons in sporadic amyotrophic lateral sclerosis.* Journal of Neuropathology & Experimental Neurology, 2011. **70**(5): p. 349-359.

347. Ryu, H.-H., et al., *Autophagy regulates amyotrophic lateral sclerosis-linked fused in sarcoma-positive stress granules in neurons.* Neurobiology of aging, 2014. **35**(12): p. 2822-2831.

348. Ying, H., et al., *Induction of autophagy in rats upon overexpression of wild-type and mutant optineurin gene.* BMC cell biology, 2015. **16**(1): p. 14.

349. Castillo, K., et al., *Trehalose delays the progression of amyotrophic lateral sclerosis by enhancing autophagy in motoneurons.* Autophagy, 2013. **9**(9): p. 1308-1320.

350. Barmada, S.J., et al., *Autophagy induction enhances TDP43 turnover and survival in neuronal ALS models.* Nature chemical biology, 2014. **10**(8): p. 677-685.

351. Watson, P. and D.J. Stephens, *ER-to-Golgi transport: form and formation of vesicular and tubular carriers.* Biochimica et Biophysica Acta (BBA)-Molecular Cell Research, 2005. **1744**(3): p. 304-315.
352. Marie, M., et al., *Membrane traffic in the secretory pathway.* Cellular and molecular life sciences, 2008. **65**(18): p. 2859-2874.
353. Preston, A., et al., *Reduced endoplasmic reticulum (ER)-to-Golgi protein trafficking contributes to ER stress in lipotoxic mouse beta cells by promoting protein overload.* Diabetologia, 2009. **52**(11): p. 2369-2373.
354. Lucocq, J., G. Warren, and J. Pryde, *Okadaic acid induces Golgi apparatus fragmentation and arrest of intracellular transport.* Journal of Cell Science, 1991. **100**(4): p. 753-759.
355. Atkin, J.D., et al., *Mutant SOD1 inhibits ER-Golgi transport in amyotrophic lateral sclerosis.* Journal of neurochemistry, 2014. **129**(1): p. 190-204.
356. Pearce, M.M., *Prion-like transmission of pathogenic protein aggregates in genetic models of neurodegenerative disease.* Current Opinion in Genetics & Development, 2017. **44**: p. 149-155.
357. Prusiner, S.B., et al., *Scrapie prions aggregate to form amyloid-like birefringent rods.* Cell, 1983. **35**(2): p. 349-358.
358. Telling, G.C., et al., *Prion propagation in mice expressing human and chimeric PrP transgenes implicates the interaction of cellular PrP with another protein.* Cell, 1995. **83**(1): p. 79-90.
359. Ravits, J., P. Paul, and C. Jorg, *Focality of upper and lower motor neuron degeneration at the clinical onset of ALS.* Neurology, 2007. **68**(19): p. 1571-1575.
360. Ayers, J.I., et al., *Prion-like propagation of mutant SOD1 misfolding and motor neuron disease spread along neuroanatomical pathways.* Acta neuropathologica, 2016. **131**(1): p. 103-114.
361. Nonaka, T., et al., *Prion-like properties of pathological TDP-43 aggregates from diseased brains.* Cell reports, 2013. **4**(1): p. 124-134.
362. Münch, C., J. O'Brien, and A. Bertolotti, *Prion-like propagation of mutant superoxide dismutase-1 misfolding in neuronal cells.* Proceedings of the National Academy of Sciences, 2011. **108**(9): p. 3548-3553.
363. Johnson, B.S., et al., *A yeast TDP-43 proteinopathy model: Exploring the molecular determinants of TDP-43 aggregation and cellular toxicity.* Proceedings of the National Academy of Sciences, 2008. **105**(17): p. 6439-6444.
364. Sun, Z., et al., *Molecular determinants and genetic modifiers of aggregation and toxicity for the ALS disease protein FUS/TLS.* PLoS biology, 2011. **9**(4): p. e1000614.
365. Coppedè, F., *An overview of DNA repair in amyotrophic lateral sclerosis.* The Scientific World Journal, 2011. **11**: p. 1679-1691.
366. Wang, W.-Y., et al., *Interaction of FUS and HDAC1 regulates DNA damage response and repair in neurons.* Nature neuroscience, 2013. **16**(10): p. 1383-1391.
367. Qiu, H., et al., *ALS-associated mutation FUS-R521C causes DNA damage and RNA splicing defects.* The Journal of clinical investigation, 2014. **124**(3): p. 981.
368. Higelin, J., et al., *FUS mislocalization and vulnerability to DNA damage in ALS patients derived hiPSCs and aging motoneurons.* Frontiers in cellular neuroscience, 2016. **10**.
369. Lopez-Gonzalez, R., et al., *Poly (GR) in C9ORF72-related ALS/FTD compromises mitochondrial function and increases oxidative stress and DNA damage in iPSC-derived motor neurons.* Neuron, 2016. **92**(2): p. 383-391.

370. Farg, M.A., et al., *The DNA damage response (DDR) is induced by the C9orf72 repeat expansion in Amyotrophic Lateral Sclerosis.* Human Molecular Genetics, 2017: p. ddx170.
371. D'Amico, E., et al., *Clinical perspective on oxidative stress in sporadic amyotrophic lateral sclerosis.* Free Radical Biology and Medicine, 2013. **65**: p. 509-527.
372. Lee, J., S. Giordano, and J. Zhang, *Autophagy, mitochondria and oxidative stress: cross-talk and redox signalling.* Biochemical Journal, 2012. **441**(2): p. 523-540.
373. Bozzo, F., A. Mirra, and M. Carrì, *Oxidative stress and mitochondrial damage in the pathogenesis of ALS: new perspectives.* Neuroscience letters, 2017. **636**: p. 3-8.
374. Duan, W., et al., *Mutant TAR DNA-binding protein-43 induces oxidative injury in motor neuron-like cell.* Neuroscience, 2010. **169**(4): p. 1621-1629.
375. Dalle-Donne, I., et al., *Biomarkers of oxidative damage in human disease.* Clinical chemistry, 2006. **52**(4): p. 601-623.
376. Ray, P.D., B.-W. Huang, and Y. Tsuji, *Reactive oxygen species (ROS) homeostasis and redox regulation in cellular signaling.* Cellular signalling, 2012. **24**(5): p. 981-990.
377. Atkin, J.D., et al., *Induction of the unfolded protein response in familial amyotrophic lateral sclerosis and association of protein-disulfide isomerase with superoxide dismutase 1.* J Biol Chem, 2006. **281**(40): p. 30152-65.
378. McCaffrey, K. and I. Braakman, *Protein quality control at the endoplasmic reticulum.* Essays in biochemistry, 2016. **60**(2): p. 227-235.
379. Wu, J. and R. Kaufman, *From acute ER stress to physiological roles of the unfolded protein response.* Cell death and differentiation, 2006. **13**(3): p. 374.
380. Ma, Y. and L.M. Hendershot, *ER chaperone functions during normal and stress conditions.* Journal of Chemical Neuroanatomy, 2004. **28**(1–2): p. 51-65.
381. Zacchi, L., et al., *Endoplasmic reticulum-associated degradation and protein quality control.* 2016.
382. Wu, Y., et al., *Contacts between the endoplasmic reticulum and other membranes in neurons.* Proceedings of the National Academy of Sciences, 2017. **114**(24): p. E4859-E4867.
383. Raffaello, A., et al., *Calcium at the center of cell signaling: interplay between endoplasmic reticulum, mitochondria, and lysosomes.* Trends in biochemical sciences, 2016. **41**(12): p. 1035-1049.
384. Borgese, N., *Getting membrane proteins on and off the shuttle bus between the endoplasmic reticulum and the Golgi complex.* J Cell Sci, 2016. **129**(8): p. 1537-1545.
385. Görlach, A., P. Klappa, and D.T. Kietzmann, *The endoplasmic reticulum: folding, calcium homeostasis, signaling, and redox control.* Antioxidants & redox signaling, 2006. **8**(9-10): p. 1391-1418.
386. Joshi, A.S., H. Zhang, and W.A. Prinz, *Organelle biogenesis in the endoplasmic reticulum.* Nature cell biology, 2017. **19**(8): p. 876-882.
387. Ramírez, O.A., S. Härtel, and A. Couve, *Location matters: the endoplasmic reticulum and protein trafficking in dendrites.* Biological research, 2011. **44**(1): p. 17-23.
388. Hetz, C., *The unfolded protein response: controlling cell fate decisions under ER stress and beyond.* Nat Rev Mol Cell Biol, 2012. **13**(2): p. 89-102.
389. Rutkowski, D.T., et al., *Adaptation to ER Stress Is Mediated by Differential Stabilities of Pro-Survival and Pro-Apoptotic mRNAs and Proteins.* PLoS Biol, 2006. **4**(11): p. e374.
390. Boyce, M., et al., *A selective inhibitor of eIF2α dephosphorylation protects cells from ER stress.* Science, 2005. **307**(5711): p. 935-939.

391. Halperin, L., J. Jung, and M. Michalak, *The many functions of the endoplasmic reticulum chaperones and folding enzymes.* IUBMB Life, 2014. **66**(5): p. 318-326.

392. Cao, S.S. and R.J. Kaufman, *Unfolded protein response.* Current Biology, 2012. **22**(16): p. R622-R626.

393. Lee, A.H., N.N. Iwakoshi, and L.H. Glimcher, *XBP-1 regulates a subset of endoplasmic reticulum resident chaperone genes in the unfolded protein response.* Mol Cell Biol, 2003. **23**(21): p. 7448-59.

394. Yoshida, H., et al., *XBP1 mRNA is induced by ATF6 and spliced by IRE1 in response to ER stress to produce a highly active transcription factor.* Cell, 2001. **107**(7): p. 881-891.

395. Schröder, M., *Endoplasmic reticulum stress responses.* Cellular and Molecular Life Sciences, 2008. **65**(6): p. 862-894.

396. Shoulders, M.D., et al., *Stress-independent activation of XBP1s and/or ATF6 reveals three functionally diverse ER proteostasis environments.* Cell reports, 2013. **3**(4): p. 1279-1292.

397. Tabas, I. and D. Ron, *Integrating the mechanisms of apoptosis induced by endoplasmic reticulum stress.* Nature cell biology, 2011. **13**(3): p. 184-190.

398. Shore, G.C., F.R. Papa, and S.A. Oakes, *Signaling cell death from the endoplasmic reticulum stress response.* Current opinion in cell biology, 2011. **23**(2): p. 143-149.

399. Urra, H., et al., *When ER stress reaches a dead end.* Biochimica et Biophysica Acta (BBA)-Molecular Cell Research, 2013. **1833**(12): p. 3507-3517.

400. Zinszner, H., et al., *CHOP is implicated in programmed cell death in response to impaired function of the endoplasmic reticulum.* Genes & development, 1998. **12**(7): p. 982-995.

401. Cregan, S.P., et al., *Bax-dependent caspase-3 activation is a key determinant in p53-induced apoptosis in neurons.* Journal of Neuroscience, 1999. **19**(18): p. 7860-7869.

402. Toshiyuki, M. and J.C. Reed, *Tumor suppressor p53 is a direct transcriptional activator of the human bax gene.* Cell, 1995. **80**(2): p. 293-299.

403. Han, J., et al., *ER-stress-induced transcriptional regulation increases protein synthesis leading to cell death.* Nat Cell Biol, 2013. **15**(5): p. 481-90.

404. Nishitoh, H., et al., *ASK1 is essential for endoplasmic reticulum stress-induced neuronal cell death triggered by expanded polyglutamine repeats.* Genes & Development, 2002. **16**(11): p. 1345-1355.

405. Hetz, C., et al., *Proapoptotic BAX and BAK modulate the unfolded protein response by a direct interaction with IRE1α.* Science, 2006. **312**(5773): p. 572-576.

406. Kim, I., W. Xu, and J.C. Reed, *Cell death and endoplasmic reticulum stress: disease relevance and therapeutic opportunities.* Nature reviews. Drug discovery, 2008. **7**(12): p. 1013.

407. Naidoo, N., et al., *Aging impairs the unfolded protein response to sleep deprivation and leads to proapoptotic signaling.* Journal of Neuroscience, 2008. **28**(26): p. 6539-6548.

408. Hoozemans, J.J.M., et al., *The unfolded protein response is activated in Alzheimer's disease.* Acta Neuropathologica, 2005. **110**(2): p. 165-72.

409. Hoozemans, J.J.M., et al., *The Unfolded Protein Response Is Activated in Pretangle Neurons in Alzheimer's Disease Hippocampus.* American Journal of Pathology, 2009. **174**(4): p. 1241-1251.

410. Chafekar, S.M., et al., *Increased Aβ1-42 production sensitizes neuroblastoma cells for ER stress toxicity.* Current Alzheimer Research, 2008. **5**(5): p. 469-474.

411. Ghribi, O., et al., *GDNF regulates the Aβ-induced endoplasmic reticulum stress response in rabbit hippocampus by inhibiting the activation of gadd 153 and the JNK and ERK kinases.* Neurobiology of Disease, 2004. **16**(2): p. 417-427.

412. Hoozemans, J.J.M., et al., *Activation of the unfolded protein response in Parkinson's disease.* Biochemical and Biophysical Research Communications, 2007. **354**(3): p. 707-711.

413. Ryu, E.J., et al., *Endoplasmic Reticulum Stress and the Unfolded Protein Response in Cellular Models of Parkinson's Disease.* Journal of Neuroscience, 2002. **22**(24): p. 10690-10698.

414. Silva, R.M., et al., *CHOP/GADD153 is a mediator of apoptotic death in substantia nigra dopamine neurons in an in vivo neurotoxin model of parkinsonism.* Journal of Neurochemistry, 2005. **95**(4): p. 974-986.

415. Duennwald, M.L. and S. Lindquist, *Impaired ERAD and ER stress are early and specific events in polyglutamine toxicity.* Genes & development, 2008. **22**(23): p. 3308-3319.

416. Carnemolla, A., et al., *Rrs1 is involved in endoplasmic reticulum stress response in Huntington disease.* Journal of Biological Chemistry, 2009. **284**(27): p. 18167-18173.

417. Vidal, R.L., et al., *Targeting the UPR transcription factor XBP1 protects against Huntington's disease through the regulation of FoxO1 and autophagy.* Human Molecular Genetics, 2012. **21**(10): p. 2245-2262.

418. Hetz, C., et al., *Caspase-12 and endoplasmic reticulum stress mediate neurotoxicity of pathological prion protein.* EMBO Journal, 2003. **22**(20): p. 5435-45.

419. Torres, M., et al., *Prion Protein Misfolding Affects Calcium Homeostasis and Sensitizes Cells to Endoplasmic Reticulum Stress.* PLoS ONE, 2010. **5**(12): p. e15658.

420. Kikuchi, H., et al., *Spinal cord endoplasmic reticulum stress associated with a microsomal accumulation of mutant superoxide dismutase-1 in an ALS model.* Proceedings of the National Academy of Sciences, 2006. **103**(15): p. 6025-6030.

421. Yamagishi, S., et al., *An in vitro model for Lewy body-like hyaline inclusion/astrocytic hyaline inclusion: induction by ER stress with an ALS-linked SOD1 mutation.* PLoS One, 2007. **2**(10): p. e1030.

422. Oh, Y.K., et al., *Superoxide dismutase 1 mutants related to amyotrophic lateral sclerosis induce endoplasmic stress in neuro2a cells.* Journal of neurochemistry, 2008. **104**(4): p. 993-1005.

423. Ilieva, E.V., et al., *Oxidative and endoplasmic reticulum stress interplay in sporadic amyotrophic lateral sclerosis.* Brain, 2007. **130**(12): p. 3111-3123.

424. Ito, Y., et al., *Involvement of CHOP, an ER-stress apoptotic mediator, in both human sporadic ALS and ALS model mice.* Neurobiology of Disease, 2009. **36**(3): p. 470-476.

425. Sasaki, S., *Endoplasmic reticulum stress in motor neurons of the spinal cord in sporadic amyotrophic lateral sclerosis.* Journal of Neuropathology & Experimental Neurology, 2010. **69**(4): p. 346-355.

426. Farg, M.A., et al., *Mutant FUS induces endoplasmic reticulum stress in amyotrophic lateral sclerosis and interacts with protein disulfide-isomerase.* Neurobiol Aging, 2012. **33**(12): p. 2855-68.

427. Walker, A.K., et al., *ALS-Associated TDP-43 Induces Endoplasmic Reticulum Stress, Which Drives Cytoplasmic TDP-43 Accumulation and Stress Granule Formation.* PLoS One, 2013. **8**(11): p.:e81170. doi: 10.1371/journal.pone.0081170. eCollection 2013.

428. Suzuki, H., et al., *ALS-linked P56S-VAPB, an aggregated loss-of-function mutant of VAPB, predisposes motor neurons to ER stress-related death by inducing aggregation*

of co-expressed wild-type VAPB. Journal of neurochemistry, 2009. **108**(4): p. 973-985.

429. Nishitoh, H., et al., *ALS-linked mutant SOD1 induces ER stress-and ASK1-dependent motor neuron death by targeting Derlin-1.* Genes & development, 2008. **22**(11): p. 1451-1464.

430. Kiskinis, E., et al., *Pathways Disrupted in Human ALS Motor Neurons Identified through Genetic Correction of Mutant SOD1.* Cell Stem Cell, 2014. **14**(6): p. 781-795.

431. Wainger, Brian J., et al., *Intrinsic Membrane Hyperexcitability of Amyotrophic Lateral Sclerosis Patient-Derived Motor Neurons.* Cell Reports, 2014. **7**(1): p. 1-11.

432. Kieran, D., et al., *Deletion of the BH3-only protein puma protects motoneurons from ER stress-induced apoptosis and delays motoneuron loss in ALS mice.* Proceedings of the National Academy of Sciences, 2007. **104**(51): p. 20606-20611.

433. Matus, S., et al., *Functional contribution of the transcription factor ATF4 to the pathogenesis of amyotrophic lateral sclerosis.* PloS one, 2013. **8**(7): p. e66672.

434. Matus, S., et al., *ER dysfunction and protein folding stress in ALS.* International journal of cell biology, 2013. **2013**.

435. Vaccaro, A., et al., *Pharmacological reduction of ER stress protects against TDP-43 neuronal toxicity in vivo.* Neurobiology of Disease, 2013. **55**(0): p. 64-75.

436. Wang, L., B. Popko, and R.P. Roos, *The unfolded protein response in familial amyotrophic lateral sclerosis.* Hum Mol Genet, 2011. **20**(5): p. 1008-15.

437. Ellgaard, L. and L.W. Ruddock, *The human protein disulphide isomerase family: substrate interactions and functional properties.* EMBO Rep, 2005. **6**(1): p. 28-32.

438. Hatahet, F. and L.W. Ruddock, *Protein disulfide isomerase: a critical evaluation of its function in disulfide bond formation.* Antioxidants & redox signaling, 2009. **11**(11): p. 2807-2850.

439. Honjo, Y., et al., *Protein disulfide isomerase-immunopositive inclusions in patients with Alzheimer disease.* Brain Research, 2010. **1349**(0): p. 90-96.

440. Honjo, Y., et al., *Protein disulfide isomerase-immunopositive inclusions in patients with amyotrophic lateral sclerosis.* Amyotrophic Lateral Sclerosis, 2011. **12**(6): p. 444-450.

441. Woehlbier, U., et al., *ALS-linked protein disulfide isomerase variants cause motor dysfunction.* The EMBO journal, 2016. **35**(8): p. 845-865.

442. Kwok, C.T., et al., *Association studies indicate that protein disulfide isomerase is a risk factor in amyotrophic lateral sclerosis.* Free Radical Biology and Medicine, 2013. **58**: p. 81-86.

443. Yang, Q. and Z.-b. Guo, *Polymorphisms in protein disulfide isomerase are associated with sporadic amyotrophic lateral sclerosis in the Chinese Han population.* International Journal of Neuroscience, 2015: p. 1-5.

444. Gonzalez-Perez, P., et al., *Identification of rare protein disulfide isomerase gene variants in amyotrophic lateral sclerosis patients.* Gene, 2015. **566**(2): p. 158-165.

445. Iwawaki, T., et al., *A transgenic mouse model for monitoring endoplasmic reticulum stress.* Nature medicine, 2004. **10**(1): p. 98-102.

446. Menéndez-Benito, V., S. Heessen, and N.P. Dantuma, *Monitoring of Ubiquitin-Dependent Proteolysis with Green Fluorescent Protein Substrates.* Methods in enzymology, 2005. **399**: p. 490-511.

447. Bence, N.F., E.J. Bennett, and R.R. Kopito, *Application and Analysis of the GFP u Family of Ubiquitin-Proteasome System Reporters.* Methods in enzymology, 2005. **399**: p. 481-490.

448.	Walker, A.K., et al., *Protein disulphide isomerase protects against protein aggregation and is S-nitrosylated in amyotrophic lateral sclerosis.* Brain, 2010. **133**(Pt 1): p. 105-16.

449.	D'Angiolella, V., M. Esencay, and M. Pagano, *A cyclin without cyclin-dependent kinases: cyclin F controls genome stability through ubiquitin-mediated proteolysis.* Trends in cell biology, 2013. **23**(3): p. 135-140.

450.	Turano, C., et al., *Proteins of the PDI family: Unpredicted non-ER locations and functions.* Journal of Cellular Physiology, 2002. **193**(2): p. 154-163.

451.	Nardo, G., et al., *Amyotrophic lateral sclerosis multiprotein biomarkers in peripheral blood mononuclear cells.* PloS one, 2011. **6**(10): p. e25545.

452.	Yang, Y.S., N.Y. Harel, and S.M. Strittmatter, *Reticulon-4A (Nogo-A) redistributes protein disulfide isomerase to protect mice from SOD1-dependent amyotrophic lateral sclerosis.* Journal of Neuroscience, 2009. **29**(44): p. 13850-13859.

453.	Bai, C., R. Richman, and S.J. Elledge, *Human cyclin F.* The EMBO journal, 1994. **13**(24): p. 6087.

454.	D'Angiolella, V., et al., *SCFCyclin F controls centrosome homeostasis and mitotic fidelity via CP110 degradation.* Nature, 2010. **466**(7302): p. 138.

455.	Walter, D., et al., *SCFCyclin F-dependent degradation of CDC6 suppresses DNA re-replication.* Nature communications, 2016. **7**.

456.	D'Angiolella, V., et al., *Cyclin F-mediated degradation of ribonucleotide reductase M2 controls genome integrity and DNA repair.* Cell, 2012. **149**(5): p. 1023-1034.

457.	Klein, D.K., et al., *Cyclin F suppresses B-Myb activity to promote cell cycle checkpoint control.* Nature communications, 2015. **6**: p. 5800.

458.	Lim, S. and P. Kaldis, *Cdks, cyclins and CKIs: roles beyond cell cycle regulation.* Development, 2013. **140**(15): p. 3079-3093.

459.	Skaar, J.R., J.K. Pagan, and M. Pagano, *Mechanisms and function of substrate recruitment by F-box proteins.* Nature reviews. Molecular cell biology, 2013. **14**(6).

460.	Yoshida, Y., et al., *E3 ubiquitin ligase that recognizes sugar chains.* Nature, 2002. **418**(6896): p. 438.

461.	Kong, M., et al., *Cyclin F regulates the nuclear localization of cyclin B1 through a cyclin–cyclin interaction.* The EMBO journal, 2000. **19**(6): p. 1378-1388.

462.	Schulman, B.A., et al., *Insights into SCF ubiquitin ligases from the structure of the Skp1-Skp2 complex.* Nature, 2000. **408**(6810): p. 381.

463.	Choudhury, R., et al., *APC/C and SCF cyclin F Constitute a Reciprocal Feedback Circuit Controlling S-Phase Entry.* Cell reports, 2016. **16**(12): p. 3359-3372.

464.	Fung, T.K., et al., *Cyclin F is degraded during G2-M by mechanisms fundamentally different from other cyclins.* Journal of Biological Chemistry, 2002. **277**(38): p. 35140-35149.

465.	Hogan, A.L., et al., *Expression of ALS/FTD-linked mutant CCNF in zebrafish leads to increased cell death in the spinal cord and an aberrant motor phenotype.* Human Molecular Genetics, 2017: p. ddx136.

466.	Terpe, K., *Overview of tag protein fusions: from molecular and biochemical fundamentals to commercial systems.* Applied microbiology and biotechnology, 2003. **60**(5): p. 523-533.

467.	Shaner, N.C., P.A. Steinbach, and R.Y. Tsien, *A guide to choosing fluorescent proteins.* Nature methods, 2005. **2**(12): p. 905.

468.	Freedman, R.B., A.D. Dunn, and L.W. Ruddock, *Protein folding: A missing redox link in the endoplasmic reticulum.* Current Biology, 1998. **8**(13): p. R468-R470.

469. Ido, A., H. Fukuyama, and M. Urushitani, *Protein misdirection inside and outside motor neurons in amyotrophic lateral sclerosis (ALS): a possible clue for therapeutic strategies.* International journal of molecular sciences, 2011. **12**(10): p. 6980-7003.

470. Tradewell, M.L., et al., *Arginine methylation by PRMT1 regulates nuclear-cytoplasmic localization and toxicity of FUS/TLS harbouring ALS-linked mutations.* Human molecular genetics, 2011. **21**(1): p. 136-149.

471. Donnelly, C.J., et al., *RNA toxicity from the ALS/FTD C9ORF72 expansion is mitigated by antisense intervention.* Neuron, 2013. **80**(2): p. 415-428.

472. Shaffer, A., et al., *XBP1, downstream of Blimp-1, expands the secretory apparatus and other organelles, and increases protein synthesis in plasma cell differentiation.* Immunity, 2004. **21**(1): p. 81-93.

473. Bence, N.F., R.M. Sampat, and R.R. Kopito, *Impairment of the ubiquitin-proteasome system by protein aggregation.* Science, 2001. **292**(5521): p. 1552-1555.

474. Slee, E.A., et al., *Ordering the Cytochrome c–initiated Caspase Cascade: Hierarchical Activation of Caspases-2, -3, -6, -7, -8, and -10 in a Caspase-9–dependent Manner.* The Journal of Cell Biology, 1999. **144**(2): p. 281-292.

475. Bernardoni, P., et al., *Reticulon1-C modulates protein disulphide isomerase function.* Cell death & disease, 2013. **4**(4): p. e581.

476. Soo, K.Y., et al., *Rab1-dependent ER–Golgi transport dysfunction is a common pathogenic mechanism in SOD1, TDP-43 and FUS-associated ALS.* Acta neuropathologica, 2015. **130**(5): p. 679-697.

477. Forrester, M.T., M. Benhar, and J.S. Stamler, *Nitrosative Stress in the ER: A New Role for S-Nitrosylation in Neurodegenerative Diseases.* ACS Chemical Biology, 2006. **1**(6): p. 355-358.

478. Lee, S.O., et al., *Protein disulphide isomerase is required for signal peptide peptidase-mediated protein degradation.* The EMBO journal, 2010. **29**(2): p. 363-375.

479. Lee, A., et al., *Pathogenic mutation in the ALS/FTD gene, CCNF, causes elevated Lys48-linked ubiquitylation and defective autophagy.* Cellular and Molecular Life Sciences, 2017: p. 1-20.

480. Cao, S.S. and R.J. Kaufman, *Endoplasmic reticulum stress and oxidative stress in cell fate decision and human disease.* Antioxidants & redox signaling, 2014. **21**(3): p. 396-413.

481. Lee, E. and D.H. Lee, *Emerging roles of protein disulfide isomerase in cancer.* BMB reports, 2017. **50**(8): p. 401.

482. Ferrari, D.M. and H.D. Soling, *The protein disulphide-isomerase family: unravelling a string of folds.* Biochem J, 1999. **339 (Pt 1)**: p. 1-10.

483. Xu, S., S. Sankar, and N. Neamati, *Protein disulfide isomerase: a promising target for cancer therapy.* Drug Discovery Today, 2014. **19**(3): p. 222-240.

484. Hatahet, F. and L.W. Ruddock, *Substrate recognition by the protein disulfide isomerases.* FEBS Journal, 2007. **274**(20): p. 5223-5234.

485. Jessop, C.E., et al., *Protein disulphide isomerase family members show distinct substrate specificity: P5 is targeted to BiP client proteins.* Journal of Cell Science, 2009. **122**(23): p. 4287-4295.

486. Tian, G., et al., *The crystal structure of yeast protein disulfide isomerase suggests cooperativity between its active sites.* Cell, 2006. **124**(1): p. 61-73.

487. Klappa, P., et al., *The b' domain provides the principal peptide-binding site of protein disulfide isomerase but all domains contribute to binding of misfolded proteins.* The EMBO journal, 1998. **17**(4): p. 927-935.

488. Darby, N.J. and T.E. Creighton, *Functional properties of the individual thioredoxin-like domains of protein disulfide isomerase.* Biochemistry, 1995. **34**(37): p. 11725-11735.

489. Gruber, C.W., et al., *Protein disulfide isomerase: the structure of oxidative folding.* Trends in Biochemical Sciences, 2006. **31**(8): p. 455-464.

490. Woycechowsky, K.J. and R.T. Raines, *Native disulfide bond formation in proteins.* Current Opinion in Chemical Biology, 2000. **4**(5): p. 533-539.

491. Liu, H., X.-Y. Dong, and Y. Sun, *Peptide disulfide RKCGCFF facilitates oxidative protein refolding by mimicking protein disulfide isomerase.* Biochemical Engineering Journal, 2013. **79**(0): p. 29-32.

492. Ren, G., et al., *Properties of the thioredoxin fold superfamily are modulated by a single amino acid residue.* Journal of Biological Chemistry, 2009. **284**(15): p. 10150-10159.

493. Moore, P., K.M. Bernardi, and B. Tsai, *The Ero1α-PDI redox cycle regulates retro-translocation of cholera toxin.* Molecular biology of the cell, 2010. **21**(7): p. 1305-1313.

494. Delom, F., et al., *Role of extracellular molecular chaperones in the folding of oxidized proteins refolding of colloidal thyroglobulin by protein disulfide isomerase and immunoglobulin heavy chain-binding protein.* Journal of Biological Chemistry, 2001. **276**(24): p. 21337-21342.

495. Klappa, P., H.C. Hawkins, and R.B. Freedman, *Interactions between protein disulphide isomerase and peptides.* European Journal of Biochemistry, 1997. **248**(1): p. 37-42.

496. Irvine, A.G., et al., *Protein disulfide-isomerase interacts with a substrate protein at all stages along its folding pathway.* PloS one, 2014. **9**(1): p. e82511.

497. Molinari, M., et al., *Sequential assistance of molecular chaperones and transient formation of covalent complexes during protein degradation from the ER.* The Journal of cell biology, 2002. **158**(2): p. 247-257.

498. Vuori, K., et al., *Characterization of the human prolyl 4-hydroxylase tetramer and its multifunctional protein disulfide-isomerase subunit synthesized in a baculovirus expression system.* Proceedings of the National Academy of Sciences, 1992. **89**(16): p. 7467-7470.

499. Park, B., et al., *Redox regulation facilitates optimal peptide selection by MHC class I during antigen processing.* Cell, 2006. **127**(2): p. 369-382.

500. Benhar, M., M.T. Forrester, and J.S. Stamler, *Nitrosative stress in the ER: a new role for S-nitrosylation in neurodegenerative diseases.* ACS Chem Biol, 2006. **1**(6): p. 355-8.

501. Wang, C., et al., *Structural insights into the redox-regulated dynamic conformations of human protein disulfide isomerase.* Antioxidants & redox signaling, 2013. **19**(1): p. 36-45.

502. Vuori, K., et al., *Expression and site-directed mutagenesis of human protein disulfide isomerase in Escherichia coli. This multifunctional polypeptide has two independently acting catalytic sites for the isomerase activity.* Journal of Biological Chemistry, 1992. **267**(11): p. 7211-7214.

503. Medraño-Fernandez, I., et al., *Different redox sensitivity of endoplasmic reticulum associated degradation clients suggests a novel role for disulphide bonds in secretory proteins.* Biochemistry and Cell Biology, 2014. **92**(2): p. 113-118.

504. Mezghrani, A., et al., *Manipulation of oxidative protein folding and PDI redox state in mammalian cells.* The EMBO journal, 2001. **20**(22): p. 6288-6296.

505. Wilkinson, B. and H.F. Gilbert, *Protein disulfide isomerase.* Biochimica et Biophysica Acta (BBA) - Proteins and Proteomics, 2004. **1699**(1–2): p. 35-44.

506. Furukawa, Y., et al., *Disulfide cross-linked protein represents a significant fraction of ALS-associated Cu, Zn-superoxide dismutase aggregates in spinal cords of model mice.* Proceedings of the National Academy of Sciences, 2006. **103**(18): p. 7148-7153.

507. Nagano, S., et al., *A cysteine residue affects the conformational state and neuronal toxicity of mutant SOD1 in mice: relevance to the pathogenesis of ALS.* Human molecular genetics, 2015. **24**(12): p. 3427-3439.

508. Jonsson, P.A., et al., *Disulphide-reduced superoxide dismutase-1 in CNS of transgenic amyotrophic lateral sclerosis models.* Brain, 2005. **129**(2): p. 451-464.

509. Banci, L., et al., *Structural and dynamic aspects related to oligomerization of apo SOD1 and its mutants.* Proceedings of the National Academy of Sciences, 2009. **106**(17): p. 6980-6985.

510. Niwa, J.-i., et al., *Disulfide bond mediates aggregation, toxicity, and ubiquitylation of familial amyotrophic lateral sclerosis-linked mutant SOD1.* Journal of Biological Chemistry, 2007. **282**(38): p. 28087-28095.

511. Wang, J., G. Xu, and D.R. Borchelt, *Mapping superoxide dismutase 1 domains of non-native interaction: roles of intra-and intermolecular disulfide bonding in aggregation.* Journal of neurochemistry, 2006. **96**(5): p. 1277-1288.

512. Cozzolino, M., et al., *Cysteine 111 affects aggregation and cytotoxicity of mutant Cu, Zn-superoxide dismutase associated with familial amyotrophic lateral sclerosis.* Journal of Biological Chemistry, 2008. **283**(2): p. 866-874.

513. Karch, C.M. and D.R. Borchelt, *A limited role for disulfide cross-linking in the aggregation of mutant SOD1 linked to familial amyotrophic lateral sclerosis.* Journal of Biological Chemistry, 2008. **283**(20): p. 13528-13537.

514. Tabata, Y., et al., *Vaticanol B, a resveratrol tetramer, regulates endoplasmic reticulum stress and inflammation.* American Journal of Physiology-Cell Physiology, 2007. **293**(1): p. C411-C418.

515. Noiva, R. *Protein disulfide isomerase: the multifunctional redox chaperone of the endoplasmic reticulum.* in *Seminars in cell & developmental biology.* 1999. Elsevier.

516. Pariser, H.P., J. Zhang, and R.E. Hausman, *The cell adhesion molecule retina cognin is a cell surface protein disulfide isomerase that uses disulfide exchange activity to modulate cell adhesion.* Experimental cell research, 2000. **258**(1): p. 42-52.

517. Wroblewski, V.J., et al., *Mechanisms involved in degradation of human insulin by cytosolic fractions of human, monkey, and rat liver.* Diabetes, 1992. **41**(4): p. 539-547.

518. Essex, D.W., K. Chen, and M. Swiatkowska, *Localization of protein disulfide isomerase to the external surface of the platelet plasma membrane.* Blood, 1995. **86**(6): p. 2168-2173.

519. Safran, M. and J.L. Leonard, *Characterization of a N-Bromoacetyl-L-Thyroxine Affinity-Labeled 55-Kilodalton Protein as Protein Disulfide Isomerase in Cultured Glial Cells.* Endocrinology, 1991. **129**(4): p. 2011-2016.

520. Jiang, X.-M., et al., *Redox control of exofacial protein thiols/disulfides by protein disulfide isomerase.* Journal of Biological Chemistry, 1999. **274**(4): p. 2416-2423.

521. Terada, K., et al., *Secretion, surface localization, turnover, and steady state expression of protein disulfide isomerase in rat hepatocytes.* Journal of Biological Chemistry, 1995. **270**(35): p. 20410-20416.

522.   Bennett, T.A., et al., *Sulfhydryl regulation of L-selectin shedding: phenylarsine oxide promotes activation-independent L-selectin shedding from leukocytes.* The Journal of Immunology, 2000. **164**(8): p. 4120-4129.

523.   Cho, J., et al., *A critical role for extracellular protein disulfide isomerase during thrombus formation in mice.* The Journal of clinical investigation, 2008. **118**(3): p. 1123.

524.   Stolf, B.S., et al., *Protein disulfide isomerase and host-pathogen interaction.* The Scientific World Journal, 2011. **11**: p. 1749-1761.

525.   Tsai, B., et al., *Protein disulfide isomerase acts as a redox-dependent chaperone to unfold cholera toxin.* Cell, 2001. **104**(6): p. 937-948.

526.   Gerner, C., et al., *Reassembling proteins and chaperones in human nuclear matrix protein fractions.* Journal of cellular biochemistry, 1999. **74**(2): p. 145-151.

527.   Clive, D.R. and J.J. Greene, *Cooperation of protein disulfide isomerase and redox environment in the regulation of NF-κB and AP1 binding to DNA.* Cell biochemistry and function, 1996. **14**(1): p. 49-55.

528.   Markus, M. and R. Benezra, *Two isoforms of protein disulfide isomerase alter the dimerization status of E2A proteins by a redox mechanism.* Journal of Biological Chemistry, 1999. **274**(2): p. 1040-1049.

529.   Hotchkiss, K.A., L.J. Matthias, and P.J. Hogg, *Exposure of the cryptic Arg-Gly-Asp sequence in thrombospondin-1 by protein disulfide isomerase.* Biochimica et Biophysica Acta (BBA)-Protein Structure and Molecular Enzymology, 1998. **1388**(2): p. 478-488.

530.   Yoshimori, T., et al., *Protein disulfide-isomerase in rat exocrine pancreatic cells is exported from the endoplasmic reticulum despite possessing the retention signal.* Journal of Biological Chemistry, 1990. **265**(26): p. 15984-15990.

531.   Halloran, M., S. Parakh, and J.D. Atkin, *The role of s-nitrosylation and s-glutathionylation of protein disulphide isomerase in protein misfolding and neurodegeneration.* International journal of cell biology, 2013. **2013**(2013): p. 797914.

532.   Kourtis, N. and N. Tavernarakis, *Cellular stress response pathways and ageing: intricate molecular relationships.* The EMBO journal, 2011. **30**(13): p. 2520-2531.

533.   Uehara, T., et al., *S-nitrosylated protein-disulphide isomerase links protein misfolding to neurodegeneration.* Nature, 2006. **441**(7092): p. 513-7.

534.   Jeon, G.S., et al., *Potential effect of S-nitrosylated protein disulfide isomerase on mutant SOD1 aggregation and neuronal cell death in amyotrophic lateral sclerosis.* Molecular neurobiology, 2014. **49**(2): p. 796-807.

535.   Selles, B., et al., *Atypical protein disulfide isomerases (PDI): Comparison of the molecular and catalytic properties of poplar PDI-A and PDI-M with PDI-L1A.* PloS one, 2017. **12**(3): p. e0174753.

536.   Galligan, J.J. and D.R. Petersen, *The human protein disulfide isomerase gene family.* Human genomics, 2012. **6**(1): p. 6.

537.   Maattanen, P., et al., *ERp57 and PDI: multifunctional protein disulfide isomerases with similar domain architectures but differing substrate–partner associations This paper is one of a selection of papers published in this Special Issue, entitled CSBMCB—Membrane Proteins in Health and Disease.* Biochemistry and cell biology, 2006. **84**(6): p. 881-889.

538.   Mazzarella, R.A., et al., *ERp72, an abundant luminal endoplasmic reticulum protein, contains three copies of the active site sequences of protein disulfide isomerase.* Journal of Biological Chemistry, 1990. **265**(2): p. 1094-1101.

539. Sato, Y., et al., *Synergistic cooperation of PDI family members in peroxiredoxin 4-driven oxidative protein folding.* Sci Rep, 2013. **3**: p. 2456.

540. Kozlov, G., et al., *A structural overview of the PDI family of proteins.* The FEBS journal, 2010. **277**(19): p. 3924-3936.

541. Grillo, C., et al., *Cooperative activity of Ref-1/APE and ERp57 in reductive activation of transcription factors.* Free Radical Biology and Medicine, 2006. **41**(7): p. 1113-1123.

542. Leach, M.R., et al., *Localization of the lectin, ERp57 binding, and polypeptide binding sites of calnexin and calreticulin.* Journal of Biological Chemistry, 2002. **277**(33): p. 29686-29697.

543. Molinari, M., et al., *Contrasting Functions of Calreticulin and Calnexin in Glycoprotein Folding and ER Quality Control.* Molecular Cell, 2004. **13**(1): p. 125-135.

544. Frickel, E.M., et al., *ERp57 is a multifunctional thiol-disulfide oxidoreductase.* J Biol Chem, 2004. **279**(18): p. 18277-87.

545. Lee, Y.M., F. Almqvist, and S.J. Hultgren, *Targeting virulence for antimicrobial chemotherapy.* Current opinion in pharmacology, 2003. **3**(5): p. 513-519.

546. Dutton, R.J., et al., *Bacterial species exhibit diversity in their mechanisms and capacity for protein disulfide bond formation.* Proceedings of the National Academy of Sciences, 2008. **105**(33): p. 11933-11938.

547. Heras, B., et al., *DSB proteins and bacterial pathogenicity.* Nature Reviews Microbiology, 2009. **7**(3): p. 215-225.

548. Bardwell, J.C., K. McGovern, and J. Beckwith, *Identification of a protein required for disulfide bond formation in vivo.* Cell, 1991. **67**(3): p. 581-589.

549. Akiyama, Y., et al., *In vitro catalysis of oxidative folding of disulfide-bonded proteins by the Escherichia coli dsbA (ppfA) gene product.* Journal of Biological Chemistry, 1992. **267**(31): p. 22440-22445.

550. Martin, J.L., *Thioredoxin—a fold for all reasons.* Structure, 1995. **3**(3): p. 245-250.

551. Martin, J.L., J. Bardwell, and J. Kuriyan, *Crystal structure of the DsbA protein required for disulphide bond formation in vivo.* Nature, 1993. **365**(6445): p. 464.

552. Kadokura, H., et al., *Snapshots of DsbA in action: detection of proteins in the process of oxidative folding.* Science, 2004. **303**(5657): p. 534-537.

553. Darby, N.J. and T.E. Creighton, *Catalytic mechanism of DsbA and its comparison with that of protein disulfide isomerase.* Biochemistry, 1995. **34**(11): p. 3576-3587.

554. Inaba, K., et al., *Crystal structure of the DsbB-DsbA complex reveals a mechanism of disulfide bond generation.* Cell, 2006. **127**(4): p. 789-801.

555. Zhou, Y., et al., *NMR solution structure of the integral membrane enzyme DsbB: functional insights into DsbB-catalyzed disulfide bond formation.* Molecular cell, 2008. **31**(6): p. 896-908.

556. Berkmen, M., D. Boyd, and J. Beckwith, *The nonconsecutive disulfide bond of Escherichia coli phytase (AppA) renders it dependent on the protein-disulfide isomerase, DsbC.* Journal of Biological Chemistry, 2005. **280**(12): p. 11387-11394.

557. Hiniker, A., J.-F. Collet, and J.C. Bardwell, *Copper stress causes an in vivo requirement for the Escherichia coli disulfide isomerase DsbC.* Journal of Biological Chemistry, 2005. **280**(40): p. 33785-33791.

558. McCarthy, A.A., et al., *Crystal structure of the protein disulfide bond isomerase, DsbC, from Escherichia coli.* Nature Structural & Molecular Biology, 2000. **7**(3): p. 196.

559.   Heras, B., et al., *Crystal structures of the DsbG disulfide isomerase reveal an unstable disulfide.* Proceedings of the National Academy of Sciences of the United States of America, 2004. **101**(24): p. 8876-8881.

560.   Rietsch, A., et al., *Reduction of the periplasmic disulfide bond isomerase, DsbC, occurs by passage of electrons from cytoplasmic thioredoxin.* Journal of Bacteriology, 1997. **179**(21): p. 6602-6608.

561.   Chen, J., et al., *Chaperone activity of DsbC.* Journal of Biological Chemistry, 1999. **274**(28): p. 19601-19605.

562.   Xu, C., B. Bailly-Maitre, and J.C. Reed, *Endoplasmic reticulum stress: cell life and death decisions.* Journal of Clinical Investigation, 2005. **115**(10): p. 2656.

563.   LaMantia, M. and W.J. Lennarz, *The essential function of yeast protein disulfide isomerase does not reside in its isomerase activity.* Cell, 1993. **74**(5): p. 899-908.

564.   Wolter, K.G., et al., *Movement of Bax from the cytosol to mitochondria during apoptosis.* The Journal of cell biology, 1997. **139**(5): p. 1281-1292.

565.   Deng, H.-X., et al., *Conversion to the amyotrophic lateral sclerosis phenotype is associated with intermolecular linked insoluble aggregates of SOD1 in mitochondria.* Proceedings of the National Academy of Sciences, 2006. **103**(18): p. 7142-7147.

566.   Fujiwara, N., et al., *Oxidative modification to cysteine sulfonic acid of Cys111 in human copper-zinc superoxide dismutase.* Journal of Biological Chemistry, 2007. **282**(49): p. 35933-35944.

567.   Guo, Y., et al., *Ultrastructural diversity of inclusions and aggregations in the lumbar spinal cord of SOD1-G93A transgenic mice.* Brain research, 2010. **1353**: p. 234-244.

568.   Polling, S., et al., *Misfolded Polyglutamine, Polyalanine, and Superoxide Dismutase 1 Aggregate via Distinct Pathways in the Cell.* Journal of Biological Chemistry, 2014. **289**(10): p. 6669-6680.

569.   Wang, X., et al., *Bcl-2 proteins regulate ER membrane permeability to luminal proteins during ER stress-induced apoptosis.* Cell Death & Differentiation, 2011. **18**(1): p. 38-47.

570.   Ayala, Y.M., et al., *Structural determinants of the cellular localization and shuttling of TDP-43.* Journal of cell science, 2008. **121**(22): p. 3778-3785.

571.   Kozutsumi, Y., et al., *The presence of malfolded proteins in the endoplasmic reticulum signals the induction of glucose-regulated proteins.* Nature, 1988. **332**(6163): p. 462-464.

572.   Cohen, T.J., et al., *Redox signalling directly regulates TDP-43 via cysteine oxidation and disulphide cross-linking.* The EMBO journal, 2012. **31**(5): p. 1241-1252.

573.   Lagier-Tourenne, C., M. Polymenidou, and D.W. Cleveland, *TDP-43 and FUS/TLS: emerging roles in RNA processing and neurodegeneration.* Human molecular genetics, 2010. **19**(R1): p. R46-R64.

574.   Kulp, M.S., et al., *Domain architecture of protein-disulfide isomerase facilitates its dual role as an oxidase and an isomerase in Ero1p-mediated disulfide formation.* Journal of Biological Chemistry, 2006. **281**(2): p. 876-884.

575.   Messens, J. and J.-F. Collet, *Pathways of disulfide bond formation in Escherichia coli.* The international journal of biochemistry & cell biology, 2006. **38**(7): p. 1050-1062.

576.   Gross, E., et al., *Structure of Ero1p, source of disulfide bonds for oxidative protein folding in the cell.* Cell, 2004. **117**(5): p. 601-610.

577.   Sevier, C.S., et al., *The prokaryotic enzyme DsbB may share key structural features with eukaryotic disulfide bond forming oxidoreductases.* Protein science, 2005. **14**(6): p. 1630-1642.

578.   Edman, J.C., et al., *Sequence of protein disulphide isomerase and implications of its relationship to thioredoxin.* Nature, 1985. **317**(6034): p. 267-270.

579.   Nakamura, H., *Thioredoxin and its related molecules: update 2005.* Antioxidants & redox signaling, 2005. **7**(5-6): p. 823-828.

580.   Haebel, P.W., et al., *The disulfide bond isomerase DsbC is activated by an immunoglobulin-fold thiol oxidoreductase: crystal structure of the DsbC–DsbDα complex.* The EMBO journal, 2002. **21**(18): p. 4774-4784.

581.   Krause, G., et al., *Mimicking the active site of protein disulfide-isomerase by substitution of proline 34 in Escherichia coli thioredoxin.* Journal of Biological Chemistry, 1991. **266**(15): p. 9494-9500.

582.   Zapun, A., J.C. Bardwell, and T.E. Creighton, *The reactive and destabilizing disulfide bond of DsbA, a protein required for protein disulfide bond formation in vivo.* Biochemistry, 1993. **32**(19): p. 5083-5092.

583.   Appenzeller-Herzog, C. and L. Ellgaard, *In vivo reduction-oxidation state of protein disulfide isomerase: the two active sites independently occur in the reduced and oxidized forms.* Antioxid Redox Signal, 2008. **10**(1): p. 55-64.

584.   Georgescu, R.E., et al., *Proline isomerization-independent accumulation of an early intermediate and heterogeneity of the folding pathways of a mixed α/β protein, Escherichia coli thioredoxin.* Biochemistry, 1998. **37**(28): p. 10286-10297.

585.   Charbonnier, J.-B., et al., *On the role of the cis-proline residue in the active site of DsbA.* Protein Science, 1999. **8**(1): p. 96-105.

586.   Maeda, K., et al., *Structural basis for target protein recognition by the protein disulfide reductase thioredoxin.* Structure, 2006. **14**(11): p. 1701-1710.

587.   Dai, S., et al., *Structural snapshots along the reaction pathway of ferredoxin–thioredoxin reductase.* Nature, 2007. **448**: p. 92-96.

588.   Horibe, T., et al., *Different contributions of the three CXXC motifs of human protein-disulfide isomerase-related protein to isomerase activity and oxidative refolding.* Journal of Biological Chemistry, 2004. **279**(6): p. 4604-4611.

589.   Huber-Wunderlich, M. and R. Glockshuber, *A single dipeptide sequence modulates the redox properties of a whole enzyme family.* Folding and design, 1998. **3**(3): p. 161-171.

590.   Quan, S., et al., *The CXXC motif is more than a redox rheostat.* Journal of Biological Chemistry, 2007. **282**(39): p. 28823-28833.

591.   Hanson, G.T., et al., *Investigating mitochondrial redox potential with redox-sensitive green fluorescent protein indicators.* Journal of Biological Chemistry, 2004. **279**(13): p. 13044-13053.

592.   Mössner, E., M. Huber-Wunderlich, and R. Glockshuber, *Characterization of Escherichia coli thioredoxin variants mimicking the active-sites of other thiol/disulfide oxidoreductases.* Protein Science, 1998. **7**(5): p. 1233-1244.

593.   Appenzeller-Herzog, C. and L. Ellgaard, *The human PDI family: versatility packed into a single fold.* Biochim Biophys Acta, 2008. **1783**(4): p. 535-48.

594.   Bessette, P.H., et al., *In Vivo and in Vitro Function of theEscherichia coli Periplasmic Cysteine Oxidoreductase DsbG.* Journal of Biological Chemistry, 1999. **274**(12): p. 7784-7792.

595.   Woycechowsky, K.J., K.D. Wittrup, and R.T. Raines, *A small-molecule catalyst of protein folding in vitro and in vivo.* Chemistry & Biology, 1999. **6**(12): p. 871-879.

596.   Kersteen, E.A. and R.T. Raines, *Catalysis of protein folding by protein disulfide isomerase and small-molecule mimics.* Antioxid Redox Signal, 2003. **5**(4): p. 413-24.

597.   Nguyen, V.D., et al., *Alternative conformations of the x region of human protein disulphide-isomerase modulate exposure of the substrate binding b'domain.* Journal of molecular biology, 2008. **383**(5): p. 1144-1155.

598.   Perri, E., S. Parakh, and J. Atkin, *Protein disulphide isomerases: emerging roles of PDI and ERp57 in the nervous system and as therapeutic targets for ALS.* Expert opinion on therapeutic targets, 2017. **21**(1): p. 37-49.

599.   Hamilos, D. and H. Wedner, *The role of glutathione in lymphocyte activation. I. Comparison of inhibitory effects of buthionine sulfoximine and 2-cyclohexene-1-one by nuclear size transformation.* The Journal of Immunology, 1985. **135**(4): p. 2740-2747.

600.   Chakravarthi, S., C.E. Jessop, and N.J. Bulleid, *The role of glutathione in disulphide bond formation and endoplasmic-reticulum-generated oxidative stress.* EMBO reports, 2006. **7**(3): p. 271-275.

601.   Darby, N.J., R.B. Freedman, and T.E. Creighton, *Dissecting the mechanism of protein disulfide isomerase: catalysis of disulfide bond formation in a model peptide.* Biochemistry, 1994. **33**(25): p. 7937-7947.

602.   Fox, A.H. and A.I. Lamond, *Paraspeckles.* Cold Spring Harbor perspectives in biology, 2010. **2**(7): p. a000687.

603.   Shelkovnikova, T.A., et al., *Compromised paraspeckle formation as a pathogenic factor in FUSopathies.* Human Molecular Genetics, 2014. **23**(9): p. 2298-2312.

604.   Nishimoto, Y., et al., *The long non-coding RNA nuclear-enriched abundant transcript 1_2 induces paraspeckle formation in the motor neuron during the early phase of amyotrophic lateral sclerosis.* Molecular brain, 2013. **6**(1): p. 31.

605.   Ceballos-Picot, I., et al., *Glutathione antioxidant system as a marker of oxidative stress in chronic renal failure.* Free Radical Biology and Medicine, 1996. **21**(6): p. 845-853.

606.   Posadino, A.M., et al., *Resveratrol alters human endothelial cells redox state and causes mitochondrial-dependent cell death.* Food and Chemical Toxicology, 2015. **78**: p. 10-16.

607.   Cai, H., C.-C. Wang, and C.-L. Tsou, *Chaperone-like activity of protein disulfide isomerase in the refolding of a protein with no disulfide bonds.* Journal of Biological Chemistry, 1994. **269**(40): p. 24550-24552.

608.   Di, L., *Strategic approaches to optimizing peptide ADME properties.* The AAPS journal, 2015. **17**(1): p. 134-143.

609.   Banting, F., et al., *Pancreatic extracts in the treatment of diabetes mellitus.* Canadian Medical Association Journal, 1922. **12**(3): p. 141.

610.   Harris, K.S., et al., *Efficient backbone cyclization of linear peptides by a recombinant asparaginyl endopeptidase.* Nature communications, 2015. **6**: p. 10199.

611.   Altura, B.M. and B.T. Altura. *Actions of vasopressin, oxytocin, and synthetic analogs on vascular smooth muscle*. in *Federation proceedings*. 1984.

612.   Ramsey, J.D. and N.H. Flynn, *Cell-penetrating peptides transport therapeutics into cells.* Pharmacology & therapeutics, 2015. **154**: p. 78-86.

613.   Lau, J.L. and M.K. Dunn, *Therapeutic peptides: Historical perspectives, current development trends, and future directions.* Bioorganic & Medicinal Chemistry, 2017.

614.   Sousa, D.A., et al., *Influence of cysteine and tryptophan substitution on DNA-binding activity on maize α-hairpinin antimicrobial peptide.* Molecules, 2016. **21**(8): p. 1062.

615.   Nolde, S.B., et al., *Disulfide-stabilized helical hairpin structure and activity of a novel antifungal peptide EcAMP1 from seeds of barnyard grass (Echinochloa crus-galli).* Journal of Biological Chemistry, 2011. **286**(28): p. 25145-25153.

616.   Walker, A.K., et al., *Functional recovery in new mouse models of ALS/FTLD after clearance of pathological cytoplasmic TDP-43.* Acta neuropathologica, 2015. **130**(5): p. 643-660.

617.   Oller-Salvia, B., et al., *Blood–brain barrier shuttle peptides: an emerging paradigm for brain delivery.* Chemical Society Reviews, 2016. **45**(17): p. 4690-4707.

618.   Upadhyay, R.K., *Drug delivery systems, CNS protection, and the blood brain barrier.* BioMed research international, 2014. **2014**.

619.   Parakh, S. and J.D. Atkin, *Novel roles for protein disulphide isomerase in disease states: a double edged sword?* Frontiers in cell and developmental biology, 2015. **3**.

620.   Hoffstrom, B.G., et al., *Inhibitors of protein disulfide isomerase suppress apoptosis induced by misfolded proteins.* Nature chemical biology, 2010. **6**(12): p. 900-906.

Appendix

Supplementary figure 1
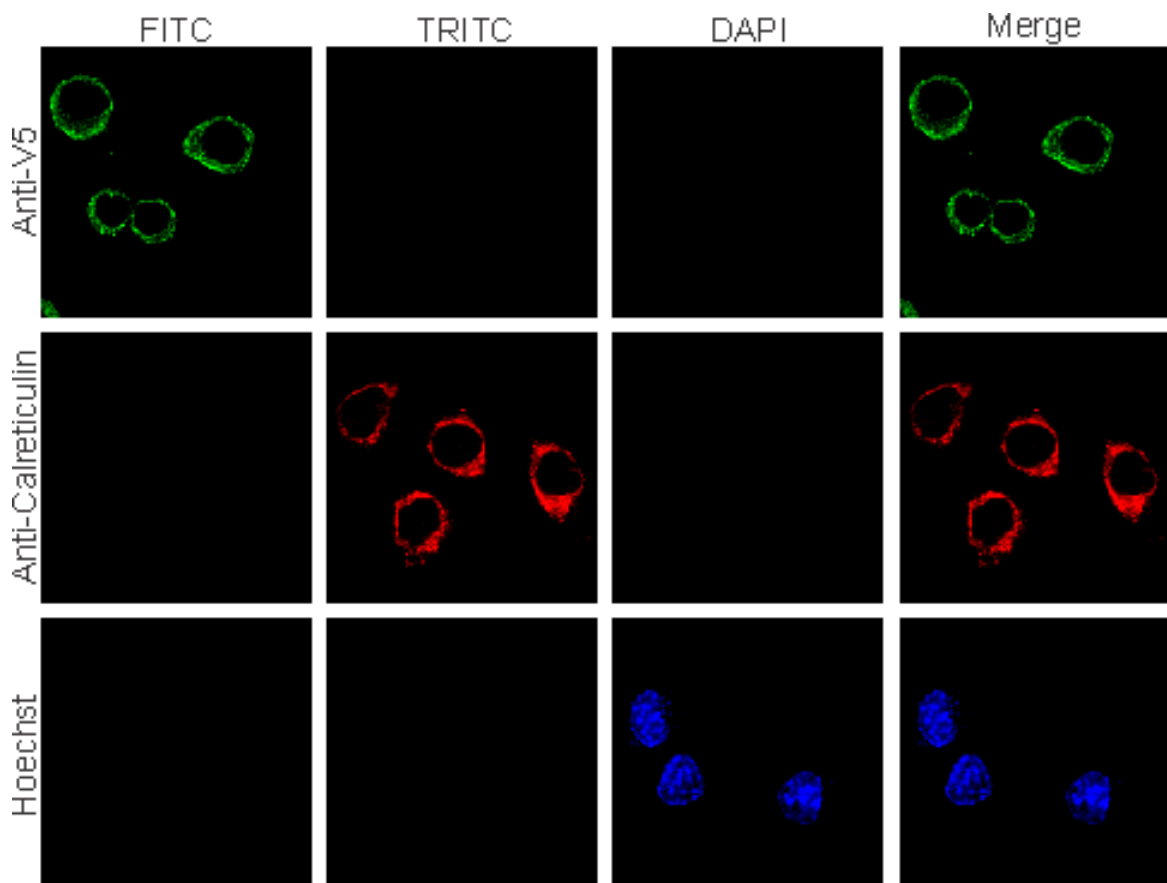
Supplementary figure 1: Single colour controls. Cells expressing PDI-V5 were stained with either Anti-Calreticulin, Anti-V5 or Hoechst and then viewed under a fluorescent microscope to ensure there was no bleed through from one channel to another. The figure demonstrates that no bleed through was evident, validating that PDI co-localises with Calreticulin in the ER.
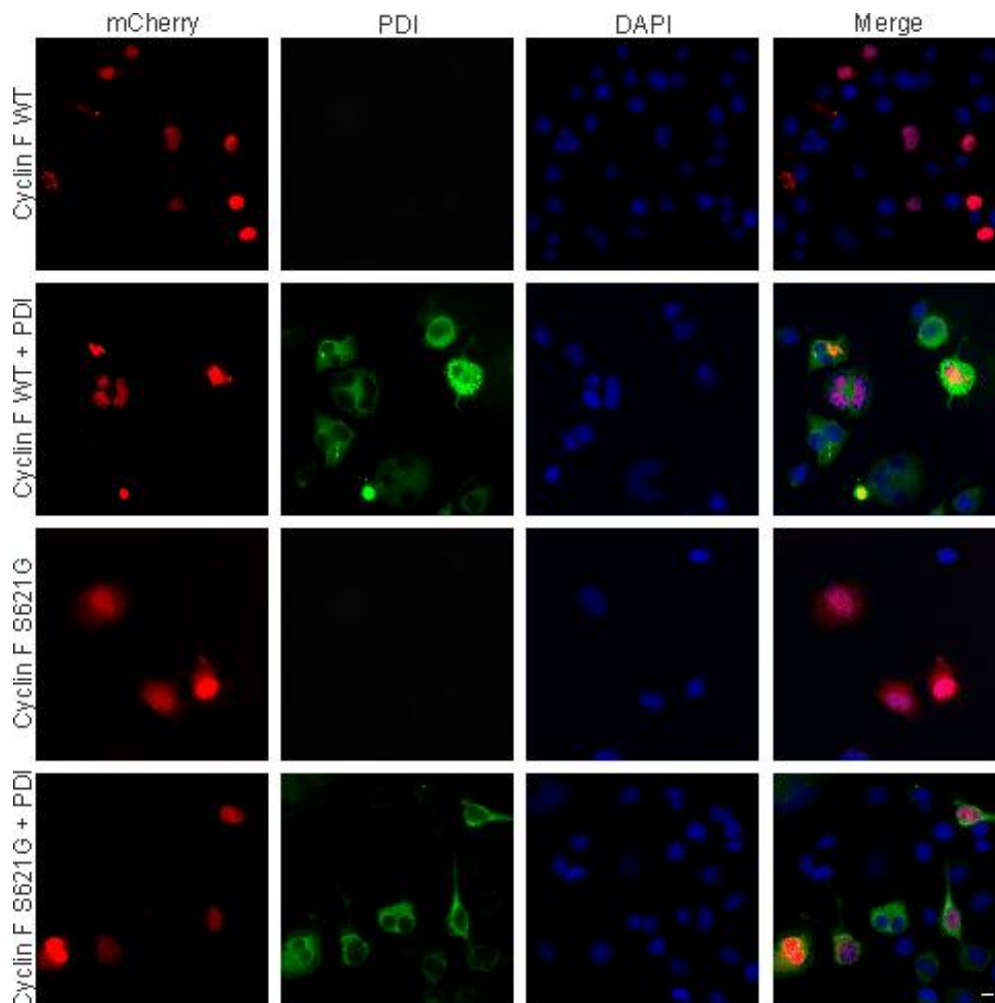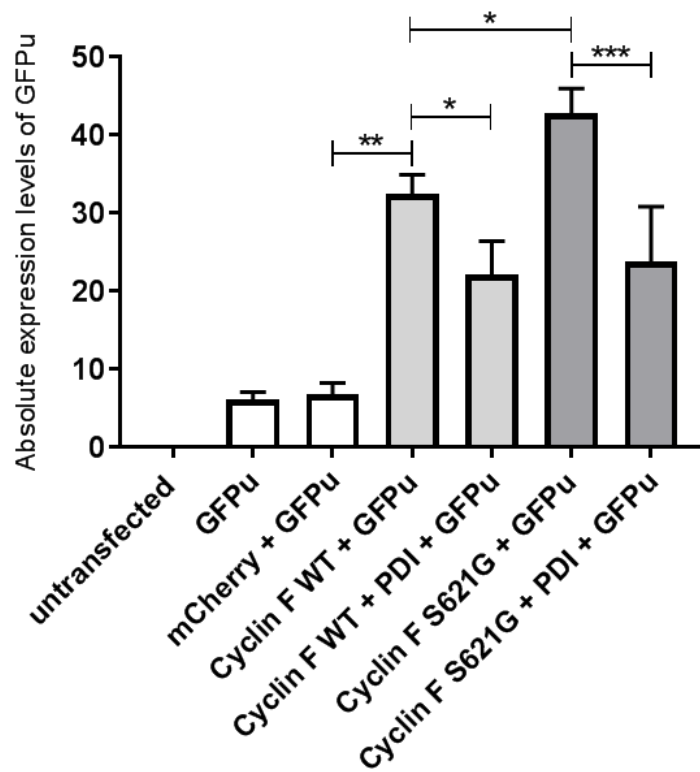
Supplementary figure 2: Low magnification images demonstrating that the overexpression of PDI inhibits ALS mutant Cyclin F localisation to the cytoplasm. The overexpression of PDI decreases the proportion of cells displaying mutant Cyclin F mislocalisation to the cytoplasm. Scale bar = 20 µM.
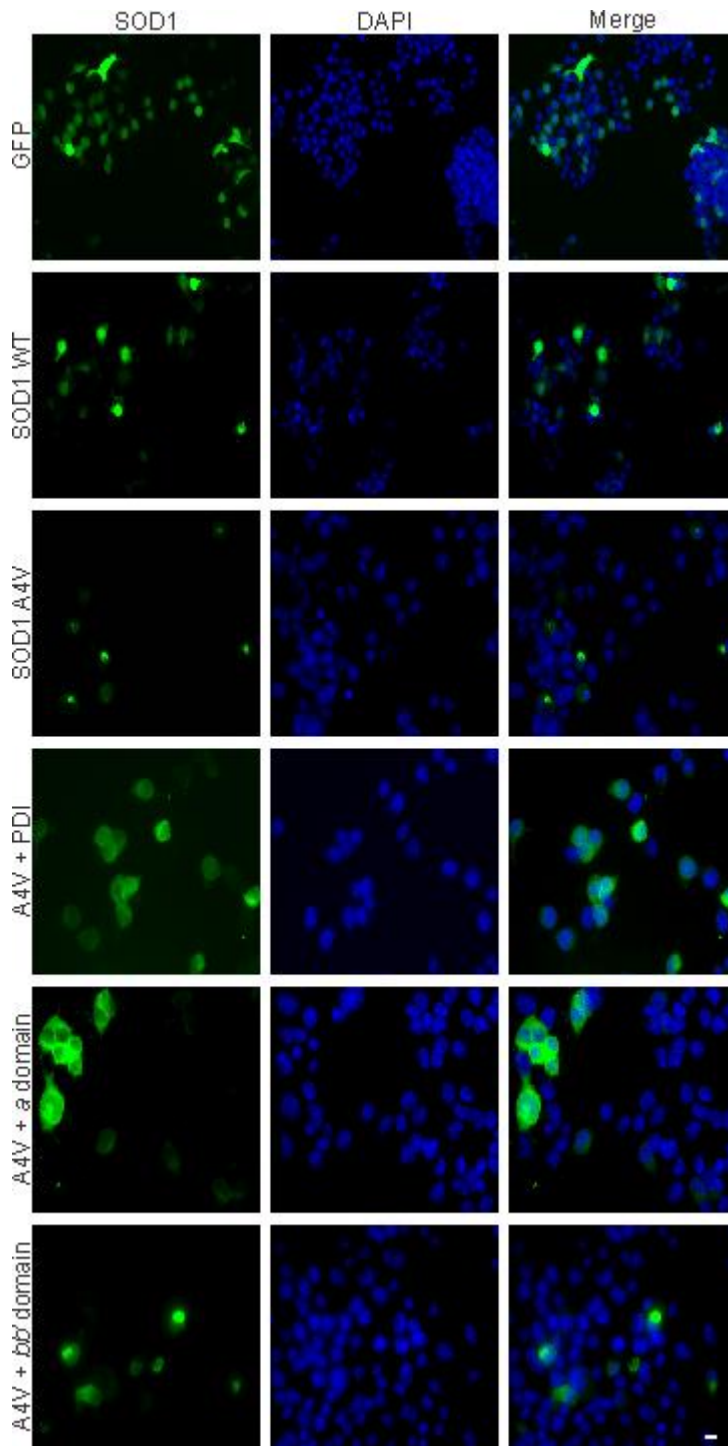
Supplementary figure 3
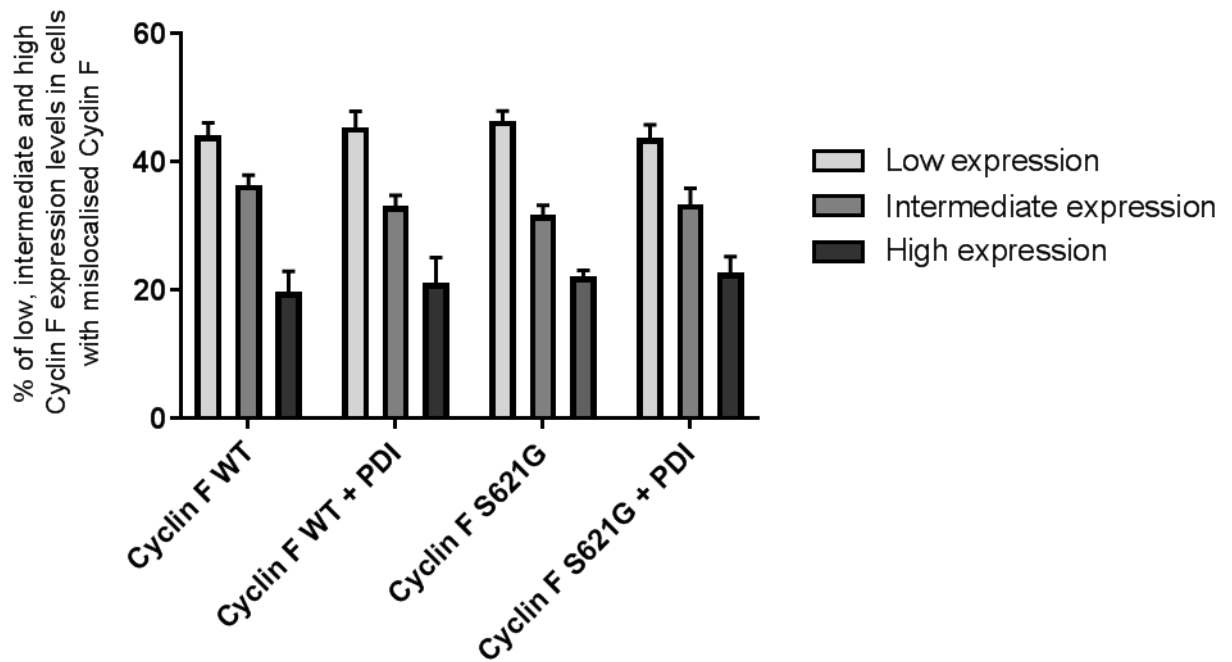
Supplementary figure 3: The percentage of low, intermediate and high Cyclin F expression levels in cells displaying Cyclin F mislocalisation. Cyclin F expression levels were similar between groups, suggesting that co-expression with PDI did not alter or decrease the expression of Cyclin F. This result validates the finding that the overexpression of PDI decreases mutant Cyclin F mislocalisation to the cytoplasm.

Supplementary figure 4: The absolute expression levels of GFPu in cells co-expressing wildtype or mutant Cyclin F with either empty pcDNA3.1 vector or PDI. In addition to analysing the percentage of Cyclin F transfected cells displaying GFPu activation, the absolute expression levels of GFPu were also examined. The overexpression of PDI decreased the absolute expression levels of GFPu in cells expressing both wildtype or mutant Cyclin F, suggesting that PDI is protective against UPS impairment induced by both wildtype and mutant forms of the protein.

Supplementary figure 5: Low magnification images demonstrating that the overexpression of PDI and the *a* domain mutant reduces mutant SOD1 inclusion formation. The overexpression of PDI and the *a* domain mutant decreases the proportion of cells displaying mutant SOD1 inclusion formation. Scale bar = 20 µM.
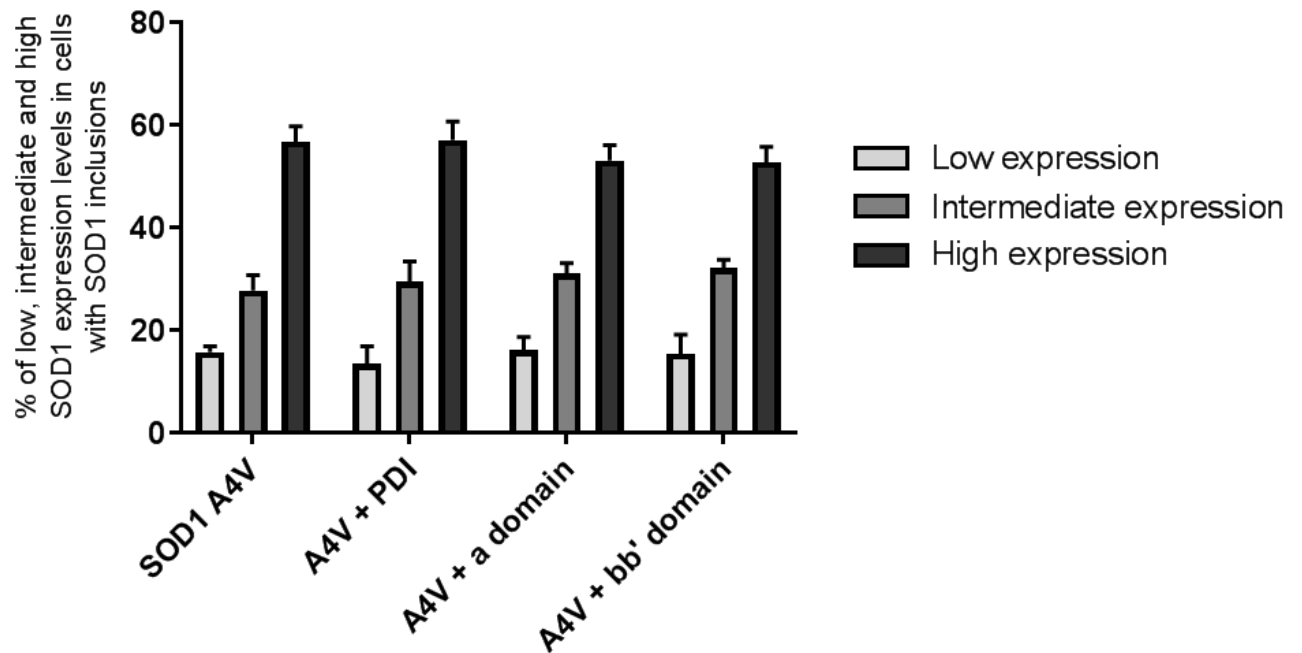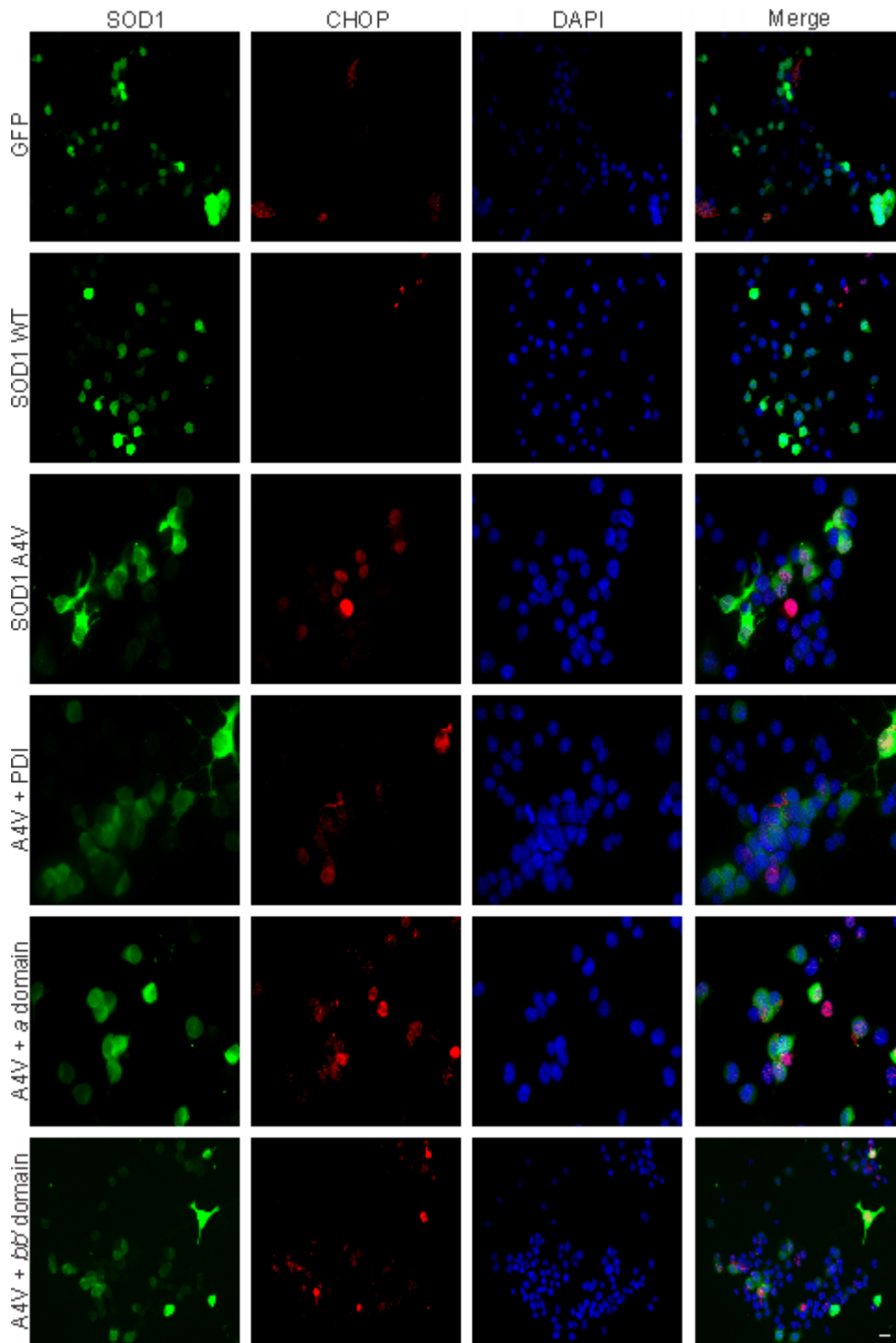
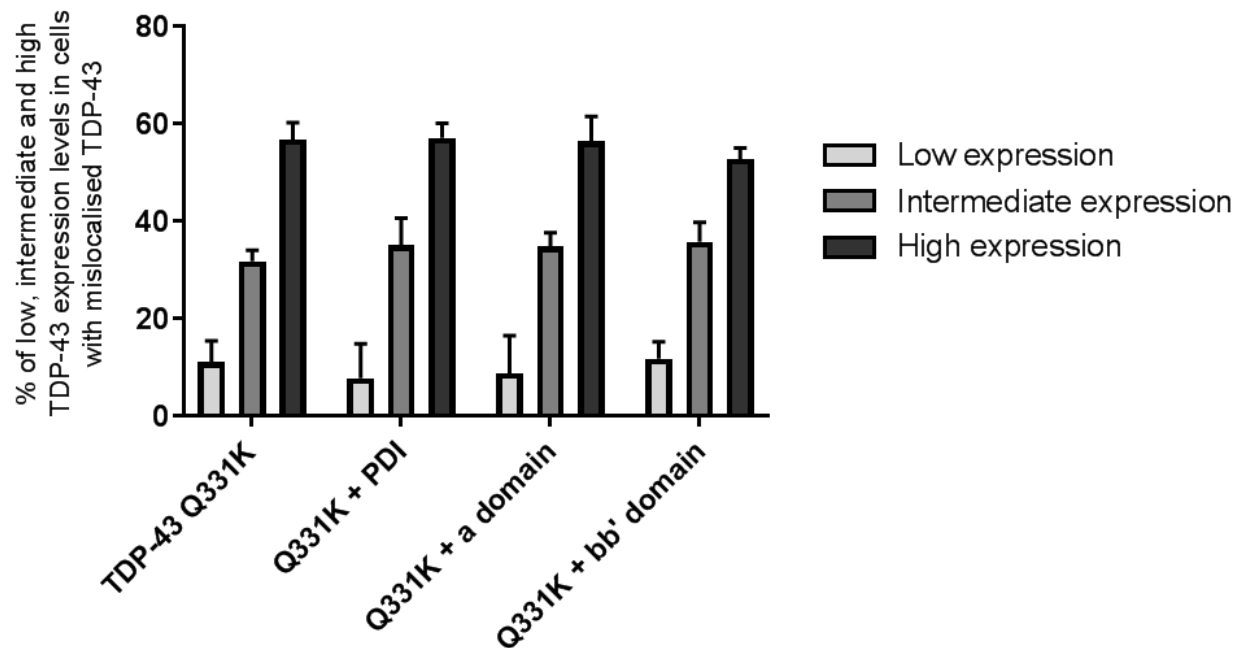**Supplementary figure 6: The percentage of low, intermediate and high mutant SOD1 A4V expression levels in cells displaying SOD1 inclusions.** Mutant SOD1 A4V expression levels were similar between groups, suggesting that co-expression with PDI or the domain mutants did not alter or decrease the expression of mutant SOD1. This result validates the finding that the overexpression of PDI and the *a* domain mutant decreases mutant SOD1 inclusion formation.

Supplementary figure 7: Low magnification images demonstrating that the overexpression of PDI's *a* and *bb'* domains decreases ER stress induced by mutant SOD1. The overexpression of PDI and the *a* and *bb'* domain mutants decreases the proportion of cells displaying CHOP activation induced by mutant SOD1. Scale bar = 20 µM.

Supplementary figure 8: The percentage of low, intermediate and high mutant TDP-43 Q331K expression levels in cells displaying TDP-43 mislocalisation to the cytoplasm.

Mutant TDP-43 Q331K expression levels were similar between groups, suggesting that co-expression with PDI or the domain mutants did not alter or decrease the expression of mutant TDP-43. This result validates the finding that the overexpression of PDI and the *a* domain mutant decreases mutant TDP-43 mislocalisation to the cytoplasm.